TESIS DE LA UNIVERSIDAD DE ZARAGOZA
2020
125

Jaime Martín González

Complejos Polihidruro de osmio con un ligando pinza P,O,P : reacciones de formación de hidrógeno y de activación de enlaces B-H y B-N

Departamento
Química Inorgánica

Director/es
Esteruelas Rodrigo, Miguel Angel
García Yebra, María Cristina

ISSN 2254-7606

Prensas de la Universidad
Universidad Zaragoza

ISSN 2254-7606

Universidad Zaragoza
1542

Tesis Doctoral

COMPLEJOS POLIHIDRURO DE OSMIO CON UN LIGANDO PINZA P,O,P : REACCIONES DE FORMACIÓN DE HIDRÓGENO Y DE ACTIVACIÓN DE ENLACES B-H Y B-N

Autor

Jaime Martín González

Director/es

Esteruelas Rodrigo, Miguel Angel
García Yebra, María Cristina

UNIVERSIDAD DE ZARAGOZA

Química Inorgánica

2020

Universidad de Zaragoza

Departamento de Química Inorgánica

COMPLEJOS POLIHIDRURO DE OSMIO CON UN LIGANDO PINZA P,O,P: REACCIONES DE FORMACIÓN DE HIDRÓGENO Y DE ACTIVACIÓN DE ENLACES B-H Y B-N

Memoria presentada en la modalidad de compendio de publicaciones para acceder al título de Doctor, por el Licenciado en Químicas

Jaime Martín González

Zaragoza, 2020

Miguel Ángel Esteruelas Rodrigo, Profesor de Investigación de Organismo Público de Investigación (Consejo Superior de Investigaciones Científicas) en el Instituto Universitario de Investigación mixto de Síntesis Química y Catálisis Homogénea (ISQCH)

y

Mª Cristina García Yebra, Profesora Titular de Universidad del Departamento de Química Orgánica y Química Inorgánica de la Universidad de Alcalá

HACEN CONSTAR:

que la presente Memoria titulada: ***"Complejos Polihidruro de Osmio con un Ligando Pinza P,O,P: Reacciones de Formación de Hidrógeno y de Activación de Enlaces B-H y B-N"*** ha sido desarrollada en el Departamento de Química Inorgánica de la Facultad de Ciencias de la Universidad de Zaragoza, y AUTORIZAN la presentación de la misma en la modalidad de compendio de publicaciones para su defensa.

Zaragoza, de Enero de 2020

Fdo. Prof. Miguel Ángel Esteruelas Fdo. Prof. Mª Cristina García Yebra

ÍNDICE

PREÁMBULO

Esta Tesis Doctoral se presenta en la modalidad de compendio de publicaciones, siguiendo la normativa establecida en el *acuerdo de 20 de diciembre de 2013, del Consejo de Gobierno de la Universidad de Zaragoza, por el que se aprueba el Reglamento de Tesis Doctorales (BOUZ 10/01/2014)*. Todos los trabajos que se exponen a continuación han sido previamente publicados en revistas científicas con un índice de impacto incluido en la relación de revistas del *Journal of Citation Reports* y constituyen una unidad temática.

La estructura de la Tesis consta de una introducción general y una memoria, en la que se especifican los objetivos, las aportaciones del doctorando, la metodología utilizada, los resúmenes de los artículos y las conclusiones finales. Las copias de los artículos publicados, así como la información suplementaria, se incluyen como apéndice de la tesis. El resumen de cada artículo está organizado en forma de capítulo con una introducción, discusión de resultados y conclusiones.

El capítulo 1 describe la preparación de nuevos complejos polihidruros de osmio estabilizados por un ligando pinza POP y la formación cinéticamente controlada de H_2 al añadir secuencialmente H^+ y H^-. El capítulo 2 muestra el mecanismo de la deshidrogenación catalítica de ácido fórmico promovida por el complejo $OsH_3(OH)\{\kappa^3$-*P,O,P*-[xant($P^iPr_2)_2$]} sobre la base del estudio de la cinética del proceso, observaciones espectroscópicas y cálculos teóricos. El capítulo 3 recoge la síntesis y caracterización de complejos σ-borano elongados y σ-borano de osmio y analiza la situación de enlace osmio-borano desde un punto de vista teórico. El capítulo 4 describe la preparación de complejos boróxido de osmio a través de un nuevo camino sintético y estudia su

reactividad frente a CO. El capítulo 5 presenta la síntesis y caracterización de los primeros anillos aromáticos de tres miembros con vértices distintos. Los complejos cicloosmatioborano preparados en este capítulo son una nueva manifestación de la aromaticidad de tipo Hückel 4*n* + 2 cuando *n* = 0.

Ls artículos que forman parte de esta Tesis Doctoral son los siguientes:

1. Esteruelas, M. A.; García-Yebra, C.; Martín, J.; Oñate, E. *mer*, *fac*, and Bidentate Coordination of an Alkyl-POP Ligand in the Chemistry of Nonclassical Osmium Hydrides. *Inorg. Chem.* **2017**, *56*, 676-683.

2. Esteruelas, M. A.; García-Yebra, C.; Martín, J.; Oñate, E. Dehydrogenation of Formic Acid Promoted by a Trihydride-Hydroxo-Osmium(IV) Complex: Kinetics and Mechanism. *ACS Catal.* **2018**, *8*, 11314-11323.

3. Esteruelas, M. A.; Fenández, I.; García-Yebra, C.; Martín, J.; Oñate, E. Elongated σ-Borane versus σ-Borane in Pincer-POP-Osmium Complexes. *Organometallics* **2017**, *36*, 2298-2307.

4. Antiñolo, A.; Esteruelas, M. A.; García-Yebra, C.; Martín, J.; Oñate, E.; Ramos, A. Reactions of an Osmium(IV)-Hydroxo Complex with Amino-Boranes: Formation of Boroxide Derivatives. *Organometallics* **2019**, *38*, 310-318.

5. Esteruelas, M. A.; Fernández, I.; García-Yebra, C.; Martín, J.; Oñate, E. Cycloosmathioborane Compounds: Other Manifestations of the Hückel Aromaticity. *Inorg. Chem.* **2019**, *58*, 2265-2269.

ABREVIATURAS

Å	Ångström
ACID	Anisotropía de la Densidad de Corriente Inducida (*Anisotropy of the Current Induced Density*)
AIM	Teoría de Átomos en Moléculas (*Atoms In Molecules*)
ASE	Energía de Estabilización Aromática (*Aromatic Stabilization Energy*)
ATR	Técnica espectroscópica de IR de Reflexión Total Atenuada (*Attenuated Total Reflection*)
a.u.	Unidad Atómica (*Hartree Atomic Units*)
BCP	Punto Crítico de Enlace (*Bond Critical Point*)
BP	Camino de Enlace (*Bond Path*)
Bu	Butilo
CCDC	Centro de Datos Cristalográficos de Cambridge (*Cambridge Crystallographic Data Centre*)
COSY	Espectroscopía de Correlación Homonuclear (*COrrelation SpectroscopY*)
Cy	Ciclohexilo
δ	Desplazamiento químico en partes por millón (RMN)
ΔE	Variación de Energía
Δ*G*	Variación de la Energía libre de Gibbs
Δ*H*	Variación de la Entalpía
Δ*S*	Variación de la Entropía
DFT	Teoría del Funcional de Densidad (*Density Functional Theory*)
EDA	Análisis de Descomposición de Energía (*Energy Decomposition Analysis*)
Et	Etilo
fac	*facial*
FT	Transformada de Fourier (*Fourier Transform*)
HMBC	Espectroscopía de correlación heteronuclear a dos o más enlaces (*Heteronuclear Multiple Bond Correlation*)
HSQC	Espectroscopía de correlación heteronuclear a un enlace (*Heteronuclear Single Quantum Correlation*)

Hz	Hercio
IR	Infrarrojo
ISE	Método de Isomeriazación (*Isomerization Method*)
^{i}Pr	Isopropilo
J	Constante de acoplamiento (RMN)
Me	Metilo
mer	*meridional*
N	Constante de acoplamiento virtual (RMN)
NBO	Orbitales Naturales de Enlace (*Natural Bond Orbitals*)
NICS	Cambio de Desplazamiento Químico Independiente del Núcleo (*Nucleus-Independent Chemical Shifts*)
NOCV	Orbital Natural para Valencia Química (*Natural Orbital for Chemical Valence*)
OLED	Diodo Orgánico de Emisión de Luz (*Organic Light-Emitting Diode*)
Ph	Fenilo
ppm	Partes por millón
RMN	Resonancia Magnética Nuclear
SPS	Sistema de Purificación de Disolventes (*Solvent Purification Systems*)
terc	terciario
TOF	Frecuencia de Conversión (*Turnover Frequency*)
WBI	Índice de Enlace de Wiberg (*Wiberg Bond Index*)

INTRODUCCIÓN

I.1. LA TECNOLOGÍA DEL HIDRÓGENO

El nivel de desarrollo de la sociedad actual está de acuerdo con una creciente demanda global de energía que, según las previsiones, experimentará un aumento significativo en los próximos años. La mayor parte de la energía que consumimos proviene de los combustibles fósiles, pero sus reservas son limitadas y su combustión produce un impacto negativo sobre el medio ambiente. Así, la tendencia actual se centra en la búsqueda de fuentes de energía renovables que complementen o sustituyan a las actuales para crear un modelo energético sostenible. Dentro de las fuentes renovables cabe destacar la energía hidráulica, que representa el 71% de la producción mundial de energía renovable, la solar o la eólica.[1] La energía hidráulica no es suficiente para cubrir las necesidades energéticas, y las energías solar y eólica son discontinuas (dependen de las condiciones meteorológicas). Almacenar la energía producida de una forma eficiente podría atenuar el problema.

La molécula de hidrógeno puede ser utilizada como un vector energético limpio, ya que su combustión proporciona alrededor de 2.5 veces más energía que la quema de los hidrocarburos habituales, formando agua como único subproducto. Este alto contenido de energía por masa hizo que en los años 70 se introdujera el concepto de *economía del hidrógeno*, coincidiendo con la primera crisis del petróleo.[2] Sin embargo, la baja densidad energética del H_2 comparada con la del propano o la gasolina es una gran desventaja para su aplicación.

La mayor parte del H_2 se genera mediante el reformado del gas natural e hidrocarburos y se utiliza principalmente en la síntesis del amoniaco (proceso Bosch-Haber) y en el cracking del petróleo. No obstante, existen métodos de producción de H_2 más sostenibles

y respetuosos con el medio ambiente. Por ejemplo, la descomposición catalizada del agua en H_2 y O_2 (water splitting) es uno de los métodos más limpios para liberar H_2, y utilizar la energía solar para este propósito sería ideal desde un punto de vista ecológico. Sin embargo, para poder reducir la dependencia actual de los combustibles fósiles, éste y otros métodos deben cubrir las necesidades energéticas existentes y ser económicamente viables.[3]

Dos de los problemas más importantes a resolver para utilizar el H_2 como vector energético son su almacenamiento y su transporte. El H_2 se puede almacenar en forma gaseosa empleando tanques presurizados y en forma líquida mediante depósitos criogénicos que mantengan la temperatura por debajo de 20 K. Otra opción son los materiales adsorbentes. Desafortunadamente, estas soluciones son poco prácticas ya que requieren de una infraestructura muy específica.[4]

Una estrategia alternativa para resolver el problema puede ser el uso de compuestos con alto contenido en hidrógeno que, a través de procesos de deshidrogenación reversibles, lo liberen según la demanda y de forma cinéticamente controlada.[5] Compuestos sólidos como el amoniaco-borano,[6] con un 19,6 % de H_2 en peso, o líquidos orgánicos portadores de hidrógeno[7] han sido muy estudiados en los últimos años. Los cicloalcanos fueron los primeros en ser considerados para este propósito debido a su contenido relativamente alto en H_2 y la facilidad para su transporte, aunque presentan la desventaja de poseer una elevada entalpía de deshidrogenación, que se puede rebajar introduciendo un heteroátomo en el anillo.[8] El ácido fórmico y el metanol también son considerados líquidos orgánicos portadores de hidrógeno interesantes ya que, además del H_2 liberado, se puede reducir el CO_2 formado para obtener compuestos de interés sintético.[9] Producir H_2 de forma

eficiente y reciclar los productos de deshidrogenación en condiciones suaves son los grandes retos a superar antes de llegar a una aplicación práctica.[10]

El H_2 generado en las reacciones de deshidrogenación es igualmente interesante debido a su naturaleza reductora,[11] y puede participar en reacciones de hidrogenación sin necesidad de utilizar hidruros metálicos, que generan una gran cantidad de residuos, o H_2 gas, haciendo que este tipo de reacciones sean más sencillas de llevar a cabo. En este sentido, la metodología de *préstamo de hidrógeno*, resumida en el esquema 1, combina reacciones de deshidrogenación, acoplamiento e hidrogenación de manera secuencial para formar nuevos enlaces C-C o C-N, generando en muchos casos agua como único subproducto en un proceso redox neto nulo.[12] Este conjunto de reacciones representa una metodología de intercambio de H_2 que permite obtener compuestos orgánicos de interés partiendo de alcoholes o aminas utilizando procesos más seguros, atómicamente eficientes y respetuosos con el medio ambiente.

Esquema 1. Metodología de *Préstamo de Hidrógeno*

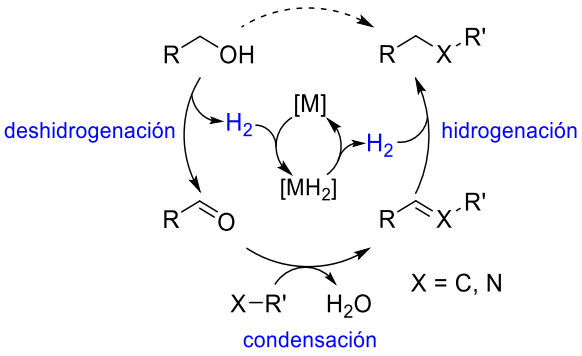

I.2. EL OSMIO Y LA TECNOLOGÍA DEL HIDRÓGENO

Los metales del grupo del platino son muy utilizados en catálisis debido principalmente a su elevada eficiencia imposible de alcanzar con otros metales de transición. Sin embargo, el osmio ha recibido poca atención a excepción de su uso en la dihidroxilación de Sharpless y en otros procesos relacionados.[13] En los últimos años, algunos compuestos de este metal se han revelado como catalizadores útiles para llevar a cabo algunas transformaciones orgánicas interesantes[14] y particularmente en procesos relacionados con la tecnología del hidrógeno.[15]

El amoniaco-borano es un sólido estable en condiciones ambientales y con un alto contenido en hidrógeno. Los catalizadores homogéneos basados en metales de transición han mostrado su eficacia en la deshidrogenación cinéticamente controlada de este compuesto, habiéndose conseguido determinar distintos mecanismos a través de los cuáles sucede el proceso, así como caracterizar los subproductos formados.[6]

El complejo pentacoordinado $OsH(SH)(CO)(P^iPr_3)_2$ (**1**)[16] promueve la liberación de 1 mol de H_2 por mol de amoniaco-borano y dimetilamina-borano.[17] El ligando SH, además, permite capturar los monómeros deshidrogenados antes de su polimerización dando lugar a los derivados hidrogenoaminoboriltiolato $OsH\{\kappa^2\text{-}H,S\text{-}[HB(S)(NR_2)]\}(CO)(P^iPr_3)_2$ (R = H, **2**; Me, **3**). Por otra parte, el complejo dihidruro $OsH_2(CO)(\eta^2\text{-}CH_2{=}CHEt)(P^iPr_3)_2$[18] (**4**) promueve la deshidrogenación del amoniaco-borano para liberar H_2 y formar poliaminoborano.[19] La ecuación de velocidad del proceso es de primer orden respecto del catalizador e independiente de la concentración de amoniaco-borano. Cálculos DFT unidos a los datos cinéticos permiten proponer el ciclo catalítico que aparece en el esquema 2. La disociación de la olefina de **4** conduce a un dihidruro

insaturado **A**. La vacante generada posibilita la coordinación del amoniaco-borano dando lugar al intermedio **B** tipo Shimoi con el enlace B-H coordinado *trans* al hidruro H_a. El amoniaco-borano se deshidrogena por transferencia directa de un protón NH al ligando hidruro H_b, generando el derivado dihidruro-dihidrógeno $OsH_2(\eta^2\text{-}H_2)(CO)(P^iPr_3)_2$ (**5a**),[20] sin que haya ningún cambio en el estado de oxidación del metal y sin la asistencia de otro ligando. El complejo **5a** isomeriza a través del correspondiente tetrahidruro al *cis*-dihidruro **5b**, que es más estable que el *trans*-dihidruro. La energía necesaria para que se produzca la disociación del ligando H_2 de **5b**, ~19 kcal·mol^{-1}, es similar a la obtenida por Caulton y colaboradores en un estudio estequiométrico anterior.[21] La especie dihidruro activa **A** se regenera tras la liberación de H_2, lo que permite cerrar el ciclo catalítico. El mecanismo a través del cual sucede la catálisis viene determinado por la transferencia directa de un protón NH a un ligando hidruro del catalizador, observado anteriormente por otros autores,[22] y difiere de los mecanismos de esfera interna y esfera externa generalmente propuestos para explicar la deshidrogenación catalítica de amoniaco-borano.[23]

Esquema 2. Ciclo Catalítico para la Deshidrogenación de Amoniaco-Borano Promovida por el Complejo 4

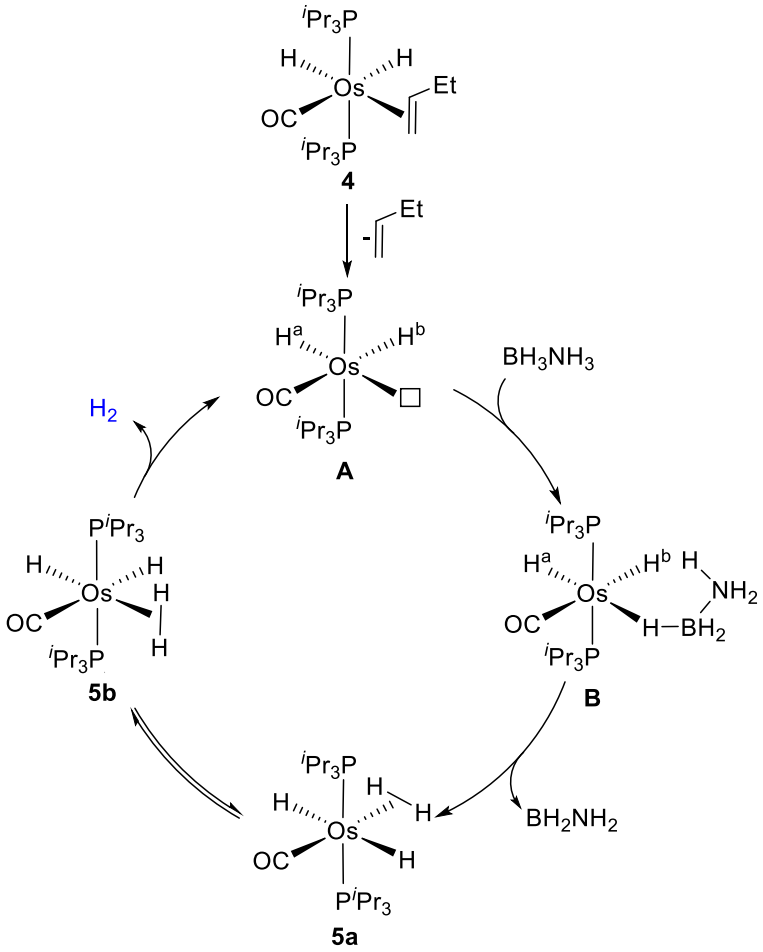

La utilización de amoníaco-borano como almacén químico de hidrógeno conduce a monómeros deshidrogenados que polimerizan fácilmente. Evidencias experimentales unidas a estudios teóricos sugieren que la polimerización ocurre fuera de la esfera de coordinación del metal, probablemente asistida por un disolvente nucleófilo, lo que rebaja la energía de activación del proceso.[24]

Otras reacciones que generan hidrógeno son la alcohólisis y la hidrólisis de boranos. El complejo $OsCl\{\kappa^2\text{-}C,C\text{-}[CN(CH_3)CHCHNCH_2C(O)]\}(P^iPr_3)_2$ (**6**) promueve tanto la alcohólisis como la hidrólisis cinéticamente controlada de pinacolborano (esquema 3).[25]

El esquema 4 muestra un ciclo catalítico para la generación de H_2 mediante la alcohólisis de pinacolborano en el que todos los intermedios han sido aislados y caracterizados. El complejo **6** promueve la activación heterolítica del enlace B-H del pinacolborano dando lugar al compuesto **7** de forma instantánea y cuantitativa. El ligando hidruro y el sustituyente Bpin del carbeno de Fischer generado activan el enlace O-H de alcoholes (y del agua) de forma heterolítica produciendo ROBpin y el derivado dihidrógeno **8**, el cual pierde la molécula de hidrógeno coordinada para regenerar **6**.

Esquema 3. Alcohólisis (a) e Hidrólisis (b) del Pinacolborano

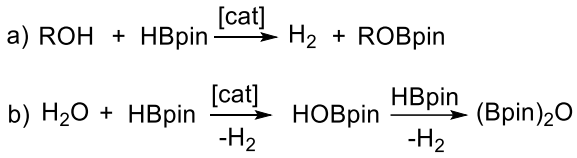

Esquema 4. Generación de H_2 Mediante la Alcohólisis de Pinacolborano Promovida por el Complejo 6

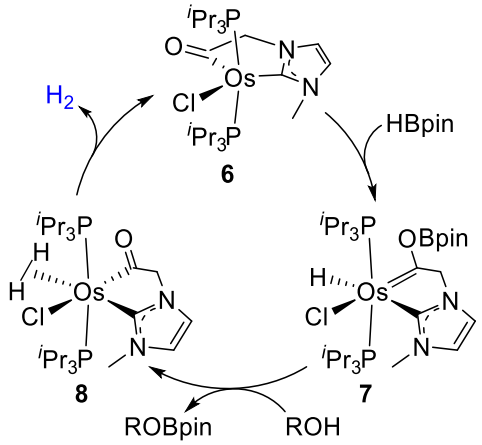

Los alcoholes son considerados una forma sencilla de almacenar y transportar H_2 y son capaces de participar en procesos de deshidrogenación-hidrogenación reversibles.[26] La deshidrogenación de alcoholes secundarios genera cetonas (esquema 5a) y la

deshidrogenación de alcoholes primarios genera aldehídos o ésteres si se produce un acoplamiento posterior (esquema 5b y 5c). La formación de aldehídos tiene la desventaja de poder provocar el envenenamiento de los catalizadores por carbonilación.[27] La hidrogenación de los productos oxidados es un proceso termodinámicamente favorable, fundamental para el reciclaje de los alcoholes y su uso como transportadores de hidrógeno. En la mayoría de los casos, por el contrario, la deshidrogenación no es favorable ($\Delta G > 0$) y se requiere de condiciones de reacción que favorezcan la liberación del gas H_2 formado para desplazar el equilibrio hacia los productos deshidrogenados.[28] Además del interés que generan los alcoholes como transportadores de hidrógeno, los compuestos oxidados producidos como resultado de la deshidrogenación pueden ser útiles desde un punto de vista sintético, al ser obtenidos de una manera atómicamente eficiente y respetuosa con el medio ambiente.[26a,27]

Esquema 5. Reacciones de Deshidrogenación de Alcoholes

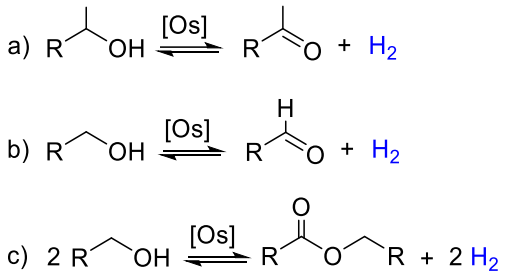

Los catalizadores *trans*-$OsCl_2$(dppf)(en) (dppf = 1,1'-bis(difenilfosfino)ferroceno; en = etilendiamina) (**9**)[29] y *trans*-$OsCl_2$(dppf)(ampy) (ampy = 2-aminometilpiridina) (**10**)[30] son capaces de deshidrogenar alcoholes secundarios lineales y cíclicos sin aceptor de hidrógeno y presentan actividades comparables a las de los derivados de rutenio (figura 1). Recientemente, se ha descrito la deshidrogenación de alcoholes primarios y secundarios para dar aldehídos y cetonas, respectivamente, promovida por los complejos

$OsH_3\{\kappa^2\text{-}N_{piridina},N_{imina}\text{-(BMePI)}\}(P^iPr_3)_2$ (BMePI = 1,3-bis(6′-metil-2′-piridilimino)isoindolinato) (**11**) y $OsH\{\kappa^2\text{-}N_{piridina},N_{imina}\text{-(BMePI)}\}(CO)(P^iPr_3)_2$ (**12**).[31]

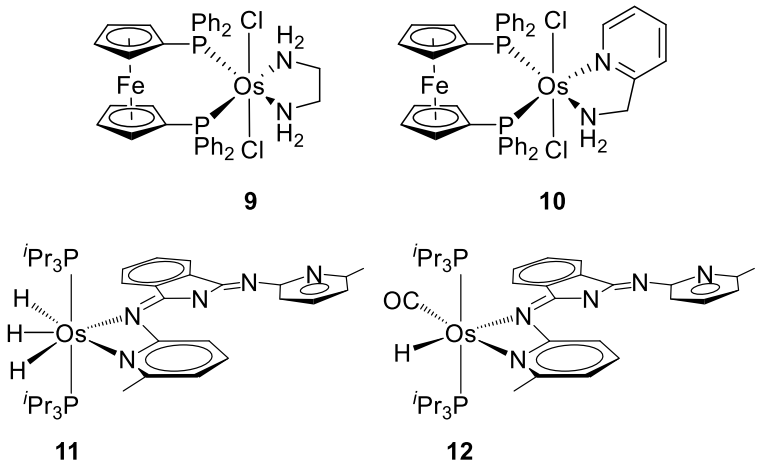

Figura 1. Complejos de osmio que promueven la deshidrogenación de alcoholes sin aceptor de hidrógeno.

Gusev ha estudiado el proceso de deshidrogenación de alcoholes y su posterior acoplamiento para formar ésteres catalizado por complejos de osmio.[32] El dímero $\{OsH(CO)[PyCH_2N(CH_2)_2P^iPr_2]\}_2$ (**13**) cataliza la transformación de alcoholes primarios en ésteres y promueve también el proceso contrario, es decir, la reducción del éster para recuperar el alcohol inicial,[32d] mostrando una actividad similar al derivado análogo de rutenio y siendo un claro ejemplo de reversibilidad en este tipo de procesos.

Los cicloalcanos contienen una cantidad de hidrógeno suficiente para ser considerados líquidos orgánicos portadores de hidrógeno. Sin embargo, como se ha comentado anteriormente, la elevada entalpía asociada a la deshidrogenación de estos sustratos es una limitación,[33] siendo la deshidrogenación de ciclodecano catalizada por el complejo $OsH(COD)(^{CF3}PCP)$ (COD = 1,4-ciclooctadieno; $^{CF3}PCP = 2,6\text{-}C_6H_3(CH_2P(CF_3)_2)_2$) (**14**) uno de los pocos ejemplos descritos con osmio.[34] La introducción de un heteroátomo en el ciclo generalmente favorece los procesos de deshidrogenación. Así, la

deshidrogenación catalizada de aminas cíclicas está más favorecida (esquema 6).[8] El trihidruro $OsH_3(acac)(P^iPr_3)_2$ (acac = acetilacetonato) (**15**),[35] y los compuestos **11** y **12** (figura 1),[31] catalizan la deshidrogenación de aminas cíclicas produciendo las correspondientes aminas aromáticas y liberando H_2.

Esquema 6. Reacciones de Deshidrogenación de Cicloalcanos y Aminas Cíclicas

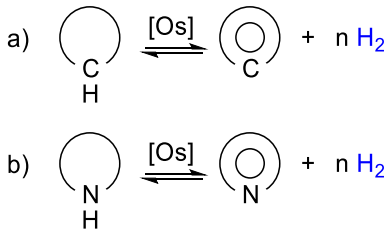

Los aldehídos formados en la deshidrogenación de alcoholes primarios son más reactivos que el alcohol. Así, pueden reaccionar con aminas primarias formando amidas al liberar una segunda molécula de H_2 (esquema 7a). Alternativamente, la reacción con aminas primarias puede liberar una molécula de agua generando iminas (esquema 7b). Ambos procesos pueden llegar a ser de gran interés para la industria.[36]

Esquema 7. Reacciones de Formación de Amidas e Iminas

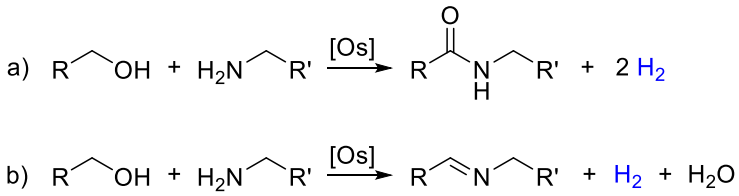

Los catalizadores $OsHX(CO)\{\kappa^3\text{-}P,N,N\text{-}[PyCH_2NHCH_2CH_2NHP^tBu_2]\}$ (X = Cl (**16**), X = H (**17**)) diseñados por Gusev permiten sintetizar amidas a partir de alcoholes primarios y aminas primarias.[32e,37] El esquema 8 muestra el mecanismo de la síntesis de amidas catalizada por el complejo **17** a través de dos ciclos relacionados. La primera etapa, descrita en el ciclo *a*, consiste en la deshidrogenación del alcohol para dar el

correspondiente aldehído. En los intermedios de reacción **C-E** se observa que el ligando NH asiste al metal en el proceso de deshidrogenación estabilizando dichos intermedios mediante puentes de hidrógeno. La formación de la amida se describe en el ciclo *b*. Una molécula de aldehído, formada en el ciclo *a*, reacciona con **17** proporcionando el intermedio alcóxido **F** que posteriormente se enlaza a una molécula de amina mediante puentes de hidrógeno dando lugar a **G**. Seguidamente, se incorpora una segunda molécula de aldehído para formar el enlace C-N del hemiaminal de **H**. Finalmente, se elimina una molécula de alcohol conduciendo a **I**, que libera la amida formada y regenera **17** cerrando el ciclo *b*. Este mecanismo muestra que solamente se utiliza un sitio de la esfera de coordinación del metal en lugar de proceder a través de la eliminación de un ligando auxiliar y posterior *β*-eliminación de hidrógeno. En el caso descrito en el esquema 8, el enlace entre el átomo de osmio y el grupo NH se mantiene durante todo el proceso.[37] Este y otros estudios sugieren que un ligando puede asistir la catálisis mediante estabilización por puentes de hidrógeno de los pasos determinantes del proceso, cuestionando otros mecanismos de esfera externa planteados hasta el momento.[38]

Esquema 8. Síntesis de Amidas Catalizada por el Complejo 17

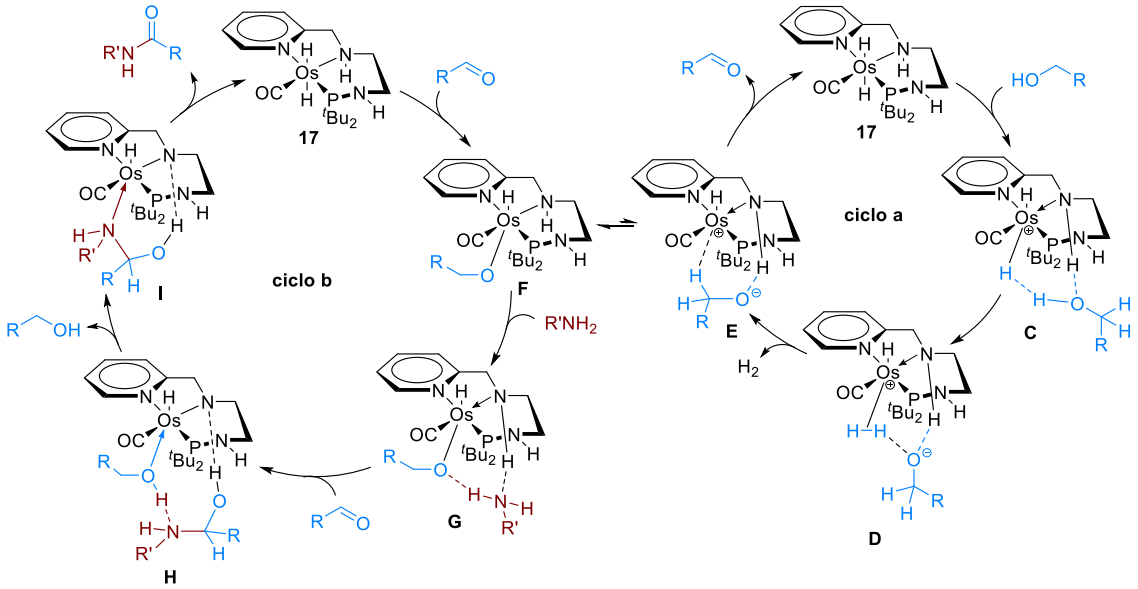

El complejo $OsH_4\{\kappa^3\text{-}P,O,P\text{-}[dbf(P^iPr_2)_2]\}$ ($dbf(P^iPr_2)_2$ = 4,6-bis(diisopropilfosfina)dibenzofurano) (**18**) promueve la formación de iminas a partir de alcoholes primarios y aminas primarias,[39] siendo más eficaz que el sistema análogo de rutenio $RuH(CO)\{\kappa^3\text{-}P,N,P\text{-}[C_5H_3N(CHP^iPr_2)_2]\}$ utilizado por Milstein.[40] El esquema 9 muestra el mecanismo de este proceso. El tetrahidruro **18** es lo suficientemente básico como para desprotonar el alcohol de partida y formar el alcóxido **J**, que se transforma en la especie insaturada **K** liberando una molécula de H_2. La *β*-eliminación de hidrógeno en el grupo alcóxido lleva a la especie **L**, que posteriormente disocia el aldehído para dar el dihidruro insaturado **M**. La vacante de coordinación originada permite activar el enlace O-H de una nueva molécula de alcohol y regenerar la especie activa **J**. El aldehído disociado reacciona con la molécula de amina produciendo la imina. El complejo $OsH_3(acac)(P^iPr_3)_2$ (**15**) también promueve el acoplamiento de alcoholes con aminas para dar iminas.[35] Este catalizador es menos activo que **18**, pero la simplicidad de sus ligandos

y el sencillo procedimiento sintético para su obtención permiten considerar a **15** como una alternativa interesante en la síntesis de iminas.

Esquema 9. Ciclo Catalítico para la Formación de Iminas a partir de Alcoholes y Aminas Promovido por el Complejo 18

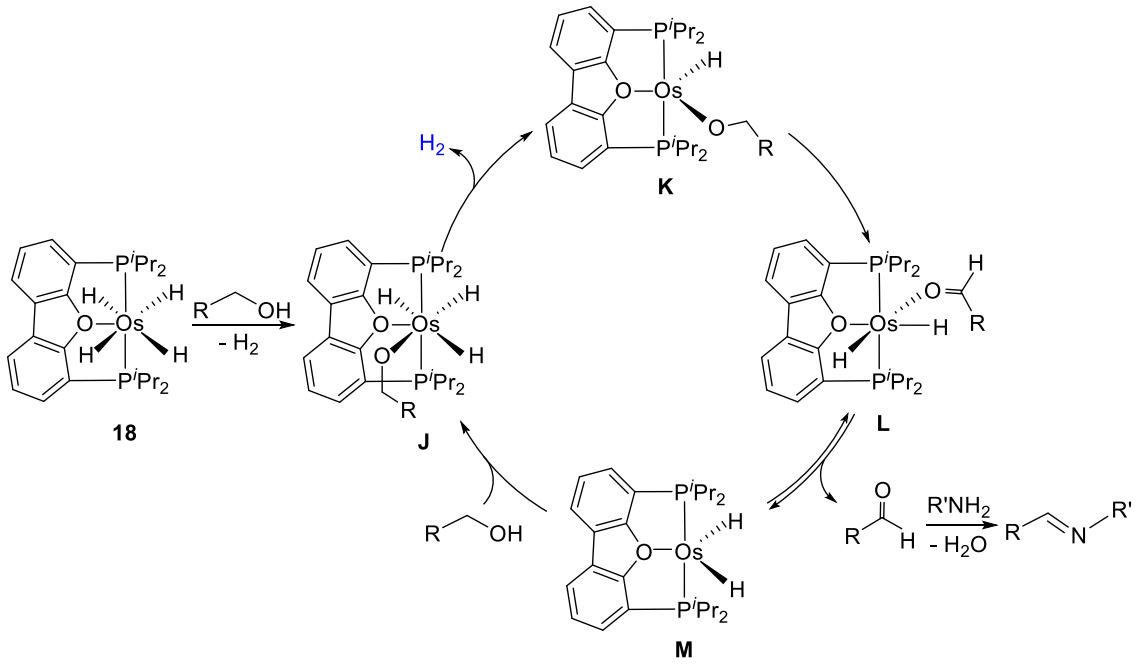

Algunos compuestos de osmio pueden participar con éxito en procesos relacionados con la metodología de *préstamo de hidrógeno*.[15d] El esquema 10 muestra distintas reacciones de alquilación promovidas por catalizadores de osmio utilizando esta metodología. El complejo $OsCl_2$(dppf)(ampy) (**10**) cataliza la alquilación de α-tetralona con alcoholes primarios de manera más eficiente que el correspondiente derivado de rutenio (esquema 10a).[30] El dihidruro $OsH_2(CO)[HN(C_2H_4P^iPr_2)_2]$ (**19**) y el tetrahidruro $OsH_4[HN(C_2H_4P^iPr_2)_2]$ (**20**)[32a,32b] promueven la alquilación de aminas primarias con alcoholes primarios (esquema 10b).

Esquema 10. Reacciones de Alquilación en la Metodología de *Préstamo de Hidrógeno*

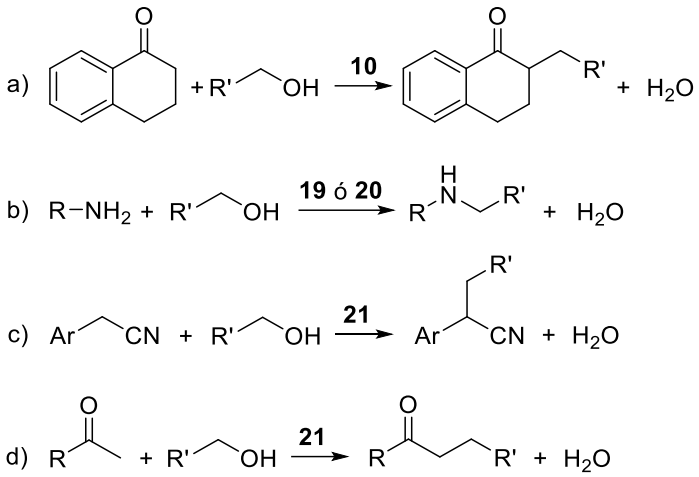

El compuesto [Os(η^6-*p*-cimeno)(OH)IPr]OTf (IPr = 1,3-bis(2,6-diisopropilfenil)-imidazolilideno, OTf = CF_3SO_3) (**21**)[41] cataliza la α-alquilación de arilacetonitrilos y metilcetonas con alcoholes (esquema 10 c y d).[42] El mecanismo propuesto para estas dos reacciones se muestra en el esquema 11. El primer paso consiste en el intercambio entre el grupo hidroxilo y el grupo alcóxido. La β-eliminación en el grupo alcóxido del intermedio **N** generado da lugar a la especie **Ñ**, que disocia una molécula de aldehído para formar el hidruro insaturado **O**. El aldehído puede experimentar una condensación de Knovenagel con un nitrilo, generando H_2O y un nitrilo α,β-insaturado, que se inserta en el enlace Os-H de **O** para dar el intermedio **P**. Por último, la adición del enlace O-H de una nueva molécula de alcohol al enlace Os-C permite liberar el producto de alquilación y regenerar la especie activa **N**. La α-alquilación de metilcetonas se puede explicar de forma similar.

Esquema 11. Ciclo Catalítico Propuesto para la α-Alquilación de Arilacetonitrilos y Metilcetonas con Alcoholes Promovida por el Complejo 21

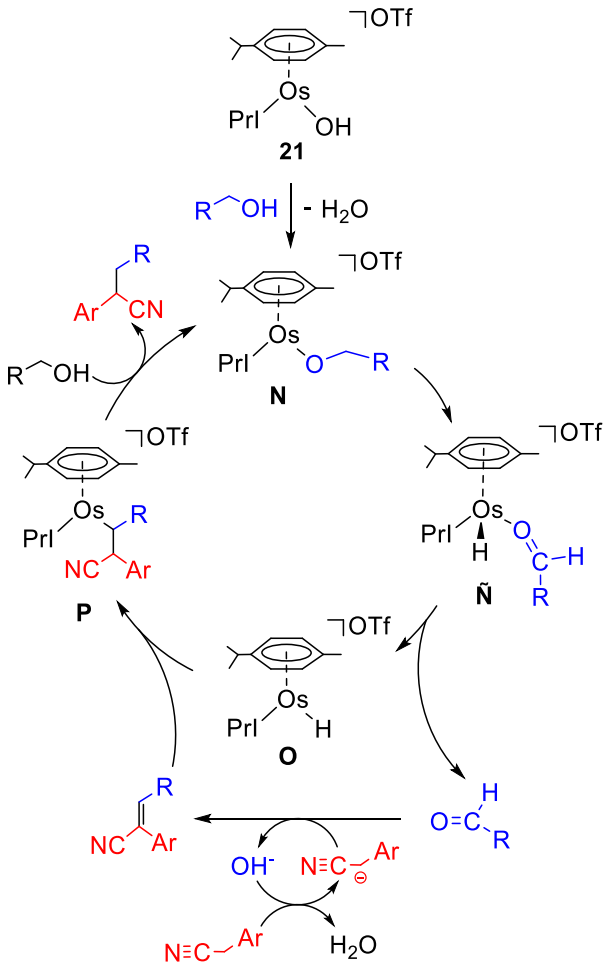

I.3. LIGANDOS PINZA

Las propiedades de un complejo metálico dependen en gran medida de los ligandos que lo componen. Una elección adecuada de los ligandos permite regular el entorno electrónico y estérico del metal proporcionando un mayor control sobre la reactividad del complejo resultante. Los ligandos pinza, llamados así por su particular forma de coordinarse al metal, son ampliamente utilizados para conseguir este objetivo.

Los trabajos de Shaw y otros autores a mediados de los años 70[43] llevaron a van Koten a introducir el término *pinza* en 1989[44] para definir a aquellos ligandos tridentados con un carbono aniónico en la posición central y dos grupos laterales dadores fosfina o amina que aseguraran una coordinación meridional al centro metálico. Sin embargo, ésta definición se ha visto ampliada debido a la gran variedad de grupos funcionales que pueden formar parte de esta estructura. Así, en la actualidad se denomina ligando pinza a cualquier ligando tridentado que se coordina habitualmente de forma meridional (figura 2).

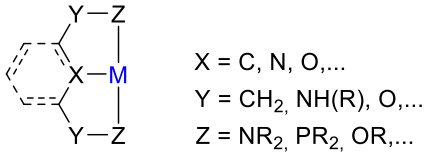

Figura 2. Estructura de un complejo tipo pinza.

Los ligandos pinza se componen fundamentalmente de un átomo central (X) y dos grupos laterales (Z) a través de los cuáles el ligando se enlaza al metal (M). Los grupos laterales están separados del átomo central por grupos espaciadores (Y) y son parte de los dos metalaciclos fusionados, habitualmente anillos de 5 ó 6 miembros, que forma el ligando pinza al coordinarse κ^3 al metal. Con frecuencia, el átomo dador central es C, N u O. Los grupos laterales ejercen un gran efecto sobre la densidad electrónica del metal, mientras que los sustituyentes de estos átomos controlan el acceso al átomo central debido al impedimento estérico que generan. Los grupos laterales más utilizados son fosfinas y aminas, con sustituyentes Ph, ^{i}Pr o ^{t}Bu. Actualmente, son muchos los grupos funcionales que pueden formar parte de los ligandos pinza y es habitual que cada año surjan nuevos ejemplos.

La creciente variedad de estos ligandos hace que establecer una clasificación adecuada sea una tarea compleja. Una propuesta razonable, utilizada por algunos autores,[45] consiste en clasificarlos i) atendiendo a si los grupos laterales (Z) son iguales o no, lo que permite dividirlos en ligandos simétricos (PCP, NNN, …) y asimétricos (NNP, PCN, …); ii) en función de su carga, siendo iónicos ($PC^{-}P$, $N^{-}N^{-}N^{-}$, …) o neutros (PCP, POP, …).

La disposición *meridional* que adopta habitualmente un ligando pinza al coordinarse al centro metálico proporciona al complejo resultante una gran estabilidad térmica. Esta propiedad permite a muchos complejos actuar como catalizadores eficientes en procesos endotérmicos consiguiendo activar enlaces inertes[46] o deshidrogenar moléculas orgánicas.[47] Además, los ligandos pinza ocupan gran parte de la esfera de coordinación del metal y limitan el espacio libre a su alrededor, aportando un mayor control sobre la reactividad del complejo.

La rigidez no es una propiedad común a todos estos ligandos. Algunos cambian su conformación de κ^3-*mer* a κ^3-*fac* adaptándose a los requerimientos electrónicos y estéricos del metal (p ej. con ligandos PNP,[48] PSiP[49] o POP[50]). En otras ocasiones los ligandos pinza presentan hemilabilidad, lo que permite a uno de los grupos dadores descoordinarse de manera reversible generando una vacante de coordinación.[51] Esta cooperación entre metal y ligando, que *a priori* puede parecer contrapuesta a las características deseables para estos ligandos, es en muchos casos el factor clave de la eficiencia catalítica de los complejos pinza.[45]

Las cualidades únicas de estos ligandos unidas a procedimientos sintéticos sencillos para preparar nuevos ejemplos o modificar los ya existentes hacen que los ligandos pinza

tengan aplicaciones en campos tan diversos como la luminiscencia, el reconocimiento molecular o la catálisis.[52]

I.3.1. Complejos de Osmio con Ligandos Pinza

La química de los complejos de osmio con ligandos pinza está significativamente menos explorada que la de los otros metales del grupo del platino. No obstante se han preparado compuestos estabilizados por una amplia gama de ligandos neutros (CNC,[53] CNO,[54] NNN,[55] PNN,[32c-f,37] PNP,[32a,32b,56] y POP[39,57]), monoaniónicos (CCC,[58] CCN,[59] CNC,[60] CNN,[60] NCN,[55i,61] NNN,[62] NNS,[63] PCP,[34,64] y PNP[65]), dianiónicos (CCN,[59] CNC,[60,66] CNN,[60,67] CNO,[68] y ONO[69]), e incluso trianiónicos (NNO[70]). Algunos de ellos tienen interés en distintos campos, debido a sus propiedades catalíticas, fotofísicas o biológicas.

Las reacciones promovidas por complejos con estos ligandos relacionadas con la tecnología del hidrógeno se han comentado en el apartado I.2 de esta introducción. Entre los procesos de interés en síntesis orgánica cabe mencionar la reducción de cetonas proquirales para dar alcoholes ópticamente activos mediante hidrogenación con hidrógeno molecular y a través de transferencia de hidrógeno de isopropanol (esquema 12). Complejos OsCl(CNN)[(*S*,*R*)-Josiphos], con un ligando dianiónico CNN derivado de 2-aminometil-6-arilpiridina y el ligando quiral (*S*,*R*)-Josiphos ((*S*)-1-[(*R*P)-2-(difenilfosfino)ferrocenil]etildiciclohexilfosfina),[67a] y compuestos *trans*-[$OsCl_2$(L){(*S*,*S*)-^{i}Pr-pybox}] (L = $P(OR)_3$, piridina; (*S*,*S*)-^{i}Pr-pybox = 2,6-bis[4'-(*S*)-isopropiloxazolin-2'-il]piridina), catalizan la reducción de estos sustratos con mejores enantioselectividades que las especies análogas de rutenio.[55h,55k]

Esquema 12. Reacciones de Formación de Alcoholes Quirales

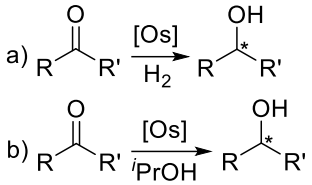

Los compuestos de osmio con propiedades luminiscentes tienen aplicación en campos emergentes como la fabricación de dispositivos OLED (diodos orgánicos emisores de luz).[71] Los complejos basados en metales de la tercera serie de transición ofrecen ventajas para este tipo de aplicaciones debido a que se favorecen los acoplamientos spin-órbita dando lugar a rendimientos cuánticos mayores,[72] y la utilización de ligandos multidentados, como los ligandos pinza, aumenta la estabilidad y la rigidez del sistema.[73] La figura 3 muestra compuestos de osmio con ligandos pinza que tienen propiedades fotofísicas. Las especies luminiscentes de osmio(II) con ligandos tridentados aniónicos se limitan a unos pocos ejemplos con ligandos NNN y CCC. El complejo $Os(fpbpy)_2$ (fpbpy = 6-(5-(trifluorometil)pirazol-3-il)-2,2'-bipiridina) (**22**) con dos ligandos NNN emite en el infrarrojo cercano.[62b] El compuesto $Os\{\kappa^3\text{-}C,C,C\text{-}[MeBzIm\text{-}CF_3C_6H_2\text{-}MeBzIm]\}_2$ (MeBzIm = 1,3-bis(3metilbencimidazol-1-il)) (**23**) con dos ligandos CCC emite en la región azul y se ha utilizado recientemente en la preparación de un dispositivo OLED.[58b] El derivado heteroléptico de osmio(II) $[Os(tpy)(Stpy)]^{2+}$ (tpy = 2,2':6',2''-terpiridina; Stpy = 4'-(2-tionil)-tpy) (**24**) con dos ligandos neutros NNN es luminiscente en la región roja del espectro.[55e] Los compuestos emisivos de osmio(IV) han recibido poca atención hasta el momento debido a su limitada estabilidad y bajos rendimientos cuánticos. Recientemente, la preparación del complejo $OsH_2\{\kappa^3\text{-}N,N',C\text{-}[pz\text{-}py\text{-}C_6H_4]\}(P^iPr_3)_2$ (**25**) con un ligando CNN aniónico que emite en la región verde-amarilla

con un 60% de eficiencia, demuestra que los complejos de osmio(IV) también pueden alcanzar buenos rendimientos cuánticos.[60]

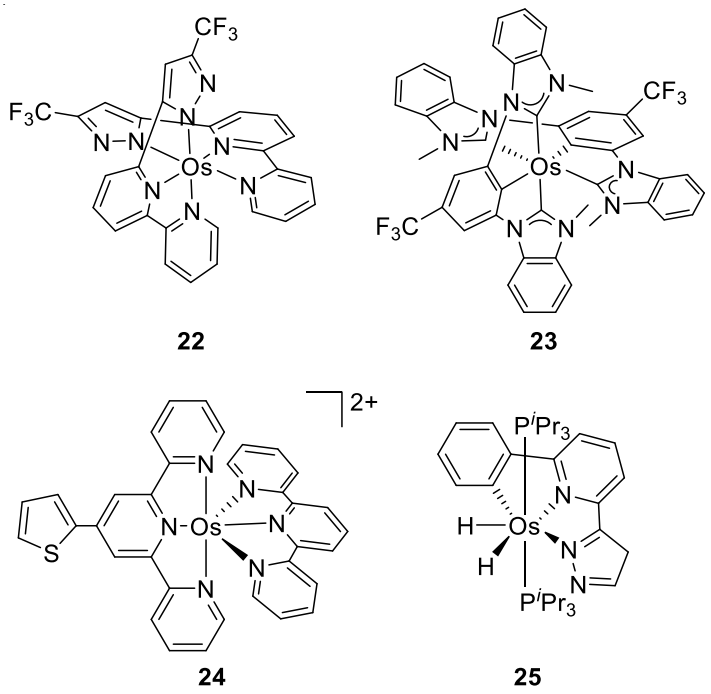

Figura 3. Complejos de osmio con ligandos pinza que presentan propiedades fotofísicas.

La diversidad estructural y características únicas de los compuestos de metales de la tercera serie de transición del grupo del platino hacen que estos sean considerados como candidatos para el tratamiento de algunos tipos de cáncer. Recientemente, se han estudiado las propiedades citotóxicas y antimicrobianas de algunos derivados de osmio.[74] Pfeffer y colaboradores han descrito compuestos de osmio con ligandos NCN dipiridilbenzoato y NNN terpiridina que presentan propiedades citotóxicas *in vitro* frente al glioblastoma con valores de IC_{50} similares a los alcanzados por análogos de rutenio.[55i] Además, el derivado nitruro de osmio(VI) $[OsCl_2N(tpy)]^+$ (**26**) exhibe actividad anticancerígena *in vivo* frente al mismo tipo de tumor, aumentando significativamente la supervivencia de ratones.[75] Compuestos del tipo *trans*-$OsCl_2(L)\{(S,S)$-^{i}Pr-pybox$\}$ con un ligando neutro NNN son activos contra microbios y células tumorales HeLa.[55j]

I.4. LIGANDOS POP

Un tipo interesante de ligandos pinza son los POP, que están formados por dos unidades PR_2 como grupos laterales y un átomo de oxígeno en la posición central. Al coordinarse a un metal de transición forman complejos M(POP) con un enlace M-O lábil, lo que permite que puedan actuar de manera tridentada o *P*,*P*-bidentada.

Las fosfinas son ligandos muy versátiles cuyas propiedades electrónicas y estéricas se modifican al cambiar el sustituyente R. Así, las fosfinas pueden variar su capacidad σ-dadora y su requerimiento estérico, que viene definido por el ángulo cónico de Tolman. Las difosfinas y otros ligandos quelato presentan un parámetro adicional, generalmente llamado ángulo de mordedura, referido en este caso al ángulo P-M-P, que influye en la flexibilidad del ligando.[76]

Los ligandos POP más habituales se presentan en la figura 4. Si se particularizan para el caso más común, donde R = Ph, se denominan POP' = bis[2-(difenilfosfino)etil]éter, DPEphos = bis(2-(difenilfosfino)fenil)éter, DBFphos = 4,6-bis(difenilfosfino)dibenzofurano, xantphos = 9,9-dimetil(4,5-bis(difenilfosfino)xanteno.

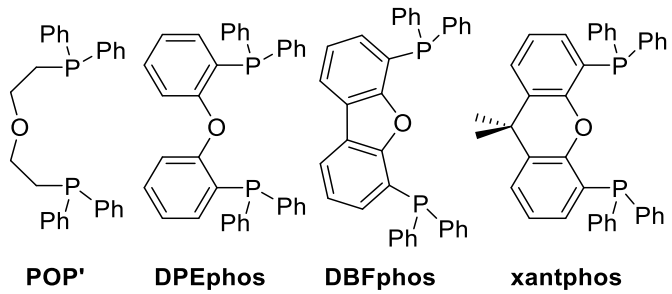

Figura 4. Ejemplos de ligandos POP.

Los primeros complejos con un ligando POP fueron descritos en los años 70, comenzando por la caracterización por difracción de rayos-X del complejo $[RhCO(POP')]PF_6$.[77] Sin

embargo, no fue hasta los años 90 cuando comenzó el verdadero desarrollo de la química de estos ligandos al utilizarse complejos M(POP) en la hidroformilación de olefinas.[78]

La hemilabilidad es una propiedad potencial de los ligandos POP. La figura 5 muestra gráficas que correlacionan el ángulo de mordedura P-M-P con la distancia M-O, para complejos caracterizados cristalográficamente con los ligandos POP más habituales, independientemente de los sustituyentes de las unidades PR_2.

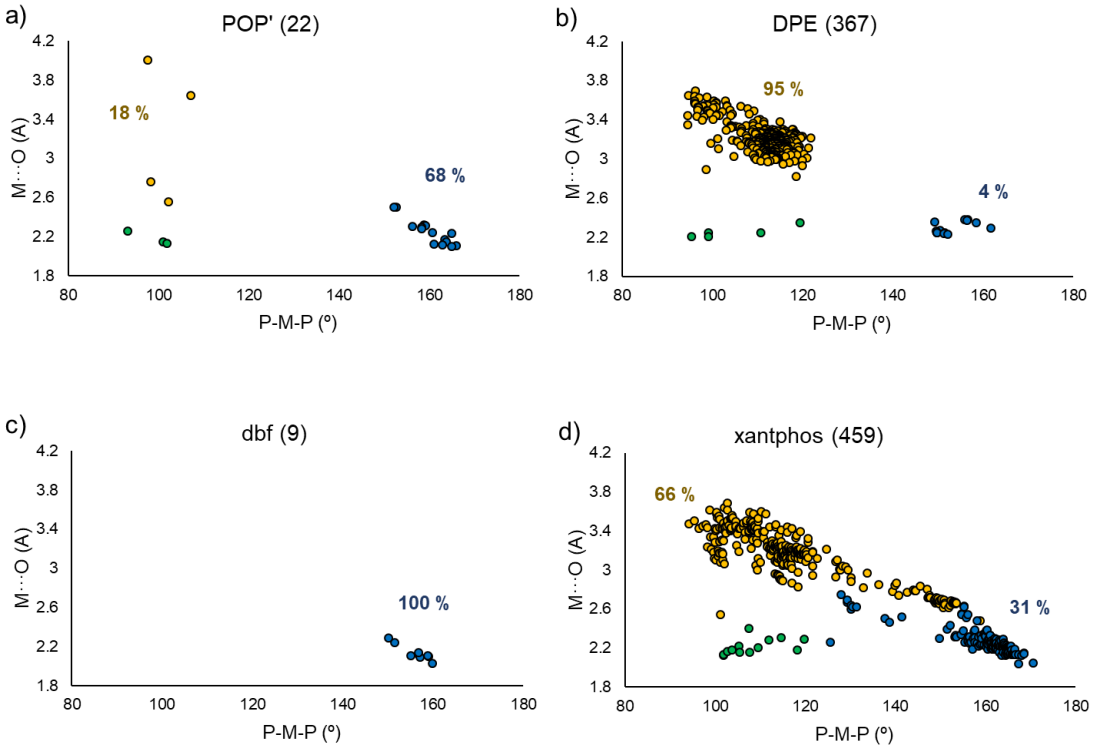

Figura 5. Relación entre la distancia M-O (Å) y ángulo de mordedura P-M-P (º) para las estructuras cristalográficas de complejos con ligandos de tipo POP'(a), DPE (b), dbf (c), y xantphos (d), independientemente de los sustituyentes PR_2. Entre paréntesis se indica el número de estructuras para cada caso en una búsqueda realizada en Abril de 2019 con la base de datos del CCDC (Cambridge Crystallographic Data Centre). ● κ^3-*mer*, ● κ^3-*fac*, ● κ^2-*P*,*P*-bidentado.

La figura 5 pone de manifiesto que los ligandos más explorados han sido del tipo DPE y xantphos, con 367 y 459 estructuras, respectivamente, mientras que los tipos POP' y dbf,

con 22 y 9 ejemplos, han sido mucho menos utilizados. También se puede observar la preferencia de cada tipo de ligando por un modo de coordinación determinado. Los ligandos DPE muestran una clara preferencia por la coordinación κ^2-*P*,*P*-bidentada (95 % de los ejemplos), mientras que los ligandos xantphos, que también prefieren coordinarse de manera κ^2-*P*,*P*-bidentada (66 % de los ejemplos), se unen al metal κ^3-*mer* en el 31 % de los ejemplos. Por otro lado, los ligandos POP' prefieren la coordinación κ^3-*mer* a la κ^2-*P*,*P*-bidentada (68 % frente a un 18 % de los ejemplos) y los ligandos dbf se coordinan exclusivamente de forma κ^3-*mer*, no conociéndose ejemplos de otro tipo. Los ligandos POP coordinados de forma κ^3-*fac* son mucho menos habituales en todos los casos, incluso inexistentes para el dbf.

Los ligandos de tipo xantphos son los más utilizados. El sustituyente de los grupos PR_2 influye de manera determinante en el modo de coordinación. La figura 6 muestra el efecto que se produce al reemplazar el grupo fenilo por el isopropilo. El ligando xantphos prefiere la coordinación κ^2-*P*,*P*-bidentada (80% de los ejemplos; figura 6a) mientras que la tendencia se invierte con el ligando 9,9-dimetil-4,5-bis(diisopropilfosfino)xanteno (xant(P^iPr_2)$_2$), mostrando una clara predilección por la coordinación κ^3-*mer* (84 % de los ejemplos; figura 6b).

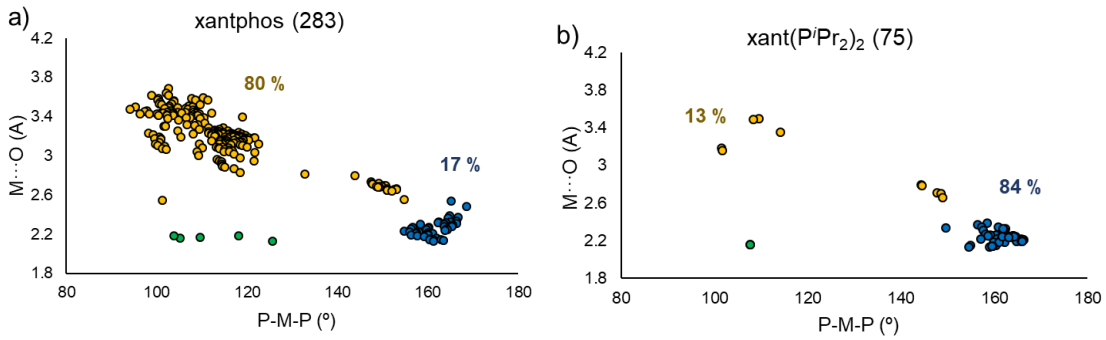

Figura 6. Relación entre la distancia M-O (Å) y ángulo de mordedura P-M-P (º) para las estructuras cristalográficas de complejos con ligandos a) xantphos y b) xant(P^iPr_2)$_2$. Entre paréntesis se indica el número de estructuras para cada caso en una búsqueda realizada en Abril de 2019 con la base de datos del CCDC. ● κ^3-*mer*, ● κ^3-*fac*, ● κ^2-*P*,*P*-bidentado.

I.5. COMPLEJOS DE METALES DEL GRUPO DEL PLATINO CON EL LIGANDO xant(P^iPr_2)$_2$

La mayoría de los complejos metálicos que incorporan el ligando xant(P^iPr_2)$_2$[57b] son ciertamente derivados de metales del grupo del platino.

I.5.1. Complejos de Rutenio y Osmio

Los ligandos dbf(P^iPr_2)$_2$, xant(P^iPr_2)$_2$ y xantphos reaccionan con las sales $MCl_3 \cdot 3H_2O$ (M = Ru, Os) para dar los derivados paramagnéticos de rutenio(III) y osmio(III) $MCl_3\{\kappa^3$-*P*,*O*,*P*-[dbf(P^iPr_2)$_2$}], $MCl_3\{\kappa^3$-*P*,*O*,*P*-[xant(P^iPr_2)$_2$]} y $MCl_3\{\kappa^3$-*P*,*O*,*P*-[xant(PPh_2)$_2$]}, respectivamente (esquema 13).[57b]

Esquema 13. Preparación de los Complejos M(POP) de Rutenio(III) y Osmio(III)

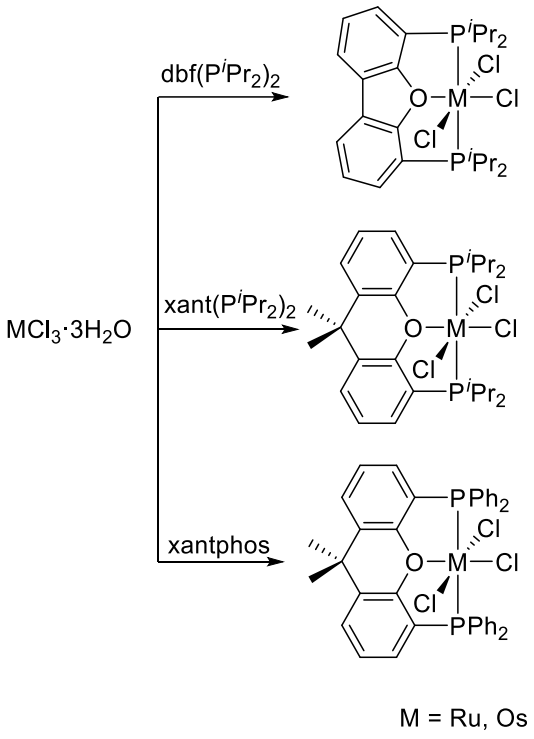

Los aductos *cis*-$RuCl_2\{\kappa^1$-*S*-$(DMSO)_4\}$ (**27**)[79] y *cis*-$OsCl_2\{\kappa^1$-*S*-$(DMSO)_4\}$ (**28**)[39] son la entrada a los derivados diamagnéticos (esquema 14).[39,57c,57d] Las reacciones con el ligando xant(P^iPr_2)$_2$ conducen a los compuestos $RuCl_2(\kappa^1$-*S*-DMSO)$\{\kappa^3$-*P,O,P*-[xant(P^iPr_2)$_2$]} (**29**) y $OsCl_2(\kappa^1$-*S*-DMSO)$\{\kappa^3$-*P,O,P*-[xant(P^iPr_2)$_2$]} (**30**), respectivamente. El aducto **28** también reacciona con el ligando dbf(P^iPr_2)$_2$ para dar el complejo $OsCl_2(\kappa^1$-*S*-DMSO)$\{\kappa^3$-*P,O,P*-[dbf(P^iPr_2)$_2$]} (**31**).

Esquema 14. Entrada a los Complejos M(POP) Diamagnéticos de Rutenio y Osmio

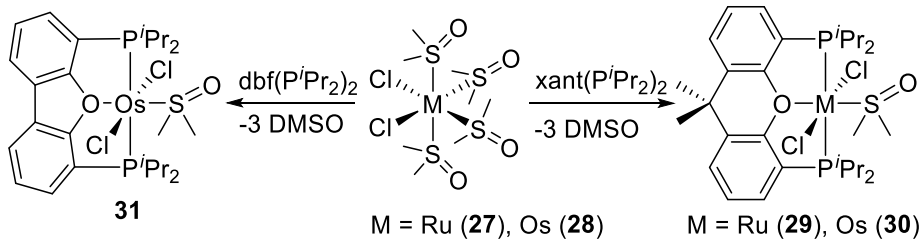

Estos compuestos diamagnéticos permiten la obtención de derivados polihidruro mediante reacciones con hidrógeno molecular en presencia de NEt_3 (esquema 15). El complejo **31** se transforma en el trihidruro $OsH_3Cl\{\kappa^3\text{-}P,O,P\text{-}[dbf(P^iPr_2)_2]\}$ (**32** en el esquema 15a). De manera similar, el compuesto **30** se convierte en el trihidruro $OsH_3Cl\{\kappa^3\text{-}P,O,P\text{-}[xant(P^iPr_2)_2]\}$ (**33**), con un rendimiento del 20% desde el $OsCl_3\cdot 3H_2O$ (esquema 15b). Esta especie se puede preparar mediante un método alternativo que mejora el rendimiento global. El tratamiento de $OsCl_3\cdot 3H_2O$ con triisopropilfosfina en isopropanol conduce a $OsH_2Cl_2(P^iPr_3)_2$ (**34**),[80] que reacciona con hidrógeno molecular en presencia de NEt_3 para dar el trihidruro $OsH_3Cl(P^iPr_3)_2$ (**35**). La sustitución de las fosfinas por el ligando $xant(P^iPr_2)_2$ produce **33** con un rendimiento del 55% desde el $OsCl_3\cdot 3H_2O$ (esquema 15c).[57c] El derivado de rutenio **29** se transforma inicialmente en el monohidruro $RuHCl(\kappa^1\text{-}S\text{-DMSO})\{\kappa^3\text{-}P,O,P\text{-}[xant(P^iPr_2)_2]\}$ (**36**). La eliminación del ligando DMSO es posible tras largos tiempos de reacción en isopropanol bajo atmósfera de H_2. Esta reacción conduce al complejo $RuHCl(\eta^2\text{-}H_2)\{\kappa^3\text{-}P,O,P\text{-}[xant(P^iPr_2)_2]\}$ (**37**), análogo al compuesto de osmio **33**, que sin embargo es una especie hidruro-dihidrógeno de acuerdo con la preferencia del rutenio por estados de oxidación más bajos (esquema 15d).

Esquema 15. Preparación de Polihidruros M(POP)

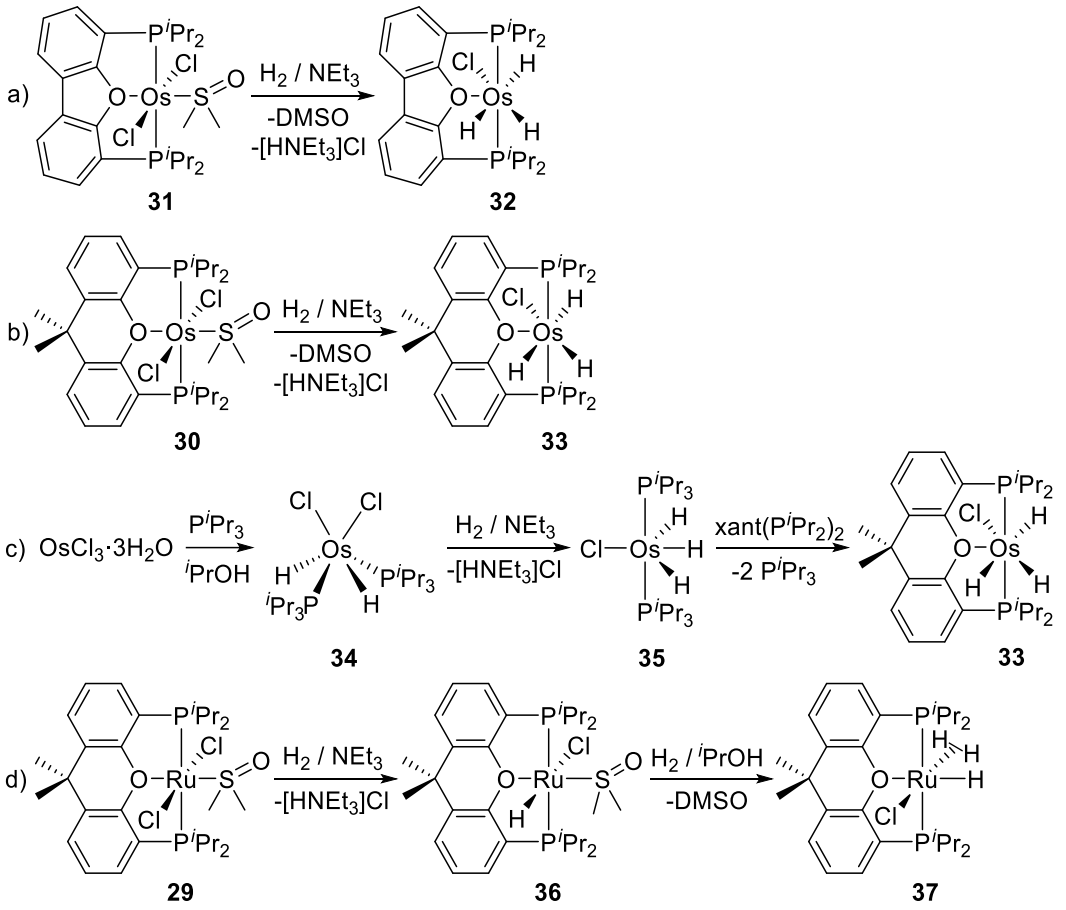

Las reacciones de los complejos **30** y **31** con hidrógeno molecular en presencia de NaH dan polihidruros diferentes. El complejo **31** conduce al tetrahidruro $OsH_4\{\kappa^3$-*P,O,P*-[dbf($P^iPr_2)_2$]} (**18** en el esquema 16a), mientras que la reacción de **30** genera el hexahidruro $OsH_6\{\kappa^2$-*P,P*-[xant($P^iPr_2)_2$]} (**38**), produciéndose el cambio en el modo de coordinación de la difosfina de κ^3-*P,O,P* a κ^2-*P,P* (esquema 16b). Este compuesto de osmio(VI) es estable bajo atmósfera de H_2, pero tras varios días bajo atmósfera de argón pierde H_2 dando lugar al tetrahidruro $OsH_4\{\kappa^3$-*P,O,P*-[xant($P^iPr_2)_2$]} (**39**) con un rendimiento del 30% desde el $OsCl_3{\cdot}3H_2O$ (esquema 16b).[57c] Alternativamente, este complejo se puede preparar a partir de **34**, que inicialmente se transforma en el hexahidruro $OsH_6(P^iPr_3)_2$ (**40**).[80] La difosfina xant($P^iPr_2)_2$ desplaza las unidades P^iPr_3 y

una molécula de H_2 para dar **39** con un rendimiento del 20% desde el $OsCl_3 \cdot 3H_2O$ (esquema 16c). Aunque el procedimiento disminuye ligeramente el rendimiento global, el tiempo sufre una reducción de 10 a 7 días.

Esquema 16. Preparación de los Complejos Tetrahidruro Os(POP)

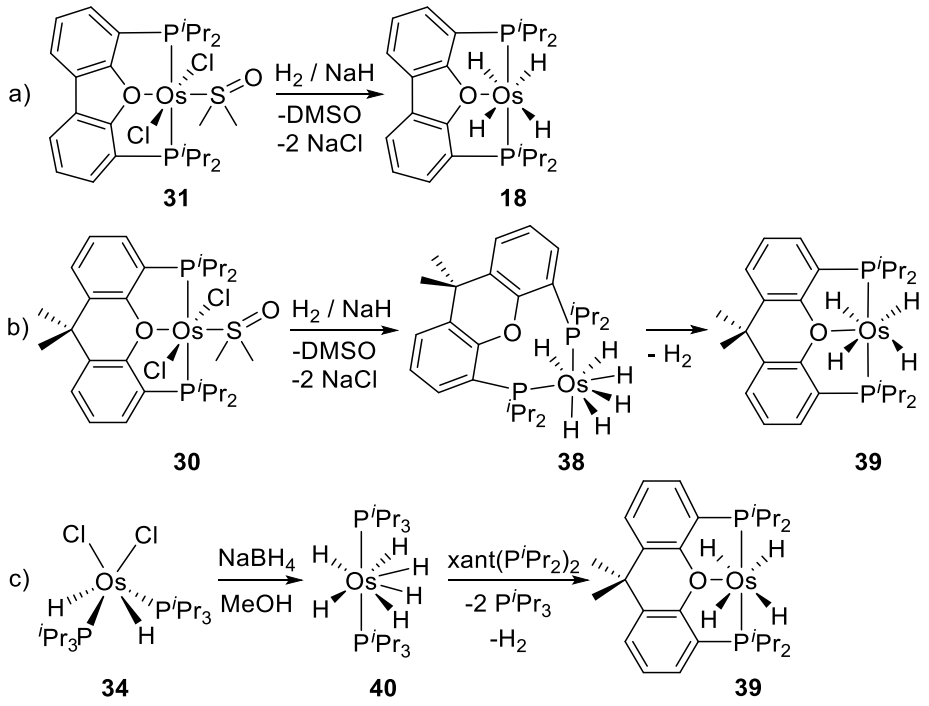

El derivado de rutenio análogo a **39** no se puede preparar siguiendo las reacciones utilizadas en la química de osmio. Sin embargo, la especie Ru(COD)(COT) (COT = 1,3,5-ciclooctatrieno) (**41**)[81] permite la formación del compuesto $RuH_2(\eta^2\text{-}H_2)\{\kappa^3\text{-}P,O,P\text{-}[xant(P^iPr_2)_2]\}$ (**42**), siguiendo un procedimiento similar al utilizado por Chaudret y colaboradores en la síntesis de complejos polihidruro $RuH_2(\eta^2\text{-}H_2)(PR_3)_2$ (esquema 17).[82] La comparación de **39** y **42** pone de manifiesto de nuevo que, como consecuencia del mayor carácter oxidante del rutenio respecto al osmio, las especies polihidruro d^4 en osmio son derivados dihidrógeno d^6 en rutenio.[57d]

Esquema 17. Formación del Complejo 42

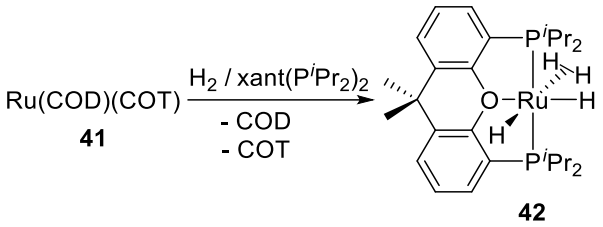

42

Un procedimiento más eficaz para obtener **42** que el que se muestra en el esquema 17 consiste en la sustitución del ligando DMSO por un fragmento hidrocarbonado insaturado que pueda ser reducido posteriormente (esquema 18).[57d] El complejo **29** se transforma en el derivado alenilideno $RuCl_2(=C=C=CPh_2)\{\kappa^3\text{-}P,O,P\text{-}[xant(P^iPr_2)_2]\}$ (**43**) por reacción con 1,1-difenil-2-propin-1-ol. Este compuesto se reduce secuencialmente en presencia de amoniaco-borano dando lugar al vinilideno $RuCl_2(=C=CHCHPh_2)\{\kappa^3\text{-}P,O,P\text{-}[xant(P^iPr_2)_2]\}$ (**44**), que posteriormente experimenta la hidrogenación del doble enlace $Ru=C_\alpha$, generando el tetrahidruroborato $RuH(\eta^2\text{-}H_2BH_2)\{\kappa^3\text{-}P,O,P\text{-}[xant(P^iPr_2)_2]\}$ (**45**) y 3,3-difenil-1-propeno. La formación de **45** tiene lugar a través del intermedio insaturado **Q**, que resulta de la sustitución de los ligandos cloruro por hidruros y la eliminación del alqueno. La hidrogenación de **45** en isopropanol proporciona la especie **42**.

Esquema 18. Ruta Sintética Alternativa para la Preparación de 42

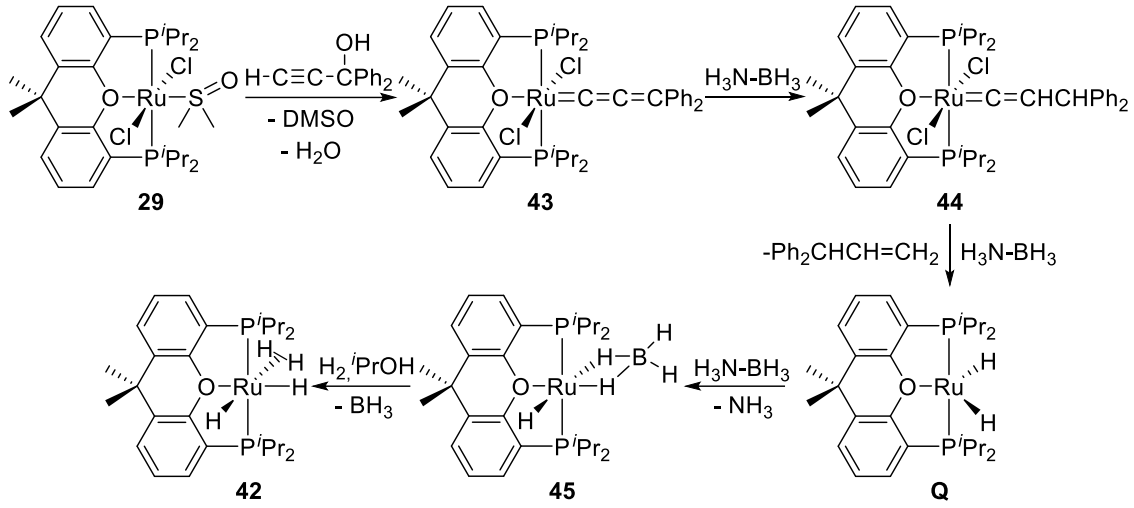

El complejo de osmio **30** análogo a **29** reacciona con 1,1-difenil-2-propin-1-ol de manera similar para dar el derivado alenilideno $OsCl_2(=C=C=CPh_2)\{\kappa^3\text{-}P,O,P\text{-}[xant(P^iPr_2)_2]\}$ (**46**). Su posterior tratamiento con amoniaco-borano reduce el doble enlace $C_\beta=C_\gamma$. Sin embargo, el vinilideno resultante $OsCl_2(=C=CHCHPh_2)\{\kappa^3\text{-}P,O,P\text{-}[xant(P^iPr_2)_2]\}$ (**47**) es inerte frente a la hidrogenación del doble enlace $Os=C_\alpha$, por lo que no es posible la preparación del tetrahidruro de osmio **39** utilizando este procedimiento (esquema 19). Esto es consistente con la preferencia del osmio por formar compuestos con una multiplicidad de enlace metal-carbono mayor que el rutenio.[83]

Esquema 19. Preparación y Reducción del Complejo Alenilideno de Osmio 46

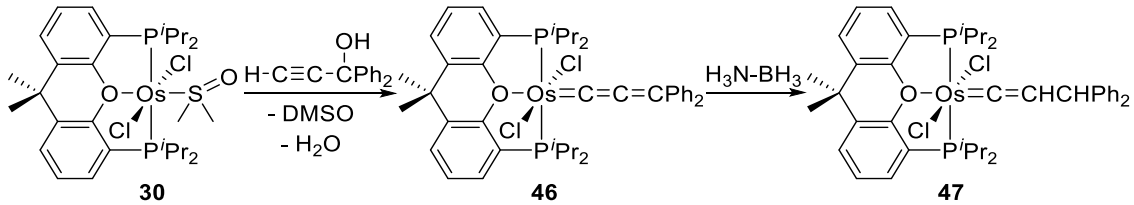

El complejo tetrahidruro de osmio **39** es un reductor capaz de promover la reducción de H^+ a pesar del alto estado de oxidación de su centro metálico (esquema 20).[57c] Este

polihidruro adiciona un protón para dar la especie $[OsH_5\{\kappa^3\text{-}P,O,P\text{-}[xant(P^iPr_2)_2]\}]^+$ (**48**), que existe como una mezcla en equilibro de dos tautómeros que difieren en energía 3.0 kcal·mol^{-1}, de acuerdo con cálculos DFT: el trihidruro-dihidruro comprimido de osmio(VI) (**48a**) y el hidruro-dihidruro comprimido-dihidrógeno de osmio(IV) (**48b**). La adición de una segunda molécula de HOTf libera H_2 y proporciona el complejo dihidruro-dihidrógeno elongado $[OsH_2(\eta^2\text{-}H_2)(OTf)\{\kappa^3\text{-}P,O,P\text{-}[xant(P^iPr_2)_2]\}]^+$ (**49**).

Esquema 20. Reducción de H^+ Promovida por 39 para dar 49

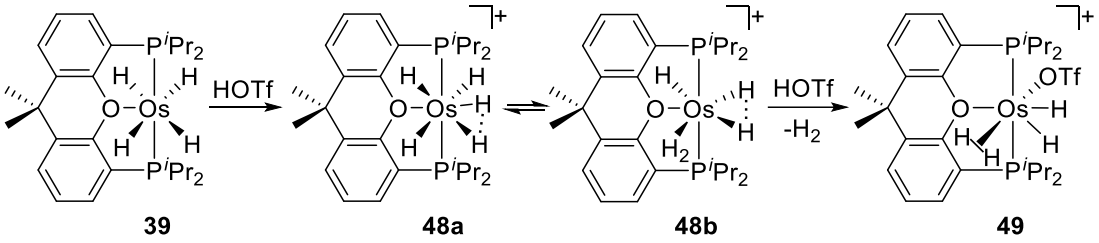

El complejo de rutenio **42** promueve la activación C-H de distintas cetonas y aldehídos (esquema 21).[57e] La liberación de H_2 desde **42** conduce al intermedio dihidruro **Q**, que reduce el grupo carbonilo (*vide infra*), por lo que estas reacciones requieren 2 equivalentes de sustrato. El tratamiento de **42** con acetofenona y benzofenona lleva a los derivados rutenaisobenzofurano $RuH\{\kappa^2\text{-}O,C\text{-}[OC(R)C_6H_4]\}\{\kappa^3\text{-}P,O,P\text{-}[xant(P^iPr_2)_2]\}$ (R = Me (**50**), Ph (**51**)), respectivamente, resultado de la activación selectiva del enlace C-H en la posición *orto* del anillo aromático. El complejo **42** activa selectivamente el enlace *orto*-C-H de cetonas aromáticas fluoradas. La reacción con 2-fluoroacetofenona genera el compuesto rutenaisobenzofurano fluorado $RuH\{\kappa^2\text{-}O,C\text{-}[OC(Me)C_6H_3F]\}\{\kappa^3\text{-}P,O,P\text{-}[xant(P^iPr_2)_2]\}$ (**52**). La especie **42** también promueve la activación selectiva del enlace vinílico C_β-H de las cetonas *α,β*-insaturadas metil vinil cetona y bencilidenacetona dando lugar a los rutenafuranos $Ru\{\kappa^2\text{-}O,C\text{-}[OC(Me)CHC(R)]\}\{\kappa^3\text{-}P,O,P\text{-}[xant(P^iPr_2)_2]\}$ (R = H (**53**), Ph (**54**)). La reacción con bencilidenacetofenona proporciona

una mezcla de RuH{κ^2-*O*,*C*-[OC(CH=CHPh)C$_6$H$_4$)]}{κ^3-*P*,*O*,*P*-[xant(P^{i}Pr$_2$)$_2$]} (**55**) y RuH{κ^2-*O*,*C*-[OC(Ph)CHCPh]}{κ^3-*P*,*O*,*P*-[xant(P^{i}Pr$_2$)$_2$]} (**56**) en una relación molar 1:1.

Esquema 21. Activación C-H de Cetonas y Aldehídos Promovidas por 42

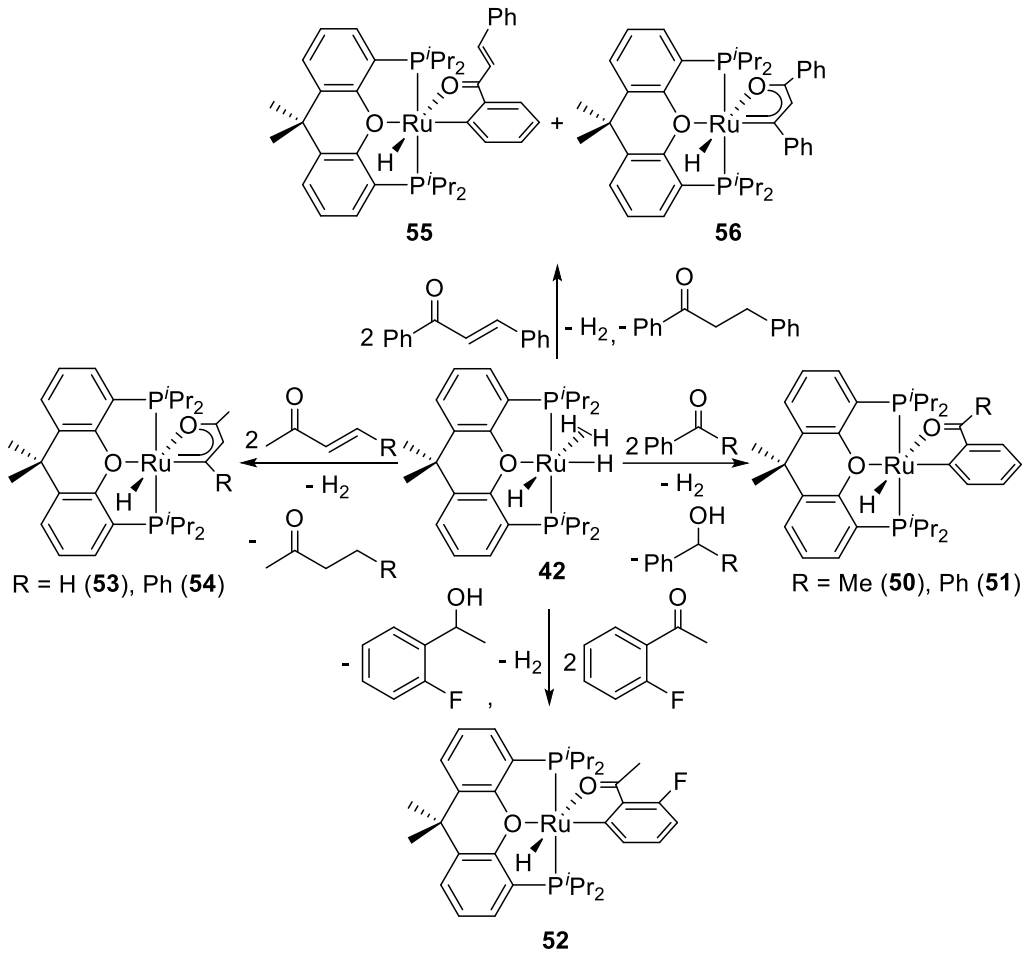

El compuesto de osmio **39** experimenta reacciones de activación C-H similares generando productos análogos (esquema 22).[57e] El complejo **39** reacciona con acetofenona y benzofenona para dar los derivados osmaisobenzofurano OsH{κ^2-*O*,*C*-[OC(R)C$_6$H$_4$]}{κ^3-*P*,*O*,*P*-[xant(P^{i}Pr$_2$)$_2$]} (R = Me (**57**), Ph (**58**)). El estudio de esta reacción con benzofenona perdeuterada sugiere que el origen de la selectividad de la activación de enlaces *orto*-C-H de estas cetonas aromáticas es únicamente termodinámico, dado que las activaciones de los enlaces C-H en posiciones *meta* y *para*

están cinéticamente favorecidas, lo que está de acuerdo con lo observado por Goldman para derivados PCP de iridio.[84] El complejo **39** se transforma en los derivados osmaisobenzofurano fluorados OsH{κ^2-*O*,*C*-[OC(Me)C_6H_3F]}{κ^3-*P*,*O*,*P*-[xant(P^{i}Pr$_2$)$_2$]} (**59**) y OsH[κ^2-*O*,*C*-[OC($C_6H_3F_2$)C_6H_4]}{κ^3-*P*,*O*,*P*-[xant(P^{i}Pr$_2$)$_2$]} (**60**) por reacción con 2-fluoroacetofenona y 2,6-difluorobenzofenona, respectivamente. El tratamiento de **39** con metil vinil cetona y bencilidenacetona produce los osmafuranos OsH{κ^2-*O*,*C*-[OC(Me)CHC(R)]}{κ^3-*P*,*O*,*P*-[xant(P^{i}Pr$_2$)$_2$]} (R = H (**61**), Ph (**62**)). La reacción de **39** con bencilidenacetofenona genera una mezcla de OsH{κ^2-*O*,*C*-[OC(CH=CHPh)C_6H_4]}{κ^3-*P*,*O*,*P*-[xant(P^{i}Pr$_2$)$_2$]} (**63**) y OsH{κ^2-*O*,*C*-[OC(Ph)CHCPh]}{κ^3-*P*,*O*,*P*-[xant(P^{i}Pr$_2$)$_2$]} (**64**) en una relación molar 2:1.

Esquema 22. Activación C-H de Cetonas y Aldehídos Promovida por 39

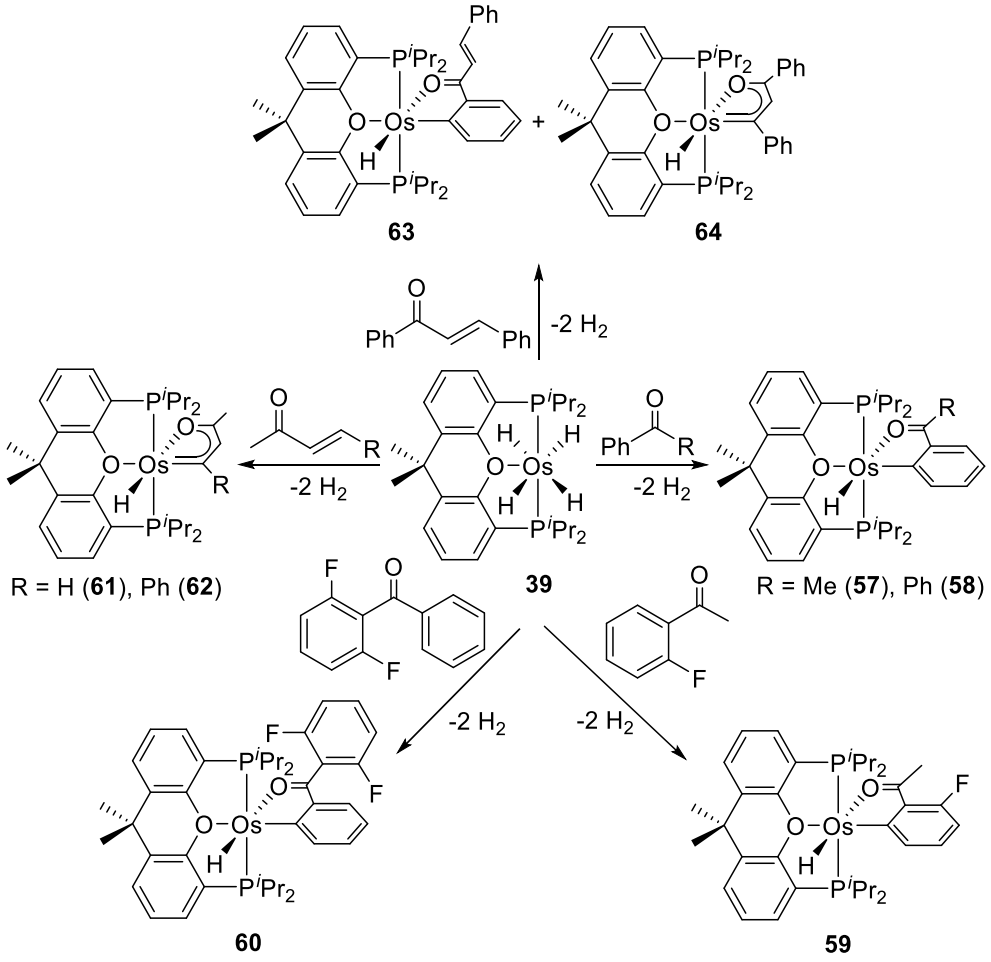

El compuesto **42** promueve selectivamente la activación del enlace OC-H de aldehídos frente a la activación C-H en posición *orto*, a pesar de que este último enlace es sólo 23 kcal/mol más fuerte que el primero (esquema 23a).[57e] Así, la reacción con benzaldehído da el intermedio hidruro-acilo insaturado **R** que evoluciona al derivado hidruro-fenilo-carbonilo RuH(Ph)(CO){κ^3-*P*,*O*,*P*-[xant(P^{i}Pr$_2$)$_2$]} (**65**) mediante la desinserción del grupo fenilo. La especie análoga de osmio **39** también favorece la activación del enlace OC-H sobre la ruptura del enlace *orto*-C-H del sustituyente fenilo. La reacción con benzaldehído genera el producto hidruro-fenilo-carbonilo OsH(Ph)(CO){κ^3-*P*,*O*,*P*-[xant(P^{i}Pr$_2$)$_2$]} (**66**) a través del intermedio **S** (esquema 23b). El complejo **39** también

activa el enlace OC-H en presencia del enlace CH vinílico de aldehídos *α,β*-insaturados (esquema 23c). La reacción con 1-ciclohexeno-1-carboxaldehído conduce al derivado ciclohexenilo $OsH(C_6H_9)(CO)\{\kappa^3\text{-}P,O,P\text{-}[xant(P^iPr_2)_2]\}$ (**67**) que evoluciona al dihidruro-carbonilo $OsH_2(CO)\{\kappa^3\text{-}P,O,P\text{-}[xant(P^iPr_2)_2]\}$ (**68**) como consecuencia de la eliminación de 1,3-ciclohexadieno.

Esquema 23. Activación del Enlace OC-H de Aldehídos

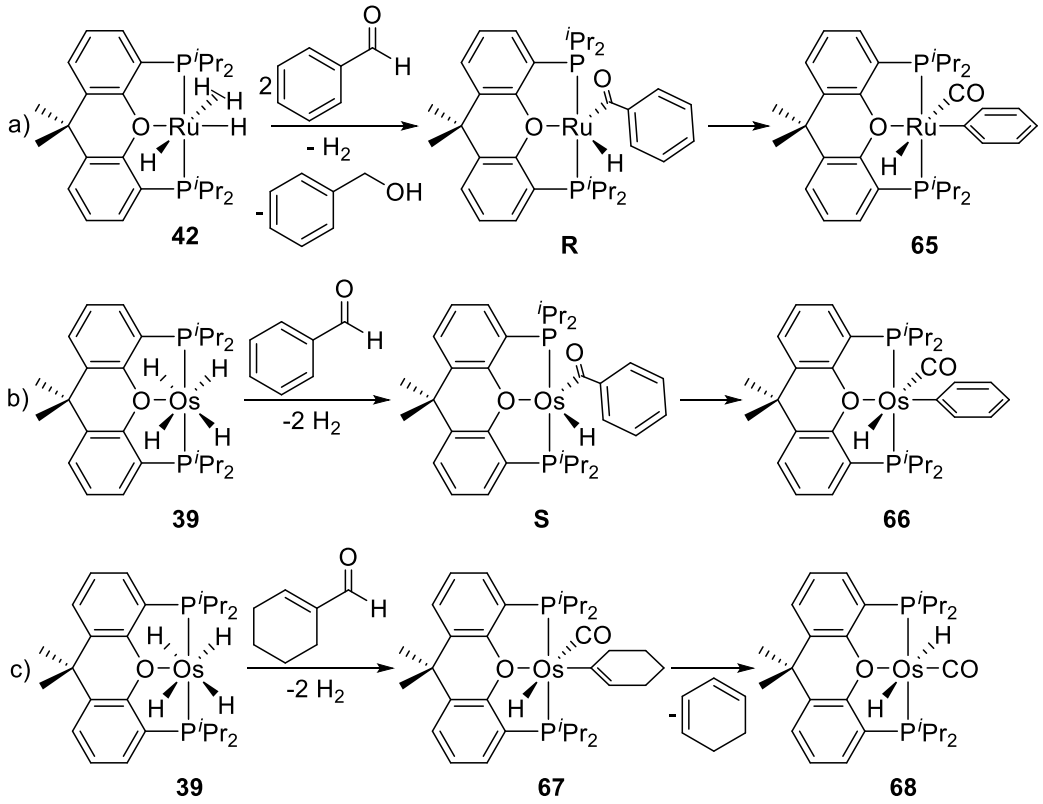

Algunos complejos de osmio y rutenio basados en los ligandos $dbf(P^iPr_2)_2$ y $xant(P^iPr_2)_2$ promueven procesos catalíticos de interés. La formación de iminas a partir de alcoholes primarios y aminas primarias catalizada por $OsH_4\{\kappa^3\text{-}P,O,P\text{-}[dbf(P^iPr_2)_2\}$ (**18**) se ha comentado en el apartado 2 de esta introducción (esquema 9).

Los compuestos **39** y **42** promueven la dimerización *Z*-cabeza-cabeza regio- y estereoselectiva de alquinos terminales para dar los correspondientes *Z*-eninos, siendo el catalizador de rutenio más activo para esta transformación (ecuación 1).[57c,57d]

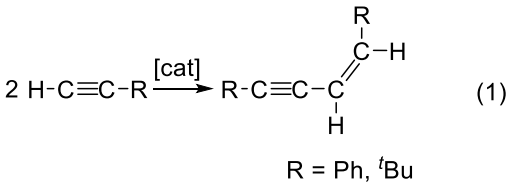

El complejo **39** reacciona con fenilacetileno y *terc*-butilacetileno generando los derivados $Os(C{\equiv}CR)_2(=C{=}CHR)\{\kappa^3\text{-}P,O,P\text{-}[xant(P^iPr_2)_2]\}$ (R = Ph (**69**), ^{t}Bu(**70**)), respectivamente, 2 equivalentes de la correspondiente olefina e H_2 (esquema 24). Sobre la base de esta reacción estequiométrica se propone el mecanismo que se muestra en el esquema 25.[57c] La inserción migratoria del ligando vinilideno en uno de los enlaces metal-alquinilo origina la especie **T**. El desplazamiento del triple enlace carbono-carbono coordinado del ligando buteninilo por una molécula de alquino conduce al intermedio **U**, que elimina el *Z*-enino para dar **V**. La coordinación de una nueva molécula de alquino regenera los derivados vinilidenos, cerrando el ciclo catalítico.

Esquema 24. Reacción Estequiométrica de 39 con Alquinos

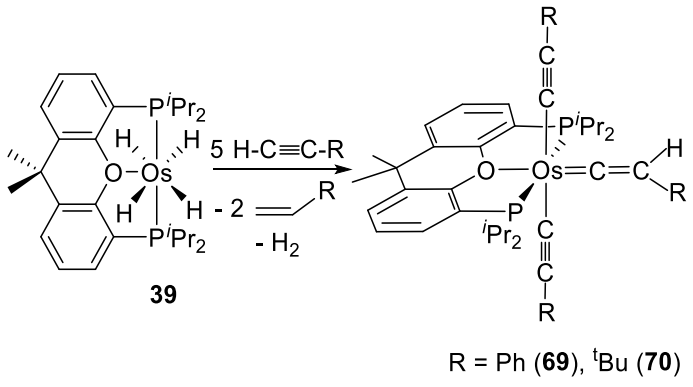

Esquema 25. Ciclo Catalítico para la Formación de *Z*-Eninos

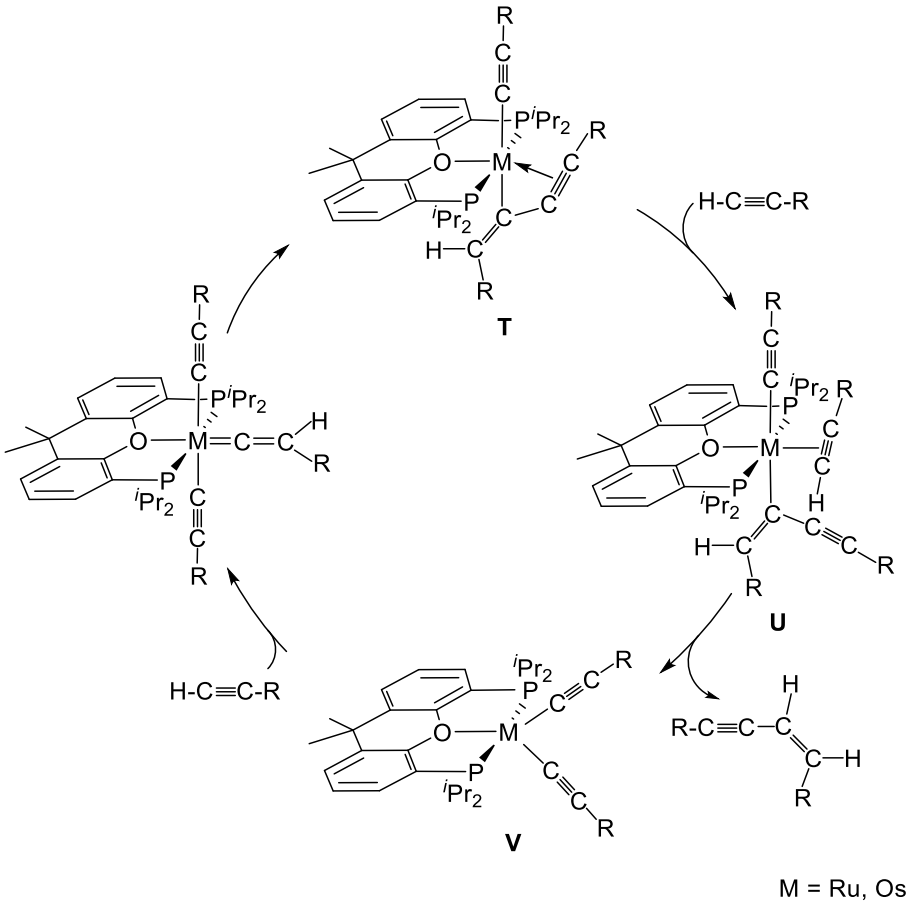

El complejo de rutenio **42** promueve la reducción de cetonas mediante transferencia de hidrógeno de isopropanol, en ausencia de base (esquema 26).[57d] Este proceso se ha propuesto que transcurra a través de un mecanismo de esfera interna.[85] Bajo las condiciones de reacción, el complejo **42** pierde H_2 para dar la especie insaturada **Q**. La coordinación de las cetonas a esta última conduce al intermedio **W**, que evoluciona al derivado alcóxido **X** mediante la migración de un ligando hidruro desde el centro metálico al átomo de carbono carbonílico. La eliminación del producto reducido mediante el intercambio entre el alcóxido resultante de la inserción e isopropanol produce **Y**. Finalmente, una reacción de *β*-eliminación regenera la especie activa **Q**, cerrando el ciclo catalítico.

Esquema 26. Reducción de Cetonas Promovida por el Complejo 42

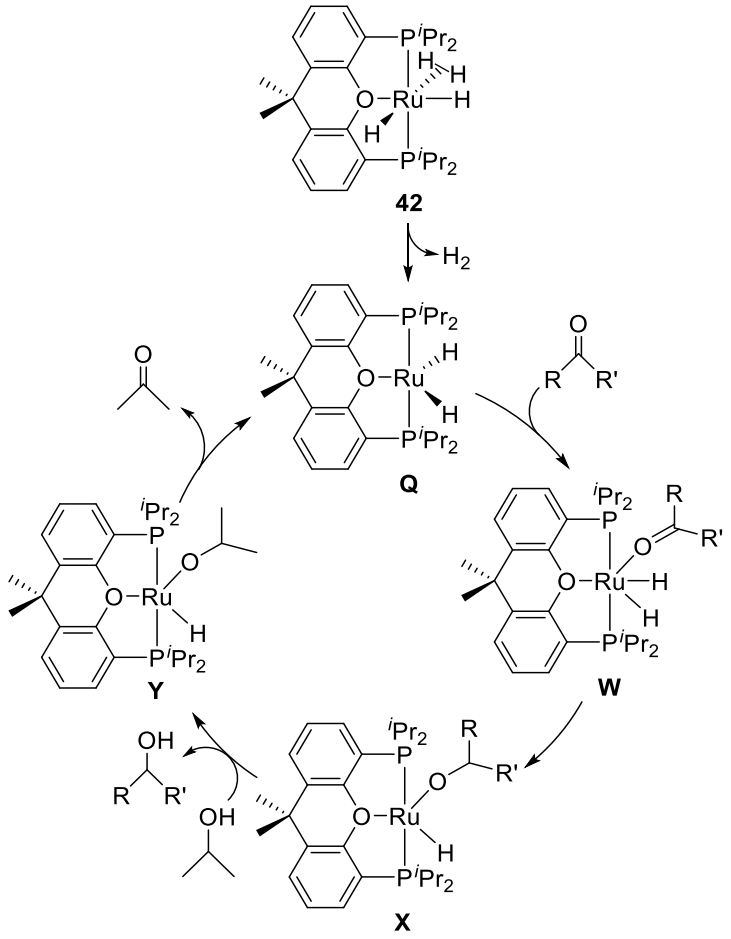

El compuesto **42** también es un precursor eficiente para la alquilación catalítica de nitrilos y cetonas, reacciones típicas en la *metodología de préstamo de hidrógeno*.[57d] Esta especie es activa en las alquilaciones de fenilacetonitrilo con alcohol bencílico y 1-octanol y en la alquilación de acetofenona con alcohol bencílico.

I.5.2. Complejos de Rodio e Iridio

El estudio comparativo de los compuestos de rodio e iridio pone de manifiesto la preferencia de este último por formar especies coordinativamente saturadas, lo que está de acuerdo con el mayor carácter reductor del iridio frente al rodio. El dímero de rodio

$[Rh(\mu\text{-}Cl)(C_8H_{14})_2]_2$ (**71**) reacciona con el ligando xant(P^iPr_2)$_2$ para dar el complejo planocuadrado insaturado $RhCl\{\kappa^3\text{-}P,O,P\text{-}[xant(P^iPr_2)_2]\}$ (**72** en el esquema 27a). El dímero correspondiente de iridio $[Ir(\mu\text{-}Cl)(C_8H_{14})_2]_2$ (**73**) reacciona con xant(P^iPr_2)$_2$ para formar el intermedio planocuadrado $IrCl\{\kappa^3\text{-}P,O,P\text{-}[xant(P^iPr_2)_2]\}$ (**Z**), análogo a **72**, que evoluciona hacia la especie octaédrica saturada $IrHCl\{\kappa^4\text{-}C,P,O,P\text{-}[CH_2CH(CH_3)P(^iPr)xant(P^iPr_2)]\}$ (**74**), resultado de la ciclometalación de uno de los sustituyentes isopropilo de la fosfina (esquema 27b).[86] La sustitución del ligando cloruro por hidruro también genera derivados insaturados de rodio y saturados de iridio. Al tratar **72** con una disolución de KOH/^{i}PrOH se forma el intermedio **AA** que da lugar al complejo monohidruro $RhH\{\kappa^3\text{-}P,O,P\text{-}[xant(P^iPr_2)_2]\}$ (**75** en el esquema 27c), mientras que un tratamiento similar de **74** conduce al trihidruro $IrH_3\{\kappa^3\text{-}P,O,P\text{-}[xant(P^iPr_2)_2]\}$ (**76** en el esquema 27d). La especie **Z** de iridio sufre la sustitución del ligando cloruro por un grupo isopropóxido para dar **AB** que evoluciona a **AC**. Este último, a diferencia de **72**, es capaz de deshidrogenar isopropanol para dar el trihidruro **76**, de acuerdo con el mayor carácter reductor del iridio.

Esquema 27. Formación de Complejos de Rodio e Iridio con el Ligando xant(P^{i}Pr$_2$)

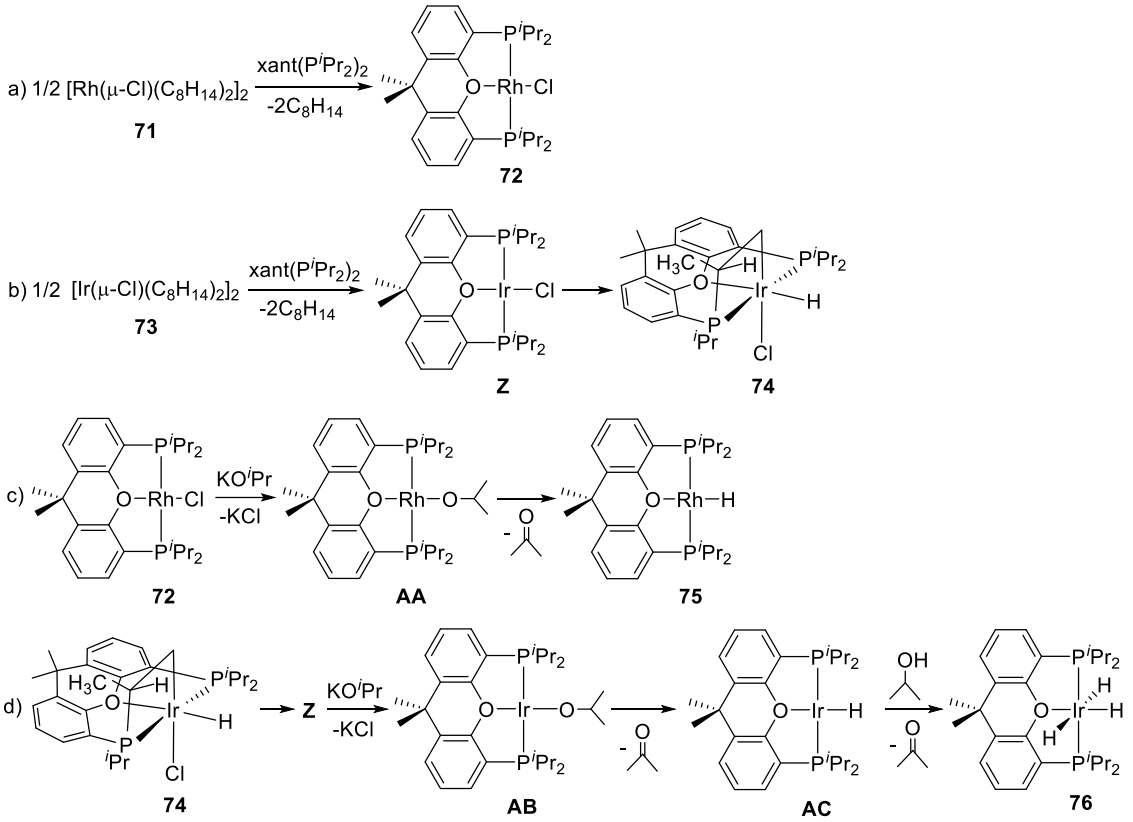

Los compuestos **72** y **74** son capaces de activar enlaces Si-H de silanos, como difenilsilano, generando las especies saturadas d^6 RhHCl(SiHPh$_2$){κ^3-*P*,*O*,*P*-[xant(P^{i}Pr$_2$)$_2$]} (**77**) y IrHCl(SiHPh$_2$){κ^3-*P*,*O*,*P*-[xant(P^{i}Pr$_2$)$_2$]} (**78**), respectivamente (esquema 28). El complejo de rodio(III) **77** no es estable en disolución y pierde H_2 para formar el derivado planocuadrado Rh(SiClPh$_2$){κ^3-*P*,*O*,*P*-[xant(P^{i}Pr$_2$)$_2$]} (**79**), resultante de la migración del ligando cloruro desde el metal al átomo de silicio (esquema 28a). El complejo de iridio **78** tampoco es estable en disolución. Sin embargo, este evoluciona a la especie octaédrica saturada *trans*-dihidruro IrH$_2$(SiClPh$_2$){κ^3-*P*,*O*,*P*-[xant(P^{i}Pr$_2$)$_2$]} (**80**) sin pérdida de H_2 (esquema 28b). El monohidruro de rodio(I) también es capaz de activar enlaces Si-H (esquema 28c). La reacción de **75** con trifenisilano proporciona el compuesto octaédrico de rodio(III) *trans*-RhH$_2$(SiPh$_3$){κ^3-*P*,*O*,*P*-[xant(P^{i}Pr$_2$)$_2$]} (**81**)

que, por pérdida de H_2, conduce a Rh(SiPh$_3$){κ^3-*P*,*O*,*P*-[xant(P^{i}Pr$_2$)$_2$]} (**82**). La eliminación reductora de H_2 en los derivados octaédricos de rodio(III) requiere de la disociación previa del átomo de oxígeno del ligando xant(P^{i}Pr$_2$)$_2$, lo que favorece la formación de intermedios dihidrógeno que evolucionan a las correspondientes especies planocuadradas. El complejo **77** se puede aislar y caracterizar completamente mientras que la especie análoga **81** sólo se detecta por RMN a baja temperatura. Esto se debe a que el ligando hidruro disminuye la nucleofilia del compuesto planocuadrado y, por lo tanto, la estabilidad de las especies saturadas de rodio(III) respecto al ligando cloruro.[87]

Esquema 28. Reacciones de Activación Si-H Promovidas por Complejos de Rodio e Iridio

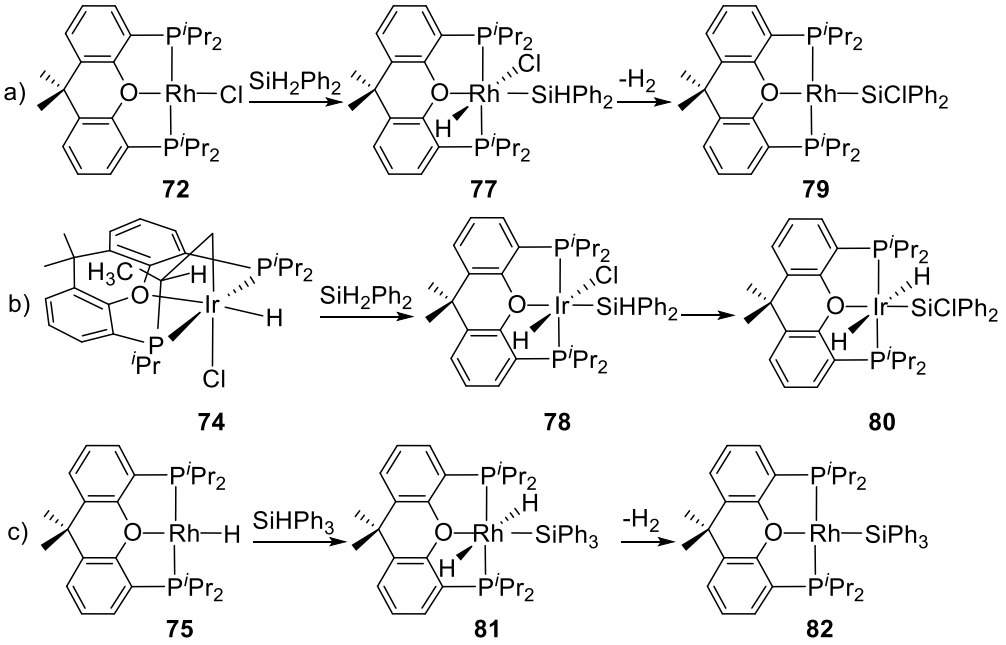

El complejo **79** es la entrada a un interesante derivado silílol (esquema 29). El tratamiento de **79** con NaBAr$^F_4$·2H$_2$O (Ar^F = 3,5-bis(trifluorometil)fenilo) provoca la abstracción del átomo de cloro del grupo silílo dando lugar al silileno **AD**, que posteriormente reacciona

con H_2O generando el derivado pentacoordinado hidruro-silílol [RhH{Si(OH)Ph_2}{κ^3-*P,O,P*-[xant(P^{i}Pr$_2$)$_2$]}]BAr$^F_4$ (**83**).[87]

Esquema 29. Formación del Derivado Silílol de Rodio(III)

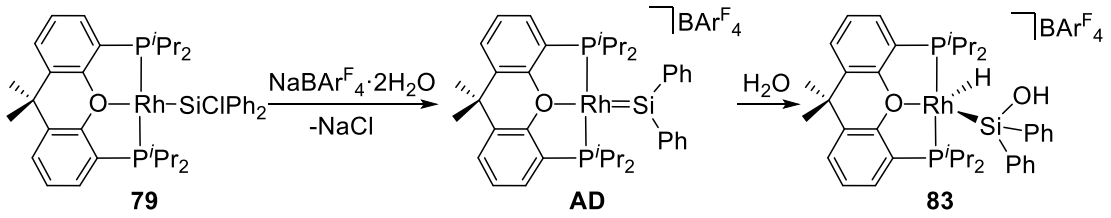

El compuesto **83** promueve la monoalcohólisis de difenilsilano de manera selectiva, de acuerdo con el esquema 30. La eliminación reductora de SiH(OH)Ph_2 proporciona la especie insaturada **AE** que, tras la adición oxidante de difenilsilano, da el derivado pentacoordinado **AF**. La formación del intermedio dihidrógeno **AG** y posterior disociación de la molécula de hidrógeno coordinada genera el silileno **AD**. Esta especie es el intermedio clave del proceso, lo que está de acuerdo con la propuesta de Tilley y colaboradores, que han demostrado que los complejos silileno de iridio son catalizadores activos en la alcohólisis de silanos.[88] La adición de una molécula de ROH a **AD** da lugar al intermedio **AH** que, tras la eliminación reductora del alcoxisilano correspondiente, regenera la especie activa **AE** cerrando el ciclo catalítico.[87]

Esquema 30. Alcohólisis de Difenilsilano Promovida por el Complejo 83

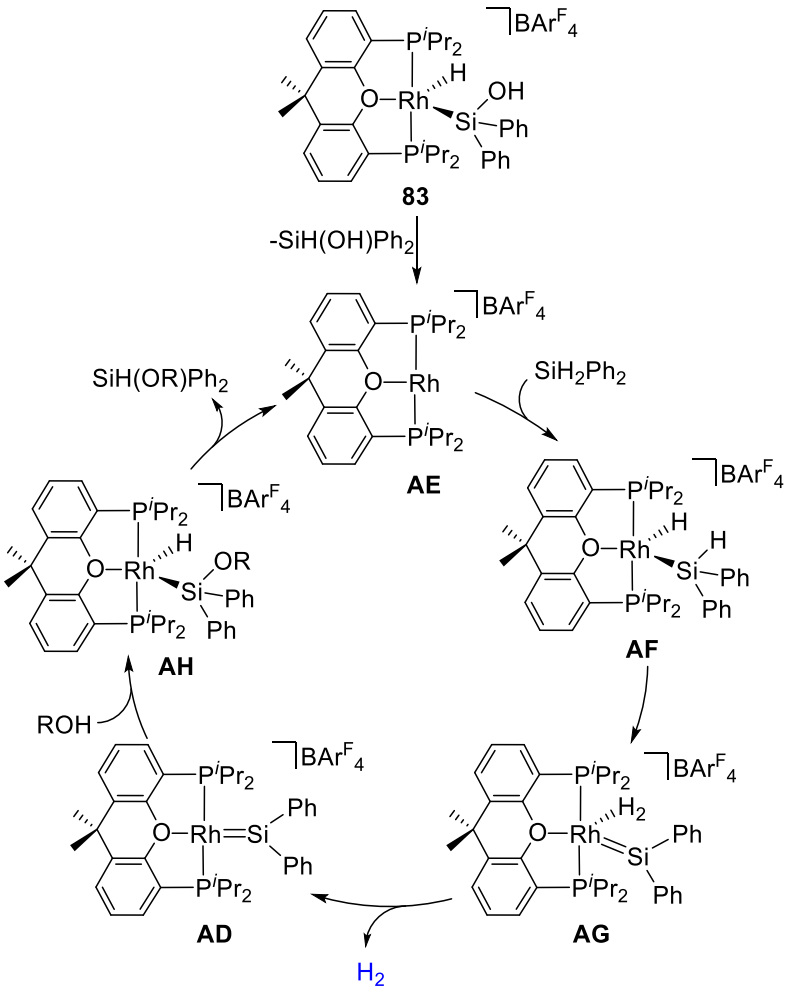

El monohidruro de rodio(I) **75** promueve la deshidrogenación cinéticamente controlada de amoniaco-borano y dimetilamina-borano.[89] Además de hidrógeno molecular, las reacciones generan poliaminoborano y el dímero $[H_2BNMe_2]_2$, respectivamente. El esquema 31 resume la propuesta mecanística para la deshidrogenación de amoniaco-borano. Inicialmente, la disociación del átomo de oxígeno de la difosfina da el intermedio **AI**. La posterior coordinación de una molécula de sustrato al centro metálico conduce a la especie tipo Shimoi **AJ**. La adición oxidante del enlace B-H al átomo de rodio proporciona **AK**, que libera amino-borano generando el hidruro-dihidrógeno **AL** mediante la transferencia de protón desde el grupo NH_3 a uno de los ligandos hidruro de

AK. Por último, la liberación de H_2 regenera la especie activa **AI**, lo que permite cerrar el ciclo catalítico.

Esquema 31. Ciclo Catalítico para la Deshidrogenación de Amoniaco-Borano Promovida por el Complejo 75

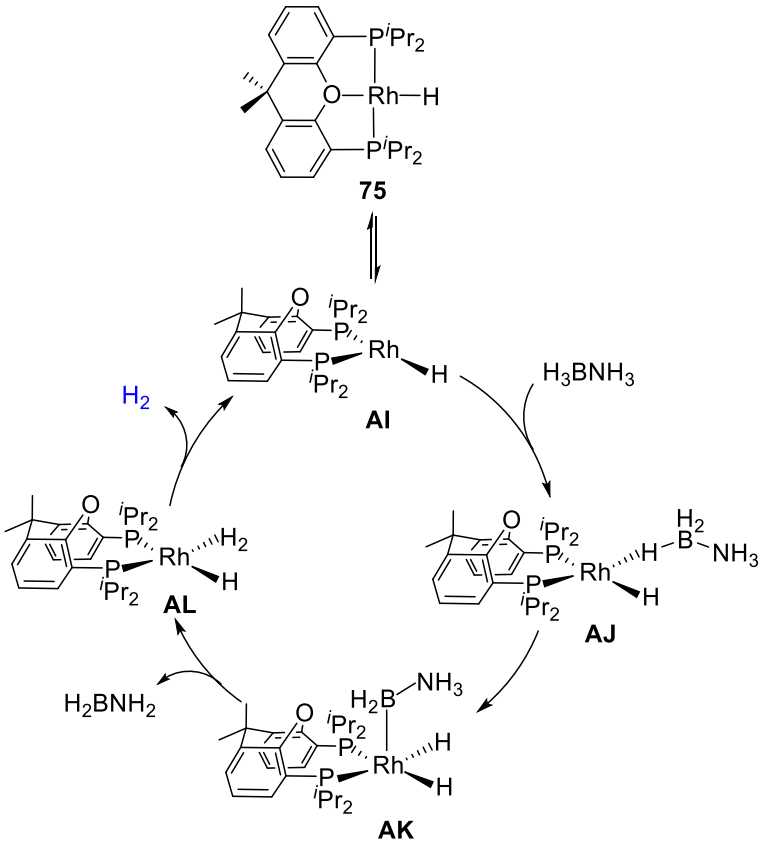

Weller y colaboradores han estudiado recientemente la reacción de deshidropolimerización de $H_3B{\cdot}NMe_2$.[90] Con el objetivo de optimizar la obtención de *N*-metil poliaminaborano han utilizado catalizadores basados en fragmentos Rh{xant(PR_2)$_2$} con diferentes sustituyentes en los grupos PR_2. Los resultados muestran que con grupos etilo se forman dímeros que son inactivos, mientras que con sustituyentes muy voluminosos como el *terc*-butilo se generan catalizadores mononucleares poco

selectivos. El ligando xant(P^iPr_2)$_2$ ofrece el comportamiento óptimo dando lugar a los sistemas más activos y selectivos.

El complejo **75** también activa el enlace B-H del catecolborano y del pinacolborano, de acuerdo con la marcada relación diagonal entre el boro y el silicio (esquema 32).[91] Estas reacciones conducen a los compuestos de rodio(III) *trans*-$RhH_2(BR_2)\{\kappa^3$-*P,O,P*-[xant(P^iPr_2)$_2$]} (BR_2 = Bcat (**84**), Bpin (**85**)). Estos se transforman en los derivados de rodio(I) $Rh(BR_2)\{\kappa^3$-*P,O,P*-[xant(P^iPr_2)$_2$]} (BR_2 = Bcat (**86**), Bpin (**87**)) tras la eliminación reductora de H_2, de manera similar a sus homólogos de silicio. El complejo **87** se puede obtener por reacción de **75** con B_2pin_2, lo que demuestra que este último también es capaz de activar el enlace B-B.

Esquema 32. Activación B-H y B-B Promovida por el Complejo de Rodio 75

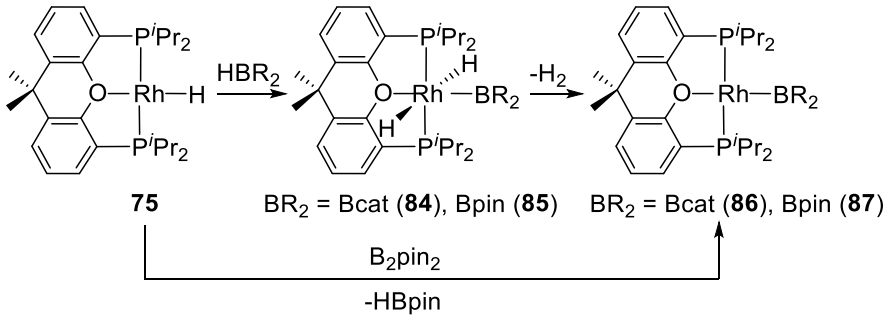

La química de iridio con ligandos borilo pone nuevamente de manifiesto las diferencias entre este metal y el rodio (esquema 33). El complejo **74** activa el enlace B-H del catecolborano generando el compuesto octaédrico IrHCl(Bcat)$\{\kappa^3$-*P,O,P*-[xant(P^iPr_2)$_2$]} (**88** en el esquema 33a). Las especies **74** y **76** activan el enlace B-B de B_2cat_2 para dar el derivado *tris*-borilo $Ir(Bcat)_3\{\kappa^3$-*P,O,P*-[xant(P^iPr_2)$_2$]} (**89** en los esquemas 33b y 33c). La formación de este compuesto de iridio(III) es notable ya que desafía el concepto de influencia *trans*.[92]

Esquema 33. Activación B-H y B-B Promovida por Complejos de Iridio

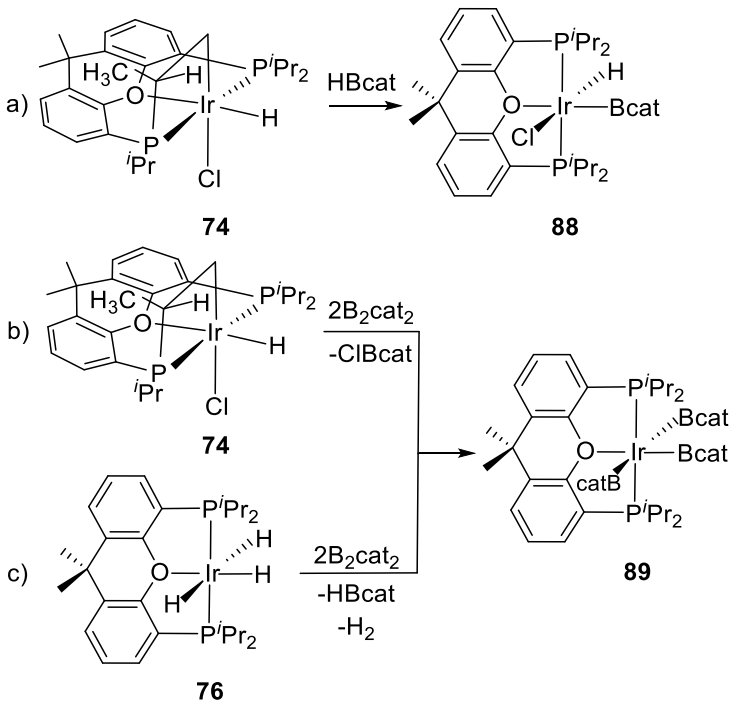

El complejo de rodio **75** promueve la activación de enlaces C-H de diferentes arenos y fluoroarenos (esquema 34). Las reacciones conducen a derivados arilo de rodio(I) planocuadrados generando H_2.[91] La selectividad del proceso depende de la posición de los sustituyentes del arilo: la activación C-H en arenos está favorecida en las posiciones *meta* y *para* con respecto al sustituyente R, mientras que en los fluoroarenos la posición favorecida es la *orto* con respecto del ligando fluoruro. Sin embargo, la reacción de **75** con cloroarenos da lugar a especies de rodio(III), que generalmente resultan de la adición oxidante del enlace C-Cl. Este hecho se debe a que la activación del enlace C-Cl está favorecida cinética y termodinámicamente frente a la ruptura C-H. La deshalogenación de estos compuestos mediante la adición de ^{t}BuOK ha permitido la preparación de una amplia gama de complejos arilo planocuadrados de rodio(I).[93]

Esquema 34. Activación de Enlaces C-H y C-Cl Promovidas por el Complejo 75

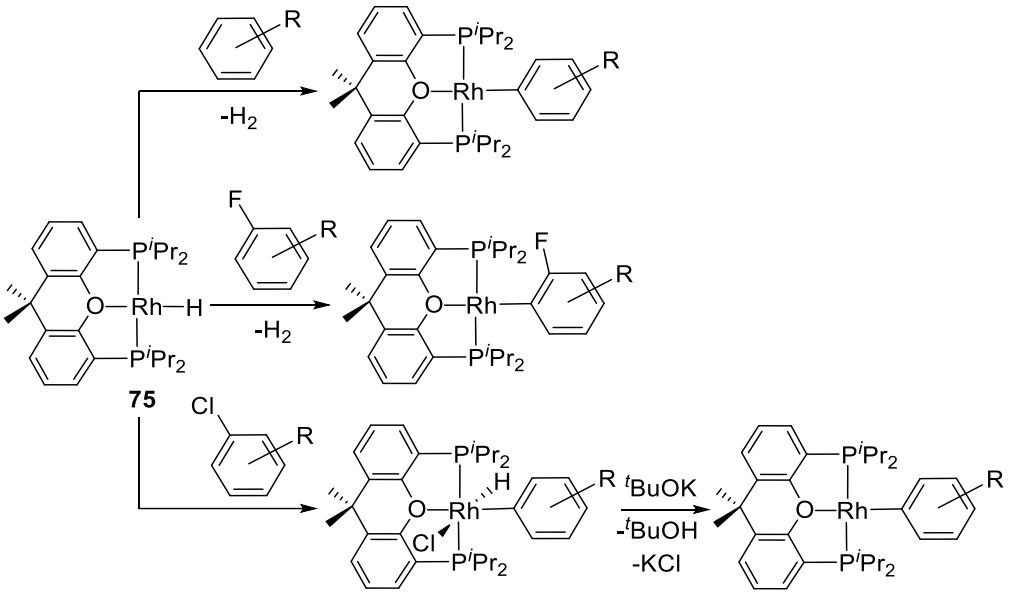

El monohidruro **75** cataliza la borilación directa de arenos.[91] La concatenación de las reacciones de activación B-H y C-H comentadas anteriormente forma ciclos que racionalizan el hecho. La borilación de arenos con HBpin se produce a través de las dos rutas que se muestran en el esquema 35. La ruta *areno* implica la activación C-H del areno por **75**, seguida de la reacción entre Rh(Ph){κ^3-*P*,*O*,*P*-[xant(P^{i}Pr$_2$)$_2$]} (**90**) y el borano. A través de la ruta *borano*, el complejo **75** inicialmente activa el enlace B-H del borano y posteriormente la especie borilo **87** reacciona con el areno.

Esquema 35. Borilación de Arenos Promovida por el Complejo 75

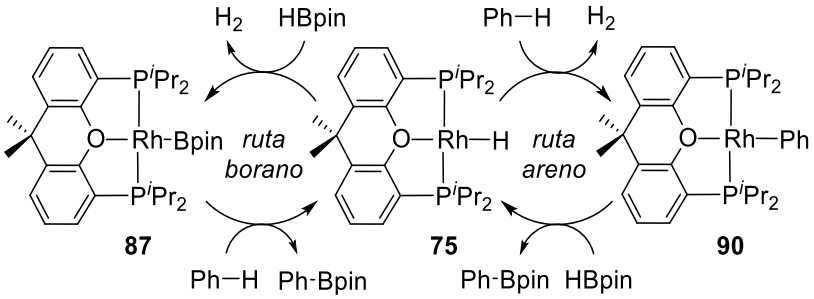

El complejo **87** promueve la borilación con descianación de aril-nitrilos[94] (ecuación 2). Estudios estequiométricos han permitido establecer de manera inequívoca el mecanismo de la catálisis, mediante el aislamiento y la caracterización de los intermedios Rh{C(R-C_6H_4)=NBpin}{κ^3-*P,O,P*-[xant(P^iPr_2)$_2$]} (R = H (**91**), *p*-CF_3 (**92**)) y Rh(R){κ^3-*P,O,P*-[xant(P^iPr_2)$_2$]} (R = Ph (**90**), *p*-CF_3-C_6H_4 (**93**)) involucrados en la reacción.[95] El esquema 36 muestra las etapas fundamentales del proceso: inserción del nitrilo en el enlace Rh-B de **87** para dar las especies planocuadradas Rh{C(R-C_6H_4)=NBpin}{κ^3-*P,O,P*-[xant(P^iPr_2)$_2$]}, extrusión del borilisocianuro que polimeriza en el medio, y reacción de los derivados arilo con B_2pin_2 para regenerar **87** y cerrar el ciclo catalítico.

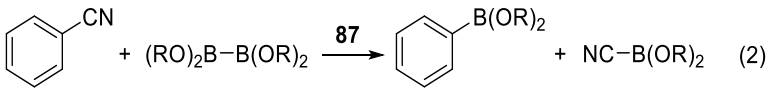

Esquema 36. Borilación con Descianación de Nitrilos Promovida por 87

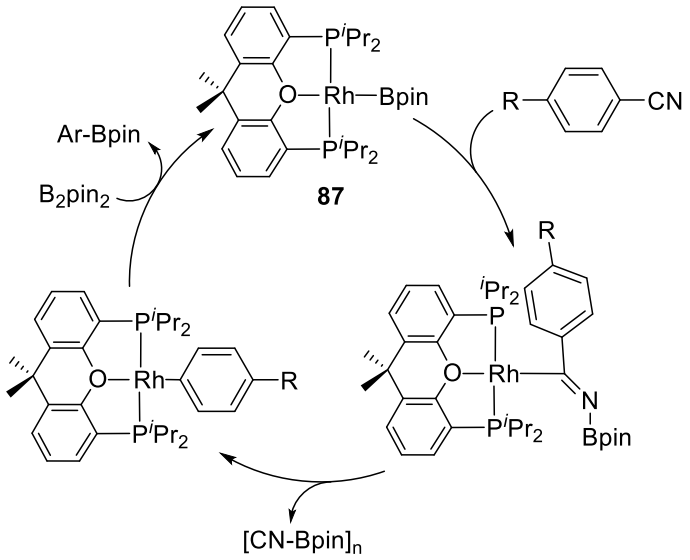

El compuesto **87** también cataliza reacciones de borilación de alquilaquinos tales como 2-butino, 3-hexino y 4-octino.[96] La borilación de 2-butino conduce al producto resultante

de la adición *cis* del enlace B-B al triple enlace del alquino (ecuación 3), de acuerdo con la tendencia generalmente observada para estas reacciones.

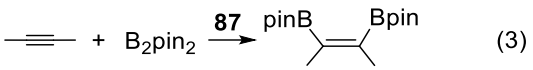

(3)

El esquema 37 muestra el ciclo catalítico para la borilación de 2-butino.[96a] El catalizador **87** promueve la activación del enlace B-B del diborano. La disociación del átomo de oxígeno de la difosfina en la especie **AM** permite la coordinación del 2-butino para dar el intermedio **AN**. La inserción del alquino en un enlace Rh-B lleva a la especie **AÑ**. Finalmente, la eliminación reductora del *Z*-diborilalqueno permite la regeneración de **87**, cerrando el ciclo catalítico.

Esquema 37. Ciclo Catalítico de la Borilación de 2-Butino Promovida por 87

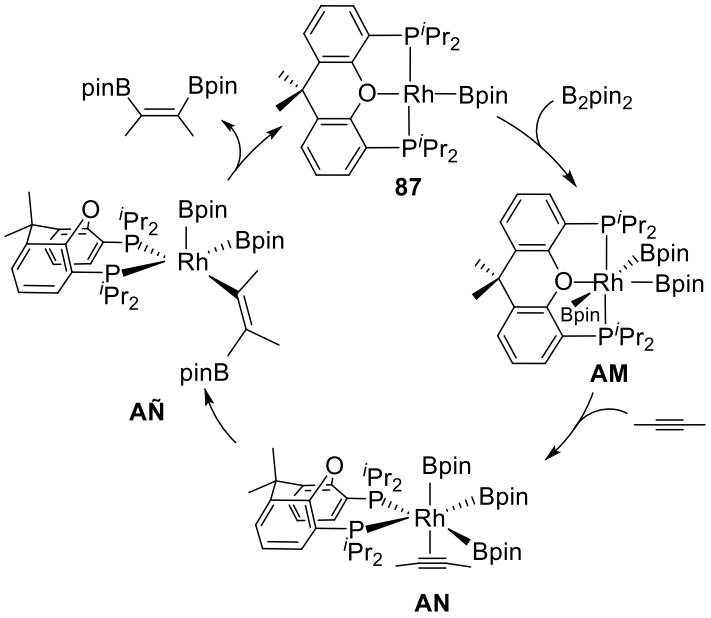

Las reacciones con alquinos de cadena alifática más larga conducen a mezclas equimolares de borildienos conjugados y borilolefinas (ecuación 4). Formalmente, estos

productos son el resultado de la adición del enlace B-B del diborano a dos moléculas diferentes de alquino y la transferencia de un hidruro de una a otra.

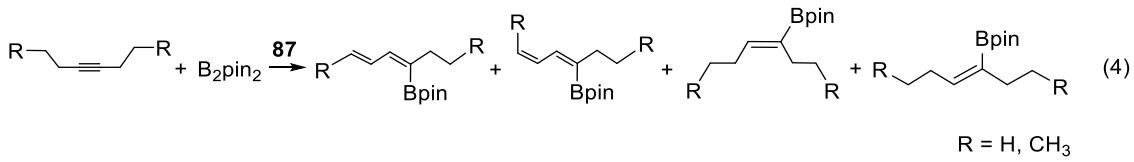

El esquema 38 racionaliza la formación de los productos de la catálisis.[96b] Los alquinos 3-hexino y 4-octino se insertan en el enlace Rh-B de **87** formando los derivados *E*-*β*-borilalquenilos Rh{(*E*)-C(R)=C(R)Bpin}{κ^3-*P*,*O*,*P*-[xant(P^{i}Pr$_2$)$_2$]} (R = Et (**94**), Pr (**95**)), que isomerizan a los correspondientes *Z*-*β*-borilalquenilos Rh{(*Z*)-C(R)=C(R)Bpin}{κ^3-*P*,*O*,*P*-[xant(P^{i}Pr$_2$)$_2$]} (R = Et (**96**), Pr (**97**)). La activación del enlace C$_\gamma$-H del sustituyente alquilo unido al átomo de carbono *α* (C$_\alpha$) del grupo *β*-borilalquenilo conduce a las especies hidruro-rodacicloalquilo **AO** (R = H) y **AP** (R = CH$_3$). La migración del ligando hidruro a C$_\alpha$ da los intermedios **AQ** (R = H) y **AR** (R = CH$_3$) que, tras una reacción de *β*-eliminación de hidrógeno, forman **AS** (R = H) y **AT** (R = CH$_3$). Los dienos de estas especies pueden presentar estereoquímica *Z* o *E* debido a que el fragmento orgánico de los intermedios **AQ** y **AR** es capaz de rotar alrededor del enlace C$_\gamma$-C$_\beta$. Una segunda molécula de alquino desplaza el dieno coordinado de **AS** y **AT** dando lugar a borildienos conjugados y el hidruro alquino correspondiente. La inserción del triple enlace del alquino en el enlace Rh-H proporciona los compuestos *E*-alquenilo Rh{(*E*)-C(R)=C(R)H}{κ^3-*P*,*O*,*P*-[xant(P^{i}Pr$_2$)$_2$]} (R = Et (**98**), Pr (**99**)), que pueden isomerizar a los correspondientes *Z*-alquenilos Rh{(*Z*)-C(R)=C(R)H}{κ^3-*P*,*O*,*P*-[xant(P^{i}Pr$_2$)$_2$]} (R = Et (**100**), Pr (**101**)). Finalmente, los complejos **98**, **99**, **100** y **101** reaccionan con el diborano para dar los productos de la hidroborilación *Z* y *E*, regenerando el catalizador **87**.

Esquema 38. Ciclo Catalítico para la Borilación de 3-Hexino y 4-Octino Promovida por 87

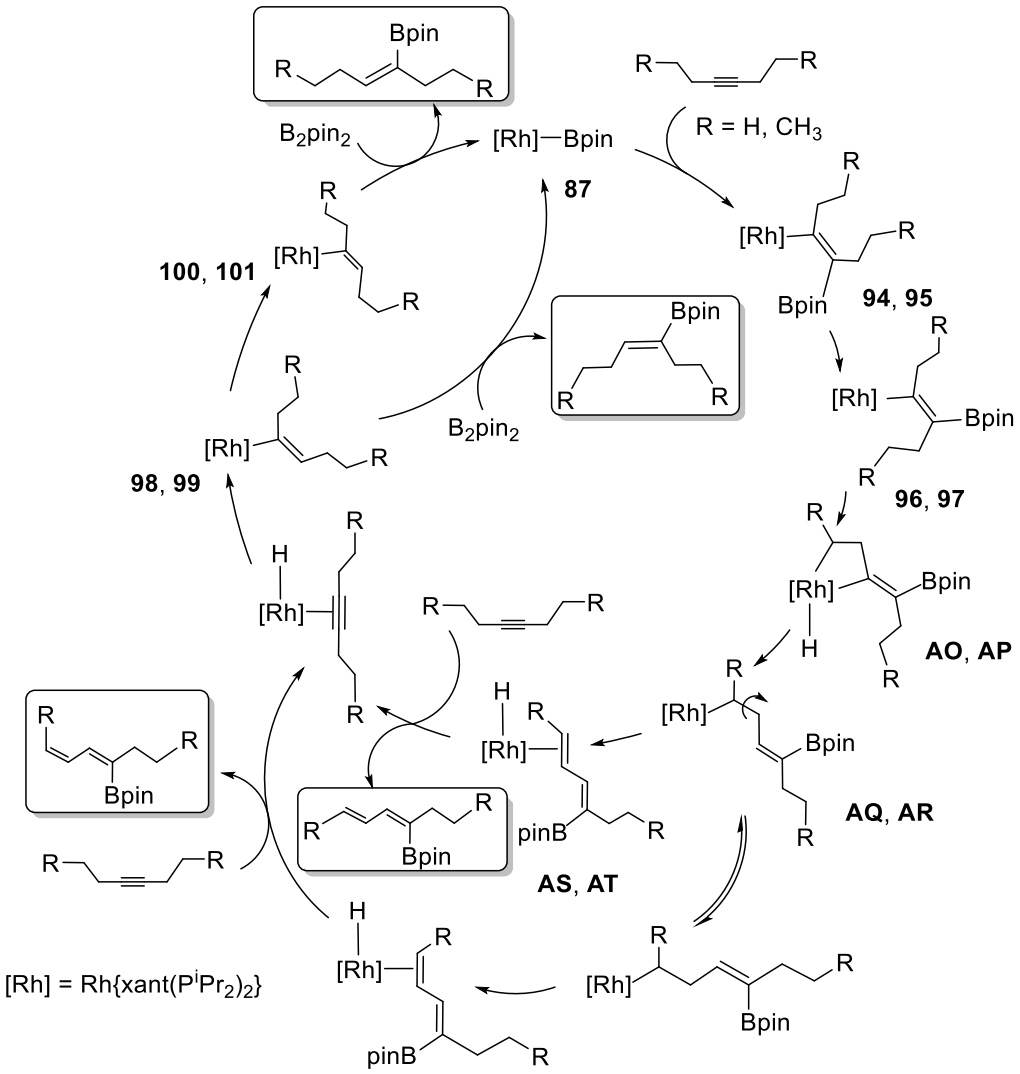

I.5.3. Complejos de Paladio

Los complejos de metales del grupo 10 con el ligando xant(P^iPr_2)$_2$ son escasos y se han utilizado en estudios de trifluorometilación de haluros de arilo desde un punto de vista computacional y experimental. El ligando xant(P^iPr_2)$_2$ estabiliza el compuesto planocuadrado de paladio(II) *trans*-Pd{(Ph)(CF_3)}{κ^2-*P*,*P*-[xant(P^iPr_2)$_2$]} (**102**) y la

especie planocuadrada de níquel(II) *trans*-Ni{(1-Np)(CF_3)}{κ^2-*P*,*P*-[xant(P^iPr_2)$_2$]} (1-Np = 1-naftil) (**103**), que muestran un modo de coordinación *trans*-κ^2-*P*,*P*-bidentado poco habitual (figura 7). A diferencia de **102** y **103**, los derivados con el ligando xantphos existen como mezclas de los isómeros *cis* y *trans*. De acuerdo con esto, la eliminación reductora de Ph-CF_3 de los compuestos con el ligando xant(P^iPr_2)$_2$ es mucho más lenta que de los derivados con el ligando xantphos.[97]

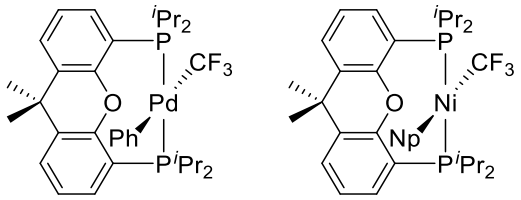

102 **103**

Figura 7. Complejos de paladio y níquel con el ligando xant(P^iPr_2)$_2$ coordinado κ^2-*P*,*P*-bidentado.

MEMORIA

M.1. OBJETIVOS DE INVESTIGACIÓN

El propósito de nuestro grupo es obtener conocimiento sobre las interacciones metal-enlace σ, determinar la naturaleza de las especies encontradas, su relación con la clase de ruptura que sufren los enlaces y aplicar el conocimiento obtenido en cuatro ámbitos de interés para la sociedad: desarrollar catalizadores para la deshidrogenación de amino-boranos y líquidos orgánicos transportadores de hidrógeno, diseñar métodos catalíticos eficientes para la deshalogenación de contaminantes orgánicos persistentes, diseñar nuevos dopantes para PHOLEDs de alta eficiencia en la región de altas energías y desarrollar procedimientos eficientes en síntesis orgánica.

La presente Tesis Doctoral se ha desarrollado dentro de este marco general, centrándose principalmente en los enlaces H-H, B-H y B-N y en el desarrollo de catalizadores para la liberación de hidrógeno. Pretendía alcanzar los siguientes objetivos concretos:

- Estudiar la protonación del ión hidruro, controlada cinéticamente por el complejo $OsH_3Cl\{\kappa^3\text{-}P,O,P\text{-}[xant(P^iPr_2)_2]\}$, determinando la influencia de los diferentes modos de coordinación del ligando $xant(P^iPr_2)_2$ sobre la naturaleza de los ligandos hidrógeno dadores en los polihidruros de osmio resultantes.

- Preparar un derivado hidróxido de osmio(IV), estudiar su actividad catalítica en la descomposición de ácido fórmico a CO_2 y H_2 y establecer el mecanismo de la reacción.

- Estudiar la coordinación de catecolborano y pinacolborano al átomo de osmio de los fragmentos $OsHX\{xant(P^iPr_2)_2\}$ (X = Cl, H), analizando la influencia del ligando X.

- Preparar derivados boróxido de osmio, los primeros de un metal del grupo del platino, mediante el desplazamiento del grupo amino de un amino-borano por la base conjugada de un hidroxiácido ($L_nOs\text{-}OH$).

- Preparar compuestos aromáticos triangulares con tres vértices diferentes. Ellos deben estar basados en dos elementos de los grupos principales, azufre y boro, y en un fragmento metálico de transición, osmio y sus ligandos asociados.

Los esfuerzos realizados para lograr estos objetivos y los resultados obtenidos se resumen en los artículos presentados a continuación. Cada objetivo se corresponde con un artículo.

M.2. METODOLOGÍA

Este apartado describe el procedimiento seguido para la preparación de los nuevos compuestos, las técnicas usadas para su caracterización y la metodología utilizada para estudiar la deshidrogenación cinéticamente controlada de ácido fórmico en presencia del complejo $OsH_3(OH)\{\kappa^3\text{-}P,O,P\text{-}[xant(P^iPr_2)_2]\}$.

Todas las reacciones se llevaron a cabo bajo rigurosa atmósfera de argón, usando técnicas de Schlenk o caja seca. Los disolventes se secaron mediante los procedimientos habituales y se destilaron en atmósfera de argón antes de su uso (acetona, THF, metanol e isopropanol) o se obtuvieron libres de oxígeno y agua de un aparato de purificación de disolventes MBraun SPS-800 (diclorometano, pentano, tolueno, éter dietílico y acetonitrilo). Para las reacciones llevadas cabo dentro de la caja seca, se procedió a un secado adicional de los disolventes, almacenando el pentano sobre P_2O_5 y el tolueno y el THF sobre Na. El agua se desoxigenó antes de ser utilizada mediante ciclos de vacío/argón.

El material de vidrio, que contiene grupos silicato y silanol que pueden actuar como centros nucleofílicos y de intercambio iónico, se trató con Me_3SiCl generando una superficie con enlaces siloxano Si-O-Si que enmascara estos grupos y disminuye la hidrofilia del material.[98]

Los reactivos se obtuvieron de fuentes comerciales y se utilizaron sin tratamiento posterior con la excepción del catecolborano, que se purificó mediante sublimación en un horno de bolas (Kugelrohr BUCHI) a presión reducida.

Los complejos $OsH_3Cl\{\kappa^3$-*P,O,P*-[dbf(P^iPr_2)$_2$]},[39] $OsH_3Cl\{\kappa^3$-*P,O,P*-[xant(P^iPr_2)$_2$]}[57c] y $OsH_4\{\kappa^3$-*P,O,P*-[xant(P^iPr_2)$_2$]}[57c] se sintetizaron siguiendo los procedimientos previamente descritos en la bibliografía.

Los **análisis elementales** de carbono, hidrógeno, nitrógeno y azufre se realizaron en un microanalizador elemental CHNS/O Perkin-Elmer EA-2400 Series II en el servicio de análisis elemental del Instituto de Síntesis Química y Catálisis Homogénea (ISQCH). Todas las muestras se prepararon y encapsularon dentro de una caja seca y fueron analizadas inmediatamente después con el objetivo de preservar el producto bajo atmósfera inerte en todo momento.

Los espectros de **infrarrojo (IR)** se registraron en disolución de diclorometano o tolueno en un espectrofotómetro Perkin-Elmer Spectrum 100 FT-IR, o en estado sólido en un espectrofotómetro Perkin-Elmer Spectrum 100 FT-IR equipado con un accesorio ATR (Attenuated Total Reflection).

Los espectros de **resonancia magnética nuclear (RMN)** se midieron en espectrómetros Bruker ARX 300, Bruker Avance 300, 400 o 500 MHz. Los disolventes deuterados se obtuvieron de fuentes comerciales y se secaron antes de su uso (tamiz molecular de 3 Å ó CaH_2 para CD_2Cl_2; Na para C_6D_6, C_7D_8 y THF-d_8). Las constantes de acoplamiento, *J* y *N* ($N = J_{H\text{-}P} + J_{H\text{-}P'}$ ó $J_{C\text{-}P} + J_{C\text{-}P'}$), se expresan en hercios (Hz). Los desplazamientos químicos (δ) se expresan en ppm y están referenciados respecto a la señal residual del disolvente deuterado en los espectros de ^1H y $^{13}C\{^1H\}$, a la señal de ácido fosfórico (H_3PO_4, 85%) en los espectros de $^{31}P\{^1H\}$ y a la señal de $BF_3{\cdot}OEt_2$ en los espectros de ^{11}B. La elucidación estructural completa se llevó a cabo con los experimentos indicados

para cada compuesto complementados con experimentos de correlación bidimensional ^{1}H-^{1}H COSY, ^{1}H–^{13}C HSQC y ^{1}H–^{13}C HMBC.

Los **espectros de ionización de masas** se registraron en un espectrómetro Bruker MicroTOF-Q con analizador híbrido Q-TOF de alta resolución.

Procedimiento general para el estudio de la deshidrogenación catalizada de ácido fórmico. Una disolución del compuesto $OsH_3(OH)\{\kappa^3$-*P,O,P*-[xant(P^iPr_2)$_2$]} en 2.5 mL de tolueno se introdujo en un matraz de 25 mL conectado a una bureta de gases provista de un reservorio de vaselina. El matraz se sumergió en un baño termostatizado de agua. Una vez que el sistema se equilibró a presión atmosférica, se inyectó una cantidad conocida de ácido fórmico a través de un septum y la mezcla se agitó a 500 rpm. Las reacciones se monitorizaron midiendo el volumen de gas total generado (H_2 y CO_2) en función del tiempo.

Estudios espectrocópicos de RMN para la descaboxilación del compuesto $OsH_3\{\kappa^1$-O-$(HCO_2)\}\{\kappa^3$-*P,O,P*-[xant(P^iPr_2)$_2$]}. La descarboxilación del complejo $OsH_3\{\kappa^1$-O-$(HCO_2)\}\{\kappa^3$-*P,O,P*-[xant(P^iPr_2)$_2$]} se siguió mediante espectroscopía de RMN de $^{31}P\{^1H\}$ en el rango de temperaturas T = 303 - 323 K. Una cantidad conocida de ácido fórmico (1.2 µL, 0.032 mmol) se inyectó en un tubo de RMN con una disolución de $OsH_3(OH)\{\kappa^3$-*P,O,P*-[xant(P^iPr_2)$_2$]} (20.8 mg, 0.032 mmol) en tolueno-d_8 (0.5 mL) y un capilar sellado que contenía una disolución de PPh_3 en tolueno-d_8 como patrón. Tras 5 min, se midió la formación de $OsH_4\{\kappa^3$-*P,O,P*-[xant(P^iPr_2)$_2$]} en función del tiempo por RMN. Los parámetros de los experimentos de RMN de $^{31}P\{^1H\}$ se modificaron para posibilitar la integración de las señales con respecto al patrón: programa del pulso (zgig), $d_1 \geq 5T_1$ (d_1 = 20 s).

M.3. APORTACIONES DEL DOCTORANDO

El autor de la presente Tesis Doctoral ha colaborado en el proceso de elaboración de los artículos que forman parte de esta memoria. Además, siendo el único autor no poseedor del título de Doctor, ninguno de estos trabajos ha formado o formará parte de otras tesis.

1. *mer*, *fac*, and Bidentate Coordination of an Alkyl-POP Ligand in the Chemistry of Nonclassical Osmium Hydrides. *Inorg. Chem.* **2017**, *56*, 676-683.

El doctorando realizó la síntesis y caracterización de todos los complejos descritos en el artículo y colaboró en la redacción y corrección del manuscrito.

2. Dehydrogenation of Formic Acid Promoted by a Trihydride-Hydroxo-Osmium(IV) Complex: Kinetics and Mechanism. *ACS Catal.* **2018**, *8*, 11314-11323.

El doctorando realizó la síntesis y caracterización de todos los complejos descritos en el artículo, llevó a cabo el estudio cinético y colaboró en la redacción y corrección del manuscrito.

3. Elongated σ-Borane versus σ-Borane in Pincer-POP-Osmium Complexes. *Organometallics* **2017**, *36*, 2298-2307.

El doctorando realizó la síntesis y caracterización de todos los complejos descritos en el artículo y colaboró en la redacción y corrección del manuscrito.

4. Reactions of an Osmium(IV)-Hydroxo Complex with Amino-Boranes: Formation of Boroxide Derivatives. *Organometallics* **2019**, *38*, 310-318.

El doctorando realizó la síntesis y caracterización de los complejos boróxido, el estudio de reactividad frente a CO, y colaboró en la redacción y corrección del manuscrito. Este

trabajo fue elegido por la revista *Organometallics* para su portada del 28 de Enero de 2019 y el doctorando participó en el diseño de la misma.

5. Cycloosmathioborane Compounds: Other Manifestations of the Hückel Aromaticity. *Inorg. Chem.* **2019**, *58*, 2265-2269.

El doctorando realizó la síntesis y caracterización de todos los complejos descritos en la comunicación y colaboró en la redacción y corrección del manuscrito.

Las estructuras de rayos-X publicadas en estos 5 artículos fueron resueltas por el Dr. Enrique Oñate, Científico Titular del CSIC. Los cálculos teóricos fueron realizados por el Dr. Enrique Oñate ó/y por el Dr. Israel Fernández, Profesor Titular de la Universidad Complutense de Madrid. Los amino-boranos ^{i}Pr(H)NBCy$_2$ y ^{i}Pr(H)NBBN utilizados en el capítulo 4 fueron sintetizados por el Dr. Alberto Ramos, investigador postdoctoral de la Universidad de Castilla la Mancha.

M4. RESUMEN DE LOS ARTÍCULOS

A continuación, se presentan resúmenes de los artículos contenidos en esta tesis doctoral. Cada resumen mantiene la numeración utilizada en los artículos para designar compuestos y esquemas. Los capítulos 1 y 2 describen la síntesis de nuevos complejos polihidruro y su relación en procesos de la tecnología del hidrógeno. Los capítulos 3, 4 y 5 muestran la reactividad de algunos de esos polihidruros frente a boranos, amino-boranos y amina-boranos, respectivamente.

Capítulo 1: Coordinación *mer, fac* y Bidentada de un Ligando POP-Alquilo en la Química de Hidruros no Clásicos de Osmio

INTRODUCCIÓN

El comportamiento químico de un complejo de un metal de transición está determinado por el ión central y por los ligandos que forman su esfera de coordinación. Los grupos que rodean el núcleo del complejo gobiernan la densidad electrónica del ión metálico y el espacio disponible a su alrededor para llevar a cabo reacciones. En algunos casos, los ligandos también cooperan con el metal mediante la participación directa en las transformaciones químicas.[25,36,99] Hay otros ligandos que cambian sus propiedades durante las reacciones. Este grupo incluye ligandos que modifican su capacidad electrodadora mientras se adaptan al medio de reacción mediante transformaciones reversibles[100] y ligandos que cambian su modo de coordinación para satisfacer los requerimientos de cada etapa en un proceso de varios pasos.

Los grupos hemilábiles son la clase de ligandos más simple con el comportamiento anterior. La coordinación-descoordinación reversible del átomo dador hemilábil permite la estabilización de centros metálicos altamente reactivos e influye significativamente en el comportamiento catalítico de los complejos.[101] Las difosfinas tridentadas aniónicas PCP presentan un comportamiento opuesto. Así, aunque la coordinación *mer* permite estabilizar complejos de reactividad inusual,[47a,102] la estabilidad y la rigidez del ligando pinza disminuye la adaptabilidad de estos ligandos a los requerimientos de los procesos secuenciales. Los éteres POP, sin embargo, son ligandos difosfina flexibles, que pueden actuar como grupos κ^3-*fac* y bidentado, además de κ^3-*mer*.[86-87,89,95,103] Weller y

colaboradores han demostrado que el ligando xantphos tiene la capacidad de cambiar su modo de coordinación en varios procesos relevantes promovidos por rodio e iridio,[50,104] como la hidroacilación[105] y carbotiolación[106] de alquenos y alquinos y la deshidrogenación de amina-boranos.[107]

Los polihidruros de los metales de transición son compuestos que tienen suficientes átomos de hidrógeno enlazados al centro metálico de un fragmento L_nM para formar al menos dos tipos diferentes de ligandos.[108] Éstos ligandos se clasifican generalmente en cuatro tipos dependiendo de la separación entre los hidrógenos coordinados: dihidrógenos de tipo Kubas (0.8 - 1.0 Å), dihidrógenos elongados (1.0 - 1.3 Å), dihidruros comprimidos (1.3 - 1.6 Å) e hidruros clásicos (> 1.6 Å).[108-109] Los polihidruros de metales del grupo del platino ofrecen nuevos y emocionantes retos conceptuales y la posibilidad de interaccionar en diferentes campos,[108] entre los que se encuentran la conversión y el almacenamiento de energía.[6a,110] En este sentido, los polihidruros de osmio son particularmente interesantes. Además de promover la deshidrogenación de amina-boranos,[17,19] su capacidad para activar enlaces C-H, N-H y C-N de un gran rango de moléculas orgánicas, que incluyen 2-azetidinonas[59,111] y nucleobases,[112] les permiten interaccionar con la química orgánica sintética,[15a,39,55g,113] el diseño de fármacos[111a] y la ciencia de los materiales.[58b,114] A pesar de la riqueza de la química de los polihidruros de osmio, los complejos de este tipo con ligandos pinza son una excepción,[108] conociéndose tan solo unos pocos ejemplos con ligandos PNP,[32a] P(olefina)P,[115] y P(C(sp^3))P.[64k] Nuestro grupo ha publicado que las reacciones de los complejos pinza POP $OsCl_2\{\kappa^1\text{-}S\text{-}(DMSO)_4\}\{\kappa^3\text{-}P,O,P\text{-}[xant(P^iPr_2)_2]\}$ y $OsCl_2(\kappa^1\text{-}S\text{-}DMSO)\{\kappa^3\text{-}P,O,P\text{-}[dbf(P^iPr_2)_2]\}$ con hidrógeno molecular, en presencia de NEt_3, conducen a los derivados trihidruro clásicos $OsH_3Cl\{\kappa^3\text{-}P,O,P\text{-}[xant(P^iPr_2)_2]\}$[57c] y $OsH_3Cl\{\kappa^3\text{-}P,O,P\text{-}[dbf(P^iPr_2)_2]\}$[39], como se

muestra en el apartado 5.1 de la Introducción de esta Tesis. Nuestro interés en determinar la influencia de los diferentes modos de coordinación de ligandos pinza flexibles en la naturaleza de los ligandos H-dadores de los polihidruros de osmio nos animó a estudiar la protonación del ión hidruro, cinéticamente controlada por el compuesto $OsH_3Cl\{\kappa^3$-*P,O,P*-[xant($P^iPr_2)_2$]}. La formación de hidrógeno molecular cinéticamente controlada mediante neutralización exotérmica del ión hidruro es un proceso de gran interés en conexión con el almacenamiento de hidrógeno en materiales sólidos, que podrían convertirse en una forma eficiente y segura de almacenar energía tanto para aplicaciones estacionarias como móviles.[116]

Este capítulo muestra que el ligando xant($P^iPr_2)_2$ cambia su modo de coordinación para estabilizar dihidrógenos de tipo Kubas, dihidrógenos elongados, dihidruros comprimidos e hidruros clásicos, que actúan como especies intermedias en la formación de hidrógeno por reacción de H^+ y H^-, en presencia de polihidruros de osmio. Además, se muestra que el modo de coordinación *mer*, a diferencia de los modos de coordinación *fac* y bidentado, favorece las interacciones no clásicas entre átomos de hidrógeno coordinados al centro metálico.

DISCUSIÓN DE RESULTADOS

El esquema 1 resume los procedimientos utilizados para generar hidrógeno molecular a partir del trihidruro clásico $OsH_3Cl\{\kappa^3$-*P,O,P*-[xant($P^iPr_2)_2$]} (**1**). La ruta *a* implica la adición secuencial de H^+ y H^-, mientras que la ruta *b* muestra la adición contraria.

Esquema 1. Formación de H_2 mediante Adición Secuencial de H^+ y H^- o H^- y H^+ al Complejo 1 en Dos Ciclos Relacionados

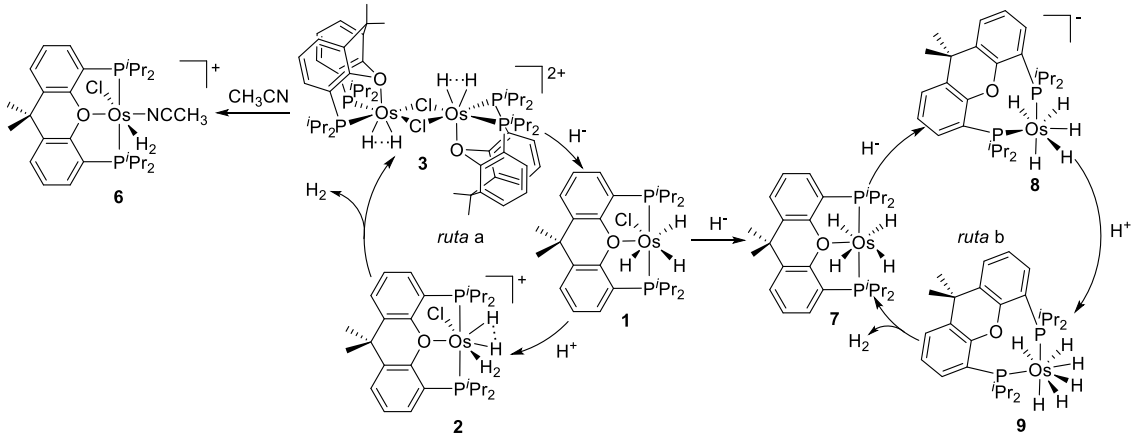

El complejo **1** adiciona un protón, de acuerdo con el carácter de base de Lewis de los polihidruros saturados. La adición de 1.0 equivalentes de $HBF_4{\cdot}OEt_2$ a **1** en diclorometano-d_2, bajo atmósfera de hidrógeno, conduce al catión dihidruro comprimido-dihidrógeno tipo Kubas $[OsCl(H\cdots H)(\eta^2\text{-}H_2)\{\kappa^3\text{-}P,O,P\text{-}[xant(P^iPr_2)_2]\}]^+$ (**2**). Cálculos DFT revelan que hay dos estructuras dihidruro comprimido-dihidrógeno que difieren en 3 kcal·mol^{-1} (ΔG, 1 atm, 298.15 K): **2a** y **2b**. La figura 1 muestra una vista de estas estructuras optimizadas mediante cálculos DFT.

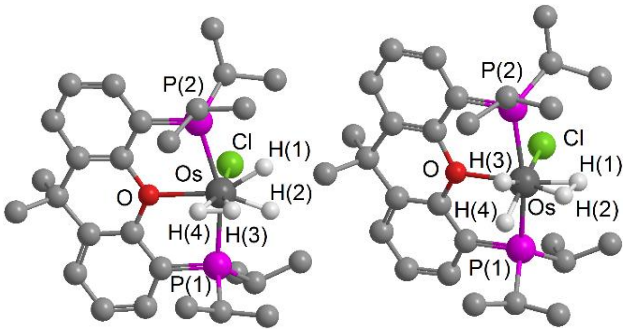

2a **2b**

Figura 1. Estructuras de **2a** y **2b** optimizadas mediante cálculos DFT.

La labilidad del ligando dihidrógeno en **2** es consistente con su naturaleza tipo Kubas aunque la separación entre los dos átomos de hidrógeno está en el límite entre dihidrógeno de tipo Kubas y dihidrógeno elongado (1.029 Å para **2a** y 1.091 Å para **2b**). Así, el complejo **2** es estable en disolución de diclorometano, bajo atmósfera de hidrógeno, durante unas pocas horas. Sin embargo, bajo atmósfera de argón, pierde el ligando dihidrógeno para dar el dímero $[(Os(H\cdots H)\{\kappa^3\text{-}P,O,P\text{-}[xant(P^iPr_2)_2]\})_2(\mu\text{-}Cl)_2]^{2+}$ (**3**), que contiene dos hidruros comprimidos unidos a cada átomo de osmio ($d_{H\text{-}H}$ = 1.36(6) Å). Éste compuesto se aisló como la sal de BF_4^- con un 95 % de rendimiento y se caracterizó mediante difracción de rayos-X (figura 2). La estructura muestra un cambio en el modo de coordinación de la difosfina de κ^3-*mer* a κ^3-*fac*.

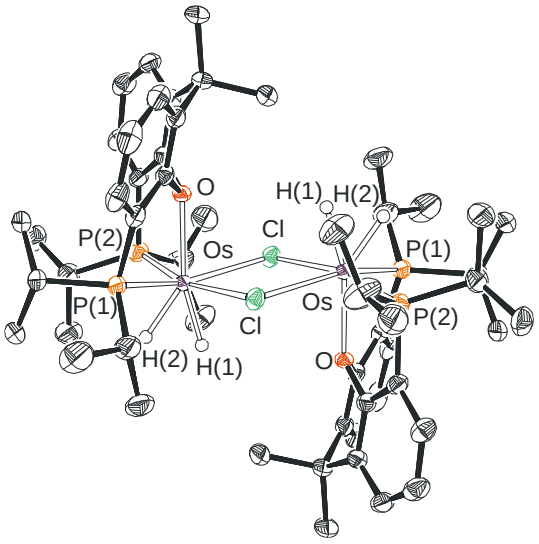

Figura 2. Diagrama molecular del complejo **3**.

La coordinación *fac* en **3**, permitida por la flexibilidad del grupo xanteno, es un factor determinante para la estabilización de la estructura dímera. En efecto, la difosfina derivada de dibenzofurano, que es un ligando más rígido, estabiliza la especie OsH_4 y evita la formación de un dímero equivalente a **3**. Así, la adición de 1.0 equivalentes de $HBF_4{\cdot}OEt_2$ a $OsH_3Cl\{\kappa^3\text{-}P,O,P\text{-}[dbf(P^iPr_2)_2]\}$ (**4**) en diclorometano, bajo argón, lleva al

complejo dihidruro comprimido-dihidrógeno [OsCl(H···H)(η^2-H_2){κ^3-*P*,*O*,*P*-[dbf(P^iPr_2)$_2$]}]BF_4 (**5**), que se aísla como sólido amarillo pálido con un 85 % de rendimiento (eq 1). A diferencia de **2**, el complejo análogo derivado de 4,6-bis(diisopropilfosfino)dibenzofurano es estable bajo argón, en estado sólido y en diclorometano, y no pierde hidrógeno molecular. El complejo **5** se caracterizó mediante difracción de rayos-X (figura 3). Su estructura está de acuerdo con la estructura optimizada del isómero más estable de **2**, el isómero **2a**. (Distancias H-H para el complejo **5** del ligando dihidrógeno H(3)-H(4) = 1.06(5) Å (rayos-X), 0.976 Å (DFT) y del dihidruro comprimido H(1)···H(2) = 1.10(7) Å (rayos-X), 1.387 Å (DFT)).

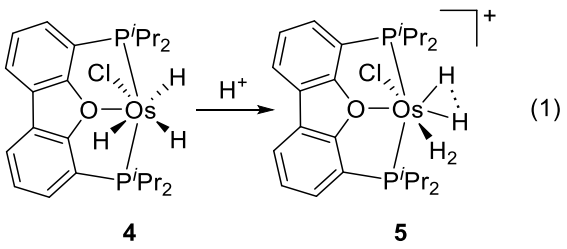

(1)

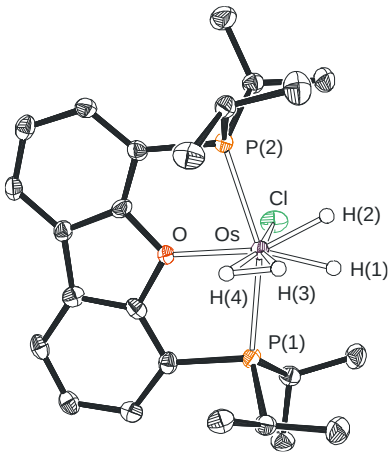

Figura 3. Diagrama molecular del complejo **5**.

El cambio en el modo de coordinación de la difosfina de κ^3-*mer* a κ^3-*fac* es un requerimiento para la formación del dímero a partir de los fragmentos [$OsClH_2${κ^3-*P*,*O*,*P*-[xant(P^iPr_2)$_2$]}]$^+$, resultantes de la disociación de hidrógeno molecular de **2**, dado que el

impedimento estérico impuesto por los sustituyentes isopropilo del ligando difosfina con disposición *mer* de los fragmentos insaturados parecen prevenir la dimerización. En cambio, la coordinación κ^3-*mer* está claramente favorecida frente a la κ^3-*fac* cuando el centro metálico de un complejo mononuclear está saturado. Como prueba ello, los puentes cloruro de **3** se rompen en presencia de acetonitrilo para formar el complejo saturado dihidrógeno tipo Kubas $[OsCl(\eta^2\text{-}H_2)(CH_3CN)\{\kappa^3\text{-}P,O,P\text{-}[xant(P^iPr_2)_2]\}]BF_4$ (**6**) (distancia (H(1)-H(2) = 1.02(6) Å (rayos-X), 0.985 Å (DFT)), en el que la difosfina se dispone κ^3-*mer*. El compuesto se aísla como un sólido blanco, con un rendimiento casi cuantitativo, y se caracterizó mediante difracción de rayos-X (figura 4).

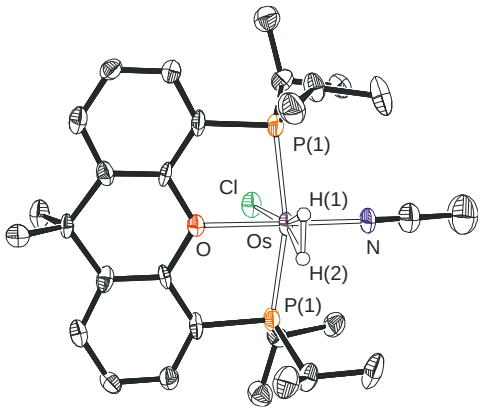

Figura 4. Diagrama molecular del complejo **6**.

El ión hidruro también rompe los puentes cloruro de **3**. La adición de KH a una disolución del dímero en tetrahidrofurano regenera **1**, cerrando un ciclo para la formación de hidrógeno molecular por reacción de H^+ y H^- en el centro metálico de **1** (ruta *a* en el esquema 1).

El ión hidruro desplaza el ligando cloruro de **1** para dar el derivado tetrahidruro $OsH_4\{\kappa^3\text{-}P,O,P\text{-}[xant(P^iPr_2)_2]\}$ (**7**). La naturaleza clásica de los átomos de hidrógeno coordinados de este compuesto, se confirmó por difracción de rayos-X y cálculos DFT.[57c] De manera

similar al cloruro, el átomo de oxígeno de la difosfina coordinada *mer* en **7** tiene tendencia a ser desplazado por el ión hidruro. La adición de KH a **7** en tetrahidrofurano llevó al pentahidruro aniónico $[OsH_5\{\kappa^2\text{-}P,P\text{-}[xant(P^iPr_2)_2]\}]^-$ (**8**), que contiene la difosfina κ^2-*P*,*P*-bidentada. La utilización del éter corona 18-crown-6 permitió obtener cristales de la sal de $[K(18\text{-crown-}6)]^+$ con un rendimiento del 66 % (figura 5). La estructura de difracción de rayos-X muestra la coordinación bidentada de la difosfina. El poliedro de coordinación alrededor del átomo de osmio puede racionalizarse como una bipirámide pentagonal con el hidruro H(5) y el átomo P(1) de la difosfina en posición axial, mientras que el átomo P(2) y el resto de hidruros están en el plano ecuatorial. La disposición de la difosfina aparece forzada por su carácter bidentado. A diferencia de **8**, el correspondiente anión $[OsH_5(P^iPr_3)_2]^-$ contiene ambas fosfinas monodentadas en las posiciones axial de la bipirámide.[117] La estructura también muestra tres hidruros apuntando hacia el átomo de potasio, que está ligeramente alejado del plano del éter corona.

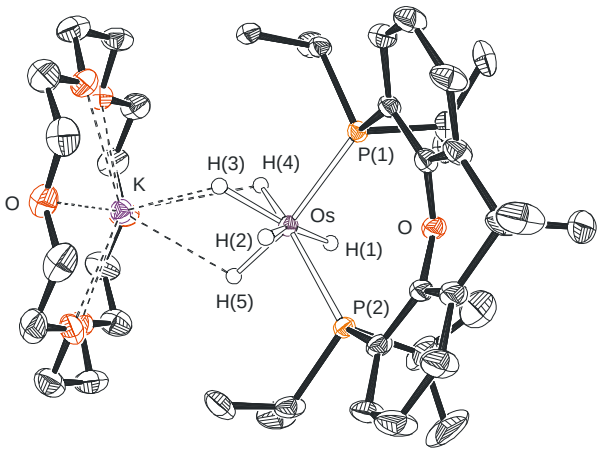

Figura 5. Diagrama molecular del complejo **8**.

El complejo **8** es una base de Brønsted fuerte que se protona incluso por trazas de agua. La protonación conduce al hexahidruro $OsH_6\{\kappa^2\text{-}P,P\text{-}[xant(P^iPr_2)_2]\}$ (**9**), que presenta la difosfina bidentada con los átomos de fósforo en los sitios B de dos planos trapezoidales

BAAB, que definen su estructura de dodecaedro distorsionado.[57c,118] El complejo **9** pierde hidrógeno molecular y coordina el átomo de oxígeno para regenerar el tetrahidruro **7**, cerrando un segundo ciclo para la formación de hidrógeno molecular por reacción de H^- y H^+ en el centro metálico del tetrahidruro **7** (ruta *b* en el esquema 1).

CONCLUSIONES

Este estudio revela que los polihidruros de osmio estabilizados por el ligando xant(P^iPr_2)$_2$ adicionan secuencialmente H^+ y H^- o H^- y H^+ para generar hidrógeno molecular de forma cíclica. Durante el proceso, la difosfina cambia su modo de coordinación de κ^3-*mer* a κ^3-*fac* y a κ^2-*P*,*P*-bidentado en función de los requerimientos electrónicos y estéricos de los intermedios involucrados para formar polihidruros con interacciones no clásicas y polihidruros clásicos. Las interacciones no clásicas están favorecidas por la coordinación tridentada, en particular por la disposición *mer*, mientras que los polihidruros clásicos generalmente se encuentran cuando la difosfina está bidentada. La flexibilidad del grupo xanteno es un factor determinante para el comportamiento de la difosfina.

Capítulo 2: Deshidrogenación de Ácido Fórmico Promovida por un Complejo Trihidruro-Hidroxo de Osmio(IV). Cinética y Mecanismo

INTRODUCCIÓN

El ácido fórmico forma parte de la familia de los líquidos orgánicos transportadores de hidrógeno. Se trata de una sustancia estable en condiciones ambientales, se produce a gran escala y es biodegradable. Tiene baja inflamabilidad y toxicidad, presenta capacidad gravimétrica y volumétrica de H_2 de 4.4 wt % y 53.4 g/L,[119] y su reciclaje mediante hidrogenación de CO_2 experimenta una constante mejora,[120] habiéndose alcanzado un valor de TOF de 1100000 h^{-1} utilizando el complejo RuHCl(PNP) (PNP = 2,6-bis(di-*terc*-butilfosfinometil)piridina) como catalizador para la reducción de formiatos.[120a]

Algunos sistemas de metales de transición homogéneos y heterogéneos han probado su eficacia en la deshidrogenación de ácido fórmico para dar H_2 y CO_2.[9,121] La mayoría de los catalizadores homogéneos son complejos de Fe,[122] Ru[123] e Ir.[124] Además, se conocen unos pocos precursores de Mo,[125] Rh,[126] Ni,[127] Cu[128] y Al.[129] Sin embargo, el conocimiento de los mecanismos que operan en estos procesos, a menudo postulados sin evidencias experimentales, es escaso. La catálisis consta de dos etapas: la formación de CO_2 y la liberación de H_2. La etapa limitante puede ser cualquiera de las dos. Las mayores diferencias se han encontrado en la primera, que puede ocurrir por abstracción de hidruro, *β*-eliminación de hidrógeno o a través de un mecanismo de esfera externa,[130] aunque este último está siendo cuestionado.[32f,37-38,131]

Los complejos hidróxido de metales del grupo del platino son muy escasos.[132] Los derivados hidruro-hidroxo son particularmente desafiantes, ya que son el resultado formal

de la adición oxidante de agua al centro metálico, proceso que generalmente está desfavorecido desde un punto de vista termodinámico; esto explica que los pocos ejemplos que se conocen se caractericen por ser reversibles.[133] Los compuestos de osmio de este tipo son especies de Os(II)[134] y, aunque el estado de oxidación + 4 es habitual para este elemento con ligandos de tamaño pequeño, los complejos hidruro-hidroxo de Os(IV) eran especies desconocidas hasta el momento.

Este capítulo presenta la preparación y caracterización de un complejo hidruro-hidroxo de Os(IV) estabilizado por el ligando xant($P^iPr_2)_2$, su actividad como catalizador en la deshidrogenación de ácido fórmico, así como la cinética y el mecanismo del proceso.

DISCUSIÓN DE RESULTADOS

Los compuestos hidróxido de osmio conocidos incluyen los complejos nitruro $Os(N)Tp(OH)_2$ (Tp = hidrurotris(1-pirazolil)borato),[135] $[Os(N)(CH_2SiMe_3)(OH)]^-$ y $[Os(N)(CH_2SiMe_3)(OH)_2]^-$,[136] el catión semi-sandwich [OsOH(η^6-*p*-cimeno)IPr]$^+$,[41] los derivados hidruro-hidroxo $OsH(OH)(PMe_3)_4$,[134a] $OsH(OH)(CO)(PR_3)_2$ (PR_3 = P^iPr_3,[134b] P^tBu_2Me[134c]), $OsH(OH)(NH_2CMe_2CMe_2NH_2)(PPh_3)_2$,[134d] y [OsH(OH)(C≡CPh)(IPr)(P^iPr_3)]OTf,[134e] y unos pocos dímeros.[137] Estos complejos se preparan siguiendo uno de estos métodos: a) hidrólisis de enlaces Os-C[134a,134c] u Os-N[134d] y b) sustitución de un ligando cloruro por uno hidróxido.[41,134a,134c,136] La utilización del segundo de los métodos con el compuesto $OsH_3Cl\{\kappa^3$-*P,O,P*-[xant($P^iPr_2)_2$]} (**1**)[57c] como producto de partida dio resultados fallidos. Sin embargo, la sustitución previa del ligando cloruro de **1** por un mejor grupo saliente, como el trifuorometanosulfonato, permitió obtener el producto deseado (esquema 1).

Esquema 1. Preparación del Complejo 3

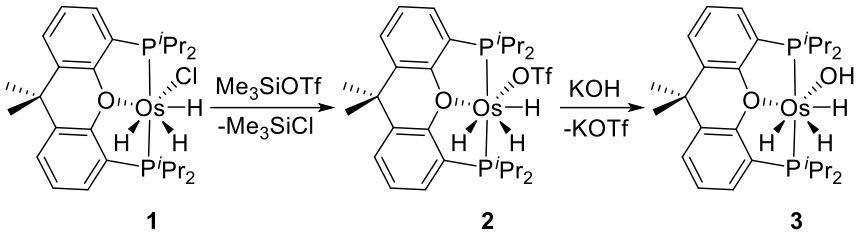

El tratamiento de una disolución de **1** en tolueno con 2.0 equivalentes de Me_3SiOTf conduce al intermedio sintético $OsH_3OTf\{\kappa^3$-*P*,*O*,*P*-[xant(P^{i}Pr$_2$)$_2$]} (**2**), que se aísla como un sólido amarillo con un 90 % de rendimiento.

El ligando trifluorometanosulfonato se desplaza fácilmente por el grupo hidróxido. La adición gota a gota de una disolución de KOH en agua a una disolución de **2** en acetona conduce al hidróxido $OsH_3OH\{\kappa^3$-*P*,*O*,*P*-[xant(P^{i}Pr$_2$)$_2$]} (**3**), que se aísla como un sólido amarillo con un 92 % de rendimiento.

El complejo trihidruro-hidroxo **3** promueve la deshidrogenación de ácido fórmico para dar H_2 y CO_2.[138] El estudio cinético de la reacción se llevó a cabo realizando sucesivos experimentos de deshidrogenación catalítica en tolueno y midiendo el volumen total de gas generado con una bureta de gases. El método de las velocidades iniciales permitió encontrar una ley de velocidad de orden 0 en el sustrato, ácido fórmico, y orden 1 en el complejo precursor **3** (ecuación 1).

$$d[H_2]/dt = k[\mathbf{3}] \qquad (1)$$

El análisis de Eyiring permitió cuantificar los parámetros de activación del proceso: $\Delta H^{\ddagger}$ = 18 ± 3 kcal·mol^{-1} y $\Delta S^{\ddagger}$ = -3 ± 8 cal·mol^{-1}·K^{-1}, que dan un valor para $\Delta G^{\ddagger}$ de 18 ± 5 kcal·mol^{-1} a 298 K. Este valor está dentro del rango publicado para la

deshidrogenación de ácido fórmico catalizada por otros sistemas homogéneos (17 – 26 kcal·mol^{-1}).[120a,122d,124f,139]

Se llevó a cabo la reacción estequiométrica de **3** con ácido fórmico con el objetivo de identificar los intermedios claves de la catálisis. La adición de 1.0 equivalentes de ácido fórmico a una disolución de **3** en tolueno-d_8 contenida en un tubo de RMN conduce cuantitativa e instantáneamente al derivado formiato $OsH_3\{\kappa^1\text{-}O\text{-}(HCO_2)\}\{\kappa^3\text{-}P,O,P\text{-}[xant(P^iPr_2)_2]\}$ (**4**), como consecuencia de la protonación del ligando hidróxido de **3** y el desplazamiento posterior de H_2O (esquema 2). El complejo **4** se caracterizó por difracción de rayos-X (figura 1).

Esquema 2. Reacción de 3 con Ácido Fórmico

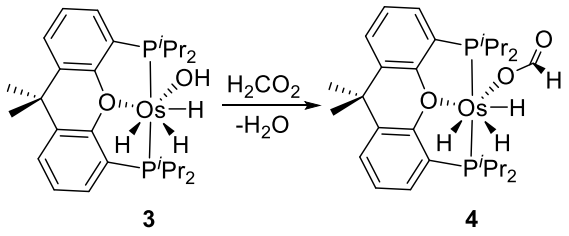

3 **4**

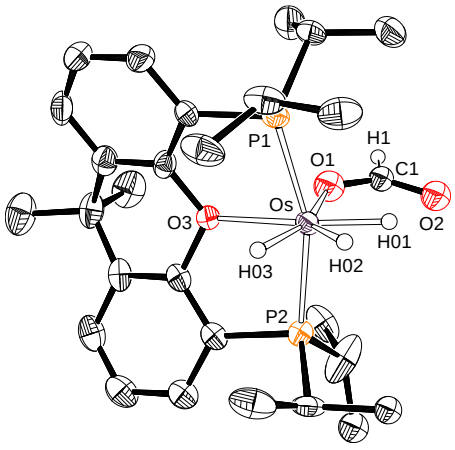

Figura 1. Diagrama molecular del complejo **4**.

El complejo **4** es inestable y pierde CO_2 para dar $OsH_4\{\kappa^3\text{-}P,O,P\text{-}[xant(P^iPr_2)_2]\}$ (**5** en el esquema 3). El estudio cinético de esta transformación por espectroscopía de RMN de

$^{31}P\{^{1}H\}$, entre 303 y 323 K, demuestra que la desaparición de **4** es una función exponencial del tiempo y se ajusta a un proceso de primer orden. Los parámetros de activación calculados a partir del análisis de Eyring son $\Delta H^{\ddagger} = 20 \pm 3$ kcal·mol^{-1} y $\Delta S^{\ddagger} = 0 \pm 8$ cal·mol^{-1}·K^{-1}. Estos valores permiten obtener un valor para $\Delta G^{\ddagger}$ de 20 ± 5 kcal·mol^{-1} a 298 K, que está de acuerdo con el valor obtenido en el proceso catalítico.

Esquema 3. Descarboxilación del complejo 4

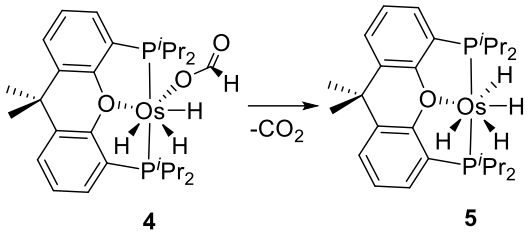

4 **5**

El complejo tetrahidruro **5** reacciona con ácido fórmico para formar hidrógeno molecular y regenerar el derivado formiato **4** (esquema 4). De acuerdo con cálculos DFT previos (ver sección 5.1 de la introducción), la protonación da el catión **A**, que tiene dos tautómeros con energías similares: el trihidruro-dihidruro comprimido **Aa** y el hidruro-dihidruro comprimido-dihidrógeno **Ab**.[57c] La disociación del ligando H_2 coordinado de este último y la coordinación del anión formiato a la especie insaturada resultante **B** debería conducir a **4**.

Esquema 4. Reacción de 5 con Ácido Fórmico

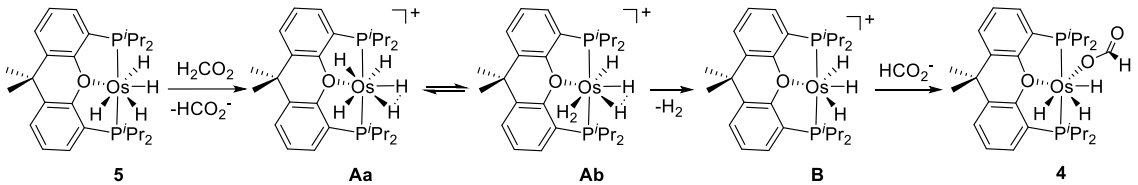

5 **Aa** **Ab** **B** **4**

Las reacciones resumidas en los esquemas 2-4 caracterizan completamente el proceso catalítico. El complejo trihidruro-hidroxo **3** es el precursor de la catálisis y, bajo

condiciones catalíticas, se transforma cuantitativamente en el verdadero catalizador, el derivado formiato **4** (esquema 2), que pierde CO_2 para formar el tetrahidruro **5** (esquema 3). Este último reacciona con ácido fórmico para dar hidrógeno molecular y regenerar **4** en un proceso en tres etapas: protonación, disociación de H_2 y coordinación del formiato (esquema 4). Dado que la deshidrogenación catalítica de ácido fórmico promovida por **3** tiene los mismos parámetros de activación que la pérdida estequiométrica de CO_2 de **4**, la formación de CO_2 es la etapa limitante de la catálisis, mientras que la formación de hidrógeno molecular es rápida.

Como se ha mencionado en la introducción de este capítulo, la formación de CO_2 puede ocurrir a través de tres caminos distintos: esfera externa, β-eliminación de hidrógeno y abstracción de hidruro. El mecanismo de esfera externa se excluye debido a que el sistema no tiene ninguna función que pueda permitir esta vía. Las reacciones de β-eliminación de hidrógeno se caracterizan por ocurrir en especies insaturadas. A diferencia de la β-eliminación de hidrógeno, la migración del hidruro sucede en dos etapas en un intermedio saturado, que implican el deslizamiento del centro metálico desde el átomo de oxígeno coordinado hasta el hidrógeno libre y la posterior eliminación de CO_2. Con el objetivo de discernir entre β-eliminación de hidrógeno y abstracción de hidruro se llevaron a cabo cálculos DFT (B3LYP(GD3)//6-31G**/SDD(f)). Los cambios en $\Delta G^{\ddagger}$ se calcularon en tolueno a 298 K y 1 atm. Aunque la reacción es ligeramente endergónica, el equilibrio se desplaza por la eliminación del gas.

La figura 2 resume el perfil de energía para la β-eliminación de hidrógeno. Dado que el complejo formiato **4** es saturado, la disociación del átomo de oxígeno del ligando pinza es necesaria para generar una vacante de coordinación en el centro metálico. La vacante permite la migración del átomo de hidrógeno del grupo formiato, que conduce al

intermedio **D**. La disociación posterior de la molécula de CO_2 coordinada sucede en dos etapas, que implican la rotura secuencial de los enlaces Os-C y Os-O. Esto supone una barrera energética de 26.8 kcal·mol^{-1} respecto a **4**, que está fuera del rango experimental y sugiere que la *β*-eliminación de hidrógeno no es un camino operativo.

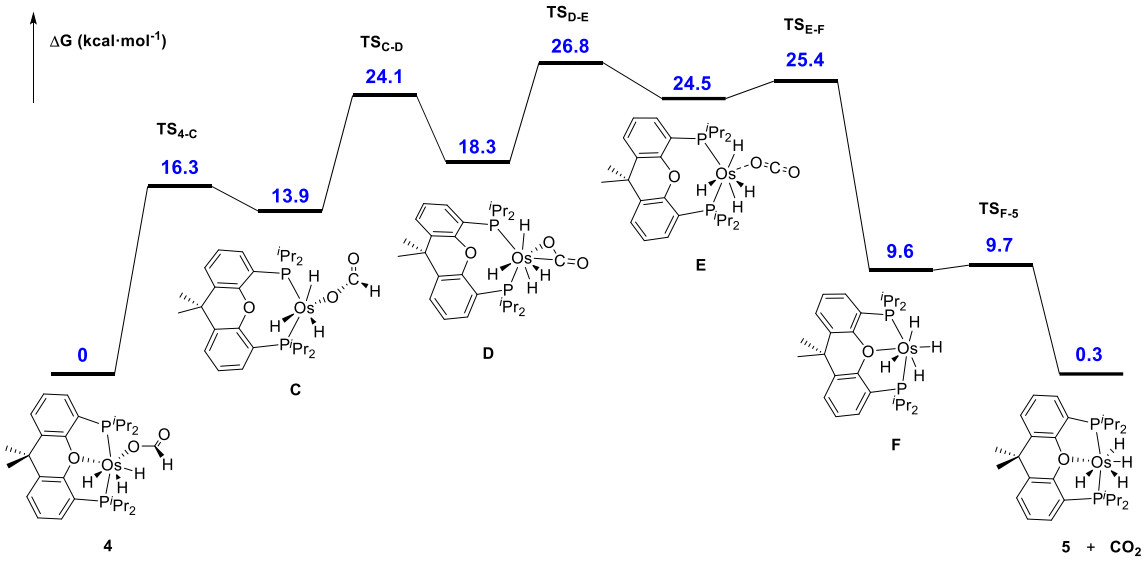

Figura 2. Perfil energético (Δ*G* in kcal·mol^{-1}) para la formación de CO_2 a través de la *β*-eliminación de hidrógeno.

La abstracción de hidruro ocurre a través del intermedio **G** (figura 3), que se puede describir como una especie Os{κ^1-H-(HCO_2)}. Este intermedio es 12.1 kcal·mol^{-1} menos estable que **4**. El intermedio **G** se genera mediante el deslizamiento del centro metálico desde el átomo de oxígeno coordinado al átomo libre de hidrógeno, siguiendo el camino O-C-H. El proceso tiene una energía de activación de 22.5 kcal·mol^{-1}. Este valor es similar a los valores experimentales obtenidos para la catálisis y para la liberación estequiométrica de CO_2 de **4**. La similitud de los tres valores apoya un mecanismo de abstracción de hidruro para la etapa de formación de CO_2 y revela que el deslizamiento del centro metálico del oxígeno al hidrógeno a través del camino O-C-H es la etapa

limitante de la formación de CO_2 y, por lo tanto, de la catálisis. La eliminación de CO_2 de **G** es un proceso prácticamente sin barreras.

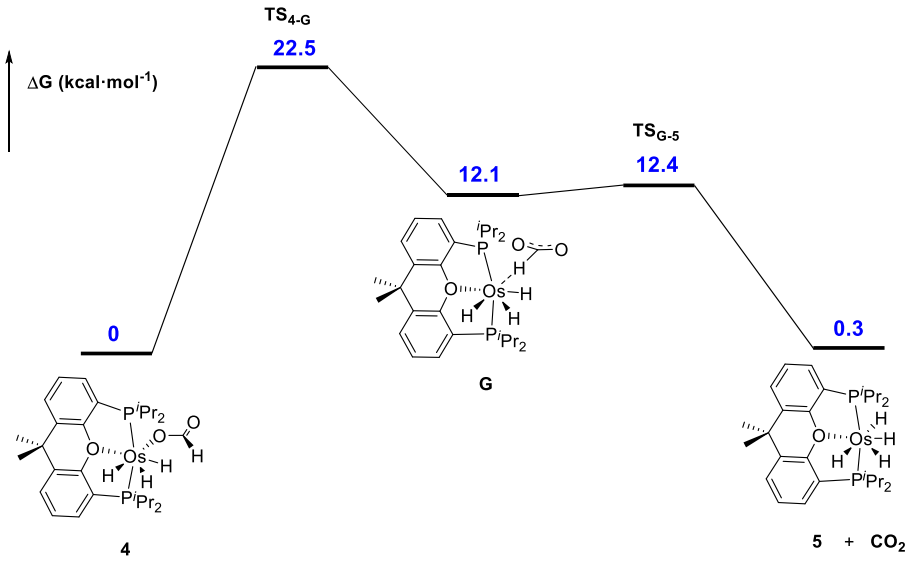

Figura 3. Perfil energético (ΔG in kcal·mol^{-1}) para la formación de CO_2 a través de la abstracción de hidruro.

CONCLUSIONES

La sustitución del ligando cloruro del trihidruro $OsH_3Cl\{\kappa^3$-*P,O,P*-[xant(P^iPr_2)$_2$]} por el grupo hidróxido proporciona el derivado trihidruo-hidroxo de osmio(IV) $OsH_3(OH)\{\kappa^3$-*P,O,P*-[xant(P^iPr_2)$_2$]}, que promueve eficazmente la deshidrogenación de ácido fórmico para dar CO_2 y H_2.

La deshidrogenación sucede a través del ciclo catalítico que se muestra en el esquema 5. Bajo condiciones catalíticas, el complejo trihidruro-hidroxo reacciona con ácido fórmico para formar el compuesto $OsH_3\{\kappa^1$-O-(HCO_2)$\}$ $\{\kappa^3$-*P,O,P*-[xant(P^iPr_2)$_2$]}, que ha podido caracterizarse por completo. Cálculos DFT sugieren que el deslizamiento del centro metálico desde el oxígeno al hidrógeno a través del camino O-C-H genera el intermedio

$OsH_3\{\kappa^1\text{-}H\text{-}(HCO_2)\}\{\kappa^3\text{-}P,O,P\text{-}[xant(P^iPr_2)_2]\}$, que pierde CO_2 para dar el tetrahidruro $OsH_4\{\kappa^3\text{-}P,O,P\text{-}[xant(P^iPr_2)_2]\}$. Este último sufre la protonación del ácido fórmico. De acuerdo con cálculos DFT previos, el catión resultante existe como una mezcla de dos tautómeros en equilibrio: el trihidruro-dihidruro comprimido $[OsH_3(H\cdots H)\{\kappa^3\text{-}P,O,P\text{-}[xant(P^iPr_2)_2]\}]^+$ y el hidruro-dihidruro comprimido-dihidrógeno $[OsH(H\cdots H)(\eta^2\text{-}H_2)\{\kappa^3\text{-}P,O,P\text{-}[xant(P^iPr_2)_2]\}]^+$. La disociación de la molécula de H_2 coordinada a este último conduce al catión insaturado $[OsH_3\{\kappa^3\text{-}P,O,P\text{-}[xant(P^iPr_2)_2]\}]^+$, que coordina el anión formiato para regenerar $OsH_3\{\kappa^1\text{-}O\text{-}(HCO_2)\}\{\kappa^3\text{-}P,O,P\text{-}[xant(P^iPr_2)_2]\}$ y cerrar el ciclo. El deslizamiento del centro metálico desde el oxígeno al hidrógeno a través del camino O-C-H es la etapa limitante de la catálisis.

Esquema 5. Ciclo Catalítico para la Deshidrogenación de Ácido Fórmico Promovida por 3

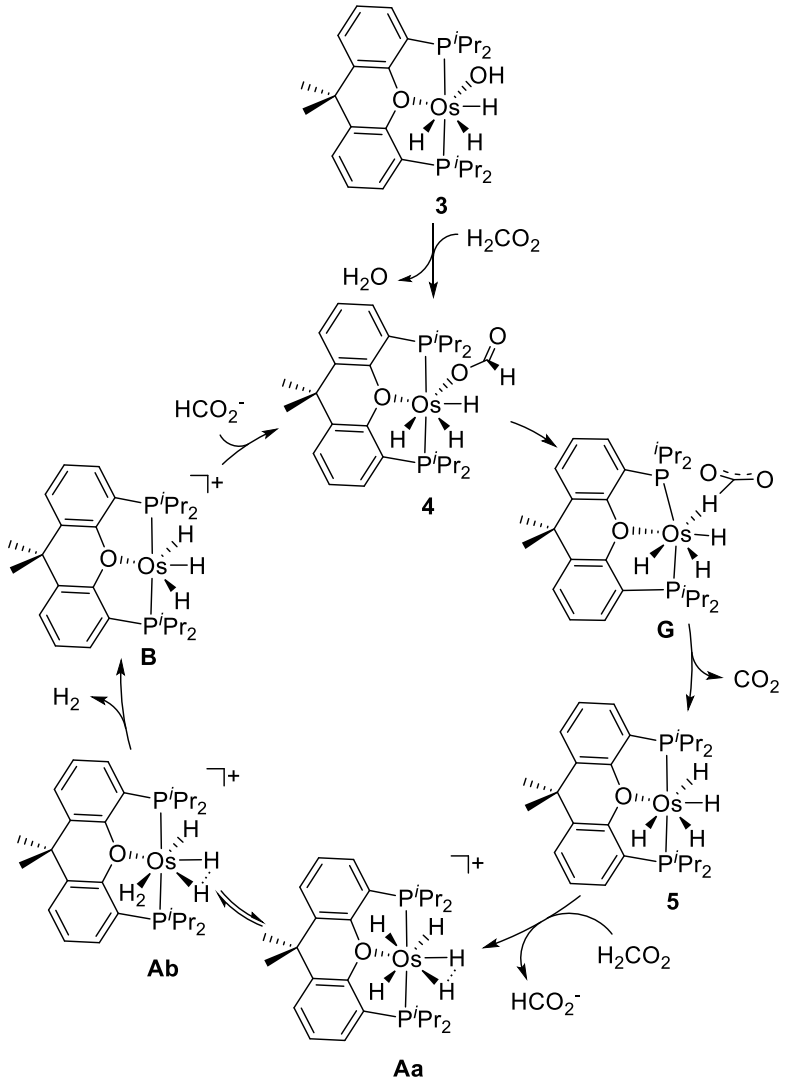

En resumen, se ha descubierto el primer catalizador de osmio que promueve la deshidrogenación de ácido fórmico a CO_2 y H_2 y se ha establecido el mecanismo de la catálisis incluyendo la caracterización completa de los intermedios clave y la elucidación de la etapa limitante del proceso.

Capítulo 3: σ-Boranos Elongados vs σ-Boranos en Complejos Pinza POP de Osmio

INTRODUCCIÓN

El primer paso en reacciones de activación de enlaces σ promovidas por metales es la coordinación del enlace al metal para formar un complejo σ. La interacción entre el metal y el enlace implica donación del orbital molecular σ del enlace coordinado a los orbitales vacíos del metal y retrodonación desde el metal al orbital molecular σ* del enlace. El balance entre donación y retrodonación determina el grado de adición del enlace al metal que, en la mayoría de los casos, es responsable de la separación entre los átomos coordinados.[108] Los compuestos dihidrógeno son el grupo de complejos mejor estudiado de éste tipo. En función de la separación entre los átomos de hidrógeno coordinados, estos se clasifican en complejos de tipo Kubas (0.8 – 1.0 Å) y dihidrógenos elongados (1.0 – 1.3 Å). Estados de oxidación altos, metales de la primera serie de transición, cargas catiónicas, ligandos ácidos y grupos tridentados que fuerzan ángulos L-M-L cercanos a 90º estabilizan complejos de tipo Kubas, mientras que estados de oxidación bajos, metales de la tercera serie de transición y ligandos π-dadores favorecen la formación de compuestos dihidrógeno elongados.[109,140]

El estudio de complejos de enlaces E-H (E = B, C, Si, etc) es mucho más difícil que el estudio de especies dihidrógeno.[141] Como consecuencia, hay poca información disponible sobre los complejos σ-E-H. En comparación con la molécula de hidrógeno, un enlace R_nE-H (n = 2 ó 3) es asimétrico y los sustituyentes en el átomo E pueden modular la acidez del enlace. Además, en algunos casos el átomo E puede disponer de orbitales

vacíos, como es el caso del átomo de boro, lo que altera el balance entre donación y retrodonación, en comparación con la situación de la molécula de hidrógeno.

La activación de enlaces B-H es una reacción de gran interés en relación con la borilación de moléculas orgánicas[142] y la deshidrogenación de amina-boranos.[6a,23,110,143] Sin embargo, se han publicado pocos ejemplos de complejos que contienen coordinación B-H no asistida.[144] Entre ellos, se incluyen compuestos de algunos metales de la primera serie de transición, como Ti,[145] Mn, Re[146] y Ni;[147] y Ru.[148] Estos complejos tienen ángulos H-M-B pequeños (32 - 38º), mientras que las distancias B-H están en un rango de 1.23 - 1.35 Å. Con metales de la tercera serie de transición, Heinekey y colaboradores han publicado la estructura de difracción de neutrones del derivado $IrH_2\{\kappa^3$-*P,C,P*-$[C_6H_3$-1,3-$(OP^tBu_2)_2]\}(\eta^2$-H-$BH_2)$, que contiene un enlace σ-B-H coordinado al átomo de iridio con una distancia B-H de 1.45(5) Å. El homólogo con pinacolborano (HBpin) pierde hidrógeno molecular para dar el derivado planocuadrado $Ir\{\kappa^3$-*P,C,P*-$[C_6H_3$-1,3-$(OP^tBu_2)_2]\}(\eta^2$-H-Bpin).[149] Nuestro grupo ha descrito la coordinación de catecolborano (HBcat) y HBpin al dihidruro de osmio $OsH_2(CO)(P^iPr_3)_2$ para dar $OsH_2(CO)(\eta^2$-H-$BR_2)(P^iPr_3)_2$.[150] También hay unos pocos complejos semi-sandwich Rh-(C_5Me_5), con ligandos hidruro y borilo, que presentan separaciones entre el boro y el hidruro en el rango 1.60 - 2.0 Å.[151] Para estos compuestos, que pueden considerarse los homólogos borano de las especies dihidrógeno elongadas atendiendo al valor de la separación entre los átomos de boro e hidrógeno, se ha propuesto la existencia de una interacción "residual" B···H, aunque no se han proporcionado evidencias claras sobre su naturaleza. Al contrario que para los complejos dihidrógeno, sigue siendo difícil asignar una formulación correcta basada en medidas de RMN de ^{11}B y ^1H.[152] Por lo tanto, es necesario

desarrollar métodos simples que permitan confirmar la naturaleza de la interacción entre el enlace B-H y el centro metálico, distinguiendo entre σ-borano y σ-borano elongado.

La capacidad del esqueleto *mer*-Os(POP) para estabilizar interacciones no clásicas[153] (ver Capítulo 1) nos animó a estudiar la coordinación de los enlaces B-H de las moléculas HBcat y HBpin a los fragmentos metálicos OsHX{κ^3-*P,O,P*-[xant(P^{i}Pr$_2$)$_2$]} (X = H y Cl) y analizar la influencia del ligando X en el grado de adición del enlace B-H al átomo de osmio.

Este capítulo describe la formación de nuevos complejos σ-borano elongados y σ-borano para un metal del grupo del platino de la tercera serie de transición, muestra las primeras estructuras de rayos-X para este tipo de compuestos en la química de osmio, y analiza la situación de enlace osmio-borano en función de X, probando que los métodos *teoría de átomos en moléculas* (AIM), *orbitales naturales de enlace* (NBO), y *análisis de descomposición energética-orbital natural para valencia química* (EDA-NOCV) son herramientas sencillas útiles para distinguir entre σ-borano y σ-borano elongado.

DISCUSIÓN DE RESULTADOS

El complejo dinuclear [(Os(H···H){κ^3-*P,O,P*-[xant(P^{i}Pr$_2$)$_2$]})$_2$(μ-Cl)$_2$][BF$_4$]$_2$ (**3**) reacciona con HBcat y HBpin. Su tratamiento en diclorometano con 5.1 equivalentes de los boranos conduce a los respectivos derivados hidruro-σ-borano elongado OsHCl(η^2-H-BR$_2$){κ^3-*P,O,P*-[xant(P^{i}Pr$_2$)$_2$]} (BR$_2$ = Bcat (**4**), Bpin (**5**)), que se aíslan como sólidos blancos con rendimientos del 56 % (**4**) y 54 % (**5**), de acuerdo con el esquema 1.

Esquema 1. Formación de los Complejos σ-Borano Elongados 4 y 5

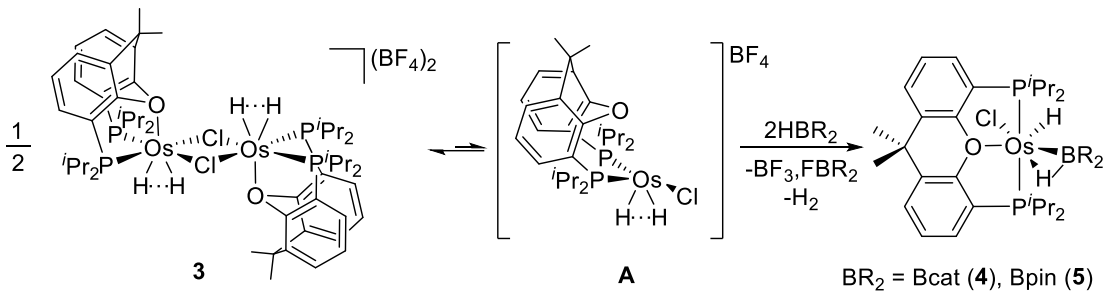

El complejo **4** se caracterizó mediante difracción de rayos-X. La estructura tiene dos moléculas que son químicamente equivalentes pero cristalográficamente independientes en la unidad asimétrica. La figura 1 muestra una de ellas. La coordinación del enlace B-H provoca su elongación. Las distancias B-H(02) de 1.68(2) y 1.67(2) Å, 1.601 Å en la estructura optimizada mediante cálculos DFT, comparan bien con las distancias B-H más cortas encontradas en el complejo de rodio $Rh(\eta^5\text{-}C_5Me_5)(Bpin)_2(\eta^2\text{-}HBpin)$ (1.53(3) y 1.69(3) Å),[151] cuya estructura también tiene dos moléculas químicamente equivalentes y cristalográficamente independientes en la unidad asimétrica. Estos valores son consistentes con el carácter σ-borano elongado de estas especies. Los ángulos B-M-H en ambos compuestos son similares, 53.6(9) y 53.1(9)º en **4** frente a 47.5(8) y 54.3(10)º en el derivado de rodio.

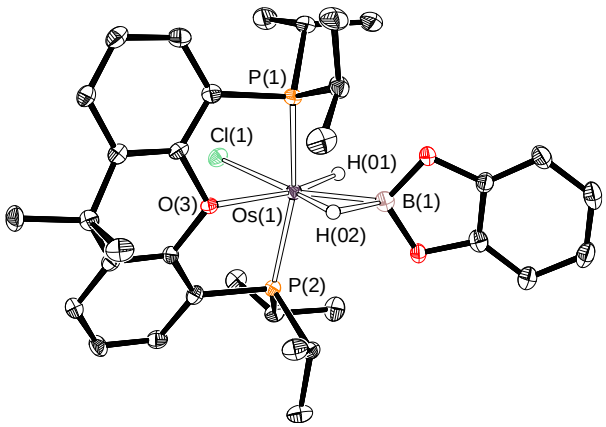

Figura 1. Diagrama molecular del complejo **4**.

La distancia B-H(02) es alrededor de 0.5 Å más larga que los enlaces B-H(Os) en el derivado tetrahidruroborato $OsH_3(\kappa^2\text{-}H_2BH_2)(IPr)(P^iPr_3)$ (1.18(3) y 1.17(3) Å; IPr = 1,3-bis(2,6-diisopropilfenilimidazolilideno)[118b] y aproximadamente 0.4 Å más larga que las distancias B-H(Os) en la especie dihidruroborato $Os(Bcat)(\kappa^2\text{-}H_2Bcat)(CO)(P^iPr_3)$ (1.26(3) y 1.27(3) Å).[150b] La distancia B-H(02) es sólo ligeramente más corta que la separación entre el átomo de boro y el ligando hidruro H(01), 1.70(2) y 1.70(2) Å; 1.770 Å en la estructura optimizada mediante cálculos DFT. Estos valores sugieren la existencia de una interacción *cis*-hidruro-σ-borano elongado. Contactos "residuales" de este tipo son comunes en especies *cis*-hidruro-dihidrógeno elongadas.[140c,154] Esto parece estar relacionado con la geometría del complejo y el tamaño de los átomos involucrados; y podría verse magnificado por el distinto signo de las cargas parciales sobre el ligando hidruro y sobre el átomo de boro del borano. La interacción entre el centro metálico y el enlace B-H es realmente fuerte. Las distancias Os-B de 2.036(4) y 2.042(4) Å, 2.054 Å en la estructura DFT-optimizada, se asemejan a las distancias Os-borilo publicadas.[150,155]

El complejo **5** también se caracterizó por difracción de rayos-X. La fuerza de la interacción entre el enlace B-H y el centro metálico es similar a la del compuesto **4**. Las distancias B-H(02) y Os-B de 1.69(2) y 2.075(3) Å, respectivamente, 1.623 y 2.071Å en la estructura optimizada mediante DFT, se asemejan a los valores de **4**.

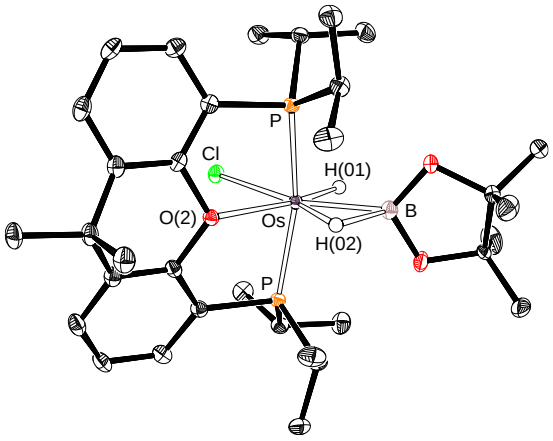

Figura 2. Diagrama molecular del complejo **5**.

El tetrahidruro clásico $OsH_4\{\kappa^3$-*P*,*O*,*P*-[xant(P^iPr_2)$_2$]} (**6**) reacciona rápidamente con HBcat, a pesar de la estabilidad térmica y la baja tendencia a la eliminación reductora de hidrógeno molecular que presenta.[57e] La adición de 1.1 equivalentes de borano a una disolución de **6** en benceno da lugar al derivado dihidruro-σ-borano elongado de osmio(II) $OsH_2(\eta^2$-H-Bcat)$\{\kappa^3$-*P*,*O*,*P*-[xant(P^iPr_2)$_2$]} (**7**), como resultado de la sustitución formal de una molécula de hidrógeno por un enlace B-H de HBcat (esquema 2).

Esquema 2. Formación del Complejo σ-Borano 7

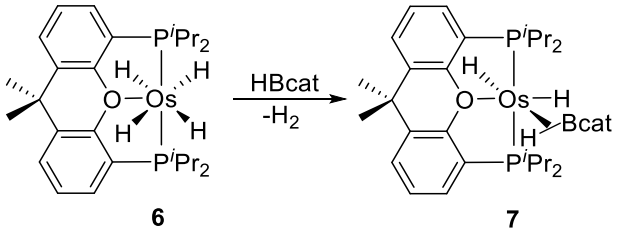

6 **7**

El complejo **7** se aísla como un sólido blanco con un 80% de rendimiento y se caracterizó por difracción de rayos-X. La sustitución del cloruro por hidruro hace que la interacción entre el centro metálico y el enlace B-H del borano sea menos fuerte. Como consecuencia, la distancia B(1)-H(01) de 1.49(4) Å, 1.434 Å en la estructura optimizada mediante DFT,

es entre 0.1 y 0.2 Å más corta que en **4**. El ángulo B(1)-Os-H(01) de 45.5(15)º también es menor. Tanto la distancia B-H como el ángulo B-Os-H son similares a los valores encontrados en el complejo de iridio Ir{κ^3-*P*,*C*,*P*-[C_6H_3-1,3-(OP^tBu_2)$_2$]}(η^2-H-Bpin) (1.47(6) Å y 45(2)°).[149] Como era de esperar y al contrario que la longitud del enlace B-H, la distancia Os-B de 2.057(4) Å, 2.088 Å en la estructura optimizada mediante cálculos DFT, es entre 0.03 y 0.04 Å más larga que en **4**. Como en el último, el átomo de boro y su hidruro *cisoide* H(02) están cerca, aunque la separación entre ellos de 1.81(4) Å, 1.926 Å en la estructura optimizada por cálculos DFT, es entre 0.1-0.2 Å más larga que en **4**; esto es, el átomo de boro se aleja del hidruro de la misma manera que se acerca al átomo de hidrógeno. Este hecho sugiere de nuevo que en estos compuestos la proximidad entre el átomo de boro y el hidruro *cis* es consecuencia de la geometría de los complejos y del tamaño de los átomos implicados.

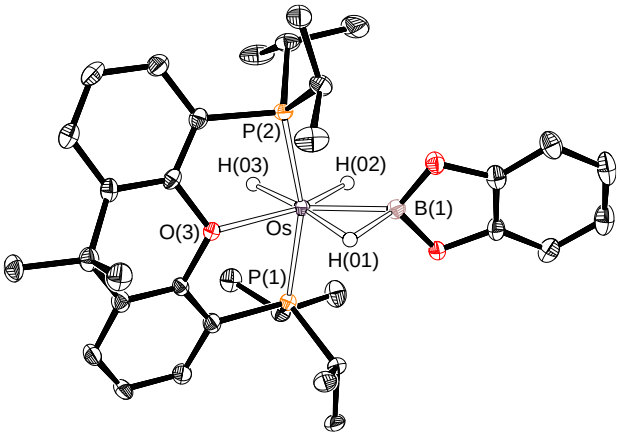

Figura 3. Diagrama molecular del complejo **7**.

La rápida formación del complejo **7** de acuerdo con el esquema 2 no es consistente ni con el carácter saturado de **6** ni con la disociación del átomo de oxígeno del grupo xanteno antes de la coordinación del borano. Dado que los complejos con hidruros metálicos son habitualmente anfóteros,[156] estos pueden experimentar autoionización. En el caso de **7**,

esto debería implicar la formación del pentahidruro $[OsH_5\{\kappa^2\text{-}P,P\text{-}[xant(P^iPr_2)_2]\}]^-$ (**8**)[153] y del catión de osmio(IV) $[OsH_3\{\kappa^3\text{-}P,O,P\text{-}[xant(P^iPr_2)_2]\}]^+$ (**B** en eq 2). El átomo de boro del borano podría sufrir el ataque nucleófilo del pentahidruro, lo que daría lugar a la liberación de un hidruro y la formación de $OsH_5(Bcat)\{\kappa^2\text{-}P,P\text{-}[xant(P^iPr_2)_2]\}$ (**C**), un fragmento boril-pentahidruro análogo al hexahidruro $OsH_6\{\kappa^2\text{-}P,P\text{-}[xant(P^iPr_2)_2]\}$[57c] (eq 3). El catión **B** puede atrapar el hidruro generado para formar de nuevo **6** (eq 4), que podría seguir reaccionando de la misma manera hasta la consumición total del borano, mientras que la coordinación del átomo de oxígeno del grupo xanteno de **C** debería producir la eliminación de hidrógeno molecular y la formación de **7** (eq 5).

$$2\ \underset{\mathbf{6}}{OsH_4\{\kappa^3\text{-}P,O,P\text{-}[xant(P^iPr_2)_2]\}} \rightleftharpoons \rightleftharpoons \underset{\mathbf{8}}{[OsH_5\{\kappa^2\text{-}P,P\text{-}[xant(P^iPr_2)_2]\}]^-} + \underset{\mathbf{B}}{[OsH_3\{\kappa^3\text{-}P,O,P\text{-}[xant(P^iPr_2)_2]\}]^+} \quad (2)$$

$$\underset{\mathbf{8}}{[OsH_5\{\kappa^2\text{-}P,P\text{-}[xant(P^iPr_2)_2]\}]^-} + HBcat \longrightarrow \underset{\mathbf{C}}{OsH_5(Bcat)\{\kappa^2\text{-}P,P\text{-}[xant(P^iPr_2)_2]\}} + H^- \quad (3)$$

$$\underset{\mathbf{B}}{[OsH_3\{\kappa^3\text{-}P,O,P\text{-}[xant(P^iPr_2)_2]\}]^+} + H^- \longrightarrow \underset{\mathbf{6}}{OsH_4\{\kappa^3\text{-}P,O,P\text{-}[xant(P^iPr_2)_2]\}} \quad (4)$$

$$\underset{\mathbf{C}}{OsH_5(Bcat)\{\kappa^2\text{-}P,P\text{-}[xant(P^iPr_2)_2]\}} \longrightarrow \underset{\mathbf{7}}{OsH_2(\kappa^2\text{-}H\text{-}Bcat)\{\kappa^3\text{-}P,O,P\text{-}[xant(P^iPr_2)_2]\}} + 2\ H_2 \quad (5)$$

La formación de **7**, de acuerdo con la secuencia mostrada en las eqs 2-5, implica la adición heterolítica del enlace B-H del HBcat a distintos centros metálicos. Para comprobar que esta secuencia de reacciones es una propuesta razonable, se llevó a cabo la reacción de **6** con ClBcat. Como se esperaba, la adición de 0.5 equivalentes del cloro-borano a una disolución de **6** en benceno inmediatamente proporciona una mezcla cuantitativa 1:1 de **7** y **1** (esquema 3).

Esquema 3. Reacción del Complejo 7 con ClBcat

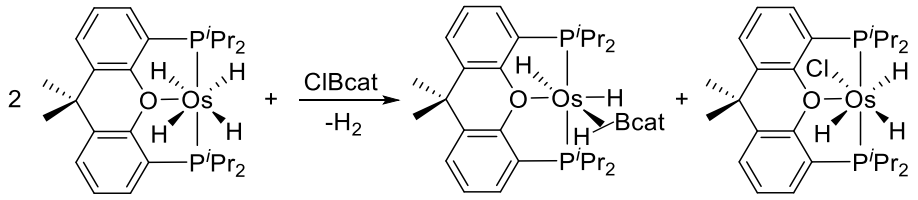

6 **7** **1**

La situación de enlace en los complejos **4** y **7** se analizó mediante cálculos DFT, al nivel BP86-D3. La naturaleza de las interacciones osmio-boro se investigó con los métodos AIM, NBO, y EDA-NOCV. La figura 5 muestra la distribución Laplaciana en el plano Os-H-B. Ambas especies exhiben una interacción Os-B significativa, como lo demuestra la existencia de un punto crítico de enlace (BCP) situado entre el metal y el átomo de boro, que se asocia a un camino de enlace (BP) entre los dos átomos. Mientras que para el complejo **4** existe un BCP entre el metal y el átomo de hidrógeno adyacente al boro, dicha interacción no se encuentra para el complejo **7**; esto es, ausencia de un BCP y el correspondiente BP entre ambos átomos. Esto es consistente con los índices de enlace de Wiberg calculados (WBI) para los enlaces Os-B y Os-H. Mientras que los WBIs para el enlace Os-B de ambos complejos son similares (WBI = 0.68 (**4**), y 0.65 (**7**)), para la interacción Os-H los índices WBI son bastante diferentes, 0.36 para **7** y 0.51 para **4**, lo que sugiere una interacción mucho más débil en el primero. Como consecuencia, no existe un BCP en el correspondiente diagrama AIM. Por lo tanto, los métodos AIM y NBO indican que, aunque la fortaleza del enlace Os-B es similar en ambos complejos, su situación de enlace es diferente. Mientras el complejo σ-borano elongado **4** se caracteriza por un ciclo de tres miembros con un punto crítico de anillo OsBH, el complejo σ-borano **7** carece de esa topología triangular.

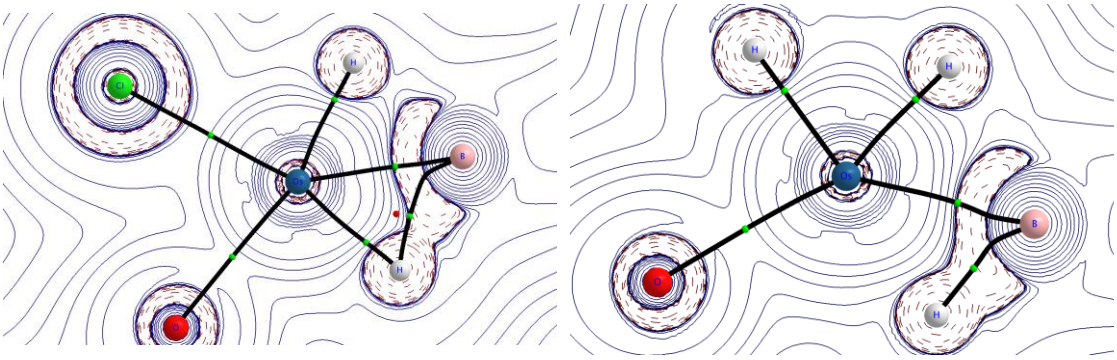

4 **7**

Figura 5. Diagrama de contorno $\nabla^2\rho(r)$ para los complejos **4** y **7** en el plano O-Os-B.

Ambos complejos se analizaron también por el método EDA-NOCV, con el objetivo de obtener una visión más cuantitativa en la situación de enlace. Este método combina esquemas de reparto de carga (NOCV) y energía (EDA) para descomponer la densidad de energía de deformación asociada a la formación de enlaces, $\Delta\rho$, en diferentes componentes del enlace químico. Los cálculos EDA-NOCV proporcionan las contribuciones energéticas para cada par u orbitales interactuantes a la energía total del enlace (ver más detalles en la sección de detalles computacionales del artículo).

Se consideró la interacción entre los fragmentos neutros de capa cerrada OsHX{κ^3-*P,O,P*-[xant(P^iPr_2)$_2$]} y HBcat (X = Cl (**4**) y H (**7**)). Los datos recogidos en la tabla 1 evidencian que la interacción Os-H más débil discutida anteriormente para el complejo σ-borano **7** conduce a una reducción significativa de la interacción entre el ligando HBcat y el fragmento metálico con respecto al complejo **4** ($\Delta\Delta E_{int}$ = 31.9 kcal·mol^{-1}). El EDA sugiere que, a pesar de la menor repulsión de Pauli, esta menor interacción en el complejo **7** se debe principalmente a atracciones electrostáticas ($\Delta\Delta E_{elstat}$ = 59.3 kcal·mol^{-1}) y orbitalarias ($\Delta\Delta E_{orb}$ = 34.7 kcal·mol^{-1}) menos estabilizantes.

Tabla 1. Resultados EDA-NOCV (en kcal·mol^{-1}) Calculados al Nivel ZORA-BP86-D3/TZ2P+//BP86-D3/def2-SVP

	4	**7**
ΔE_{int}	-118.2	-86.3
ΔE_{Pauli}	298.3	234.7
ΔE_{elstat}[a]	-244.1 (58.6%)	-184.8 (57.6%)
ΔE_{orb}[a]	-160.8 (38.6%)	-126.1 (39.3%)
$\Delta E(\rho_1)$[b]	-47.2 (29.3%)	-28.9 (22.9%)
$\Delta E(\rho_2)$[b]	-83.9 (52.2%)	-71.6 (56.8%)
ΔE_{rest}[b]	-29.7 (18.5%)	-25.6 (20.3%)
ΔE_{disp}[a]	-11.5 (2.8%)	-10.1 (3.1%)

[a] Los valores entre paréntesis indican la contribución porcentual de interacciones atractoras a la energía total, $\Delta E_{int} = \Delta E_{Pauli} + \Delta E_{elstat} + \Delta E_{orb} + \Delta E_{disp.}$ [b] Los valores entre paréntesis son las contribuciones porcentuales de las interacciones orbitalarias ΔE_{orb} a la energía total.

El método NOCV proporciona información cuantitativa adicional sobre las contribuciones a las atracciones orbitalarias totales, que ilustran las diferentes situaciones de enlace en estos complejos. La figura 6 muestra las densidades de energía de deformación $\Delta\rho$ calculadas, que indican el flujo de carga en estas especies (el flujo de carga tiene lugar en la dirección rojo → azul). A partir de los datos de la figura 6, dos interacciones orbitalarias principales describen la situación de enlace σ-borano, a saber, la interacción dador-aceptor que involucra el orbital molecular σ(B-H) y un orbital d atómico vacante del metal (ρ1) y la retrodonación (ρ2) desde el orbital atómico d(Os) hasta el orbital molecular σ*(B-H). Según las energías asociadas calculadas, ambas interacciones orbitalarias son significativamente más fuertes en el complejo **4**, lo que se

traduce en las interacciones orbitalarias totales (ΔE_{orb}) más altas calculadas para este complejo (ver tabla 1). La donación desde el orbital molecular σ(B-H) es significativamente más fuerte en **4** que en **7** ($\Delta\Delta E(\rho_1)$ = 18.3 kcal·mol^{-1}) debido a la mayor capacidad electro-atractora del ligando cloruro con respecto del ligando hidruro. Como consecuencia de esta fuerte donación y la alta población del correspondiente orbital molecular σ*(B-H) ($\Delta\Delta E(\rho_2)$ = 12.3 kcal·mol^{-1}), el enlace B-H es significativamente más largo en **4** que en **7**. La coordinación del dimetilaminoborano al fragmento de rutenio $RuHX(P^iPr_3)_2$ (X = H y Cl) presenta un efecto similar.[157]

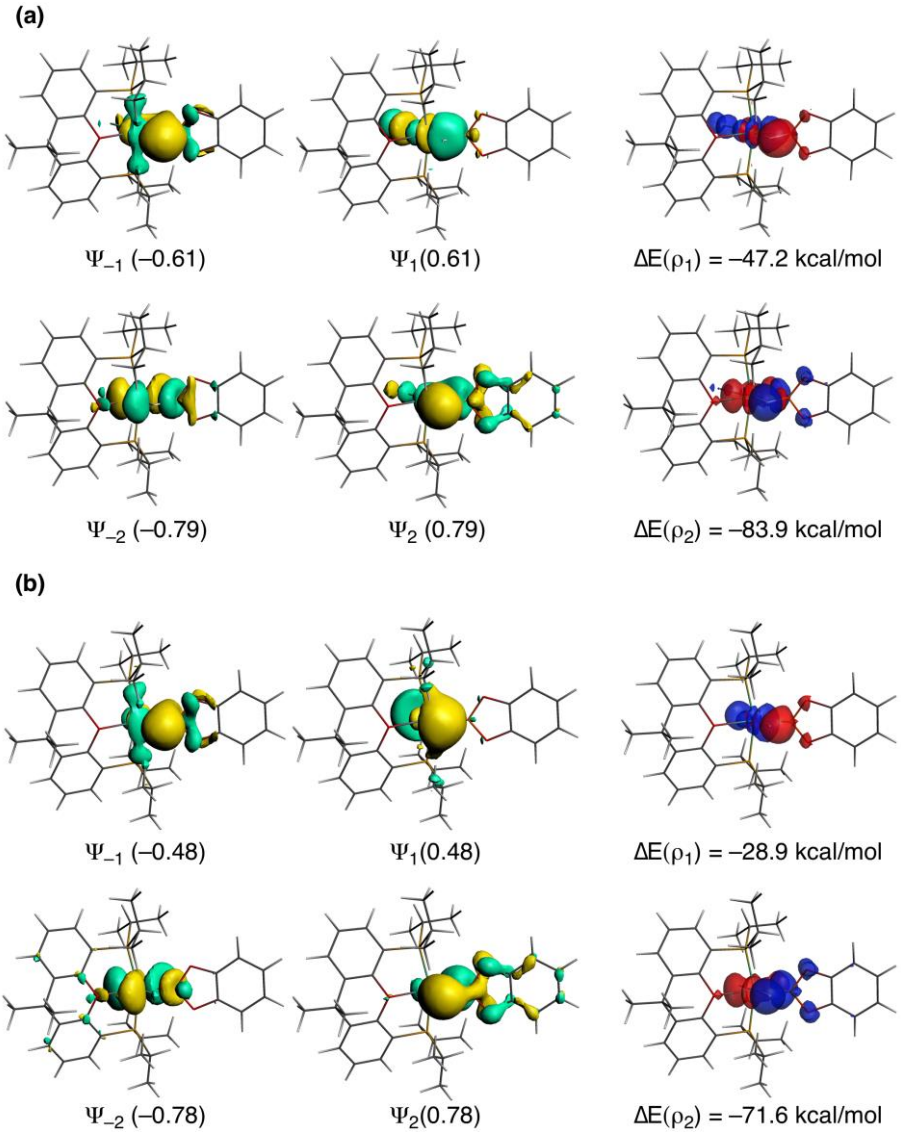

Figura 6. Pares de orbitales NOCV más importantes Ψ_{-k}, Ψ_k con sus valores propios $-\upsilon_k$, υ_k entre paréntesis y las densidades de energía de deformación asociadas $\Delta\rho_k$ y las energías de estabilización orbital ΔE para los complejos **4** (a) y **7** (b). El flujo de carga en las densidades de energía de deformación tiene lugar de rojo a azul.

CONCLUSIONES

Este estudio muestra que los fragmentos OsHX{κ^3-*P*,*O*,*P*-[xant(P^{i}Pr$_2$)$_2$]} (X = Cl y H) estabilizan la coordinación del enlace B-H de boranos *trans* al ligando X. La fortaleza de

la interacción entre el centro metálico y el borano depende de la naturaleza de X, siendo más fuerte para el cloruro que para el hidruro La capacidad electro-atractora del ligando cloruro tiene un efecto positivo sobre ambos componentes del enlace Os(η^2-H-B) al favorecer tanto la donación desde el orbital σ(B-H) al átomo de osmio como la retrodonación d(Os) → σ*(B-H). Como resultado de ello, el enlace B-H coordinado es significativamente más largo en el complejo **4** (X = Cl) que en **7** (X = H). El análisis EDA-NOCV sugiere que la fortaleza significativamente menor calculada para la interacción entre el fragmento $OsH_2\{\kappa^3$-*P,O,P*-[xant($P^iPr_2)_2$]} y el borano es debida principalmente a la existencia de atracciones electrostáticas y orbitalarias menos estabilizantes.

La coordinación del borano al fragmento metálico $OsHCl\{\kappa^3$-*P,O,P*-[xant($P^iPr_2)_2$]} da especies σ-borano elongadas, mientras que la coordinación al fragmento dihidruro $OsH_2\{\kappa^3$-*P,O,P*-[xant($P^iPr_2)_2$]} proporciona un compuesto σ-borano. El análisis NBO-AIM muestra situaciones de enlace marcadamente diferentes para ambos tipos de derivados. Mientras que los complejos σ-borano elongados se caracterizan por poseer un ciclo de tres miembros con un punto crítico de anillo OsBH, el compuesto σ-borano carece de dicha topología triangular.

En resumen, nuevos complejos σ-borano y σ-borano elongados estabilizados por fragmentos metálicos $OsHX\{\kappa^3$-*P,O,P*-[xant($P^iPr_2)_2$]} se han aislado y caracterizado por completo, y la interacción entre los fragmentos metálicos y el enlace B-H coordinado se ha analizado en función de X a partir de datos espectroscópicos, de difracción de rayos-X y mediante estudios teóricos.

Capítulo 4: Reacciones de un Complejo de Osmio(IV)-Hidróxido con Amino-Boranos: Formación de Derivados Boróxido

INTRODUCCIÓN

Los complejos hidróxido de metales del grupo del platino[132,158] son un grupo escaso y particularmente interesante de hidroxiácidos débiles, que tienen un derivado oxo como base conjugada, y son al mismo tiempo la base conjugada fuerte de un acuo complejo (esquema 1). El interés de estas especies no se corresponde, sin embargo, con una química abundante, en particular para el osmio. Además de unos pocos dímeros,[137] los compuestos hidróxido mononucleares de éste elemento incluyen complejos nitruro,[135-136] especies semi-sandwich,[41-42,159] y derivados hidruro-hidróxido[134,160], como se vio en la introducción del Capítulo 2. Estos últimos son particularmente raros debido a que la eliminación reductora de agua está generalmente favorecida desde un punto de vista termodinámico.[133] Los compuestos de este tipo son generalmente derivados de osmio(II). El complejo $OsH_3(OH)\{\kappa^3$-*P,O,P*-[xant(P^iPr_2)$_2$]} presentado en el Capítulo 2 es el único complejo de osmio(IV) aislado y caracterizado.[160]

Esquema 1. Equilibrio de Brønsted-Lowry para un Hidroxiácido Metálico

$$[L_nM(OH_2)]^n \overset{-H^+}{\rightleftharpoons} [L_nM(OH)]^{n-1} \overset{-H^+}{\rightleftharpoons} [L_nM(O)]^{n-2}$$

La dualidad de los complejos hidróxido se manifiesta en la respectiva nucleofilia y electrofilia de los átomos de oxígeno e hidrógeno del grupo hidróxido en las escasas reacciones que se han llevado a cabo,[161] como la adición de aldehídos a [OsH(OH)(CPh)(IPr)(P^iPr_3)]OTf (IPr = 1,3-bis(2,6-diisopropilfenil)imidazolilideno,

OTf = CF_3SO_3), que conduce a los correspondientes derivados carboxilato e hidrógeno molecular (esquema 2).[162]

Esquema 2. Reacción de un Complejo Hidróxido de Osmio con Aldehídos

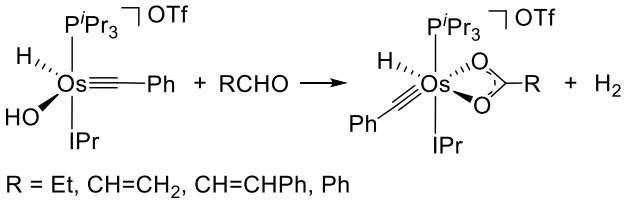

Los grupos boróxido se han propuesto como una alternativa prometedora a los ligandos alcóxido, ya que permiten modular las propiedades electrónicas y estéricas de precursores catalíticos en reacciones de interés en síntesis orgánica.[163] El orbital p vacío del átomo de boro permite aceptar electrones de un par no compartido del oxígeno, lo que da lugar a un oxígeno menos donador. Además, aunque el ligando boróxido tiene el doble de sustituyentes de carbono que un grupo alcóxido, la presencia de un espacio adicional lo convierte en un ligando estéricamente menos impedido.[164] Se conocen compuestos boróxido de metales de los bloques s y p[165] y complejos de todos los grupos del bloque d.[163,166] Sin embargo, los derivados boróxido de metales del grupo del platino eran desconocidos hasta ahora. La preparación de este tipo de compuestos se lleva a cabo principalmente a través de dos procedimientos: reacción de un haluro metálico con un boróxido de litio y protonolisis de un enlace metal-carbono, -nitrógeno, u –oxígeno con un ácido borónico[164] (*a* y *b* en el esquema 3).

Esquema 3. Procedimientos Sintéticos para la Preparación de Compuestos Boróxido

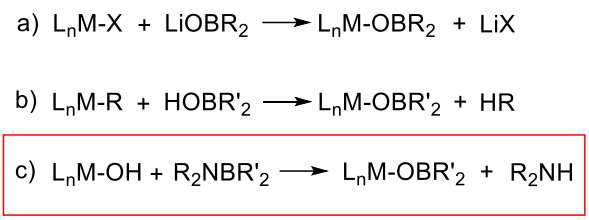

El boro tiene mayor afinidad por el oxígeno que por el nitrógeno, lo que es consistente con una mayor energía de disociación del enlace B-O respecto del N-O en especies de boro tricoordinadas.[167] Este hecho, unido a la nucleofilia del oxígeno y a la electrofilia del hidrógeno, nos animó a intentar preparar especies boróxido mediante el desplazamiento de un grupo amino de un amino-borano por la base conjugada de un hidroxiácido (*c* en el esquema 3). Este capítulo muestra un procedimiento novedoso que nos ha permitido aislar los primeros complejos boróxido de un metal del grupo del platino.

DISCUSIÓN Y RESULTADOS

Los iones metálicos en alto estado de oxidación forman enlaces fuertes con el oxígeno, incrementando la electrofilia del átomo de hidrógeno del grupo hidróxido. De acuerdo con esto, el tratamiento de una disolución del complejo de osmio(IV) $OsH_3(OH)\{\kappa^3$-*P,O,P*-[xant($P^iPr_2)_2$]} (**1**) en tolueno con 1.0 equivalentes de los amino-boranos $^iPr(H)NBCy_2$ y $^iPr(H)NBBN$ (BBN = 9-borabiciclo[3.3.1]nonano) produce la liberación de isopropilamina y la formación de los derivados boróxido de osmio(IV) $OsH_3(OBR_2)\{\kappa^3$-*P,O,P*-[xant($P^iPr_2)_2$]} (BR_2 = BCy_2 (**2**), BBN (**3**)), que se aíslan como sólidos amarillos con un rendimiento de 50-60 % (esquema 4).

Esquema 4. Formación de los Complejos Boróxido 2 y 3

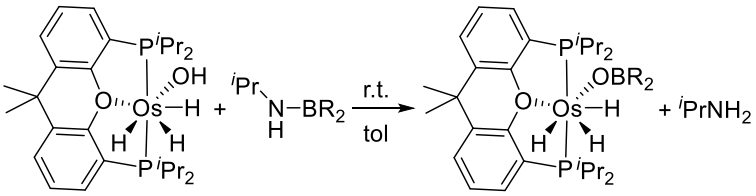

1 BR_2 = BCy_2 (**2**), BBN (**3**)

El compuesto **2** se caracterizó por difracción de rayos-X (figura 1). La distancia osmio-boróxido de 2.089(3) Å se encuentra en la parte superior del rango de distancias osmio(IV)-alcóxido (1.90-2.10 Å).[168] El ángulo Os-O1-B1 de 137.9(3)º se desvía significativamente del valor esperado para un átomo de oxígeno con hibridación sp^2, y es aproximadamente 20º mayor que el ángulo Os-S-B en los compuestos borotiolato $OsH(SBR_2)(\eta^2\text{-}H_2)(CO)(P^iPr_3)_2$ (113-119º).[150a] Esto es consistente con lo observado por Braunschweig y colaboradores para los ángulos M-calcógeno-B en los complejos borocalcógeno $Cp(CO)_2Mn[EB^tBu(IMe)]$ (E = S, Se, Te), que aumenta al ir hacia arriba en el grupo; esto es, en la secuencia Te < Se < S.[169]

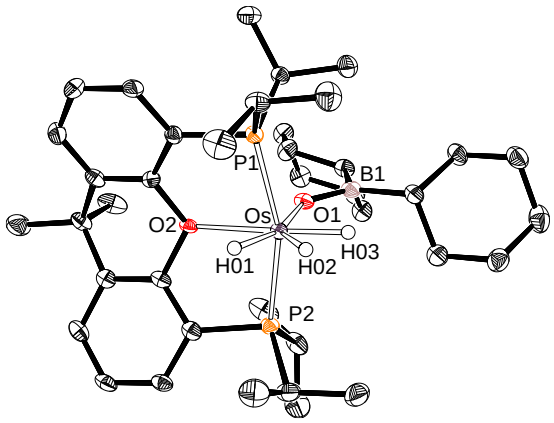

Figura 1. Diagrama molecular del complejo **2**.

La estabilidad de la unidad H-Os-OBR_2 en los compuestos **2** y **3** es notable. La eliminación reductora de hidrógeno molecular está cinéticamente favorecida frente a la

liberación del ácido borínico. Estos complejos reaccionan bajo atmósfera de CO a temperatura ambiente para dar los respectivos derivados boróxido de osmio(II) *cis*-dicarbonilo-hidruro $OsH(OBR_2)(CO)_2\{\kappa^2\text{-}P,P\text{-}[xant(P^iPr_2)_2]\}$ (BR_2 = BCy_2 (**4**), BBN (**5**)), e hidrógeno molecular (esquema 5). La eliminación del ácido borínico es posterior y requiere alta temperatura y largos tiempos de reacción. Así, el complejo **4** libera $HOBCy_2$, tras 4 días bajo atmósfera de CO a 110 ºC, para dar el compuesto tricarbonilo de osmio(0) $Os(CO)_3\{\kappa^2\text{-}P,P\text{-}[xant(P^iPr_2)_2]\}$ (**6**), que se aísla como un sólido amarillo con un rendimiento del 41 %. Los sustituyentes del átomo de boro influyen en la velocidad de eliminación del ácido borínico. El sistema bicíclico de **5** favorece la eliminación reductora con respecto a los sustituyentes ciclohexilo de **4**. Como consecuencia, el complejo **5** no se pueda aislar como un sólido puro ya que se forma cierta proporción del derivado **6** en la transformación de **3** a **5**, incluso a temperatura ambiente.

Esquema 5. Carbonilación de los Complejos 2 y 3

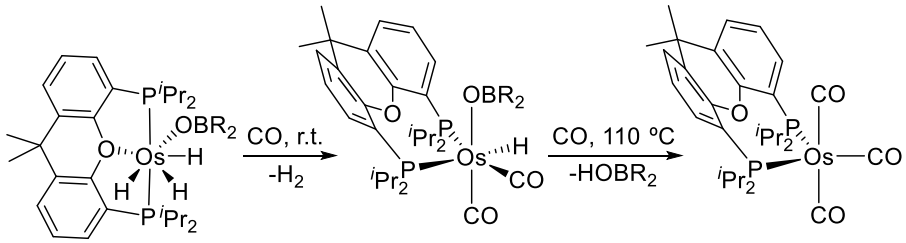

2, 3 **4, 5** **6**

El complejo **4** se aísla como un sólido blanco con un 64 % de rendimiento y se caracterizó mediante difracción de rayos-X (figura 2). La estructura confirma la reducción del centro metálico de +4 a +2, que implica la sustitución de dos ligandos hidruro por dos grupos carbonilo. La reducción provoca un cambio en el modo de coordinación de la difosfina de $\kappa^3\text{-}P,O,P$ a $\kappa^2\text{-}P,P$, que está de acuerdo con la flexibilidad de los ligandos éter-difosfina.[50,57c,57e,104,106,153,170] La formación de **4** y **5** amplía a osmio(II) el rango de

especies de osmio(VI) y osmio(IV) estabilizadas por ligandos éter-difosfina coordinados en modo κ^2-*P*,*P*.

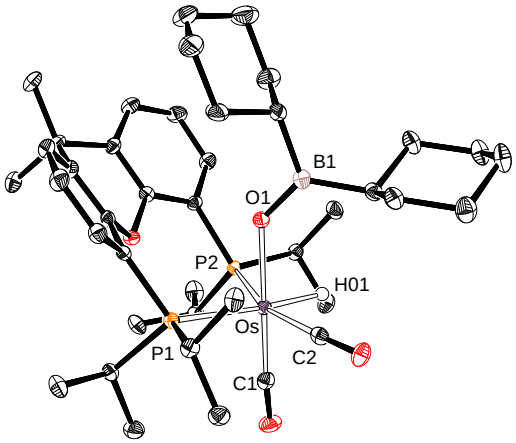

Figura 2. Diagrama molecular del complejo **4**.

El complejo **6** tricarbonilo de osmio(0) se caracterizó por difracción de rayos-X. La figura 3 muestra una vista de la molécula. El poliedro de coordinación alrededor del centro metálico se puede racionalizar como una bipirámide trigonal distorsionada con dos grupos carbonilos en las posiciones apicales. Los átomos de fósforo de la difosfina y el grupo carbonilo restante se encuentran en el plano ecuatorial. El complejo **6** es relevante por dos motivos: (i) amplía a osmio(0) el rango de compuestos con ligandos éter-difosfina coordinados en modo κ^2-*P*,*P* y (ii) es un ejemplo singular de compuesto $Os(CO)_3P_2$ con los átomos de fósforo situados en el plano ecuatorial de la bipirámide, ya que siempre ocupan las posiciones apicales en los complejos de este tipo previamente publicados.[171]

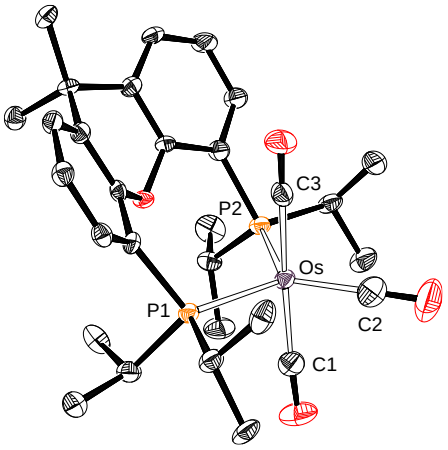

Figura 3. Diagrama molecular del complejo **6**.

El precursor hidróxido **1** presenta diferente reactividad frente a CO, respecto de los derivados boróxidos **2** y **3**. El complejo **1** elimina el grupo oxígeno dador y un ligando hidruro para dar el compuesto *trans*-dihidruro $OsH_2(CO)\{\kappa^3$-*P*,*O*,*P*-[xant(P^iPr_2)$_2$]} (**7**)[57e] y agua (esquema 6). El complejo **7** se transforma en el derivado *cis*-dicarbonilo $OsH_2(CO)_2\{\kappa^2$-*P*,*P*-[xant(P^iPr_2)$_2$]} (**8**), bajo atmósfera de CO a 110º C, como resultado del desplazamiento del átomo de oxígeno de la difosfina por una segunda molécula de CO y la isomerización de *trans* a *cis* de los ligandos hidruro. El complejo **8**, que es un nuevo ejemplo de especies de osmio(II) con el ligando xant(P^iPr_2)$_2$ coordinado en modo κ^2-*P*,*P*, es la réplica dihidruro de **4** y **5**. Este compuesto experimenta eliminación reductora de H_2 bajo atmósfera de CO para dar el derivado **6**.

Esquema 6 Carbonilación del Complejo 1

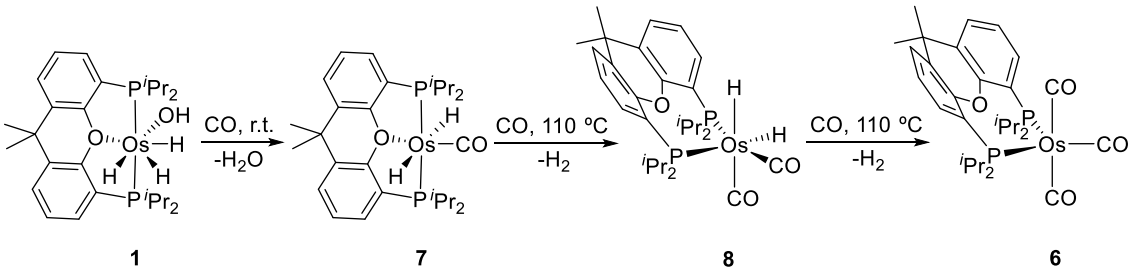

CONCLUSIONES

El estudio presenta una nueva reacción en la química de los complejos hidróxido de metales de transición, revela la existencia de derivados boróxido de metales del grupo del platino, demuestra que la eliminación reductora de ácidos borínicos desde los compuestos hidruro-boróxido está desfavorecida frente a la eliminación de hidrógeno molecular y amplia el rango de compuestos con ligandos éter-difosfina coordinados en modo κ^2-*P*,*P*.

La nucleofilia del oxígeno y la electrofilia del hidrógeno en los ligandos hidróxido coordinados a metales de transición permiten al ligando hidróxido desplazar el grupo amino de amino-boranos $R_2NBR'_2$. Las reacciones conducen a derivados boróxidos, incluyendo compuestos de metales del grupo del platino como el osmio. Complejos de este tipo con ligandos hidruro son estables frente a la eliminación de ácidos borínicos, al contrario que las especies hidruro-hidróxido que tienden a liberar agua. Bajo atmósfera de CO se observa la eliminación de hidrógeno molecular. La eliminación de ácido borínico sucede en una etapa posterior, en condiciones de alta temperatura tras largos tiempos de reacción. El ligando xant(P^iPr_2)$_2$ estabiliza estas especies de osmio adaptando su modo de coordinación a los requerimientos electrónicos y estéricos de cada complejo. Como consecuencia, se amplía el rango de compuestos estabilizados por la difosfina coordinada κ^2-*P*,*P* a derivados de osmio(II) y osmio(0).

Capítulo 5: Compuestos Cicloosmatioborano: Otras Manifestaciones de la Aromaticidad de Hückel

INTRODUCCIÓN

La aromaticidad es un concepto clásico que está en continua evolución.[172] Inicialmente se introdujo para explicar propiedades especiales de algunos hidrocarburos insaturados y heterociclos conjugados. En 1979, Thorn y Hoffmann propusieron su extensión a compuestos aromáticos orgánicos, donde una unidad CH se reemplaza por un fragmento isolobal de un metal de transición.[173] Tres años después, el grupo de Roper publicó la preparación y caracterización del primer metalabenceno.[174] Desde entonces, se han descrito un gran número de derivados aromáticos basados en elementos de transición y carbono,[175] muchos de ellos como especies aromáticas de tipo Hückel.[175c]

Recientemente, Frogley y Wright han definido los compuestos metalaromáticos como aquellos que tienen al menos un metal de transición en el anillo.[175d] Previamente, en 1979, Bursten y Fenske habían usado el término "metaloaromaticidad" para describir el comportamiento que inducía en el ciclobutadieno la coordinación del fragmento metálico $Fe(CO)_3$.[176] Aunque desde un punto de vista conceptual ambas acepciones son diferentes, la metaloaromaticidad ha sido empleada por algunos autores sin distinguir entre ambas situaciones.[177] El término *aromaticidad totalmente metálica* se ha propuesto para abordar diferentes aspectos del comportamiento de los elementos de los grupos principales y de los metales de transición.[178] El dianión ciclogaleno $[Ga_3L_3]^{2-}$ (L = $Mes_2C_6H_3$) fue el primer compuesto de esa clase.[179] En la actualidad, se conocen anillos aromáticos homolépticos de 3-10 miembros formados por elementos del grupo 2 y de los grupos 13-

16,[180] además de cationes tripaladio[181] y trioro.[182] Sin duda, los compuestos con anillos de tres miembros son los más desafiantes debido a la tensión impuesta por el pequeño tamaño del anillo. Estudios computacionales revelan que la aromaticidad en compuestos del grupo 14 análogos al ciclopropenilo ($E_3H_3^+$) disminuye según la secuencia C > Si > Ge > Sn > Pb.[183] Además de especies homolépticas, se conocen unas pocas especies heterolépticas con dos elementos de los grupos principales. Cummins y colaboradores publicaron triángulos EP_2 (E = Ge, Sn, Pb) estabilizados dentro de la esfera de coordinación de una unidad de diniobio protegida estéricamente,[184] mientras que el grupo de Guha ha predicho mediante un estudio computacional que la sustitución de un átomo de boro del triángulo $[B_3H_3]^{2-}$ por un elemento del grupo 15 debería proporcionar anillos neutros aromáticos H_2B_2XH (X = N, P).[185] En este capítulo, damos un paso más en este fascinante campo describiendo la preparación y completa caracterización de los primeros triángulos aromáticos formados por tres elementos distintos. Dos de ellos pertenecen a los grupos principales y el tercero es un metal de transición con sus ligandos.

DISCUSIÓN DE RESULTADOS

El esquema 1 resume la preparación de los nuevos compuestos, que parte del complejo $OsH_3(OTf)\{\kappa^3$-*P,O,P*-[xant($P^iPr_2)_2$]} (**1**) y tiene lugar a través del derivado hidrogenosulfuro $OsH_3(SH)\{\kappa^3$-*P,O,P*-[xant($P^iPr_2)_2$]} (**2**). La preparación del compuesto **2** está inspirada en la síntesis del complejo hidróxido análogo $OsH_3(OH)\{\kappa^3$-*P,O,P*-[xant($P^iPr_2)_2$]}.[186] Al igual que el grupo OH^-, el ligando SH^- desplaza el anión trifluorurometanosulfonato (OTf^-) de **1** para dar **2**, que se aísla como cristales rojos con un 47 % de rendimiento.

Esquema 1. Estrategia Sintética para la Preparación de los Complejos Cicloosmatioborano

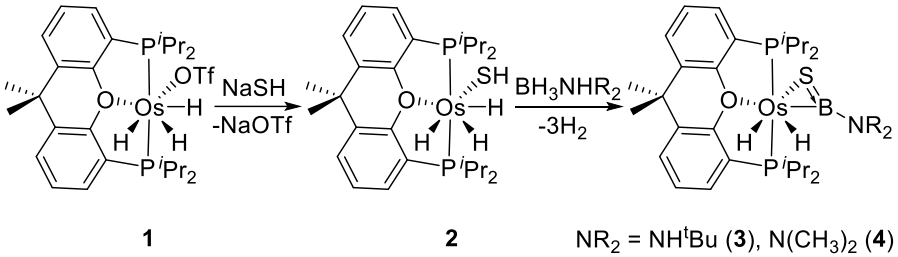

La estructura de difracción de rayos-X muestra la coordinación del grupo SH al átomo de Os (figura 1). Los complejos de metales del grupo del platino que contienen ligandos hidrogenosulfuro terminales son escasos debido a la alta tendencia que tiene éste grupo para actuar como ligando puente.[187] El derivado pentacoordinado catecolboril Os(Bcat)(SH)(CO)(P^{i}Pr$_3$)$_2$ fue el primer complejo SH mononuclear de un metal del grupo del platino caracterizado por difracción de rayos-X.[150a] Recientemente, Braun y colaboradores han preparado el derivado de rodio(I) Rh(SH){κ^3-*P*,*O*,*P*-[xant(^{t}Bu$_2$)$_2$]}, que también se ha caracterizado mediante difracción de rayos-X.[188]

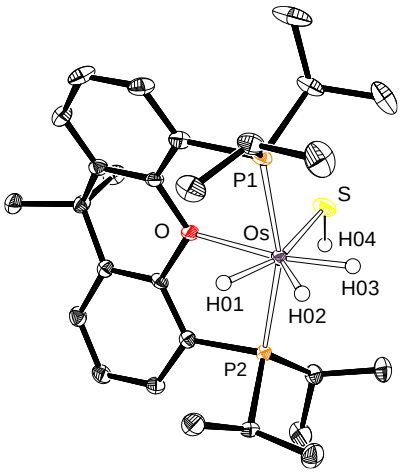

Figura 1. Diagrama molecular del complejo **2**.

El complejo **2** reacciona con amina-boranos BH_3NHR_2 para dar los derivados cicloosmatioboranos $OsH_2\{\kappa^2\text{-}S,B\text{-}[SBNR_2]\}\{\kappa^3\text{-}P,O,P\text{-}[xant(P^iPr_2)_2]\}$ ($NR_2 = NH^tBu$ (**3**), NMe_2 (**4**)), como resultado de la eliminación de H_2 de ambos, el centro metálico y los amina-boranos. La deshidrogenación está favorecida por el carácter polihidruro de **2**[19,108] y la presencia de un ligando hidrogenosulfuro, que atrapa el monómero amino-borano resultante de la pérdida de hidrógeno del amina-borano.[17] La captura facilita la extracción completa de los átomos de H unidos al átomo de B. Los complejos **3** y **4** se aislaron como sólidos amarillos con rendimientos del 60 %.

La estructura de **3** obtenida mediante difracción de rayos-X (figura 2) demuestra la forma triangular del anillo formado por los átomos de Os, S y B. La característica más llamativa del triángulo es la distancia B-S de 1.782(6) Å, que sugiere cierto carácter de doble enlace. Esta es sólo 0.03 Å más larga que la distancia B-S encontrada en el complejo de manganeso $Mn(\eta^5\text{-}C_5H_5)\{S=B(^tBu)IMe\}(CO)_2$ (IMe = 1,3-dimetilimidazolilideno; 1.747(3) Å)[189] y en los tioxoboranos $S=B\{\kappa^2\text{-}N,N\text{-}[N(2,6\text{-}Me_2C_6H_3)C(Me)CHC(Me)N(2,6\text{-}Me_2C_6H_3)]\}$ (1.741(2) Å)[190] y $S=B\{\kappa^2\text{-}N,N\text{-}[N(2,4,6\text{-}Me_3C_6H_2)P(Ph)_2NP(Ph)_2N(2,4,6\text{-}Me_3C_6H_2)]\}$ (1.752(5) Å)[191] y alrededor de 0.07 Å más larga que la longitud de enlace S=B encontrada en el catión $S=B\{\kappa^2\text{-}N,N\text{-}[N(L^{Mes})CH_2CH_2N(L^{Mes})]\}^+$ (L^{Mes} = 1,3-dimesitilimidazolinilideno; 1.710(5) Å);[192] especies que se han descrito como las primeras con un enlace doble B=S. Los anillos de tres miembros de **3** y **4** recuerdan al intermedio recientemente propuesto por Braunschweig y colaboradores para la reacción del complejo alquilborileno $Mn(\eta^5\text{-}C_5H_5)(=B^tBu)(CO)_2$ con $SPPh_3$, que proporciona el producto de metátesis $Mn(\eta^5\text{-}C_5H_5)(CO)_2(PPh_3)$. Este trabajo sugiere que el intermedio de la reacción es un derivado $\kappa^2\text{-}S,B\text{-}[SB^tBu]$.[193]

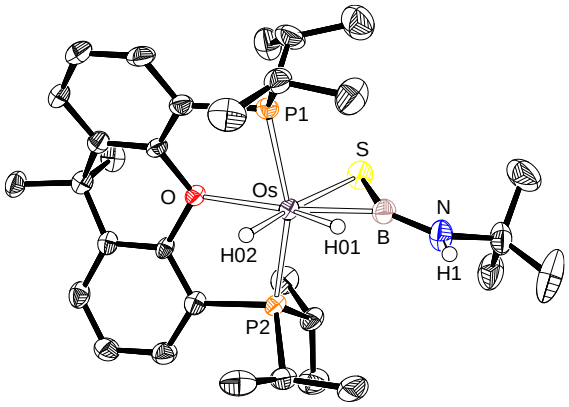

Figura 2. Diagrama molecular del complejo **3**.

La situación de enlace en el anillo de tres miembros del complejo **3** se estudió mediante cálculos DFT (BP86-D3/def2-TZVPP). El índice de Wiberg para el enlace B-S de 1.40 y la forma de los HOMO-7 y HOMO-8 apoyan un cierto carácter de doble enlace. Estos orbitales, que se extienden hasta el par no compartido del átomo de nitrógeno del grupo amino-borano, son orbitales moleculares π deslocalizados sobre el anillo de tres miembros (figura 3). El carácter múltiple del enlace B-S deriva de la deslocalización del par no compartido del átomo de S en el orbital atómico p_z vacío del átomo de B (energía de perturbación de segundo orden asociada de -55.7 kcal·mol^{-1}). Además, el método NBO también encuentra una deslocalización significativa de un orbital atómico doblemente ocupado d_π(Os) en el orbital vacante p_z(B) (energía asociada de -21.3 kcal·mol^{-1}), lo que es totalmente consistente con la figura 3.

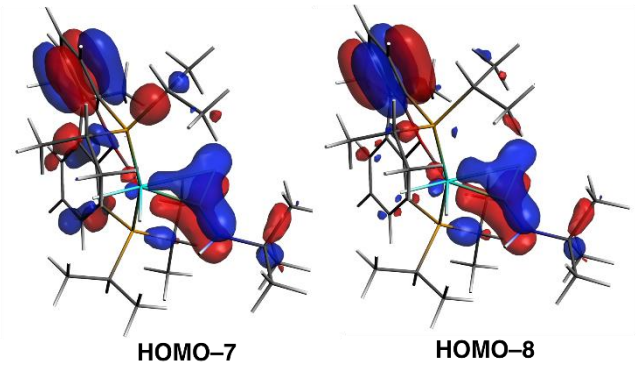

Figura 3. Orbitales moleculares π calculados deslocalizados en el metalaciclo Os-S-B del complejo **3** (valor de isosuperficie 0.04 a.u.).

Estos hallazgos son consistentes con un sistema aromático de tipo Hückel 4*n* + 2 en el que n = 0 y donde los dos electrones π del anillo provienen del átomo de S. Con el objetivo de confirmar la aromaticidad del novedoso anillo de tres miembros Os-S-B, se calcularon los valores de *cambio de desplazamiento químico independiente del núcleo* (NICS) en el centro del anillo. El valor negativo encontrado del NICS(0) = -32.1 ppm apoya, a primera vista, la naturaleza aromática del metalaciclo. No obstante, valores isotrópicos de los NICS, particularmente en anillos pequeños, están generalmente contaminados por los efectos de protección local de los enlaces cercanos y, por lo tanto, no siempre son fiables.[183a] Esta situación es aún más importante cuando un metal de transición forma parte del anillo.[175c] Por esta razón, también se calculó la contribución del tensor fuera del plano al valor de los NICS 1 Å por encima y por debajo del centro del anillo.[194] Los valores negativos obtenidos, $NICS(1)_{zz}$ = -17.9 y -18.4 ppm, confirman la naturaleza aromática del metalaciclo Os-S-B. Además, se aplicó el método de *anisotropía de la densidad de corriente inducida* (ACID)[195] para visualizar la corriente del anillo aromático en el metalaciclo. El método ACID, calculado para un sistema modelo donde los grupos voluminosos isopropilo y *terc*-butilo se reemplazaron por átomos de H ($NICS(1)_{zz}$ = -15.9 ppm), muestra claramente la aparición de una corriente de anillo diatrópica (vectores

en el sentido de las agujas del reloj) dentro del anillo de tres miembros, lo que confirma la naturaleza aromática de este novedoso metalaciclo (figura 4).

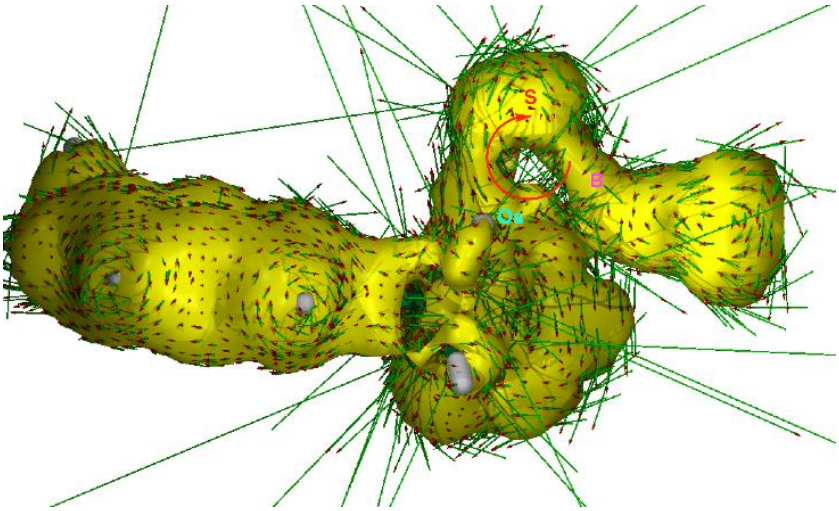

Figura 4. Gráfico ACID para el compuesto modelo $OsH_2\{\kappa^2\text{-}S,B\text{-}[SBNH_2]\{xant(PH_2)_2\}$ con un valor de 0.4 a.u. de isosuperficie.

Los descriptores energéticos apoyan el carácter aromático de los complejos **3** y **4**. Sin embargo, la aplicación de los métodos energéticos típicamente utilizados en otros compuestos aromáticos (métodos ASE o ISE),[175c] incluidos aquellos que tienen metales de transición en sus estructuras, no es posible para estas especies. Por ello, se llevaron a cabo dos reacciones isodésmicas alternativas, a saber, la hidrogenación y la eliminación reductora, representadas en el esquema 2. Para ambas reacciones, se calcula que la escisión del anillo de tres miembros es endotérmica, lo que es totalmente consistente con la estabilidad termodinámica (debido a la aromaticidad) del metalaciclo.

Esquema 2. Reacciones Isodésmicas Calculadas para el Complejo 3

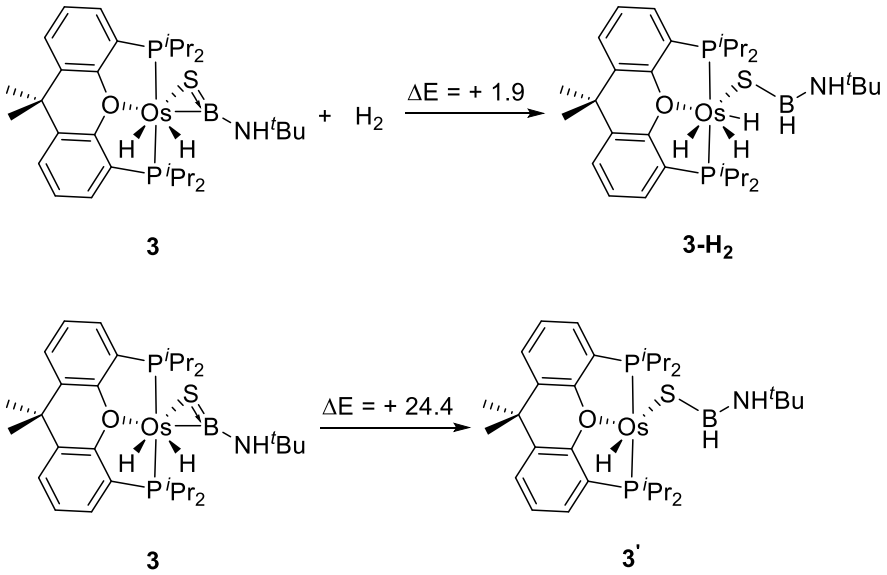

3 **3-H$_2$**

3 **3'**

[a]Las energías, en kcal·mol^{-1}, se calcularon en el Nivel BP86-D3/def2-TZVPP.

CONCLUSIONES

La unión de un fragmento metálico de 16 electrones de valencia L_5Os^{IV}, un átomo de S y una unidad B-NR_2 da lugar a anillos π-aromáticos de tres miembros, que están formados por diferentes vértices y representan una novedosa manifestación de la aromaticidad de tipo Hückel 4*n* + 2 en el que *n* = 0. Estos compuestos cicloosmatioborano se forman tras la deshidrogenación simultánea de un complejo trihidruro hidrogenosulfuro de osmio(IV) y un amina-borano BH_3NHR_2.

M.5. CONCLUSIONES GENERALES

Este estudio ha revelado que los polihidruros estabilizados por el fragmento metálico Os{xant(P^iPr_2)$_2$} añaden H^+ y H^- para generar H_2 de manera cíclica, catalizan la descomposición de ácido fórmico a H_2 y CO_2, coordinan el enlace B-H de boranos, estabilizan complejos boróxido y, cuando el centro metálico tiene 16 electrones de valencia, se ensamblan con un átomo de azufre y una unidad B-NR_2 para dar anillos aromáticos de tres miembros distintos.

La flexibilidad de la difosfina juega un papel fundamental en esta riqueza de funciones, al cambiar su modo de coordinación de κ^3-*mer* a κ^3-*fac* y κ^2-*P*,*P*, para adaptar el fragmento metálico a las necesidades electrónicas y al requerimiento espacial que demandan las especies implicadas en cada proceso particular. Así, hemos demostrado, por ejemplo, que las interacciones no clásicas entre los átomos de hidrógeno coordinados al centro metálico se favorecen con una disposición κ^3-*mer* de la difosfina, mientras que la coordinación κ^2-*P*,*P* parece generar polihidruros clásicos.

Otros ligandos, como cloruro, hidróxido o hidrogenosulfuro, también han jugado un papel determinante en casos particulares. El ligando cloruro incrementa la fortaleza entre el enlace B-H de los boranos y el átomo de osmio en los complejos σ-boranos descubiertos; su electronegatividad favorece la cesión de densidad electrónica del orbital σ-(B-H) del borano al átomo de osmio, mientras que su poder π-dador estimula la retrodonación desde los orbitales *d* del metal al orbital σ*(B-H) del borano. El ligando hidróxido, además de estabilizar el primer precursor catalítico de osmio para la descomposición de ácido fórmico a H_2 y CO_2, genera un hidroxiácido con el metal que nos ha permitido diseñar un camino sintético original para preparar y aislar los primeros complejos boróxido de un

metal del grupo del platino. El procedimiento se basa en el desplazamiento del grupo amino de amino-boranos $R_2B\text{-}NR'_2$ por la base conjugada del hidroxiácido, es consecuencia de la nucleofilia del átomo de oxígeno y la electrofilia del átomo de hidrógeno y tiene su razón termodinámica en la mayor energía de disociación de los enlaces B-O respecto a los enlaces B-N en especies de boro tricoordinadas. Estos polihidruros son estables frente a la eliminación reductora del ácido borónico. El ligando hidrogenosulfuro es el precursor de un vértice de los triángulos aromáticos descubiertos, donde el átomo de azufre aporta los dos electrones necesarios para que los cicloosmatioboranos cumplan la regla $4n + 2$ ($n = 0$) en otra original manifestación de la aromaticidad de Hückel.

Finalmente, debe señalarse que de las dos etapas que forman el ciclo catalítico para la descomposición de ácido fórmico, formación de H_2 y formación de CO_2, esta última es la que determina la velocidad del proceso, de acuerdo con los resultados del estudio cinético de la catálisis, del estudio cinético del paso estequiométrico clave y de los cálculos DFT llevados a cabo. Los cálculos sugieren, además, que el deslizamiento del centro metálico desde el átomo de oxígeno al átomo de hidrógeno de un ligando formiato coordinado es la reacción elemental de mayor energía de activación y, por tanto, la determinante de la velocidad de la etapa de formación de CO_2.

En resumen, queda demostrada una vez más la riqueza de la química de los complejos polihidruro de metales del grupo del platino, en particular la de los compuestos de osmio de esta clase, y su relevancia para el desarrollo de la tecnología del hidrógeno.

REFERENCIAS

(1) (a) Panwar, N. L.; Kaushik, S. C.; Kothari, S. Role of Renewable Energy Sources in Environmental Protection: A Review. *Renew. Sust. Energ. Rev.* **2011**, *15*, 1513-1524. (b) Moran, E. F.; Lopez, M. C.; Moore, N.; Müller, N.; Hyndman, D. W. Sustainable Hydropower in the 21st Century. *Proc. Natl. Acad. Sci. USA* **2018**, *115*, 11891-11898.

(2) Bockris, J. O. M. Hydrogen Economy. *Science* **1972**, *176*, 1323.

(3) Turner, J. A. Sustainable Hydrogen Production. *Science* **2004**, *305*, 972-974.

(4) Schlapbach, L.; Züttel, A. Hydrogen-Storage Materials for Mobile Applications. *Nature* **2001**, *414*, 353-358.

(5) Chamoun, R.; Demirci, U. B.; Miele, P. Cyclic Dehydrogenation-(Re)Hydrogenation with Hydrogen-Storage Materials: An Overview. *Energy Technol.* **2015**, *3*, 100-117.

(6) (a) Rossin, A.; Peruzzini, M. Ammonia-Borane and Amine-Borane Dehydrogenation Mediated by Complex Metal Hydrides. *Chem. Rev.* **2016**, *116*, 8848-8872. (b) Bhunya, S.; Malakar, T.; Ganguly, G.; Paul, A. Combining Protons and Hydrides by Homogeneous Catalysis for Controlling the Release of Hydrogen from Ammonia-Borane: Present Status and Challenges. *ACS Catal.* **2016**, *6*, 7907-7934.

(7) Aakko-Saksa, P. T.; Cook, C.; Kiviaho, J.; Repo, T. Liquid Organic Hydrogen Carriers for Transportation and Storing of Renewable Energy - Review and Discussion. *J. Power Sources* **2018**, *396*, 803-823.

(8) Crabtree, R. H. Hydrogen Storage in Liquid Organic Heterocycles. *Energy Environ. Sci.* **2008**, *1*, 134-138.

(9) Sordakis, K.; Tang, C. H.; Vogt, L. K.; Junge, H.; Dyson, P. J.; Beller, M.; Laurenczy, G. Homogeneous Catalysis for Sustainable Hydrogen Storage in Formic Acid and Alcohols. *Chem. Rev.* **2018**, *118*, 372-433.

(10) Gianotti, E.; Taillades-Jacquin, M.; Rozière, J.; Jones, D. J. High-Purity Hydrogen Generation via Dehydrogenation of Organic Carriers: A Review on the Catalytic Process. *ACS Catal.* **2018**, *8*, 4660-4680.

(11) Blaser, H. U.; Malan, C.; Pugin, B.; Spindler, F.; Steiner, H.; Studer, M. Selective Hydrogenation for Fine Chemicals: Recent Trends and New Developments. *Adv. Synth. Catal.* **2003**, *345*, 103-151.

(12) (a) Nixon, T. D.; Whittlesey, M. K.; Williams, J. M. J. Transition Metal Catalysed Reactions of Alcohols Using Borrowing Hydrogen Methodology. *Dalton Trans.* **2009**, 753-762. (b) Guillena, G.; Ramón, D. J.; Yus, M. Hydrogen Autotransfer in the N-Alkylation of Amines and Related Compounds using Alcohols and Amines as Electrophiles. *Chem. Rev.* **2010**, *110*, 1611-1641. (c) Corma, A.; Navas, J.; Sabater, M. J. Advances in One-Pot Synthesis through Borrowing Hydrogen Catalysis. *Chem. Rev.* **2018**, *118*, 1410-1459.

(13) (a) Kolb, H. C.; VanNieuwenhze, M. S.; Sharpless, K. B. Catalytic Asymmetric Dihydroxylation. *Chem. Rev.* **1994**, *94*, 2483-2547. (b) Döbler, C.; Mehltretter, G. M.; Sundermeier, U.; Beller, M. Osmium-Catalyzed Dihydroxylation of Olefins Using Dioxygen or Air as the Terminal Oxidant. *J. Am. Chem. Soc.* **2000**, *122*, 10289-10297. (c) Döbler, C.; Mehltretter, G. M.; Sundermeier, U.; Beller, M. Dihydroxylation of Olefins Using Air as the Terminal Oxidant. *J. Organomet. Chem.* **2001**, *621*, 70-76. (d) Heravi, M. M.; Zadsirjan, V.; Esfandyari, M.; Lashaki, T. B. Applications of Sharpless Asymmetric Dihydroxylation in the Total Synthesis of Natural Products. *Tetrahedron: Asymmetry* **2017**, *28*, 987-1043.

(14) (a) Sánchez-Delgado, R. A.; Rosales, M.; Esteruelas, M. A.; Oro, L. A. Homogeneous Catalysis by Osmium Complexes. A Review. *J. Mol. Catal. A: Chem.* **1995**, *96*, 231-243. (b) Esteruelas, M. A.; Herrero, J.; López, A. M.; Oliván, M. Alkyne-Coupling Reactions Catalyzed by $OsHCl(CO)(P^iPr_3)_2$ in the Presence of Diethylamine. *Organometallics* **2001**, *20*, 3202-3205. (c) Castarlenas, R.; Esteruelas, M. A.; Oñate, E. N-Heterocyclic Carbene-Osmium Complexes for Olefin Metathesis Reactions. *Organometallics* **2005**, *24*, 4343-4346. (d) Esteruelas, M. A.; García-Yebra, C.; Oliván, M.; Oñate, E.; Valencia, M. Osmium-Catalyzed Allylic Alkylation. *Organometallics* **2008**, *27*, 4892-4902. (e) Batuecas, M.; Esteruelas, M. A.; García-Yebra, C.; Oñate, E. Redox Isomerization of Allylic Alcohols Catalyzed by Osmium and Ruthenium Complexes Containing a Cyclopentadienyl Ligand with a Pendant Amine or Phosphoramidite Group: X-ray Structure of an η^3-1-Hydroxyallyl-Metal-Hydride Intermediate. *Organometallics* **2010**, *29*, 2166-2175. (f) Varela-Fernández, A.; García-Yebra, C.; Varela, J. A.; Esteruelas, M. A.; Saá, C. Osmium-Catalyzed 7-*endo* Heterocyclization of Aromatic Alkynols into Benzoxepines. *Angew. Chem., Int. Ed.* **2010**, *49*, 4278-4281. (g) Álvarez-Pérez, A.; González-Rodríguez, C.; García-Yebra, C.; Varela, J. A.; Oñate, E.; Esteruelas, M. A.; Saá, C. Catalytic Cyclization of *o*-Alkynyl Phenethylamines via Osmacyclopropene Intermediates: Direct Access to Dopaminergic 3-Benzazepines. *Angew. Chem., Int. Ed.* **2015**, *54*, 13357-13361. (h) Wu, L. P.; Liu, Q.; Spannenberg, A.; Jackstell, R.; Beller, M. Highly Regioselective Osmium-Catalyzed Hydroformylation. *Chem. Commun.* **2015**, *51*, 3080-3082. (i) Batuecas, M.; Castro-Rodrigo, R.; Esteruelas, M. A.; García-Yebra, C.; López, A. M.; Oñate, E. Aromatic Osmacyclopropenefuran Bicycles and Their Relevance for the Metal-Mediated Hydration of Functionalized Allenes. *Angew. Chem., Int. Ed.* **2016**, *55*, 13749-13753. (j) González-Fernández, R.; Crochet, P.; Cadierno, V.; Menéndez, M. I.; López, R. Phosphinous Acid-Assisted Hydration of Nitriles: Understanding the Controversial Reactivity of Osmium and Ruthenium Catalysts. *Chem. - Eur. J.* **2017**, *23*, 15210-15221.

(15) (a) Barrio, P.; Esteruelas, M. A.; Oñate, E. Reactions of a Hexahydride-Osmium Complex with Aldehydes: Double C-H_α Activation-Decarbonylation and Single C-H_α Activation-Hydroxylation Tandem Processes and Catalytic Tishchenko Reactions. *Organometallics* **2004**, *23*, 1340-1348. (b) Chelucci, G.; Baldino, S.; Baratta, W. Ruthenium and Osmium Complexes Containing 2-(aminomethyl)pyridine (Ampy)-Based Ligands in Catalysis. *Coord. Chem. Rev.* **2015**, *300*, 29-85. (c) Chelucci, G.; Baldino, S.; Baratta, W. Recent Advances in Osmium-Catalyzed Hydrogenation and Dehydrogenation Reactions. *Acc. Chem. Res.* **2015**, *48*, 363-379. (d) Chelucci, G. Ruthenium and Osmium Complexes in C-C Bond-Forming Reactions by Borrowing Hydrogen Catalysis. *Coord. Chem. Rev.* **2017**, *331*, 1-36.

(16) Buil, M. L.; Elipe, S.; Esteruelas, M. A.; Oñate, E.; Peinado, E.; Ruiz, N. Five-Coordinate Complexes $MHCl(CO)(P^iPr_3)_2$ (M = Os, Ru) as Precursors for the Preparation of New Hydrido−

and Alkenyl−Metallothiol and Monothio−*β*-Diketonato Derivatives. *Organometallics* **1997**, *16*, 5748-5755.

(17) Esteruelas, M. A.; Fernández, I.; López, A. M.; Mora, M.; Oñate, E. Osmium-Promoted Dehydrogenation of Amine-Boranes and B-H Bond Activation of the Resulting Amino-Boranes. *Organometallics* **2014**, *33*, 1104-1107.

(18) Albéniz, M. J.; Buil, M. L.; Esteruelas, M. A.; López, A. M.; Oro, L. A.; Zeier, B. Synthesis and Protonation of the Dithioformato Complex $OsH(\eta^2\text{-}S_2CH)(CO)(P^iPr_3)_2$. *Organometallics* **1994**, *13*, 3746-3748.

(19) Esteruelas, M. A.; López, A. M.; Mora, M.; Oñate, E. Ammonia-Borane Dehydrogenation Promoted by an Osmium Dihydride Complex: Kinetics and Mechanism. *ACS Catal.* **2015**, *5*, 187-191.

(20) Werner, H.; Esteruelas, M. A.; Meyer, U.; Wrackmeyer, B. (η^2-Tetrahydroborato)Ruthenium(II) and Osmium(II) Complexes with Fluxional Structure. *Chem. Ber.* **1987**, *120*, 11-15.

(21) Gusev, D. G.; Kuhlman, R. L.; Renkema, K. B.; Eisenstein, O.; Caulton, K. G. Structure and H_2-Loss Energies of $OsHX(H2)(CO)L_2$ Complexes (L = $P(^tBu)_2Me$, $P(^iPr)_3$; X = Cl, I, H): Attempted Correlation of ^1J(H−D), T_1min, and $\Delta G^{\ddagger}$. *Inorg. Chem.* **1996**, *35*, 6775-6783.

(22) (a) Paul, A.; Musgrave, C. B. Catalyzed Dehydrogenation of Ammonia-Borane by Iridium Dihydrogen Pincer Complex Differs from Ethane Dehydrogenation. *Angew. Chem., Int. Ed.* **2007**, *46*, 8153-8156. (b) Yang, X. Z.; Hall, M. B. The Catalytic Dehydrogenation of Ammonia-Borane Involving an Unexpected Hydrogen Transfer to Ligated Carbene and Subsequent Carbon-Hydrogen Activation. *J. Am. Chem. Soc.* **2008**, *130*, 1798-1799.

(23) Waterman, R. Mechanisms of Metal-Catalyzed Dehydrocoupling Reactions. *Chem. Soc. Rev.* **2013**, *42*, 5629-5641.

(24) Malakar, T.; Roy, L.; Paul, A. The Role of Solvent and of Species Generated in Situ on the Kinetic Acceleration of Aminoborane Oligomerization. *Chem. - Eur. J.* **2013**, *19*, 5812-5817.

(25) Bolaño, T.; Esteruelas, M. A.; Gay, M. P.; Oñate, E.; Pastor, I. M.; Yus, M. An Acyl-NHC Osmium Cooperative System: Coordination of Small Molecules and Heterolytic B-H and O-H Bond Activation. *Organometallics* **2015**, *34*, 3902-3908.

(26) (a) Friedrich, A.; Schneider, S. Acceptorless Dehydrogenation of Alcohols: Perspectives for Synthesis and H_2 Storage. *ChemCatChem* **2009**, *1*, 72-73. (b) Trincado, M.; Banerjee, D.; Grützmacher, H. Molecular Catalysts for Hydrogen Production from Alcohols. *Energy Environ. Sci.* **2014**, *7*, 2464-2503.

(27) Gunanathan, C.; Milstein, D. Applications of Acceptorless Dehydrogenation and Related Transformations in Chemical Synthesis. *Science* **2013**, *341*, 249.

(28) Crabtree, R. H. Homogeneous Transition Metal Catalysis of Acceptorless Dehydrogenative Alcohol Oxidation: Applications in Hydrogen Storage and to Heterocycle Synthesis. *Chem. Rev.* **2017**, *117*, 9228-9246.

(29) Baratta, W.; Bossi, G.; Putignano, E.; Rigo, P. Pincer and Diamine Ru and Os Diphosphane Complexes as Efficient Catalysts for the Dehydrogenation of Alcohols to Ketones. *Chem. - Eur. J.* **2011**, *17*, 3474-3481.

(30) Putignano, E.; Bossi, G.; Rigo, P.; Baratta, W. MCl_2(ampy)(dppf) (M = Ru, Os): Multitasking Catalysts for Carbonyl Compound/Alcohol Interconversion Reactions. *Organometallics* **2012**, *31*, 1133-1142.

(31) Buil, M. L.; Esteruelas, M. A.; Gay, M. P.; Gómez-Gallego, M.; Nicasio, A. I.; Oñate, E.; Santiago, A.; Sierra, M. A. Osmium Catalysts for Acceptorless and Base-Free Dehydrogenation of Alcohols and Amines: Unusual Coordination Modes of a BPI Anion. *Organometallics* **2018**, *37*, 603-617.

(32) (a) Bertoli, M.; Chouale, A.; Gusev, D. G.; Lough, A. J.; Major, Q.; Moore, B. PNP Pincer Osmium Polyhydrides for Catalytic Dehydrogenation of Primary Alcohols. *Dalton Trans.* **2011**, *40*, 8941-8949. (b) Bertoli, M.; Choualeb, A.; Lough, A. J.; Moore, B.; Spasyuk, D.; Gusev, D. G. Osmium and Ruthenium Catalysts for Dehydrogenation of Alcohols. *Organometallics* **2011**, *30*, 3479-3482. (c) Spasyuk, D.; Gusev, D. G. Acceptorless Dehydrogenative Coupling of Ethanol and Hydrogenation of Esters and Imines. *Organometallics* **2012**, *31*, 5239-5242. (d) Spasyuk, D.; Smith, S.; Gusev, D. G. From Esters to Alcohols and Back with Ruthenium and Osmium Catalysts. *Angew. Chem., Int. Ed.* **2012**, *51*, 2772-2775. (e) Spasyuk, D.; Vicent, C.; Gusev, D. G. Chemoselective Hydrogenation of Carbonyl Compounds and Acceptorless Dehydrogenative Coupling of Alcohols. *J. Am. Chem. Soc.* **2015**, *137*, 3743-3746. (f) Gusev, D. G. Dehydrogenative Coupling of Ethanol and Ester Hydrogenation Catalyzed by Pincer-Type YNP Complexes. *ACS Catal.* **2016**, *6*, 6967-6981.

(33) Pez, G. P.; Scott, A.; Cooper A.; Cheng, H. US Pat., 7101530, 2006.

(34) Gruver, B. C.; Adams, J. J.; Arulsamy, N.; Roddick, D. M. Acceptor Pincer Chemistry of Osmium: Catalytic Alkane Dehydrogenation by (^{CF3}PCP)Os(cod)(H). *Organometallics* **2013**, *32*, 6468-6475.

(35) Esteruelas, M. A.; Lezáun, V.; Martínez, A.; Oliván, M.; Oñate, E. Osmium Hydride Acetylacetonate Complexes and Their Application in Acceptorless Dehydrogenative Coupling of Alcohols and Amines and for the Dehydrogenation of Cyclic Amines. *Organometallics* **2017**, *36*, 2996-3004.

(36) Gunanathan, C.; Milstein, D. Metal-Ligand Cooperation by Aromatization-Dearomatization: A New Paradigm in Bond Activation and "Green" Catalysis. *Acc. Chem. Res.* **2011**, *44*, 588-602.

(37) Gusev, D. G. Rethinking the Dehydrogenative Amide Synthesis. *ACS Catal.* **2017**, *7*, 6656-6662.

(38) (a) Dub, P. A.; Henson, N. J.; Martin, R. L.; Gordon, J. C. Unravelling the Mechanism of the Asymmetric Hydrogenation of Acetophenone by [RuX_2(diphosphine)(1,2-diamine)] Catalysts. *J. Am. Chem. Soc.* **2014**, *136*, 3505-3521. (b) Dub, P. A.; Gordon, J. C. Metal Ligand Bifunctional Catalysis: The "Accepted" Mechanism, the Issue of Concertedness, and the Function of the Ligand in Catalytic Cycles Involving Hydrogen Atoms. *ACS Catal.* **2017**, *7*, 6635-6655.

(39) Esteruelas, M. A.; Honczek, N.; Oliván, M.; Oñate, E.; Valencia, M. Direct Access to POP-Type Osmium(II) and Osmium(IV) Complexes: Osmium a Promising Alternative to Ruthenium for the Synthesis of Imines from Alcohols and Amines. *Organometallics* **2011**, *30*, 2468-2471.

(40) Gnanaprakasam, B.; Zhang, J.; Milstein, D. Direct Synthesis of Imines from Alcohols and Amines with Liberation of H_2. *Angew. Chem., Int. Ed.* **2010**, *49*, 1468-1471.

(41) Castarlenas, R.; Esteruelas, M. A.; Oñate, E. Preparation, X-ray Structure, and Reactivity of an Osmium-Hydroxo Complex Stabilized by an N-Heterocyclic Carbene Ligand: A Base-Free Catalytic Precursor for Hydrogen Transfer from 2-Propanol to Aldehydes. *Organometallics* **2008**, *27*, 3240-3247.

(42) Buil, M. L.; Esteruelas, M. A.; Herrero, J.; Izquierdo, S.; Pastor, I. M.; Yus, M. Osmium Catalyst for the Borrowing Hydrogen Methodology: α-Alkylation of Arylacetonitriles and Methyl Ketones. *ACS Catal.* **2013**, *3*, 2072-2075.

(43) (a) Moulton, C. J.; Shaw, B. L. Transition Metal-Carbon Bonds. Part XLII. Complexes of Nickel, Palladium, Platinum, Rhodium and Iridium with the Tridentate Ligand 2,6-Bis[(Di-T-Butylphosphino)Methyl]Phenyl. *J. Chem. Soc., Dalton Trans.* **1976**, 1020-1024. (b) van Koten, G.; Timmer, K.; Noltes, J. G.; Spek, A. L. A Novel Type of Pt-C Interaction and a Model for the Final Stage in Reductive Elimination Processes Involving C-C Coupling at Pt; Synthesis and Molecular-Geometry of [1,*N*,*N*'-η-2,6-Bis{Dimethylamino)Methyl}-Toluene]Iodoplatinum(II) Tetrafluoroborate. *J. Chem. Soc., Chem. Comm.* **1978**, 250-252.

(44) van Koten, G. Tuning the Reactivity of Metals Held in a Rigid Ligand Environment. *Pure Appl Chem* **1989**, *61*, 1681-1694.

(45) Peris, E.; Crabtree, R. H. Key Factors in Pincer Ligand Design. *Chem. Soc. Rev.* **2018**, *47*, 1959-1968.

(46) Gunanathan, C.; Milstein, D. Bond Activation and Catalysis by Ruthenium Pincer Complexes. *Chem. Rev.* **2014**, *114*, 12024-12087.

(47) (a) Choi, J.; MacArthur, A. H. R.; Brookhart, M.; Goldman, A. S. Dehydrogenation and Related Reactions Catalyzed by Iridium Pincer Complexes. *Chem. Rev.* **2011**, *111*, 1761-1779. (b) Kumar, A.; Bhatti, T. M.; Goldman, A. S. Dehydrogenation of Alkanes and Aliphatic Groups by Pincer-Ligated Metal Complexes. *Chem. Rev.* **2017**, *117*, 12357-12384. (c) Alig, L.; Fritz, M.; Schneider, S. First-Row Transition Metal (De)Hydrogenation Catalysis Based On Functional Pincer Ligands. *Chem. Rev.* **2019**, *119*, 2681-2751.

(48) Gunanathan, C.; Gnanaprakasam, B.; Iron, M. A.; Shimon, L. J. W.; Milstein, D. "Long-Range" Metal-Ligand Cooperation in H_2 Activation and Ammonia-Promoted Hydride Transfer with a Ruthenium-Acridine Pincer Complex. *J. Am. Chem. Soc.* **2010**, *132*, 14763-14765.

(49) Suárez, E.; Plou, P.; Gusev, D. G.; Martín, M.; Sola, E. Cationic, Neutral, and Anionic Hydrides of Iridium with PSiP Pincers. *Inorg. Chem.* **2017**, *56*, 7190-7199.

(50) Pontiggia, A. J.; Chaplin, A. B.; Weller, A. S. Cationic Iridium Complexes of the Xantphos Ligand. Flexible Coordination Modes and the Isolation of the Hydride Insertion Product with an Alkene. *J. Organomet. Chem.* **2011**, *696*, 2870-2876.

(51) Younus, H. A.; Ahmad, N.; Su, W.; Verpoort, F. Ruthenium Pincer Complexes: Ligand Design and Complex Synthesis. *Coord. Chem. Rev.* **2014**, *276*, 112-152.

(52) (a) Albrecht, M.; van Koten, G. Platinum Group Organometallics Based on "Pincer" Complexes: Sensors, Switches, and Catalysts. *Angew. Chem., Int. Ed.* **2001**, *40*, 3750-3781. (b) Valdés, H.; García-Eleno, M. A.; Canseco-González, D.; Morales-Morales, D. Recent Advances in Catalysis with Transition-Metal Pincer Compounds. *ChemCatChem* **2018**, *10*, 3136-3172. (c) *Pincer Compounds: Chemistry and Applications*, 1st Edition; Morales-Morales, D., Ed.; Elsevier: Amsterdam, 2018.

(53) (a) Wong, C.-Y.; Lai, L.-M.; Pat, P.-K.; Chung, L.-H. Osmium Complexes Containing N-Heterocyclic Carbene-Based C,N,C-Pincer Ligands. *Organometallics* **2010**, *29*, 2533-2539. (b) Chung, L.-H.; Cho, K.-S.; England, J.; Chan, S.-C.; Wieghardt, K.; Wong, C.-Y. Ruthenium(II) and Osmium(II) Complexes Bearing Bipyridine and the N-Heterocyclic Carbene-Based C^N^C Pincer Ligand: An Experimental and Density Functional Theory Study. *Inorg. Chem.* **2013**, *52*, 9885-9896.

(54) Castarlenas, R.; Esteruelas, M. A.; Oñate, E. Preparation of [C,N,O]-Pincer Osmium Complexes by Alkylidene Metathesis with a Methyl Group of 2,6-Diacetylpyridine. *Organometallics* **2007**, *26*, 3082-3084.

(55) (a) Sauvage, J. P.; Collin, J. P.; Chambron, J. C.; Guillerez, S.; Coudret, C.; Balzani, V.; Barigelletti, F.; De Cola, L.; Flamigni, L. Ruthenium(II) and Osmium(II) Bis(terpyridine) Complexes in Covalently-Linked Multicomponent Systems: Synthesis, Electrochemical Behavior, Absorption Spectra, and Photochemical and Photophysical Properties. *Chem. Rev.* **1994**, *94*, 993-1019. (b) Huynh, M. H. V.; Lee, D. G.; White, P. S.; Meyer, T. J. Intramolecular, Oxidatively Induced Substitution on a Coordinated Terpyridyl Ligand. *J. Am. Chem. Soc.* **1999**, *121*, 10446-10447. (c) Huynh, M. H. V.; White, P. S.; Meyer, T. J. Formation and O-Atom Reactivity of the Os(IV)−Sulfilimido and Os(IV)−Sulfoximido Complexes, *cis*-/*trans*-[OsIV(tpy)Cl_2($NSC_6H_3Me_2$)] and *cis*-/*trans*-[OsIV(tpy)Cl_2($NS(O)C_6H_3Me_2$)]. *J. Am. Chem. Soc.* **2001**, *123*, 9170-9171. (d) Huynh, M. H. V.; White, P. S.; John, K. D.; Meyer, T. J. Isolation and Characterization of the Osmium(V)–Imido Complex [OsV(Tp)Cl_2(NH)]. *Angew. Chem., Int. Ed.* **2001**, *40*, 4049-4051. (e) Encinas, S.; Flamigni, L.; Barigelletti, F.; Constable, E. C.; Housecroft, C. E.; Schofield, E. R.; Figgemeier, E.; Fenske, D.; Neuburger, M.; Vos, J. G.; Zehnder, M. Electronic Energy Transfer and Collection in Luminescent Molecular Rods Containing Ruthenium(II) and Osmium(II) 2,2′:6′,2″-Terpyridine Complexes Linked by Thiophene-2,5-diyl Spacers. *Chem. - Eur. J.* **2002**, *8*, 137-150. (f) Huynh, M. H. V.; Baker, R. T.; Morris, D. E.; White, P. S.; Meyer, T. J. [OsIII(tpy)(Cl)($NCCH_3$)(NSAr)]: Reversible Reduction of Acetonitrile by OsIII–Sulfilimido Complexes. *Angew. Chem., Int. Ed.* **2002**, *41*, 3870-3873. (g) Esteruelas, M. A.; Masamunt, A. B.; Oliván, M.; Oñate, E.; Valencia, M. Aromatic Diosmatricyclic Nitrogen-Containing Compounds. *J. Am. Chem. Soc.* **2008**, *130*, 11612-11613. (h) Vega, E.; Lastra, E.; Gamasa, M. P. Asymmetric Transfer Hydrogenation of Ketones Catalyzed by Enantiopure Osmium(II) Pybox Complexes. *Inorg. Chem.* **2013**, *52*, 6193-6198. (i) Boff, B.; Gaiddon, C.; Pfeffer, M. Cancer Cell Cytotoxicity of Cyclometalated Compounds Obtained with Osmium(II) Complexes. *Inorg. Chem.* **2013**, *52*, 2705-2715. (j) Menéndez-Pedregal, E.; Manteca, A.; Sánchez, J.; Díez, J.; Gamasa, M. P.; Lastra, E. Antimicrobial and Antitumor Activity of Enantiopure Pybox-Osmium Complexes. *Eur. J. Inorg. Chem.* **2015**, 1424-1432. (k) de Julián, E.; Fernández, N.; Díez, J.; Lastra, E.; Gamasa, M. P. Osmium(II)/R-Pybox vs Ruthenium(II)/R-

Pybox Complexes in the Catalytic Asymmetric Transfer Hydrogenation of Arylketones. *Mol. Catal.* **2018**, *456*, 75-86.

(56) (a) Jia, G. C.; Lee, H. M.; Williams, I. D.; Lau, C. P.; Chen, Y. Z. Synthesis, Characterization, and Acidity Properties of $[MCl(H_2)(L)(PMP)]BF_4$ (M=Ru, L=PPh_3, CO; M=Os, L=PPh_3; PMP=2,6-$(Ph_2PCH_2)_2C_5H_3N$). *Organometallics* **1997**, *16*, 3941-3949. (b) Liu, S. H.; Lo, S. T.; Wen, T. B.; Zhou, Z. Y.; Lau, C. P.; Jia, G. C. Preparation, Characterization, and Reactivity of an Osmium-Alkenyl Dihydrogen Complex. *Organometallics* **2001**, *20*, 667-672. (c) Acosta-Ramirez, A.; Bertoli, M.; Gusev, D. G.; Schlaf, M. Homogeneous Catalytic Hydrogenation of Long-Chain Esters by an Osmium Pincer Complex and its Potential Application in the Direct Conversion of Triglycerides into Fatty Alcohols. *Green Chem.* **2012**, *14*, 1178-1188.

(57) (a) Holscher, M.; Prechtl, M. H. G.; Leitner, W. Can $[M(H)_2(H_2)(PXP)]$ Pincer Complexes (M = Fe, Ru, Os; X = N, O, S) Serve as Catalyst Lead Structures for NH_3 Synthesis from N_2 and H_2? *Chem. - Eur. J.* **2007**, *13*, 6636-6643. (b) Asensio, G.; Cuenca, A. B.; Esteruelas, M. A.; Medio-Simón, M.; Oliván, M.; Valencia, M. Osmium(III) Complexes with POP Pincer Ligands: Preparation from Commercially Available $OsCl_3 \cdot 3H_2O$ and Their X-ray Structures. *Inorg. Chem.* **2010**, *49*, 8665-8667. (c) Alós, J.; Bolaño, T.; Esteruelas, M. A.; Oliván, M.; Oñate, E.; Valencia, M. POP-Pincer Osmium-Polyhydrides: Head-to-Head (*Z*)-Dimerization of Terminal Alkynes. *Inorg. Chem.* **2013**, *52*, 6199-6213. (d) Alós, J.; Bolaño, T.; Esteruelas, M. A.; Oliván, M.; Oñate, E.; Valencia, M. POP-Pincer Ruthenium Complexes: d^6 Counterparts of Osmium d^4 Species. *Inorg. Chem.* **2014**, *53*, 1195-1209. (e) Alós, J.; Esteruelas, M. A.; Oliván, M.; Oñate, E.; Puylaert, P. C-H Bond Activation Reactions in Ketones and Aldehydes Promoted by POP-Pincer Osmium and Ruthenium Complexes. *Organometallics* **2015**, *34*, 4908-4921.

(58) (a) Chung, L.-H.; Chan, S.-C.; Lee, W.-C.; Wong, C.-Y. Emissive Osmium(II) Complexes Supported by N-Heterocyclic Carbene-based C∧C∧C-Pincer Ligands and Aromatic Diimines. *Inorg. Chem.* **2012**, *51*, 8693-8703. (b) Alabau, R. G.; Eguillor, B.; Esler, J.; Esteruelas, M. A.; Oliván, M.; Oñate, E.; Tsai, J. Y.; Xia, C. J. CCC-Pincer-NHC Osmium Complexes: New Types of Blue-Green Emissive Neutral Compounds for Organic Light-Emitting Devices (OLEDs). *Organometallics* **2014**, *33*, 5582-5596. (c) Eguillor, B.; Esteruelas, M. A.; Lezáun, V.; Oliván, M.; Oñate, E.; Tsai, J.-Y.; Xia, C. A Capped Octahedral MHC6 Compound of a Platinum Group Metal. *Chem. - Eur. J.* **2016**, *22*, 9106-9110. (d) Alabau, R. G.; Esteruelas, M. A.; Oliván, M.; Oñate, E.; Palacios, A. U.; Tsai, J.-Y.; Xia, C. Osmium(II) Complexes Containing a Dianionic CCCC-Donor Tetradentate Ligand. *Organometallics* **2016**, *35*, 3981-3995.

(59) Casarrubios, L.; Esteruelas, M. A.; Larramona, C.; Muntaner, J. G.; Oñate, E.; Sierra, M. A. 2-Azetidinones as Precursors of Pincer Ligands: Preparation, Structure, and Spectroscopic Properties of CC'N-Osmium Complexes. *Inorg. Chem.* **2015**, *54*, 10998-11006.

(60) Alabau, R. G.; Esteruelas, M. A.; Oliván, M.; Oñate, E. Preparation of Phosphorescent Osmium(IV) Complexes with N,N′,C- and C,N,C′-Pincer Ligands. *Organometallics* **2017**, *36*, 1848-1859.

(61) Shao, J.-Y.; Zhong, Y.-W. Monometallic Osmium(II) Complexes with Bis(N-methylbenzimidazolyl)benzene or -pyridine: A Comparison Study with Ruthenium(II) Analogues. *Inorg. Chem.* **2013**, *52*, 6464-6472.

(62) (a) Das, C.; Peng, S. M.; Lee, G. H.; Goswami, S. Osmium(II) Complexes of 2-[(Arylamido)Phenylazo]Pyridines. New Examples of Deamination Reactions: X-ray Structure and Redox Properties. *New J. Chem.* **2002**, *26*, 222-228. (b) Chen, K.; Cheng, Y.-M.; Chi, Y.; Ho, M.-L.; Lai, C.-H.; Chou, P.-T.; Peng, S.-M.; Lee, G.-H. Osmium Complexes with Tridentate 6-Pyrazol-3-yl 2,2′-Bipyridine Ligands: Coarse Tuning of Phosphorescence from the Red to the Near-Infrared Region. *Chem. - Asian J.* **2007**, *2*, 155-163. (c) Samanta, S.; Singh, P.; Fiedler, J.; Zális, S.; Kaim, W.; Goswami, S. Singlet Diradical Complexes of Ruthenium and Osmium: Geometrical and Electronic Structures and their Unexpected Changes on Oxidation. *Inorg. Chem.* **2008**, *47*, 1625-1633. (d) Betley, T. A.; Qian, B. A.; Peters, J. C. Group VIII Coordination Chemistry of a Pincer-Type Bis(8-quinolinyl)amido Ligand. *Inorg. Chem.* **2008**, *47*, 11570-11582. (e) Chen, J.-L.; Chi, Y.; Chen, K.; Cheng, Y.-M.; Chung, M.-W.; Yu, Y.-C.; Lee, G.-H.; Chou, P.-T.; Shu, C.-F. New Series of Ruthenium(II) and Osmium(II) Complexes Showing Solid-State Phosphorescence in Far-Visible and Near-Infrared. *Inorg. Chem.* **2010**, *49*, 823-832. (f) Müller, A. L.; Wadepohl, H.; Gade, L. H. Bis(Pyridylimino)Isoindolato (BPI) Osmium Complexes: Structural Chemistry and Reactivity. *Organometallics* **2015**, *34*, 2810-2818.

(63) Santra, B. K.; Munshi, P.; Das, G.; Bharadwaj, P.; Lahiri, G. K. Osmium Mediated Selective Aromatic Thiolation Reaction in the Complexes [OsII{*o*-$SC_6H_3(R)N{=}NC_5H_4N$}$_2$]. Synthesis, Spectroscopic Characterization, Electron-Transfer Properties and Crystal Structure of the Complex where R=H. *Polyhedron* **1999**, *18*, 617-630.

(64) (a) Hoskins, S. V.; Rckard, C. E. F.; Roper, W. R. Electrophilic Addition of an Osminim-Bound Chloromethylene Ligand to the Benzene Ring of a Triphenylphosphine Ligand. Synthesis of Metallacyclic and Metallabicyclic Complexes. X-Ray Structures of [$OsCl(CO)_2$(*o*-$PPh_2C_6H_4CHCl$)(PPh_3)] and [$OsCl(CO)_2$(*o*-$PPh_2C_6H_4CHC_6H_4PPh_2$-*o*)]. *J. Chem. Soc., Chem. Comm.* **1984**, 1000-1002. (b) Wen, T. B.; Cheung, Y. K.; Yao, J.; Wong, W.-T.; Zhou, Z. Y.; Jia, G. Vinylidene and Carbyne Complexes Derived from the Reactions of $OsCl(PPh_3)$(PCP) (PCP = 2,6-$(PPh_2CH_2)_2C_6H_3$) with Terminal Acetylenes. *Organometallics* **2000**, *19*, 3803-3809. (c) Gusev, D. G.; Dolgushin, F. M.; Antipin, M. Y. Cyclometalated Osmium Complexes Containing a Tridentate PCP Ligand. *Organometallics* **2001**, *20*, 1001-1007. (d) Gauvin, R. M.; Rozenberg, H.; Shimon, L. J. W.; Milstein, D. Synthesis and Structure of New Osmium−PCP Complexes. Osmium-Mediated C−C Bond Activation. *Organometallics* **2001**, *20*, 1719-1724. (e) Gusev, D. G.; Maxwell, T.; Dolgushin, F. M.; Lyssenko, M.; Lough, A. J. Alkylidene and Vinylidene "Pincer" Complexes from Reactions of Alkynes with Ruthenium and Osmium Hydrides. *Organometallics* **2002**, *21*, 1095-1100. (f) Gusev, D. G.; Lough, A. J. Double C−H Activation on Osmium and Ruthenium Centers: Carbene vs Olefin Products. *Organometallics* **2002**, *21*, 2601-2603. (g) Liu, S. H.; Lo, S. T.; Wen, T. B.; Williams, I. D.; Zhou, Z. Y.; Lau, C. P.; Jia, G. Reactions of Hydrogen with Ruthenium and Osmium Complexes Containing Tridentate Ligands $Cy_2PCH_2CH(CH_2)_2PCy_2$ and 2,6-$(Ph_2PCH_2)_2C_6H_3$. *Inorg. Chim. Acta.* **2002**, *334*, 122-130. (h) Gusev, D. G.; Fontaine, F.-G.; Lough, A. J.; Zargarian, D. Polyhydrido(silylene)osmium and Silyl(dinitrogen)ruthenium Products Through Redistribution of Phenylsilane with Osmium and Ruthenium Pincer Complexes. *Angew. Chem., Int. Ed.* **2003**, *42*, 216-219. (i) Wen, T. B.; Zhou, Z. Y.; Jia, G. Coupling Reaction of Phenylacetylene with $OsH_n(PPh_3)$(2,6-$(PPh_2CH_2)_2C_6H_3$) (n = 1, 3). *Organometallics* **2003**, *22*, 4947-4951. (j) Wen, T. B.; Zhou, Z. Y.; Jia, G. Osmium-Mediated Hexamerization of Phenylacetylene. *Angew. Chem., Int. Ed.* **2006**, *45*, 5842-5846. (k) Kuznetsov, V. F.; Gusev, D. G. Chiral Hydride and Dihydrogen Pincer-Type Complexes of Osmium. *Organometallics* **2007**, *26*, 5661-5666. (l) Gauvin, R. M.; Rozenberg, H.; Shimon, L. J.

W.; Ben-David, Y.; Milstein, D. Osmium-Mediated C·H and C·C Bond Cleavage of a Phenolic Substrate: *p*-Quinone Methide and Methylene Arenium Pincer Complexes. *Chem. - Eur. J.* **2007**, *13*, 1382-1393.

(65) (a) Lee, J. H.; Pink, M.; Caulton, K. G. Triple Benzylic Dehydrogenation by Osmium in an Amide Ligand Environment. *Organometallics* **2006**, *25*, 802-804. (b) Lee, J. H.; Fan, H. J.; Pink, M.; Caulton, K. G. Reactivity of (NO)-N-Center Cot with an Osmium Polyhydride: Reductive Elimination and Reductive Nitrosylation on the Path from Odd- to Even-Electron Molecules. *New J. Chem.* **2007**, *31*, 838-840. (c) Lee, J. H.; Pink, M.; Tomaszewski, J.; Fan, H. J.; Caulton, K. G. Facile Hydrogenation of N_2O by an Operationally Unsaturated Osmium Polyhydride. *J. Am. Chem. Soc.* **2007**, *129*, 8706-8707. (d) Tsvetkov, N.; Pink, M.; Fan, H. J.; Lee, J. H.; Caulton, K. G. Redox and Lewis Acid Reactivity of Unsaturated Os-II. *Eur. J. Inorg. Chem.* **2010**, 4790-4800. (e) Tsvetkov, N.; Fan, H. J.; Caulton, K. G. An Evaluation of Monovalent Osmium Supported by the PNP Ligand Environment. *Dalton Trans.* **2011**, *40*, 1105-1110. (f) Schendzielorz, F. S.; Finger, M.; Volkmann, C.; Wurtele, C.; Schneider, S. A Terminal Osmium(IV) Nitride: Ammonia Formation and Ambiphilic Reactivity. *Angew. Chem., Int. Ed.* **2016**, *55*, 11417-11420.

(66) (a) Esteruelas, M. A.; Fernández, I.; Herrera, A.; Martín-Ortiz, M.; Martínez-Álvarez, R.; Oliván, M.; Oñate, E.; Sierra, M. A.; Valencia, M. Multiple C−H Bond Activation of Phenyl-Substituted Pyrimidines and Triazines Promoted by an Osmium Polyhydride: Formation of Osmapolycycles with Three, Five, and Eight Fused Rings. *Organometallics* **2010**, *29*, 976-986. (b) Esteruelas, M. A.; Fernández, I.; Gómez-Gallego, M.; Martín-Ortíz, M.; Molina, P.; Oliván, M.; Otón, F.; Sierra, M. A.; Valencia, M. Mono- and dinuclear osmium N,N′-di- and tetraphenylbipyridyls and extended bipyridyls. Synthesis, structure and electrochemistry. *Dalton Trans.* **2013**, *42*, 3597-3608. (c) Eguillor, B.; Esteruelas, M. A.; Lezáun, V.; Oliván, M.; Oñate, E. Elongated Dihydrogen versus Compressed Dihydride in Osmium Complexes. *Chem. - Eur. J.* **2017**, *23*, 1526-1530.

(67) (a) Baratta, W.; Ballico, M.; Chelucci, G.; Siega, K.; Rigo, P. Osmium(II) CNN Pincer Complexes as Efficient Catalysts for both Asymmetric Transfer and H_2 Hydrogenation of Ketones. *Angew. Chem., Int. Ed.* **2008**, *47*, 4362-4365. (b) Baratta, W.; Fanfoni, L.; Magnolia, S.; Siega, K.; Rigo, P. Benzo[h]quinoline Pincer Ruthenium and Osmium Catalysts for Hydrogenation of Ketones. *Eur. J. Inorg. Chem.* **2010**, *2010*, 1419-1423. (c) Bossi, G.; Putignano, E.; Rigo, P.; Baratta, W. Pincer Ru and Os Complexes as Efficient Catalysts for Racemization and Deuteration of Alcohols. *Dalton Trans.* **2011**, *40*, 8986-8995.

(68) (a) Majumder, K.; Peng, S. M.; Bhattacharya, S. Cyclometallation and N=N Bond Cleavage of 2-(Arylazo)Phenols by Osmium. Synthesis, Structure and Redox Properties. *J. Chem. Soc., Dalton Trans.* **2001**, 284-288. (b) Gupta, P.; Butcher, R. J.; Bhattacharya, S. Chemically Induced Cyclometalation of 2-(Arylazo)Phenols. Synthesis, Characterization, and Redox Properties of a Family of Organoosmium Complexes. *Inorg. Chem.* **2003**, *42*, 5405-5411. (c) Acharyya, R.; Peng, S. M.; Lee, G. H.; Bhattacharya, S. An Unprecedented Oxidative Migration of a Methyl Group from 2-(2 ',6 '-Dimethylphenylazo)-4-Methylphenol Mediated by Ruthenium and Osmium. *Inorg. Chem.* **2003**, *42*, 7378-7380.

(69) (a) Li, Z.-Y.; Yu, W.-Y.; Che, C.-M.; Poon, C.-K.; Wang, R.-J.; Mak, T. C. W. Oxo-, Nitrido- and Imido-Osmium(VI) Complexes with a Sterically Bulky Chelating Alkoxide Ligand. *J. Chem. Soc., Dalton Trans.* **1992**, 1657-1661. (b) Xiang, J.; Man, W.-L.; Yiu, S.-M.; Peng, S.-

M.; Lau, T.-C. Reaction of an Osmium(VI) Nitrido Complex with Cyanide: Formation and Reactivity of an Osmium(III) Hydrogen Cyanamide Complex. *Chem. - Eur. J.* **2011**, *17*, 13044-13051.

(70) Collins, T. J.; Lai, T.; Peake, G. T. A Novel Nonplanar Amido-N ligand Type. Nonplanarity in the Amido-N ligand Induced by Steric Effects. *Inorg. Chem.* **1987**, *26*, 1674-1677.

(71) Chou, P.-T.; Chi, Y. Osmium- and Ruthenium-Based Phosphorescent Materials: Design, Photophysics, and Utilization in OLED Fabrication. *Eur. J. Inorg. Chem.* **2006**, *2006*, 3319-3332.

(72) Baldo, M. A.; O'Brien, D. F.; You, Y.; Shoustikov, A.; Sibley, S.; Thompson, M. E.; Forrest, S. R. Highly Efficient Phosphorescent Emission from Organic Electroluminescent Devices. *Nature* **1998**, *395*, 151-154.

(73) Lu, C. W.; Wang, Y.; Chi, Y. Metal Complexes with Azolate-Functionalized Multidentate Ligands: Tactical Designs and Optoelectronic Applications. *Chem. - Eur. J.* **2016**, *22*, 17892-17908.

(74) Konkankit, C. C.; Marker, S. C.; Knopf, K. M.; Wilson, J. J. Anticancer Activity of Complexes of the Third Row Transition Metals, Rhenium, Osmium, and Iridium. *Dalton Trans.* **2018**, *47*, 9934-9974.

(75) Berger, G.; Grauwet, K.; Zhang, H.; Hussey, A. M.; Nowicki, M. O.; Wang, D. I.; Chiocca, E. A.; Lawler, S. E.; Lippard, S. J. Anticancer Activity of Osmium(VI) Nitrido Complexes in Patient-Derived Glioblastoma Initiating Cells and *in vivo* Mouse Models. *Cancer Lett.* **2018**, *416*, 138-148.

(76) Crabtree, R. H. *The Organometallic Chemistry of the Transition Metals*, 6th ed.; Wiley, 2014.

(77) Alcock, N. W.; Brown, J. M.; Jeffery, J. C. Structural and Chemical Aspects of Phosphino-Ethers as Chelating Ligands in Rhodium(I) Cationic Complexes. X-Ray Crystal-Structures of Two Phosphino-Ether Rhodium Carbonyl-Complexes. *J. Chem. Soc., Chem. Comm.* **1974**, 829-830.

(78) Kranenburg, M.; Vanderburgt, Y. E. M.; Kamer, P. C. J.; Van Leeuwen, P. W. N. M.; Goubitz, K.; Fraanje, J. New Diphosphine Ligands Based on Heterocyclic Aromatics Inducing Very High Regioselectivity in Rhodium-Catalyzed Hydroformylation: Effect of the Bite Angle. *Organometallics* **1995**, *14*, 3081-3089.

(79) Evans, I. P.; Spencer, A.; Wilkinson, G. Dichlorotetrakis(Dimethyl Sulphoxide)Ruthenium(II) and its Use as a Source Material for Some New Ruthenium(II) Complexes. *J. Chem. Soc., Dalton Trans.* **1973**, 204-209.

(80) Aracama, M.; Esteruelas, M. A.; Lahoz, F. J.; Lopez, J. A.; Meyer, U.; Oro, L. A.; Werner, H. Synthesis, Reactivity, Molecular-Structure, and Catalytic Activity of the Novel Dichlorodihydridoosmium(IV) Complexes $OsH_2Cl_2(PR_3)_2$ (PR_3 = P^iPr_3, PMe^tBu_2). *Inorg. Chem.* **1991**, *30*, 288-293.

(81) Pertici, P.; Vitulli, G.; Paci, M.; Porri, L. A New Synthetic Method for the Preparation of Cyclo-Olefin Ruthenium Complexes. *J. Chem. Soc., Dalton Trans.* **1980**, 1961-1964.

(82) Chaudret, B.; Poilblanc, R. Preparation of Polyhydride Complexes of Ruthenium by Direct Hydrogenation of Zerovalent Olefinic Derivatives. Mononuclear Complexes of the Type RuH_6I_2 and RuH_4I_3. Spontaneous H-D Exchange between the Phosphine Protons and the Solvent Catalyzed by RuH_4I_3. *Organometallics* **1985**, *4*, 1722-1726.

(83) (a) Esteruelas, M. A.; Oro, L. A. The Chemical and Catalytic Reactions of Hydrido-Chloro-Carbonylbis (Triisopropylphosphine)Osmium(II) and its Major Derivatives. *Adv. Organomet. Chem.* **2001**, *47*, 1-59. (b) Esteruelas, M. A.; López, A. M. C−C Coupling and C−H Bond Activation Reactions of Cyclopentadienyl−Osmium Compounds: The Rich and Varied Chemistry of $Os(\eta^5\text{-}C_5H_5)Cl(P^iPr_3)_2$ and Its Major Derivatives. *Organometallics* **2005**, *24*, 3584-3613. (c) Esteruelas, M. A.; López, A. M.; Oliván, M. Osmium–Carbon Double Bonds: Formation and Reactions. *Coord. Chem. Rev.* **2007**, *251*, 795-840. (d) Bolaño, T.; Esteruelas, M. A.; Oñate, E. Osmium–Carbon Multiple Bonds: Reduction and C–C Coupling Reactions. *J. Organomet. Chem.* **2011**, *696*, 3911-3923.

(84) Zhang, X. W.; Kanzelberger, M.; Emge, T. J.; Goldman, A. S. Selective Addition to Iridium of Aryl C-H Bonds *ortho* to Coordinating Groups. Not Chelation-Assisted. *J. Am. Chem. Soc.* **2004**, *126*, 13192-13193.

(85) Esteruelas, M. A.; Valero, C.; Oro, L. A.; Meyer, U.; Werner, H. Insertion Reaction of Acetone-d6 into the Os-H Bond of $[OsHCl(CO)(P^iPr_3)_2]$. Experimental-Evidence for the Hydrogen-Transfer Mechanism from Alcohols to Ketones. *Inorg. Chem.* **1991**, *30*, 1159-1160.

(86) Esteruelas, M. A.; Oliván, M.; Vélez, A. Xantphos-Type Complexes of Group 9: Rhodium versus Iridium. *Inorg. Chem.* **2013**, *52*, 5339-5349.

(87) Esteruelas, M. A.; Oliván, M.; Vélez, A. POP-Pincer Silyl Complexes of Group 9: Rhodium versus Iridium. *Inorg. Chem.* **2013**, *52*, 12108-12119.

(88) Calimano, E.; Tilley, T. D. Reactions of Cationic PNP-Supported Iridium Silylene Complexes with Polar Organic Substrates. *Organometallics* **2010**, *29*, 1680-1692.

(89) Esteruelas, M. A.; Nolis, P.; Oliván, M.; Oñate, E.; Vallribera, A.; Vélez, A. Ammonia Borane Dehydrogenation Promoted by a Pincer-Square-Planar Rhodium(I) Monohydride: A Stepwise Hydrogen Transfer from the Substrate to the Catalyst. *Inorg. Chem.* **2016**, *55*, 7176-7181.

(90) Adams, G. M.; Colebatch, A. L.; Skornia, J. T.; McKay, A. I.; Johnson, H. C.; Lloyd-Jones, G. C.; Macgregor, S. A.; Beattie, N. A.; Weller, A. S. Dehydropolymerization of $H_3B.NMeH_2$ To Form Polyaminoboranes Using [Rh(Xantphos-alkyl)] Catalysts. *J. Am. Chem. Soc.* **2018**, *140*, 1481-1495.

(91) Esteruelas, M. A.; Oliván, M.; Vélez, A. POP-Rhodium-Promoted C-H and B-H Bond Activation and C-B Bond Formation. *Organometallics* **2015**, *34*, 1911-1924.

(92) Esteruelas, M. A.; Fernández, I.; Martínez, A.; Oliván, M.; Oñate, E.; Vélez, A. Iridium-Promoted B–B Bond Activation: Preparation and X-ray Diffraction Analysis of a *mer*-Tris(boryl) Complex. *Inorg. Chem.* **2019**, *58*, 4712-4717.

(93) Curto, S. G.; Esteruelas, M. A.; Oliván, M.; Oñate, E.; Vélez, A. Selective C-Cl Bond Oxidative Addition of Chloroarenes to a POP-Rhodium Complex. *Organometallics* **2017**, *36*, 114-128.

(94) Tobisu, M.; Kinuta, H.; Kita, Y.; Rémond, E.; Chatani, N. Rhodium(I)-Catalyzed Borylation of Nitriles through the Cleavage of Carbon–Cyano Bonds. *J. Am. Chem. Soc.* **2012**, *134*, 115-118.

(95) Esteruelas, M. A.; Oliván, M.; Vélez, A. Conclusive Evidence on the Mechanism of the Rhodium-Mediated Decyanative Borylation. *J. Am. Chem. Soc.* **2015**, *137*, 12321-12329.

(96) (a) Curto, S. G.; Esteruelas, M. A.; Oliván, M.; Oñate, E.; Vélez, A. β-Borylalkenyl *Z-E* Isomerization in Rhodium-Mediated Diboration of Nonfunctionalized Internal Alkynes. *Organometallics* **2018**, *37*, 1970-1978. (b) Curto, S. G.; Esteruelas, M. A.; Oliván, M.; Oñate, E. Rhodium-Mediated Dehydrogenative Borylation–Hydroborylation of Bis(alkyl)alkynes: Intermediates and Mechanism. *Organometallics* **2019**, *38*, 2062-2074.

(97) (a) Bakhmutov, V. I.; Bozoglian, F.; Gómez, K.; González, G.; Grushin, V. V.; Macgregor, S. A.; Martin, E.; Miloserdov, F. M.; Novikov, M. A.; Panetier, J. A.; Romashov, L. V. CF_3-Ph Reductive Elimination from [(Xantphos)Pd(CF_3)(Ph)]. *Organometallics* **2012**, *31*, 1315-1328. (b) Jover, J.; Miloserdov, F. M.; Benet-Buchholz, J.; Grushin, V. V.; Maseras, F. On the Feasibility of Nickel-Catalyzed Trifluoromethylation of Aryl Halides. *Organometallics* **2014**, *33*, 6531-6543.

(98) Seed, B. Silanizing Glassware. *Curr. Protoc. Cell Bio.* **2000**, *8*, A.3E.1-A.3E.2.

(99) (a) Noyori, R.; Ohkuma, T. Asymmetric Catalysis by Architectural and Functional Molecular Engineering: Practical Chemo- and Stereoselective Hydrogenation of Ketones. *Angew. Chem., Int. Ed.* **2001**, *40*, 40-73. (b) Clapham, S. E.; Hadzovic, A.; Morris, R. H. Mechanisms of the H_2-Hydrogenation and Transfer Hydrogenation of Polar Bonds Catalyzed by Ruthenium Hydride Complexes. *Coord. Chem. Rev.* **2004**, *248*, 2201-2237. (c) Conley, B. L.; Pennington-Boggio, M. K.; Boz, E.; Williams, T. J. Discovery, Applications, and Catalytic Mechanisms of Shvo's Catalyst. *Chem. Rev.* **2010**, *110*, 2294-2312. (d) Bajo, S.; Esteruelas, M. A.; López, A. M.; Oñate, E. Osmium-Acyl Decarbonylation Promoted by Tp-Mediated Allenylidene Abstraction: A New Role of the Tp Ligand. *Organometallics* **2014**, *33*, 4057-4066.

(100) (a) Periana, R. A.; Taube, D. J.; Gamble, S.; Taube, H.; Satoh, T.; Fujii, H. Platinum Catalysts for the High-Yield Oxidation of Methane to a Methanol Derivative. *Science* **1998**, *280*, 560-564. (b) Hashiguchi, B. G.; Young, K. J. H.; Yousufuddin, M.; Goddard, W. A.; Periana, R. A. Acceleration of Nucleophilic CH Activation by Strongly Basic Solvents. *J. Am. Chem. Soc.* **2010**, *132*, 12542-12545. (c) Crabtree, R. H. Creating Ligands with Multiple Personalities. *Science* **2010**, *330*, 455-456. (d) Kaim, W. Manifestations of Noninnocent Ligand Behavior. *Inorg. Chem.* **2011**, *50*, 9752-9765.

(101) (a) Braunstein, P.; Naud, F. Hemilability of Hybrid Ligands and the Coordination Chemistry of Oxazoline-Based Systems. *Angew. Chem., Int. Ed.* **2001**, *40*, 680-699. (b) Angell, S. E.; Rogers, C. W.; Zhang, Y.; Wolf, M. O.; Jones, W. E. Hemilabile Coordination Complexes for Sensing Applications. *Coord. Chem. Rev.* **2006**, *250*, 1829-1841. (c) Braunstein, P. Bonding and Organic and Inorganic Reactivity of Metal-Coordinated Phosphinoenolates and Related Functional Phosphine-Derived Anions. *Chem. Rev.* **2006**, *106*, 134-159. (d) Weng, Z. Q.; Teo, S.

H.; Hor, T. S. A. Metal Unsaturation and Ligand Hemilability in Suzuki Coupling. *Acc. Chem. Res.* **2007**, *40*, 676-684. (e) Zhang, W. H.; Chien, S. W.; Hor, T. S. A. Recent Advances in Metal Catalysts with Hybrid Ligands. *Coord. Chem. Rev.* **2011**, *255*, 1991-2024. (f) Annibale, V. T.; Song, D. T. Multidentate Actor Ligands as Versatile Platforms for Small Molecule Activation and Catalysis. *RSC Adv.* **2013**, *3*, 11432-11449.

(102) (a) van der Boom, M. E.; Milstein, D. Cyclometalated Phosphine-Based Pincer Complexes: Mechanistic Insight in Catalysis, Coordination, and Bond Activation. *Chem. Rev.* **2003**, *103*, 1759-1792. (b) Haibach, M. C.; Kundu, S.; Brookhart, M.; Goldman, A. S. Alkane Metathesis by Tandem Alkane-Dehydrogenation-Olefin-Metathesis Catalysis and Related Chemistry. *Acc. Chem. Res.* **2012**, *45*, 947-958. (c) Kumar, A.; Zhou, T.; Emge, T. J.; Mironov, O.; Saxton, R. J.; Krogh-Jespersen, K.; Goldman, A. S. Dehydrogenation of *n*-Alkanes by Solid-Phase Molecular Pincer-Iridium Catalysts. High Yields of *α*-Olefin Product. *J. Am. Chem. Soc.* **2015**, *137*, 9894-9911.

(103) (a) Boone, M. P.; Brown, C. C.; Ancelet, T. A.; Stephan, D. W. Interconversion of Ruthenium-O($CH_2CH_2PCy_2$)$_2$ Alkylidene and Alkylidyne Hydride Complexes. *Organometallics* **2010**, *29*, 4369-4374. (b) Lumbroso, A.; Koschker, P.; Vautravers, N. R.; Breit, B. Redox-Neutral Atom-Economic Rhodium-Catalyzed Coupling of Terminal Alkynes with Carboxylic Acids Toward Branched Allylic Esters. *J. Am. Chem. Soc.* **2011**, *133*, 2386-2389. (c) Pawley, R. J.; Huertos, M. A.; Lloyd-Jones, G. C.; Weller, A. S.; Willis, M. C. Intermolecular Alkyne Hydroacylation. Mechanistic Insight from the Isolation of the Vinyl Intermediate that Precedes Reductive Elimination. *Organometallics* **2012**, *31*, 5650-5659.

(104) Dallanegra, R.; Chaplin, A. B.; Weller, A. S. Rhodium Cyclopentyl Phosphine Complexes of Wide-Bite-Angle Ligands DPEphos and Xantphos. *Organometallics* **2012**, *31*, 2720-2728.

(105) Pawley, R. J.; Moxham, G. L.; Dallanegra, R.; Chaplin, A. B.; Brayshaw, S. K.; Weller, A. S.; Willis, M. C. Controlling Selectivity in Intermolecular Alkene or Aldehyde Hydroacylation Reactions Catalyzed by {Rh(L_2)}$^+$ Fragments. *Organometallics* **2010**, *29*, 1717-1728.

(106) Ren, P.; Pike, S. D.; Pernik, I.; Weller, A. S.; Willis, M. C. Rh-POP Pincer Xantphos Complexes for C-S and C-H Activation. Implications for Carbothiolation Catalysis. *Organometallics* **2015**, *34*, 711-723.

(107) Johnson, H. C.; Leitao, E. M.; Whitten, G. R.; Manners, I.; Lloyd-Jones, G. C.; Weller, A. S. Mechanistic Studies of the Dehydrocoupling and Dehydropolymerization of Amine-Boranes Using a [Rh(Xantphos)]$^+$ Catalyst. *J. Am. Chem. Soc.* **2014**, *136*, 9078-9093.

(108) Esteruelas, M. A.; López, A. M.; Oliván, M. Polyhydrides of Platinum Group Metals: Nonclassical Interactions and *σ*-Bond Activation Reactions. *Chem. Rev.* **2016**, *116*, 8770-8847.

(109) Crabtree, R. H. Dihydrogen Complexation. *Chem. Rev.* **2016**, *116*, 8750-8769.

(110) Bhunya, S.; Malakar, T.; Ganguly, G.; Paul, A. Combining Protons and Hydrides by Homogeneous Catalysis for Controlling the Release of Hydrogen from Ammonia–Borane: Present Status and Challenges. *ACS Catal.* **2016**, *6*, 7907-7934.

(111) (a) Casarrubios, L.; Esteruelas, M. A.; Larramona, C.; Muntaner, J. G.; Oliván, M.; Oñate, E.; Sierra, M. A. Chelated Assisted Metal-Mediated N-H Bond Activation of *β*-Lactams:

Preparation of Irida-, Rhoda-, Osma-, and Ruthenatrinems. *Organometallics* **2014**, *33*, 1820-1833. (b) Casarrubios, L.; Esteruelas, M. A.; Larramona, C.; Lledós, A.; Muntaner, J. G.; Oñate, E.; Ortuño, M. A.; Sierra, M. A. Mechanistic Insight into the Facilitation of β-Lactam Fragmentation through Metal Assistance. *Chem. - Eur. J.* **2015**, *21*, 16781-16785.

(112) (a) Esteruelas, M. A.; García-Raboso, J.; Oliván, M.; Oñate, E. N-H and N-C Bond Activation of Pyrimidinic Nucleobases and Nucleosides Promoted by an Osmium Polyhydride. *Inorg. Chem.* **2012**, *51*, 5975-5984. (b) Esteruelas, M. A.; García-Raboso, J.; Oliván, M. Reactions of an Osmium-Hexahydride Complex with Cytosine, Deoxycytidine, and Cytidine: The Importance of the Minor Tautomers. *Inorg. Chem.* **2012**, *51*, 9522-9528.

(113) Esteruelas, M. A.; Herrero, J.; López, A. M.; Oliván, M. Alkyne-Coupling Reactions Catalyzed by OsHCl(CO)(P^iPr_3) in the Presence of Diethylamine. *Organometallics* **2001**, *20*, 3202-3205.

(114) (a) Crespo, O.; Eguillor, B.; Esteruelas, M. A.; Fernández, I.; García-Raboso, J.; Gómez-Gallego, M.; Martín-Ortiz, M.; Oliván, M.; Sierra, M. A. Synthesis and Characterisation of [6]-Azaosmahelicenes: the First d^4-Heterometallahelicenes. *Chem. Commun.* **2012**, *48*, 5328-5330. (b) Eguillor, B.; Esteruelas, M. A.; Fernández, I.; Gómez-Gallego, M.; Lledós, A.; Martín-Ortiz, M.; Oliván, M.; Oñate, E.; Sierra, M. A. Azole Assisted C-H Bond Activation Promoted by an Osmium-Polyhydride: Discerning between N and NH. *Organometallics* **2015**, *34*, 1898-1910.

(115) Liu, S. H.; Huang, X.; Lin, Z. Y.; Lau, C. P.; Jia, G. C. Synthesis and Characterization of Dihydrogen(olefin)osmium Complexes with (E)-$Ph_2P(CH_2)_2CH{=}CH(CH_2)_2PPh_2$. *Eur. J. Inorg. Chem.* **2002**, 1697-1702.

(116) (a) Kong, V. C. Y.; Foulkes, F. R.; Kirk, D. W.; Hinatsu, J. T. Development of Hydrogen Storage for Fuel Cell Generators. I: Hydrogen Generation Using Hydrolysis Hydrides. *Int. J. Hydrogen Energy* **1999**, *24*, 665-675. (b) Kong, V. C. Y.; Kirk, D. W.; Foulkes, F. R.; Hinatsu, J. T. Development of Hydrogen Storage for Fuel Cell Generators II: Utilization of Calcium Hydride and Lithium Hydride. *Int. J. Hydrogen Energy* **2003**, *28*, 205-214. (c) Dincer, I. Green Methods for Hydrogen Production. *Int. J. Hydrogen Energy* **2012**, *37*, 1954-1971. (d) Dincer, I.; Acar, C. Review and Evaluation of Hydrogen Production Methods for Better Sustainability. *Int. J. Hydrogen Energy* **2015**, *40*, 11094-11111.

(117) (a) Gusev, D. G.; Lough, A. J.; Morris, R. H. New Polyhydride Anions and Proton-Hydride Hydrogen Bonding in their Ion Pairs. X-ray Crystal Structure Determinations of Q[*mer*-$Os(H)_3(CO)(P^iPr_3)_2$], Q = [K(18-crown-6)] and Q = [K(1-aza-18-crown-6)]. *J. Am. Chem. Soc.* **1998**, *120*, 13138-13147. (b) Abdur-Rashid, K.; Gusev, D. G.; Lough, A. J.; Morris, R. H. Intermolecular Proton-Hydride Bonding in Ion Pairs: Synthesis and Structural Properties of [K(Q)][$MH_5((P^iPr_3)_2)$] (M = Os, Ru; Q=18-crown-6, 1-aza-18-crown-6, 1,10-diaza-18-crown-6). *Organometallics* **2000**, *19*, 834-843.

(118) (a) Howard, J. A. K.; Johnson, O.; Koetzle, T. F.; Spencer, J. L. Crystal and Molecular Structure of Bis(diisopropylphenylphosphine)hexahydridoosmium, [$OsH_6(PC_{12}H_{19})_2$]: Single-Crystal Neutron Diffraction Study at 20 K. *Inorg. Chem.* **1987**, *26*, 2930-2933. (b) Buil, M. L.; Cardo, J. J. F.; Esteruelas, M. A.; Fernández, I.; Oñate, E. An Entry to Stable Mixed Phosphine-Osmium-NHC Polyhydrides. *Inorg. Chem.* **2016**, *55*, 5062-5070.

(119) (a) Grasemann, M.; Laurenczy, G. Formic Acid as a Hydrogen Source - Recent Developments and Future Trends. *Energy Environ. Sci.* **2012**, *5*, 8171-8181. (b) Kawanami, H.; Himeda, Y.; Laurenczy, G. Formic Acid as a Hydrogen Carrier for Fuel Cells Toward a Sustainable Energy System. *Adv. Inorg. Chem.* **2017**, *70*, 395-427. (c) Eppinger, J.; Huang, K. W. Formic Acid as a Hydrogen Energy Carrier. *ACS Energy Lett.* **2017**, *2*, 188-195.

(120) (a) Filonenko, G. A.; van Putten, R.; Schulpen, E. N.; Hensen, E. J. M.; Pidko, E. A. Highly Efficient Reversible Hydrogenation of Carbon Dioxide to Formates Using a Ruthenium PNP-Pincer Catalyst. *ChemCatChem* **2014**, *6*, 1526-1530. (b) Wang, W. H.; Himeda, Y.; Muckerman, J. T.; Manbeck, G. F.; Fujita, E. CO_2 Hydrogenation to Formate and Methanol as an Alternative to Photo- and Electrochemical CO_2 Reduction. *Chem. Rev.* **2015**, *115*, 12936-12973. (c) Bernskoetter, W. H.; Hazari, N. Reversible Hydrogenation of Carbon Dioxide to Formic Acid and Methanol: Lewis Acid Enhancement of Base Metal Catalysts. *Acc. Chem. Res.* **2017**, *50*, 1049-1058. (d) Artz, J.; Müller, T. E.; Thenert, K.; Kleinekorte, J.; Meys, R.; Sternberg, A.; Bardow, A.; Leitner, W. Sustainable Conversion of Carbon Dioxide: An Integrated Review of Catalysis and Life Cycle Assessment. *Chem. Rev.* **2018**, *118*, 434-504.

(121) (a) Singh, A. K.; Singh, S.; Kumar, A. Hydrogen Energy Future with Formic Acid: a Renewable Chemical Hydrogen Storage System. *Catal. Sci. Technol.* **2016**, *6*, 12-40. (b) Mellmann, D.; Sponholz, P.; Junge, H.; Beller, M. Formic Acid as a Hydrogen Storage Material – Development of Homogeneous Catalysts for Selective Hydrogen Release. *Chem. Soc. Rev.* **2016**, *45*, 3954-3988. (c) Wang, X.; Meng, Q. L.; Gao, L. Q.; Jin, Z.; Ge, J. J.; Liu, C. P.; Xing, W. Recent Progress in Hydrogen Production from Formic Acid Decomposition. *Int. J. Hydrogen Energy* **2018**, *43*, 7055-7071.

(122) (a) Boddien, A.; Gärtner, F.; Jackstell, R.; Junge, H.; Spannenberg, A.; Baumann, W.; Ludwig, R.; Beller, M. *ortho*-Metalation of Iron(0) Tribenzylphosphine Complexes: Homogeneous Catalysts for the Generation of Hydrogen from Formic Acid. *Angew. Chem., Int. Ed.* **2010**, *49*, 8993-8996. (b) Boddien, A.; Loges, B.; Gärtner, F.; Torborg, C.; Fumino, K.; Junge, H.; Ludwig, R.; Beller, M. Iron-Catalyzed Hydrogen Production from Formic Acid. *J. Am. Chem. Soc.* **2010**, *132*, 8924-8934. (c) Boddien, A.; Mellmann, D.; Gärtner, F.; Jackstell, R.; Junge, H.; Dyson, P. J.; Laurenczy, G.; Ludwig, R.; Beller, M. Efficient Dehydrogenation of Formic Acid Using an Iron Catalyst. *Science* **2011**, *333*, 1733-1736. (d) Zell, T.; Butschke, B.; Ben-David, Y.; Milstein, D. Efficient Hydrogen Liberation from Formic Acid Catalyzed by a Well-Defined Iron Pincer Complex under Mild Conditions. *Chem. - Eur. J.* **2013**, *19*, 8068-8072. (e) Zell, T.; Milstein, D. Hydrogenation and Dehydrogenation Iron Pincer Catalysts Capable of Metal Ligand Cooperation by Aromatization/Dearomatization. *Acc. Chem. Res.* **2015**, *48*, 1979-1994. (f) Mellone, I.; Gorgas, N.; Bertini, F.; Peruzzini, M.; Kirchner, K.; Gonsalvi, L. Selective Formic Acid Dehydrogenation Catalyzed by Fe-PNP Pincer Complexes Based on the 2,6-Diaminopyridine Scaffold. *Organometallics* **2016**, *35*, 3344-3349.

(123) (a) Gan, W. J.; Snelders, D. J. M.; Dyson, P. J.; Laurenczy, G. Ruthenium(II)-Catalyzed Hydrogen Generation from Formic Acid using Cationic, Ammoniomethyl-Substituted Triarylphosphine Ligands. *ChemCatChem* **2013**, *5*, 1126-1132. (b) Mellone, I.; Peruzzini, M.; Rosi, L.; Mellmann, D.; Junge, H.; Beller, M.; Gonsalvi, L. Formic Acid Dehydrogenation Catalysed by Ruthenium Complexes Bearing the Tripodal Ligands Triphos and NP_3. *Dalton Trans.* **2013**, *42*, 2495-2501. (c) Guerriero, A.; Bricout, H.; Sordakis, K.; Peruzzini, M.; Monflier, E.; Hapiot, F.; Laurenczy, G.; Gonsalvi, L. Hydrogen Production by Selective Dehydrogenation

of HCOOH Catalyzed by Ru-Biaryl Sulfonated Phosphines in Aqueous Solution. *ACS Catal.* **2014**, *4*, 3002-3012. (d) Czaun, M.; Goeppert, A.; Kothandaraman, J.; May, R. B.; Haiges, R.; Prakash, G. K. S.; Olah, G. A. Formic Acid As a Hydrogen Storage Medium: Ruthenium-Catalyzed Generation of Hydrogen from Formic Acid in Emulsions. *ACS Catal.* **2014**, *4*, 311-320. (e) Pan, Y. P.; Pan, C. L.; Zhang, Y. F.; Li, H. F.; Min, S. X.; Guo, X. M.; Zheng, B.; Chen, H. L.; Anders, A.; Lai, Z. P.; Zheng, J. R.; Huang, K. W. Selective Hydrogen Generation from Formic Acid with Well-Defined Complexes of Ruthenium and Phosphorus-Nitrogen PN^3-Pincer Ligand. *Chem. - Asian J.* **2016**, *11*, 1357-1360. (f) Mellone, I.; Bertini, F.; Peruzzini, M.; Gonsalvi, L. An Active, Stable and Recyclable Ru(II) Tetraphosphine-Based Catalytic System for Hydrogen Production by Selective Formic Acid Dehydrogenation. *Catal. Sci. Technol.* **2016**, *6*, 6504-6512. (g) Anderson, N. H.; Boncella, J. M.; Tondreau, A. M. Reactivity of Silanes with (^{tBu}PONOP)Ruthenium Dichloride: Facile Synthesis of Chloro-Silyl Ruthenium Compounds and Formic Acid Decomposition. *Chem. - Eur. J.* **2017**, *23*, 13617-13622. (h) Piola, L.; Fernández-Salas, J. A.; Nahra, F.; Poater, A.; Cavallo, L.; Nolan, S. P. Ruthenium-Catalysed Decomposition of Formic Acid: Fuel Cell and Catalytic Applications. *Mol. Catal.* **2017**, *440*, 184-189. (i) Guan, C.; Zhang, D. D.; Pan, Y. P.; Iguchi, M.; Ajitha, M. J.; Hu, J. S.; Li, H. F.; Yao, C. G.; Huang, M. H.; Min, S. X.; Zheng, J. R.; Himeda, Y.; Kawanami, H.; Huang, K. W. Dehydrogenation of Formic Acid Catalyzed by a Ruthenium Complex with an *N,N'*-Diimine Ligand. *Inorg. Chem.* **2017**, *56*, 438-445.

(124) (a) Celaje, J. J. A.; Lu, Z. Y.; Kedzie, E. A.; Terrile, N. J.; Lo, J. N.; Williams, T. J. A Prolific Catalyst for Dehydrogenation of Neat Formic Acid. *Nat. Commun.* **2016**, *7*, 11308. (b) Papp, G.; Ölveti, G.; Horváth, H.; Kathó, A.; Joó, F. Highly Efficient Dehydrogenation of Formic Acid in Aqueous Solution Catalysed by an Easily Available Water-Soluble Iridium(III) Dihydride. *Dalton Trans.* **2016**, *45*, 14516-14519. (c) Iguchi, M.; Himeda, Y.; Manaka, Y.; Kawanami, H. Development of an Iridium-Based Catalyst for High-Pressure Evolution of Hydrogen from Formic Acid. *ChemSusChem* **2016**, *9*, 2749-2753. (d) Li, J. J.; Li, J. H.; Zhang, D. J.; Liu, C. B. DFT Study on the Mechanism of Formic Acid Decomposition by a Well-Defined Bifunctional Cyclometalated Iridium(III) Catalyst: Self-Assisted Concerted Dehydrogenation via Long-Range Intermolecular Hydrogen Migration. *ACS Catal.* **2016**, *6*, 4746-4754. (e) Czaun, M.; Kothandaraman, J.; Goeppert, A.; Yang, B.; Greenberg, S.; May, R. B.; Olah, G. A.; Prakash, G. K. S. Iridium-Catalyzed Continuous Hydrogen Generation from Formic Acid and Its Subsequent Utilization in a Fuel Cell: Toward a Carbon Neutral Chemical Energy Storage. *ACS Catal.* **2016**, *6*, 7475-7484. (f) Iguchi, M.; Zhong, H.; Himeda, Y.; Kawanami, H. Kinetic Studies on Formic Acid Dehydrogenation Catalyzed by an Iridium Complex towards Insights into the Catalytic Mechanism of High-Pressure Hydrogen Gas Production. *Chem. - Eur. J.* **2017**, *23*, 17017-17021. (g) Wang, L.; Onishi, N.; Murata, K.; Hirose, T.; Muckerman, J. T.; Fujita, E.; Himeda, Y. Efficient Hydrogen Storage and Production Using a Catalyst with an Imidazoline-Based, Proton-Responsive Ligand. *ChemSusChem* **2017**, *10*, 1071-1075. (h) Cohen, S.; Borin, V.; Schapiro, I.; Musa, S.; De-Botton, S.; Belkova, N. V.; Gelman, D. Ir(III)-PC(sp^3)P Bifunctional Catalysts for Production of H_2 by Dehydrogenation of Formic Acid: Experimental and Theoretical Study. *ACS Catal.* **2017**, *7*, 8139-8146. (i) Iguchi, M.; Zhong, H.; Himeda, Y.; Kawanami, H. Effect of the *ortho*-Hydroxyl Groups on a Bipyridine Ligand of Iridium Complexes for the High-Pressure Gas Generation from the Catalytic Decomposition of Formic Acid. *Chem. - Eur. J.* **2017**, *23*, 17788-17793. (j) Lu, S. M.; Wang, Z. J.; Wang, J. J.; Li, J.; Li, C. Hydrogen Generation from Formic

Acid Decomposition on a Highly Efficient Iridium Catalyst Bearing a Diaminoglyoxime Ligand. *Green Chem.* **2018**, *20*, 1835-1840.

(125) Neary, M. C.; Parkin, G. Dehydrogenation, Disproportionation and Transfer Hydrogenation Reactions of Formic Acid Catalyzed by Molybdenum Hydride Compounds. *Chem. Sci.* **2015**, *6*, 1859-1865.

(126) Fink, C.; Laurenczy, G. CO_2 as a Hydrogen Vector - Transition Metal Diamine Catalysts for Selective HCOOH Dehydrogenation. *Dalton Trans.* **2017**, *46*, 1670-1676.

(127) Enthaler, S.; Brück, A.; Kammer, A.; Junge, H.; Irran, E.; Gülak, S. Exploring the Reactivity of Nickel Pincer Complexes in the Decomposition of Formic Acid to CO_2/H_2 and the Hydrogenation of $NaHCO_3$ to HCOONa. *ChemCatChem* **2015**, *7*, 65-69.

(128) Correa, A.; Cascella, M.; Scotti, N.; Zaccheria, F.; Ravasio, N.; Psaro, R. Mechanistic Insights into Formic Acid Dehydrogenation Promoted by Cu-Amino Based Systems. *Inorg. Chim. Acta.* **2018**, *470*, 290-294.

(129) Myers, T. W.; Berben, L. A. Aluminium-Ligand Cooperation Promotes Selective Dehydrogenation of Formic Acid to H_2 and CO_2. *Chem. Sci.* **2014**, *5*, 2771-2777.

(130) Iglesias, M.; Oro, L. A. Mechanistic Considerations on Homogeneously Catalyzed Formic Acid Dehydrogenation. *Eur. J. Inorg. Chem.* **2018**, 2125–2138.

(131) (a) Dub, P. A.; Gordon, J. C. The Mechanism of Enantioselective Ketone Reduction with Noyori and Noyori-Ikariya Bifunctional Catalysts. *Dalton Trans.* **2016**, *45*, 6756-6781. (b) Morris, S. A.; Gusev, D. G. Rethinking the Claisen-Tishchenko Reaction. *Angew. Chem., Int. Ed.* **2017**, *56*, 6228-6231.

(132) Nelson, D. J.; Nolan, S. P. Hydroxide Complexes of the Late Transition Metals: Organometallic Chemistry and Catalysis. *Coord. Chem. Rev.* **2017**, *353*, 278-294.

(133) Ozerov, O. V. Oxidative Addition of Water to Transition Metal Complexes. *Chem. Soc. Rev.* **2009**, *38*, 83-88.

(134) (a) Gotzig, J.; Werner, R.; Werner, H. Basic Metals: 53. Ruthenium- and Osmium-Complexes with Dimethylphosphinomethanide-Anion as Ligands. *J. Organomet. Chem.* **1985**, *290*, 99-114. (b) Edwards, A. J.; Elipe, S.; Esteruelas, M. A.; Lahoz, F. J.; Oro, L. A.; Valero, C. Synthesis and Reactivity of the Unusual Five-Coordinate Hydrido-Hydroxo Complex $OsH(OH)(CO)(P^iPr_3)_2$. *Organometallics* **1997**, *16*, 3828-3836. (c) Renkema, K. B.; Huffman, J. C.; Caulton, K. G. Characterization and Structure of $OsH(OH)(CO)(PBu_2Me)^tBu_2$. *Polyhedron* **1999**, *18*, 2575-2578. (d) Prokopchuk, D. E.; Collado, A.; Lough, A. J.; Morris, R. H. Structural Properties of *trans* Hydrido-Hydroxo $M(H)(OH)(NH_2CMe_2CMe_2NH_2)(PPh_3)_2$ (M = Ru, Os) Complexes and their Proton Exchange Behaviour with Water in Solution. *Dalton Trans.* **2013**, *42*, 10214-10220. (e) Buil, M. L.; Cardo, J. J. F.; Esteruelas, M. A.; Fernández, I.; Oñate, E. Hydroboration and Hydrogenation of an Osmium-Carbon Triple Bond: Osmium Chemistry of a Bis-*σ*-Borane. *Organometallics* **2015**, *34*, 547-550.

(135) Wu, A.; Dehestani, A.; Saganic, E.; Crevier, T. J.; Kaminsky, W.; Cohen, D. E.; Mayer, J. M. Reactions of Tp-Os Nitrido Complexes with the Nucleophiles Hydroxide and Thiosulfate. *Inorg. Chim. Acta.* **2006**, *359*, 2842-2849.

(136) Kiefer, A. M.; Giles, J. A.; Shapley, P. A. Synthesis, Structure, and Reactivity of Organometallic Osmium(VI) Hydroxo Compounds. *Organometallics* **2007**, *26*, 1881-1887.

(137) (a) Gould, R. O.; Jones, C. L.; Stephenson, T. A.; Tocher, D. A. Structural Characterization of Hydroxo-Bridged Arene-Ruthenium and -Osmium Complexes: Further Reactions of Hydroxo-Bridged Complexes. *J. Organomet. Chem.* **1984**, *264*, 365-378. (b) Cabeza, J. A.; Mann, B. E.; Maitlis, P. M.; Brevard, C. The Synthesis of Di-Nuclear and Tetra-Nuclear *p*-Cymene-Osmium Hydride Complexes - Characterization by ^{1}H (^{187}Os) Reverse INEPT Two-Dimensional Nuclear Magnetic-Resonance Spectroscopy. *J. Chem. Soc., Dalton Trans.* **1988**, 629-634. (c) Esteruelas, M. A.; García-Yebra, C.; Oliván, M.; Oñate, E. Reaction of a Cationic Osmium(IV) Dihydride with Ethylene: Formation and Structure of the Novel Tetraethylene Dimer Complex $[\{(P^{i}Pr_3)(\eta^2\text{-}C_2H_4)_2Os\}_2(\mu\text{-}OH)_2(\mu\text{-}O_2CCH_3)]BF_4$. *Organometallics* **2000**, *19*, 3260-3262. (d) Peacock, A. F. A.; Habtemariam, A.; Fernández, R.; Walland, V.; Fabbiani, F. P. A.; Parsons, S.; Aird, R. E.; Jodrell, D. I.; Sadler, P. J. Tuning the Reactivity of Osmium(II) and Ruthenium(II) Arene Complexes under Physiological Conditions. *J. Am. Chem. Soc.* **2006**, *128*, 1739-1748.

(138) No se forma CO. En este contexto, tanto los compuestos 3 como 5 reaccionan con éste gas para dar la especie $Os(CO)_3\{\kappa^2\text{-}P,P\text{-}[xant(P^{i}Pr_2)_2]\}$, que no es activa.

(139) (a) Scholten, J. D.; Prechtl, M. H. G.; Dupont, J. Decomposition of Formic Acid Catalyzed by a Phosphine-Free Ruthenium Complex in a Task-Specific Ionic Liquid. *ChemCatChem* **2010**, *2*, 1265-1270. (b) Wang, W. H.; Xu, S.; Manaka, Y.; Suna, Y.; Kambayashi, H.; Muckerman, J. T.; Fujita, E.; Himeda, Y. Formic Acid Dehydrogenation with Bioinspired Iridium Complexes: A Kinetic Isotope Effect Study and Mechanistic Insight. *ChemSusChem* **2014**, *7*, 1976-1983. (c) Wang, W. H.; Ertem, M. Z.; Xu, S. A.; Onishi, N.; Manaka, Y.; Suna, Y.; Kambayashi, H.; Muckerman, J. T.; Fujita, E.; Himeda, Y. Highly Robust Hydrogen Generation by Bioinspired Ir Complexes for Dehydrogenation of Formic Acid in Water: Experimental and Theoretical Mechanistic Investigations at Different pH. *ACS Catal.* **2015**, *5*, 5496-5504. (d) Ertem, M. Z.; Himeda, Y.; Fujita, E.; Muckerman, J. T. Interconversion of Formic Acid and Carbon Dioxide by Proton-Responsive, Half-Sandwich Cp*Ir-III Complexes: A Computational Mechanistic Investigation. *ACS Catal.* **2016**, *6*, 600-609.

(140) (a) Kubas, G. J. *Metal Dihydrogen and σ-Bond Complexes: Structure, Theory and Reactivity;* Kluwer: New York, 2001. (b) Kubas, G. J. Metal-Dihydrogen and *σ*-Bond Coordination: the Consummate Extension of the Dewar-Chatt-Duncanson Model for Metal-Olefin *π* Bonding. *J. Organomet. Chem.* **2001**, *635*, 37-68. (c) Kubas, G. J. Fundamentals of H_2 Binding and Reactivity on Transition Metals Underlying Hydrogenase Function and H_2 Production and Storage. *Chem. Rev.* **2007**, *107*, 4152-4205.

(141) (a) Lin, Z. Y. Structural and Bonding Characteristics in Transition Metal-Silane Complexes. *Chem. Soc. Rev.* **2002**, *31*, 239-245. (b) Lachaize, S.; Sabo-Etienne, S. *σ*-Silane Ruthenium Complexes: The Crucial Role of Secondary Interactions. *Eur. J. Inorg. Chem.* **2006**, 2115-2127. (c) Perutz, R. N.; Sabo-Etienne, S. The *σ*-CAM Mechanism: *σ* Complexes as the Basis of *σ*-Bond Metathesis at Late-Transition-Metal Centers. *Angew. Chem., Int. Ed.* **2007**, *46*, 2578-2592.

(142) (a) Miyaura, N. Metal-Catalyzed Reactions of Organoboronic Acids and Esters. *Bull. Chem. Soc. Jpn.* **2008**, *81*, 1535-1553. (b) Crudden, C. M.; Glasspoole, B. W.; Lata, C. J. Expanding the Scope of Transformations of Organoboron Species: Carbon-Carbon Bond

Formation with Retention of Configuration. *Chem. Commun.* **2009**, 6704-6716. (c) Dang, L.; Lin, Z. Y.; Marder, T. B. Boryl Ligands and their Roles in Metal-Catalysed Borylation Reactions. *Chem. Commun.* **2009**, 3987-3995. (d) Mkhalid, I. A. I.; Barnard, J. H.; Marder, T. B.; Murphy, J. M.; Hartwig, J. F. C-H Activation for the Construction of C-B Bonds. *Chem. Rev.* **2010**, *110*, 890-931. (e) Ros, A.; Fernández, R.; Lassaletta, J. M. Functional Group Directed C-H Borylation. *Chem. Soc. Rev.* **2014**, *43*, 3229-3243.

(143) (a) Hamilton, C. W.; Baker, R. T.; Staubitz, A.; Manners, I. B-N Compounds for Chemical Hydrogen Storage. *Chem. Soc. Rev.* **2009**, *38*, 279-293. (b) St John, A.; Goldberg, K. I.; Heinekey, D. M. Pincer Complexes as Catalysts for Amine Borane Dehydrogenation. *Top. Organomet. Chem.* **2013**, *40*, 271-287.

(144) Pandey, K. K. Transition Metal-σ-Borane Complexes. *Coord. Chem. Rev.* **2009**, *253*, 37-55.

(145) (a) Hartwig, J. F.; Muhoro, G. N.; He, X. M.; Eisenstein, O.; Bosque, R.; Maseras, F. Catecholborane Bound to Titanocene. Unusual Coordination of Ligand σ-Bonds. *J. Am. Chem. Soc.* **1996**, *118*, 10936-10937. (b) Muhoro, C. N.; Hartwig, J. F. Synthesis, Structure, and Reactivity of [$Cp_2Ti(HBcat)(PMe_3)$]: A Monoborane σ Complex. *Angew. Chem., Int. Ed. Engl.* **1997**, *36*, 1510-1512. (c) Muhoro, C. N.; He, X. M.; Hartwig, J. F. Titanocene Borane σ-Complexes. *J. Am. Chem. Soc.* **1999**, *121*, 5033-5046. (d) Lam, W. H.; Lin, Z. Y. Bonding Analysis of Titanocene Borane σ-Complexes. *Organometallics* **2000**, *19*, 2625-2628.

(146) Schlecht, S.; Hartwig, J. F. σ-Borane Complexes of Manganese and Rhenium. *J. Am. Chem. Soc.* **2000**, *122*, 9435-9443.

(147) Crestani, M. G.; Muñoz-Hernández, M.; Arévalo, A.; Acosta-Ramírez, A.; García, J. J. σ-Borane Coordinated to Nickel(0) and Some Related Nickel(II) Trihydride Complexes. *J. Am. Chem. Soc.* **2005**, *127*, 18066-18073.

(148) (a) Montiel-Palma, V.; Lumbierres, M.; Donnadieu, B.; Sabo-Etienne, S.; Chaudret, B. σ-Borane and Dihydroborate Complexes of Ruthenium. *J. Am. Chem. Soc.* **2002**, *124*, 5624-5625. (b) Lachaize, S.; Essalah, W.; Montiel-Palma, V.; Vendier, L.; Chaudret, B.; Barthelat, J. C.; Sabo-Etienne, S. Coordination Modes of Boranes in Polyhydride Ruthenium Complexes: σ-Borane versus Dihydridoborate. *Organometallics* **2005**, *24*, 2935-2943. (c) Alcaraz, G.; Grellier, M.; Sabo-Etienne, S. Bis σ-Bond Dihydrogen and Borane Ruthenium Complexes: Bonding Nature, Catalytic Applications, and Reversible Hydrogen Release. *Acc. Chem. Res.* **2009**, *42*, 1640-1649.

(149) Hebden, T. J.; Denney, M. C.; Pons, V.; Piccoli, P. M. B.; Koetzle, T. F.; Schultz, A. J.; Kaminsky, W.; Goldberg, K. I.; Heinekey, D. M. σ-Borane Complexes of Iridium: Synthesis and Structural Characterization. *J. Am. Chem. Soc.* **2008**, *130*, 10812-10820.

(150) (a) Esteruelas, M. A.; López, A. M.; Mora, M.; Oñate, E. B-H Activation and H-H Formation: Two Consecutive Heterolytic Processes on an Osmium-Hydrogensulfide Bond. *Chem. Commun.* **2013**, *49*, 7543-7545. (b) Esteruelas, M. A.; López, A. M.; Mora, M.; Oñate, E. Boryl-Dihydrideborate Osmium Complexes: Preparation, Structure, and Dynamic Behavior in Solution. *Organometallics* **2015**, *34*, 941-946.

(151) Hartwig, J. F.; Cook, K. S.; Hapke, M.; Incarvito, C. D.; Fan, Y. B.; Webster, C. E.; Hall, M. B. Rhodium Boryl Complexes in the Catalytic, Terminal Functionalization of Alkanes. *J. Am. Chem. Soc.* **2005**, *127*, 2538-2552.

(152) Alcaraz, G.; Sabo-Etienne, S. NMR: A Good Tool to Ascertain σ-Silane or σ-Borane Formulations? *Coord. Chem. Rev.* **2008**, *252*, 2395-2409.

(153) Esteruelas, M. A.; García-Yebra, C.; Martín, J.; Oñate, E. *mer*, *fac*, and Bidentate Coordination of an Alkyl-POP Ligand in the Chemistry of Nonclassical Osmium Hydrides. *Inorg. Chem.* **2017**, *56*, 676-683.

(154) Jessop, P. G.; Morris, R. H. Reactions of Transition-Metal Dihydrogen Complexes. *Coord. Chem. Rev.* **1992**, *121*, 155-284.

(155) (a) Irvine, G. J.; Roper, W. R.; Wright, L. J. Five-coordinate ruthenium(II) and osmium(II) boryl complexes. *Organometallics* **1997**, *16*, 2291-2296. (b) Rickard, C. E. F.; Roper, W. R.; Williamson, A.; Wright, L. J. Crystal structure of Os(Bcat)Cl(CO)(PPh3)(2) and the syntheses and structural studies of derived cationic and neutral osmium boryl complexes. *Organometallics* **1998**, *17*, 4869-4874. (c) Rickard, C. E. F.; Roper, W. R.; Williamson, A.; Wright, L. J. Synthesis and structures of cis- and trans-[Os(Bcat)(aryl)(CO)(2)(PPh3)(2)]: Compounds of relevance to the metal-catalyzed hydroboration reaction and the metal-mediated borylation of arenes. *Angew. Chem., Int. Ed.* **1999**, *38*, 1110-1113. (d) Rickard, C. E. F.; Roper, W. R.; Williamson, A.; Wright, L. J. Reactions of cis and trans Bcat, aryl osmium complexes (cat=1,2-O2C6H4). Bis(Bcat) complexes of osmium and ruthenium and a structural comparison of cis and trans isomers of Os(Bcat)I(CO)(2)(PPh3)(2). *Organometallics* **2000**, *19*, 4344-4355. (e) Irvine, G. J.; Rickard, C. E. F.; Roper, W. R.; Williamson, A.; Wright, L. J. A base-stabilized terminal borylene complex of osmium derived from reaction between a dichloroboryl complex and 8-aminoquinoline. *Angew. Chem., Int. Ed.* **2000**, *39*, 948-950. (f) Rickard, C. E. F.; Roper, W. R.; Williamson, A.; Wright, L. J. Tethered Osmium Boryl Complexes from the Reaction of $Os(BCl_2)Cl(CO)(PPh_3)_2$ with 2-Hydroxypyridine. *Organometallics* **2002**, *21*, 1714-1718. (g) Rickard, C. E. F.; Roper, W. R.; Williamson, A.; Wright, L. J. Tethered Boryl and Base-Stabilized Borylene Osmium Complexes from the Reaction of $Os(BCl_2)Cl(CO)(PPh_3)_2$ with 2-Aminopyridine. *Organometallics* **2002**, *21*, 4862-4872. (h) Rickard, C. E. F.; Roper, W. R.; Williamson, A.; Wright, L. J. Exchange of Boryl Ligand Substituents in $Os[B(OEt)_2]Cl(CO)(PPh_3)_2$. *J. Organomet. Chem.* **2004**, *689*, 1609-1616. (i) Buil, M. L.; Esteruelas, M. A.; Garcés, K.; Oñate, E. From Tetrahydroborate- to Aminoborylvinylidene Osmium Complexes via Alkynyl-Aminoboryl Intermediates. *J. Am. Chem. Soc.* **2011**, *133*, 2250-2263. (j) Esteruelas, M. A.; López, A. M.; Mora, M.; Oñate, E. Reactions of Osmium-Pinacolboryl Complexes: Preparation of the First Vinylideneboronate Esters. *Organometallics* **2012**, *31*, 2965-2970. (k) Esteruelas, M. A.; Fernández, I.; López, A. M.; Mora, M.; Oñate, E. Preparation, Structure, Bonding, and Preliminary Reactivity of a Six-Coordinate d(4) Osmium-Boryl Complex. *Organometallics* **2012**, *31*, 4646-4649. (l) Buil, M. L.; Esteruelas, M. A.; Fernández, I.; Izquierdo, S.; Oñate, E. Cationic Dihydride Boryl and Dihydride Silyl Osmium(IV) NHC Complexes: A Marked Diagonal Relationship. *Organometallics* **2013**, *32*, 2744-2752. (m) Braunschweig, H.; Légare, M. A.; Matler, A.; Wennemann, B. Silylosmium Anions for the Synthesis of Borylosmium(II) Complexes by Salt Elimination. *Eur. J. Inorg. Chem.* **2016**, 3376-3379. (n) McQueen, C. M. A.; Hill, A. F.; Sharma, M.; Singh, S. K.; Ward, J. S.; Willis, A. C.; Young, R. D. Synthesis and

reactivity of osmium and ruthenium PBP-LXL boryl pincer complexes. *Polyhedron* **2016**, *120*, 185-195.

(156) Morris, R. H. Bronsted-Lowry Acid Strength of Metal Hydride and Dihydrogen Complexes. *Chem. Rev.* **2016**, *116*, 8588-8654.

(157) Bénac-Lestrille, G.; Helmstedt, U.; Vendier, L.; Alcaraz, G.; Clot, E.; Sabo-Etienne, S. Dimethylaminoborane (H_2BNMe_2) Coordination to Late Transition Metal Centers: Snapshots of the B-H Oxidative Addition Process. *Inorg. Chem.* **2011**, *50*, 11039-11045.

(158) Roesky, H. W.; Singh, S.; Yusuff, K. K. M.; Maguire, J. A.; Hosmane, N. S. Organometallic Hydroxides of Transition Elements. *Chem. Rev.* **2006**, *106*, 3813-3843.

(159) Buil, M. L.; Cadierno, V.; Esteruelas, M. A.; Gimeno, J.; Herrero, J.; Izquierdo, S.; Oñate, E. Selective Hydration of Nitriles to Amides Promoted by an Os-NHC Catalyst: Formation and X-ray Characterization of κ^2-Amidate Intermediates. *Organometallics* **2012**, *31*, 6861-6867.

(160) Esteruelas, M. A.; García-Yebra, C.; Martín, J.; Oñate, E. Dehydrogenation of Formic Acid Promoted by a Trihydride-Hydroxo-Osmium(IV) Complex: Kinetics and Mechanism. *ACS Catal.* **2018**, *8*, 11314-11323.

(161) Cuesta, L.; Hevia, E.; Morales, D.; Pérez, J.; Riera, L.; Miguel, D. Reactivity of Molybdenum and Rhenium Hydroxo Complexes toward Organic Electrophiles: Reactions that Afford Carboxylato Products. *Organometallics* **2006**, *25*, 1717-1722.

(162) Buil, M. L.; Cardo, J. J. F.; Esteruelas, M. A.; Oñate, E. Dehydrogenative Addition of Aldehydes to a Mixed NHC-Osmium-Phosphine Hydroxide Complex: Formation of Carboxylate Derivatives. *Organometallics* **2016**, *35*, 2171-2173.

(163) (a) Cole, S. C.; Coles, M. P.; Hitchcock, P. B. A Step too Far? Assessment of the Boroxide Ligand in Ring-Opening Polymerization. *Organometallics* **2004**, *23*, 5159-5168. (b) Cole, S. C.; Coles, M. P.; Hitchcock, P. B. Boroxide Complexes of the Group 4 Metals: A "Noninnocent" Ligand in Olefin Polymerization. *Organometallics* **2005**, *24*, 3279-3289. (c) Nasr, A.; Breuil, P. A. R.; Silva, D. C.; Berthod, M.; Dellus, N.; Jeanneau, E.; Lemaire, M.; Olivier-Bourbigou, H. New Boron-Containing Molybdenum Imido Alkylidene Complexes for Linear Olefin Homometathesis. *Organometallics* **2013**, *32*, 5320-5325.

(164) Coles, M. P. Metal Compounds of Boron-Substituted Alkoxide ('Boroxide') Ligands. *Coord. Chem. Rev.* **2016**, *323*, 52-59.

(165) (a) Beck, G.; Hitchcock, P. B.; Lappert, M. F.; Mackinnon, I. A. Lipophilic Lithium Alkoxides or Dialkylboroxides - X-Ray Structures of $[Li(\mu\text{-}OR')]_2$ and $Li(OBR_2)(tmeda)$, [tmeda = $(Me_2NCH_2)_2$, R = $CH(SiMe_3)_2$, R' = C^tBu_3 or BR_2]. *J. Chem. Soc., Chem. Comm.* **1989**, 1312-1314. (b) Murphy, D.; Sheehan, J. P.; Spalding, T. R.; Ferguson, G.; Lough, A. J.; Gallagher, J. F. Compounds Containing B-O-X Bonds (X = Si, Ge, Sn, Pb). Part 4. Crystal-Structures of $B(SiPh_3)_3$, $PhB(OSiPh_3)_2$ and $PhB(OGePh_3)_2$. *J. Mater. Chem.* **1993**, *3*, 1275-1283. (c) Anulewicz-Ostrowska, R.; Luliński, S.; Serwatowski, J. Synthesis and Characterization of Dialkylmetal Boryloxides $[(\mu\text{-}9\text{-}BBN\text{-}9\text{-}O)MMe_2]_2$, M = Al, Ga, In. *Inorg. Chem.* **1999**, *38*, 3796-3800. (d) Anulewicz-Ostrowska, R.; Luliński, S.; Serwatowski, J.; Suwińska, K. Diverse Reactivity of Dialkylaluminum Dimesitylboryloxides $[(\mu\text{-}Mes_2BO)AlR_2]_2$. Synthetic and

Structural Study. *Inorg. Chem.* **2000**, *39*, 5763-5767. (e) Vidovic, D.; Moore, J. A.; Jones, J. N.; Cowley, A. H. Synthesis and Characterization of a Coordinated Oxoborane: Lewis Acid Stabilization of a Boron-Oxygen Double Bond. *J. Am. Chem. Soc.* **2005**, *127*, 4566-4567. (f) Le Coz, E.; Dorcet, V.; Roisnel, T.; Tobisch, S.; Carpentier, J. F.; Sarazin, Y. Low-Coordinate Barium Boryloxides: Synthesis and Dehydrocoupling Catalysis for the Production of Borasiloxanes. *Angew. Chem., Int. Ed.* **2018**, *57*, 11747-11751. (g) Someşan, A. A.; Le Coz, E.; Roisnel, T.; Silvestru, C.; Sarazin, Y. Stable Lead(II) Boroxides. *Chem. Commun.* **2018**, *54*, 5299-5302.

(166) (a) Weese, K. J.; Bartlett, R. A.; Murray, B. D.; Olmstead, M. M.; Power, P. P. Synthesis and Spectroscopic and Structural Characterization of Derivatives of the Quasi-Alkoxide Ligand [$OBMes_2$]- (Mes = 2,4,6-$Me_3C_6H_2$). *Inorg. Chem.* **1987**, *26*, 2409-2413. (b) Chen, H.; Power, P. P.; Shoner, S. C. Synthesis and Spectroscopic and X-Ray Structural Characterization of the First Homoleptic Transition-Metal Boryloxides [$Mn(OBTrip_2)(\mu\text{-}OBTrip_2)]_2$ and [$Fe(OBMes_2)(\mu\text{-}OBMes_2)]_2$. *Inorg. Chem.* **1991**, *30*, 2884-2888. (c) Chisholm, M. H.; Folting, K.; Haubrich, S. T.; Martin, J. D. Triple Bonds between Tungsten Atoms with Ancillary Dimesitylboroalkoxide Ligands. Preparations, Properties and Structures of $W_2(NMe_2)_4[OB(Mes)_2]_2$ and $W_2(OBu^t)_4[OB(Mes)_2]_2$ *Inorg. Chim. Acta.* **1993**, *213*, 17-24. (d) Gibson, V. C.; Redshaw, C.; Clegg, W.; Elsegood, M. R. J. Synthesis and Structural Characterization of some Novel Metalloboroxides Bearing Boron-Bound Mesityl and Fluoromesityl Substituents: The Molecular Structure of the First Metallaboroxane Complex. *Polyhedron* **1997**, *16*, 2637-2641. (e) Cole, S. C.; Coles, M. P.; Hitchcock, P. B. Transition-Metal Imido-Boroxide Complexes: a Structural and Spectroscopic Investigation of the Influence of Boron. *J. Chem. Soc., Dalton Trans.* **2002**, 4168-4174. (f) Cole, S. C.; Coles, M. P.; Hitchcock, P. B. Neutral and Zwitterionic Group 4 Metal Alkyls with Ancillary Boroxide Ligands. *Dalton Trans.* **2004**, 3428-3430.

(167) Luo, Y. R. *Comprehensive Handbook of Chemical Bond Energies;* CRC Press: Boca Raton, FL, 2007.

(168) (a) Che, C. M.; Huang, J. S.; Li, Z. Y.; Poon, C. K.; Tong, W. F.; Lai, T. F.; Cheng, M. C.; Wang, C. C.; Wang, Y. Dialkoxyosmium(IV) Porphyrins. Crystal and Molecular-Structures of Diethoxy-, Diphenoxy-, and Bis(2-propanolato) (*meso*-tetraphenylporphyrinato)osmium(IV). *Inorg. Chem.* **1992**, *31*, 5220-5225. (b) Kuhlman, R.; Streib, W. E.; Huffman, J. C.; Caulton, K. G. Site Selectivity in Electrophilic (H^+,CH_3^+) abstraction on $Os(H)_2X_2(P^iPr_3)_2$. *J. Am. Chem. Soc.* **1996**, *118*, 6934-6945. (c) Cheung, W. M.; Zhang, Q. F.; Williams, I. D.; Leung, W. H. Synthesis, Crystal Structures, and Reactivity of Osmium(II) an -(IV) Complexes Containing a Dithioimidodiphosphinate Ligand. *Inorg. Chem.* **2007**, *46*, 5754-5762. (d) Esteruelas, M. A.; García-Raboso, J.; Oliván, M. Preparation of Half-Sandwich Osmium Complexes by Deprotonation of Aromatic and Pro-aromatic Acids with a Hexahydride Brønsted Base. *Organometallics* **2011**, *30*, 3844-3852.

(169) Liu, S. Y.; Légaré, M. A.; Auerhammer, D.; Hofmann, A.; Braunschweig, H. The First Boron-Tellurium Double Bond: Direct Insertion of Heavy Chalcogens into a Mn=B Double Bond. *Angew. Chem., Int. Ed.* **2017**, *56*, 15760-15763.

(170) (a) Johnson, H. C.; Torry-Harris, R.; Ortega, L.; Theron, R.; McIndoe, J. S.; Weller, A. S. Exploring the Mechanism of the Hydroboration of Alkenes by Amine-Boranes Catalysed by $[Rh(Xantphos)]^+$. *Catal. Sci. Technol.* **2014**, *4*, 3486-3494. (b) Johnson, H. C.; Leitao, E. M.;

Whittell, G. R.; Manners, I.; Lloyd-Jones, G. C.; Weller, A. S. Mechanistic Studies of the Dehydrocoupling and Dehydropolymerization of Amine-Boranes Using a $[Rh(Xantphos)]^+$ Catalyst. *J. Am. Chem. Soc.* **2014**, *136*, 9078-9093. (c) Johnson, H. C.; Weller, A. S. P-C-Activated Bimetallic Rhodium Xantphos Complexes: Formation and Catalytic Dehydrocoupling of Amine-Boranes. *Angew. Chem., Int. Ed.* **2015**, *54*, 10173-10177. (d) Adams, G. M.; Weller, A. S. POP-Type Ligands: Variable Coordination and Hemilabile Behaviour. *Coord. Chem. Rev.* **2018**, *355*, 150-172. (e) Adams, G. M.; Colebatch, A. L.; Skornia, J. T.; McKay, A. I.; Johnson, H. C.; Lloyd-Jones, G. C.; Macgregor, S. A.; Beattie, N. A.; Weller, A. S. Dehydropolymerization of $H_3B{\cdot}NMeH_2$ To Form Polyaminoboranes Using [Rh(Xantphos-alkyl)] Catalysts. *J. Am. Chem. Soc.* **2018**, *140*, 1481-1495.

(171) (a) Stalick, J. K.; Ibers, J. A. Crystal and Molecular Structure of Tricarbonylbis(triphenylphosphine)osmium(0), $Os(CO)_3(P(C_6H_5)_3)_2$. *Inorg. Chem.* **1969**, *8*, 419-423. (b) Fiedler, T.; Bhuvanesh, N.; Hampel, F.; Reibenspies, J. H.; Gladysz, J. A. Gyroscope Like Molecules Consisting of Trigonal or Square Planar Osmium Rotators within Three-Spoked Dibridgehead Diphosphine Stators: Syntheses, Substitution Reactions, Structures, and Dynamic Properties. *Dalton Trans.* **2016**, *45*, 7131-7147. (c) Bissert, R.; Braunschweig, H.; Dewhurst, R. D.; Schneider, C. Metal-Only Lewis Pairs Based on Zerovalent Osmium. *Organometallics* **2016**, *35*, 2567-2573.

(172) (a) Stanger, A. What is ... Aromaticity: a Critique of the Concept of Aromaticity-Can it Really be Defined? *Chem. Commun.* **2009**, 1939-1947. (b) Solà, M. Why Aromaticity Is a Suspicious Concept? Why? *Front. Chem.* **2017**, *5*, 22.

(173) Thorn, D. L.; Hoffmann, R. Delocalization in Metallocycles. *Nouv. J. Chim.* **1979**, *3*, 39-45.

(174) Elliott, G. P.; Roper, W. R.; Waters, J. M. Metallacyclohexatrienes or "Metallabenzenes". Synthesis of Osmabenzene Derivatives and X-Ray Crystal Structure of $[Os(CSCHCHCHCH)(CO)(PPh_3)_2]$. *J. Chem. Soc., Chem. Comm.* **1982**, 811-813.

(175) (a) Bleeke, J. R. Metallabenzenes. *Chem. Rev.* **2001**, *101*, 1205-1227. (b) Cao, X.-Y.; Zhao, Q.; Lin, Z.; Xia, H. The Chemistry of Aromatic Osmacycles. *Acc. Chem. Res.* **2014**, *47*, 341-354. (c) Fernández, I.; Frenking, G.; Merino, G. Aromaticity of Metallabenzenes and Related Compounds. *Chem. Soc. Rev.* **2015**, *44*, 6452-6463. (d) Frogley, B. J.; Wright, L. J. Recent Advances in Metallaaromatic Chemistry. *Chem. - Eur. J.* **2018**, *24*, 2025-2038. (e) Zhu, C.; Xia, H. Carbolong Chemistry: A Story of Carbon Chain Ligands and Transition Metals. *Acc. Chem. Res.* **2018**, *51*, 1691-1700.

(176) Bursten, B. E.; Fenske, R. F. Molecular Orbital Studies on Cyclobutadiene Metal Complexes: Concept of Metalloaromaticity. *Inorg. Chem.* **1979**, *18*, 1760-1765.

(177) (a) Masui, H. Metalloaromaticity. *Coord. Chem. Rev.* **2001**, *219*, 957-992. (b) Feixas, F.; Matito, E.; Poater, J.; Solà, M. Metalloaromaticity. *WIREs Comput. Mol. Sci.* **2013**, *3*, 105-122.

(178) (a) Boldyrev, A. I.; Wang, L. S. All-Metal Aromaticity and Antiaromaticity. *Chem. Rev.* **2005**, *105*, 3716-3757. (b) Tsipis, C. A. DFT Study of "All-Metal" Aromatic Compounds. *Coord. Chem. Rev.* **2005**, *249*, 2740-2762. (c) Zubarev, D. Y.; Averkiev, B. B.; Zhai, H.-J.; Wang, L.-S.; Boldyrev, A. I. Aromaticity and Antiaromaticity in Transition-Metal Systems. *Phys. Chem.*

Chem. Phys. **2008**, *10*, 257-267. (d) Li, L.-J.; Ali, B.; Chen, Z.; Sun, Z.-M. Recent Advances in Aromatic Antimony Clusters. *Chin. J. Chem.* **2018**, *36*, 955-960.

(179) (a) Li, X.-W.; Pennington, W. T.; Robinson, G. H. A Metallic System with Aromatic Character. Synthesis and Molecular Structure of $Na_2[(Mes_2C_6H_3)Ga]_3$ (Mes=2,4,6-$Me_3C_6H_2$): The First Cyclogallane. *J. Am. Chem. Soc.* **1995**, *117*, 7578-7579. (b) Li, X. W.; Xie, Y. M.; Schreiner, P. R.; Gripper, K. D.; Critendon, R. C.; Campana, C. F.; Schaefer, H. F.; Robinson, G. H. Cyclogallanes and Metalloaromaticity. Synthesis and Molecular Structure of Dipotassium Tris((2,6-dimesityphenyl)cyclogallene), $K_2[(Mes_2C_6H_3)Ga]_3$ (Mes=2,4,6-$Mes_2C_6H_3$): A Structural and Theoretical Examination. *Organometallics* **1996**, *15*, 3798-3803. (c) Robinson, G. H. Gallanes, Gallenes, Cyclogallenes, and Gallynes: Organometallic Chemistry about the Gallium−Gallium Bond. *Acc. Chem. Res.* **1999**, *32*, 773-782. (d) Wang, Y. Z.; Robinson, G. H. Organometallics of the Group 13 M-M Bond (M = Al, Ga, In) and the Concept of Metalloaromaticity. *Organometallics* **2007**, *26*, 2-11.

(180) Maslowsky, E. Inorganic Metallocenes: The Structures and Aromaticity of Sandwich Compounds of the Transition Elements with Inorganic Rings. *Coord. Chem. Rev.* **2011**, *255*, 2746-2763.

(181) Blanchard, S.; Fensterbank, L.; Gontard, G.; Lacôte, E.; Maestri, G.; Malacria, M. Synthesis of Triangular Tripalladium Cations as Noble-Metal Analogues of the Cyclopropenyl Cation. *Angew. Chem., Int. Ed.* **2014**, *53*, 1987-1991.

(182) Robilotto, T. J.; Bacsa, J.; Gray, T. G.; Sadighi, J. P. Synthesis of a Trigold Monocation: An Isolobal Analogue of $[H_3]^+$. *Angew. Chem., Int. Ed.* **2012**, *51*, 12077-12080.

(183) (a) Fernández, I.; Duvall, M.; I-Chia Wu, J.; Schleyer, P. v. R.; Frenking, G. Aromaticity in Group 14 Homologues of the Cyclopropenylium Cation. *Chem. - Eur. J.* **2011**, *17*, 2215-2224. (b) Fernández, I.; Wu, J. I.; Schleyer, P. v. R. Substituent Effects on "Hyperconjugative" Aromaticity and Antiaromaticity in Planar Cyclopolyenes. *Org. Lett.* **2013**, *15*, 2990-2993.

(184) Figueroa, J. S.; Cummins, C. C. Triatomic EP_2 Triangles (E = Ge, Sn, Pb) as μ^2: η^3,η^3-Bridging Ligands. *Angew. Chem., Int. Ed.* **2005**, *44*, 4592-4596.

(185) Ullah, S. S.; Mazumder, L. J.; Kaushik, S.; Das, N.; Brahma, M. S.; Sharma, P. K.; Guha, A. K. Electronic Structure, Stability, and Aromaticity of H_2B_2XH (X=N, P) molecules: A Theoretical Study. *Comput. Theor. Chem.* **2017**, *1113*, 120-125.

(186) Esteruelas, M. A.; García-Yebra, C.; Martín, J.; Oñate, E. Dehydrogenation of Formic Acid Promoted by a Trihydride-Hydroxo-Osmium(IV) Complex: Kinetics and Mechanism. *ACS Catal.* **2018**, *8*, 11314-11323.

(187) (a) Au, Y.-K.; Cheung, K.-K.; Wong, W.-T. Synthesis and Structural Characterization of Ruthenium and Osmium Carbonyl Clusters Containing 4,6-Dimethylpyrimidine-2-thione. *Inorg. Chim. Acta.* **1995**, *228*, 267-275. (b) Au, Y.-K.; Cheung, K.-K.; Wong, W.-T. Synthesis, Structural Characterization and Thermal Reactivities of Osmium Carbonyl Clusters Containing 4,6-Dimethylpyrimidine-2-thione. *J. Chem. Soc., Dalton Trans.* **1995**, 1047-1057. (c) Reyes-López, O. R.; Leyva, M. A.; Rosales-Hoz, M. J. Structural Characterization of [(μ-H)$Os_3(CO)_{10}$(μ-NH_2)] and a New Polymorphic form of [(μ-H)$Os_3(CO)_{10}$(μ-SH)]. Influence of the Bridging Group on the Geometry of Compounds [(μ-H)$Os_3(CO)_{10}$(μ-X)] (X=NH_2, NRH, PRH,

SbR_2, OH, SH, SR, SeR, Cl, Br). Reactions of [(μ-H)$Os_3(CO)_{10}$(μ-X)] (X=OH and SH) with Proton Sponge. *J. Mol. Struct.* **2011**, *985*, 134-138.

(188) Wozniak, M.; Braun, T.; Ahrens, M.; Braun-Cula, B.; Wittwer, P.; Herrmann, R.; Laubenstein, R. Activation of SF6 at a Xantphos-Type Rhodium Complex. *Organometallics* **2018**, *37*, 821-828.

(189) Liu, S. Y.; Légaré, M.-A.; Auerhammer, D.; Hofmann, A.; Braunschweig, H. The First Boron-Tellurium Double Bond: Direct Insertion of Heavy Chalcogens into a Mn=B Double Bond. *Angew. Chem., Int. Ed.* **2017**, *56*, 15760-15763.

(190) Wang, H.; Zhang, J. Y.; Hu, H. F.; Cui, C. M. Access to B=S and B=Se Double Bonds via Sulfur and Selenium Insertion into a B-H Bond and Hydrogen Migration. *J. Am. Chem. Soc.* **2010**, *132*, 10998-10999.

(191) Jaiswal, K.; Prashanth, B.; Ravi, S.; Shamasundar, K. R.; Singh, S. Reactivity of a Dihydroboron Species: Synthesis of a Hydroborenium Complex and an Expedient Entry into Stable Thioxo- and Selenoxo-Boranes. *Dalton Trans.* **2015**, *44*, 15779-15785.

(192) Franz, D.; Irran, E.; Inoue, S. Isolation of a Three-Coordinate Boron Cation with a Boron-Sulfur Double Bond. *Angew. Chem., Int. Ed.* **2014**, *53*, 14264-14268.

(193) Bauer, J.; Braunschweig, H.; Damme, A.; Carlos, J. O.; Kramer, J.-H. T.; Radacki, K.; Shang, R.; Siedler, E.; Ye, Q. Metathesis Reactions of a Manganese Borylene Complex with Polar Heteroatom-Carbon Double Bonds: A Pathway to Previously Inaccessible Carbene Complexes. *J. Am. Chem. Soc.* **2013**, *135*, 8726-8734.

(194) Fallah-Bagher-Shaidaei, H.; Wannere, C. S.; Corminboeuf, C.; Puchta, R.; Schleyer, P. v. R. Which NICS Aromaticity Index for Planar π Rings is Best? *Org. Lett.* **2006**, *8*, 863-866.

(195) (a) Herges, R.; Geuenich, D. Delocalization of Electrons in Molecules. *J. Phys. Chem. A.* **2001**, *105*, 3214-3220. (b) Geuenich, D.; Hess, K.; Köhler, F.; Herges, R. Anisotropy of the Induced Current Density (ACID), a General Method to Quantify and Visualize Electronic Delocalization. *Chem. Rev.* **2005**, *105*, 3758-3772.

AGRADECIMIENTOS

- Grupo de Organometálicos y Catálisis del Instituto de Síntesis Química y Catálisis Homogénea (ISQCH) por financiar mi contratación por parte de la Universidad de Zaragoza a través de los contratos PUI14/244.2 (periodo 15/01/2015 – 31/03/2018) y PUI18/47.2 (periodo 01/04/2018 – 31/03/2019).

- Universidad de Zaragoza y Consejo Superior de Investigaciones Científicas por poner a mi disposición todos los medios necesarios para realizar la presente Tesis.

- Diputación General de Aragón (proyectos E35 y E06_17R) y Ministerio de Economía y Competitividad (proyectos CTQ2014-52799-P, CTQ2017-82935-P, y Red de Excelencia Consolider CTQ2014-51912-REDC, CTQ2016-81797-REDC) por financiar la investigación llevada acabo en la presente Tesis.

APÉNDICE

A continuación, se presenta el factor de impacto y el área temática al que pertenecen las revistas donde están publicados los trabajos que constituyen esta tesis.

- *ACS Catalysis*

Índice de Impacto: 12,221 (Journal Citation Reports 2018)

Rank.: 11/148. Q1 (Chemistry, Physical)

- *Inorganic Chemistry*

Índice de Impacto: 4,850 (Journal Citation Reports 2018)

Rank.: 4/45. Q1 (Chemistry, Inorganic & Nuclear)

- *Organometallics*

Índice de Impacto: 4,100 (Journal Citation Reports 2018)

Rank.: 5/45. Q1 (Chemistry, Inorganic & Nuclear)

COPIA DE LAS PUBLICACIONES

Mer-, Fac-, and Bidentate-Coordination of an Alkyl-POP Ligand in the Chemistry of Nonclassical Osmium-Hydrides

Miguel A. Esteruelas, Cristina García-Yebra, Jaime Martín, and Enrique Oñate*

Departamento de Química Inorgánica, Instituto de Síntesis Química y Catálisis Homogénea (ISQCH), Centro de Innovación en Química Avanzada (ORFEO−CINQA), Universidad de Zaragoza−CSIC, 50009 Zaragoza, Spain

ABSTRACT

Nonclassical and classical osmium polyhydrides containing the diphosphine 9,9-dimethyl-4,5-bis(diisopropylphosphino)xanthene (xant(P^iPr_2)$_2$), coordinated κ^3-*mer*, κ^3-*fac*, and κ^2-P,P, have been isolated during the cyclic formation of H_2 by means of the sequential addition of H^+ and H^- or H^- and H^+ to the classical trihydride $OsH_3Cl\{xant(P^iPr_2)_2\}$ (**1**). This complex adds H^+ to form the compressed dihydride-dihydrogen $[OsCl(H\cdots H)(\eta^2\text{-}H_2)\{xant(P^iPr_2)_2\}]^+$ (**2**). Under argon, cation **2** losses H_2 and the resulting unsaturated fragment dimerizes to give $[(Os(H\cdots H)\{xant(P^iPr_2)_2\})_2(\mu\text{-}Cl)_2]^{2+}$ (**3**). During the transformation the phosphine changes its coordination mode from *mer* to *fac*. The benzofuran counterpart of **1**, $OsH_3Cl\{dbf(P^iPr_2)_2\}$ (**4**)

(dbf(P^iPr_2)$_2$ = 4,6-bis(diisopropylphosphino)dibenzofuran), also adds H^+ to afford the benzofuran counterpart of **2**, $[OsCl(H\cdots H)(\eta^2\text{-}H_2)\{xant(P^iPr_2)_2\}]^+$ (**5**), which in contrast to the latter is stable and does not dimerize. Acetonitrile breaks the chloride bridge of **3** to form the dihydrogen $[OsCl(\eta^2\text{-}H_2)(CH_3CN)\{xant(P^iPr_2)_2\}]^+$ (**6**), regenerating the *mer* coordination of the diphosphine. The hydride ion also breaks the chloride bridge of **3**. The addition of KH to **3** leads to **1**, closing a cycle for the formation of H_2. Complex **1** reacts with a second hydride ion to give $OsH_4\{xant(P^iPr_2)_2\}$ (**7**) as consequence of the displacement of the chloride. Similarly to the latter, the oxygen atom of the *mer*-coordinate diphosphine of **7** has tendency to be displaced by the hydride ion. Thus the addition of KH to **7** yields $[OsH_5\{xant(P^iPr_2)_2\}]^-$ (**8**), containing a κ^2-P,P-diphosphine. Complex **8** is easily protonated to afford $OsH_6\{xant(P^iPr_2)_2\}$ (**9**), which releases H_2 to regenerate **7**, closing a second cycle for the formation of molecular hydrogen.

INTRODUCTION

The chemical behavior of a transition metal complex is determined by the central ion and by the ligands forming its coordination sphere. The groups surrounding the core govern the available electron density of the metal ion and the accessible space for performing the reactions. In some cases, the ligands also cooperate with the metal by means of a direct participation in the chemical transformations.[1] There are other ligands that change their properties during the reactions. This group includes ligands that modify their electronic donor ability while are adapted to the reaction medium by means of reversible transformations[2] and ligands that change their coordination mode to meet with the requirements of each stage of a multi-step process.

Hemilabile groups are the simplest class of ligands with the latter behavior. The reversible coordination-decoordination of the hemilabile donor atom allows the stabilization of highly reactive metal centers, which has a significant influence in the catalytic behavior of the complexes.[3] Tridentate anionic PCP-diphosphines are situated in the opposite position. Although their *mer*-coordination allows them to stabilize complexes with unusual reactivity,[4] the stability and rigidity of the pincer diminishes the adaptability of these ligands to the requirement of the sequential processes. In the search for more versatile diphosphines that could act as κ^3-*fac* and bidentate groups, in addition to κ^3-*mer*, flexible POP ethers have been also employed.[5] Thus, Weller and co-workers have demonstrated that 4,5-bis(diphenylphosphino)-9,9-dimethylxanthene (xantphos) has the ability of changing its coordination fashion in several relevant rhodium- and iridium-mediated processes,[6] such as the hydroacylation[7] and carbothiolation[8] of alkenes and alkynes and the dehydrocoupling of amineboranes.[9]

Transition metal polyhydrides are compounds having enough hydrogen atoms bonded to the metal center of a L_nM fragment to form at least two different types of ligands.[10] These ligands are generally classified in four types depending upon the separation between the coordinated hydrogens: Kubas type dihydrogens (0.8 – 1.0 Å), elongated dihydrogens (1.0 – 1.3 Å), compressed dihydrides (1.3 – 1.6 Å), and classical hydrides (> 1.6 Å).[10,11] Polyhydrides of the platinum group metals offer new exciting conceptual challenges and the possibility of interacting with different fields,[10] including the conversion and storage of regenerative energy.[12] In this respect, osmium polyhydrides are of particular interest. In addition to promote the dehydrocoupling of amineboranes,[13] their ability to activate C-H, N-H, and C-N bonds of a wide range of organic molecules, including 2-azetidinones[14] and nucleobases[15], allow them to interact with organic synthetic chemistry,[16] drugs design,[14a] and material science.[17] Although the

chemistry of the osmium polyhydrides is rich, the complexes of this type with pincer ligands are a noticeable exception,[10] being reduced to a few complexes with PNP,[18] P(olefin)P[19] and P(Csp^3)P[20] ligands. Recently, we have reported that the reactions of complexes $OsCl_2$\{xant(P^iPr_2)$_2$\}(κ-S-DMSO) (xant(P^iPr_2)$_2$ = 9,9-dimethyl-4,5-bis(diisopropylphosphino)xanthene) and $OsCl_2$\{dbf(P^iPr_2)$_2$\}(κ-S-DMSO) (dbf(P^iPr_2)$_2$ = 4,6-bis(diisopropylphosphino)dibenzofuran) with molecular hydrogen, in the presence of Et_3N, lead to the classical trihydride derivatives OsH_3Cl\{xant(P^iPr_2)$_2$\}[21] and OsH_3Cl\{dbf(P^iPr_2)$_2$\}[16d] containing a pincer POP-ligand. Our interest in determining the influence of the different coordination modes of flexible pincer ligands on the nature of the H-donor ligands of Osmium polyhydrides prompted us to study the protonation of the hydride ion, kinetically controlled by OsH_3Cl\{xant(P^iPr_2)$_2$\}. The kinetically controlled formation of molecular hydrogen by the exothermic neutralization of the hydride ion is a process of great interest in connection with the storage of hydrogen in solid materials, which would become a safe and efficient way to store energy for both stationary and mobile applications.[22]

This paper shows that the ligand 9,9-dimethyl-4,5-bis(diisopropylphosphino)xanthene changes its coordination mode to stabilize Kubas type dihydrogens, elongated dihydrogens, compressed dihydrides, and classical hydrides, which act as intermediates to generate molecular hydrogen from H^+ and H^-, in the presence of osmium polyhydrides. In addition, it proves that the *mer* coordination favors nonclassical interactions between the coordinated hydrogen atoms, with regard to the *fac* and bidentate coordination modes.

RESULTS AND DISCUSSION

Scheme 1 sumarizes the procedures used to generate molecular hydrogen starting from the classical trihydride $OsH_3Cl\{xant(P^iPr_2)_2\}$ (**1**). The ***route a*** involves the sequential addition of H^+ and H^- whereas the ***route b*** involves the opposite addition.

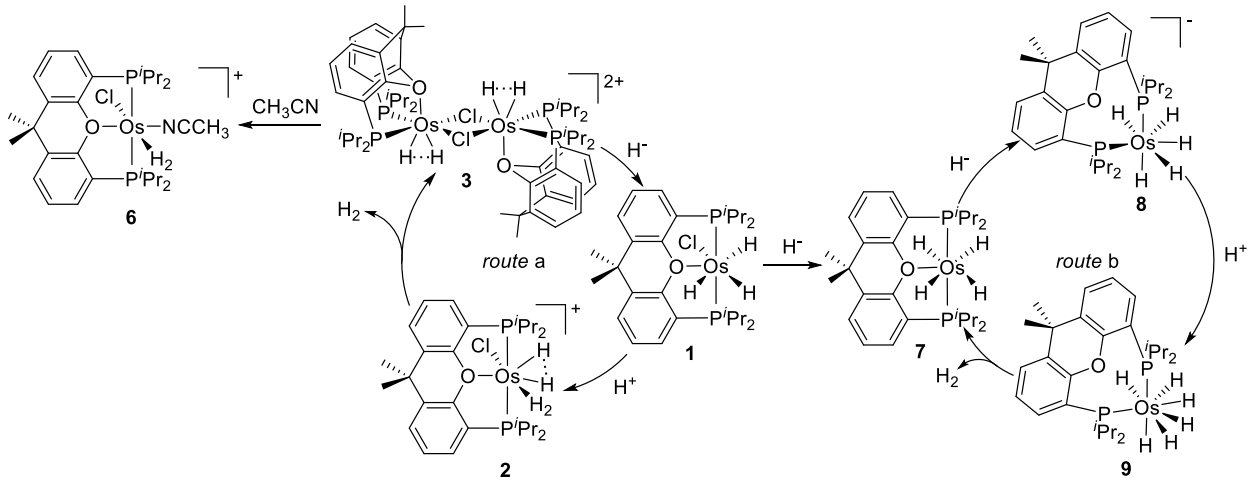

Scheme 1. Formation of H_2 by sequential addition of H^+ and H^- or H^- and H^+ to $OsH_3Cl\{xant(P^iPr_2)_2\}$ (**1**) in two related cycles.

Complex **1** adds a proton in agreement with the Lewis base character of the saturated polyhydrides. Under hydrogen atmosphere, the addition of 1.0 equiv of $HBF_4{\cdot}OEt_2$ to **1** in dichloromethane-d_2 leads to the cation $[OsCl(H\cdots H)(\eta^2\text{-}H_2)\{xant(P^iPr_2)_2\}]^+$ (**2**). The presence of four hydrogen atoms bonded to the metal center is supported by the ^1H NMR spectrum of the resulting solution, which contains a broad signal at -10.71 ppm with an integrated intensity of 4. According to the existence of nonclassical interactions between the coordinated hydrogen atoms, this resonance exhibits a 400 MHz T_1(min) value of 40 ± 2 ms at 203 K. The $^{31}P\{^1H\}$ NMR spectrum shows a singlet at 62.6 ppm. DFT calculations (energies calculated at the B3LYP(GD3)//6-31G(d,p)/SDD level with the Gaussian 09 program[23]) reveal that there are two compressed dihydride-dihydrogen structures differing by 3.0 kcal.mol^{-1} (ΔG, 1 atm, 298.15 K):

2a and **2b**. Figure 1 shows a view of these DFT-optimized structures. In both cases, the diphoshpine is *mer*-coordinated with P(1)-Os-P(2), O-Os-P(1), and O-Os-P(2) angles of 160.2°, 80.0°, and 80.2° for **2a** and 165.5°, 82.6°, and 82.4° for **2b**. The most stable structure **2a** shows the dihydrogen ligand (1.029 Å) at the perpendicular plane to the P-Os-P direction, *trans* disposed to the chloride, whereas the compressed dihydride (1.427 Å) lies *trans* to the oxygen atom of the diphosphine, almost parallel to the P-Os-P direction. In **2b**, the dihydrogen (1.091 Å) and the compressed dihydride (1.358 Å) ligands exchange their positions.

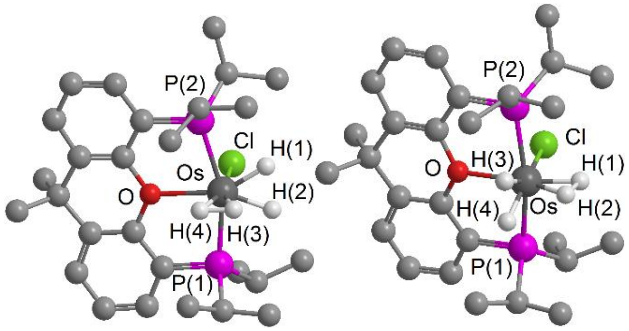

2a **2b**

Figure 1 DFT optimized structures of **2a** and **2b**. Hydrogen atoms (except hydrides) are omitted for clarity. Selected bond lengths (Å) and angles (°): for **2a** Os-O = 2.307, Os-P(1) = 2.381, Os-P(2) = 2.384, Os-Cl = 2.438, H(1)-H(2) = 1.427, H(3)-H(4) = 1.029, O-Os-P(1) = 80.0, O-Os-P(2) = 80.2, P(1)-Os-P(2) = 160.2; for **2b** Os-O = 2.224, Os-P(1) = 2.390, Os-P(2) = 2.391, Os-Cl = 2.474, H(1)-H(2) = 1.091, H(3)-H(4) = 1.358, O-Os-P(1) = 82.6, O-Os-P(2) = 82.4, P(1)-Os-P(2) = 165.5.

The lability of the dihydrogen ligand in **2** suggests that it is of the Kubas type even though the separation between the two hydrogen atoms lies at the border between a Kubas-type dihydrogen and an elongated dihydrogen.Thus, complex **2** can be kept in dichloromethane, under hydrogen atmosphere, at room temperature, for a few hours. However, under argon, it losses the

dihydrogen ligand to afford the dimer $[(Os(H\cdots H)\{xant(P^iPr_2)_2\})_2(\mu\text{-}Cl)_2]^{2+}$ (**3**) which was isolated as its yellow BF_4-salt in 95% yield and characterized by X-ray diffraction analysis.[24] The structure (Figure 2) shows a change in the coordination mode of the diphosphine, which now coordinates in a κ^3-*fac* fashion with O-Os-P(1), O-Os-P(2) and P(1)-Os-P(2) angles of 80.45(9)°, 82.32(9)° and 107.72(5)°, respectively. The coordinated hydrogen atoms, separated by 1.36(6) (Å), lie *trans* to the oxygen atoms of the diphoshines forming a compressed dihydride. The nonclassical nature of the OsH_2-units was confirmed by the ^1H NMR spectrum in dichloromethane-d_2, which shows a triplet ($^2J_{H\text{-}P}$ = 14.5 Hz) at -9.53 ppm. In agreement with the H-H separation found by X-ray- diffraction analysis, this resonance exhibits a 400 MHz T_1(min) value of 63 ± 3 ms, at 243 K, and a $J_{H\text{-}D}$ value of 7 Hz which fit with H-H separations of 1.35 Å and 1.32 Å, respectively.[25] The $^{31}P\{^1H\}$ NMR spectrum shows a signal at 42.9 ppm.

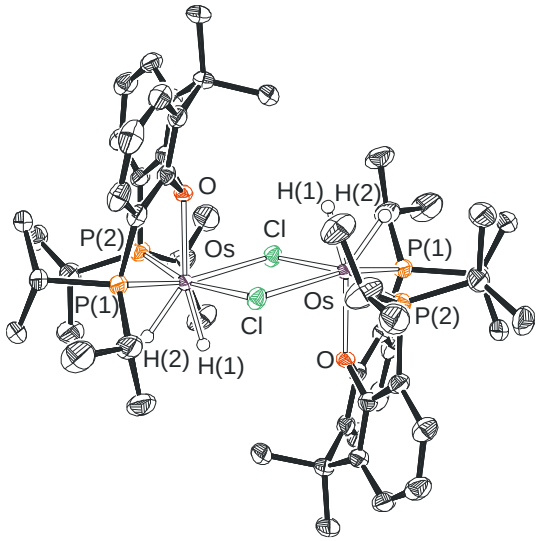

Figure 2 ORTEP diagram of complex **3** with 50% probability ellipsoids. The counteranions, solvent molecules, and hydrogen atoms (except hydrides) are omitted for clarity. Selected bond lengths (Å) and angles (°): Os-O = 2.156(3), Os-P(1) = 2.316(1), Os-P(2) = 2.295(1), H(1)-H(2) = 1.36(6), O-Os-centroid H(1)-H(2) = 169.65, O-Os-P(1) = 80.45(9); O-Os-P(2) = 82.32(9), P(1)-Os-P(2) = 107.72(5).

The *fac*-coordination of the diphosphine in **3** is a determinant factor for the stabilization of the dimeric structure with regard to **2**, which is related to the flexibility of the xanthene group. In fact, the most rigid benzofuran stabilizes the OsH_4-species and prevents the formation of a counterpart dimer of **3**. Thus, under argon, the addition of 1.0 equiv of $HBF_4{\cdot}OEt_2$ to $OsH_3Cl\{dbf(P^iPr_2)_2\}$ (**4**) in dichloromethane leads to the compressed dihydride-dihydrogen $[OsCl(H\cdots H)(\eta^2\text{-}H_2)\{dbf(P^iPr_2)_2\}]BF_4$ (**5**), which was isolated as a pale yellow solid in 85% yield (eq.1). In contrast to **2**, this 4,6-bis(diisopropylphosphino)dibenzofuran counterpart is moderately stable under argon, in the solid state, and in dichloromethane and does not release molecular hydrogen to dimerize. Complex **5** was characterized by X-ray diffraction analysis. Its structure (Figure 3) is in full agreement with the optimized structure of the most stable isomer of **2**. As in the latter, the diphosphine is *mer*-coordinated with O-Os-P(1), O-Os-P(2) and P(1)-Os-P(2) angles of 78.66(9)°, 78.72(9)° and 157.23(4)° respectively. The dihydrogen ligand (H(3)-H(4) = 1.06(5) Å (X-ray), 0.976 Å (DFT)) lies at the perpendicular plane to the P-Os-P direction, *trans*-disposed to the chloride; and the compressed dihydride (1.10(7) Å (X-ray), 1.387 Å (DFT)) is situated *trans* to the oxygen atom of the diphosphine, almost parallel to the P-Os-P direction. In the ^1H NMR spectrum in dichloromethane-d_2, the OsH_4-unit displays a broad signal at -10.60 ppm, which exhibits a 400 MHz T_1(min) value of 40 ± 2 ms at 203 K, in agreement with **2**. The $^{31}P\{^1H\}$ NMR spectrum contains a singlet at 65.3 ppm.

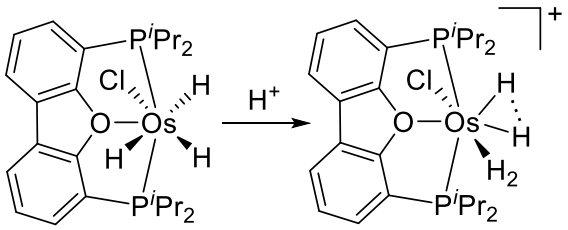

4 **5** (1)

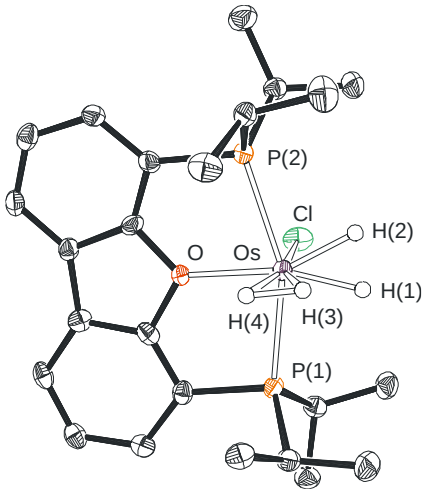

Figure 3. ORTEP diagram of complex **5** with 50% probability ellipsoids. The counteranions, solvent molecules, and hydrogen atoms (except hydrides) are omitted for clarity. Selected bond lengths (Å) and angles (°): Os-O = 2.092(3), Os-P(1) = 2.400(1), Os-P(2) = 2.403(1), H(3)-H(4) = 1.06(5), H(1)-H(2) = 1.10(7), Os-Cl = 2.415(1), O-Os-centroid H(1)-H(2) = 171.37, Cl-Os-centroid H(3)-H(4) = 178.09, O-Os-P(1) = 78.66(9), O-Os-P(2) = 78.72(9), P(1)-Os-P(2) = 157.23(4).

The coordination changes from κ^3-*mer* to κ^3-*fac* of the diphosphine is a requirement for the coordinative saturation of the metal center on the $[OsClH_2\{xant(P^iPr_2)\}]^+$ fragment resulting from the dissociation of molecular hydrogen from **2**, since the steric hindrance experienced by the isopropyl substituents of the *mer*-coordinated diphosphines of two unsaturated fragments appears to prevent the dimerization. However, the coordination κ^3-*mer* is clearly favored over the κ^3-*fac*, when the metal center of a mononuclear complex is saturated. As a proof of concept, it should be mentioned that the chloride bridges of **3** are broken in acetonitrile to form the saturated dihydrogen complex $[OsCl(\eta^2\text{-}H_2)(CH_3CN)\{xant(P^iPr_2)_2\}]BF_4$ (**6**), which contains a κ^3-*mer* coordinated diphosphine. This compound was isolated as a white solid, in almost quantitative yield, and characterized by X-ray diffraction analysis. The structure[26] (Figure 4) proves the *mer*-

coordination (O-Os-P(1) = 83.08(6)°, 83.13(7)°; P(1)-Os-P(1) = 165.85(13)°, 165.81(14)°) of the diphosphine. The dihydrogen ligand (1.02(6) Å (X-ray), 0.985 Å (DFT)), which is almost parallel to the P-Os-P direction, lies *trans* to the chloride. In the ^{1}H NMR spectrum, in dichloromethane-d_2, the coordinated hydrogen molecule displays a triplet ($^{2}J_{H-P}$ = 6 Hz) at -9.86 ppm. As expected for its Kubas type dihydrogen nature, this resonance exhibits a 300 MHz T_1(min) value of 21 ± 1 ms, at 203 K, whereas the H-D coupling constant in the partially deuterated species is 20 Hz. These values allow to calculate H-H separations of 0.94 Å and 1.09 Å, respectively,[25] which agree well with that obtained by X-ray diffraction analysis. The ^{31}P{^{1}H} NMR spectrum shows a singlet at 27.2 ppm.

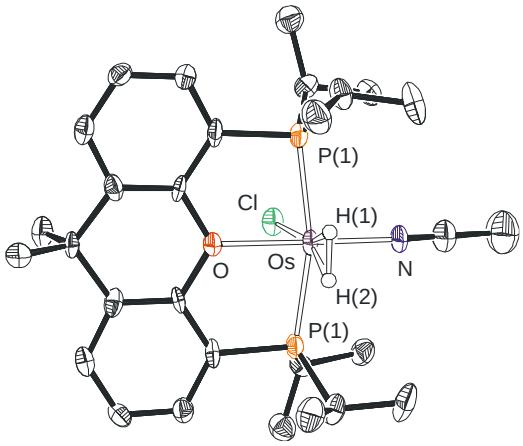

Figure 4. ORTEP diagram for one of the two molecules in the symmetry unit of complex **6** with 50% probability ellipsoids. The counteranions, solvent molecules, and hydrogen atoms (except hydrides) are omitted for clarity. Selected bond lengths (Å) and angles (°): Os-O = 2.131(9), Os-P(1) = 2.338(3), Os-Cl = 2.441(4), Os-N = 2.024(16), H(1)-H(2) = 1.02(6), Cl-Os-centroid H(1)-H(2) = 174.96, O-Os-P(1) = 83.08(6), P(1)-Os-P(1) = 165.85(13).

The hydride ion also breaks the chloride bridges of **3**. The addition of KH to the tetrahydrofuran solutions of the dimer regenerates **1**, closing a cycle for the formation of molecular hydrogen by reaction of H^+ and H^- on the osmium center of **1** (***route* a** in **Scheme 1**).

The hydride ion displaces the chloride ligand of **1** to afford the tetrahydride derivative $OsH_4\{xant(P^iPr_2)_2\}$ (**7**). The classical nature of the coordinated hydrogen atoms of this previously reported compound was confirmed by X-ray diffraction analysis and DFT calculations.[21] Similarly to chloride, the oxygen atom of the *mer*-coordinate diphosphine of the latter has tendency to be displaced by the hydride ion. The addition of KH to **7** in tetrahydrofuran leads to the anionic pentahydride $[OsH_5\{xant(P^iPr_2)_2\}]^-$ (**8**), containing a κ^2-P,P-bidentate diphosphine. In the presence of the crown ether 18-crown-6, yellow crystals of the [K(18-crown-6)]$^+$-salt were obtained in 66% yield. The X-ray diffraction structure (Figure 5) proves the bidentate coordination of the diphosphine, which acts with a P-Os-P bite angle of 109.46(3)°. The coordination polyhedron around the osmium atom can be idealized as a pentagonal bipyramid with the hydride H(5) and the P(1) atom of the diphosphine in axial positions (P(1)-Os-H(5) = 165.6(16)°), whereas the P(2) atom and the remaining hydrides lie in the equatorial plane. The disposition of the phosphorous atoms is certainly enforced by the bidentate character of the diphosphine. In contrast to **8**, the related anion $[OsH_5(P^iPr_3)_2]^-$ contains both monodentated phosphines at the axial positions of the bipyramid.[27] The structure also shows three hydrides pointing towards the potassium cation, which is slightly out of the plane of the crown ether. The ion pair is helped together through electrostatic interactions, enhanced by the ionic nature of cation and anion. In tetrahydrofuran the hydride ligands, as well as the phosphorous atoms of the diphosphine, rapidly exchange their positions even at 183 K. In agreement with this, the ^{1}H NMR spectrum shows a broad signal at -12.46 ppm, whereas the $^{31}P\{^1H\}$ NMR spectrum contains a singlet at 20.6 ppm. The classical hydride character of the coordinated hydrogen atoms is strongly supported by the 400MHz T_1(min) of the hydride resonance, 248 ms, at 208 K.

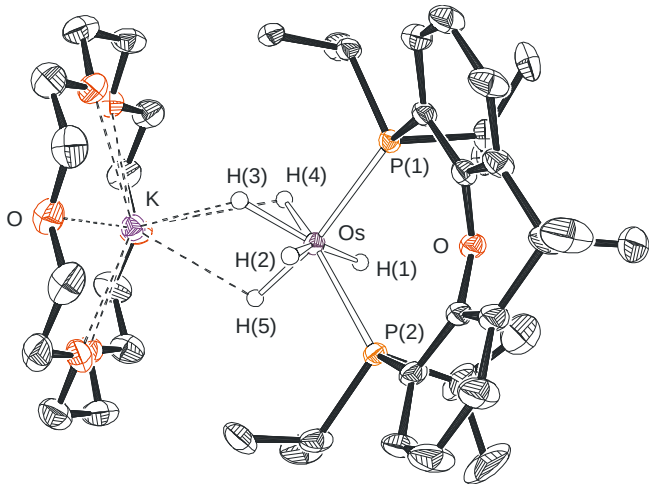

Figure 5. ORTEP diagram of complex **8** with 50% probability ellipsoids. The solvent molecules, and hydrogen atoms (except hydrides) are omitted for clarity. Selected bond lengths (Å) and angles (°): Os-O = 3.496(3), Os-P(1) = 2.309(1), Os-P(2) = 2.322(1), Os-K = 3.624(1), P(1)-Os-P(2) = 109.46(3), P(1)-Os-H(5) = 165.6(16).

Complex **8** is a strong Brønsted base which is even protonated by traces of water. The protonation leads to the hexahydride $OsH_6\{xant(P^iPr_2)_2\}$ (**9**), also containing a P,P-bidentate diphosphine with the P atoms at a B site of the BAAB trapezoidal planes, which define its dodecaedral structure.[21, 28] Complex **9** releases molecular hydrogen and coordinates the oxygen atom to regenerate the tetrahydride **7**, closing a second cycle for the formation of molecular hydrogen by reaction of H^- with H^+ on the metal center of the tetrahydride **7** (***route* b** in **Scheme 1**).

CONCLUDING REMARKS

This study reveals that osmium-polyhydrides stabilized by the POP-pincer ligand 9,9-dimethyl-4,5-bis(diisopropylphosphine)xanthene sequentially add H^+ and H^- or H^- and H^+ to generate molecular hydrogen in a cyclic manner. During the process the diphosphine changes its coordination mode from κ^3-*mer* to κ^3-*fac* and κ^2-P,P-bidentate, depending upon the electronic

and steric requirements of the involved intermediates, to form both polyhydrides with nonclassical interactions and classical polyhydrides. The nonclassical interactions are favored by the tridentate coordination, in particular by the *mer*-disposition, whereas the classical polyhydrides are usual when the diphosphine is bidentate. The flexibility of the central xanthene group is a determinant factor for the behavior of the diphosphine.

EXPERIMENTAL SECTION

General Information. All reactions were carried out under argon with rigorous exclusion of air using Schlenk tube or glovebox techniques. Solvents were dried by the usual procedures and distilled under argon prior to use or obtained oxygen- and water-free from an MBraun solvent purification apparatus. The starting materials $[OsH_3Cl\{xant(P^iPr_2)_2\}]$ (**1**),[21] $[OsH_3Cl\{dbf(P^iPr_2)_2\}]$ (**4**)[16d] and $[OsH_4\{xant(P^iPr_2)_2\}]$ (**7**)[21] were prepared according to published methods. ^1H, $^{31}P\{^1H\}$, and $^{13}C\{^1H\}$ NMR spectra were recorded on either a Bruker 300 ARX, Bruker Avance 300 MHz or a Bruker Avance 400 MHz instrument. Chemical shifts (expressed in parts per million) are referenced to residual solvent peaks (^1H, $^{13}C\{^1H\}$) or external H_3PO_4 ($^{31}P\{^1H\}$). Coupling constants, J and N ($N = J_{PH} + J_{P'H}$ for ^1H; $N = J_{PC} + J_{P'C}$ for ^{13}C) are given in hertz. Spectral assignments were achieved by ^1H-^1H COSY, $^1H\{^{31}P\}$, ^{13}C APT, ^1H-^{13}C HSQC and ^1H-^{13}C HMBC experiments. Infrared spectra were recorded on a Perkin-Elmer Spectrum One or Perkin-Elmer Spectrum 100 FT-IR spectrometer, equipped with an ATR accessory, as neat solids. C, H, and N analyses were carried out in a Perkin-Elmer 2400 CHNS/O analyzer. High-resolution electrospray mass spectra were acquired using a MicroTOF-Q hybrid quadrupole time-of-flight spectrometer (Bruker Daltonics, Bremen, Germany).

Formation of $[OsCl(H\cdots H)(\eta^2\text{-}H_2)\{xant(P^iPr_2)_2\}]BF_4$ (2). A solution of $[OsH_3Cl\{xant(P^iPr_2)_2\}]$ (**1**) (50 mg; 0.073 mmol) in dichloromethane-d_2 (0.6 mL) was placed in a

screw-top NMR tube under H_2 atmosphere, and $HBF_4{\cdot}OEt_2$ (11 μL; 0.081 mmol) was added. NMR spectra of the reaction solution showed immediate and quantitative formation of **2**. All attempts to isolate the new species were unsuccessful due to easy loss of hydrogen to form the dinuclear complex **3**.

HRMS (*electrospray, m/z*): calcd. for $C_{27}H_{44}ClOOsP_2$ $[M]^+$: 673.2158, found: 673.2155. ^{1}H NMR (400 MHz, CD_2Cl_2, 233K): δ 7.76 (d, $^3J_{HH}$ = 7.5, 2H, C*H*-arom), 7.67 (m, 2H, C*H*-arom), 7.53 (dd, $^3J_{HH}$ = 7.6, $^3J_{HH}$ = 7.5, 2H, C*H*-arom), 3.09 (m, 2H, PC*H*$(CH_3)_2$), 2.79 (m, 2H, PC*H*$(CH_3)_2$), 1.81 (s, 3H, C(C*H*$_3)_2$), 1.60 (dvt, *N* = 16.4, $^3J_{HH}$ = 7.0, 6H, PCH(C*H*$_3)_2$), 1.56 (s, 3H, C(C*H*$_3)_2$), 1.45 (dvt, *N* = 18.4, $^3J_{HH}$ = 7.6, 6H, PCH(C*H*$_3)_2$), 1.30 (dvt, *N* = 18.1, $^3J_{HH}$ = 7.1, 6H, PCH(C*H*$_3)_2$), 0.75 (dvt, *N* = 17.2, $^3J_{HH}$ = 7.1, 6H, PCH(C*H*$_3)_2$), -10.71 (br, 4H, Os*H*). ^{13}C{^{1}H}-APT NMR (100.62 MHz, CD_2Cl_2, 233K): δ 155.4 (vt, *N* = 12.5, *C*-arom), 132.4 (vt, *N* = 5.9, *C*-arom), 132.0 (s, *C*H-arom), 131.9 (s, *C*H-arom), 127.7 (vt, *N* = 6.2, *C*H-arom), 119.8 (vt, *N* = 39.4, *C*-arom), 35.0 (s, C(*C*H$_3)_2$), 34.0 (s, *C*$(CH_3)_2$), 30.3 (s, C(*C*H$_3)_2$), 26.6 (vt, *N* = 33.1, P*C*H$(CH_3)_2$), 26.0 (vt, *N* = 35.4, P*C*H$(CH_3)_2$), 22.1 (s, PCH(*C*H$_3)_2$), 19.8 (s, PCH(*C*H$_3)_2$), 19.2 (s, PCH(*C*H$_3)_2$), 18.3 (s, PCH(*C*H$_3)_2$). ^{31}P{^{1}H} NMR (161.98 MHz, CD_2Cl_2, 233K): δ 62.6 (s, POP). $T_{1(min)}$ (ms, Os*H*, 400MHz, CD_2Cl_2, 203K): 40 ± 2 (-10.64 ppm).

Synthesis of [(Os(H···H){xant(P^{i}Pr$_2)_2$})$_2$(μ-Cl)$_2$][BF$_4$]$_2$ (3). $HBF_4{\cdot}OEt_2$ (37 μl; 0.272 mmol) was added to a solution of [OsH_3Cl{xant(P^{i}Pr$_2)_2$}] (**1**) (130 mg; 0,194 mmol) in dichloromethane (5 ml). After stirring for 1 hour, the solvent was evaporated and the residue was treated with cold pentane (2 x 1 ml) to afford a pale yellow solid which was dried overnight under reduced pressure. Yield: 113 mg (95%). Yellow crystals suitable for X-ray diffraction were obtained by vapor diffusion of pentane into a CH_2Cl_2 solution. Anal. Calcd. for $C_{54}H_{84}B_2Cl_2F_8O_2Os_2P_4$: C, 42.84; H, 5.59. Found: C, 42.60; H, 5.82. IR (ATR, cm^{-1}): *ν*(BF) 1050 (s). ^{1}H NMR (500 MHz,

CD_2Cl_2, 293K): δ 7.83 (m, 4H, C*H*-arom), 7.55 (m, 8H, C*H*-arom), 2.58 (m, 4H, PC*H*$(CH_3)_2$), 2.11 (s, 3H, C(CH_3)$_2$), 2.08 (s, 3H, C(CH_3)$_2$), 1.99 (m, 4H, PC*H*$(CH_3)_2$), 1.24 (dd, $^3J_{HP}$ = 17.5, $^3J_{HH}$ = 7.0, 12H, PCH(CH_3)$_2$), 1.12 (dd, $^3J_{HP}$ = 17.0, $^3J_{HH}$ = 7.0, 12H, PCH(CH_3)$_2$), 1.02 (dd, $^3J_{HP}$ = 17.0, $^3J_{HH}$ = 7.3, 12H, PCH(CH_3)$_2$), 0.85 (dd, $^3J_{HP}$ = 15.1, $^3J_{HH}$ = 6.9, 12H, PCH(CH_3)$_2$), -9.53 (t, $^2J_{HP}$ = 14.5, 4H, Os*H*). ^{13}C {^{1}H} NMR-APT (75.47 MHz, CD_2Cl_2, 293K): δ 159.7 (d, $^2J_{CP}$ = 8.7, *C*-arom), 137.8 (d, $^3J_{CP}$ = 4.6, *C*-arom), 130.9, 130.1 (both s, *C*H-arom), 128.3 (d, $^2J_{CP}$ = 6.1, *C*H-arom), 120.1 (d, $^1J_{CP}$ = 40.7, *C*-arom), 38.5 (s, *C*$(CH_3)_2$), 32.2 (s, C(*C*H_3)$_2$), 32.0 (d, $^1J_{CP}$ = 33.8, P*C*H$(CH_3)_2$), 25.0 (d, $^1J_{CP}$ = 36.3, P*C*H$(CH_3)_2$), 23.3 (s, C(*C*H_3)$_2$), 22.1 (s, PCH(*C*H_3)$_2$), 21.4 (s, PCH(*C*H_3)$_2$), 19.0 (s, PCH(*C*H_3)$_2$), 18.4 (d, $^2J_{CP}$ = 4.2, PCH(*C*H_3)$_2$). ^{31}P {^{1}H} NMR (202.46 MHz, CD_2Cl_2, 293K): δ 42.9 (br, POP). $T_{1(min)}$ (ms, Os*H*, 400MHz, CD_2Cl_2, 243K): 63 ± 3 (-9.53 ppm).

Determination of the $J_{H\text{-}D}$ value for complex 3. A solution of $DBF_4 \cdot D_2O$ was prepared by stirring HBF_4 (1 ml) and D_2O (1 ml) for 1 hour. Then, a solution of [OsH_3Cl{xant(P^{i}Pr$_2$)$_2$}] (**1**) (45 mg, 0.067 mmol) was placed in an NMR tube and treated with the freshly prepared solution of DBF_4 in D_2O (22 µl; 0.080 mmol). After 24 hours, the ^{1}H{^{31}P} NMR spectrum of the reaction mixture showed a triplet ($J_{H\text{-}D}$ = 7.0 Hz), at -9.53 ppm, corresponding to the deuterated isotopomer of complex **3**.

Synthesis of [OsCl(H···H)(η^2-H$_2$){dbf(P^{i}Pr$_2$)$_2$}]BF$_4$ (5). $HBF_4 \cdot OEt_2$ (14 µL; 0.103 mmol) was added to a solution of [OsH_3Cl{dbf(P^{i}Pr$_2$)$_2$}] (**4**) (60 mg, 0,095 mmol) in dichloromethane (3 mL). After stirring for 15 min, at room temperature, the solvent was evaporated under reduced pressure and cold pentane (1 mL) was added to afford a pale yellow solid which was washed once with cold pentane (3 mL) and dried overnight under vacuum. Yield: 58 mg (85%). In order to confirm the structure of the cation, crystals suitable for X-ray diffraction analysis were

obtained by slow diffusion of pentane into a dichloromethane solution of complex [OsCl(H···H)(η^2-H_2){dbf(P^iPr_2)$_2$}][OTf]. Anal. Calcd. for $C_{24}H_{38}BClF_4OOsP_2$: C, 40.20; H, 5.34. Found: C, 39.99; H, 5.43. HRMS (*electrospray, m/z*): calcd. for $C_{24}H_{37}OOsP_2$ $[M\text{-}HCl]^+$: 595.1930, found: 595.1935. IR (ATR, cm^{-1}): ν(B-F) 1049 (m). ^{1}H NMR (300 MHz, CD_2Cl_2, 293K): δ 8.25. (d, $^3J_{HH}$ = 7.7, 2H, C*H*-arom), 8.00 (m, 2H, C*H*-arom), 7.77 (dd, $^3J_{HH}$ = 7.7, $^3J_{HH}$ = 7.6, 2H, C*H*-arom), 3.27 (m, 2H, PC*H*$(CH_3)_2$), 2.89 (m, 2H, PC*H*$(CH_3)_2$), 1.75 (dvt, *N* = 16.2, $^3J_{HH}$ = 7.3, 6H, PCH(C*H*$_3)_2$), 1.57 (dvt, *N* = 19.9, $^3J_{HH}$ = 7.5, 6H, PCH(C*H*$_3)_2$), 1.39 (dvt, *N* = 19.0, $^3J_{HH}$ = 6.9, 6H, PCH(C*H*$_3)_2$), 0.91 (dvt, *N* = 18.1, $^3J_{HH}$= 7.0, 6H, PCH(C*H*$_3)_2$), -10.60 (br, 4H, Os*H*). ^{13}C{^{1}H}-APT NMR (75.47 MHz, CD_2Cl_2, 293K): δ 161.0 (vt, *N* = 13.1, *C*-arom), 131.1 (s, *C*H-arom), 128.7 (vt, *N* = 5.4, *C*H-arom), 127.8 (s, *C*H-arom), 123.8 (vt, *N* = 6.5, *C*-arom), 115.0 (vt, *N* = 37.6, *C*-arom), 25.8 (vt, *N* = 30.7, P*C*H$(CH_3)_2$), 25.2 (vt, *N* = 29.3, P*C*H$(CH_3)_2$), 22.2 (s, PCH(*C*H$_3)_2$), 20.9 (vt, *N* = 4.5, PCH(*C*H$_3)_2$), 20.2 (s, PCH(*C*H$_3)_2$), 18.0 (s, PCH(*C*H$_3)_2$). ^{31}P{^{1}H} NMR (121.49 MHz, CD_2Cl_2, 293K): δ 65.3 (s, POP). $T_{1(min)}$ (ms, Os*H*, 400MHz, CD_2Cl_2, 203K): 40 ± 2 (-10.60 ppm).

Synthesis of [OsCl(η^2-H_2)(CH_3CN){xant(P^iPr_2)$_2$}][BF_4] (6): [(Os(H···H){xant(P^iPr_2)$_2$})$_2$(μ-Cl)$_2$][BF_4]$_2$ (**3**) (100 mg; 0.066 mmol) was dissolved in CH_3CN (3 mL) and stirred for 30 min after which the solvent was evaporated. The residue was precipitated with cold pentane (2 x 1 ml) to afford a white solid which was dried overnight under reduced pressure. Yield: 93 mg (99 %). Colorless crystals suitable for X-ray diffraction were obtained by vapor diffusion of pentane into a CH_2Cl_2 solution. Anal. Calcd. for $C_{29}H_{45}BClF_4NOOsP_2$: C, 43.64; H, 5.68; N, 1.76. Found: C, 43.26; H, 5.72; N, 1.79. IR (ATR, cm^{-1}): ν (C-N) 2288 cm^{-1}; ν(BF) 1048 (s). ^{1}H NMR (300 MHz, CD_2Cl_2, 293K): δ 7.64 (m, 2H, C*H*-arom), 7.57 (dd, $^3J_{HH}$ = 7.6, $^4J_{HH}$ = 1.3, 2H, C*H*-arom), 7.40 (dd, $^3J_{HH}$ = 7.6, $^3J_{HH}$ = 7.5, 2H, C*H*-arom), 3.32 (m, 2H, PC*H*$(CH_3)_2$), 2.86 (m,

2H, PC*H*(CH_3)$_2$), 2.77 (s, 3H, CH_3CN), 1.65 (dvt, *N* = 15.1, $^3J_{HH}$ = 7.2, 6H, PCH(C*H*$_3$)$_2$), 1.61 (s, 3H, C(C*H*$_3$)$_2$), 1.59 (s, 3H, C(C*H*$_3$)$_2$), 1.54 (dvt, *N* = 16.9, $^3J_{HH}$ = 7.5, 6H, PCH(C*H*$_3$)$_2$), 1.42 (dvt, *N* = 17.2, $^3J_{HH}$ = 6.9, 6H, PCH(C*H*$_3$)$_2$), 0.94 (dvt, *N* = 16.4, $^3J_{HH}$ = 6.1, 6H, PCH(C*H*$_3$)$_2$), -9.86 (t, $^2J_{HP}$ = 6.0, 2H, Os*H*). ^{13}C {^{1}H} NMR-APT (75.47 MHz, CD_2Cl_2, 293K): δ 158.2 (vt, *N* = 11.6, *C*-arom), 132.4 (vt, *N* = 6.0, *C*-arom), 132.1 (s, *C*H-arom), 131.2 (s, *C*H-arom), 127.3 (vt, *N* = 6.3, *C*H-arom), 124.4 (s, CH_3*C*N), 123.7 (vt, *N* = 38.4, *C*-arom), 34.2 (s, *C*(CH_3)$_2$) 34.1 (s, C(*C*H$_3$)$_2$), 33.1 (s, C(*C*H$_3$)$_2$), 28.0 (vt, *N* = 28.1, P*C*H(CH_3)$_2$), 27.9 (vt, *N* = 32.0, P*C*H(CH_3)$_2$), 21.8 (s, PCH(*C*H$_3$)$_2$), 19.8 (vt, *N* = 5.9, PCH(*C*H$_3$)$_2$), 19.8 (s, PCH(*C*H$_3$)$_2$), 18.7 (s, PCH(*C*H$_3$)$_2$), 4.2 (s, *C*H$_3$CN). ^{31}P {^{1}H} NMR (121.49 MHz, CD_2Cl_2, 293K): δ 27.2 (s, POP). $T_{1(min)}$ (ms, Os*H*, 300 MHz, CD_2Cl_2, 203K): 21 ± 1 (-10.51 ppm).

Determination of the J_{HD} value for complex 6. DOTf (3 μL; 0.034 mmol) was added to a solution of [OsH_3Cl{xant(P^{i}Pr$_2$)$_2$}] (**1**) (23 mg; 0.034 mmol) in CD_2Cl_2 (0.5 mL). Then, CH_3CN (2 μL; 0.038 mmol) was added. The ^{1}H{^{31}P} NMR spectrum of this solution showed a triplet (J_{HD} = 20 Hz) at -9.87 ppm, corresponding to the deuterated isotopomer.

Synthesis of [K(18-crown-6)][OsH_5{xant(P^{i}Pr$_2$)$_2$}] (8): To a THF (0.6 mL) solution of [OsH_4{xant(P*i*Pr$_2$)$_2$}] (**7**) (40 mg, 0.063 mmol) were added KH (8 mg, 0.200 mmol) and 18-crown-6 (50 mg, 0.190 mmol). The reaction mixture was heated at 70 ºC for 14 h and then filtered while hot. The filtrate was cooled at room temperature to afford yellow crystals, which were isolated after removal of the supernatant by decantation, and dried overnight under reduced pressure. Yield: 39 mg (66%). Complex **8** can be recrystallized by slow vapor diffusion of pentane into a solution of the compound in THF. Anal. Calcd. for $C_{39}H_{69}KO_7OsP_2$·C, 49.77; H, 7.39. Found: C, 50.17; H, 7.65. HRMS (*electrospray, m/z*): calcd. for $C_{27}H_{44}OOsP_2$ [M-H]$^+$: 638.2478, found: 638.2479. ^{1}H NMR (400.13 MHz, THF-*d*$_8$, 293K): 7.19 (d, $^3J_{HH}$ = 7.5, 2H, C*H*-

arom), 7.13 (m, 2H, C*H*-arom) 6.89 (dd, $^{3}J_{HH}$ = 7.5, $^{3}J_{HH}$ = 7.5, 2H, C*H*-arom), 3.51 (s, 24H, CH_2-18-crown-6), 2.18 (m, 4H, PC*H*(CH_3)$_2$), 1.53 (s, 6H, C(CH_3)$_2$), 1.16 (dvt, $^{3}J_{HH}$ = 7.0, *N* = 13.0, 12H, PCH(CH_3)$_2$), 1.13 (dvt, *N* = 11.9, $^{3}J_{HH}$ = 6.5, 12H, PCH(CH_3)$_2$), -12.46 (br, 5H, Os*H*). ^{13}C{^{1}H} NMR-APT (100.62 MHz, THF-d_8, 343K): δ 158.0 (vt, *N* = 8.0, *C*-arom), 135.0 (s, *C*-arom), 132.2 (m, *C*-arom), 127.6 (s, *C*H-arom), 121.7 (s, *C*H-arom), 120.0 (s, *C*H-arom), 70.5 (s, *C*H_2-18-crown-6), 36.0 (s, *C*(CH_3)$_2$), 29.2 (d, $^{1}J_{CP}$ = 27.1, P*C*H(CH_3)$_2$), 26.6 (s, C(*C*H_3)$_2$), 20.9 (vt, *N* = 4.6, PCH(*C*H_3)$_2$), 19.1 (s, PCH(*C*H_3)$_2$). ^{31}P{^{1}H} NMR (161.98 MHz, THF-d_8, 293K): δ 20.6 (s, POP).

Reaction of [(Os(H···H){xant(P^{i}Pr$_2$)$_2$})$_2$(μ-Cl)$_2$][BF$_4$]$_2$ (3) with KH: [(Os(H···H){xant(P^{i}Pr$_2$)$_2$})$_2$(μ-Cl)$_2$][BF$_4$]$_2$ (**3**) (100 mg, 0.066 mmol) and KH (6 mg, 0.15 mmol) were placed in a schlenk tube and THF (5 mL) was added to form a suspension. The reaction mixture was stirred and monitored by NMR showing complete conversion into [OsH$_3$Cl{xant(P^{i}Pr$_2$)$_2$}] (**1**) after 1 h.

Computational details and Cartesian coordinates of 2, 5 and 6: All calculations were performed at the DFT level using the B3LYP functional[29] supplemented with the Grimme's dispersion correction D3[30] as implemented in Gaussian09[23]. Os atom was described by means of an effective core potential SDD for the inner electron[31] and its associated double-ζ basis set for the outer ones, complemented with a set of f-polarization functions.[32] The 6-31G** basis set was used for the H, C, O, N, Cl and P atoms.[33] All minima were verified to have no negative frequencies. All geometries were fully optimized in vacuo.

Structural Analysis of Complexes 3, 5, 6 and 8. X-ray data were collected on a Bruker Smart APEX CCD (**5**, **6**, and **8**) and a Smart APEX CCD DUO (**3**) diffractometers using graphite monochromated Mo Kα radiation (λ = 0.71073 Å). Data were collected over the complete sphere

and were corrected for absorption by using a multiscan method applied with the SADABS program. The structures were solved by Patterson or direct methods and refined by full-matrix least squares on F^2 with SHELXL97, including isotropic and subsequently anisotropic displacement parameters. The hydrogen atoms were observed in the least Fourier Maps or calculated, and refined freely or using a restricted riding model.

However, the hydride ligands were observed in the difference fourier maps but does not refined properly, therefore the osmium-hydride distance was fixed in the refinement (1.59 Å, CCDC). Complex **8** is twined by pseudomerohedry. The structure simulates orthorhombic but was properly refined in the monoclinic symmetry system with beta approximately 90º and refined with the twin law 1 0 0 0 -1 0 0 0 -1 plus one BASF parameter of ≈ 0.5. Due to the difficulty of the refinement restrictions in the displacement parameters were used. In the four structures there are anions and crystallization molecules observed disordered and refined with different moieties, restrained geometry and isotropic thermal parameters.

Crystal data for **3**: $C_{54}H_{84}Cl_2O_2Os_2P_4$, 2($BF_4$), CH_2Cl_2, M_W 1598.94, irregular block, yellow (0.19 x 0.12 x 0.08), monoclinic, space group P21/c, *a*: 12.9473(15) Å, *b*: 20.565(2) Å, *c*: 12.0926(14) Å, β: 93.005(2)°, *V* = 3215.4(6) $Å^3$, *Z* = 2, *Z'* = 0.5, D_{calc}: 1.651 g cm^{-3}, F(000): 1588, T = 100(2) K, μ 4.275 mm^{-1}. 41253 measured reflections (2θ: 3-58º, ω scans 0.3º), 8442 unique (R_{int} = 0.0411); min./max. transm. factors 0.633/0.862. Final agreement factors were R^1 = 0.0394 (6950 observed reflections, I > 2σ(I)) and wR^2 = 0.1061; data/restraints/parameters 8442/35/379; GoF = 0.949. Largest peak and hole: 2.66 (close to osmium atoms) and -1.705 e/ $Å^3$.

Crystal data for **5**: $C_{24}H_{38}ClOOsP_2$, CF_3O_3S, CHF_3O_3 S, M_W 929.28, irregular block, colorless (0.19 x 0.14 x 0.08), monoclinic, space group Cc, *a*: 16.2471(10) Å, *b*: 21.4146(13) Å, *c*:

10.2694(6) Å, β: 104.6620(10)°, V = 3456.6(4) Å^3, Z = 4, Z' = 1. D_{calc}: 1.786 g cm^{-3}, F(000): 1840, T = 100(2) K, μ 4.053 mm^{-1}. 19163 measured reflections (2θ: 3-58°, ω scans 0.3°), 7949 unique (R_{int} = 0.0320); min./max. transm. factors 0.687/0.862. Final agreement factors were R^1 = 0.0277 (7384 observed reflections, I > 2σ(I)) and wR^2 = 0.0555; data/restraints/parameters 7949/6/ 428; GoF = 1.022. Largest peak and hole: 0.827 and -0.846 e/ Å^3.

Crystal data for **6**: $C_{29}H_{45}ClNOOsP_2$, BF_4, $C_4H_{10}O$, M_W 872.18, irregular block, colorless (0.15 x 0.10 x 0.07), monoclinic, space group $P2_1/m$, a: 11.843(3) Å, b: 22.139(5) Å, c: 14.179(3) Å, β: 89.988(3)°, V = 3717.4(14) Å^3, Z = 4, Z' = 1, D_{calc}: 1.558 g cm^{-3}, F(000): 1760, T = 100(2) K, μ 3.638 mm^{-1}. 32991 measured reflections (2θ: 3-58°, ω scans 0.3°), 7908 unique (R_{int} = 0.0876); min./max. transm. factors 0.590/0.862. Final agreement factors were R^1 = 0.0521 (5862 observed reflections, I > 2σ(I)) and wR^2 = 0.1289; data/restraints/parameters 7908/256/417; GoF = 1.135. Largest peak and hole: 1.785 (close to osmium atoms) and -1.406 e/ Å^3.

Crystal data for **8**: $C_{27}H_{45}OOsP_2$, $C_{12}H_{24}KO_6$, 0.5(C_4H_8O), 0.5(C_5H_{12}), M_W 1013.31, irregular block, yellow (0.25 x 0.06 x 0.06), monoclinic, space group $P2_1/n$, a: 17.0875(9) Å, b: 15.2536(8) Å, c: 19.5724(10) Å, β: 109.6270(10)°, V = 4805.1(4) Å^3, Z = 4, Z' = 1, D_{calc}: 1.401 g cm^{-3}, F(000): 2100, T = 100(2) K, μ 2.852 mm^{-1}. 82792 measured reflections (2θ: 3-58°, ω scans 0.3°), 11705 unique (R_{int} = 0.0583); min./max. transm. factors 0.679/ 0.862. Final agreement factors were R^1 = 0.0386 (9412 observed reflections, I > 2σ(I)) and wR^2 = 0.0946; data/restraints/parameters 11705/17/510; GoF = 1.032. Largest peak and hole: 2.348 (close to osmium atoms) and -1.381 e/ Å^3.

ASSOCIATED CONTENT

Supporting Information. The Supporting Information is available free of charge on the ACS Publications website at DOI:

·Crystallographic details for **3**, **5**, **6** and **8** (CIF).

Theoretical complexes coordinates (XYZ).

AUTHOR INFORMATION

Corresponding Author

*E-mail: maester@unizar.es.

Author Contributions

The manuscript was written through contributions of all authors.

Notes

The authors declare no competing financial interest.

ACKNOWLEDGMENT

(Financial support from the MINECO of Spain (Projects CTQ2014-52799-P and CTQ2014-51912-REDC), Gobierno de Aragón (E35), FEDER, and the European Social Fund is acknowledged.

REFERENCES

(1) (a) Noyori, R.; Ohkuma, T. Asymmetric Catalysis by Architectural and Functional Molecular Engineering: Practical Chemo- and Stereoselective Hydrogenation of Ketones. *Angew. Chem., Int. Ed.* **2001**, *40*, 40-73. (b) Clapham, S. E.; Hadzovic, A.; Morris, R. H. Mechanisms of the H_2-Hydrogenation and Transfer Hydrogenation of Polar Bonds Catalyzed by Ruthenium Hydride Complexes. *Coord. Chem. Rev.* **2004**, *248*, 2201-2237. (c) Conley, B. L.; Pennington-Boggio, M. K.; Boz, E.; Williams, T. J. Discovery, Applications, and Catalytic

Mechanisms of Shvo's Catalyst. *Chem. Rev.* **2010**, *110*, 2294-2312. (d) Gunanathan, C.; Milstein, D. Metal-Ligand Cooperation by Aromatization-Dearomatization: A New Paradigm in Bond Activation and "Green" Catalysis. *Acc. Chem. Res.* **2011**, *44*, 588-602. (e) Bajo, S.; Esteruelas, M. A.; López, A. M.; Oñate, E. Osmium-Acyl Decarbonylation Promoted by Tp-Mediated Allenylidene Abstraction: A New Role of the Tp Ligand. *Organometallics* **2014**, *33*, 4057-4066. (f) Bolaño, T.; Esteruelas, M. A.; Gay, M. P.; Oñate, E.; Pastor, I. M.; Yus, M. An Acyl-NHC Osmium Cooperative System: Coordination of Small Molecules and Heterolytic B-H and O-H Bond Activation. *Organometallics* **2015**, *34*, 3902-3908.

(2) (a) Periana, R. A.; Taube, D. J.; Gamble, S.; Taube, H.; Satoh, T.; Fujii, H. Platinum Catalysts for the High-Yield Oxidation of Methane to a Methanol Derivative. *Science* **1998**, *280*, 560-564. (b) Hashiguchi, B. G.; Young, K. J. H.; Yousufuddin, M.; Goddard, W. A.; Periana, R. A. Acceleration of Nucleophilic CH Activation by Strongly Basic Solvents. *J. Am. Chem. Soc.* **2010**, *132*, 12542-12545. (c) Crabtree, R. H. Creating Ligands with Multiple Personalities. *Science* **2010**, *330*, 455-456. (d) Kaim, W. Manifestations of Noninnocent Ligand Behavior. *Inorg. Chem.* **2011**, *50*, 9752-9765.

(3) (a) Braunstein, P.; Naud, F. Hemilability of Hybrid Ligands and the Coordination Chemistry of Oxazoline-Based Systems. *Angew. Chem., Int. Ed.* **2001**, *40*, 680-699. (b) Angell, S. E.; Rogers, C. W.; Zhang, Y.; Wolf, M. O.; Jones, W. E. Hemilabile Coordination Complexes for Sensing Applications. *Coord. Chem. Rev.* **2006**, *250*, 1829-1841. (c) Braunstein, P. Bonding and Organic and Inorganic Reactivity of Metal-Coordinated Phosphinoenolates and Related Functional Phosphine-Derived Anions. *Chem. Rev.* **2006**, *106*, 134-159. (d) Weng, Z. Q.; Teo, S. H.; Hor, T. S. A. Metal Unsaturation and Ligand Hemilability in Suzuki Coupling. *Acc. Chem. Res.* **2007**, *40*, 676-684. (e) Zhang, W. H.; Chien, S. W.; Hor, T. S. A. Recent Advances in Metal

Catalysts with Hybrid Ligands. *Coord. Chem. Rev.* **2011**, *255*, 1991-2024. (f) Annibale, V. T.; Song, D. T. Multidentate Actor Ligands as Versatile Platforms for Small Molecule Activation and Catalysis. *RSC Adv.* **2013**, *3*, 11432-11449.

(4) (a) van der Boom, M. E.; Milstein, D. Cyclometalated Phosphine-Based Pincer Complexes: Mechanistic Insight in Catalysis, Coordination, and Bond Activation. *Chem. Rev.* **2003**, *103*, 1759-1792. (b) Choi, J.; MacArthur, A. H. R.; Brookhart, M.; Goldman, A. S. Dehydrogenation and Related Reactions Catalyzed by Iridium Pincer Complexes. *Chem. Rev.* **2011**, *111*, 1761-1779. (c) Haibach, M. C.; Kundu, S.; Brookhart, M.; Goldman, A. S. Alkane Metathesis by Tandem Alkane-Dehydrogenation-Olefin-Metathesis Catalysis and Related Chemistry. *Acc. Chem. Res.* **2012**, *45*, 947-958. (d) Kumar, A.; Zhou, T.; Emge, T. J.; Mironov, O.; Saxton, R. J.; Krogh-Jespersen, K.; Goldman, A. S. Dehydrogenation of *n*-Alkanes by Solid-Phase Molecular Pincer-Iridium Catalysts. High Yields of *α*-Olefin Product. *J. Am. Chem. Soc.* **2015**, *137*, 9894-9911.

(5) (a) Boone, M. P.; Brown, C. C.; Ancelet, T. A.; Stephan, D. W. Interconversion of Ruthenium-O($CH_2CH_2PCy_2$)$_2$ Alkylidene and Alkylidyne Hydride Complexes. *Organometallics* **2010**, *29*, 4369-4374. (b) Lumbroso, A.; Koschker, P.; Vautravers, N. R.; Breit, B. Redox-Neutral Atom-Economic Rhodium-Catalyzed Coupling of Terminal Alkynes with Carboxylic Acids Toward Branched Allylic Esters. *J. Am. Chem. Soc.* **2011**, *133*, 2386-2389. (c) Pawley, R. J.; Huertos, M. A.; Lloyd-Jones, G. C.; Weller, A. S.; Willis, M. C. Intermolecular Alkyne Hydroacylation. Mechanistic Insight from the Isolation of the Vinyl Intermediate that Precedes Reductive Elimination. *Organometallics* **2012**, *31*, 5650-5659. (d) Esteruelas, M. A.; Oliván, M.; Vélez, A. Xantphos-Type Complexes of Group 9: Rhodium versus Iridium. *Inorg. Chem.* **2013**, *52*, 5339-5349. (e) Esteruelas, M. A.; Oliván, M.; Vélez, A. POP-Pincer Silyl Complexes of

Group 9: Rhodium versus Iridium. *Inorg. Chem.* **2013**, *52*, 12108-12119. (f) Esteruelas, M. A.; Oliván, M.; Vélez, A. Conclusive Evidence on the Mechanism of the Rhodium-Mediated Decyanative Borylation. *J. Am. Chem. Soc.* **2015**, *137*, 12321-12329. (g) Esteruelas, M. A.; Nolis, P.; Oliván, M.; Oñate, E.; Vallribera, A.; Vélez, A. Ammonia Borane Dehydrogenation Promoted by a Pincer-Square-Planar Rhodium(I) Monohydride: A Stepwise Hydrogen Transfer from the Substrate to the Catalyst. *Inorg. Chem.* **2016**, *55*, 7176-7181.

(6) (a) Pontiggia, A. J.; Chaplin, A. B.; Weller, A. S. Cationic Iridium Complexes of the Xantphos Ligand. Flexible Coordination Modes and the Isolation of the Hydride Insertion Product with an Alkene. *J. Organomet. Chem.* **2011**, *696*, 2870-2876. (b) Dallanegra, R.; Chaplin, A. B.; Weller, A. S. Rhodium Cyclopentyl Phosphine Complexes of Wide-Bite-Angle Ligands DPEphos and Xantphos. *Organometallics* **2012**, *31*, 2720-2728.

(7) Pawley, R. J.; Moxham, G. L.; Dallanegra, R.; Chaplin, A. B.; Brayshaw, S. K.; Weller, A. S.; Willis, M. C. Controlling Selectivity in Intermolecular Alkene or Aldehyde Hydroacylation Reactions Catalyzed by $\{Rh(L_2)\}^+$ Fragments. *Organometallics* **2010**, *29*, 1717-1728.

(8) Ren, P.; Pike, S. D.; Pernik, I.; Weller, A. S.; Willis, M. C. Rh-POP Pincer Xantphos Complexes for C-S and C-H Activation. Implications for Carbothiolation Catalysis. *Organometallics* **2015**, *34*, 711-723.

(9) Johnson, H. C.; Leitao, E. M.; Whitten, G. R.; Manners, I.; Lloyd-Jones, G. C.; Weller, A. S. Mechanistic Studies of the Dehydrocoupling and Dehydropolymerization of Amine-Boranes Using a $[Rh(Xantphos)]^+$ Catalyst. *J. Am. Chem. Soc.* **2014**, *136*, 9078-9093.

(10) Esteruelas, M. A.; López, A. M.; Oliván, M. Polyhydrides of Platinum Group Metals: Nonclassical Interactions and σ-Bond Activation Reactions. *Chem. Rev.* **2016**, *116*, 8770-8847.

(11) Crabtree, R. H. Dihydrogen Complexation. *Chem. Rev.* **2016**, *116*, 8750-8769.

(12) (a) Rossin, A.; Peruzzini, M. Ammonia-Borane and Amine-Borane Dehydrogenation Mediated by Complex Metal Hydrides. *Chem. Rev.* **2016**, *116*, 8848-8872. (b) Bhunya, S.; Malakar, T.; Ganguly, G.; Paul, A. Combining Protons and Hydrides by Homogeneous Catalysis for Controlling the Release of Hydrogen from Ammonia–Borane: Present Status and Challenges. *ACS Catal.* **2016**, *6*, 7907-7934.

(13) (a) Esteruelas, M. A.; Fernández, I.; López, A. M.; Mora, M.; Oñate, E. Osmium-Promoted Dehydrogenation of Amine-Boranes and B-H Bond Activation of the Resulting Amino-Boranes. *Organometallics* **2014**, *33*, 1104-1107. (b) Esteruelas, M. A.; López, A. M.; Mora, M.; Oñate, E. Ammonia-Borane Dehydrogenation Promoted by an Osmium Dihydride Complex: Kinetics and Mechanism. *ACS Catal.* **2015**, *5*, 187-191.

(14) (a) Casarrubios, L.; Esteruelas, M. A.; Larramona, C.; Muntaner, J. G.; Oliván, M.; Oñate, E.; Sierra, M. A. Chelated Assisted Metal-Mediated N-H Bond Activation of *β*-Lactams: Preparation of Irida-, Rhoda-, Osma-, and Ruthenatrinems. *Organometallics* **2014**, *33*, 1820-1833. (b) Casarrubios, L.; Esteruelas, M. A.; Larramona, C.; Lledós, A.; Muntaner, J. G.; Oñate, E.; Ortuño, M. A.; Sierra, M. A. Mechanistic Insight into the Facilitation of *β*-Lactam Fragmentation through Metal Assistance. *Chem. Eur. J.* **2015**, *21*, 16781-16785. (c) Casarrubios, L.; Esteruelas, M. A.; Larramona, C.; Muntaner, J. G.; Oñate, E.; Sierra, M. A. 2-Azetidinones as Precursors of Pincer Ligands: Preparation, Structure, and Spectroscopic Properties of CC'N-Osmium Complexes. *Inorg. Chem.* **2015**, *54*, 10998-11006.

(15) (a) Esteruelas, M. A.; García-Raboso, J.; Oliván, M.; Oñate, E. N-H and N-C Bond Activation of Pyrimidinic Nucleobases and Nucleosides Promoted by an Osmium Polyhydride.

Inorg. Chem. **2012**, *51*, 5975-5984. (b) Esteruelas, M. A.; García-Raboso, J.; Oliván, M. Reactions of an Osmium-Hexahydride Complex with Cytosine, Deoxycytidine, and Cytidine: The Importance of the Minor Tautomers. *Inorg. Chem.* **2012**, *51*, 9522-9528.α

(16) (a) Esteruelas, M. A.; Herrero, J.; López, A. M.; Oliván, M. Alkyne-Coupling Reactions Catalyzed by OsHCl(CO)(P^iPr_3) in the Presence of Diethylamine. *Organometallics* **2001**, *20*, 3202-3205. (b) Barrio, P.; Esteruelas, M. A.; Oñate, E. Reactions of a Hexahydride-Osmium Complex with Aldehydes: Double C-H_α Activation-Decarbonylation and Single C-H_α Activation-Hydroxylation Tandem Processes and Catalytic Tishchenko Reactions. *Organometallics* **2004**, *23*, 1340-1348. (c) Esteruelas, M. A.; Masamunt, A. B.; Oliván, M.; Oñate, E.; Valencia, M. Aromatic Diosmatricyclic Nitrogen-Containing Compounds. *J. Am. Chem. Soc.* **2008**, *130*, 11612-11613. (d) Esteruelas, M. A.; Honczek, N.; Oliván, M.; Oñate, E.; Valencia, M. Direct Access to POP-Type Osmium(II) and Osmium(IV) Complexes: Osmium a Promising Alternative to Ruthenium for the Synthesis of Imines from Alcohols and Amines. *Organometallics* **2011**, *30*, 2468-2471.

(17) (a) Crespo, O.; Eguillor, B.; Esteruelas, M. A.; Fernández, I.; García-Raboso, J.; Gómez-Gallego, M.; Martín-Ortiz, M.; Oliván, M.; Sierra, M. A. Synthesis and Characterisation of [6]-Azaosmahelicenes: the First d^4-Heterometallahelicenes. *Chem. Commun.* **2012**, *48*, 5328-5330. (b) Alabau, R. G.; Eguillor, B.; Esler, J.; Esteruelas, M. A.; Oliván, M.; Oñate, E.; Tsai, J. Y.; Xia, C. J. CCC-Pincer-NHC Osmium Complexes: New Types of Blue-Green Emissive Neutral Compounds for Organic Light-Emitting Devices (OLEDs). *Organometallics* **2014**, *33*, 5582-5596. (c) Eguillor, B.; Esteruelas, M. A.; Fernández, I.; Gómez-Gallego, M.; Lledós, A.; Martín-Ortiz, M.; Oliván, M.; Oñate, E.; Sierra, M. A. Azole Assisted C-H Bond Activation Promoted

by an Osmium-Polyhydride: Discerning between N and NH. *Organometallics* **2015**, *34*, 1898-1910.

(18) Bertoli, M.; Chouale, A.; Gusev, D. G.; Lough, A. J.; Major, Q.; Moore, B. PNP Pincer Osmium Polyhydrides for Catalytic Dehydrogenation of Primary Alcohols. *Dalton Trans.* **2011**, *40*, 8941-8949.

(19) Liu, S. H.; Huang, X.; Lin, Z. Y.; Lau, C. P.; Jia, G. C. Synthesis and Characterization of Dihydrogen(olefin)osmium Complexes with (E)-$Ph_2P(CH_2)_2CH=CH(CH_2)_2PPh_2$. *Eur. J. Inorg. Chem.* **2002**, 1697-1702.

(20) Kuznetsov, V. F.; Gusev, D. G. Chiral Hydride and Dihydrogen Pincer-Type Complexes of Osmium. *Organometallics* **2007**, *26*, 5661-5666.

(21) Alós, J.; Bolaño, T.; Esteruelas, M. A.; Oliván, M.; Oñate, E.; Valencia, M. POP-Pincer Osmium-Polyhydrides: Head-to-Head (*Z*)-Dimerization of Terminal Alkynes. *Inorg. Chem.* **2013**, *52*, 6199-6213.

(22) (a) Kong, V. C. Y.; Foulkes, F. R.; Kirk, D. W.; Hinatsu, J. T. Development of Hydrogen Storage for Fuel Cell Generators. I: Hydrogen Generation Using Hydrolysis Hydrides. *Int. J. Hydrogen. Energ.* **1999**, *24*, 665-675. (b) Kong, V. C. Y.; Kirk, D. W.; Foulkes, F. R.; Hinatsu, J. T. Development of Hydrogen Storage for Fuel Cell Generators II: Utilization of Calcium Hydride and Lithium Hydride. *Int. J. Hydrogen. Energ.* **2003**, *28*, 205-214. (c) Dincer, I. Green Methods for Hydrogen Production. *Int. J. Hydrogen. Energ.* **2012**, *37*, 1954-1971. (d) Dincer, I.; Acar, C. Review and Evaluation of Hydrogen Production Methods for Better Sustainability. *Int. J. Hydrogen. Energ.* **2015**, *40*, 11094-11111.

(23) Frisch, M. J.; Trucks, G. W.; Schlegel, H. B.; Scuseria, G. E.; Robb, M. A.; Cheeseman, J. R.; Scalmani, G.; Barone, V.; Mennucci, B.; Petersson, G. A.; Nakatsuji, H.; Caricato, M.; Li, X.; Hratchian, H. P.; Izmaylov, A. F.; Bloino, J.; Zheng, G.; Sonnenberg, J. L.; Hada, M.; Ehara, M.; Toyota, K.; Fukuda, R.; Hasegawa, J.; Ishida, M.; Nakajima, T.; Honda, Y.; Kitao, O.; Nakai, H.; Vreven, T.; Montgomery, J. A., Jr.; Peralta, J. E.; Ogliaro, F.; Bearpark, M.; Heyd, J. J.; Brothers, E.; Kudin, K. N.; Staroverov, V. N.; Kobayashi, R.; Normand, J.; Raghavachari, K.; Rendell, A.; Burant, J. C.; Iyengar, S. S.; Tomasi, J.; Cossi, M.; Rega, N.; Millam, N. J.; Klene, M.; Knox, J. E.; Cross, J. B.; Bakken, V.; Adamo, C.; Jaramillo, J.; Gomperts, R.; Stratmann, R. E.; Yazyev, O.; Austin, A. J.; Cammi, R.; Pomelli, C.; Ochterski, J. W.; Martin, R. L.; Morokuma, K.; Zakrzewski, V. G.; Voth, G. A.; Salvador, P.; Dannenberg, J. J.; Dapprich, S.; Daniels, A. D.; Farkas, Ö.; Foresman, J. B.; Ortiz, J. V.; Cioslowski, J.; Fox, D. J. *Gaussian 09, Revision B.01*; Gaussian, Inc.: Wallingford, CT, **2009**.

(24) In addition to reference 21, for osmium complexes previously described with this diphosphine see: (a) Asensio, G.; Cuenca, A. B.; Esteruelas, M. A.; Medio-Simón, M.; Oliván, M.; Valencia, M. Osmium(III) Complexes with POP Pincer Ligands: Preparation from Commercially Available $OsCl_3 \cdot 3H_2O$ and Their X-ray Structures. *Inorg. Chem.* **2010**, *49*, 8665-8667. (b) Alós, J.; Bolaño, T.; Esteruelas, M. A.; Oliván, M.; Oñate, E.; Valencia, M. POP-Pincer Ruthenium Complexes: d^6 Counterparts of Osmium d^4 Species. *Inorg. Chem.* **2014**, *53*, 1195-1209. (c) Alós, J.; Esteruelas, M. A.; Oliván, M.; Oñate, E.; Puylaert, P. C-H Bond Activation Reactions in Ketones and Aldehydes Promoted by POP-Pincer Osmium and Ruthenium Complexes. *Organometallics* **2015**, *34*, 4908-4921.

(25) $d_{H\text{-}H}$ = 5.815 $(T_{1\ (min)}/\nu)^{1/6}$ and $d_{H\text{-}H}$ = 1.44-0.0168 ($J_{H\text{-}D}$). Morris, R. H. Dihydrogen, Dihydride and in Between: NMR and Structural Properties of Iron Group Complexes. *Coord. Chem. Rev.* **2008**, *252*, 2381-2394.

(26) The structure has two chemically equivalent but crystallographically independent molecules in the symmetry unit.

(27) (a) Gusev, D. G.; Lough, A. J.; Morris, R. H. New Polyhydride Anions and Proton-Hydride Hydrogen Bonding in their Ion Pairs. X-ray Crystal Structure Determinations of Q[*mer*-$Os(H)_3(CO)(P^iPr_3)_2$], Q = [K(18-crown-6)] and Q = [K(1-aza-18-crown-6)]. *J. Am. Chem. Soc.* **1998**, *120*, 13138-13147. (b) Abdur-Rashid, K.; Gusev, D. G.; Lough, A. J.; Morris, R. H. Intermolecular Proton-Hydride Bonding in Ion Pairs: Synthesis and Structural Properties of [K(Q)][$MH_5((P^iPr_3)_2)$] (M = Os, Ru; Q=18-crown-6, 1-aza-18-crown-6, 1,10-diaza-18-crown-6). *Organometallics* **2000**, *19*, 834-843.

(28) (a) Howard, J. A. K.; Johnson, O.; Koetzle, T. F.; Spencer, J. L. Crystal and Molecular Structure of Bis(diisopropylphenylphosphine)hexahydridoosmium, [$OsH_6(PC_{12}H_{19})_2$]: Single-Crystal Neutron Diffraction Study at 20 K. *Inorg. Chem.* **1987**, *26*, 2930-2933. (b) Buil, M. L.; Cardo, J. J. F.; Esteruelas, M. A.; Fernández, I.; Oñate, E. An Entry to Stable Mixed Phosphine-Osmium-NHC Polyhydrides. *Inorg. Chem.* **2016**, *55*, 5062-5070.

(29) (a) Lee, C. T.; Yang, W. T.; Parr, R. G. Development of the Colle-Salvetti Correlation-Energy Formula into a Functional of the Electron-Density. *Phys Rev B* **1988**, *37*, 785-789. (b) Becke, A. D. A New Mixing of Hartree-Fock and Local Density-Functional Theories. *J. Chem. Phys.* **1993**, *98*, 1372-1377. (c) Stephens, P. J.; Devlin, F. J.; Chabalowski, C. F.; Frisch, M. J. Ab-Initio Calculation of Vibrational Absorption and Circular-Dichroism Spectra Using Density-

Functional Force-Fields. *J. Phys. Chem.* **1994**, *98*, 11623-11627. (1) Alós, J.; Bolaño, T.; Esteruelas, M. A.; Oliván, M.; Oñate, E.; Valencia, M. POP-Pincer Osmium-Polyhydrides: Head-to-Head (*Z*)-Dimerization of Terminal Alkynes. *Inorg. Chem.* 2013, *52*, 6199-6213.

(30) Grimme, S.; Antony, J.; Ehrlich, S.; Krieg, H. A Consistent and Accurate *ab initio* Parametrization of Density Functional Dispersion Correction (DFT-D) for the 94 Elements H-Pu. *J. Chem. Phys.* **2010**, *132*.

(31) Andrae, D.; Haussermann, U.; Dolg, M.; Stoll, H.; Preuss, H. Energy-Adjusted Abinitio Pseudopotentials for the 2nd and 3rd Row Transition-Elements. *Theoretica Chimica Acta* **1990**, *77*, 123-141.

(32) Ehlers, A. W.; Bohme, M.; Dapprich, S.; Gobbi, A.; Hollwarth, A.; Jonas, V.; Kohler, K. F.; Stegmann, R.; Veldkamp, A.; Frenking, G. A Set of F-Polarization Functions for Pseudo-Potential Basis-Sets of the Transition-Metals Sc-Cu, Y-Ag and La-Au. *Chem. Phys. Lett.* **1993**, *208*, 111-114.

(33) (a) Hehre, W. J.; Ditchfield, R.; Pople, J. A. Self-Consistent Molecular-Orbital Methods. XII. Further Extensions of Gaussian-Type Basis Sets for Use in Molecular-Orbital Studies of Organic-Molecules. *J. Chem. Phys.* **1972**, *56*, 2257-2261. (b) Francl, M. M.; Pietro, W. J.; Hehre, W. J.; Binkley, J. S.; Gordon, M. S.; Defrees, D. J.; Pople, J. A. Self-Consistent Molecular-Orbital Methods .23. A Polarization-Type Basis Set for 2nd-Row Elements. *J. Chem. Phys.* **1982**, *77*, 3654-3665.

TABLE OF CONTENTS SYNOPSIS

New dihydrogen-, compressed dihydride-, and classical hydride-osmium compounds containing the diphosphine 9,9-dimethyl-4,5-bis(diisopropylphosphino)xanthene, coordinated κ^3-*mer*, κ^3-*fac*, and κ^2-P,P, have been isolated during the cyclic formation of H_2 by means of the sequential addition of H^+ and H^- or H^- and H^+ to the classical trihydride $OsH_3Cl\{xant(P^iPr_2)_2\}$.

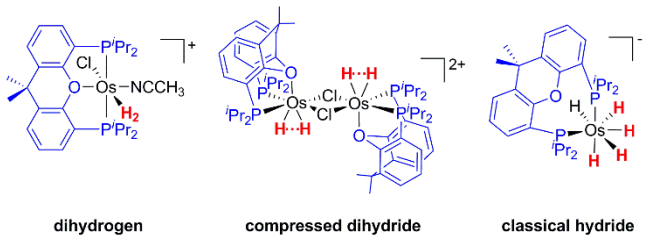

Mer-, Fac-, and Bidentate-Coordination of an Alkyl-POP Ligand in the Chemistry of Nonclassical Osmium-Hydrides

Miguel A. Esteruelas, Cristina García-Yebra, Jaime Martín, and Enrique Oñate

Departamento de Química Inorgánica, Instituto de Síntesis Química y Catálisis Homogénea (ISQCH), Centro de Innovación en Química Avanzada (ORFEO-CINQA)
Universidad de Zaragoza – CSIC
50009 Zaragoza, Spain
E-mail: maester@unizar.es

Supporting Information

Index

I. Computational details and Cartesian coordinates of 2, 5 and 6: All calculations were performed at the DFT level using the B3LYP functional[1] supplemented with the Grimme's dispersion correction D3[2] as implemented in Gaussian09[3]. Os atom was described by means of an effective core potential SDD for the inner electron[4] and its associated double-ζ basis set for the outer ones, complemented with a set of f-polarization functions.[5] The 6-31G** basis set was used for the H, C, O, N, Cl and P atoms.[6] All minima were verified to have no negative frequencies. All geometries were fully optimized in vacuo.

Cartesian coordinates:

2

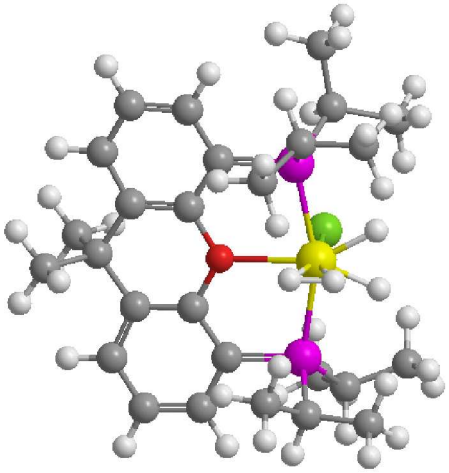

Os	-0.15254400	-1.23754200	-0.09871000
H	0.34441500	-2.74337300	0.11986700
H	-1.06728100	-2.53473600	0.10182700
H	-0.16111900	-0.94115900	-1.72461500
Cl	-0.08490600	-0.91520500	2.31696100
P	2.22642800	-1.17164900	-0.16831100
P	-2.41701800	-0.49192300	-0.06975600
O	0.18664100	1.04447600	-0.06718400
C	2.55048000	0.62491800	-0.09238100
C	1.50195400	1.55742800	-0.03256600
C	1.73950800	2.93065500	0.03580700
C	3.07807300	3.34919100	0.04307400
H	3.29154900	4.41007800	0.10606900
C	4.13789800	2.45417400	-0.03353700
H	5.16077600	2.81442900	-0.03248800
C	3.86986200	1.09214400	-0.10576100
H	4.69058500	0.38381900	-0.15938800
C	0.62600900	3.97003800	0.10172200
C	0.72979300	4.73606000	1.44726400
H	-0.04851300	5.50006500	1.52117300
H	1.69608500	5.23944900	1.53500300
H	0.62093400	4.05139000	2.29271700
C	0.78325600	4.95494500	-1.08690600
H	0.71092300	4.42698900	-2.04187800
H	1.74915300	5.46375200	-1.04911300
H	0.01085100	5.72676600	-1.06265000
C	-0.74286400	3.30049900	0.02103000
C	-0.92229100	1.91720900	-0.02866200
C	-2.20085100	1.33017800	-0.07518200
C	-3.31781900	2.17278600	-0.13541100
H	-4.30951100	1.74762300	-0.22426700
C	-3.17038400	3.55453200	-0.09303000
H	-4.04067500	4.20050300	-0.13087900
C	-1.89643800	4.09755300	0.00068700
H	-1.78702200	5.17502900	0.04678700
C	3.23050000	-2.01424100	1.17996200
H	4.18621300	-2.24291000	0.68909800
C	2.56234600	-3.33542200	1.60314600
H	3.23689400	-3.87618800	2.27404700
H	2.33981400	-3.99485000	0.75973900
H	1.63388300	-3.13330400	2.14255900
C	3.50120200	-1.12899700	2.40819900
H	2.56798400	-0.82859700	2.88688500
H	4.07063200	-0.23093700	2.16350300
H	4.08579600	-1.70837800	3.12986200
C	3.04285300	-1.69916400	-1.76484800
H	4.10149500	-1.44303700	-1.62444400
C	2.92751900	-3.21584000	-1.98141800
H	1.87936800	-3.53066300	-2.03153100
H	3.42091000	-3.78937600	-1.19344700
H	3.40083600	-3.48640600	-2.93012000
C	2.51229000	-0.91599700	-2.97305500
H	3.11697000	-1.15496800	-3.85313000
H	2.55568800	0.16559500	-2.81936100
H	1.47919400	-1.19134700	-3.20496800
C	-3.46058200	-0.84209900	-1.57707500
H	-4.41312500	-0.33120900	-1.39241300
C	-2.83434600	-0.25160600	-2.84923000
H	-1.90265100	-0.76271200	-3.11045000
H	-2.62722200	0.81748500	-2.75466300
H	-3.52521400	-0.38718500	-3.68687500
C	-3.72963200	-2.34704900	-1.73287600
H	-4.30765100	-2.52135900	-2.64548400
H	-4.30017600	-2.75934300	-0.89824700
H	-2.79400900	-2.90963800	-1.81846600
C	-3.40299200	-0.92609700	1.46851600
H	-2.90072900	-0.32330000	2.23263800
C	-4.88798900	-0.53668700	1.40117500

H	-5.42239000	-1.08727800	0.62071600
H	-5.04200400	0.53213200	1.24439600
H	-5.36033000	-0.79008000	2.35506400
C	-3.23748800	-2.40591300	1.85747300
H	-3.77635600	-2.58197600	2.79352500
H	-2.19190300	-2.66268300	2.02825000
H	-3.65722600	-3.08253900	1.10820300
H	-0.25253600	-1.95530600	-1.57765600

Zero-point correction= 0.649899 (Hartree/Particle)
Thermal correction to Energy= 0.687651
Thermal correction to Enthalpy= 0.688595
Thermal correction to Gibbs Free Energy= 0.583842
Sum of electronic and zero-point Energies= -2363.675537
Sum of electronic and thermal Energies= -2363.637785
Sum of electronic and thermal Enthalpies= -2363.636841
Sum of electronic and thermal Free Energies= -2363.741594

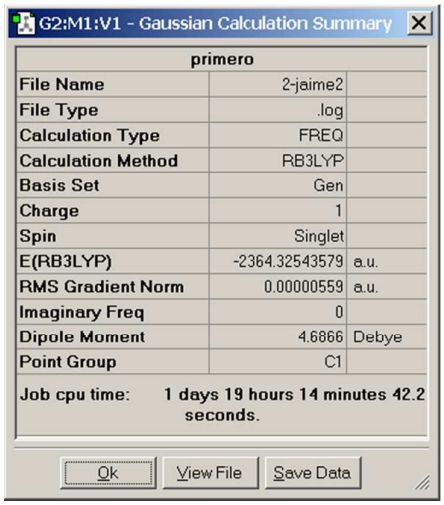

2b

Os	0.12478300	-1.17064000	0.26029900
H	0.35347900	-2.66090200	0.85908000
H	0.28364500	-2.70490800	-0.22901600
H	-0.53853700	-1.17935900	1.72783400
Cl	0.04466000	-0.79328700	-2.18392500
P	-2.25987200	-1.16605500	0.10366900
P	2.42665800	-0.56812200	0.02836600
O	-0.16296100	1.03349900	0.19042500
C	-2.53996600	0.63762800	-0.03422500
C	-1.47268200	1.55470800	0.01073700
C	-1.67834800	2.93168700	-0.06788600
C	-3.00500100	3.37803500	-0.16308700
H	-3.19439700	4.44420700	-0.21056700
C	-4.08295300	2.50284400	-0.18566600
H	-5.09631500	2.88321500	-0.25312900
C	-3.84540700	1.13460900	-0.12337000
H	-4.68126200	0.44273800	-0.14393900
C	-0.54466000	3.95194900	-0.03330800
C	-0.65743200	4.87389000	-1.27675100
H	0.13016700	5.63023400	-1.27820200
H	-1.61086900	5.40631000	-1.28699200
H	-0.57777100	4.29186600	-2.19864900
C	-0.66186100	4.79262000	1.26534500
H	-0.58372100	4.15563400	2.15110900
H	-1.62113200	5.31546200	1.30338700
H	0.13042100	5.54434100	1.31349700
C	0.81350700	3.25630600	-0.05503700
C	0.96976300	1.87198600	0.01267400
C	2.23786700	1.25796000	-0.03713300
C	3.36967300	2.08005900	-0.09891400
H	4.35729100	1.63532300	-0.09647600
C	3.24640700	3.46407200	-0.14248800
H	4.12888400	4.09303900	-0.18554500
C	1.98006100	4.03168500	-0.13065900
H	1.88850000	5.11112100	-0.16678300
C	-3.15357800	-2.07627000	-1.28163100
H	-4.11247800	-2.35126400	-0.82268100
C	-2.39116300	-3.36804200	-1.63078700
H	-3.00445000	-3.97429600	-2.30460200
H	-2.16369500	-3.97688700	-0.75124300
H	-1.45433600	-3.13230300	-2.13995900
C	-3.43918100	-1.24256000	-2.54039700
H	-2.51370000	-0.93232200	-3.02584500
H	-4.03285900	-0.35102700	-2.33015300
H	-4.00635500	-1.86186000	-3.24299500
C	-3.24243800	-1.64050400	1.62780100
H	-4.28585300	-1.43841100	1.35135200
C	-3.08948500	-3.13893500	1.93066900
H	-2.04345700	-3.39165100	2.13528700

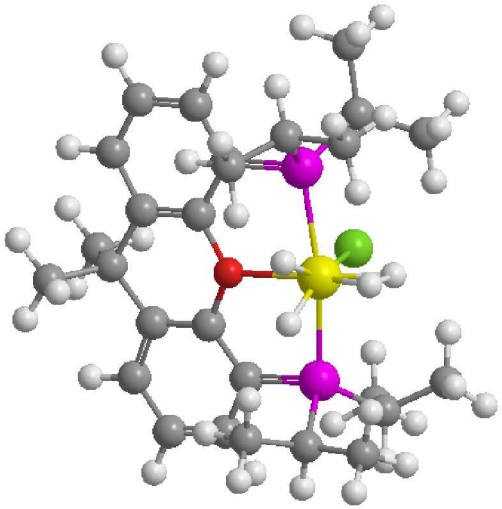

H	-3.44246600	-3.77204400	1.11315200
H	-3.67280300	-3.39511900	2.82030500
C	-2.89458400	-0.78367300	2.85140900
H	-3.57414900	-1.03330200	3.67200100
H	-2.98700400	0.28646500	2.64946700
H	-1.87715800	-0.98154300	3.20664600
C	3.57664600	-0.86601800	1.47161600
H	4.54214200	-0.45154500	1.15939200
C	3.12668700	-0.12962600	2.74110200
H	2.17841400	-0.52434200	3.12306700
H	3.01233500	0.94523700	2.58142200
H	3.87481700	-0.27755600	3.52591100
C	3.74183000	-2.37207000	1.73095600
H	4.40620900	-2.52558500	2.58676200
H	4.17476500	-2.90056300	0.87908800
H	2.77907600	-2.83720100	1.96932800
C	3.31613000	-1.11273000	-1.53282200
H	2.83007800	-0.50492200	-2.30173800
C	4.82719900	-0.83362300	-1.54264600
H	5.35764900	-1.41219500	-0.78018500
H	5.06916600	0.22275200	-1.41083500
H	5.23071800	-1.13454800	-2.51443200
C	3.02696200	-2.59167900	-1.84692200
H	3.48509400	-2.84315500	-2.80846400
H	1.95682900	-2.78150800	-1.93024600
H	3.45239500	-3.26414000	-1.09700800
H	0.80793800	-1.00018400	1.71020500

Zero-point correction= 0.649941 (Hartree/Particle)
Thermal correction to Energy= 0.687642
Thermal correction to Enthalpy= 0.688586
Thermal correction to Gibbs Free Energy= 0.584480
Sum of electronic and zero-point Energies= -2363.670602
Sum of electronic and thermal Energies= -2363.632901
Sum of electronic and thermal Enthalpies= -2363.631957
Sum of electronic and thermal Free Energies= -2363.736062

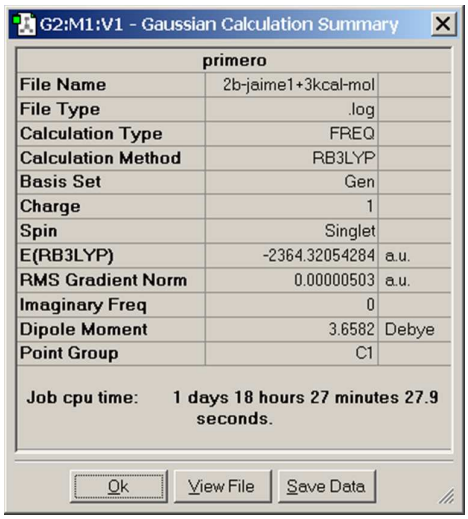

5

H	-0.69332000	-2.38938500	-0.30628700
H	0.69447200	-2.38925000	-0.30483800
H	-0.00102100	-1.84419700	1.46509300
H	0.00065100	-0.89944200	1.71027500
P	-2.39753600	-0.45022700	0.09367800
P	2.39742100	-0.45019600	0.09382000
O	-0.00004700	1.16297200	0.22045300
C	-1.11433600	1.96178800	0.08344900
C	-2.37552400	1.40553500	0.04744700
C	-3.40461600	2.35613600	-0.06688700
H	-4.44323600	2.04822300	-0.09158500
C	-3.10025000	3.72639300	-0.16012200
H	-3.91989700	4.43145900	-0.25227100
C	-1.78794800	4.21732700	-0.15839500
H	-1.59995300	5.28095100	-0.25747000
C	-0.73569300	3.30238500	-0.03563000
C	0.73560300	3.30238400	-0.03564900
C	1.78784300	4.21730200	-0.15870000
H	1.59983400	5.28091900	-0.25783500
C	3.10014200	3.72635000	-0.16061100
H	3.91978300	4.43138900	-0.25301800
C	3.40451900	2.35610100	-0.06725300
H	4.44312900	2.04818300	-0.09214000
C	2.37543200	1.40554200	0.04740800
C	1.11424400	1.96179000	0.08344800
C	-3.40448600	-0.99393400	-1.38635000
H	-3.07705300	-0.29062900	-2.15990100
C	-4.91862300	-0.85016000	-1.17339700
H	-5.43167700	-1.05272400	-2.11900800
H	-5.21264000	0.15283000	-0.85457300
H	-5.29320100	-1.56796100	-0.43702700
C	-3.03211200	-2.41123100	-1.84732200
H	-3.24725800	-3.16528400	-1.08416800
H	-1.97834600	-2.47601600	-2.12364500
H	-3.62476300	-2.66189000	-2.73340400

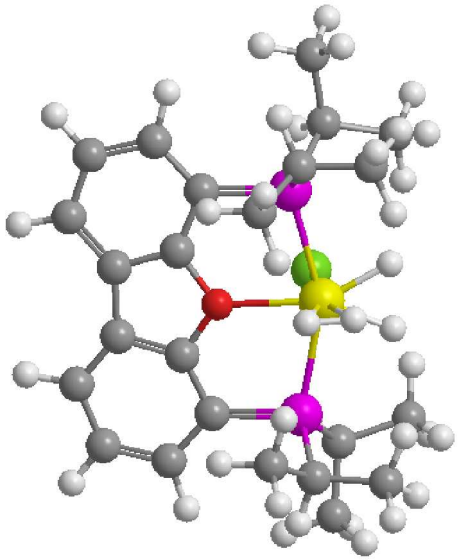

C	-3.31599000	-0.89006100	1.65388000
H	-4.33174100	-0.50349200	1.50932200
C	-3.37637000	-2.41329200	1.83084400
H	-2.37181400	-2.84289400	1.91294500
H	-3.89163900	-2.90826200	1.00449100
H	-3.91846600	-2.65496000	2.75090500
C	-2.70449100	-0.19755000	2.87918500
H	-3.30077800	-0.43865700	3.76511400
H	-2.68904200	0.89113200	2.77490800
H	-1.68147700	-0.53733300	3.07124300
C	3.40455800	-0.99376200	-1.38612900
H	3.07721400	-0.29034500	-2.15961100
C	3.03232900	-2.41096000	-1.84737100
H	3.62482200	-2.66131400	-2.73364100
H	1.97850100	-2.47586800	-2.12344500
H	3.24778200	-3.16515200	-1.08442700
C	4.91866200	-0.84990300	-1.17290500
H	5.29328800	-1.56838000	-0.43722400
H	5.21252500	0.15279700	-0.85298000
H	5.43182700	-1.05138000	-2.11869300
C	3.31580100	-0.89019400	1.65397900
H	4.33161900	-0.50384600	1.50939400
C	2.70473100	-0.19772100	2.87949700
H	1.68208300	-0.53814400	3.07229100
H	2.68856700	0.89094500	2.77504300
H	3.30176000	-0.43829900	3.76507400
C	3.37581400	-2.41346500	1.83082000
H	3.91836700	-2.65535400	2.75055800
H	3.89042000	-2.90859600	1.00416600
H	2.37113700	-2.84266700	1.91350600
Os	0.00004900	-0.98246700	0.04592900
Cl	0.00014600	-0.44575400	-2.35195700

Zero-point correction= 0.565829 (Hartree/Particle)
Thermal correction to Energy= 0.615169
Thermal correction to Enthalpy= 0.616334
Thermal correction to Gibbs Free Energy= 0.481529
Sum of electronic and zero-point Energies= -2245.847111
Sum of electronic and thermal Energies= -2245.797771
Sum of electronic and thermal Enthalpies= -2245.796606
Sum of electronic and thermal Free Energies= -2245.931410

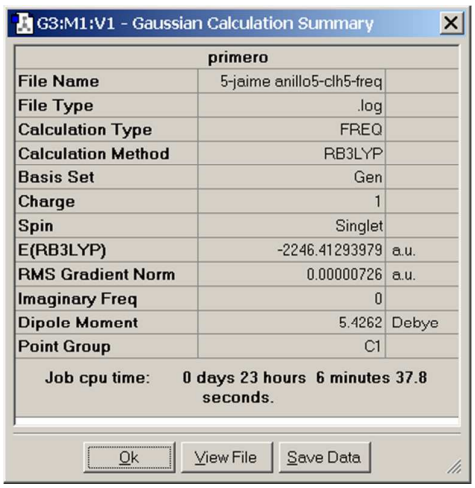

6

Os	0.89464400	-0.21006200	0.20710200
H	0.87011900	-0.67434700	1.80497300
Cl	0.68373000	-0.20202000	-2.23878000
P	0.09876500	-2.44705000	0.13646700
P	1.05298900	2.15780100	0.04888600
O	-1.28182900	0.23319900	0.11832800
C	-1.69766400	-2.14124100	-0.00866000
C	-2.21065800	-0.83132600	-0.00970700
C	-3.58094700	-0.57973900	-0.09077400
C	-4.43613300	-1.68929000	-0.15837000
H	-5.50513700	-1.51952400	-0.21771000
C	-3.96338200	-2.99496300	-0.14050900
H	-4.65477000	-3.82929500	-0.18704600
C	-2.59329600	-3.21493900	-0.06395100
H	-2.21043600	-4.23040000	-0.05035900
C	-4.17869000	0.82198400	-0.09145100
C	-5.02770100	1.00845100	-1.37714300
H	-5.48485100	2.00029400	-1.40577500
H	-5.83838600	0.27733500	-1.42220100
H	-4.40776700	0.88958400	-2.26976300
C	-5.07123200	0.98928900	1.16688100
H	-4.48257300	0.86274400	2.08006600
H	-5.87725200	0.25107800	1.17476200
H	-5.53102300	1.98048900	1.19116100
C	-3.08015900	1.87906800	-0.06722500
C	-1.71853100	1.57677400	-0.00361800
C	-0.73158600	2.58329600	-0.00774500
C	-1.14676100	3.92031000	-0.01722500
H	-0.40797300	4.71057200	0.02823500
C	-2.49586400	4.25133600	-0.06360400

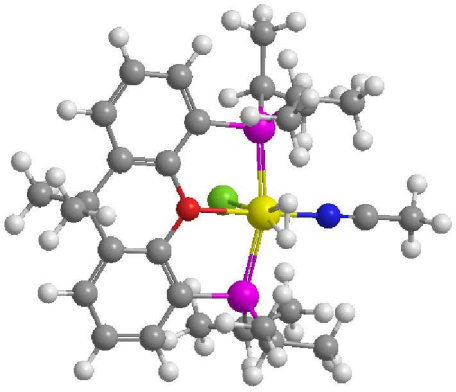

H	-2.80778800	5.29008700	-0.07072100
C	-3.43914900	3.23433000	-0.10070200
H	-4.49064400	3.49465300	-0.14292900
C	0.61940200	-3.65663200	-1.21139800
H	0.51509600	-4.64276100	-0.73898200
C	2.10259000	-3.43418100	-1.56283800
H	2.43135400	-4.22364600	-2.24629200
H	2.75355100	-3.46145700	-0.68470900
H	2.23262900	-2.47012200	-2.05908700
C	-0.24734600	-3.62594600	-2.48050700
H	-0.19279900	-2.65144000	-2.96726400
H	-1.29587100	-3.85260700	-2.28001300
H	0.12896400	-4.38180400	-3.17799000
C	0.21407100	-3.47892600	1.69846700
H	-0.33549900	-4.40135500	1.46849000
C	1.67565100	-3.83531700	2.00936300
H	2.27642100	-2.92928500	2.14775000
H	2.13600100	-4.43633000	1.22127600
H	1.72708200	-4.41422300	2.93679900
C	-0.46158900	-2.80491300	2.89957000
H	-0.45645400	-3.49057400	3.75263100
H	-1.49919300	-2.53106700	2.69215500
H	0.07548000	-1.90207800	3.21004300
C	1.69672300	3.12098700	1.51796100
H	1.59946200	4.17946000	1.25006100
C	0.86553900	2.87092600	2.78439200
H	0.95814700	1.83538100	3.13005100
H	-0.19496400	3.08849700	2.63636400
H	1.23341000	3.51251900	3.59124800
C	3.18054200	2.80264900	1.76040500
H	3.53444600	3.33941100	2.64617000
H	3.81261100	3.09905200	0.92059700
H	3.32525000	1.73106900	1.93682200
C	1.84092300	2.88801200	-1.49456400
H	1.12461500	2.60055900	-2.27089300
C	2.00643400	4.41449200	-1.49060000
H	2.69844400	4.75050000	-0.71176100
H	1.06104800	4.94641600	-1.37078900
H	2.42808200	4.72566500	-2.45178100
C	3.17515900	2.19146300	-1.81777000
H	3.54067600	2.56004800	-2.78163000
H	3.04882600	1.11259200	-1.89917100
H	3.94539900	2.41091700	-1.07209500
H	1.02371200	0.29817200	1.78623100
N	2.81725300	-0.60398800	0.14740300
C	3.94739900	-0.83669200	0.04081400
C	5.36372000	-1.12827600	-0.12704600
H	5.84175700	-0.33396700	-0.70838000
H	5.85772700	-1.20025500	0.84637400
H	5.48948800	-2.07633400	-0.65882500

Zero-point correction= 0.680230 (Hartree/Particle)
Thermal correction to Energy= 0.722115
Thermal correction to Enthalpy= 0.723059
Thermal correction to Gibbs Free Energy= 0.608022
Sum of electronic and zero-point Energies= -2495.249648
Sum of electronic and thermal Energies= -2495.207763
Sum of electronic and thermal Enthalpies= -2495.206819
Sum of electronic and thermal Free Energies= -2495.321856

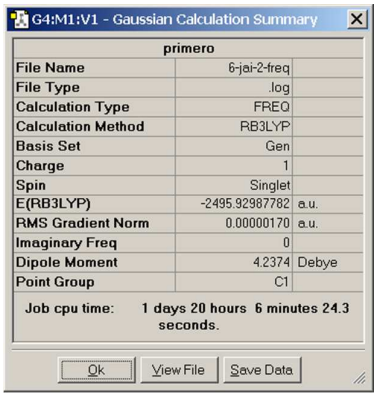

II. References

(1) (a) Lee, C. T.; Yang, W. T.; Parr, R. G. Development of the Colle-Salvetti Correlation-Energy Formula into a Functional of the Electron-Density. *Phys Rev B* **1988**, *37*, 785-789. (b) Becke, A. D. A New Mixing of Hartree-Fock and Local Density-Functional Theories. *J. Chem. Phys.* **1993**, *98*, 1372-1377. (c) Stephens, P. J.; Devlin, F. J.; Chabalowski, C. F.; Frisch, M. J. Ab-Initio Calculation of Vibrational Absorption and Circular-Dichroism Spectra Using Density-Functional Force-Fields. *J. Phys. Chem.* **1994**, *98*, 11623-11627.

(2) Grimme, S.; Antony, J.; Ehrlich, S.; Krieg, H. A Consistent and Accurate *ab initio* Parametrization of Density Functional Dispersion Correction (DFT-D) for the 94 Elements H-Pu. *J. Chem. Phys.* **2010**, *132*.

(3) Frisch, M. J.; Trucks, G. W.; Schlegel, H. B.; Scuseria, G. E.; Robb, M. A.; Cheeseman, J. R.; Scalmani, G.; Barone, V.; Mennucci, B.; Petersson, G. A.; Nakatsuji, H.; Caricato, M.; Li, X.; Hratchian, H. P.; Izmaylov, A. F.; Bloino, J.; Zheng, G.; Sonnenberg, J. L.; Hada, M.; Ehara, M.; Toyota, K.; Fukuda, R.; Hasegawa, J.; Ishida, M.; Nakajima, T.; Honda, Y.; Kitao, O.; Nakai, H.; Vreven, T.; Montgomery, J. A. Jr.; Peralta, J. E.; Ogliaro, F.; Bearpark, M.; Heyd, J. J.; Brothers, E.; Kudin, K. N.; Staroverov, V. N.; Keith, T.; Kobayashi, R.; Normand, J.; Raghavachari, K.; Rendell, A.; Burant, J. C.; Iyengar, S. S.; Tomasi, J.; Cossi, M.; Rega, N.; Millam, J. M.; Klene, M.; Knox, J. E.; Cross, J. B.; Bakken, V.; Adamo, C.; Jaramillo, J.; Gomperts, R.; Stratmann, R. E.; Yazyev, O.; Austin, A. J.; Cammi, R.; Pomelli, C.; Ochterski, J. W.; Martin, R. L.; Morokuma, K.; Zakrzewski, V. G.; Voth, G. A.; Salvador, P.; Dannenberg, J. J.; Dapprich, S.; Daniels, A. D.; Farkas, O.; Foresman, J. B.; Ortiz, J. V.; Cioslowski, J.; Fox, D. J. Gaussian 09 (v.D.01) Gaussian, Inc., Wallingford CT, 2013.

(4) Andrae, D.; Haussermann, U.; Dolg, M.; Stoll, H.; Preuss, H. Energy-Adjusted Abinitio Pseudopotentials for the 2nd and 3rd Row Transition-Elements. *Theoretica Chimica Acta* **1990**, *77*, 123-141.

(5) Ehlers, A. W.; Bohme, M.; Dapprich, S.; Gobbi, A.; Hollwarth, A.; Jonas, V.; Kohler, K. F.; Stegmann, R.; Veldkamp, A.; Frenking, G. A Set of F-Polarization Functions for Pseudo-Potential Basis-Sets of the Transition-Metals Sc-Cu, Y-Ag and La-Au. *Chem. Phys. Lett.* **1993**, *208*, 111-114.

(6) (a) Hehre, W. J.; Ditchfield, R.; Pople, J. A. Self-Consistent Molecular-Orbital Methods. XII. Further Extensions of Gaussian-Type Basis Sets for Use in Molecular-Orbital Studies of Organic-Molecules. *J. Chem. Phys.* **1972**, *56*, 2257-2261. (b) Francl, M. M.; Pietro, W. J.; Hehre, W. J.; Binkley, J. S.; Gordon, M. S.; Defrees, D. J.; Pople, J. A. Self-Consistent Molecular-Orbital Methods .23. A Polarization-Type Basis Set for 2nd-Row Elements. *J. Chem. Phys.* **1982**, *77*, 3654-3665.

Dehydrogenation of Formic Acid Promoted by a Trihydride-Hydroxo-Osmium (IV) Complex: Kinetics and Mechanism

Miguel A. Esteruelas, Cristina García-Yebra, Jaime Martín, and Enrique Oñate*

Departamento de Química Inorgánica, Instituto de Síntesis Química y Catálisis Homogénea (ISQCH), Centro de Innovación en Química Avanzada (ORFEO-CINQA), Universidad de Zaragoza-CSIC, 50009 Zaragoza, Spain

ABSTRACT

The preparation of the hydroxo-osmium(IV) complex $OsH_3(OH)\{xant(P^iPr_2)_2\}$ ($xant(P^iPr_2)_2$ = 9,9-dimethyl-4,5-bis(diisopropylphosphino)xanthene) and its catalytic efficiency for the dehydrogenation of formic acid to H_2 and CO_2 are reported. The mechanism of the dehydrogenation has been unambiguously stablished by combining the kinetic analysis of the catalysis, the isolation of the intermediates and the kinetic analysis of their decomposition, and DFT calculations on the rate-determining step. Under catalytic conditions the trihydride-hydroxo complex reacts with formic acid to afford $OsH_3\{\kappa^1\text{-}O\text{-}(HCO_2)\}\{xant(P^iPr_2)_2\}$, which isomerizes into $OsH_3\{\kappa^1\text{-}H\text{-}(HCO_2)\}\{xant(P^iPr_2)_2\}$ by means of the slippage of the metal center through a formate O-C-H path. The κ^1-H-formate intermediate releases CO_2 to give the previously reported

tetrahydride $OsH_4\{xant(P^iPr_2)_2\}$, which undergoes protonation with formic acid. The resulting OsH_5-cation exists as an equilibrium mixture of the tautomers trihydride-compressed dihydride $[OsH_3(H\cdots H)\{xant(P^iPr_2)_2\}]^+$ and hydride-compressed dihydride-dihydrogen $[OsH(H\cdots H)(\eta^2\text{-}H_2)\{xant(P^iPr_2)_2\}]^+$. The dissociation of H_2 from the latter leads to $[OsH_3\{xant(P^iPr_2)_2\}]^+$, which coordinates HCO_2^- to regenerate the trihydride-(κ^1-O-formate) complex and to close the cycle. The release of CO_2 from the κ^1-H-formate intermediate is the rate-determining step of the catalysis.

INTRODUCTION

Hydrogen gas is a promising energy carrier as clean alternative to conventional fossil fuels. It can be produced from any primary energy source, has an energy content per mass that is about three times that of the carbon-based fuels, can be used by direct introduction into either an internal combustion engine or to a fuel cell, and its oxidation with O_2 gives water.[1] However, its energy content per volume is very low at standard temperature and pressure. To overcome this difficulty, several methods are being investigated.[2]

The concept of chemical storage is an attractive strategy; in particular the use of organic liquids since they can be transported through the liquid-fuel infrastructures. In these compounds, hydrogen does not exist in its molecular form but is covalently bound. At the time and place of energy demand, H_2 is released via dehydrogenation. The hydrogen carrying liquid itself is not consumed but is reloaded and used in further cycles.[3] Formic acid is a reputed family member of liquid organic hydrogen carriers. It is stable under ambient conditions, produced in large-scale, and biodegradable. Furthermore, it has low flammability and toxicity, its gravimetric and volumetric H_2 capacity of 4.4 wt. % and 53.4 g/L are reasonable,[4] and its recyclability by means

CO_2 hydrogenation undergoes a constant improvement,[5] reaching complex RuHCl(CO)(PNP) (PNP = 2,6-bis(di-*ter*-buthylphosphinomethyl)pyridine) a TOF of 1100000 h^{-1} for the reduction to formates in 2014.[5a]

Both homogeneous and heterogeneous transition metal systems have proven to have the ability of promoting the formic acid (FA) dehydrogenation to H_2 and CO_2.[6] The majority of the homogeneous catalysts are complexes of Fe,[7] Ru,[8] and Ir.[9] In addition, a few precursors of Mo,[10] Rh,[11] Ni,[12] Cu,[13] and Al[14] have been also reported. Further research needs to be focused on the mechanism of the whole catalytic process. Most of them are only postulated and experimental support is necessary. The catalysis has two stages, CO_2 formation and H_2 formation. The rate-limiting step can be any of them. The main divergences are found in the former, which may happen by hydride abstraction, β-hydride elimination, or by an outer-sphere mechanism.[15] Although the latter is currently questioned.[16]

The use of Os in homogeneous catalysis has received significantly less attention than the use of its group congeners Fe and Ru. With the exception of Sharpless dihydroxylation and processes akin,[17] it has been centered in some particular reactions of organic synthesis.[18] However, in the last years, it is being revealed as a promising alternative for processes related to the hydrogen economy.[19] Of special relevance are its polyhydride derivatives,[20] which have shown to have the ability of carrying out the dehydrogenation of amineboranes[21] and liquid organic hydrogen carriers such as alcohols and cyclic amines.[22] Other ligand with good performance is the hydroxo group. For instance, complex [Os(OH)(η^6-*p*-cymene)IPr]OTf (IPr = 1,3-bis(2,6-diisopropylphenyl)imidazolylidene; OTf = CF_3SO_3) has shown great efficiency in the hydrogen transfer from 2-propanol to aldehydes,[23] the α-alkylation of arylacetonitriles and methyl ketones,[24] and the hydration of nitriles to amides.[25]

Hydroxo complexes of the platinum group metals are very scarce and their chemistry is underdeveloped.[26] Hydride-hydroxo derivatives are particularly challenging since formally result from the oxidative addition of water, which is generally disfavored from a thermodynamic point of view and thus the limited known examples display reversibility.[27] Compounds of Os of this class are Os(II)-species[28] and, although the oxidation state +4 is usual for this element when bears small size ligands, the hydride-hydroxo-Os(IV) complexes are unknown until now.

Pincer ligands show a marked ability to stabilize uncommon complexes due to the disposition of their donor atoms.[29] Ether-diphosphines have particular interest due to their flexibility, which grant the ability of changing between κ^3-*mer*-, κ^3-*fac*, and κ^2 coordination modes. This allows them to adapt to the requirements of the participating intermediates of the catalytic cycles.[30] In the search for efficient catalysts for processes related to hydrogen economy and also for reactions of interest in organic synthesis, some years ago we initiated a research program on POP complexes of groups 8[19c,30c,30i,31] and 9,[30h,32] which has yielded us to discover notable catalysts for dehydrogenation of ammonia borane,[30h] monoalcoholysis of disilanes,[32b] synthesis of imines from alcohols and amines with liberation of H_2,[19c] hydrogen transfer from 2-propanol to ketones, α-alkylation of phenylacetonitrile and acetophenone with alcohols,[31b] regio- and stereoseletive head-to-head (*Z*)-dimerization of terminal alkynes,[30c,31b] borylation of arenes,[32c] and decyanative borylation of arylnitriles.[32d] Now, we have discovered that the ether-diphosphine 9,9-dimethyl-4,5-bis(diisopropylphosphino)xanthene (xant(P^iPr_2)$_2$) stabilizes a hydride-hydroxo-Os(IV) complex, which efficiently promotes the FA dehydrogenation. This paper reports the preparation and characterization of this novel catalyst precursor, its activity in the dehydrogenation process, and the kinetics and mechanism of the same one.

RESULTS AND DISCUSSION

Preparation and Characterization of the Catalyst Precursor. The known hydroxo compounds of osmium include the nitrido complexes $Os(N)Tp(OH)_2$ (Tp = hydridotris(1-pyrazolyl)borate),[33] $[Os(N)(CH_2SiMe_3)(OH)]^-$, and $[Os(N)(CH_2SiMe_3)(OH)_2]^-$,[34] the previously mentioned cation $[Os(OH)(\eta^6\text{-}p\text{-cymene})IPr]^+$,[23] the hydride-hydroxo derivatives $OsH(OH)(PMe_3)_4$,[28a] $OsH(OH)(CO)(PR_3)_2$ (PR_3 = P^iPr_3,[28b] P^tBu_2Me[28c]), $OsH(OH)(NH_2CMe_2CMe_2NH_2)(PPh_3)_2$,[28d] and $[OsH(OH)(C{\equiv}CPh)(IPr)(P^iPr_3)]OTf$,[28e] and a few dimers.[35] They were prepared by one of these methods: hydrolysis of Os-C[28a,28c] or Os-N[28d] bonds and replacement of chloride by hydroxo.[23,28a,28c,34] The first method is not suitable in our case by the lack of an appropriate starting compound. So, we tried the substitution of chloride by hydroxo employing the previously reported[30c] trihydride $OsH_3Cl\{xant(P^iPr_2)_2\}$ (**1**) as a precursor. However, all attempts were unsuccessful, reaching a partial substitution in the best of cases. Then, we decided to replace the chloride ligand of **1** by a better leaving group as trifluoromethanesulfonate (Scheme 1).

Scheme 1. Preparation of complex 3

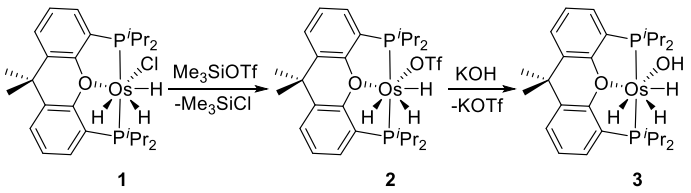

Treatment of a toluene solution of **1** with 2.0 equiv of Me_3SiOTf, at room temperature, for 10 min affords the synthetic intermediate $OsH_3(OTf)\{xant(P^iPr_2)_2\}$ (**2**), which was isolated as a yellow solid in 90 % yield. The substitution reaction is supported by the ^{19}F NMR spectrum, in toluene-d_8, which shows a singlet at -77.7 ppm due to the coordinated OTf^- anion. Like observed

for its chloride precursor, the ^{1}H NMR spectrum of **2** in toluende-d_8 shows a resonance at -13.82 ppm for the inequivalent hydride ligands, which indicates the operation of two thermally activated site exchange processes within the OsH_3 unit. Between 233 and 223 K, decoalescence occurs and two signals at -12.12 and -17.02 ppm in a 2:1 intensity ratio are observed. Although at lower temperatures than 223 K the resonance at -12.12 ppm displays broad, the expected second decoalescence is not reached even at 183 K. According to the trihydride character of the compound, 400 MHz T_1(min) values of 89 ± 4 and 69 ± 3 ms were found at 223 K for the hydride resonances. The $^{31}P\{^{1}H\}$ NMR spectrum shows a singlet at 54.6 ppm between 298 and 183 K.

Trifluromethanesulfonate is easily displaced by a hydroxo group, in contrast to the chloride ligand of **1**. Dropwise addition of a water KOH solution to an acetone solution of **2** at room temperature leads to the hydroxo $OsH_3(OH)\{xant(P^iPr_2)_2\}$ (**3**), which was isolated as a yellow solid in 92 % yield. The presence of the hydroxo ligand in this novel osmium(IV) species is supported by the IR and ^{1}H NMR spectrum. The IR contains the characteristic ν(OH) band at 3672 cm^{-1}, whereas the ^{1}H NMR spectrum in toluene-d_8 shows a broad resonance at 2.87 ppm corresponding to the OH-hydrogen atom. Like the ^{1}H NMR spectrum of **2**, the spectrum contains a signal (δ_{1H}, -12.25) for the hydrides, indicating that are also involved in two thermally activated site exchange processes. At about 273 K, a first decoalescence occurs to give two resonances at -12.46 and -13.08 ppm in a 2:1 intensity ratio. Between 203 and 193 K, the lower field signal splits into an AB system. The J_{AB} coupling constant decreases from 151.9 to 146.8 Hz as the temperature does from 193 to 173 K. These unusually high value for two hydrides disposed *cis* and their dependence with the temperature can be rationalized in terms of quantum-mechanical

exchange coupling between the involved hydrides.[20] The $^{31}P\{^{1}H\}$ NMR spectrum shows a singlet at 49.9 ppm.

FA Dehydrogenation Promoted by 3: Kinetic Study. Trihydride-hydroxo complex **3** promotes the FA dehydrogenation to H_2 and CO_2.[36] It works well with diluted solutions and also dehydrogenates neat formic acid, but rapidly decomposes under the latter conditions. The reactions were performed in toluene, under atmospheric pressure, between 298 to 318 K. The partial volume of hydrogen formed (V_{H_2}) was determined from the total volume (V_T) of gas generated according to eq 1, where $V_{m(H_2)}$ and $V_{m(CO_2)}$ are the partial molar volumes of H_2 and CO_2, respectively. The total volume was measured by displacing vaseline oil from a gas burette.

$$V_{H_2} = [V_T/(V_{m(H_2)} + V_{m(CO_2)})]V_{m(H_2)} \qquad (1)$$

The kinetics of the catalysis was studied to gain insight into the process. Initial rates (Table 1) were determined from the gas evolution experiments (Figure 1) by using eq 2, where P is the atmospheric pressure (atm), *R* is the molar gas constant, T is the temperature (K) and V_{sol} is the total volume of the reaction solution.

$$d[H_2]/dt = (dV_{H_2}/dt)P/RTV_{sol} \qquad (2)$$

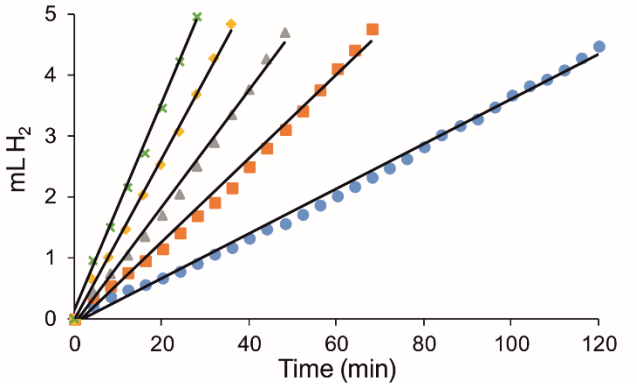

Figure 1. V_{H_2} Generated from the catalytic dehydrogenation of H_2CO_2 (0.53 M) promoted by **3** in toluene at 298 K. 10^2[**3**]: 0.61 M (blue circle), 1.23 (orange square), 1.86 (grey triangle), 2.48 (yellow diamond), 3.06 (green cross).

Table 1. Kinetic data for the dehydrogenation of formic acid promoted by 3[a]

T (K)	10^2[**3**] (M)	$[H_2CO_2]_0$ (M)	$10^2 d[H_2]/dt$ [b] ($M \cdot min^{-1}$)	k (min^{-1})
298	0.61	0.53	0.057	0.094
298	1.23	0.53	0.123	0.100
298	1.86	0.53	0.155	0.083
298	2.48	0.53	0.228	0.092
298	3.06	0.53	0.278	0.091
298	1.23	0.42	0.118	0.096
298	1.23	0.64	0.124	0.101
298	1.23	0.74	0.128	0.104
298	1.23	0.95	0.128	0.104
303	1.24	0.53	0.216	0.174
308	1.24	0.53	0.370	0.298
313	1.23	0.53	0.503	0.409
318	1.23	0.53	0.914	0.743

[a] Reactions were quantitative yielding TON between 17 and 87. [b] Calculated at 20% conversion.

A rate law for the dehydrogenation of formic acid promoted by **3** is

$$d[H_2]/dt = k[H_2CO_2]_0^a[\mathbf{3}]^b \qquad (3)$$

The rate dependence on formic acid concentration was determined at 298 K, for a constant concentration of **3** of $1.23 \cdot 10^{-2}$ M, by measuring initial rates with variable initial concentrations of formic acid ($[H_2CO_2]_0$ in Table 1) from 0.42 to 0.95 M. Under these conditions, the rate is independent of $[H_2CO_2]_0$ within the experimental error (Figure 2), in agreement with a = 0 in eq 3. The rate dependence on the catalyst precursor **3** was also determined at 298 K, for a fixed initial concentration of formic acid of 0.53 M, by varying the concentration of **3** from $0.61 \cdot 10^{-2}$ to $3.06 \cdot 10^{-2}$ M. Now, the plot of $\ln(d[H_2]/dt)$ versus ln[**3**] affords a straight line of slope 0.96 ± 0.17 (Figure 3), according to a first order in osmium concentration (b = 1 in eq 3). Therefore, the rate law is:

$$d[H_2]/dt = k[\mathbf{3}] \qquad (4)$$

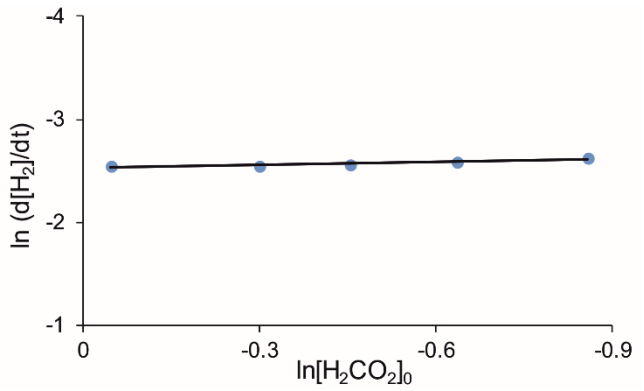

Figure 2. Plot of $\ln(d[H_2]/dt)$ vs $\ln[H_2CO_2]_0$ in toluene at 298 K, for a constant [**3**] of $1.23 \cdot 10^{-2}$ M.

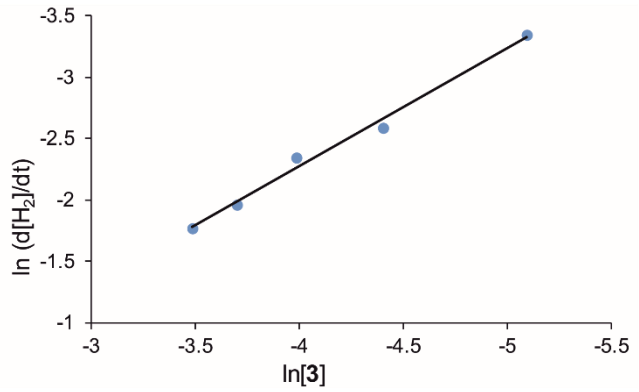

Figure 3. Plot of $\ln(d[H_2]/dt)$ vs ln[**3**] in toluene at 298 K, for a constant $[H_2CO_2]_0$ of 0.53 M.

A plot of $d[H_2]/dt$ versus [**3**] (Figure 4) provides a value of $9.0 \pm 1.0 \cdot 10^{-2}$ min^{-1} for *k* at 298 K. The activation parameters obtained from the Eyring analysis (Figure 5) are $\Delta H^{\ddagger}$ = 18 ± 3 kcal·mol^{-1} and $\Delta S^{\ddagger}$ = -3 ± 8 cal·mol^{-1}K^{-1}, which yield a $\Delta G^{\ddagger}$ value of 18 ± 5 kcal·mol^{-1} at 298 K in agreement with the values reported for the dehydrogenation of formic acid catalyzed by other homogeneous systems (17 – 26 kcal·mol^{-1}).[5a, 7d, 9f, 37]

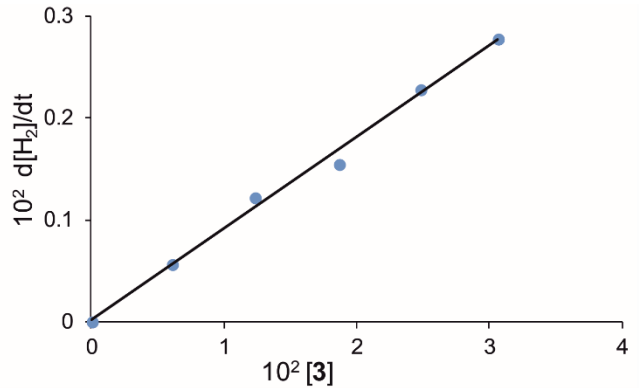

Figure 4. Plot of $d[H_2]/dt$ vs [**3**] using 0.53 M of H_2CO_2 in toluene at 298 K.

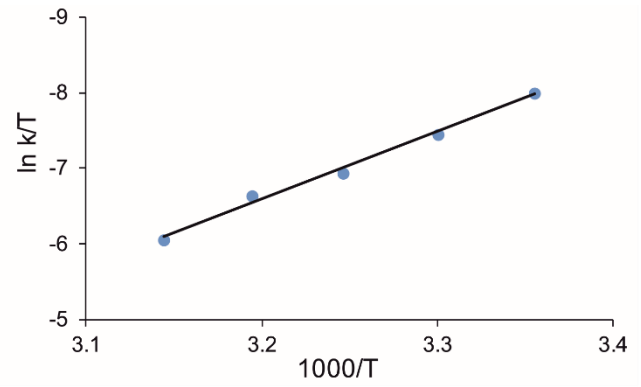

Figure 5. Eyring plot for the dehydrogenation of formic acid (0.53 M) promoted by **3** ($1.23 \cdot 10^{-2}$ M) in toluene.

Stoichometric Reactions. In order to have access to the key intermediates of the catalysis, we studied the stoichiometric reaction of **3** with formic acid in addition to the stages of CO_2 and H_2 formation.

The addition of 1.0 equiv of formic acid to a toluene-d_8 solution of **3** contained in a NMR tube quantitatively and instantly leads to the formate derivative $OsH_3\{\kappa^1\text{-O-}(HCO_2)\}\{xant(P^iPr_2)_2\}$ (**4**), as a consequence of the protonation of the hydroxo ligand of **3** and the subsequent displacement of the generated H_2O by a formate anion (Scheme 2).

Scheme 2. Reaction of 3 with H_2CO_2

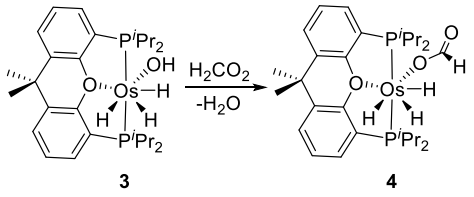

3 **4**

The presence of a formate group in the osmium coordination sphere is supported by $^{13}C\{^1H\}$ and ^1H NMR spectra of the new species at 253 K. The $^{13}C\{^1H\}$ NMR spectrum shows at 167.8 ppm a singlet due to the HCO_2-carbon atom, whereas the ^1H NMR spectrum contains a singlet at 8.91

ppm corresponding to the HCO_2-hydrogen atom. Like in **2** and **3**, the hydrides of **4** experience position exchange thermally activated. Thus, they display a broad signal at -12.55 ppm. At about 213 K, a first decoalescence occurs to afford two signals at -12.00 and -13.32 ppm. At 193 K, the expected second decoalescence can be intuited from the very broad form of the resonance at -11.93 ppm. In the $^{31}P\{^{1}H\}$ NMR spectrum, the diphosphine gives rise to a singlet at 51.2 ppm. These spectroscopic features are consistent with the stereochemistry proposed for **4** in Scheme 2, which was confirmed by the X-ray diffraction analysis of a single crystal obtained from the toluene-d_8 solution (Figure 6). The Os{xant(P^iPr_2)$_2$} skeleton is T-shaped with the metal center situated in the common vertex and P1-Os-P2, P1-Os-O3, and P2-Os-O3 angles of 159.84(7)º, 83.08(12)º, and 82.63(12)º, respectively. The geometry around the osmium atom can be described as a distorted pentagonal bipyramid with axial P^iPr_2 groups and the oxygen atoms of the diphosphine and formate in the perpendicular plane, mutually *cisoid* disposed, along with the hydrides.

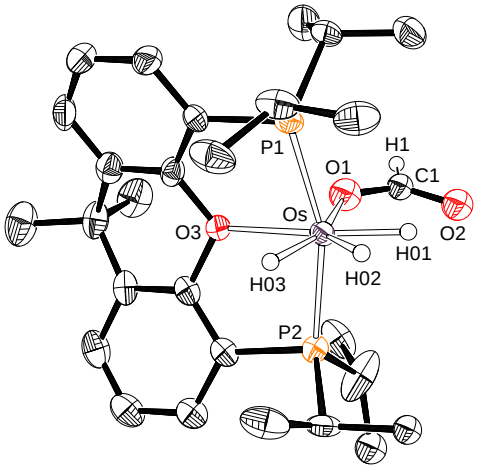

Figure 6. Molecular drawing of **4** with 50% probability ellipsoids. Hydrogen atoms (except hydrides and H1) are omitted. Selected distances (Å) and angles (deg): Os-O3 = 2.231(4), Os-O1

= 2.137(6), Os-P1 = 2.2915(19), Os-P2 = 2.2848 (18); P1-Os-P2 = 159.84(7), P1-Os-O3 = 83.08(12), P2-Os-O3 = 82.63(12), O1-Os-O3 = 76.1(3)

Complex **4** is unstable and releases CO_2 to afford $OsH_4\{xant(P^iPr_2)_2\}$ (**5**), according to Scheme 3. The transformation was monitored by $^{31}P\{^1H\}$ NMR spectroscopy as a function of time between 303 and 323 K. Figure 7 shows the transformation at 323 K. The decrease of **4** is an exponential function of time, in agreement with a first-order process, which fits to the expression

$$\ln([\mathbf{4}]/[\mathbf{4}]_0) = k_{st}t \qquad (5)$$

where $[\mathbf{4}]_0$ is the initial concentration of **4** and [**4**] is the concentration at time t. The values for the stoichiometric rate constant k_{st} are collected in Table 2. The activation parameters calculated by means of the Eyring analysis (Figure 8) are $\Delta H^{\ddagger} = 20 \pm 3$ kcal·mol^{-1} and $\Delta S^{\ddagger} = 0 \pm 8$ cal·mol^{-1}K^{-1}. They affords a $\Delta G^{\ddagger}$ value of 20 ± 5 kcal·mol^{-1} at 298 K, which compares well with that obtained for the catalytic process.

Scheme 3. Decarboxylation of complex 4

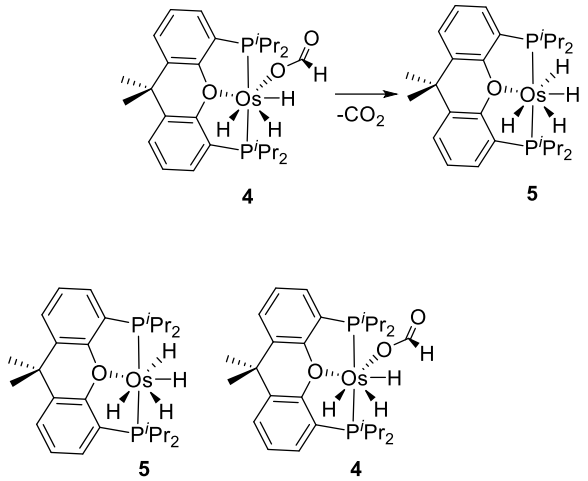

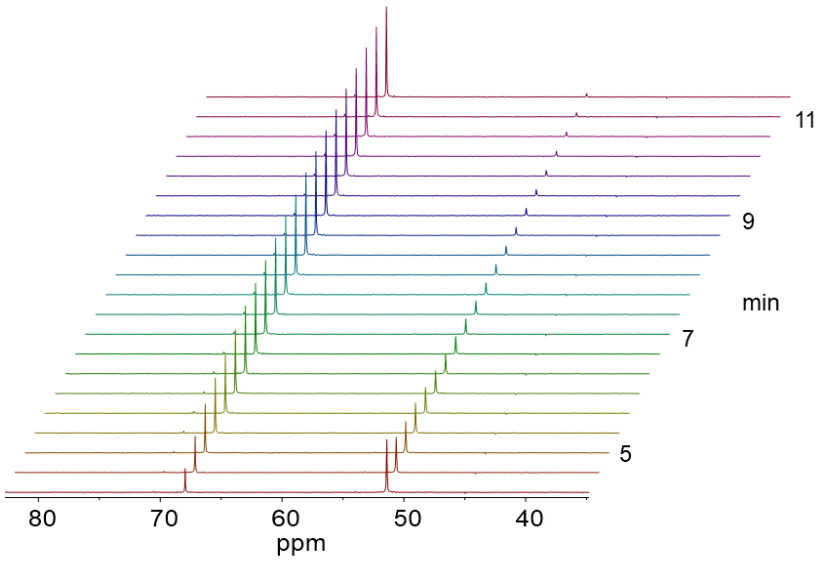

Figure 7. $^{31}P\{^{1}H\}$ spectra (161.98 MHz, in toluene-d_8) for the transformation of **4** into **5** at 323 K.

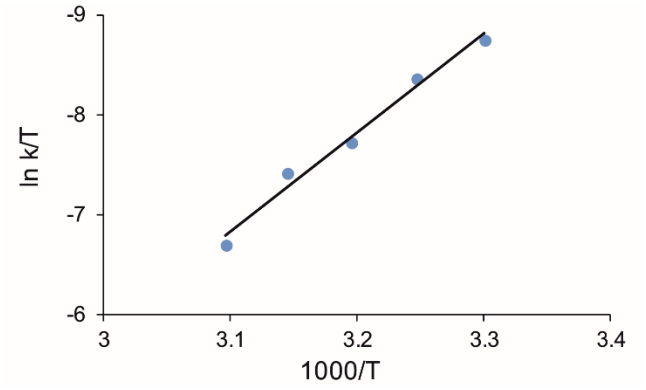

Figure 8. Eyring plot for the decarboxylation of **4** ($6.4 \cdot 10^{-2}$ M) in toluene-d_8.

Table 2. **Rate Constants k_{st} for the Decarboxylation of 4**

T (K)	k_{st} (min^{-1})
303	0.048
308	0.072
313	0.138

318	0.192
323	0.396

Tetrahydride complex **5** reacts with FA to form molecular hydrogen and to regenerate the formate derivative **4** (Scheme 4). At 243 K, the addition of 1.0 equiv of formic acid to a toluene-d_8 solution of **5** rapidly gives **4** and H_2 in quantitative yield. According to previous studies, the reaction initially implies the protonation of **4** to afford an OsH_5-cation **A**. DFT-Calculations revealed that this cation has two tautomers with similar energies: the trihydride compressed dihydride **Aa** and the hydride-compressed dihydride-dihydrogen **Ab**.[30c] The dissociation of the coordinated H_2 ligand from the latter and the coordination of the formate anion to the resulting unsaturated species **B** should lead to **4**.

Scheme 4. Reaction of 5 with H_2CO_2

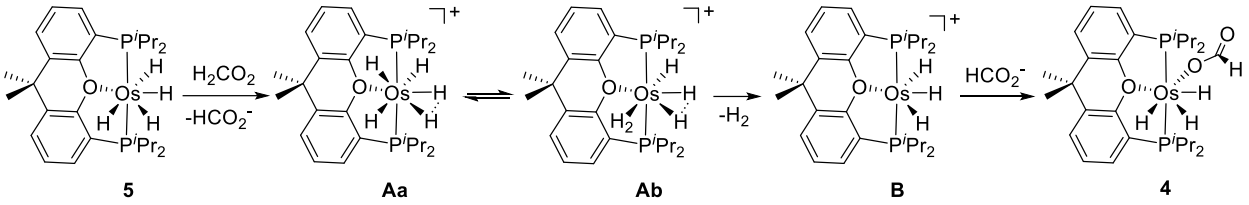

The reactions summarized in Schemes 2-4, fully characterize the catalysis. The trihydride-hydroxo complex **3** is the precursor of the catalyst and, under catalytic conditions, is quantitatively transformed into the true catalyst, the formate derivative **4** (Scheme 2), which releases CO_2 to form the tetrahydride **5** (Scheme 3). The latter reacts with FA to produce molecular hydrogen and regenerate **4** in a three step process: protonation, H_2 dissociation, and formate coordination (Scheme 4). Because the catalytic FA dehydrogenation promoted by **3** has

the same activation parameters as the stoichiometric release of CO_2 from **4**, the CO_2 formation is the rate determining step of the catalysis, while the molecular hydrogen formation is fast.

Mechanism of the CO_2 Formation Stage. As previously mentioned the CO_2 formation stage can occur through three different pathways: outer-sphere, *β*-hydride elimination, and hydride abstraction. An outer-sphere pathway must be excluded in this case because the system does not bear any function which could allow such catalysis class. *β*-Hydride elimination reactions have been proposed in cycles initiated by half-sandwich iridium(III) derivatives;[9f, 9i,] ruthenium complexes bearing pincer PNP ligands;[8e] iron species stabilized by PPP groups;[7c] and catalysts generated in situ from $Fe_3(CO)_{12}$, 2,2':6'2''-terpyridine or 1,10-phenanthroline, and triphenylphosphine working under visible light irradiation,[7b] among others. A distinctive fact of this mechanism is that the *β*-hydride elimination step occurs on unsaturated species. Hydride abstraction has been mainly proposed in reactions catalyzed by aluminum bis(imino)pyridine compounds,[14] ruthenium tetraphosphine derivatives,[8f] and iron complexes bearing PNP pincer ligands.[7d, 7f] In contrast to *β*-hydride elimination, the hydride migration takes place in two-steps, on a saturated intermediate, which involve the slippage of the metal center from the coordinated oxygen into the free hydrogen and the subsequent CO_2 release. In order to discern between *β*-hydride elimination and hydride abstraction, DFT calculations (B3LYP(GD3)//6-31G**/SDD(f)) were carried out. The changes in $\Delta G^{\ddagger}$ were calculated in toluene at 298 K and 1 atmosphere. Although the reaction is slightly endergonic, the equilibrium is driven by removal of the gas.

Figure 9 summarizes the energy profile for the *β*-hydride elimination pathway. Because the formate complex **4** is saturated, the dissociation of the oxygen atom of the pincer is necessary in order to generate a coordination vacancy at the metal center, which allows the migration of the hydrogen atom of the formate group. The dissociation has an activation energy of 16.3

kcal·mol^{-1}, which is lower than the experimental values obtained for the activation energies of the catalysis and for the stoichiometric decarboxylation of **4**, and leads to a 16 e$^-$ trihydride-hydroxo-osmium (IV) intermediate **C**. The latter is 13.9 kcal·mol^{-1} less stable than **4**. The migration leads to the Os (η^2-O=CO)-derivative **D**. Its barrier of 24.1 kcal·mol^{-1} with regard to **4** lies at the experimental upper limit. Intermediate **D** is 4.4 kcal·mol^{-1} less stable than **C**. The dissociation of the coordinated CO_2 molecule occurs in two steps, involving the sequential cleavage of the Os-C and Os-O bonds. Initially, intermediate **D** frees the carbon atom to afford **E**, which subsequently undergoes the Os-O rupture. The barrier for the first step of 26.8 kcal·mol^{-1}, with regard to **4**, is out of the experimental range and suggests that the *β*-hydride elimination is also a non-operating pathway. The release of the CO_2 molecule leads to **F**, which is a structural isomer of **5**.

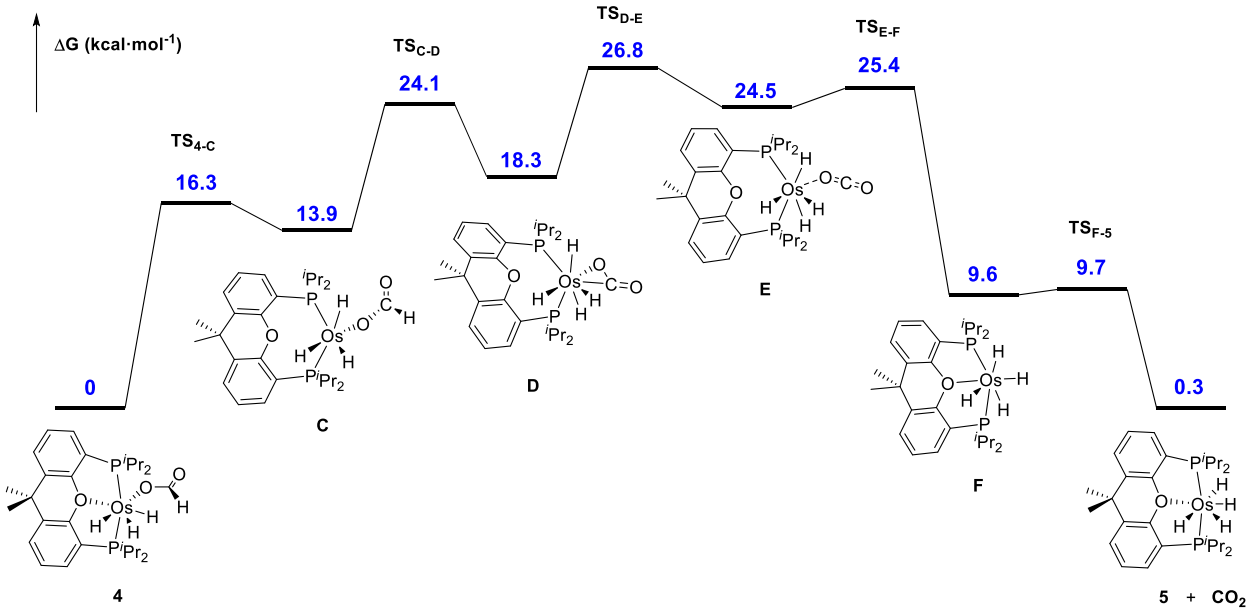

Figure 9. Energy profile (Δ*G* in kcal·mol^{-1}) for the CO_2 formation via *β*-hydride elimination.

The hydride abstraction takes place via intermediate **G** (Figure 10), which can be described as an Os{κ^1-H-(HCO$_2$)}-species and lies 12.1 kcal·mol^{-1} above **4**. Intermediate **G** is generated by means of the slippage of the metal center from the coordinated oxygen into the free hydrogen, following a formate O-C-H path. The process has an activation energy of 22.5 kcal·mol^{-1}, which compares well with the experimental values obtained for the catalysis and for the stoichiometric release of the CO_2 molecule from **4**. The agreement between the three values strongly supports a hydride abstraction mechanism for the CO_2 formation stage and reveals that the slippage of the metal center from the oxygen to the hydrogen through the formate O-C-H path is the rate determining step of the CO_2 formation stage and therefore of the catalysis. According to this, the release of CO_2 from **G** is a barrierless process.

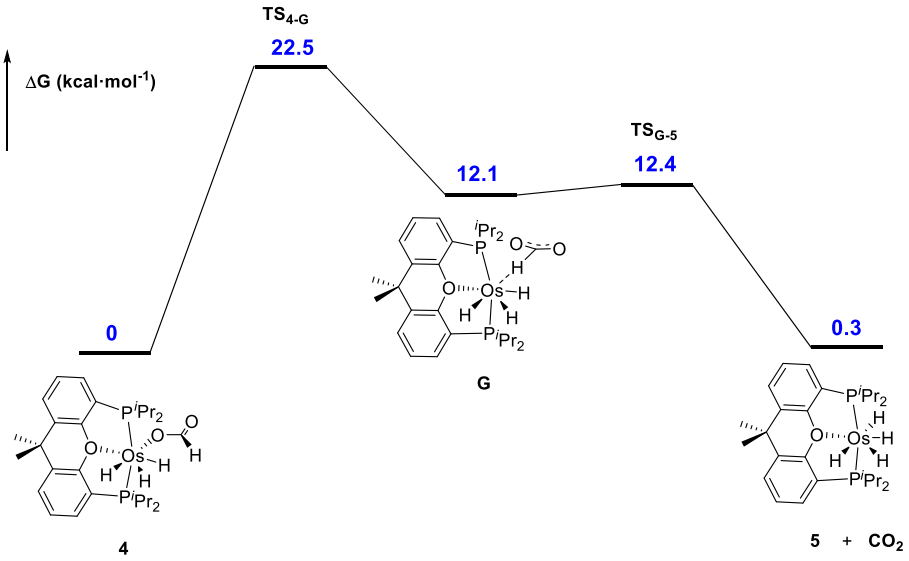

Figure 10. Energy profile (Δ*G* in kcal·mol^{-1}) for the CO_2 formation via hydride abstraction.

CONCLUDING REMARKS

Replacement of the chloride ligand of the trihydride $OsH_3Cl\{xant(P^iPr_2)_2\}$ by a hydroxo group affords the trihydride-hydroxo-osmium(IV) derivative $OsH_3(OH)\{xant(P^iPr_2)_2\}$ which efficiently promotes the FA dehydrogenation to CO_2 and H_2.

The dehydrogenation takes place through the catalytic cycle shown in Scheme 5. Under catalytic conditions the trihydride-hydroxo complex reacts with FA to form the compound $OsH_3\{\kappa^1\text{-}O\text{-}(HCO_2)\}\{xant(P^iPr_2)_2\}$, which has been isolated and fully characterized. DFT calculations suggest that the slippage of the metal center from the oxygen to the hydrogen through the formate O-C-H path affords an $OsH_3\{\kappa^1\text{-}H\text{-}(HCO_2)\}\{xant(P^iPr_2)_2\}$ intermediate, which releases CO_2 to give the previously described tetrahydride $OsH_4\{xant(P^iPr_2)_2\}$. The latter undergoes protonation with formic acid. According to previous DFT calculations, the resulting OsH_5-cation exists as an equilibrium mixture of two tautomers: the trihydride-compressed dihydride $[OsH_3(H\cdots H)\{xant(P^iPr_2)_2\}]^+$ and the hydride-compressed dihydride-dihydrogen $[OsH(H\cdots H)(\eta^2\text{-}H_2)\{xant(P^iPr_2)_2\}]^+$. The dissociation of the coordinated H_2 molecule from the latter affords the unsaturated cation $[OsH_3\{xant(P^iPr_2)_2\}]^+$, which coordinates the formate anion to regenerate the trihydride-formate and to close the cycle. The slippage of the metal center from the oxygen to the hydrogen through the formate O-C-H path is the rate-determining step of the catalysis.

Scheme 5. Catalytic Cycle for the Formic Acid Dehydrogenation Promoted by 3

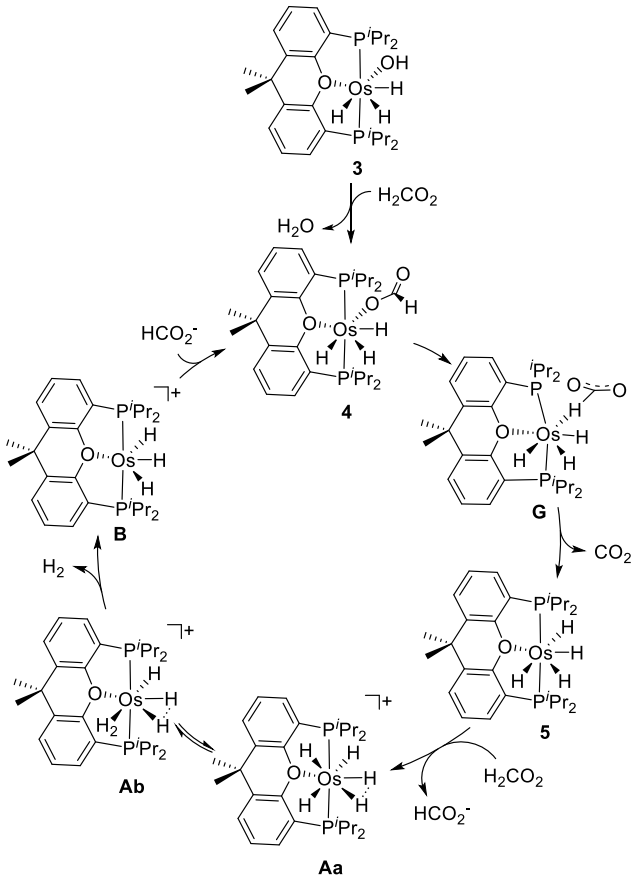

In conclusion, the first osmium catalyst for the FA dehydrogenation to CO_2 and H_2 has been discovered and the mechanism of the catalysis has been established, including the full characterization of the key intermediates and the elucidation of the rate-determining step.

EXPERIMENTAL SECTION

Preparation and characterization of complexes **2**, **3** and **4**, instrumental methods, NMR spectra, X-ray diffraction analysis information and DFT computational details are included in the Supporting Information.

General Methods for Formic Acid Dehydrogenation Studies. A solution of $OsH_3(OH)\{xant(P^iPr_2)_2\}$ (**3**) in 2.5 mL of toluene was syringed through a septum into a 25 mL flask immersed into a thermostatted bath, which was connected to a gas burette provided with a

vaseline oil reservoir. Once the system had equilibrated to atmospheric pressure, formic acid was syringed and the solution was shaken (500 rpm). The reaction was followed by measuring the volume of the formed gas (H_2 + CO_2) with the time.

NMR Spectroscopic Studies of the Decarboxylation of $OsH_3\{\kappa^1\text{-}O\text{-}(HCO_2)\}\{xant(P^iPr_2)_2\}$ (4). The decarboxylation of complex **4** was followed by $^{31}P\{^1H\}$ NMR spectroscopy, in the temperature range T = 303 to 323 K. To a screw-top NMR tube containing a solution of $OsH_3(OH)\{xant(P^iPr_2)_2\}$ (**3**) (20.8 mg, 0.032 mmol) in toluene-d_8 (0.5 mL), and a capillary tube with a solution of PPh_3 in toluene-d_8 as internal standard, was added H_2CO_2 (1.2 μL, 0.032 mmol) via syringe. After 5 min, NMR spectra were recorded at the desired temperature, to show the formation of $OsH_4\{xant(P^iPr_2)_2\}$ (**5**) as a function of the time. The parameters of the $^{31}P\{^1H\}$ NMR experiment were modified to allow the integration of the signals: pulse program (zgig), $d_1 \geq 5T_1$ (d_1 = 20 s). The k_{st} value was obtained for each temperature from a plot Ln[**4**] / Ln[**4**]$_0$ vs time (eq 5).

ASSOCIATED CONTENT

Supporting Information

The Suporting Information is available free of charge.

Preparation and characterization of complexes **2**, **3** and **4**, instrumental methods, NMR spectra, X-ray diffraction analysis information and DFT computational details (PDF)

Cartesian coordinates of the calculated structures (XYZ)

AUTHOR INFORMATION

Corresponding Author

*E-mail for M.A.E.: maester@unizar.es.

ORCID

Miguel A. Esteruelas: 0000-0002-4829-7590

Cristina García-Yebra: 0000-0002-5545-5112

Jaime Martín: 0000-0003-0909-3509

Enrique Oñate: 0000-0003-2094-719X

Notes

The authors declare no competing financial interest.

ACKNOWLEDGMENT

We thank MINECO of Spain (Projects CTQ2017-82935-P and Red de Excelencia Consolider CTQ2016-81797-REDC), Diputación General de Aragón (E06_17R), FEDER, and the European Social Fund for financial support.

REFERENCES

(1) (a) Marbán, G.; Valdés-Solís, T. Towards the Hydrogen Economy? *Int. J. Hydrogen. Energ.* **2007**, *32*, 1625-1637. (b) Nikolaidis, P.; Poullikkas, A. A Comparative Overview of Hydrogen Production Processes. *Renew. Sust. Energ. Rev.* **2017**, *67*, 597-611.

(2) (a) Schlapbach, L.; Züttel, A. Hydrogen-Storage Materials for Mobile Applications. *Nature* **2001**, *414*, 353-358. (b) Yadav, M.; Xu, Q. Liquid-Phase Chemical Hydrogen Storage Materials. *Energy Environ. Sci.* **2012**, *5*, 9698-9725. (c) Dalebrook, A. F.; Gan, W. J.; Grasemann, M.; Moret, S.; Laurenczy, G. Hydrogen Storage: Beyond Conventional Methods. *Chem. Commun.* **2013**, *49*, 8735-8751. (d) Niaz, S.; Manzoor, T.; Pandith, A. H. Hydrogen Storage: Materials,

Methods and Perspectives. *Renew. Sust. Energ. Rev.* **2015**, *50*, 457-469. (e) He, T.; Pachfule, P.; Wu, H.; Xu, Q.; Chen, P. Hydrogen Carriers. *Nat. Rev. Mater.* **2016**, *1*, 16059.

(3) Gianotti, E.; Taillades-Jacquin, M.; Rozière, J.; Jones, D. J. High-Purity Hydrogen Generation via Dehydrogenation of Organic Carriers: A Review on the Catalytic Process. *ACS Catal.* **2018**, *8*, 4660-4680.

(4) (a) Grasemann, M.; Laurenczy, G. Formic Acid as a Hydrogen Source – Recent Developments and Future Trends. *Energy Environ. Sci.* **2012**, *5*, 8171-8181. (b) Kawanami, H.; Himeda, Y.; Laurenczy, G. Formic Acid as a Hydrogen Carrier for Fuel Cells Toward a Sustainable Energy System. *Adv. Inorg. Chem.* **2017**, *70*, 395-427. (c) Eppinger, J.; Huang, K. W. Formic Acid as a Hydrogen Energy Carrier. *ACS Energy Lett.* **2017**, *2*, 188-195.

(5) (a) Filonenko, G. A.; van Putten, R.; Schulpen, E. N.; Hensen, E. J. M.; Pidko, E. A. Highly Efficient Reversible Hydrogenation of Carbon Dioxide to Formates Using a Ruthenium PNP-Pincer Catalyst. *ChemCatChem* **2014**, *6*, 1526-1530. (b) Wang, W. H.; Himeda, Y.; Muckerman, J. T.; Manbeck, G. F.; Fujita, E. CO_2 Hydrogenation to Formate and Methanol as an Alternative to Photo- and Electrochemical CO_2 Reduction. *Chem. Rev.* **2015**, *115*, 12936-12973. (c) Bernskoetter, W. H.; Hazari, N. Reversible Hydrogenation of Carbon Dioxide to Formic Acid and Methanol: Lewis Acid Enhancement of Base Metal Catalysts. *Acc. Chem. Res.* **2017**, *50*, 1049-1058. (d) Artz, J.; Müller, T. E.; Thenert, K.; Kleinekorte, J.; Meys, R.; Sternberg, A.; Bardow, A.; Leitner, W. Sustainable Conversion of Carbon Dioxide: An Integrated Review of Catalysis and Life Cycle Assessment. *Chem. Rev.* **2018**, *118*, 434-504.

(6) (a) Singh, A. K.; Singh, S.; Kumar, A. Hydrogen Energy Future with Formic Acid: a Renewable Chemical Hydrogen Storage System. *Catal. Sci. Technol.* **2016**, *6*, 12-40. (b)

Mellmann, D.; Sponholz, P.; Junge, H.; Beller, M. Formic Acid as a Hydrogen Storage Material – Development of Homogeneous Catalysts for Selective Hydrogen Release. *Chem. Soc. Rev.* **2016**, *45*, 3954-3988. (c) Sordakis, K.; Tang, C. H.; Vogt, L. K.; Junge, H.; Dyson, P. J.; Beller, M.; Laurenczy, G. Homogeneous Catalysis for Sustainable Hydrogen Storage in Formic Acid and Alcohols. *Chem. Rev.* **2018**, *118*, 372-433. (d) Wang, X.; Meng, Q. L.; Gao, L. Q.; Jin, Z.; Ge, J. J.; Liu, C. P.; Xing, W. Recent Progress in Hydrogen Production from Formic Acid Decomposition. *Int. J. Hydrogen. Energ.* **2018**, *43*, 7055-7071.

(7) See for example: (a) Boddien, A.; Gärtner, F.; Jackstell, R.; Junge, H.; Spannenberg, A.; Baumann, W.; Ludwig, R.; Beller, M. *ortho*-Metalation of Iron(0) Tribenzylphosphine Complexes: Homogeneous Catalysts for the Generation of Hydrogen from Formic Acid. *Angew. Chem., Int. Ed.* **2010**, *49*, 8993-8996. (b) Boddien, A.; Loges, B.; Gärtner, F.; Torborg, C.; Fumino, K.; Junge, H.; Ludwig, R.; Beller, M. Iron-Catalyzed Hydrogen Production from Formic Acid. *J. Am. Chem. Soc.* **2010**, *132*, 8924-8934. (c) Boddien, A.; Mellmann, D.; Gärtner, F.; Jackstell, R.; Junge, H.; Dyson, P. J.; Laurenczy, G.; Ludwig, R.; Beller, M. Efficient Dehydrogenation of Formic Acid Using an Iron Catalyst. *Science* **2011**, *333*, 1733-1736. (d) Zell, T.; Butschke, B.; Ben-David, Y.; Milstein, D. Efficient Hydrogen Liberation from Formic Acid Catalyzed by a Well-Defined Iron Pincer Complex under Mild Conditions. *Chem. - Eur. J.* **2013**, *19*, 8068-8072. (e) Zell, T.; Milstein, D. Hydrogenation and Dehydrogenation Iron Pincer Catalysts Capable of Metal Ligand Cooperation by Aromatization/Dearomatization. *Acc. Chem. Res.* **2015**, *48*, 1979-1994. (f) Mellone, I.; Gorgas, N.; Bertini, F.; Peruzzini, M.; Kirchner, K.; Gonsalvi, L. Selective Formic Acid Dehydrogenation Catalyzed by Fe-PNP Pincer Complexes Based on the 2,6-Diaminopyridine Scaffold. *Organometallics* **2016**, *35*, 3344-3349.

(8) See for example: (a) Gan, W. J.; Snelders, D. J. M.; Dyson, P. J.; Laurenczy, G. Ruthenium(II)-Catalyzed Hydrogen Generation from Formic Acid using Cationic, Ammoniomethyl-Substituted Triarylphosphine Ligands. *ChemCatChem* **2013**, *5*, 1126-1132. (b) Mellone, I.; Peruzzini, M.; Rosi, L.; Mellmann, D.; Junge, H.; Beller, M.; Gonsalvi, L. Formic Acid Dehydrogenation Catalysed by Ruthenium Complexes Bearing the Tripodal Ligands Triphos and NP_3. *Dalton Trans.* **2013**, *42*, 2495-2501. (c) Guerriero, A.; Bricout, H.; Sordakis, K.; Peruzzini, M.; Monflier, E.; Hapiot, F.; Laurenczy, G.; Gonsalvi, L. Hydrogen Production by Selective Dehydrogenation of HCOOH Catalyzed by Ru-Biaryl Sulfonated Phosphines in Aqueous Solution. *ACS Catal.* **2014**, *4*, 3002-3012. (d) Czaun, M.; Goeppert, A.; Kothandaraman, J.; May, R. B.; Haiges, R.; Prakash, G. K. S.; Olah, G. A. Formic Acid As a Hydrogen Storage Medium: Ruthenium-Catalyzed Generation of Hydrogen from Formic Acid in Emulsions. *ACS Catal.* **2014**, *4*, 311-320. (e) Pan, Y. P.; Pan, C. L.; Zhang, Y. F.; Li, H. F.; Min, S. X.; Guo, X. M.; Zheng, B.; Chen, H. L.; Anders, A.; Lai, Z. P.; Zheng, J. R.; Huang, K. W. Selective Hydrogen Generation from Formic Acid with Well-Defined Complexes of Ruthenium and Phosphorus-Nitrogen PN^3-Pincer Ligand. *Chem. - Asian J.* **2016**, *11*, 1357-1360. (f) Mellone, I.; Bertini, F.; Peruzzini, M.; Gonsalvi, L. An Active, Stable and Recyclable Ru(II) Tetraphosphine-Based Catalytic System for Hydrogen Production by Selective Formic Acid Dehydrogenation. *Catal. Sci. Technol.* **2016**, *6*, 6504-6512. (g) Anderson, N. H.; Boncella, J. M.; Tondreau, A. M. Reactivity of Silanes with (^{tBu}PONOP)Ruthenium Dichloride: Facile Synthesis of Chloro-Silyl Ruthenium Compounds and Formic Acid Decomposition. *Chem. - Eur. J.* **2017**, *23*, 13617-13622. (h) Piola, L.; Fernández-Salas, J. A.; Nahra, F.; Poater, A.; Cavallo, L.; Nolan, S. P. Ruthenium-Catalysed Decomposition of Formic Acid: Fuel Cell and Catalytic Applications. *Mol. Catal.* **2017**, *440*, 184-189. (i) Guan, C.; Zhang, D. D.; Pan, Y. P.; Iguchi, M.; Ajitha, M. J.;

Hu, J. S.; Li, H. F.; Yao, C. G.; Huang, M. H.; Ming, S. X.; Zheng, J. R.; Himeda, Y.; Kawanami, H.; Huang, K. W. Dehydrogenation of Formic Acid Catalyzed by a Ruthenium Complex with an *N,N'*-Diimine Ligand. *Inorg. Chem.* **2017**, *56*, 438-445.

(9) See for example: (a) Celaje, J. J. A.; Lu, Z. Y.; Kedzie, E. A.; Terrile, N. J.; Lo, J. N.; Williams, T. J. A Prolific Catalyst for Dehydrogenation of Neat Formic Acid. *Nat. Commun.* **2016**, *7*, 11308. (b) Papp, G.; Ölveti, G.; Horváth, H.; Kathó, A.; Joó, F. Highly Efficient Dehydrogenation of Formic Acid in Aqueous Solution Catalysed by an Easily Available Water-Soluble Iridium(III) Dihydride. *Dalton Trans.* **2016**, *45*, 14516-14519. (c) Iguchi, M.; Himeda, Y.; Manaka, Y.; Kawanami, H. Development of an Iridium-Based Catalyst for High-Pressure Evolution of Hydrogen from Formic Acid. *ChemSusChem* **2016**, *9*, 2749-2753. (d) Li, J. J.; Li, J. H.; Zhang, D. J.; Liu, C. B. DFT Study on the Mechanism of Formic Acid Decomposition by a Well-Defined Bifunctional Cyclometalated Iridium(III) Catalyst: Self-Assisted Concerted Dehydrogenation via Long-Range Intermolecular Hydrogen Migration. *ACS Catal.* **2016**, *6*, 4746-4754. (e) Czaun, M.; Kothandaraman, J.; Goeppert, A.; Yang, B.; Greenberg, S.; May, R. B.; Olah, G. A.; Prakash, G. K. S. Iridium-Catalyzed Continuous Hydrogen Generation from Formic Acid and Its Subsequent Utilization in a Fuel Cell: Toward a Carbon Neutral Chemical Energy Storage. *ACS Catal.* **2016**, *6*, 7475-7484. (f) Iguchi, M.; Zhong, H.; Himeda, Y.; Kawanami, H. Kinetic Studies on Formic Acid Dehydrogenation Catalyzed by an Iridium Complex towards Insights into the Catalytic Mechanism of High-Pressure Hydrogen Gas Production. *Chem. - Eur. J.* **2017**, *23*, 17017-17021. (g) Wang, L.; Onishi, N.; Murata, K.; Hirose, T.; Muckerman, J. T.; Fujita, E.; Himeda, Y. Efficient Hydrogen Storage and Production Using a Catalyst with an Imidazoline-Based, Proton-Responsive Ligand. *ChemSusChem* **2017**, *10*, 1071-1075. (h) Cohen, S.; Borin, V.; Schapiro, I.; Musa, S.; De-Botton, S.; Belkova, N. V.;

Gelman, D. Ir(III)-PC(sp^3)P Bifunctional Catalysts for Production of H_2 by Dehydrogenation of Formic Acid: Experimental and Theoretical Study. *ACS Catal.* **2017**, *7*, 8139-8146. (i) Iguchi, M.; Zhong, H.; Himeda, Y.; Kawanami, H. Effect of the *ortho*-Hydroxyl Groups on a Bipyridine Ligand of Iridium Complexes for the High-Pressure Gas Generation from the Catalytic Decomposition of Formic Acid. *Chem. - Eur. J.* **2017**, *23*, 17788-17793. (j) Lu, S. M.; Wang, Z. J.; Wang, J. J.; Li, J.; Li, C. Hydrogen Generation from Formic Acid Decomposition on a Highly Efficient Iridium Catalyst Bearing a Diaminoglyoxime Ligand. *Green Chem.* **2018**, *20*, 1835-1840.

(10) Neary, M. C.; Parkin, G. Dehydrogenation, Disproportionation and Transfer Hydrogenation Reactions of Formic Acid Catalyzed by Molybdenum Hydride Compounds. *Chem. Sci.* **2015**, *6*, 1859-1865.

(11) Fink, C.; Laurenczy, G. CO_2 as a Hydrogen Vector – Transition Metal Diamine Catalysts for Selective HCOOH Dehydrogenation. *Dalton Trans.* **2017**, *46*, 1670-1676.

(12) Enthaler, S.; Brück, A.; Kammer, A.; Junge, H.; Irran, E.; Gülak, S. Exploring the Reactivity of Nickel Pincer Complexes in the Decomposition of Formic Acid to CO_2/H_2 and the Hydrogenation of $NaHCO_3$ to HCOONa. *ChemCatChem* **2015**, *7*, 65-69.

(13) Correa, A.; Cascella, M.; Scotti, N.; Zaccheria, F.; Ravasio, N.; Psaro, R. Mechanistic Insights into Formic Acid Dehydrogenation Promoted by Cu-Amino Based Systems. *Inorg. Chim. Acta.* **2018**, *470*, 290-294.

(14) Myers, T. W.; Berben, L. A. Aluminium-Ligand Cooperation Promotes Selective Dehydrogenation of Formic Acid to H_2 and CO_2. *Chem. Sci.* **2014**, *5*, 2771-2777.

(15) Iglesias, M.; Oro, L. A. Mechanistic Considerations on Homogeneously Catalyzed Formic Acid Dehydrogenation. *Eur. J. Inorg. Chem.* **2018**, 2125-2138.

(16) (a) Dub, P. A.; Henson, N. J.; Martin, R. L.; Gordon, J. C. Unravelling the Mechanism of the Asymmetric Hydrogenation of Acetophenone by [RuX_2(diphosphine)(1,2-diamine)] Catalysts. *J. Am. Chem. Soc.* **2014**, *136*, 3505-3521. (b) Dub, P. A.; Gordon, J. C. The Mechanism of Enantioselective Ketone Reduction with Noyori and Noyori-Ikariya Bifunctional Catalysts. *Dalton Trans.* **2016**, *45*, 6756-6781. (c) Gusev, D. G. Dehydrogenative Coupling of Ethanol and Ester Hydrogenation Catalyzed by Pincer-Type YNP Complexes. *ACS Catal.* **2016**, *6*, 6967-6981. (d) Morris, S. A.; Gusev, D. G. Rethinking the Claisen-Tishchenko Reaction. *Angew. Chem., Int. Ed.* **2017**, *56*, 6228-6231. (e) Dub, P. A.; Gordon, J. C. Metal Ligand Bifunctional Catalysis: The "Accepted" Mechanism, the Issue of Concertedness, and the Function of the Ligand in Catalytic Cycles Involving Hydrogen Atoms. *ACS Catal.* **2017**, *7*, 6635-6655. (f) Gusev, D. G. Rethinking the Dehydrogenative Amide Synthesis. *ACS Catal.* **2017**, *7*, 6656-6662.

(17) (a) Kolb, H. C.; VanNieuwenhze, M. S.; Sharpless, K. B. Catalytic Asymmetric Dihydroxylation. *Chem. Rev.* **1994**, *94*, 2483-2547. (b) Döbler, C.; Mehltretter, G. M.; Sundermeier, U.; Beller, M. Osmium-Catalyzed Dihydroxylation of Olefins Using Dioxygen or Air as the Terminal Oxidant. *J. Am. Chem. Soc.* **2000**, *122*, 10289-10297. (c) Döbler, C.; Mehltretter, G. M.; Sundermeier, U.; Beller, M. Dihydroxylation of Olefins Using Air as the Terminal Oxidant. *J. Organomet. Chem.* **2001**, *621*, 70-76. (d) Heravi, M. M.; Zadsirjan, V.; Esfandyari, M.; Lashaki, T. B. Applications of Sharpless Asymmetric Dihydroxylation in the Total Synthesis of Natural Products. *Tetrahedron: Asymmetry* **2017**, *28*, 987-1043.

(18) See for example: (a) Sánchez-Delgado, R. A.; Rosales, M.; Esteruelas, M. A.; Oro, L. A. Homogeneous Catalysis by Osmium Complexes - a Review. *J. Mol. Catal. A: Chem.* **1995**, *96*, 231-243. (b) Esteruelas, M. A.; Herrero, J.; López, A. M.; Oliván, M. Alkyne-Coupling Reactions Catalyzed by $OsHCl(CO)(P^iPr_3)_2$ in the Presence of Diethylamine. *Organometallics* **2001**, *20*, 3202-3205. (c) Castarlenas, R.; Esteruelas, M. A.; Oñate, E. N-Heterocyclic Carbene-Osmium Complexes for Olefin Metathesis Reactions. *Organometallics* **2005**, *24*, 4343-4346. (d) Esteruelas, M. A.; García-Yebra, C.; Oliván, M.; Oñate, E.; Valencia, M. Osmium-Catalyzed Allylic Alkylation. *Organometallics* **2008**, *27*, 4892-4902. (e) Batuecas, M.; Esteruelas, M. A.; García-Yebra, C.; Oñate, E. Redox Isomerization of Allylic Alcohols Catalyzed by Osmium and Ruthenium Complexes Containing a Cyclopentadienyl Ligand with a Pendant Amine or Phosphoramidite Group: X-ray Structure of an η^3-1-Hydroxyallyl-Metal-Hydride Intermediate. *Organometallics* **2010**, *29*, 2166-2175. (f) Varela-Fernández, A.; García-Yebra, C.; Varela, J. A.; Esteruelas, M. A.; Saá, C. Osmium-Catalyzed 7-*endo* Heterocyclization of Aromatic Alkynols into Benzoxepines. *Angew. Chem., Int. Ed.* **2010**, *49*, 4278-4281. (g) Wu, L. P.; Liu, Q.; Spannenberg, A.; Jackstell, R.; Beller, M. Highly Regioselective Osmium-Catalyzed Hydroformylation. *Chem. Commun.* **2015**, *51*, 3080-3082. (h) Álvarez-Pérez, A.; González-Rodríguez, C.; García-Yebra, C.; Varela, J. A.; Oñate, E.; Esteruelas, M. A.; Saá, C. Catalytic Cyclization of *o*-Alkynyl Phenethylamines via Osmacyclopropene Intermediates: Direct Access to Dopaminergic 3-Benzazepines. *Angew. Chem., Int. Ed.* **2015**, *54*, 13357-13361. (i) Batuecas, M.; Castro-Rodrigo, R.; Esteruelas, M. A.; García-Yebra, C.; López, A. M.; Oñate, E. Aromatic Osmacyclopropenefuran Bicycles and Their Relevance for the Metal-Mediated Hydration of Functionalized Allenes. *Angew. Chem., Int. Ed.* **2016**, *55*, 13749-13753. (j) González-Fernández, R.; Crochet, P.; Cadierno, V.; Menéndez, M. I.; López, R. Phosphinous Acid-Assisted Hydration

of Nitriles: Understanding the Controversial Reactivity of Osmium and Ruthenium Catalysts. *Chem. - Eur. J.* **2017**, *23*, 15210-15221.

(19) See for example: (a) Esteruelas, M. A.; Oro, L. A.; Valero, C. Hydrogenation of Benzylideneacetone Catalyzed by $OsHCl(CO)(PR_3)_2$ (PR_3 = P^iPr_3, PMe-$^tBu_2$) - New Roles of Dihydrogen Complexes in Homogeneous Catalytic-Hydrogenation. *Organometallics* **1992**, *11*, 3362-3369. (b) Barrio, P.; Esteruelas, M. A.; Oñate, E. Reactions of a Hexahydride-Osmium Complex with Aldehydes: Double C-H_α Activation-Decarbonylation and Single C-H_α Activation-Hydroxylation Tandem Processes and Catalytic Tishchenko Reactions. *Organometallics* **2004**, *23*, 1340-1348. (c) Esteruelas, M. A.; Honczek, N.; Oliván, M.; Oñate, E.; Valencia, M. Direct Access to POP-Type Osmium(II) and Osmium(IV) Complexes: Osmium a Promising Alternative to Ruthenium for the Synthesis of Imines from Alcohols and Amines. *Organometallics* **2011**, *30*, 2468-2471. (d) Baratta, W.; Bossi, G.; Putignano, E.; Rigo, P. Pincer and Diamine Ru and Os Diphosphane Complexes as Efficient Catalysts for the Dehydrogenation of Alcohols to Ketones. *Chem. - Eur. J.* **2011**, *17*, 3474-3481. (e) Bertoli, M.; Choualeb, A.; Lough, A. J.; Moore, B.; Spasyuk, D.; Gusev, D. G. Osmium and Ruthenium Catalysts for Dehydrogenation of Alcohols. *Organometallics* **2011**, *30*, 3479-3482. (f) Spasyuk, D.; Gusev, D. G. Acceptorless Dehydrogenative Coupling of Ethanol and Hydrogenation of Esters and Imines. *Organometallics* **2012**, *31*, 5239-5242. (g) Spasyuk, D.; Vicent, C.; Gusev, D. G. Chemoselective Hydrogenation of Carbonyl Compounds and Acceptorless Dehydrogenative Coupling of Alcohols. *J. Am. Chem. Soc.* **2015**, *137*, 3743-3746. (h) Chelucci, G.; Baldino, S.; Baratta, W. Ruthenium and Osmium Complexes Containing 2-(aminomethyl)pyridine (Ampy)-Based Ligands in Catalysis. *Coord. Chem. Rev.* **2015**, *300*, 29-85. (i) Chelucci, G.; Baldino, S.; Baratta, W. Recent Advances in Osmium-Catalyzed Hydrogenation and Dehydrogenation

Reactions. *Acc. Chem. Res.* **2015**, *48*, 363-379. (j) Bolaño, T.; Esteruelas, M. A.; Gay, M. P.; Oñate, E.; Pastor, I. M.; Yus, M. An Acyl-NHC Osmium Cooperative System: Coordination of Small Molecules and Heterolytic B-H and O-H Bond Activation. *Organometallics* **2015**, *34*, 3902-3908. (k) Chelucci, G. Ruthenium and Osmium Complexes in C-C Bond-Forming Reactions by Borrowing Hydrogen Catalysis. *Coord. Chem. Rev.* **2017**, *331*, 1-36.

(20) Esteruelas, M. A.; López, A. M.; Oliván, M. Polyhydrides of Platinum Group Metals: Nonclassical Interactions and *σ*-Bond Activation Reactions. *Chem. Rev.* **2016**, *116*, 8770-8847.

(21) (a) Esteruelas, M. A.; Fernández, I.; López, A. M.; Mora, M.; Oñate, E. Osmium-Promoted Dehydrogenation of Amine-Boranes and B-H Bond Activation of the Resulting Amino-Boranes. *Organometallics* **2014**, *33*, 1104-1107. (b) Esteruelas, M. A.; López, A. M.; Mora, M.; Oñate, E. Ammonia-Borane Dehydrogenation Promoted by an Osmium Dihydride Complex: Kinetics and Mechanism. *ACS Catal.* **2015**, *5*, 187-191.

(22) (a) Esteruelas, M. A.; Lezáun, V.; Martínez, A.; Oliván, M.; Oñate, E. Osmium Hydride Acetylacetonate Complexes and Their Application in Acceptorless Dehydrogenative Coupling of Alcohols and Amines and for the Dehydrogenation of Cyclic Amines. *Organometallics* **2017**, *36*, 2996-3004. (b) Buil, M. L.; Esteruelas, M. A.; Gay, M. P.; Gómez-Gallego, M.; Nicasio, A. I.; Oñate, E.; Santiago, A.; Sierra, M. A. Osmium Catalysts for Acceptorless and Base-Free Dehydrogenation of Alcohols and Amines: Unusual Coordination Modes of a BPI Anion. *Organometallics* **2018**, *37*, 603-617.

(23) Castarlenas, R.; Esteruelas, M. A.; Oñate, E. Preparation, X-ray Structure, and Reactivity of an Osmium-Hydroxo Complex Stabilized by an N-Heterocyclic Carbene Ligand: A Base-Free

Catalytic Precursor for Hydrogen Transfer from 2-Propanol to Aldehydes. *Organometallics* **2008**, *27*, 3240-3247.

(24) Buil, M. L.; Esteruelas, M. A.; Herrero, J.; Izquierdo, S.; Pastor, I. M.; Yus, M. Osmium Catalyst for the Borrowing Hydrogen Methodology: *α*-Alkylation of Arylacetonitriles and Methyl Ketones. *ACS Catal.* **2013**, *3*, 2072-2075.

(25) Buil, M. L.; Cadierno, V.; Esteruelas, M. A.; Gimeno, J.; Herrero, J.; Izquierdo, S.; Oñate, E. Selective Hydration of Nitriles to Amides Promoted by an Os-NHC Catalyst: Formation and X-ray Characterization of κ^2-Amidate Intermediates. *Organometallics* **2012**, *31*, 6861-6867.

(26) Nelson, D. J.; Nolan, S. P. Hydroxide Complexes of the Late Transition Metals: Organometallic Chemistry and Catalysis. *Coord. Chem. Rev.* **2017**, *353*, 278-294.

(27) Ozerov, O. V. Oxidative Addition of Water to Transition Metal Complexes. *Chem. Soc. Rev.* **2009**, *38*, 83-88.

(28) (a) Gotzig, J.; Werner, R.; Werner, H. Basic Metals: 53. Ruthenium- and Osmium-Complexes with Dimethylphosphinomethanide-Anion as Ligands. *J. Organomet. Chem.* **1985**, *290*, 99-114. (b) Edwards, A. J.; Elipe, S.; Esteruelas, M. A.; Lahoz, F. J.; Oro, L. A.; Valero, C. Synthesis and Reactivity of the Unusual Five-Coordinate Hydrido-Hydroxo Complex $OsH(OH)(CO)(P^iPr_3)_2$. *Organometallics* **1997**, *16*, 3828-3836. (c) Renkema, K. B.; Huffman, J. C.; Caulton, K. G. Characterization and Structure of $OsH(OH)(CO)(PBu_2Me)^tBu_2$. *Polyhedron* **1999**, *18*, 2575-2578. (d) Prokopchuk, D. E.; Collado, A.; Lough, A. J.; Morris, R. H. Structural Properties of *trans* Hydrido-Hydroxo $M(H)(OH)(NH_2CMe_2CMe_2NH_2)(PPh_3)_2$ (M = Ru, Os) Complexes and their Proton Exchange Behaviour with Water in Solution. *Dalton Trans.* **2013**,

42, 10214-10220. (e) Buil, M. L.; Cardo, J. J. F.; Esteruelas, M. A.; Fernández, I.; Oñate, E. Hydroboration and Hydrogenation of an Osmium-Carbon Triple Bond: Osmium Chemistry of a Bis-*σ*-Borane. *Organometallics* **2015**, *34*, 547-550.

(29) *Pincer Compounds: Chemistry and Applications*; Ed.: Morales-Morales, D. Elsevier, 2018.

(30) (a) Pontiggia, A. J.; Chaplin, A. B.; Weller, A. S. Cationic Iridium Complexes of the Xantphos Ligand. Flexible Coordination Modes and the Isolation of the Hydride Insertion Product with an Alkene. *J. Organomet. Chem.* **2011**, *696*, 2870-2876. (b) Dallanegra, R.; Chaplin, A. B.; Weller, A. S. Rhodium Cyclopentyl Phosphine Complexes of Wide-Bite-Angle Ligands DPEphos and Xantphos. *Organometallics* **2012**, *31*, 2720-2728. (c) Alós, J.; Bolaño, T.; Esteruelas, M. A.; Oliván, M.; Oñate, E.; Valencia, M. POP-Pincer Osmium-Polyhydrides: Head-to-Head (*Z*)-Dimerization of Terminal Alkynes. *Inorg. Chem.* **2013**, *52*, 6199-6213. (d) Johnson, H. C.; Torry-Harris, R.; Ortega, L.; Theron, R.; McIndoe, J. S.; Weller, A. S. Exploring the Mechanism of the Hydroboration of Alkenes by Amine-Boranes Catalysed by $[Rh(xantphos)]^+$. *Catal. Sci. Technol.* **2014**, *4*, 3486-3494. (e) Johnson, H. C.; Leitao, E. M.; Whitten, G. R.; Manners, I.; Lloyd-Jones, G. C.; Weller, A. S. Mechanistic Studies of the Dehydrocoupling and Dehydropolymerization of Amine-Boranes Using a $[Rh(Xantphos)]^+$ Catalyst. *J. Am. Chem. Soc.* **2014**, *136*, 9078-9093. (f) Johnson, H. C.; Weller, A. S. P-C-Activated Bimetallic Rhodium Xantphos Complexes: Formation and Catalytic Dehydrocoupling of Amine-Boranes. *Angew. Chem., Int. Ed.* **2015**, *54*, 10173-10177. (g) Ren, P.; Pike, S. D.; Pernik, I.; Weller, A. S.; Willis, M. C. Rh-POP Pincer Xantphos Complexes for C-S and C-H Activation. Implications for Carbothiolation Catalysis. *Organometallics* **2015**, *34*, 711-723. (h) Esteruelas, M. A.; Nolis, P.; Oliván, M.; Oñate, E.; Vallribera, A.; Vélez, A. Ammonia Borane Dehydrogenation Promoted by a Pincer-Square-Planar Rhodium(I) Monohydride: A Stepwise

Hydrogen Transfer from the Substrate to the Catalyst. *Inorg. Chem.* **2016**, *55*, 7176-7181. (i) Esteruelas, M. A.; García-Yebra, C.; Martín, J.; Oñate, E. *mer*, *fac*, and Bidentate Coordination of an Alkyl-POP Ligand in the Chemistry of Nonclassical Osmium Hydrides. *Inorg. Chem.* **2017**, *56*, 676-683. (j) Adams, G. M.; Weller, A. S. POP-type ligands: Variable Coordination and Hemilabile Behaviour. *Coord. Chem. Rev.* **2018**, *355*, 150-172. (k) Adams, G. M.; Colebatch, A. L.; Skornia, J. T.; McKay, A. I.; Johnson, H. C.; Lloyd-Jones, G. C.; Macgregor, S. A.; Beattie, N. A.; Weller, A. S. Dehydropolymerization of $H_3B{\cdot}NMeH_2$ To Form Polyaminoboranes Using [Rh(Xantphos-alkyl)] Catalysts. *J. Am. Chem. Soc.* **2018**, *140*, 1481-1495.

(31) (a) Asensio, G.; Cuenca, A. B.; Esteruelas, M. A.; Medio-Simón, M.; Oliván, M.; Valencia, M. Osmium(III) Complexes with POP Pincer Ligands: Preparation from Commercially Available $OsCl_3{\cdot}3H_2O$ and Their X-ray Structures. *Inorg. Chem.* **2010**, *49*, 8665-8667. (b) Alós, J.; Bolaño, T.; Esteruelas, M. A.; Oliván, M.; Oñate, E.; Valencia, M. POP-Pincer Ruthenium Complexes: d^6 Counterparts of Osmium d^4 Species. *Inorg. Chem.* **2014**, *53*, 1195-1209. (c) Alós, J.; Esteruelas, M. A.; Oliván, M.; Oñate, E.; Puylaert, P. C-H Bond Activation Reactions in Ketones and Aldehydes Promoted by POP-Pincer Osmium and Ruthenium Complexes. *Organometallics* **2015**, *34*, 4908-4921. (d) Esteruelas, M. A.; Fenández, I.; García-Yebra, C.; Martín, J.; Oñate, E. Elongated σ-Borane versus σ-Borane in Pincer-POP-Osmium Complexes. *Organometallics* **2017**, *36*, 2298-2307. (e) Esteruelas, M. A.; Oliván, M. Osmium Complexes with POP Pincer Ligands. In *Pincer Compounds*; 1st ed.; Morales-Morales, D.; Elsevier: 2018.

(32) (a) Esteruelas, M. A.; Oliván, M.; Vélez, A. Xantphos-Type Complexes of Group 9: Rhodium versus Iridium. *Inorg. Chem.* **2013**, *52*, 5339-5349. (b) Esteruelas, M. A.; Oliván, M.; Vélez, A. POP-Pincer Silyl Complexes of Group 9: Rhodium versus Iridium. *Inorg. Chem.* **2013**, *52*, 12108-12119. (c) Esteruelas, M. A.; Oliván, M.; Vélez, A. POP-Rhodium-Promoted C-H and

B-H Bond Activation and C-B Bond Formation. *Organometallics* **2015**, *34*, 1911-1924. (d) Esteruelas, M. A.; Oliván, M.; Vélez, A. Conclusive Evidence on the Mechanism of the Rhodium-Mediated Decyanative Borylation. *J. Am. Chem. Soc.* **2015**, *137*, 12321-12329. (e) Curto, S. G.; Esteruelas, M. A.; Oliván, M.; Oñate, E.; Vélez, A. Selective C-Cl Bond Oxidative Addition of Chloroarenes to a POP-Rhodium Complex. *Organometallics* **2017**, *36*, 114-128.

(33) Wu, A.; Dehestani, A.; Saganic, E.; Crevier, T. J.; Kaminsky, W.; Cohen, D. E.; Mayer, J. M. Reactions of Tp-Os Nitrido Complexes with the Nucleophiles Hydroxide and Thiosulfate. *Inorg. Chim. Acta.* **2006**, *359*, 2842-2849.

(34) Kiefer, A. M.; Giles, J. A.; Shapley, P. A. Synthesis, Structure, and Reactivity of Organometallic Osmium(VI) Hydroxo Compounds. *Organometallics* **2007**, *26*, 1881-1887.

(35) (a) Gould, R. O.; Jones, C. L.; Stephenson, T. A.; Tocher, D. A. Structural Characterization of Hydroxo-Bridged Arene-Ruthenium and Arene-Osmium Complexes - Further Reactions of Hydroxo-Bridged Complexes. *J. Organomet. Chem.* **1984**, *264*, 365-378. (b) Cabeza, J. A.; Mann, B. E.; Maitlis, P. M.; Brevard, C. The Synthesis of Di-Nuclear and Tetra-Nuclear *p*-Cymene-Osmium Hydride Complexes - Characterization by ^{1}H (^{187}Os) Reverse INEPT Two-Dimensional Nuclear Magnetic-Resonance Spectroscopy. *J. Chem. Soc., Dalton Trans.* **1988**, 629-634. (c) Esteruelas, M. A.; García-Yebra, C.; Oliván, M.; Oñate, E. Reaction of a Cationic Osmium(IV) Dihydride with Ethylene: Formation and Structure of the Novel Tetraethylene Dimer Complex $[\{(P^{i}Pr_3)(\eta^2\text{-}C_2H_4)_2Os\}_2(\mu\text{-}OH)_2(\mu\text{-}O_2CCH_3)]BF_4$. *Organometallics* **2000**, *19*, 3260-3262. (d) Peacock, A. F. A.; Habtemariam, A.; Fernández, R.; Walland, V.; Fabbiani, F. P. A.; Parsons, S.; Aird, R. E.; Jodrell, D. I.; Sadler, P. J. Tuning the Reactivity of Osmium(II) and

Ruthenium(II) Arene Complexes Under Physiological Conditions. *J. Am. Chem. Soc.* **2006**, *128*, 1739-1748.

(36) CO is not formed. In this context, it should be mentioned that both **3** and **5** react with this gas to afford $Os(CO)_3\{\kappa^2\text{-P,P-[xant(P}^i\text{Pr}_2)_2]\}$ which is not active.

(37) See for example: (a) Scholten, J. D.; Prechtl, M. H. G.; Dupont, J. Decomposition of Formic Acid Catalyzed by a Phosphine-Free Ruthenium Complex in a Task-Specific Ionic Liquid. *ChemCatChem* **2010**, *2*, 1265-1270. (b) Wang, W. H.; Xu, S.; Manaka, Y.; Suna, Y.; Kambayashi, H.; Muckerman, J. T.; Fujita, E.; Himeda, Y. Formic Acid Dehydrogenation with Bioinspired Iridium Complexes: A Kinetic Isotope Effect Study and Mechanistic Insight. *ChemSusChem* **2014**, *7*, 1976-1983. (c) Wang, W. H.; Ertem, M. Z.; Xu, S. A.; Onishi, N.; Manaka, Y.; Suna, Y.; Kambayash, H.; Muckerman, J. T.; Fujita, E.; Himeda, Y. Highly Robust Hydrogen Generation by Bioinspired Ir Complexes for Dehydrogenation of Formic Acid in Water: Experimental and Theoretical Mechanistic Investigations at Different pH. *ACS Catal.* **2015**, *5*, 5496-5504. (d) Ertem, M. Z.; Himeda, Y.; Fujita, E.; Muckerman, J. T. Interconversion of Formic Acid and Carbon Dioxide by Proton-Responsive, Half-Sandwich Cp*Ir-III Complexes: A Computational Mechanistic Investigation. *ACS Catal.* **2016**, *6*, 600-609.

SYNOPSIS

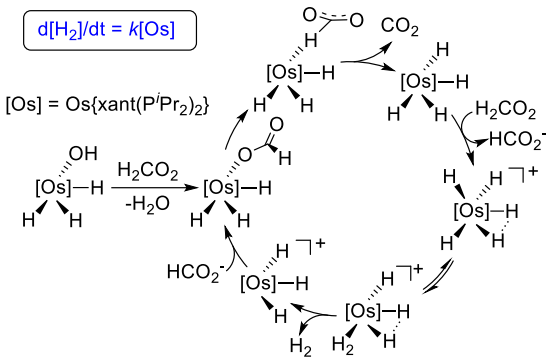

Supporting Information For

Dehydrogenation of Formic Acid Promoted by a Trihydride-Hydroxo-Osmium (IV) Complex: Kinetics and Mechanism

Miguel A. Esteruelas, Cristina García-Yebra, Jaime Martín, and Enrique Oñate*

Departamento de Química Inorgánica, Instituto de Síntesis Química y Catálisis Homogénea (ISQCH), Centro de Innovación en Química Avanzada (ORFEO – CINQA), Universidad de Zaragoza – CSIC, 50009 Zaragoza, Spain

*Corresponding author's e-mail address: maester@unizar.es

Contents:

Instrumental Methods. All reactions were performed under argon using Schlenk tube or glovebox techniques. Solvents were dried using standard procedures and distilled under argon atmosphere or obtained dry from an MBraun solvent purification apparatus. Pentane and dichloromethane were subsequently stored over P_2O_5 in the glovebox. Toluene, THF and benzene were stored over sodium in the glovebox. Commercial chemicals were used as received, except where otherwise noted. NMR spectra were recorded on either a Bruker Avance 300 MHz or 400 MHz instrument. Signals were assigned using also bidimensional NMR experiments (^{1}H-^{1}H COSY, ^{1}H-^{13}C{^{1}H} HMBC and ^{1}H-^{13}C{^{1}H} HSQC). Chemical shifts (expressed in parts per million) are referenced to residual solvent peaks (^{1}H, ^{13}C{^{1}H}) or external H_3PO_4 (^{31}P{^{1}H}). Coupling constants, J and N ($N = J_{PH} + J_{P'H}$ for ^{1}H; $N = J_{PC} + J_{P'C}$ for ^{13}C) are given in Hz. Elemental analyses were carried out using a Perkin-Elmer 2400 CHNS/O analyzer, and IR spectra were measured using a PerkinElmer Spectrum 100 FT-IR spectrometer, equipped with an ATR accessory, as pure solids.

Preparation and characterization of complexes 2, 3 and 4. The complexes $OsH_3Cl\{xant(P^iPr_2)_2\}$ (**1**), and $OsH_4\{xant(P^iPr_2)_2\}$ (**5**), were prepared as published.[1]

Synthesis of $OsH_3(OTf)\{xant(P^iPr_2)_2\}$ (2). A solution of $OsH_3Cl\{xant(P^iPr_2)_2\}$ (**1**) (500 mg; 0.745mmol) in toluene (10 mL) was treated with trimethylsilyl trifluoromethanesulfonate (270 µl; 1.492 mmol). After 10 min, the obtained yellow solution was taken to dryness. Addition of pentane (3 mL) to the residue afforded a pale yellow solid, which was washed with pentane (3 mL) and dried under vacuum. Yield: 527 mg (90 %). Anal. Calcd. for $C_{28}H_{43}F_3O_4OsP_2S$: C, 42.85; H, 5.52; S, 4.08. Found: C, 42.65; H, 5.53; S, 3.95. ^{1}H NMR (400.16 MHz, C_6D_6, 298 K): δ 7.18 (m, 2H, C*H*-arom POP), 7.13 (dd, $^3J_{HH}$ = 7.7, $^4J_{HH}$ = 1.5, 2H, C*H*-arom POP), 6.93 (dd, $^3J_{HH}$ = 7.6, $^3J_{HH}$ = 7.5, 2H, C*H*-arom POP), 2.88 (m, 2H, PC*H*(CH_3)$_2$), 2.00 (m, 2H, PC*H*(CH_3)$_2$), 1.61 (dvt, $^3J_{HH}$ = 7.7, N = 17.9, 6H, PCH(CH_3)$_2$), 1.54 (s, 3H, CH_3 POP), 1.40 (s, 3H, CH_3 POP), 1.21 (dvt, $^3J_{HH}$ = 6.9, N = 12.9, 6H, PCH(CH_3)$_2$), 1.02 (dvt, $^3J_{HH}$ = 6.9, N = 17.1, 6H, PCH(CH_3)$_2$), 0.60 (dvt, $^3J_{HH}$ = 7.0, N = 15.3, 6H, PCH(CH_3)$_2$), -13.82 (br, 3H, Os*H*). ^{1}H NMR (400.16 MHz, C_7D_8, 223K): δ -12.12 (br, 2H, Os*H*), -17.02 (br, 1H, Os*H*). ^{13}C{^{1}H}-APT NMR (100.62 MHz, C_7D_8, 233 K): δ 160.4 (vt, N = 14.2, *C*-arom POP), 133.1 (vt, N = 6.0, *C*-arom POP), 130.2 (s, *C*H-arom POP), 128.0 (s, *C*-arom POP, overlapped), 127.9 (s, *C*H-arom POP), 126.2 (s, *C*H-arom POP), 119.9 (q, $^1J_{C\text{-}F}$ = 319.0, CF_3), 35.5 (s, C(*C*H_3)$_2$ POP), 35.0 (s, *C*(CH_3)$_2$ POP), 28.4 (vt, N = 22.7, P*C*H(CH_3)$_2$), 24.5 (s, C(*C*H_3)$_2$ POP), 23.5 (vt, N = 9.8, PCH(*C*H_3)$_2$), 22.3 (vt, N = 32.1, P*C*H(CH_3)$_2$), 20.3 (s, PCH(*C*H_3)$_2$), 20.1 (s, PCH(*C*H_3)$_2$), 17.1 (s, PCH(*C*H_3)$_2$). ^{31}P{^{1}H} NMR (161.99 MHz, C_6D_6, 298 K): δ 54.6 (s, POP). ^{19}F NMR (376.49 MHz, C_6D_6, 298 K): δ -77.7 (s, CF_3SO_3). $T_{1(min)}$ (ms, Os*H*, 400.16 MHz, C_7D_8, 223 K): 89 ± 4 (-12.12 ppm), 69 ± 3 (-17.02 ppm).

Synthesis of $OsH_3(OH)\{xant(P^iPr_2)_2\}$ (3). A titrated solution of KOH in deoxygenated water (20 ml; 0.583 M) was added dropwise to a second solution of $OsH_3(OTf)\{xant(P^iPr_2)_2\}$ (**2**) (0.48 g; 0.61 mmol) in acetone (5 mL). The initially yellow solution turned into red and then a yellow solid precipitates. After stirring for 1 hour, the solid was isolated by filtration, washed with deoxygenated water (the liquors reaching pH = 7) and dried under reduced pressure. Yield: 366 mg (92%). Anal. Calcd. for $C_{27}H_{44}O_2OsP_2$: C, 49.68; H, 6.79. Found: C, 49.39; H, 6.69. IR (ATR, cm^{-1}): ν(OH) 3672 (w). ^{1}H NMR (400.16 MHz, C_7D_8, 298 K): δ 7.14-7.07 (6H, C*H*-arom POP), 2.87 (br, 1H, O*H*), 2.43 (m, 2H, PC*H*$(CH_3)_2$), 1.89 (m, 2H, PC*H*$(CH_3)_2$), 1.44 (dvt, $^3J_{HH}$ = 7.1, *N* = 14.9, 6H, PCH(C*H*$_3)_2$), 1.37 (dvt, $^3J_{HH}$ = 7.4, *N* = 14.5, 6H, PCH(C*H*$_3)_2$), 1.37 (s, 3H, C*H*$_3$ POP), 1.29 (s, 3H, C*H*$_3$ POP), 1.16 (dvt, $^3J_{HH}$ = 7.0, *N* = 16.5, 6H, PCH(C*H*$_3)_2$), 0.79 (dvt, $^3J_{HH}$ = 7.0, *N* = 14.5, 6H, PCH(C*H*$_3)_2$), -12.26 (br, 3H, Os*H*). ^{1}H NMR (400.13 MHz, C_7D_8, 183 K): δ 4.20 (br, 1H, O*H*), υ_A = -10.75 and υ_B = -12.96 (AB system, $^2J_{AB}$ = 145.0, 2H, Os*H*), -12.30 (t, $^2J_{HP}$ = 10.0, 1H, Os*H*). ^{13}C{^{1}H}-APT NMR (100.62 MHz, THF-d_8, 253 K): δ 158.3 (vt, *N* = 13.6, *C*-arom POP), 132.5 (vt, *N* = 5.6, *C*-arom POP), 131.2 (s, *C*H-arom POP), 130.4 (vt, *N* = 27.7, *C*-arom POP), 128.4 (s, *C*H-arom POP), 125.6 (s, *C*H-arom POP), 35.4 (s, C(*C*H$_3)_2$ POP), 35.2 (s, *C*(CH$_3)_2$ POP), 28.0 (s, C(*C*H$_3)_2$ POP), 27.9 (vt, *N* = 21.8, P*C*H(CH$_3)_2$), 26.8 (vt, *N* = 31.3, P*C*H(CH$_3)_2$), 22.5 (s, PCH(*C*H$_3)_2$), 20.8 (vt, *N* = 10.9, PCH(*C*H$_3)_2$), 20.7 (s, PCH(*C*H$_3)_2$), 20.2 (vt, *N* = 6.3, PCH(*C*H$_3)_2$). ^{31}P{^{1}H} NMR (161.99 MHz, C_7D_8, 298 K): δ 49.9 (s, POP). $T_{1(min)}$ (ms, Os*H*, 400.13 MHz, C_7D_8, 243 K): 107 ± 5 (-12.12 ppm), 107 ± 5 (-12.50 ppm).

Preparation of $OsH_3\{\kappa^1\text{-}O\text{-}(HCO_2)\}\{xant(P^iPr_2)_2\}$ (4). A solution of $OsH_3(OH)\{xant(P^iPr_2)_2\}$ (**3**) (41.5 mg; 0.064 mmol) in toluene-d_8 (0.6 mL) was placed in a screw-top NMR tube, and H_2CO_2 (2.4 µL; 0.064 mmol) was added. After 5 minutes at room temperature, the NMR tube was cooled at -40ºC and an NMR spectrum of the reaction solution showed quantitative formation of **4**. A single colorless crystal suitable for X-ray diffraction analysis was obtained from the toluene-d_8 solution at -20ºC. ^{1}H NMR (400.13 MHz, C_7D_8, 253 K): δ 8.91 (s, 1H, OCO*H*), 7.11-6.98 (6H, C*H*-arom POP), 2.27 (m, 2H, PC*H*$(CH_3)_2$), 1.82 (m, 2H, PC*H*$(CH_3)_2$), 1.36 (s, 3H, C*H*$_3$ POP), 1.27 (dvt, $^3J_{HH}$ = 7.0, *N* = 14.3, 6H, PCH(C*H*$_3)_2$), 1.20 (s, 3H, C*H*$_3$ POP), 1.15 (dvt, $^3J_{HH}$ = 7.3, *N* = 14.9, 6H, PCH(C*H*$_3)_2$), 1.11 (dvt, $^3J_{HH}$ = 8.0, *N* = 16.7, 6H, PCH(C*H*$_3)_2$), 0.70 (dvt, $^3J_{HH}$ = 7.0, *N* = 14.0, 6H, PCH(C*H*$_3)_2$), -12.55 (br, 3H, Os*H*). ^{1}H NMR (400.13 MHz, C_7D_8, 203 K): δ -11.93 (br, 2H, Os*H*), -13.30 (br, 1H, Os*H*). ^{13}C{^{1}H}-APT NMR (100.62 MHz, C_7D_8, 253 K): δ 167.8 (s, O*C*OH), 159.9 (vt, *N* = 13.7, *C*-arom POP), 132.5 (vt, *N* = 5.2, *C*-arom POP), 130.3 (s, *C*H-arom POP), 129.1 (*C*-arom POP, overlapped signal), 127.3 (s, *C*H-arom POP), 35.3 (s, C(*C*H$_3)_2$ POP), 34.7 (s, *C*(CH$_3)_2$ POP), 28.8 (vt, *N* = 22.2, P*C*H(CH$_3)_2$), 26.1 (vt, *N* = 32.5, P*C*H(CH$_3)_2$), 25.5 (s, C(*C*H$_3)_2$ POP), 21.3 (s, PCH(*C*H$_3)_2$), 20.8 (vt, *N* = 10.3, PCH(*C*H$_3)_2$), 20.5 (s, PCH(*C*H$_3)_2$), 19.7 (vt, *N* = 4.9, PCH(*C*H$_3)_2$). ^{31}P{^{1}H} NMR (161.98 MHz, C_7D_8, 253 K): δ 51.2

(s, POP). $T_{1(min)}$ (ms, Os*H*, 400.13 MHz, C_7D_8, 203 K): 222 ± 11 (-11.93 ppm), 216 ± 11 (-13.30 ppm).

.

Experimental Details for the Dehydrogenation of Formic Acid

Table S1. Experimental details for the dehydrogenation of formic acid promoted by **3** in toluene solutions (2.5 mL).

T	P	**3**	10^2**3**	10^2[**3**]	H_2CO_2	H_2CO_2	$[H_2CO_2]_0$	dV_T/dt	dV_{H_2}/dt	$10^2 d[H_2]/dt$	k
K	atm	mg	mmol	M	µl	mmol	M	mL/min	mL/min	M/min	min^{-1}
298	0.9948	10.0	1.53	0.61	50.0	1.33	0.53	0.07	0.035	0.057	0.094
298	0.9973	20.0	3.06	1.23	50.0	1.33	0.53	0.15	0.075	0.123	0.100
298	0.9948	30.3	4.64	1.86	50.0	1.33	0.53	0.19	0.095	0.155	0.083
298	0.9948	40.4	6.19	2.48	50.0	1.33	0.53	0.28	0.140	0.228	0.092
298	0.9958	50.0	7.66	3.06	50.0	1.33	0.53	0.34	0.170	0.278	0.091
298	0.9910	20.0	3.06	1.23	40.0	1.06	0.42	0.15	0.073	0.118	0.096
298	0.9910	20.0	3.06	1.23	60.0	1.59	0.64	0.15	0.077	0.124	0.101
298	0.9973	19.9	3.05	1.23	70.0	1.86	0.74	0.16	0.078	0.128	0.104
298	0.9968	19.7	3.02	1.23	90.0	2.39	0.95	0.16	0.078	0.128	0.104
303	0.9914	20.3	3.11	1.24	50.0	1.33	0.53	0.27	0.135	0.216	0.174
308	0.9914	20.2	3.09	1.24	50.0	1.33	0.53	0.47	0.236	0.370	0.298
313	0.9914	20.0	3.06	1.23	50.0	1.33	0.53	0.65	0.326	0.503	0.409
318	0.9914	20.0	3.06	1.23	50.0	1.33	0.53	1.20	0.602	0.914	0.743

The calculation of the partial molar volumes of H_2 and CO_2 were carried out using Van der Waals equations:

$$V_{m(H_2)} = \frac{RT}{P} + b_{H_2} - \frac{a_{H_2}}{RT} \qquad (1)$$

$$V_{m(CO_2)} = \frac{RT}{P} + b_{CO_2} - \frac{a_{CO_2}}{RT} \qquad (2)$$

R: 0.08206 atm·L·mol^{-1}·K^{-1}

a_{H_2}= 0.24436 atm·L^{2}mol^{-2}

b_{H_2}= 0.02661 L·mol^{-1}

a_{CO_2}= 3.61017 atm·L^{2}mol^{-2}

b_{CO_2}= 0.04267 L·mol^{-1}

The activation parameters were calculated from the Eying analysis:

$$\ln\frac{k}{T} = \frac{-\Delta H^{\ddagger}}{RT} + \ln\frac{k_B}{h} + \frac{\Delta S^{\ddagger}}{R} \qquad (3)$$

k_B= Boltzmann constant

h= Planck constant

NMR Spectra of Complexes 2, 3 and 4

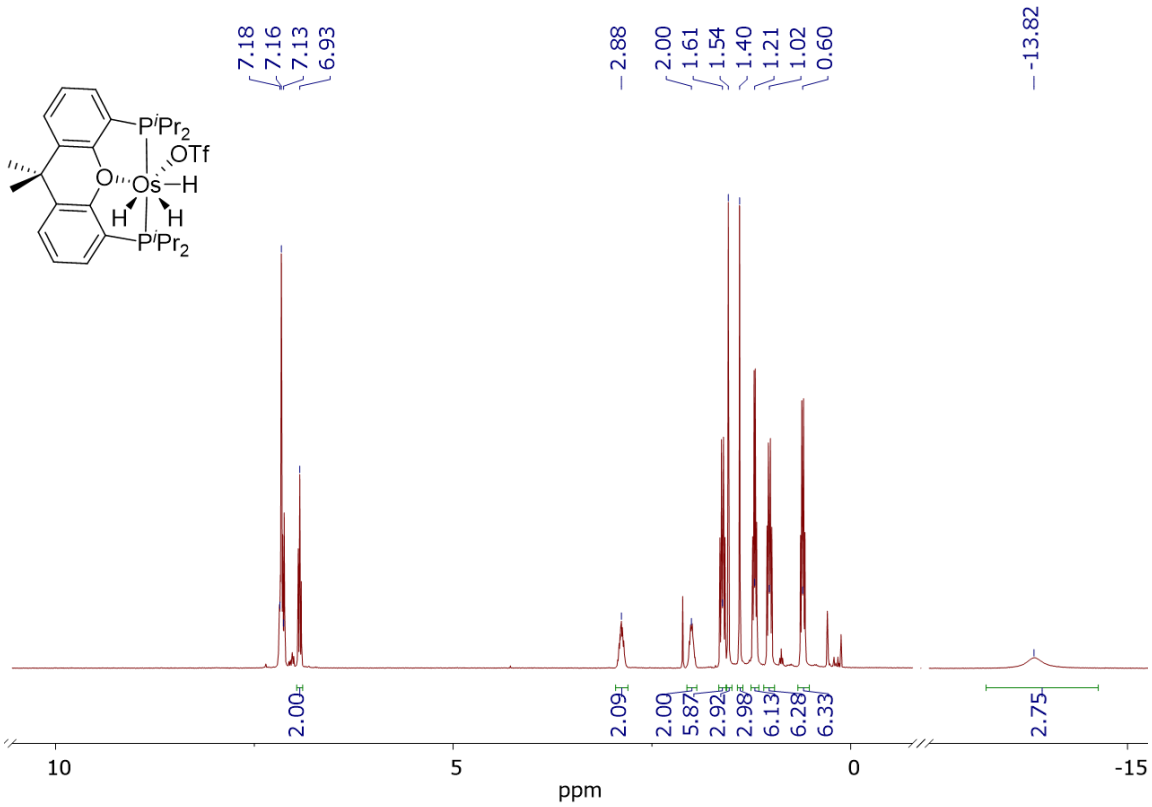

Figure S1. ^{1}H NMR (400.16 MHz, C_6D_6, 298 K) spectrum of complex **2**.

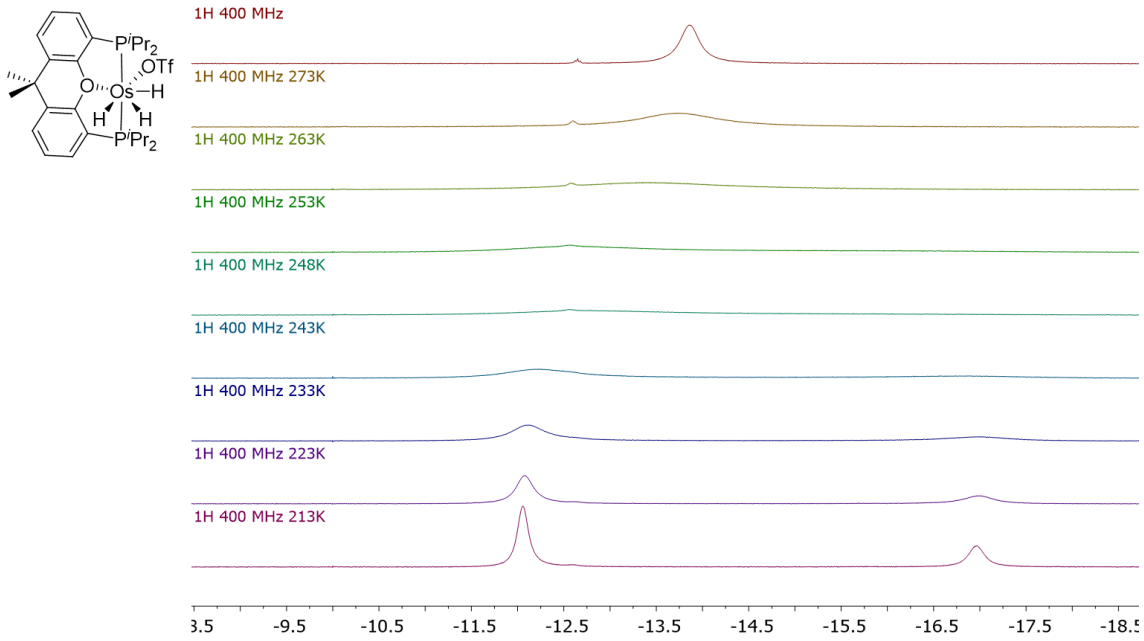

Figure S2. High-field region of the ^{1}H NMR (400.16 MHz, C_7D_8) spectrum of complex **2** between 298 and 213 K

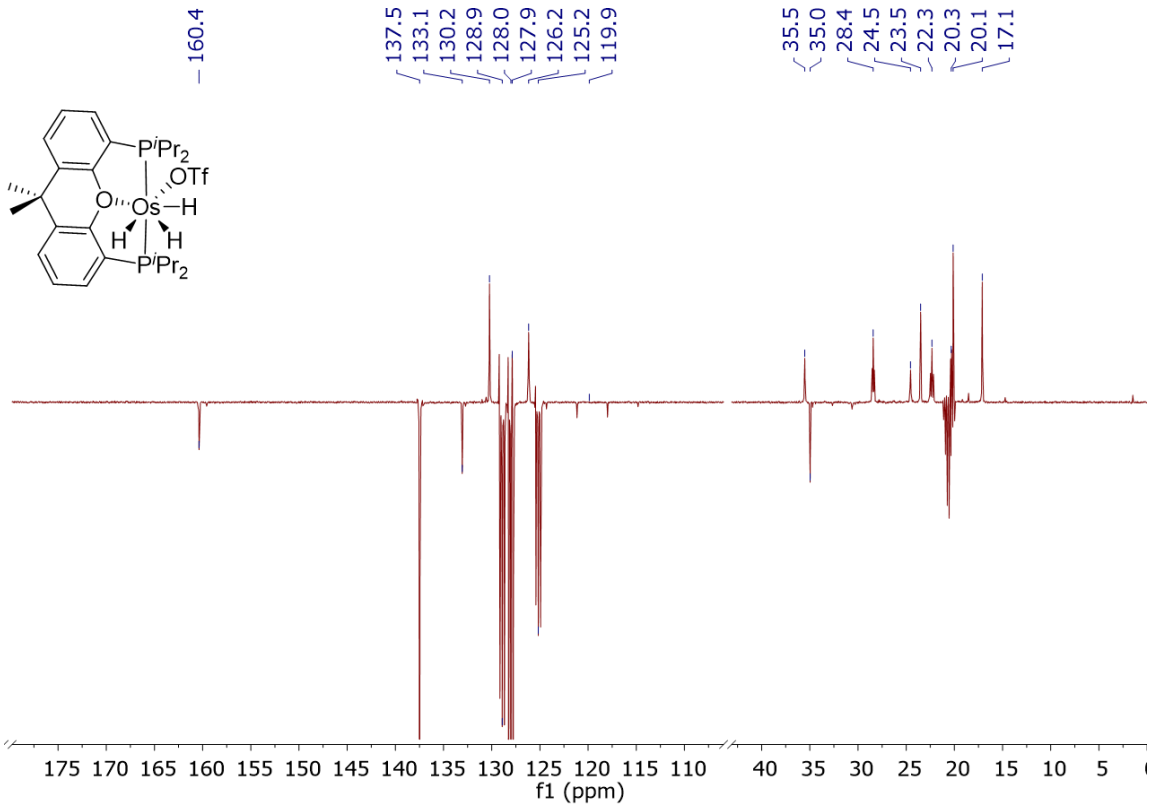

Figure S3. $^{13}C\{^1H\}$ APT NMR (100.62 MHz, C_7D_8, 233 K) spectrum of complex **2.**

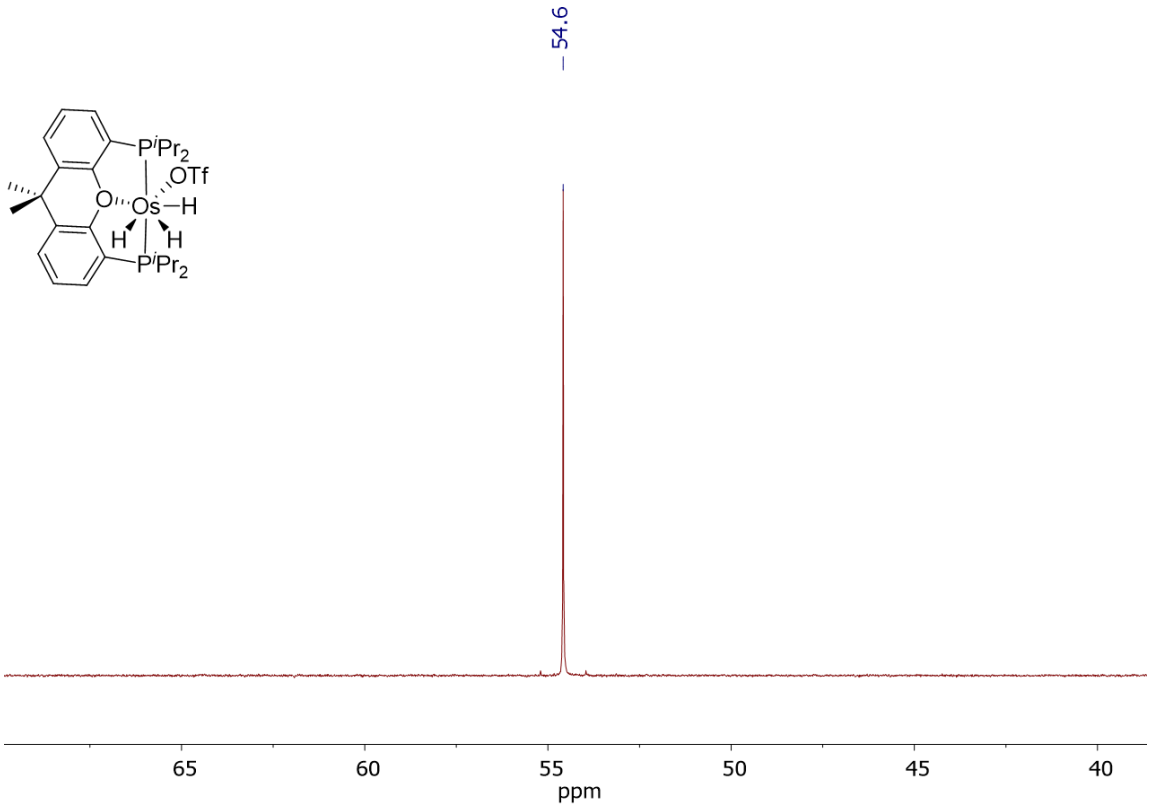

Figure S4. $^{31}P\{^1H\}$ NMR (161.99 MHz, C_6D_6, 298 K) spectrum of complex **2**.

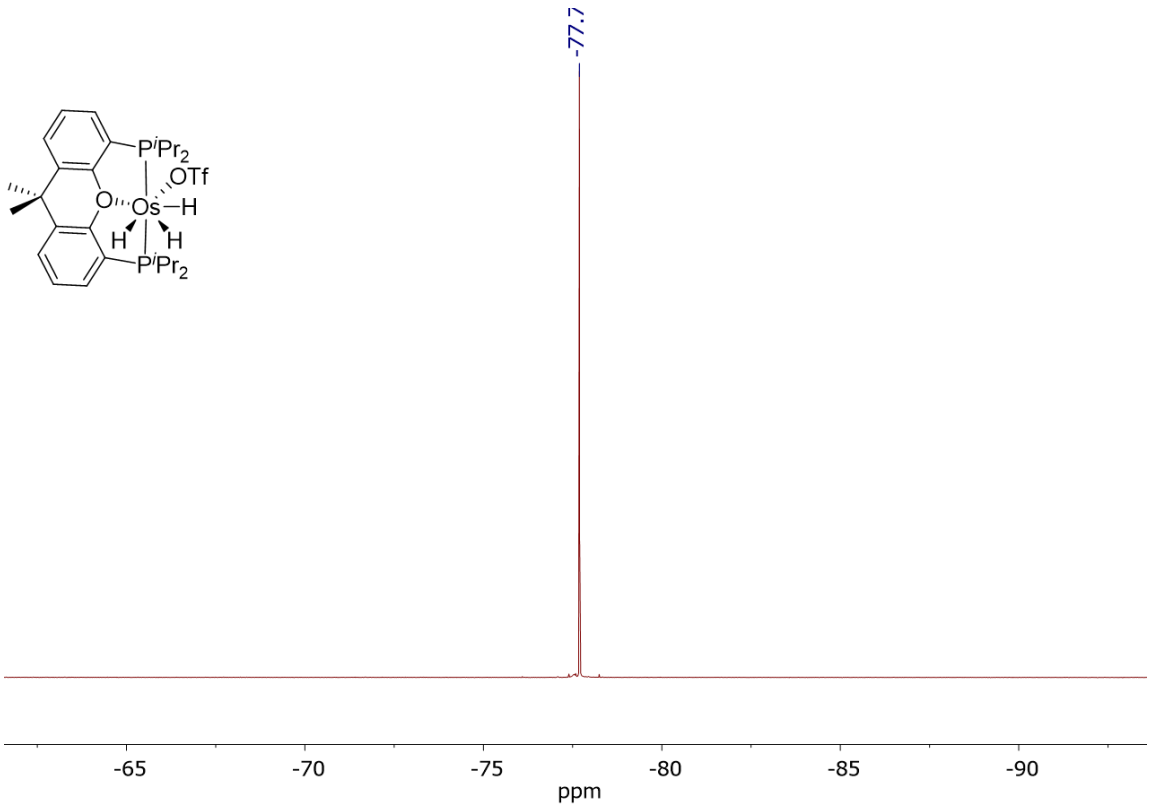

Figure S5. ^{19}F NMR (376.49 MHz, C_6D_6, 298 K) spectrum of complex **2**.

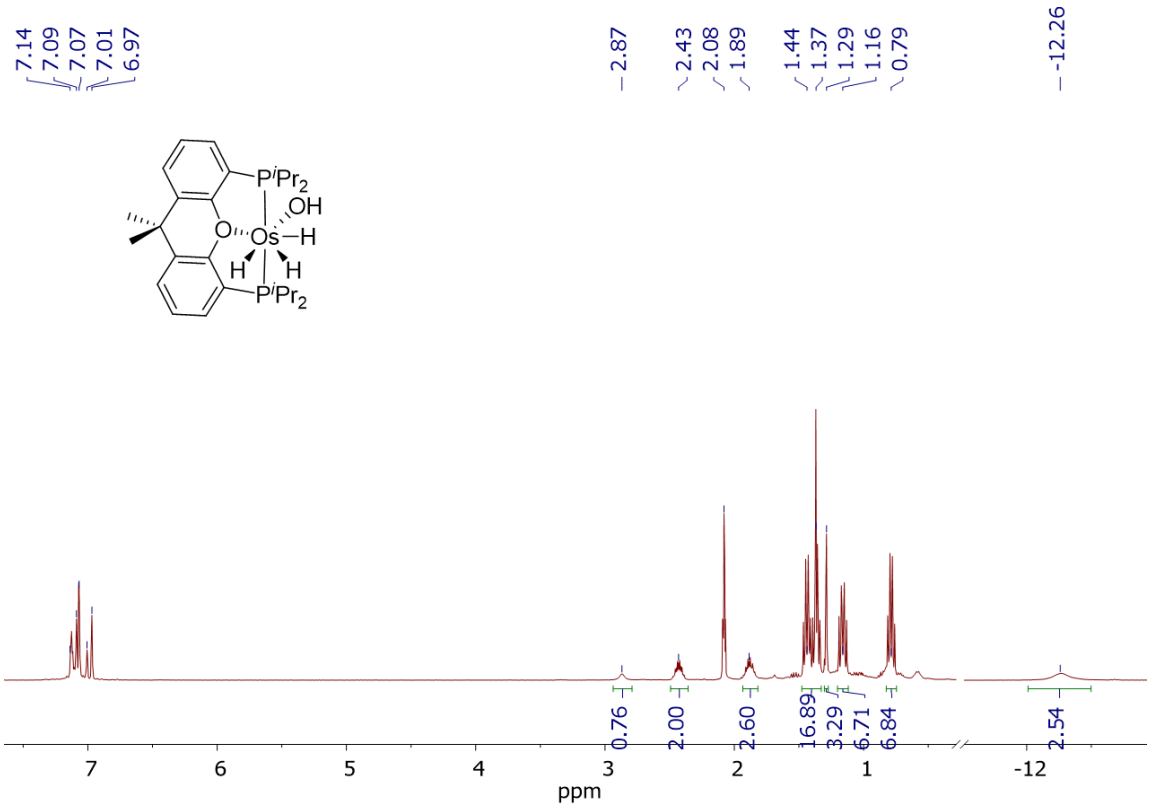

Figure S6. ^{1}H NMR (400.13 MHz, C_7D_8, 298 K) spectrum of complex **3.**

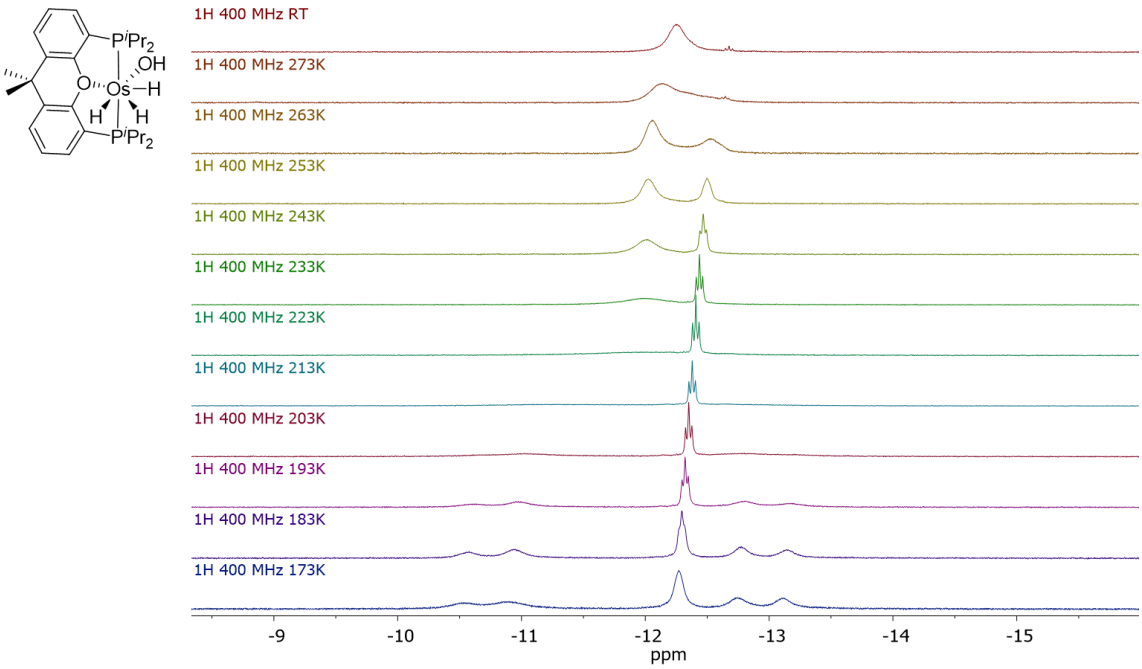

Figure S7. High-field region of the ^{1}H NMR (400.16 MHz, C_7D_8) spectrum of complex **3** between 298 and 173 K.

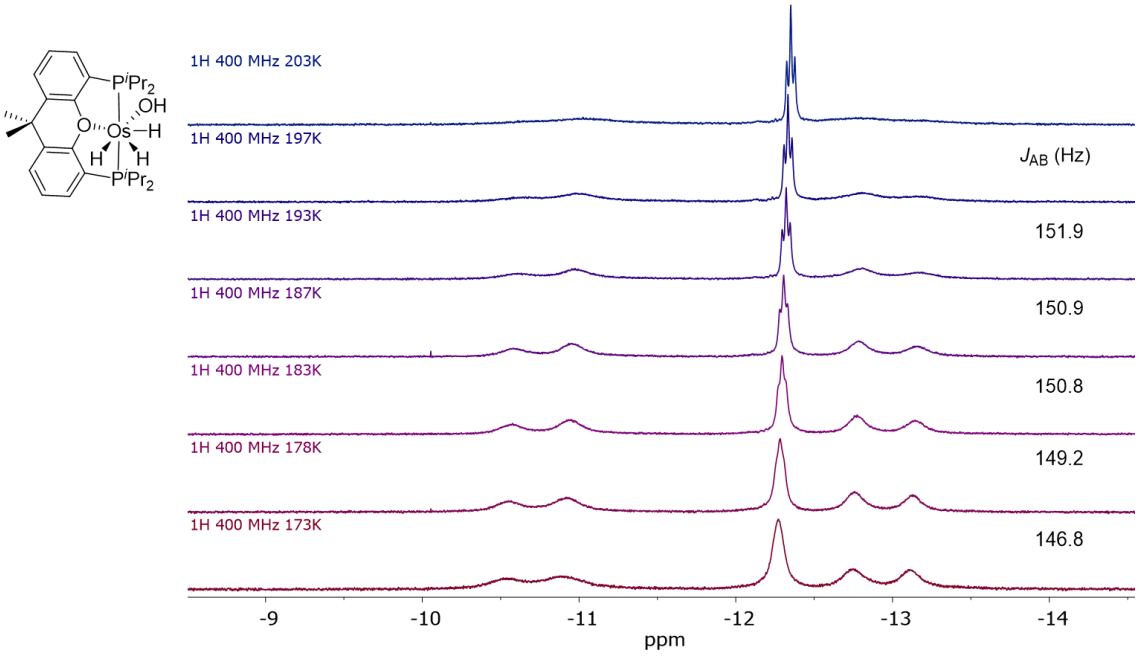

Figure S8. High-field region of the ^{1}H NMR (400.16 MHz, C_7D_8) spectrum of complex **3** between 203 and 173 K.

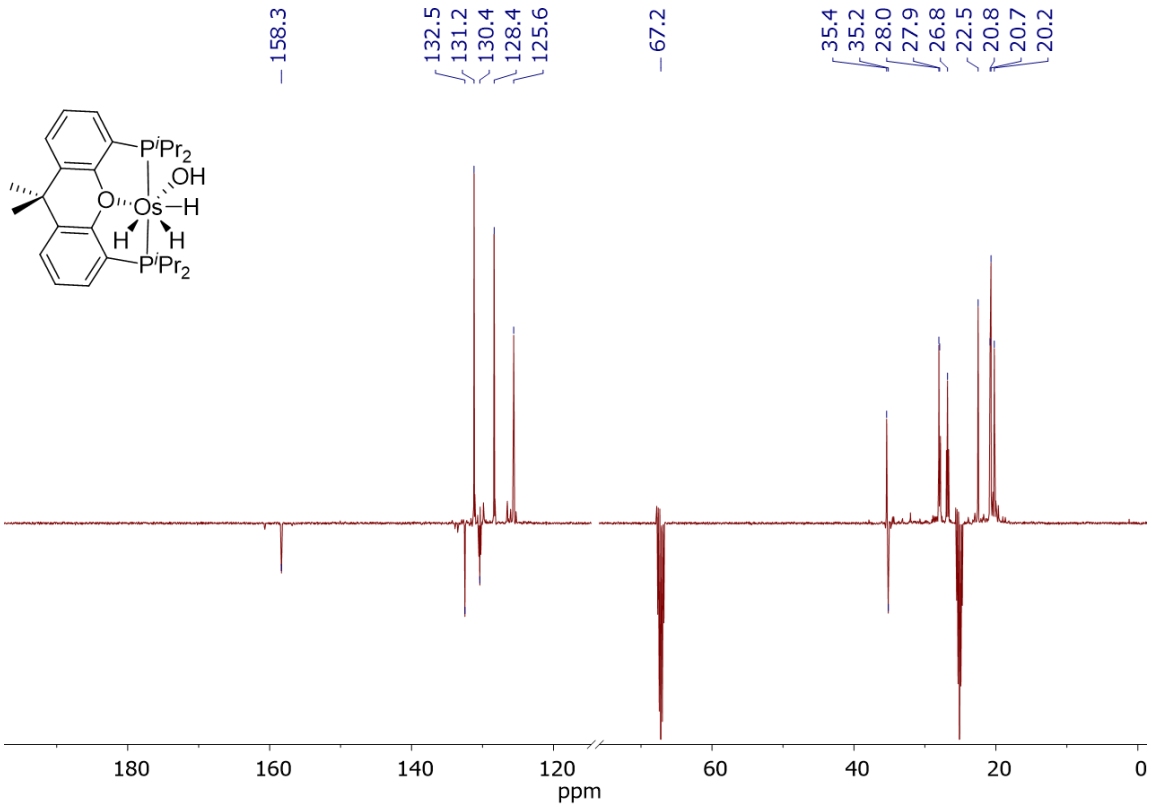

Figure S9. $^{13}C\{^1H\}$-APT NMR (100.62 MHz, THF-d_8, 253 K) spectrum of complex **3.**

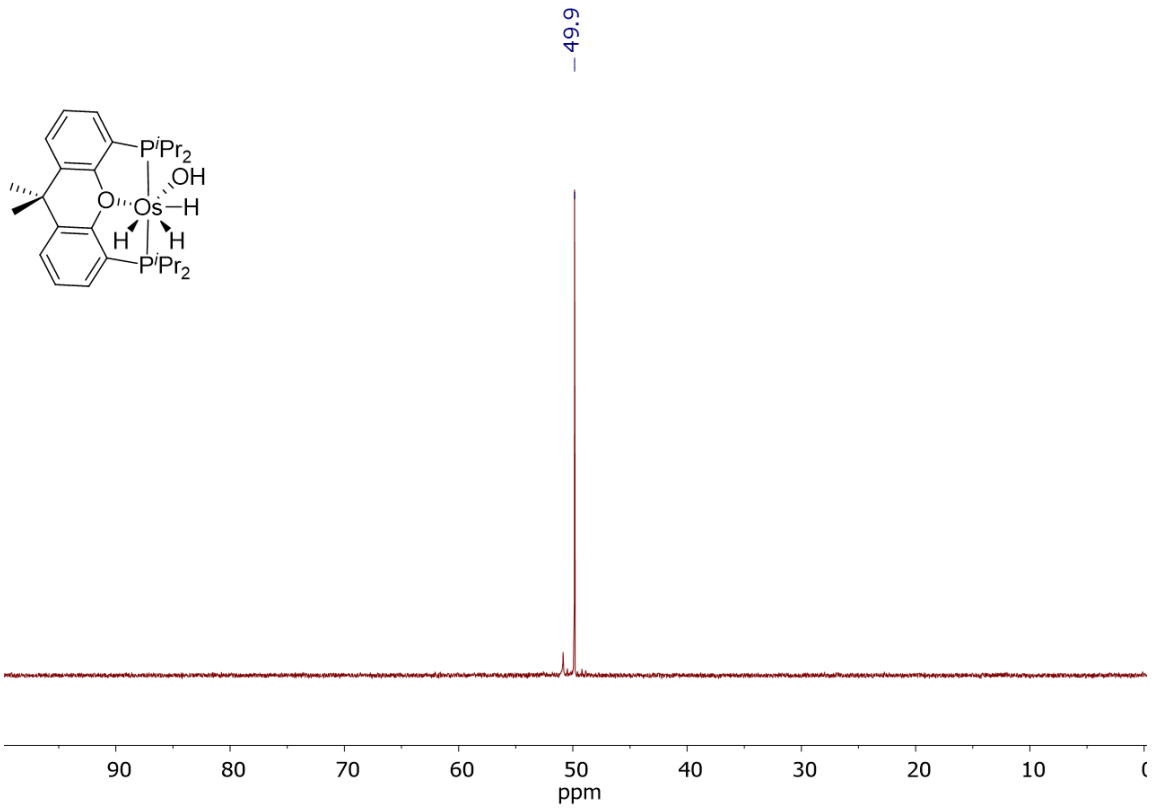

Figure S10. $^{31}P\{^1H\}$ NMR (161.99 MHz, C_7D_8, 298 K) spectrum of complex **3**.

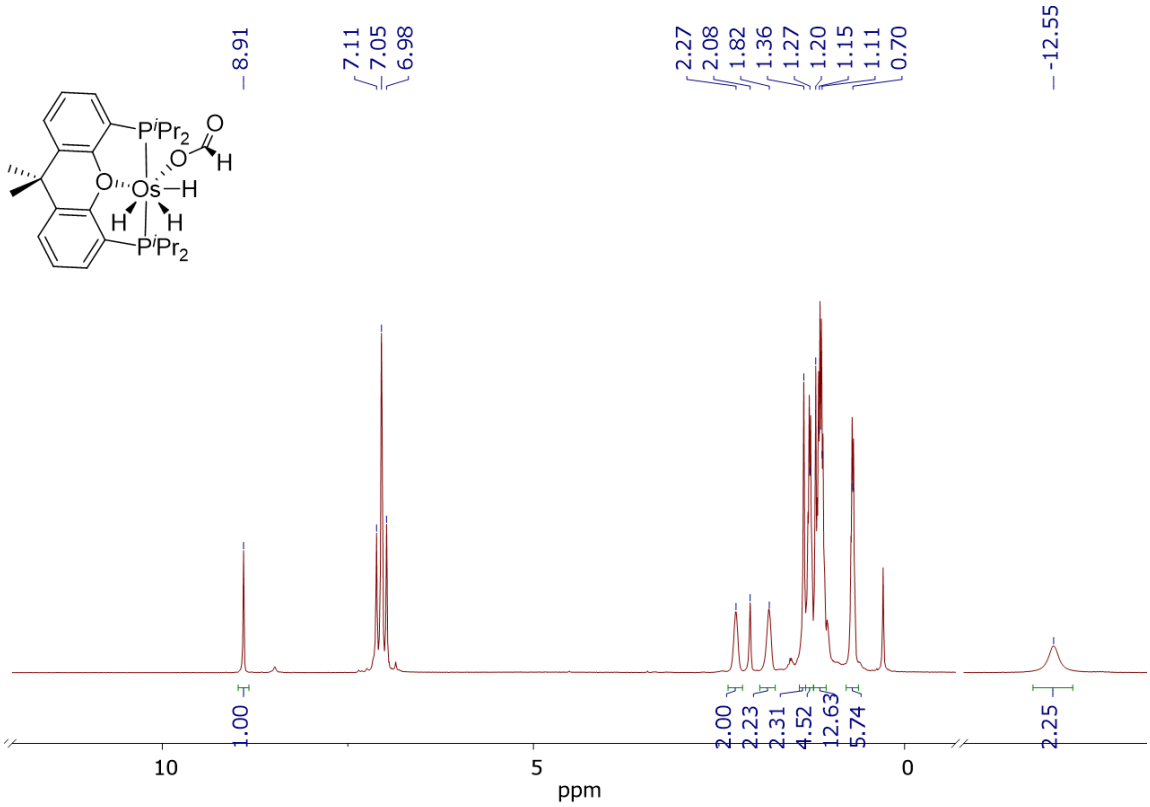

Figure S11. ^{1}H NMR (400.13 MHz, C_7D_8, 253 K) spectrum of complex **4.**

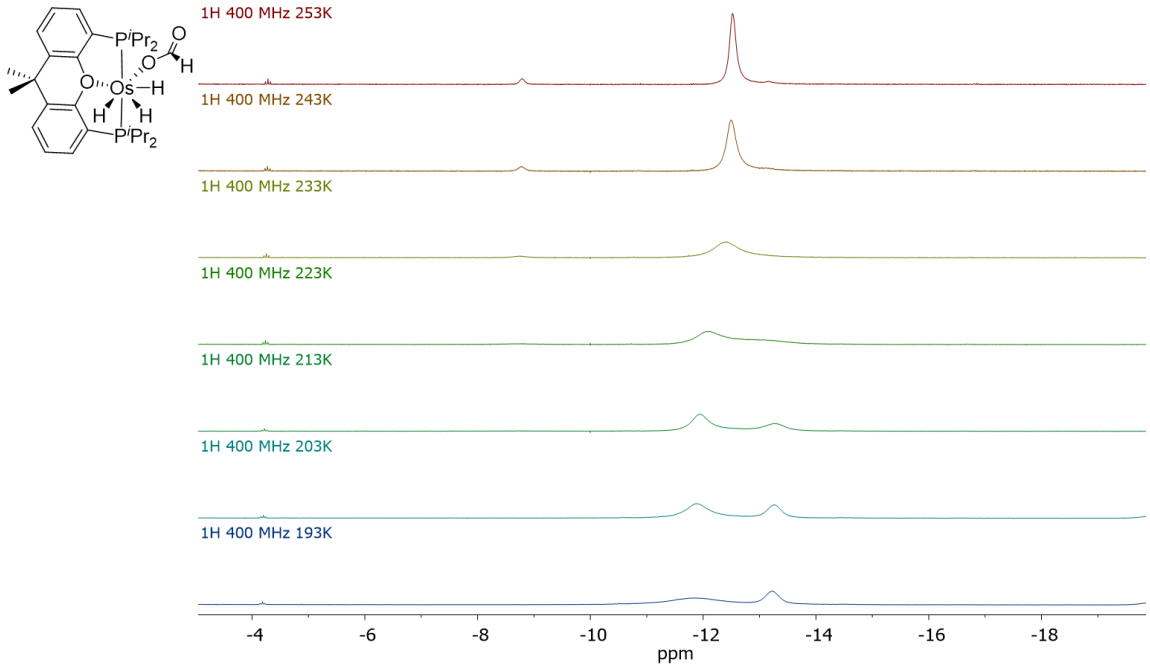

Figure S12. High-field region of the ^{1}H NMR (400.13 MHz, C_7D_8) spectrum of complex **4** between 253 and 193 K.

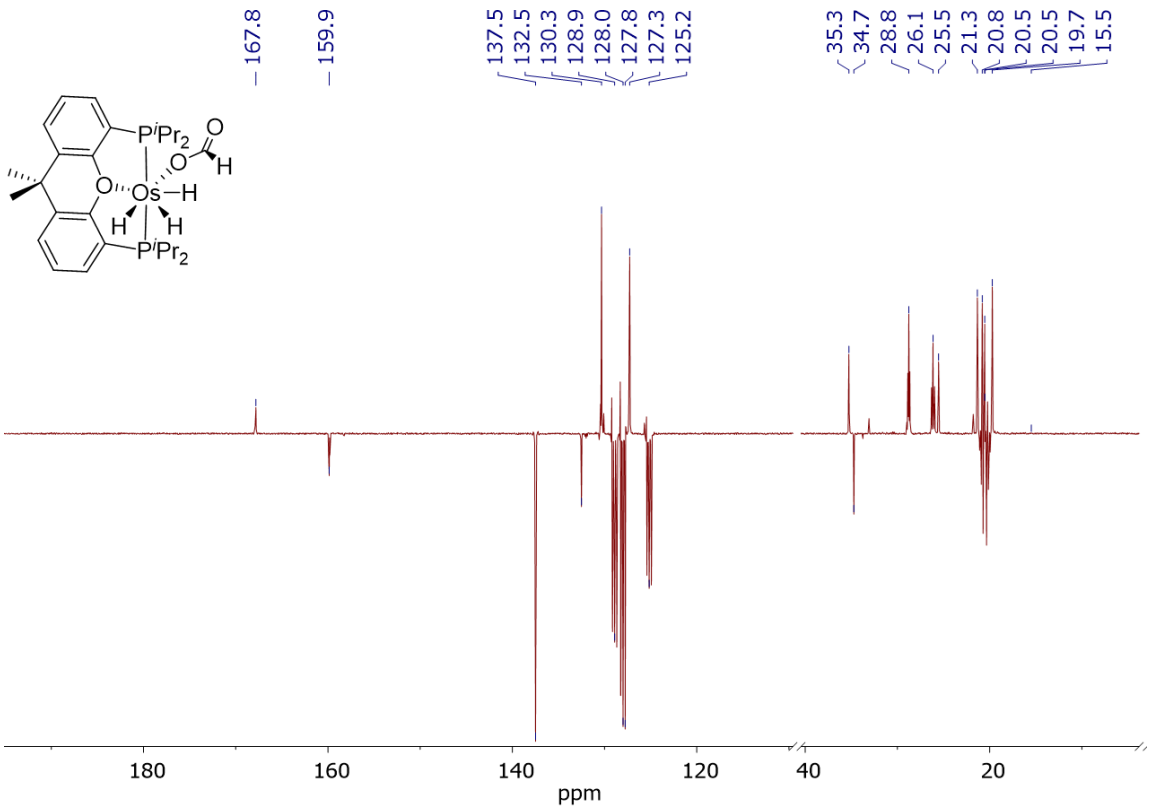

Figure S13. $^{13}C\{^{1}H\}$-APT NMR (100.62 MHz, C_7D_8, 253 K) spectrum of complex **4.**

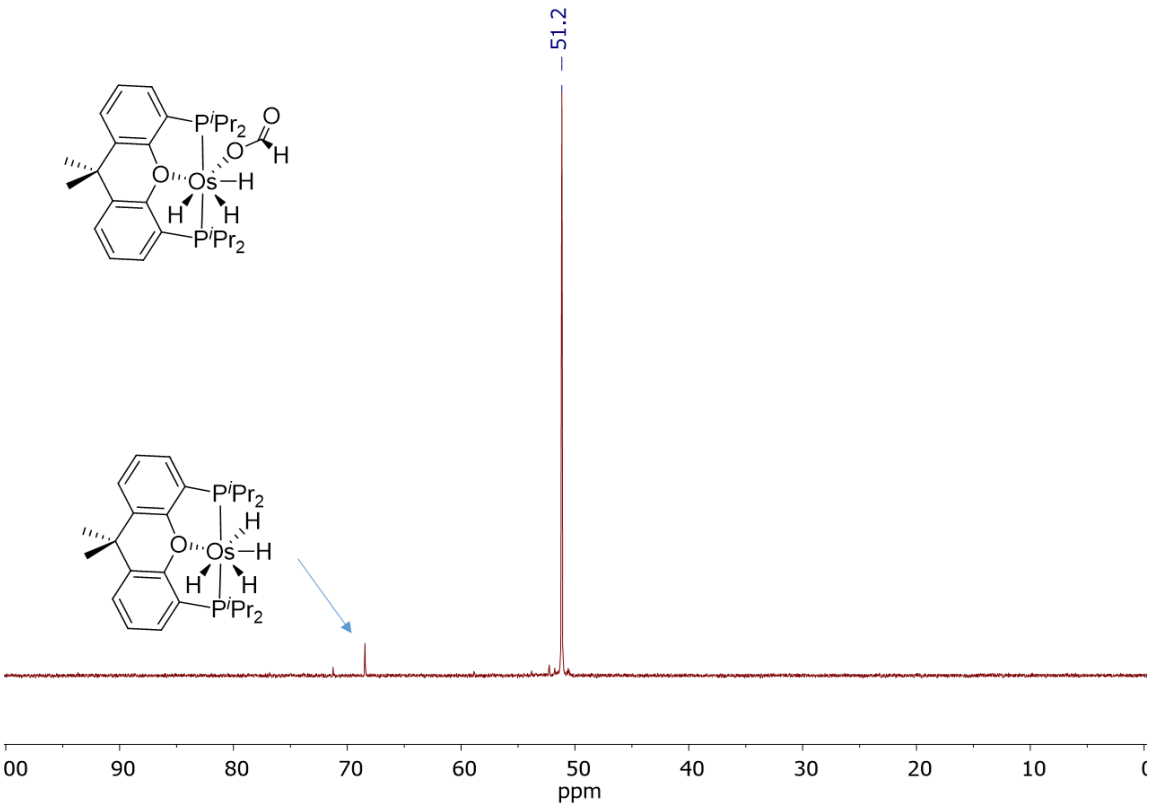

Figure S14. $^{31}P\{^{1}H\}$ NMR (161.98 MHz, C_7D_8, 253 K) spectrum of complex **4**.

$^{31}P\{^{1}H\}$ NMR Spectra of the Decarboxylation Process of Complex 4 as Function of Time

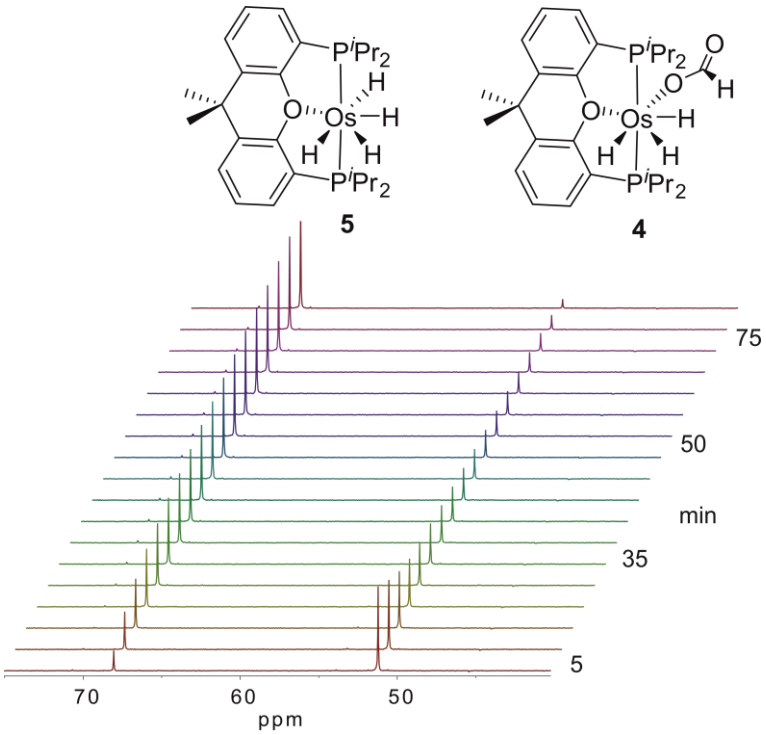

Figure S15. Stacked $^{31}P\{^{1}H\}$ spectra (161.98 MHz, in toluene-d_8) showing the course of the transformation of **4** into **5** at 303 K.

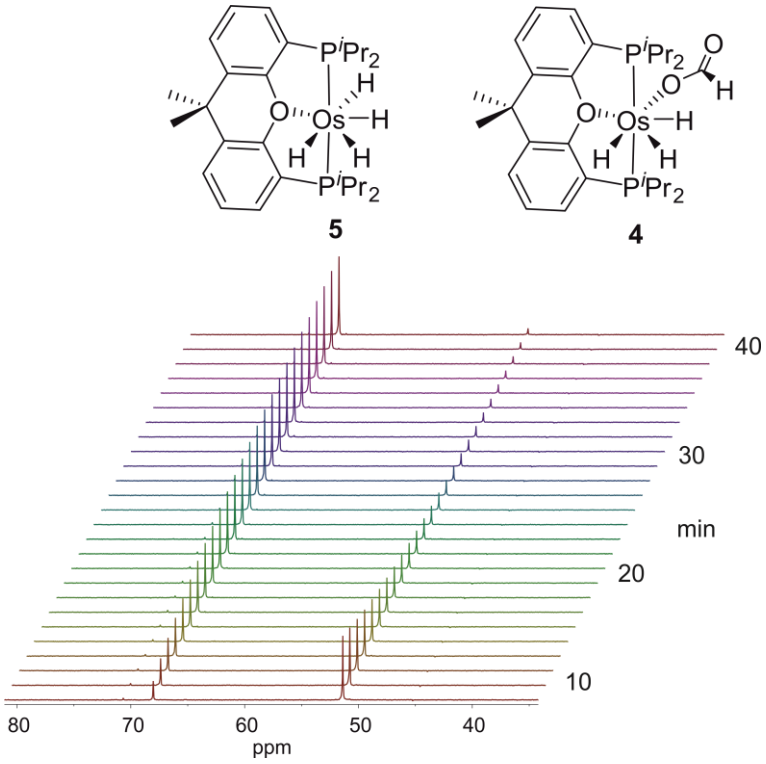

Figure S16. Stacked $^{31}P\{^{1}H\}$ spectra (161.98 MHz, in toluene-d_8) showing the course of the transformation of **4** into **5** at 308 K.

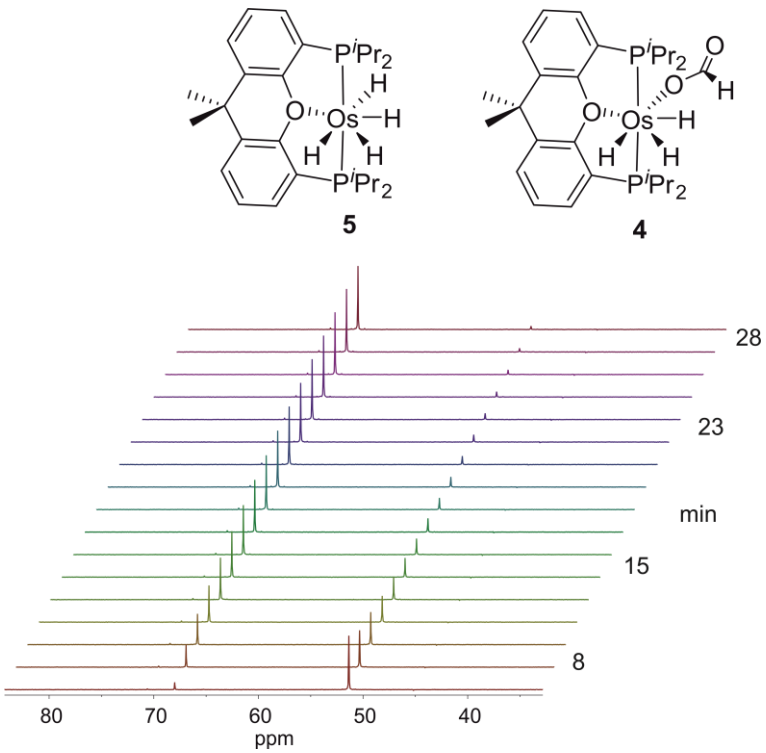

Figure S17. Stacked $^{31}P\{^1H\}$ spectra (161.98 MHz, in toluene-d_8) showing the course of the transformation of **4** into **5** at 313 K.

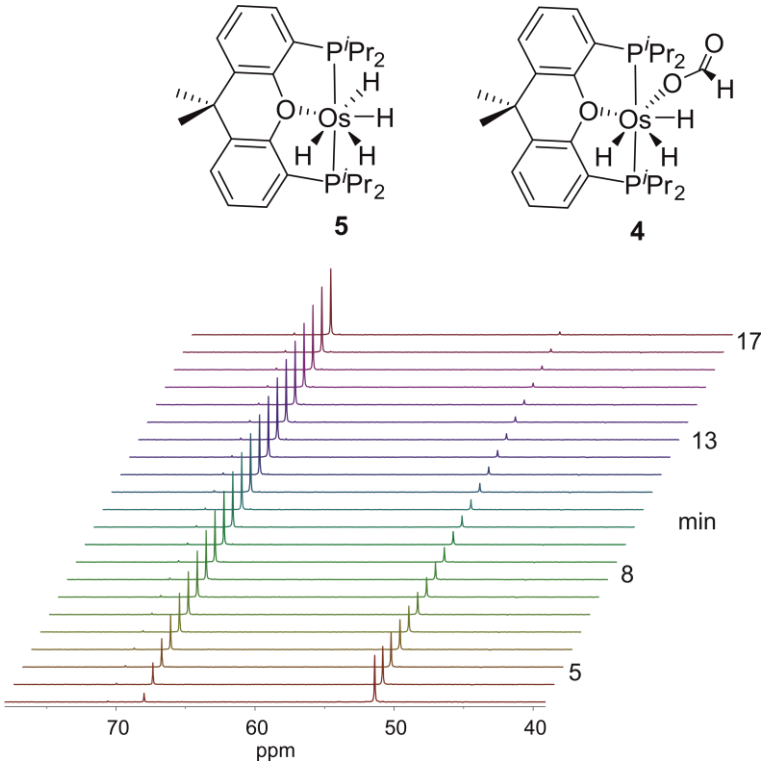

Figure S18. Stacked $^{31}P\{^1H\}$ spectra (161.98 MHz, in toluene-d_8) showing the course of the transformation of **4** into **5** at 318 K.

Structural Analysis of Complex 4.

CCDC 1849096 contains the supplementary crystallographic data for this paper. These data can be obtained free of charge via www.ccdc.cam.ac.uk/data_request/cif, or by emailing data_request@ccdc.cam.ac.uk, or by contacting The Cambridge Crystallographic Data Centre, 12 Union Road, Cambridge CB2 1EZ, UK; fax: +44 1223 336033 X-ray data were collected for the complexes on a Bruker Smart APEX-DUO diffractometer equipped with a normal focus, and 2.4 kW sealed tube source (Mo radiation, λ = 0.71073 Å).

Data were collected over the complete sphere covering 0.3° in ω. Data were corrected for absorption by using a multiscan method applied with the SADABS program.[2] The structure was solved by direct methods and refined by full-matrix least squares on F[3] with SHELXL2016,[3] including isotropic and subsequently anisotropic displacement parameters. The hydrogen atoms were observed in the least Fourier Maps or calculated, and refined freely or using a restricted riding model. The hydrides were observed but refined inadequately, so a restrained refinement was used (d(Os-H) 1.59(1) Å) resulting in a geometry in agreement with the obtained by theoretical calculations. The formate ligand was observed disordered in two positions (a, 0.8: b, 0.2, Figure S15), and refined with restrained geometry, complementary occupancy factors and isotropic thermal parameters. Two isopropyl groups were also found disordered and refined in the same way.

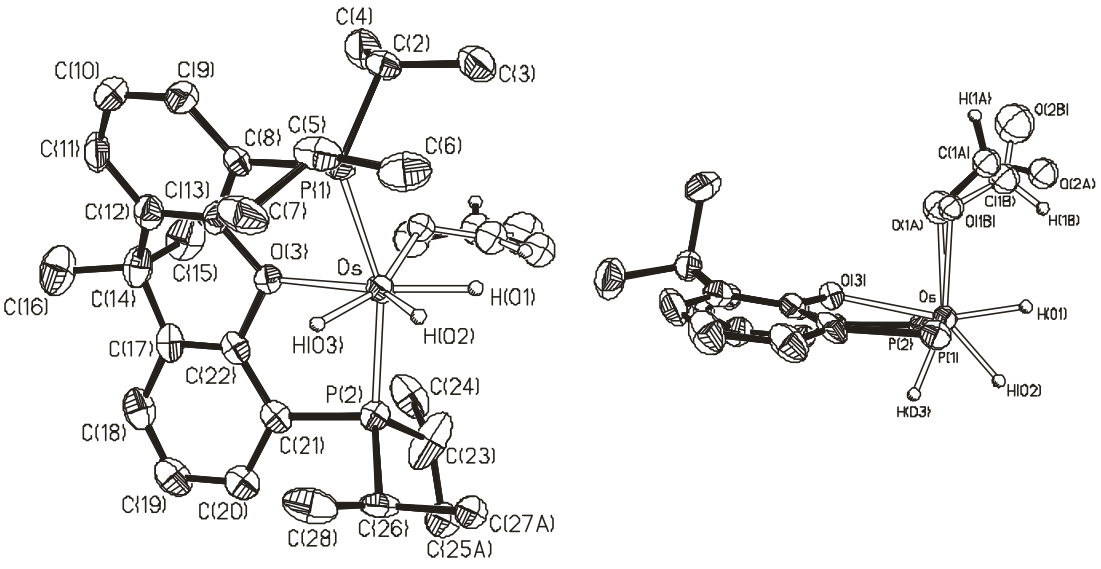

Figure S15. Molecular diagram of complex **4** at 50% probability.

Crystal data for **4**: $C_{28}H_{44}O_3OsP_2$, M_W 680.77, colourless, irregular block (0.189 x 0.134 x 0.092 mm^3), monoclinic, space group $P2_1/c$, *a*: 15.878(2) Å, *b*: 10.9673(15) Å, *c*: 16.462(2) Å, *β*: 90.174(2)°, *V* = 2866.5(7) Å^3, *Z* = 4, *Z'* = 1, D_{calc}: 1.577 g cm^{-3}, F(000): 1368, T = 100(2) K, μ

1368 mm^{-1}. 27934 measured reflections (2θ: 3-51°, ω scans 0.3°), 5335 unique (R_{int} = 0.0540); min./max. transm. Factors 0.673/0.862. Final agreement factors were R^1 = 0.0363 (3419 observed reflections, I > 2σ(I)) and wR^2 = 0.1004; data/restraints/parameters 5335/13/323; GoF = 1.062. Largest peak and hole 3.186 (close to osmium atoms) and -0.962 e/ $Å^3$.

Computational details and energy of calculated complexes. All calculations in the mechanistic studies were performed at the DFT level using the B3LYP functional[4] supplemented with the Grimme's dispersion correction D3[5] as implemented in Gaussian09.[6] Os atom was described by means of an effective core potential SDD for the inner electron[7] and its associated double-ζ basis set for the outer ones, complemented with a set of f-polarization functions.[8] The 6-31G** basis set was used for the H, C, O and P atoms.[9] All geometries were fully optimized in toluene (ε = 2.37) solvent using the continuum SMD model.[10] Transition states were identified by having one imaginary frequency in the Hessian matrix. It was confirmed that transition states connect with the corresponding intermediates by means of application of an eigenvector corresponding to the imaginary frequency and subsequent optimization of the resulting structures. Gibbs energies were computed at 298.15 K and 1 atmosphere. All values collected in schemes and figures correspond to Gibbs energies in toluene in kcal mol^{-1}.

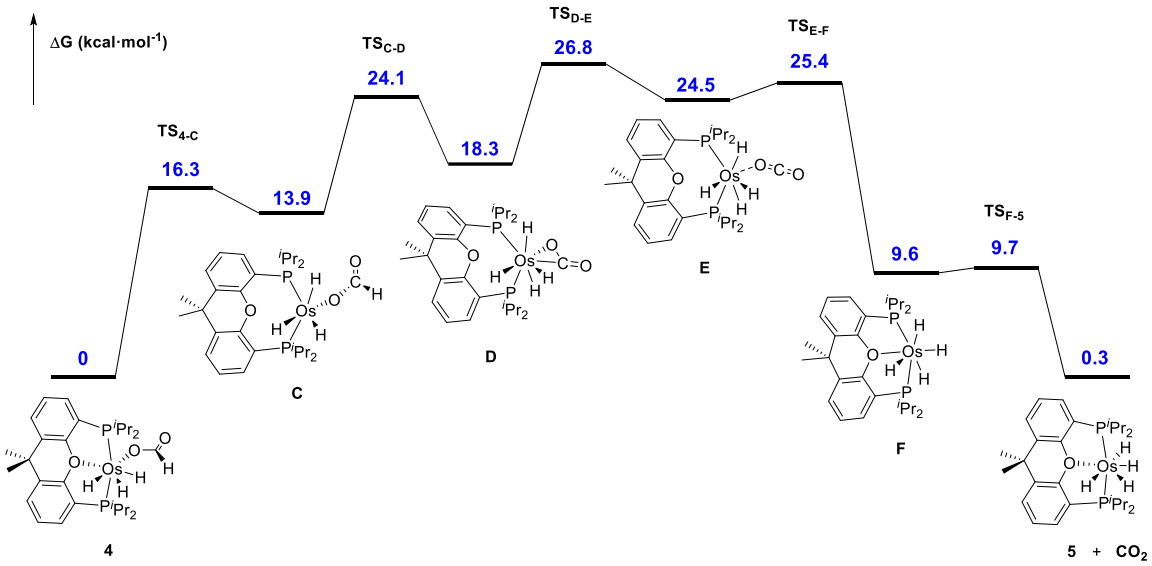

Figure S16. Energy profile for the dehydrogenation of H_2CO_2 at RT in toluene: *β*-hydride elimination pathway.

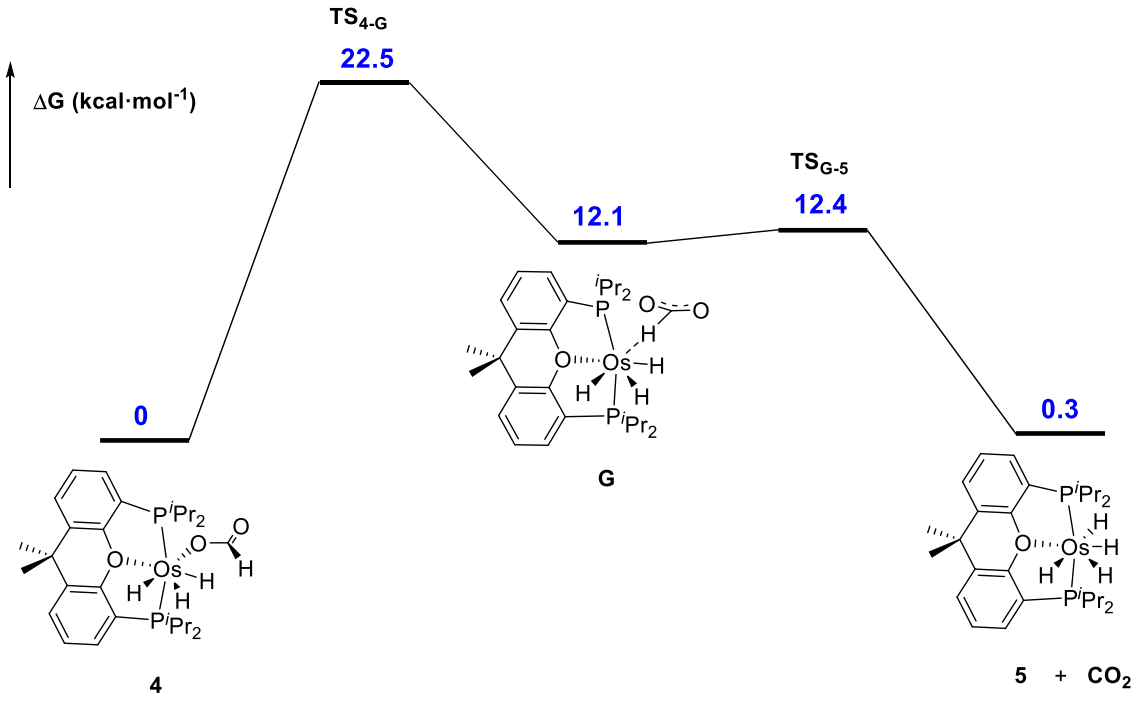

Figure S17. Energy profile for the dehydrogenation of H_2CO_2 at RT in toluene: hydride abstraction pathway.

4

Zero-point correction= 0.663705 (Hartree/Particle)

Thermal correction to Energy= 0.702825

Thermal correction to Enthalpy= 0.703769

Thermal correction to Gibbs Free Energy= 0.595412

Sum of electronic and zero-point Energies= -2092.231463

Sum of electronic and thermal Energies= -2092.192343

Sum of electronic and thermal Enthalpies= -2092.191399

Sum of electronic and thermal Free Energies= -2092.299756

$TS_{4\text{-}C}$

Zero-point correction= 0.662676 (Hartree/Particle)

Thermal correction to Energy= 0.701404

Thermal correction to Enthalpy= 0.702348

Thermal correction to Gibbs Free Energy= 0.594713

Sum of electronic and zero-point Energies= -2092.205859

Sum of electronic and thermal Energies= -2092.167130

Sum of electronic and thermal Enthalpies= -2092.166186

Sum of electronic and thermal Free Energies= -2092.273822

C

Zero-point correction= 0.663250 (Hartree/Particle)

Thermal correction to Energy= 0.702535

Thermal correction to Enthalpy= 0.703479

Thermal correction to Gibbs Free Energy= 0.594772

Sum of electronic and zero-point Energies= -2092.209119

Sum of electronic and thermal Energies= -2092.169834

Sum of electronic and thermal Enthalpies= -2092.168890

Sum of electronic and thermal Free Energies= -2092.277596

$TS_{C\text{-}D}$

Zero-point correction= 0.659485 (Hartree/Particle)

Thermal correction to Energy= 0.698023

Thermal correction to Enthalpy= 0.698967

Thermal correction to Gibbs Free Energy= 0.592186

Sum of electronic and zero-point Energies= -2092.193987

Sum of electronic and thermal Energies= -2092.155449

Sum of electronic and thermal Enthalpies= -2092.154505

Sum of electronic and thermal Free Energies= -2092.261286

D

Zero-point correction= 0.661637 (Hartree/Particle)

Thermal correction to Energy= 0.700207

Thermal correction to Enthalpy= 0.701152

Thermal correction to Gibbs Free Energy= 0.595423

Sum of electronic and zero-point Energies= -2092.204433

Sum of electronic and thermal Energies= -2092.165863

Sum of electronic and thermal Enthalpies= -2092.164919

Sum of electronic and thermal Free Energies= -2092.270648

TS_{D-E}

Zero-point correction= 0.658968 (Hartree/Particle)

Thermal correction to Energy= 0.697894

Thermal correction to Enthalpy= 0.698839

Thermal correction to Gibbs Free Energy= 0.591826

Sum of electronic and zero-point Energies= -2092.189920

Sum of electronic and thermal Energies= -2092.150994

Sum of electronic and thermal Enthalpies= -2092.150050

Sum of electronic and thermal Free Energies= -2092.257062

E

Zero-point correction= 0.658964 (Hartree/Particle)

Thermal correction to Energy= 0.698846

Thermal correction to Enthalpy= 0.699790

Thermal correction to Gibbs Free Energy= 0.589276

Sum of electronic and zero-point Energies= -2092.191067

Sum of electronic and thermal Energies= -2092.151186

Sum of electronic and thermal Enthalpies= -2092.150242

Sum of electronic and thermal Free Energies= -2092.260756

TS_{E-F}

Zero-point correction= 0.658924 (Hartree/Particle)

Thermal correction to Energy= 0.698068

Thermal correction to Enthalpy= 0.699012

Thermal correction to Gibbs Free Energy= 0.590386

Sum of electronic and zero-point Energies= -2092.190749

Sum of electronic and thermal Energies= -2092.151605

Sum of electronic and thermal Enthalpies= -2092.150661

Sum of electronic and thermal Free Energies= -2092.259286

F

Zero-point correction= 0.645685 (Hartree/Particle)

Thermal correction to Energy= 0.681447

Thermal correction to Enthalpy= 0.682391

Thermal correction to Gibbs Free Energy= 0.581911

Sum of electronic and zero-point Energies= -1903.630303

Sum of electronic and thermal Energies= -1903.594542

Sum of electronic and thermal Enthalpies= -1903.593598

Sum of electronic and thermal Free Energies= -1903.694077

TS_{F-5}

Zero-point correction= 0.643761 (Hartree/Particle)

Thermal correction to Energy= 0.679336

Thermal correction to Enthalpy= 0.680280

Thermal correction to Gibbs Free Energy= 0.580034

Sum of electronic and zero-point Energies= -1903.630320

Sum of electronic and thermal Energies= -1903.594745

Sum of electronic and thermal Enthalpies= -1903.593801

Sum of electronic and thermal Free Energies= -1903.694047

5

Zero-point correction= 0.645120 (Hartree/Particle)

Thermal correction to Energy= 0.681200

Thermal correction to Enthalpy= 0.682144

Thermal correction to Gibbs Free Energy= 0.580043

Sum of electronic and zero-point Energies= -1903.643758

Sum of electronic and thermal Energies= -1903.607679

Sum of electronic and thermal Enthalpies= -1903.606735

Sum of electronic and thermal Free Energies= -1903.708836

$TS_{4\text{-}G}$

Zero-point correction= 0.662220 (Hartree/Particle)

Thermal correction to Energy= 0.700738

Thermal correction to Enthalpy= 0.701682

Thermal correction to Gibbs Free Energy= 0.595078

Sum of electronic and zero-point Energies= -2092.196783

Sum of electronic and thermal Energies= -2092.158264

Sum of electronic and thermal Enthalpies= -2092.157320

Sum of electronic and thermal Free Energies= -2092.263924

G

Zero-point correction= 0.658734 (Hartree/Particle)

Thermal correction to Energy= 0.698175

Thermal correction to Enthalpy= 0.699120

Thermal correction to Gibbs Free Energy= 0.590593

Sum of electronic and zero-point Energies= -2092.212260

Sum of electronic and thermal Energies= -2092.172819

Sum of electronic and thermal Enthalpies= -2092.171875

Sum of electronic and thermal Free Energies= -2092.280401

TS_{G-5}

Zero-point correction= 0.658033 (Hartree/Particle)

Thermal correction to Energy= 0.696872

Thermal correction to Enthalpy= 0.697817

Thermal correction to Gibbs Free Energy= 0.590975

Sum of electronic and zero-point Energies= -2092.212858

Sum of electronic and thermal Energies= -2092.174019

Sum of electronic and thermal Enthalpies= -2092.173075

Sum of electronic and thermal Free Energies= -2092.279917

CO_2

Zero-point correction= 0.011506 (Hartree/Particle)

Thermal correction to Energy= 0.014170

Thermal correction to Enthalpy= 0.015114

Thermal correction to Gibbs Free Energy= -0.009220

Sum of electronic and zero-point Energies= -188.569692

Sum of electronic and thermal Energies= -188.567028

Sum of electronic and thermal Enthalpies= -188.566084

Sum of electronic and thermal Free Energies= -188.590418

References

(1) Alós, J.; Bolaño, T.; Esteruelas, M. A.; Oliván, M.; Oñate, E.; Valencia, M. POP-Pincer Osmium-Polyhydrides: Head-to-Head (*Z*)-Dimerization of Terminal Alkynes. *Inorg. Chem.* **2013**, *52*, 6199-6213.

(2) Blessing, R. H. An Empirical Correction for Absorption Anisotropy. *Acta Crystallogr., Sect. A: Found. Crystallogr.* **1995**, *51*, 33-38.

(3) Sheldrick, G. M. A Short History of SHELX. *Acta Crystallogr., Sect. A: Found. Crystallogr.* **2008**, *64*, 112-122.

(4) (a) Lee, C. T.; Yang, W. T.; Parr, R. G. Development of the Colle-Salvetti Correlation-Energy Formula into a Functional of the Electron-Density. *Phys. Rev. B* **1988**, *37*, 785-789. (b) Becke, A. D. A New Mixing of Hartree-Fock and Local Density-Functional Theories. *J. Chem. Phys.* **1993**, *98*, 1372-1377. (c) Stephens, P. J.; Devlin, F. J.; Chabalowski, C. F.; Frisch, M. J. Ab-Initio Calculation of Vibrational Absorption and Circular-Dichroism Spectra Using Density-Functional Force-Fields. *J. Phys. Chem.* **1994**, *98*, 11623-11627.

(5) Grimme, S.; Antony, J.; Ehrlich, S.; Krieg, H. A Consistent and Accurate *ab initio* Parametrization of Density Functional Dispersion Correction (DFT-D) for the 94 Elements H-Pu. *J. Chem. Phys.* **2010**, *132*.

(6) Gaussian 09, Revision D.01, Frisch, M. J.; Trucks, G. W.; Schlegel H. B.; Scuseria, G. E.; Robb, M. A.; Cheeseman, J. R.; Scalmani, G.; Barone, V.; Mennucci, B.; Petersson, G. A.; Nakatsuji, H.; Caricato, M.; Li, X.; Hratchian, H. P.; Izmaylov, A. F.; Bloino, J.; Zheng, G.; Sonnenberg, J. L.; Hada, M.; Ehara, M.; Toyota, K.; Fukuda, R.; Hasegawa, J.; Ishida, M.; Nakajima, T.; Honda, Y.; Kitao, O.; Nakai, H.; Vreven, T.; Montgomery, J. A.; Peralta, Jr., J. E.; Ogliaro, F.; Bearpark, M.; Heyd, J. J.; Brothers, E.; Kudin, K. N.; Staroverov, V. N.; Keith, T.; Kobayashi, R.; Normand, J.; Raghavachari, K.; Rendell, A.; Burant, J. C.; Iyengar, S. S.; Tomasi, J.; Cossi, M.; Rega, N.; Millam, J. M.; Klene, M.; Knox, J. E.; Cross, J. B.; Bakken, V.; Adamo, C.; Jaramillo, J.; Gomperts, R.; Stratmann, R. E.; Yazyev, O.; Austin, A. J.; Cammi, R.; Pomelli, C.; Ochterski, J. W.; Martin, R. L.; Morokuma, K.; Zakrzewski, V. G.; Voth, G. A.; Salvador, P.; Dannenberg, J. J.; Dapprich, S.; Daniels, A. D.; Farkas, O.; Foresman, J. B.; Ortiz, J. V.; Cioslowski, J.; Fox, D. J. Gaussian, Inc., Wallingford CT, 2013.

(7) Andrae, D.; Häußermann, U.; Dolg, M.; Stoll, H.; Preuß, H. Energy-Adjusted *ab initio* Pseudopotentials for the Second and Third Row Transition Elements. *Theor. Chim. Acta* **1990**, *77*, 123-141.

(8) Ehlers, A. W.; Bohme, M.; Dapprich, S.; Gobbi, A.; Hollwarth, A.; Jonas, V.; Kohler, K. F.; Stegmann, R.; Veldkamp, A.; Frenking, G. A Set of F-Polarization Functions for Pseudo-Potential Basis-Sets of the Transition-Metals Sc-Cu, Y-Ag and La-Au. *Chem. Phys. Lett.* **1993**, *208*, 111-114.

(9) (a) Hehre, W. J.; Ditchfield, R.; Pople, J. A. Self-Consistent Molecular-Orbital Methods. XII. Further Extensions of Gaussian-Type Basis Sets for Use in Molecular-Orbital Studies of Organic-Molecules. *J. Chem. Phys.,* **1972**, *56*, 2257-2261. (b) Francl, M. M.; Pietro, W. J.; Hehre, W. J.; Binkley, J. S.; Gordon, M. S.; Defrees, D. J.; Pople, J. A. Self-Consistent Molecular-Orbital Methods .23. A Polarization-Type Basis Set for 2nd-Row Elements. *J. Chem. Phys.* **1982**, *77*, 3654-3665.

(10) Marenich, A. V.; Cramer, C. J.; Truhlar, D. G. Universal Solvation Model Based on Solute Electron Density and on a Continuum Model of the Solvent Defined by the Bulk Dielectric Constant and Atomic Surface Tensions. *J. Phys. Chem. B* **2009**, *113*, 6378-6396.

Elongated σ-Borane versus σ-Borane in Pincer-POP-Osmium Complexes

Miguel A. Esteruelas,,† Israel Fernández,‡ Cristina García-Yebra,† Jaime Martín,† and Enrique Oñate†*

†Departamento de Química Inorgánica, Instituto de Síntesis Química y Catálisis Homogénea (ISQCH), Centro de Innovación en Química Avanzada (ORFEO-CINQA), Universidad de Zaragoza-CSIC, 50009 Zaragoza, Spain

‡Departamento de Química Orgánica I, Facultad de Ciencias Químicas, Centro de Innovación en Química Avanzada (ORFEO-CINQA), Universidad Complutense de Madrid, 28040 Madrid, Spain

Supporting Information Placeholder

ABSTRACT: Square pyramidal metal fragments $OsHX\{\kappa^3\text{-}P,O,P\text{-}[xant(P^iPr_2)_2]\}$ (X = Cl, H; $xant(P^iPr_2)_2$ = 9,9-dimethyl-4,5-bis(diisopropylphosphine)xanthene) coordinate the B-H bond of boranes *trans* to the ligand X. As a consequence, elongated σ-borane and σ-borane pincer-POP-osmium complexes have been isolated and fully characterized. The interaction between the metal fragment and the coordinated B-H has been analyzed as a function of X, from spectroscopic, X-ray diffraction, and theoretical points of view. The dinuclear complex $[(Os(H\cdots H)\{\kappa^3\text{-}P,O,P\text{-}[xant(P^iPr_2)_2]\})_2(\mu\text{-}Cl)_2][BF_4]_2$ (**3**) reacts with catecholborane (HBcat) and pinacolborane (HBpin) to give the elongated σ-borane derivative $OsHCl(\eta^2\text{-}H\text{-}BR_2)\{\kappa^3\text{-}P,O,P\text{-}[xant(P^iPr_2)_2]\}$ (BR_2 = Bcat (**4**), Bpin (**5**)), H_2, FBR_2, and BF_3. The elongated σ-borane character of **4** and **5** is supported by X-ray diffraction analysis and DFT-optimized structures of both compounds, which show distances between the coordinated B and H atoms of the borane in the range 1.6-1.7 Å. AIM analysis of **4** reveals a triangular topology for the OsHB unit involving Os-B, Os-H, and B-H bond critical points and a ring critical point. In contrast to **3**, the reaction of the tetrahydride complex $OsH_4\{\kappa^3\text{-}P,O,P\text{-}[xant(P^iPr_2)_2]\}$ (**6**) with HBcat leads to the σ-borane derivative $OsH_2(\eta^2\text{-}H\text{-}Bcat)\{\kappa^3\text{-}P,O,P\text{-}[xant(P^iPr_2)_2]\}$ (**7**), which shows a distance between the atoms of the coordinated B-H bond in the range 1.4-1.5 Å. AIM analysis for the OsHB unit of **7** only displays Os-B and B-H bond critical points therefore lacking a similar topology.

INTRODUCTION

Metal-promoted σ-bond activation reactions are the origin of a great number of processes in the current chemistry. The first step is the coordination of the σ-bond to the metal to form a σ-complex. The metal-bond interaction involves σ-donation from the σ-molecular orbital of the coordinated bond to empty orbitals of the metal and back bonding from the metal to the σ*-molecular orbital of the bond. The balance between donation and back-donation determines the degree of addition of the bond to the metal, which in the majority of cases fits to the separation between the coordinated atoms.[1] Dihydrogen compounds form the best-known group of complexes of this type. Depending upon the separation between the coordinated hydrogens, they are classified in Kubas-type complexes (0.8-1.0 Å) and elongated dihydrogens (1.0-1.3 Å). High oxidation states, first-row metals, cationic charges, acidic ligands and tridentate groups enforcing L-M-L angles close to 90º stabilize Kubas-type complexes while low oxidation states, third-row metals, and π-donor ligands favor the formation of elongated dihydrogen compounds.[2]

The stabilization of σ-E-H bond activation intermediates (B, C, Si, etc) is much more difficult than the stabilization of dihydrogen species.[3] As a consequence, very little information is available for σ-E-H complexes. By comparison to the hydrogen molecule, an R_nE-H bond (n = 2 or 3) is dissymmetric and the substituents at the E atom may tune the acidity of the bond. In addition, in some cases the E atom can possess available empty orbitals, as boron, which alter the balance between donation and back-donation in comparison with the dihydrogen situation.

The B-H bond activation is a reaction of great interest in connection with the borylation of organic molecules[4] and the dehydrocoupling of amineboranes.[5] However, scarce examples of complexes containing non-assisted B-H coordination have been reported.[6] They include some first-row metals; such as Ti,[7] Mn, Re,[8] Ni;[9] and Ru.[10] These compounds contain small H-M-B angles (32º-38º), whereas the B-H distances are in the range 1.23-1.35 Å. For third-row metals, Heinekey and coworkers have reported the neutron diffraction structure of $IrH_2\{\kappa^3\text{-}P,C,P\text{-}[C_6H_3\text{-}1,3\text{-}(OP^tBu_2)_2]\}(\eta^2\text{-}H\text{-}BH_2)$, which contains a B-H σ-bond coordinated to iridium with a B-H distance of 1.45(5) Å. The pinacolborane (HBpin) counterpart losses molecular hydrogen to afford the square planar derivative $Ir\{\kappa^3\text{-}P,C,P\text{-}[C_6H_3\text{-}1,3\text{-}(OP^tBu_2)_2]\}(\eta^2\text{-}H\text{-}Bpin)$.[11] Our group has described the coordination of catecholborane (HBcat) and HBpin to the osmium dihydride $OsH_2(CO)(P^iPr_3)_2$ to give $OsH_2(CO)(\eta^2\text{-}H\text{-}BR_2)(P^iPr_3)_2$.[12] There are also a few (C_5Me_5)Rh-complexes bearing hydride and boryl ligands, which show separations between the boron and a hydride in the range 1.60-2.0 Å.[13] For these compounds, which could be considered the borane counterparts of the elongated dihydrogen species on the base of this separation, a "residual" B···H interaction has been suggested, although no clear evidence on

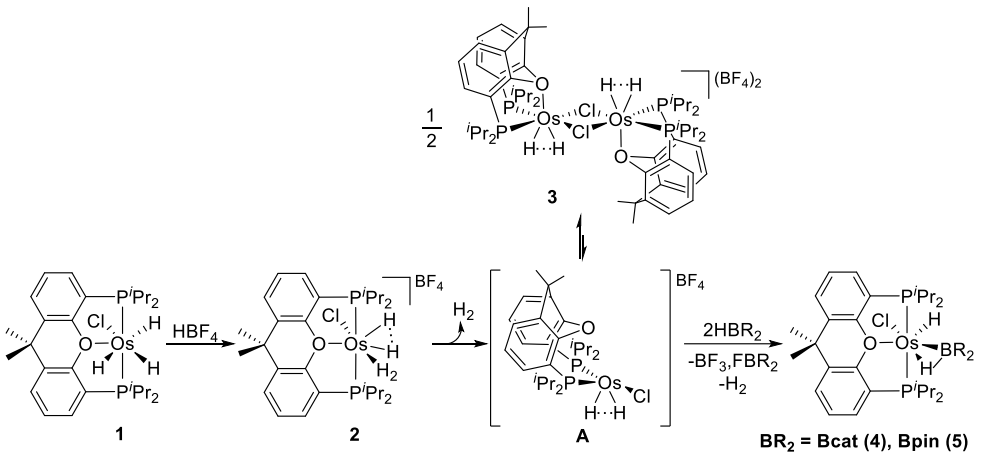

Scheme 1. Formation of Elongated σ-Borane complexes **4** and **5.**

their nature has been provided. In contrast to dihydrogen complexes, it remains difficult to assign a correct formulation on the basis of ^{11}B and ^{1}H NMR.[14] Thus, the development of simple methods to assert nature of the interaction of the B-H bond with the metal center, discerning between σ-borane and elongated σ-borane, is a need of the field.

Ether-diphosphines (POP) are flexible, which allows them to change their coordination fashion for adapting to the requirement of the participating intermediates in multistep processes.[15] As a consequence of this ability, platinum group metals containing these ligands are playing a main role in homogeneous catalysis.[16] In addition, we have recently shown that osmium polyhydrides bearing 9,9-dimethyl-4,5-bis(diisopropylphosphine)xanthene (xant(P^iPr_2)$_2$) sequentially add H^+ and H^- or H^- and H^+ to generate molecular hydrogen in a cyclic manner. During the process the ether-diphosphine changes its coordination mode to stabilize both dihydride and dihydrogen species. Dihydrogens are favored by a *mer* disposition of its donor atoms.[17] The ability of the *mer*-Os(POP) skeleton to stabilize non-classical interactions prompted us to study the coordination of HBcat and HBpin to OsHX(POP) metal fragments (X=H, Cl), in order to analyze the influence of the X ligand on the addition degree of the B-H bond to the osmium atom.

This paper describes the formation of new elongated σ-borane and σ-borane complexes for a third-row metal of the platinum group; shows the first X-ray structures for this type of compounds in the osmium chemistry; and analyzes the osmium-borane bonding situation as a function of X, proving that Atom in Molecules (AIM), Natural Bond Orbital (NBO), and Energy Decomposition Analysis-Natural Orbital for Chemical Valence (EDA-NOCV) methods are a simple tool to distinguish between σ-borane and elongated σ-borane.

RESULTS AND DISCUSSION

Elongated σ-Boranes. We have recently shown that the trihydride derivative $OsH_3Cl\{\kappa^3$-*P,O,P*-[xant(P^iPr_2)$_2$]} (**1**) adds the proton of HBF_4 to afford the compressed dihydride-dihydrogen cation $[Os(H\cdots H)(\eta^2$-$H_2)Cl\{\kappa^3$-*P,O,P*-[xant(P^iPr_2)$_2$]}]$^+$ (**2**), which is stable under hydrogen atmosphere. Under argon, it dissociates the coordinated hydrogen molecule and the resulting unsaturated dihydride $[OsH_2Cl\{\kappa^2$-*P,P*-[xant(P^iPr_2)$_2$]}]$^+$ (**A**) rapidly reaches an equilibrium with the dimer $[(Os(H\cdots H)\{\kappa^3$-*P,O,P*-[xant($P^iPr_2$)$_2$]})$_2(\mu$-$Cl)_2]^{2+}$ (**3**). During the dimerization process, the ether-diphosphine changes its coordination fashion from κ^3-*mer* to κ^3-*fac*.[17] Now, we have observed that HBcat and HBpin trap the unsaturated dihydride **A**. In addition, the metal center promotes the heterolytic H-B bond activation of a borane molecule by using a fluoride of the $[BF_4]^-$ anion as an external base. Thus, the treatment of dichloromethane solutions of the BF_4-salt of **3** with 5.1 mol of HBcat and HBpin, at room temperature, for 10 min leads to the hydride-elongated σ-borane derivatives $OsHCl(\eta^2$-H-$BR_2)\{\kappa^3$-*P,O,P*-[xant(P^iPr_2)$_2$]}(BR_2 = Bcat (**4**), Bpin (**5**)), which were isolated as white solids in 50-60% yield, together with FBR_2 ($\delta_{11B,}$ 22.5), BF_3 (δ_{11B}, 0.0), and H_2 (Scheme 1).

Complex **4** was characterized by X-ray diffraction analysis. The structure has two molecules chemically equivalent but crystallographically independent in the asymmetric unit. Figure 1 shows a view of one of them. The ether-diphosphine is *mer* coordinated with P(1)-Os-P(2), P(1)-Os-O(3), and P(2)-Os-O(3) angles of 161.98(3)° and 161.85(3)°, 80.98(6)° and 81.30(6), and 81.27(6) and 80.90(6), respectively. Thus, the coordination polyhedron around the metal center can be rationalized as a distorted octahedron. The perpendicular plane to the P(1)-Os-P(2) direction contains the hydride H(01) ligand disposed trans to the oxygen atom of the ether-diphosphine (H(01)-Os-O(3) = 165.6(9)° and 166.2(9)°) and the coordinated catecholborane molecule situated trans to the chloride ligand with the hydrogen atom H(02) pointing out the ether. The coordination of the B-H bond promotes its elongation. The B-H(02) distances of 1.68(2) and 1.67(2) Å, 1.601 Å in the DFT-optimized structure, agree well with the shortest B-H distance in the rhodium complex $Rh(\eta^5$-$C_5Me_5)(Bpin)_2(\eta^2$-HBpin) (1.53(3) and 1.69(3) Å)[13] and support the elongated σ-borane character of this species. The B-M-H angles in both compounds are also similar, 53.6(9)° and 53.1(9)° in **4** *versus* 47.5(8)° and 54.3(10)° in the rhodium derivative. The B-H(02) distance is about 0.5 Å longer than the B-H(Os) bond lengths in the tetrahydridoborate derivative $OsH_3(\kappa^2$-$H_2BH_2)(IPr)(P^iPr_3)$ (1.18(3) and 1.17(3) Å. IPr = 1,3-bis(2,6-diisopropylphenylimidazolylidene)[18] and about 0.4 Å longer than the B-H(Os) distances in the dihydrideborate species $Os(Bcat)(\kappa^2$-$H_2Bcat)(CO)(P^iPr_3)$ (1.26(3) and 1.27(3) Å).[12b] However, interestingly, the B-H(02) distance is only slightly shorter than the separation between the boron atom and the hydride ligand H(01), 1.70(2) and 1.70(2) Å; 1.770 Å in the

DFT-optimized structure. This is consistent with a *cis*-hydride-elongated σ-borane interaction. "Residual" contacts of this type are common in *cis*-hydride-elongated dihydrogen species.[2c,19] Nevertheless, in this case, it does not appear to involve a true covalent bond (*vide infra*). It seems to be related to the geometry of the complex and the size of the involved atoms and could be magnified by the different sign of the partial charges on the hydride and on the boron atom of the borane. The interaction between the metal center and the coordinated B-H bond is certainly strong. Thus, the Os-B bond lengths of 2.036(4) and 2.042(4) Å, 2.054 Å in the DFT-optimized structure, compare well with the reported Os-boryl distances.[12,20]

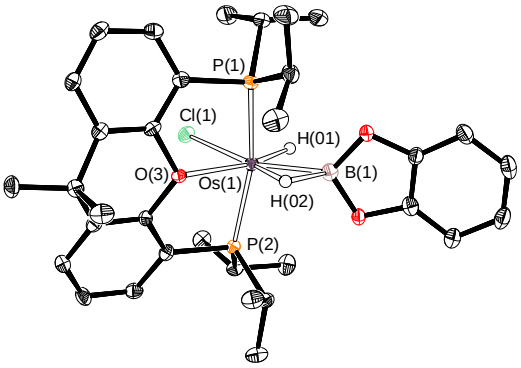

Figure 1. ORTEP diagram of one of the two molecules chemically equivalent but crystallographically independent in the asymmetric unit of the complex **4** with 50 % probability ellipsoids. The solvent molecule and hydrogen atoms (except H(01) and H(02)) are omitted for clarity. Selected bond lengths (Å) and angles (deg): Os(1)-B(1) = 2.036(4) and 2.042(4), Os(1)-O(3) = 2.259(2) and 2.251(2), Os(1)-P(2) = 2.3047(8) and 2.3175(8), Os(1)-P(1) = 2.3167(8) and 2.3046(8), Os(1)-Cl(1) = 2.4694(8) and 2.4694(8), Os(1)-H(01) = 1.582(10) and 1.588(10), Os(1)-H(02) = 1.590(10) and 1.585(10), B(1)-H(01) = 1.70(2) and 1.70(2), B(1)-H(02) = 1.68(2) and 1.67(2), P(1)-Os(1)-P(2) = 161.98(3) and 161.85(3), P(2)-Os(1)-O(3) = 81.27(6) and 80.90(6), P(1)-Os(1)-O(3) = 80.98(6) and 81.30(6), B(1)-Os(1)-H(02) = 53.6(9) and 53.1(9), O(3)-Os(1)-H(01) = 165.6(9) and 166.2(9).

Complex **5** was also characterized by X-ray diffraction analysis. Figure 2 shows a view of the molecule. The coordination polyhedron around the osmium atom resembles that of **4** with a H-Bpin group instead of the H-Bcat ligand and P-Os-P, P-Os-O(2), and H(01)-Os-O(2) angles of 163.05(2)°, 81.577(11)°, and 165.9(10)°, respectively. The strength of the interaction between the B-H bond and the metal center is similar in both compounds. Thus, the B-H(02) and Os-B distances of 1.69(2) and 2.075(3) Å, respectively, 1.623 and 2.071 Å in the DFT-optimized structure, compare well with those of **4**.

The $^{31}P\{^{1}H\}$, ^{1}H, and ^{11}B NMR spectra of **4** and **5** are consistent with the structures depicted in Figures 1 and 2. In agreement with the *mer*-coordination of the ether-diphosphine, the $^{31}P\{^{1}H\}$ NMR spectra, in benzene-d_6, at room temperature contain a singlet at about 36 ppm. Under the same conditions, the hydride ligand of **4** gives rise to a broad signal at -11.44 ppm in the ^{1}H NMR spectrum, which splits into a triplet ($^{2}J_{H\text{-}P}$ = 11.0 Hz) in dichloromethane-d_2 at 243 K, whereas the hydride ligand of **5** displays a triplet ($^{2}J_{H\text{-}P}$ = 11.0 Hz) at -12.99 ppm. In contrast to the hydride ligand, the coordinated BH-hydrogen atom gives rise to a broad resonance at -16.59 ppm for **4** and -16.99 ppm for **5**, at 243 K and at room temperature. The ^{11}B NMR spectra, in benzene-d_6, at room temperature shows a broad signal at 52.0 ppm for **4** and 46.5 pm for **5**.

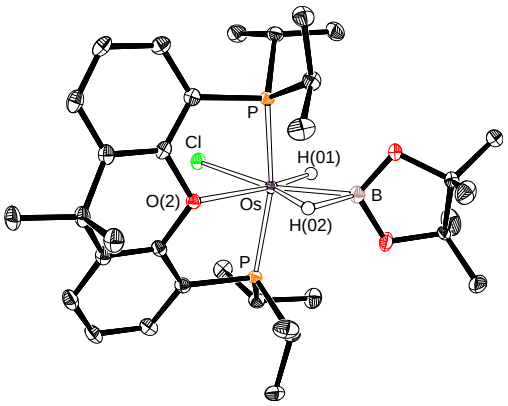

Figure 2. ORTEP diagram of complex **5** with 50 % probability ellipsoids. Hydrogen atoms (except H(01) and H(02)) are omitted for clarity. Selected bond lengths (Å) and angles (deg): Os-B(1) = 2.075(3), Os-O(2) = 2.2644(15), Os-P = 2.2989(4), Os-Cl = 2.4603(5), Os-H(01) = 1.577(10), Os-H(02) = 1.586(10), B(1)-H(01) = 1.75(3), B(1)-H(02) = 1.69(2), P-Os-P = 163.05(2), P-Os-O(2) = 81.577(11), H(01)-Os-O(2) = 165.9(10), B(1)-Os-H(02) = 53.1(9).

σ-Borane. In spite of its thermal stability and low tendency to undergo reductive elimination of molecular hydrogen,[21] the classical tetrahydride $OsH_4\{\kappa^3\text{-}P,O,P\text{-}[xant(P^iPr_2)_2]\}$ (**6**) rapidly reacts with HBcat. The addition of 1.1 mol of the borane to benzene solutions of **6** leads to the osmium(II)-dihydride-σ-borane derivative $OsH_2(\eta^2\text{-H-Bcat})\{\kappa^3\text{-}P,O,P\text{-}[xant(P^iPr_2)_2]\}$ (**7**), as a result of the formal replacement of a hydrogen molecule by the B-H bond of HBcat (eq. 1).

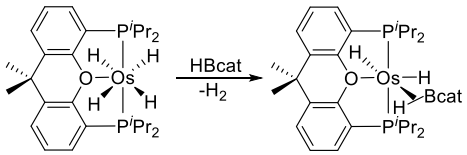

6 **7** (1)

Complex **7** was isolated as a white solid in 80% yield and characterized by X-ray diffraction analysis. Figure 3 shows a view of the molecule. The ether-diphosphine is *mer*-coordinated with P(1)-Os-P(2), P(1)-Os-O(3), and P(2)-Os-O(3) angles of 161.89(4)°, 82.06(7)°, and 81.29(7)°, respectively. Thus, the coordination polyhedron around the metal center is similar to that found for **4** with a hydride ligand (H(03)) in the position of the chloride anion and a H(02)-Os-O(3) angle of 162.6(17)°. The chloride by hydride replacement decreases the strength of the interaction between the metal center and the borane. As a consequence, the B-H distance of 1.49(4) Å (B(1)-H(01)), 1.434 Å in the DFT-optimized structure, is between 0.1 and 0.2 Å shorter than in **4**. The B-Os-H angle of 45.5(15)° (B(1)-Os-H(01)) is also smaller. Both the B-H distance and the B-M-H angle are similar to those reported for the iridium complex $Ir\{\kappa^3\text{-}P,C,P\text{-}[C_6H_3\text{-}1,3\text{-}(OP^tBu_2)_2]\}(\eta^2\text{-H-Bpin})$ (1.47(6) Å and 45(2)°).[11] As expected, and in contrast to the B-H bond length, the Os-B distance of 2.057(4) Å, 2.088 Å in the DFT-optimized structure, is between 0.02 and 0.04 Å longer than in **4**. Like in the later, the boron atom and its *cisoid* hydride H(02) are close, although

the separation between them of 1.81(4) Å, 1.926 Å in the DFT-optimized structure, is about 0.1-0.2 Å longer than in **4**; i.e., the boron atom moves away from the hydride the same as approaches the hydrogen atom. This again suggests that in these compounds the proximity between the boron atom and the hydride is a consequence of the geometry of the complexes and the size of the involved atoms.

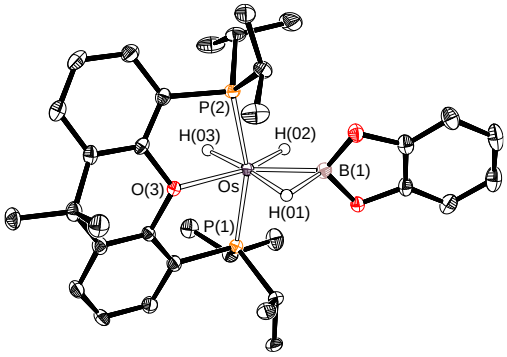

Figure 3. ORTEP diagram of complex **7** with 50 % probability ellipsoids. Hydrogen atoms (except H(01), H(02) and H(03)) are omitted for clarity. Selected bond lengths (Å) and angles (deg): Os-B(1) = 2.057(4), Os-O(3) = 2.271(3), Os-P(1) = 2.2832(10), Os-P(2) = 2.2808(10), Os-H(01) = 1.69(5), Os-H(02) = 1.579(14), Os-H(03) = 1.590(14), B(1)-H(01) = 1.49(4), B(1)-H(02) = 1.81(4), P(1)-Os-P(2) = 161.89(4), P(1)-Os-O(3) = 82.06(7), P(2)-Os-O(3) = 81.29(7), H(02)-Os-O(3) = 162.6(17), B(1)-Os-H(01) = 45.5(15).

The ^{1}H, ^{11}B, and ^{31}P{^{1}H} NMR spectra of **7** are consistent with the structure shown in the Figure 3. The ^{1}H NMR spectrum, in toluene-d_8, at 193 K shows the B-H resonance at -1.9 ppm along with the signals corresponding to the inequivalent hydrides at -5.60 and -18.8 ppm. The B-H resonance is temperature invariant between 193 and 298 K. However, the hydride signals are temperature dependent (Figure 4). Thus, they coalesce at 233 K and a hydride signal is observed above this temperature. Figure 4 reveals that the hydride ligands undergo a thermally activated site exchange process, which takes place with an activation barrier of 9 kcal·mol^{-1}.[22] This behavior agrees well with that observed for the iridium complex IrH$_2${κ^3-*P*,*C*,*P*-[C$_6$H$_3$-1,3-(OP^{t}Bu$_2$)$_2$]}(η^2-HBpin)[11] and the osmium-carbonyl derivatives OsH$_2$(CO)(η^2-H-BR$_2$)(P^{i}Pr$_3$)$_2$ (BR$_2$ = Bcat, Bpin).[12] The presence of the coordinated H-B bond is also supported by the ^{11}B NMR spectrum at room temperature, which contains a broad resonance centered at 45.5 ppm. A singlet at 56.0 ppm in the ^{31}P{^{1}H} NMR spectrum is another characteristic feature of this complex.

The promptly formation of **7** according to eq 1 is not consistent with the saturated character of **6** neither with a dissociation of the xanthene-ether group prior to the borane coordination. Because transition metal hydride complexes are usually amphoteric,[23] they can experience autoionization. In the case of **7**, this should imply the formation of the previously described pentahydride [OsH$_5${κ^2-*P*,*P*-[xant(P^{i}Pr$_2$)$_2$]}]$^-$ (**8**),[17] containing a *P*,*P*-bidentate ether-diphosphine, and the unsaturated osmium (IV) cation [OsH$_3${κ^3-*P*,*O*,*P*-[xant(P^{i}Pr$_2$)$_2$]}]$^+$ (**B** in eq 2). Thus, the boron atom of the borane could undergo the nucleophilic attack of the pentahydride, which should give rise to the release of a hydride and the formation of OsH$_5$(Bcat){κ^2-*P*,*P*-[xant(P^{i}Pr$_2$)$_2$]} (**C**), a boryl-pentahydride counterpart of the previously reported hexahydride OsH$_6${κ^2-

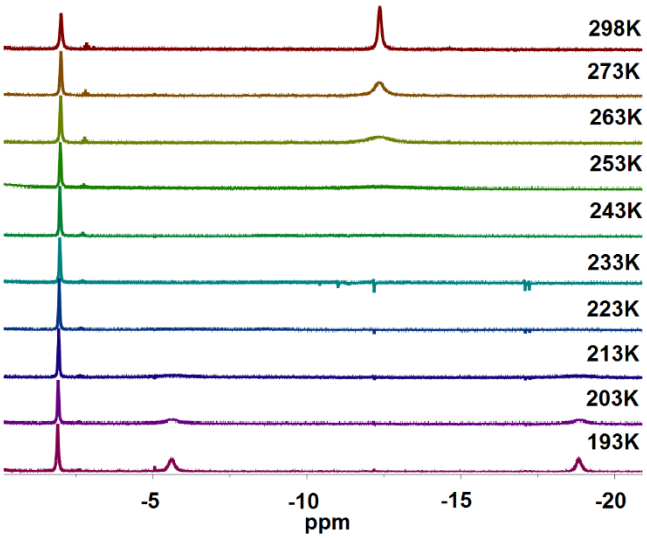

Figure 4. High-field region of the ^{1}H NMR spectrum of **7** between 298 and 193 K.

P,*P*-[xant(P^{i}Pr$_2$)$_2$]}[16d] (eq 3). Then, the generated hydride should be trapped by the cation **B** to again afford **6** (eq 4), which could further react in the same way until the consumption of the borane, whereas the coordination of the oxygen atom of the xanthene group of **C** should produce the release of molecular hydrogen and the formation of **7** (eq 5).

$$2\ \underset{\mathbf{6}}{OsH_4\{\kappa^3\text{-}P,O,P\text{-}[xant(P^iPr_2)_2]\}} \rightleftharpoons$$

$$\rightleftharpoons \underset{\mathbf{8}}{[OsH_5\{\kappa^2\text{-}P,P\text{-}[xant(P^iPr_2)_2]\}]^-} + \underset{\mathbf{B}}{[OsH_3\{\kappa^3\text{-}P,O,P\text{-}[xant(P^iPr_2)_2]\}]^+} \quad (2)$$

$$\underset{\mathbf{8}}{[OsH_5\{\kappa^2\text{-}P,P\text{-}[xant(P^iPr_2)_2]\}]^-} + HBcat \longrightarrow$$

$$\longrightarrow \underset{\mathbf{C}}{OsH_5(Bcat)\{\kappa^2\text{-}P,P\text{-}[xant(P^iPr_2)_2]\}} + H^- \quad (3)$$

$$\underset{\mathbf{B}}{[OsH_3\{\kappa^3\text{-}P,O,P\text{-}[xant(P^iPr_2)_2]\}]^+} + H^- \longrightarrow$$

$$\longrightarrow \underset{\mathbf{6}}{OsH_4\{\kappa^3\text{-}P,O,P\text{-}[xant(P^iPr_2)_2]\}} \quad (4)$$

$$\underset{\mathbf{C}}{OsH_5(Bcat)\{\kappa^2\text{-}P,P\text{-}[xant(P^iPr_2)_2]\}} \longrightarrow$$

$$\longrightarrow \underset{\mathbf{7}}{OsH_2(\eta^2\text{-}H\text{-}Bcat)\{\kappa^3\text{-}P,O,P\text{-}[xant(P^iPr_2)_2]\}} + H_2 \quad (5)$$

The formation of **7** according to the 2-5 reactions sequence involves the heterolytic addition of the H-B bond of HBcat to different metal centers. In order to prove that this reactions sequence is a reasonable proposal, we carried out the reaction of **6** with ClBcat. As expected, the addition of 0.5 equiv of the boron reagent to a benzene-d_6 solution of the tetrahydride immediately gives a quantitative 1:1 mixture of **7** and **1** (eq 6).

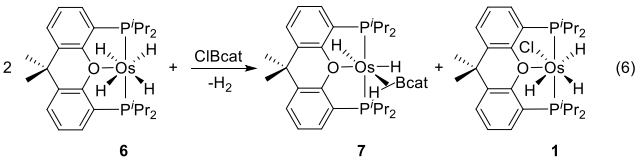

(6)

Bonding Situation. The bonding situation in complexes **4** and **7** was analyzed by means of DFT calculations, using the dispersion corrected BP86-D3 functional. The nature of the osmium-boron interactions was investigated using AIM, NBO, and EDA-NOCV methods. Figure 5 shows the Laplacian

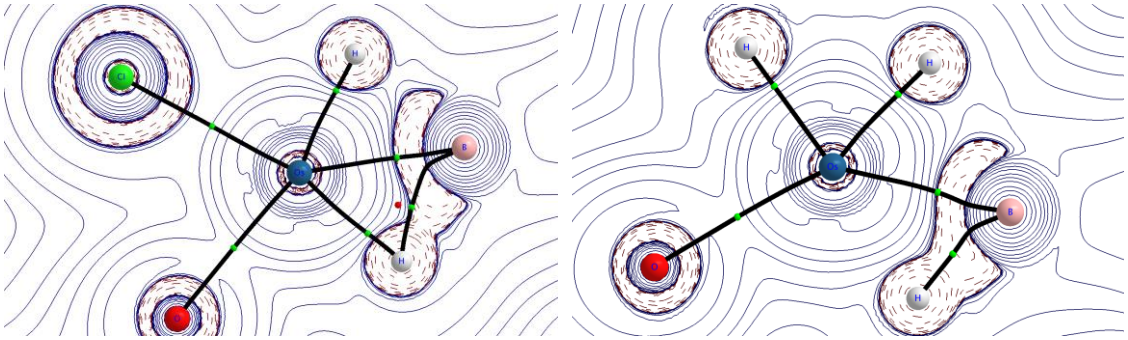

4 **7**

Figure 5. Contour line diagrams $\nabla^2\rho(r)$ for complexes **4** and **7** in the O−Os−B plane. Solid lines indicate areas of charge concentration ($\nabla^2\rho(r) < 0$) while dashed lines show areas of charge depletion ($\nabla^2\rho(r) > 0$). The solid lines connecting the atomic nuclei are the bond paths while the small green and red spheres indicate the corresponding bond critical points and ring critical points, respectively.

distributions in the Os−H−B plane for complexes **4** and **7**. Both species exhibit a significant Os−B interaction as revealed by the occurrence of a bond critical point (BCP) located between the transition metal and the boron atom, which is associated with a bond path (BP) running between both atoms. Interestingly, whereas a BCP between the osmium and the adjacent hydrogen atom close to the boron is located in complex **4**, no such Os−H interaction is found for complex **7** (i.e. absence of a BCP and corresponding BP between both atoms). This finding is consistent with the calculated Wiberg Bond Indices (WBI) for the respective Os–B and Os–H bonds. Thus, whereas similar WBIs were computed for the Os–B bond of both complexes (WBI = 0.68 and 0.65, for compounds **4** and **7**, respectively), rather different indices were computed for the Os–H interaction. Indeed, the much lower WBI value of 0.36 computed for **7** (WBI = 0.51 for **4**) clearly suggests that the Os–H interaction is much weaker in **7** than in **4**. As a consequence, no BCP was located in the corresponding AIM diagram. Therefore, the NBO and AIM methods indicate that although the Os–B bond strength is rather similar in both complexes, their bonding situations are markedly different. While the elongated σ-borane complex **4** is characterized by a three-membered cyclic species possessing one OsBH ring critical point, the σ-borane compound **7** lacks this triangular topology.

In order to gain more quantitative insight into the bonding situation of complexes **4** and **7**, the EDA-NOCV method was applied next. This method combines charge (NOCV) and energy (EDA) partitioning schemes to decompose the deformation density which is associated with the bond formation, Δρ, into different components of the chemical bond. The EDA-NOCV calculations provide pairwise energy contributions for each pair or interacting orbitals to the total bond energy (see further details in the computational details section).

The interaction between the neutral, closed-shell fragments OsHX(POP) and HBcat (X = Cl(**4**), H(**7**)) was considered for both complexes **4** and **7**. From the data in Table 1, it becomes evident that the above discussed weaker Os–H interaction in the σ-borane complex **7** leads to a significant reduction of the interaction between the HBcat ligand and the transition metal moiety with respect to complex **4** ($\Delta\Delta E_{int}$ = 31.9 kcal/mol). The EDA suggests that, despite the lower Pauli repulsion, this reduced interaction in complex **7** is mainly due to less stabilizing electrostatic ($\Delta\Delta E_{elstat}$ = 59.3 kcal/mol) and orbital ($\Delta\Delta E_{orb}$ = 34.7 kcal/mol) attractions.

Table 1. EDA-NOCV results (in kcal/mol) computed at the ZORA-BP86-D3/TZ2P+//BP86-D3/def2-SVP level.

	4	**7**
ΔE_{int}	-118.2	-86.3
ΔE_{Pauli}	298.3	234.7
ΔE_{elstat}[a]	-244.1 (58.6%)	-184.8 (57.6%)
ΔE_{orb}[a]	-160.8 (38.6%)	-126.1 (39.3%)
$\Delta E(\rho_1)$[b]	-47.2 (29.3%)	-28.9 (22.9%)
$\Delta E(\rho_2)$[b]	-83.9 (52.2%)	-71.6 (56.8%)
ΔE_{rest}[b]	-29.7 (18.5%)	-25.6 (20.3%)
ΔE_{disp}[a]	-11.5 (2.8%)	-10.1 (3.1%)

[a] Values within parentheses indicate the percentage to the total interaction energy, $\Delta E_{int} = \Delta E_{Pauli} + \Delta E_{elstat} + \Delta E_{orb} + \Delta E_{disp}$. [b] Values in parentheses are the percentage contributions to the total orbital interactions ΔE_{orb}.

The NOCV method provides further quantitative insight into the contributions to the total orbital attractions, which illustrate the different bonding situations in these complexes. Figure 6 shows the computed deformation densities Δρ, which indicate the charge flow in these species (the charge flow takes place in the direction red→blue). From the data in Figure 6, two main orbital interactions describe the σ-borane bonding situation, namely the donor-acceptor interaction involving the doubly-occupied σ(B–H) molecular orbital and a vacant d atomic orbital of the transition metal (ρ_1) and the reverse d(Os)→σ*(B–H) back-donation (ρ_2). According to the computed associated energies, both orbital interactions are significantly stronger in complex **4**, which is translated into the computed higher total orbital interactions (ΔE_{orb}) for this complex (see Table 1). Not surprisingly, the donation from the σ(B–H) molecular orbital is significantly stronger in complex **4** ($\Delta\Delta E(\rho_1)$ = 18.3 kcal/mol) due to the much higher electron withdrawing ability of the chloride ligand as compared to the hydride ligand in complex **7**. As a consequence of this stronger donation and the higher population of the corresponding σ*(B–H) molecular orbital ($\Delta\Delta E(\rho_2)$ = 12.3 kcal/mol), the B–

H bond is significantly longer in complex **4** (1.601 Å, exp. 1.68(2) and 1.67(2) Å) than in complex **7** (1.434 Å, exp. 1.49(4) Å). A similar effect has been observed for the coordination of dimethylaminoborane to the ruthenium fragments $RuHX(P^iPr_3)_2$ (X = H, Cl).[24]

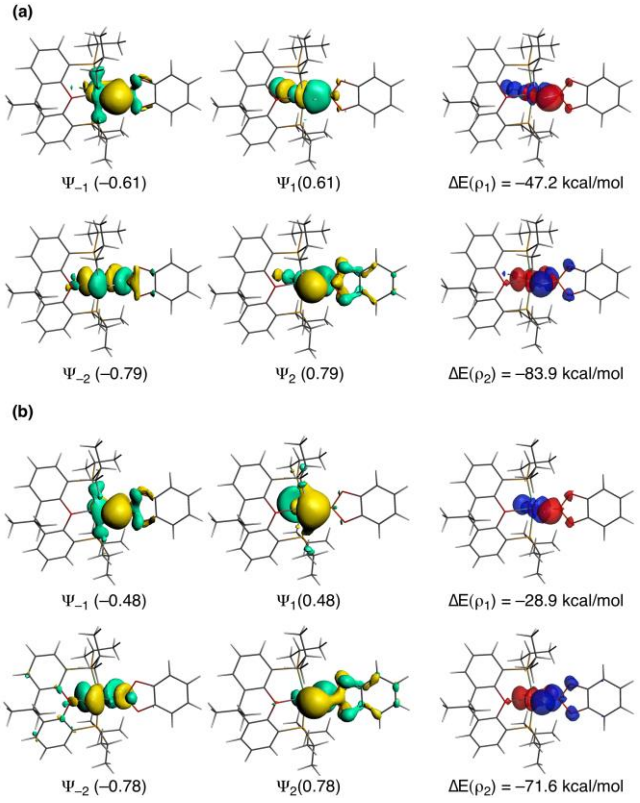

Figure 6. Most important NOCV pairs of orbitals Ψ_{-k}, Ψ_k with their eigenvalues $-\upsilon_k$, υ_k given in parentheses, and the associated deformation densities $\Delta\rho_k$ and orbital stabilization energies ΔE for the complexes **4** (a) and **7** (b). The charge flow in the deformation densities takes place in the direction red to blue.

CONCLUDING REMARKS

This study has revealed that the square pyramidal metal fragments $OsHX\{\kappa^3\text{-}P,O,P\text{-}[xant(P^iPr_2)_2]\}$ (X = Cl, H) stabilize the coordination of the B-H bond of boranes *trans* to the X ligand. The strength of the interaction between the metal center and the borane, which involves σ-donation from the doubly occupied σ(B-H) orbital to a vacant d atomic orbital of the metal and d(Os)→σ*(B-H) back-donation, is sensitive to the nature of X, being favored for chloride with regard to hydride. The electron withdrawing ability of the chloride ligand increases the donation from the σ(B-H) orbital to the osmium atom, whereas its π-donor power favors the d(Os)→σ*(B-H) back-donation. As a result, the coordinated B-H bond is significantly longer for complex **4** (X = Cl) than for **7** (X = H). The EDA-NOCV analysis suggests that the computed much lower interaction strength between the metal fragment $OsH_2\{\kappa^3\text{-}P,O,P\text{-}[xant(P^iPr_2)_2]\}$ and the borane is mainly due to less stabilizing electrostatic and orbital attractions.

The coordination of the borane to the metal fragment $OsHCl\{\kappa^3\text{-}P,O,P\text{-}[xant(P^iPr_2)_2]\}$ affords elongated σ-borane species, whereas the coordination to the dihydride counterpart $OsH_2\{\kappa^3\text{-}P,O,P\text{-}[xant(P^iPr_2)_2]\}$ gives a σ-borane compound. NBO-AIM analysis shows marked differences in the bonding situation of both types of derivatives. While elongated σ-borane complexes are characterized by a three-membered cycle possessing one OsBH ring critical point, the σ-borane compound lacks this triangular topology.

In conclusion, related elongated σ-borane and σ-borane complexes stabilized by OsHX(POP) metal fragments have been isolated, fully characterized, and the interaction between the metal fragments and the coordinated B-H analyzed as a function of X, from spectroscopic, X-ray diffraction, and theoretical points of view.

EXPERIMENTAL SECTION

General Information. All reactions were carried out under argon with rigorous exclusion of air using Schlenk tube or glovebox techniques. Solvents were dried by the usual procedures and distilled under argon prior to use or obtained oxygen- and water-free from an MBraun solvent purification apparatus. Pentane and dichloromethane were further stored over P_2O_5 in the glovebox. Toluene and benzene were stored over sodium in the glovebox. Pinacolborane was purchased from commercial sources and used without further purification. Catecholborane was purchased from commercial sources and distilled in a Kugelrohr distillation oven. Complexes $OsH_3Cl\{\kappa^3\text{-}P,O,P\text{-}[xant(P^iPr_2)_2]\}$ (**1**),[16d] $[(Os(H\cdots H)\{\kappa^3\text{-}P,O,P\text{-}[xant(P^iPr_2)_2]\})_2(\mu\text{-}Cl)_2][BF_4]_2$ (**3**),[17] and $OsH_4\{\kappa^3\text{-}P,O,P\text{-}[xant(P^iPr_2)_2]\}$ (**6**),[16d] were prepared according to published methods. ^1H, $^{31}P\{^1H\}$, ^{11}B and $^{13}C\{^1H\}$ NMR spectra were recorded on either a Bruker 300 ARX, Bruker Avance 300 MHz or a Bruker Avance 400 MHz instrument. Chemical shifts (expressed in parts per million) are referenced to residual solvent peaks (^1H, $^{13}C\{^1H\}$) or external H_3PO_4 ($^{31}P\{^1H\}$) and $BF_3{\cdot}OEt_2$ (^{11}B). Coupling constants, *J* and *N* ($N = J_{PH} + J_{P'H}$ for ^1H; $N = J_{PC} + J_{P'C}$ for ^{13}C) are given in hertz. Spectral assignments were achieved by ^1H-^1H COSY, $^1H\{^{31}P\}$, ^{13}C APT, ^1H-^{13}C HSQC and ^1H-^{13}C HMBC experiments. C and H analyses were carried out in a Perkin-Elmer 2400 CHNS/O analyzer. High-resolution electrospray mass spectra were acquired using a Micro-TOF-Q hybrid quadrupole time-of-flight spectrometer (Bruker Daltonics, Bremen, Germany).

Synthesis of $OsHCl(\eta^2\text{-H-Bcat})\{\kappa^3\text{-}P,O,P\text{-}[xant(P^iPr_2)_2]\}$ (4). To a suspension of $[(Os(H\cdots H)\{\kappa^3\text{-}P,O,P\text{-}[xant(P^iPr_2)_2]\})_2(\mu\text{-}Cl)_2][BF_4]_2$ (**3**) (50 mg; 0.033 mmol) in CH_2Cl_2 (3 mL) was added HBcat (18 µl; 0.169 mmol). After 10 min, the colorless solution obtained was taken to dryness. Addition of pentane (1mL) to the residue allowed the precipitation of a white solid, which was washed twice with pentane (2 mL) and dried under vacuum. Yield: 29 mg (56 %). Colorless crystals suitable for X-ray diffraction analysis were obtained by vapor diffusion of pentane into a toluene solution of the complex. Anal. Calcd. for $C_{33}H_{46}BClO_3OsP_2$: C, 50.23; H, 5.88. Found: C, 50.03; H, 5.95. HRMS (electrospray, m/z): calcd. for $C_{33}H_{46}BClNaO_3OsP_2$ $[M + Na]^+$: 813.2207, found: 831.2185. HRMS (electrospray, m/z): calcd. for $C_{33}H_{46}BO_3OsP_2$ $[M\text{-}Cl]^+$: 755.2632, found: 755.2600. ^1H NMR (300.13 MHz, C_6D_6, 293K): δ 7.32 (m, 2H, C*H*-arom), 7.16 (m, 2H, C*H*-arom), 7.15 (m, 2H, C*H*-arom Bcat), 7.03 (dd, $^3J_{HH}$ = 7.6, $^3J_{HH}$ = 7.5, 2H, C*H*-arom), 6.92 (m, 2H, C*H*-arom Bcat), 3.12 (m, 2H, PC*H*$(CH_3)_2$), 3.00 (m, 2H, PC*H*$(CH_3)_2$), 1.83 (dvt, $^3J_{HH}$ = 7.1, *N* = 14.5, 6H, PCH(C*H*$_3)_2$), 1.74 (dvt, $^3J_{HH}$ = 7.5, *N* = 16.1, 6H, PCH(C*H*$_3)_2$), 1.45 (s, 3H, C*H*$_3$), 1.11 (s, 3H, C*H*$_3$), 1.23-0.92 (12H, PCH(C*H*$_3)_2$), -11.44 (br, 1H, Os*H*), -15.73 (br, 1H, Os*H*). ^1H NMR (400.13 MHz, CD_2Cl_2, 243K): δ -12.53 (t, 1H, $^2J_{HP}$ = 11.0, Os*H*), -16.59 (br, 1H, Os(η^2-*H*-Bcat)). $^{13}C\{^1H\}$-APT NMR (75.47 MHz, C_6D_6, 293K): δ 158.9 (vt, *N* = 12.5, *C*-arom), 152.5 (s, *C* Bcat), 132.6 (vt, *N* = 5.6, *C*-arom), 130.8 (s, *C*H-arom), 126.9 (s, *C*H-arom), 126.3 (vt, *N* = 27.9, *C*-arom), 124.9 (vt, *N* = 4.8, *C*H-arom), 120.6 (s, *C*H-arom Bcat), 110.2 (s, *C*H-arom Bcat), 35.1 (s, C(*C*H$_3)_2$), 34.2 (s, *C*$(CH_3)_2$), 28.0 (vt, *N* = 29.6, P*C*H$(CH_3)_2$), 25.3 (vt, *N* = 25.5, P*C*H$(CH_3)_2$), 24.5 (s, C(*C*H$_3)_2$), 21.0 (s, PCH(*C*H$_3)_2$), 19.5 (s, PCH(*C*H$_3)_2$), 19.4 (vt, *N* = 9.4, PCH(*C*H$_3)_2$), 16.6 (s, PCH(*C*H$_3)_2$). $^{31}P\{^1H\}$ NMR (121.49 MHz, C_6D_6, 293K): δ 36.0 (s). ^{11}B NMR (96.29 MHz, C_6D_6, 293K): δ 52.0 (br).

Synthesis of OsHCl(η²-H-Bpin){κ³-*P,O,P*-[xant(P^{i}Pr$_2$)$_2$]} (5). To a suspension of [(Os(H···H){κ³-*P,O,P*-[xant(P^{i}Pr$_2$)$_2$]})$_2$(μ-Cl)$_2$][BF$_4$]$_2$ (**3**) (51 mg; 0.034 mmol) in CH_2Cl_2 (3 mL) was added HBpin (25 μl; 0.172 mmol). After 10 min, the colorless solution obtained was taken to dryness. Addition of pentane (1mL) to the residue allowed the precipitation of a white solid, which was washed twice with pentane (2 mL) and dried under vacuum. Yield: 30 mg (54 %). Colorless crystals suitable for X-ray diffraction analysis were obtained by vapor diffusion of pentane into a toluene solution of the complex. Anal. Calcd. for $C_{33}H_{54}BClO_3OsP_2$: C, 49.72; H, 6.83. Found: C, 49.83; H, 6.69. HRMS (electrospray, m/z): calcd. for $C_{33}H_{54}BClO_3NaOsP_2$ $[M + Na]^+$: 821.2833, found: 821.2833. HRMS (electrospray, m/z): calcd. for $C_{33}H_{54}BO_3OsP_2$ $[M - Cl]^+$: 763.3258, found: 763.3261. ^{1}H NMR (300.13 MHz, C_6D_6, 293K): δ 7.25 (m, 2H, C*H*-arom), 7.06 (dd, $^3J_{HH}$ = 7.6, $^4J_{HH}$ = 1.6, 2H, C*H*-arom), 6.93 (dd, $^3J_{HH}$ = 7.6, $^3J_{HH}$ = 7.4, 2H, C*H*-arom), 3.03 (m, 2H, PC*H*(CH$_3$)$_2$), 2.90 (m, 2H, PC*H*(CH$_3$)$_2$), 1.75 (dvt, $^3J_{HH}$ = 7.1, *N* = 14.7, 6H, PCH(C*H*$_3$)$_2$), 1.62 (dvt, $^3J_{HH}$ = 7.1, *N* = 17.0, 6H, PCH(C*H*$_3$)$_2$), 1.35 (s, 3H, C*H*$_3$), 1.18 (s, 12H, C*H*$_3$ Bpin), 1.06 (s, 3H, C*H*$_3$), 1.06 (m, 6H, PCH(C*H*$_3$)$_2$), 1.10 (m, 6H, PCH(C*H*$_3$)$_2$), -12.99 (t, $^2J_{HP}$ = 11.0, 1H, Os*H*), -16.99 (br, 1H, Os(η²-*H*-Bcat)). ^{13}C{^{1}H}-APT NMR (75.48 MHz, C_6D_6, 293K): δ 159.3 (vt, *N* = 12.5, *C*-arom), 132.6 (vt, *N* = 5.4, *C*-arom), 131.2 (s, *C*H-arom), 127.4 (vt, *N* = 26.1, *C*-arom), 127.0 (s, *C*H-arom), 124.8 (vt, *N* = 4.9, *C*H-arom), 82.4 (s, *C* Bpin), 35.6 (s, C(*C*H$_3$)$_2$), 34.4 (s, *C*(CH$_3$)$_2$), 27.6 (vt, *N* = 29.2, P*C*H(CH$_3$)$_2$), 25.8 (vt, *N* = 24.5, P*C*H(CH$_3$)$_2$), 25.1 (s, C(*C*H$_3$)$_2$), 24.9 (s, *C*H$_3$ Bpin), 21.4 (s, PCH(*C*H$_3$)$_2$), 19.9 (s, PCH(*C*H$_3$)$_2$), 19.8 (vt, *N* = 10.0, PCH(*C*H$_3$)$_2$), 16.9 (s, PCH(*C*H$_3$)$_2$). ^{31}P{^{1}H} NMR (121.49 MHz, C_6D_6, 293K): δ 35.6 (s). ^{11}B NMR (96.29 MHz, C_6D_6, 293K): δ 46.5 (br).

Synthesis of OsH$_2$(η²-H-Bcat){κ³-*P,O,P*-[xant(P^{i}Pr$_2$)$_2$]} (7). HBcat (44 μl; 0.400 mmol) was added to a solution of OsH$_4${κ³-*P,O,P*-[xant(P^{i}Pr$_2$)$_2$]} (**6**) (230 mg; 0.360 mmol) in C_6H_6 (3 mL). After 15 min stirring, the solvent was evaporated and pentane (1 mL) was added to afford a white solid which was washed once with pentane (1 mL) and dried under reduced pressure. Yield: 221 mg (80 %). Colorless crystals suitable for X-ray diffraction analysis were obtained by vapor diffusion of pentane into a toluene solution of the complex. Anal. Calcd. for $C_{33}H_{47}BO_3OsP_2$: C, 52.52; H, 6.28. Found: C, 52.74; H, 6.32. HRMS (electrospray, m/z): calcd. for $C_{33}H_{47}BO_3OsP_2$ $[M]^+$: 755.2632, found: 755.2651. ^{1}H NMR (300.13 MHz, C_6D_6, 298K): δ 7.26 (m, 2H, C*H*-arom), 7.11 (m, 2H, C*H*-arom Bcat), 6.89 (m, 4H, C*H*-arom), 6.82 (m, 2H, C*H*-arom Bcat), 3.24 (m, 2H, PC*H*(CH$_3$)$_2$), 2.37 (m, 2H, PC*H*(CH$_3$)$_2$), 1.44 (dvt, $^3J_{HH}$ = 7.9, *N* = 16.6, 6H, PCH(C*H*$_3$)$_2$), 1.30 (s, 3H, C*H*$_3$), 1.21 (m. 18H, PCH(C*H*$_3$)$_2$,), 0.93 (s, 3H, C*H*$_3$), -1.87 (br, 1H, Os*H*), -12.23 (br, 2H, Os*H*). ^{1}H NMR (400 MHz, C_7D_8, 193K): δ -1.90 (br, 1H, Os*H*), -5.60 (br, 1H, Os*H*), -18.83 (br, 1H, Os*H*). ^{13}C{^{1}H}-APT NMR (100.62 MHz, C_7D_8, 298K): δ 161.9 (vt, *N* = 13.7, *C*-arom), 153.1 (s, *C* Bcat), 133.2 (vt, *N* = 5.4, *C*-arom), 129.6 (s, *C*H-arom), 127.6 (vt, *N* = 25.5, *C*-arom), 125.4 (s, *C*H-arom), 125.2 (vt, *N* = 4.5, *C*H-arom), 120.1 (s, *C*H-arom Bcat), 110.0 (s, *C*H-arom Bcat), 34.7 (s, *C*(CH$_3$)$_2$), 33.7 (s, C(*C*H$_3$)$_2$), 27.4 (vt, *N* = 23.5, P*C*H(CH$_3$)$_2$), 23.0 (vt, *N* = 31.6, P*C*H(CH$_3$)$_2$), 22.8 (s, C(*C*H$_3$)$_2$), 20.3 (s, PCH(*C*H$_3$)$_2$), 19.7 (vt, *N* = 11.1, PCH(*C*H$_3$)$_2$), 19.2 (vt, *N* = 11.1, PCH(*C*H$_3$)$_2$), 16.7 (s, PCH(*C*H$_3$)$_2$). ^{31}P{^{1}H} NMR (161.98 MHz, C_7D_8, 298K): δ 56.0 (s). ^{11}B NMR (96.29 MHz, C_7D_8, 298K): δ 45.5 (br).

Reaction of OsH$_4${κ³-*P,O,P*-[xant(P^{i}Pr$_2$)$_2$]} with ClBcat. In a nmr tube, a solution of ClBcat (5 mg; 0.032 mmol) in C_6D_6 (0.6 mL) was added to OsH$_4${κ³-*P,O,P*-[xant(P^{i}Pr$_2$)$_2$]} (**6**; 0.041 mg; 0.064 mmol). Immediate quantitative formation of a 1:1 mixture of complexes OsH$_2$(η²-H-Bcat){κ³-*P,O,P*-[xant(P^{i}Pr$_2$)$_2$]} (**7**) and OsH$_3$Cl{κ³-*P,O,P*-[xant(P^{i}Pr$_2$)$_2$]} (**1**) was observed according to NMR measurements.

Computational Details and Cartesian Coordinates of 4, 5, and 7. Geometry optimizations were performed without symmetry constraints using the Gaussian09[25] suite of programs at the BP86[26]/def2-SVP[27] level of theory using the D3 dispersion correction suggested by Grimme et al.[28] This level is denoted BP86-D3/def2-SVP. Complexes **4**, **5** and **7** were characterized by frequency calculations, and have positive definite Hessian matrices thus confirming that the computed structures are minima on the potential energy surface. WBIs have been computed using the NBO method.[29]

All AIM results described in this work correspond to calculations performed at the BP86-D3/6-31+G(d)/WTBS(for Os) level on the optimized geometry obtained at the BP86-D3/def2-SVP level. The WTBS (well-tempered basis sets)[30] have been recommended for AIM calculations involving transition metals.[31] The topology of the electron density was conducted using the AIMAll program package.[32]

The interaction between the transition metal fragment and the borane and HBcat in complexes **4** and **7** has been investigated with the EDA-NOCV method,[33] which combines the energy decomposition analysis (EDA)[34] with the natural orbitals for chemical valence (NOCV)[35] methods. Within this approach, the interaction energy can be decomposed into the following physically meaningful terms:

$\Delta E_{int} = \Delta E_{elstat} + \Delta E_{Pauli} + \Delta E_{orb} + \Delta E_{disp}$

The term ΔE_{elstat} corresponds to the classical electrostatic interaction between the unperturbed charge distributions of the deformed reactants and is usually attractive. The Pauli repulsion ΔE_{Pauli} comprises the destabilizing interactions between occupied orbitals and is responsible for any steric repulsion. The orbital interaction ΔE_{orb} accounts for charge transfer (interaction between occupied orbitals on one moiety with unoccupied orbitals on the other, including HOMO–LUMO interactions) and polarization (empty-occupied orbital mixing on one fragment due to the presence of another fragment). Finally, the ΔE_{disp} term takes into account the interactions which are due to dispersion forces.

The EDA-NOCV method makes it possible to further partition the total orbital interactions into pairwise contributions of the orbital interactions. Details of the method can be found in the literature.[36]

The EDA-NOCV calculations were carried out using the BP86-D3/def2-SVP optimized geometries with the program package ADF 2016.01 using the same functional (BP86-D3) in conjunction with a triple-ζ-quality basis set using uncontracted Slater-type orbitals (STOs) augmented by two sets of polarization function with a frozen-core approximation for the core electrons. An auxiliary set of s, p, d, f, and g STOs were used to fit the molecular densities and to represent the Coulomb and exchange potentials accurately in each SCF cycle.[37] Scalar relativistic effects were incorporated by applying the zeroth-order regular approximation (ZORA).[38] This level of theory is denoted BP86-D3/TZ2P//BP86-D3/def2-SVP.

Structural Analysis of Complexes 4, 5, and 7. The cif files of **4**, **5**, and **7** have been deposited with the Cambridge Crystallographic Data Center (Nos. CCDC 1552854 (**4**), CCDC 1552855 (**5**), and CCDC 1552856 (**7**)). X-ray data were collected for the complexes on a Bruker Smart APEX DUO (**5**) or Bruker Smart APEX CCD (**4**, **7**) diffractometers equipped with a normal focus, 2.4 kW sealed tube source (Mo radiation, λ = 0.71073 Å) operating at 50 kV and 40 mA (**4**) or 30 mA (**5** and **7**). Data were collected over the complete sphere. Each frame exposure time was 10 s (**5** and **7**), or 20 s (**4**) covering 0.3º in ω. Data were corrected for absorption by using a multiscan method applied with the SADABS program.[39] The structures were solved by Patterson or direct methods and refined by full-matrix least squares on F^2 with SHELXL2016,[40] including isotropic and subsequently anisotropic displacement parameters. The hydrogen atoms were observed in the least Fourier Maps or calculated, and refined freely or using a restricted riding model. The hydrogen bonded to metal atoms were observed in the last cycles of refinement but refined too close to metals, so a restricted refinement model was used for all of them (d(Os-H = 1.59(1) Å).

Crystal data for **4**: $C_{33}H_{46}BClO_3OsP_2$, 2(CH_2Cl_2), M_W 958.95, colourless, irregular block (0.238 x 0.188 x 0.082), triclinic, space group P-1, *a*: 11.8674(6) Å, *b*: 16.6502(8) Å, *c*: 20.7567(10) Å, *α*: 104.9620(10)°, *β*: 96.3580(10)°, *γ*: 90.0110(10)°, *V* = 3936.2(3) Å^3, *Z* = 4, *Z'* = 2, D_{calc}: 1.618 g cm^{-3}, F(000): 1920, T = 100(2) K, μ 3.694 mm^{-1}. 67147 measured reflections (2θ: 3-58º, ω scans 0.3º), 18814 unique (R_{int} = 0.0368); min./max. transm. Factors 0.659/0.862. Final agreement factors were R^1 = 0.0287 (15471 observed reflections, I > 2σ(I)) and wR^2 = 0.0659; data/restraints/parameters 18814/8/881; GoF = 0.998. Largest peak and hole 1.169 (close to osmium atom) and -1.063 e/ Å^3.

Crystal data for **5**: $C_{33}H_{54}BClO_3OsP_2$, M_W 797.16, colourless, irregular block (0.191 x 0.185 x 0.134), orthorhombic, space group

Pnma, *a*: 18.7529(17) Å, *b*: 18.1959(17) Å, *c*: 10.5608(10)Å, *V* = 3603.6(6) Å^3, *Z* = 4, *Z'* = 0.5, D_{calc}: 1.469 g cm^{-3}, F(000): 1616, T = 100(2) K, μ 3.731 mm^{-1}. 39075 measured reflections (2θ: 3-58º, ω scans 0.3º), 5004 unique (R_{int} = 0.0291); min./max. transm. Factors 0.739/0.862. Final agreement factors were R^1 = 0.0161 (4661 observed reflections, I > 2σ(I)) and wR^2 = 0.0424; data/restraints/parameters 5004/14/235; GoF = 0.998. Largest peak and hole 0.883 (close to osmium atoms) and -0.756 e/ Å^3.

Crystal data for **7**: $C_{33}H_{47}BO_3OsP_2$, M_W 754.65, colourless, irregular block (0.261 x 0.186 x 0.160), orthorhombic, space group Pna21, *a*: 19.3235(11) Å, *b*: 19.7359(11) Å, *c*: 8.6538(5) Å, *V* = 3300.3(3) Å^3, *Z* = 4, *Z'* = 1, D_{calc}: 1.519 g cm^{-3}, F(000): 1520, T = 100(2) K, μ 3.992 mm^{-1}. 31075 measured reflections (2θ: 3-57º, ω scans 0.3º), 7781 unique (R_{int} = 0.0284); min./max. transm. Factors 0.601/0.746. Final agreement factors were R^1 = 0.0193 (7372 observed reflections, I > 2σ(I)) and wR^2 = 0.0513; data/restraints/parameters 7781/3/381; GoF = 0.795. Largest peak and hole 0.806 (close to osmium atoms) and -0.644 e/ Å^3.

ASSOCIATED CONTENT

Supporting Information

The Supporting Information is available free of charge on the ACS Publications website.

NMR spectra and Total energies of **4**, **5** and **7**. (PDF)

Theoretical complex coordinates. (XYZ)

AUTHOR INFORMATION

Corresponding Author

*E-mail for M.A.E.: maester@unizar.es

Notes

The authors declare no competing financial interest.

ACKNOWLEDGMENT

Financial support from MINECO of Spain (Projects CTQ2013-44303-P, CTQ2014-52799-P, CTQ2016-78205-P and CTQ2016-81797-REDC), Diputación General de Aragón (E35), FEDER, and European Social Fund is acknowledged.

REFERENCES

(1) Esteruelas, M. A.; López, A. M.; Oliván, M. *Chem. Rev.* **2016**, *116*, 8770-8847.

(2) (a) Kubas, G. J. *Metal Dihydrogen and σ-Bond Complexes: Structure, Theory and Reactivity*; Kluwer: New York, 2001. (b) Kubas, G. J. *J. Organomet. Chem.* **2001**, *635*, 37-68. (c) Kubas, G. J. *Chem. Rev.* **2007**, *107*, 4152-4205. (d) Kubas, G. J. *J. Organomet. Chem.* **2014**, *751*, 33-49. (e) Crabtree, R. H. *Chem. Rev.* **2016**, *116*, 8750-8769.

(3) (a) Lin, Z. Y. *Chem. Soc. Rev.* **2002**, *31*, 239-245. (b) Lachaize, S.; Sabo-Etienne, S. *Eur. J. Inorg. Chem.* **2006**, 2115-2127. (c) Perutz, R. N.; Sabo-Etienne, S. *Angew. Chem., Int. Ed.* **2007**, *46*, 2578-2592.

(4) (a) Miyaura, N. *Bull. Chem. Soc. Jpn.* **2008**, *81*, 1535-1553. (b) Crudden, C. M.; Glasspoole, B. W.; Lata, C. J. *Chem. Commun.* **2009**, 6704-6716. (c) Dang, L.; Lin, Z. Y.; Marder, T. B. *Chem. Commun.* **2009**, 3987-3995. (d) Mkhalid, I. A. I.; Barnard, J. H.; Marder, T. B.; Murphy, J. M.; Hartwig, J. F. *Chem. Rev.* **2010**, *110*, 890-931. (e) Ros, A.; Fernández, R.; Lassaletta, J. M. *Chem. Soc. Rev.* **2014**, *43*, 3229-3243.

(5) (a) Hamilton, C. W.; Baker, R. T.; Staubitz, A.; Manners, I. *Chem. Soc. Rev.* **2009**, *38*, 279-293. (b) Waterman, R. *Chem. Soc. Rev.* **2013**, *42*, 5629-5641. (c) St John, A.; Goldberg, K. I.; Heinekey, D. M. *Top. Organomet. Chem.* **2013**, *40*, 271-287. (d) Rossin, A.; Peruzzini, M. *Chem. Rev.* **2016**, *116*, 8848-8872. (e) Bhunya, S.; Malakar, T.; Ganguly, G.; Paul, A. *ACS Catal.* **2016**, *6*, 7907-7934.

(6) Pandey, K. K. *Coord. Chem. Rev.* **2009**, *253*, 37-55.

(7) (a) Hartwig, J. F.; Muhoro, G. N.; He, X. M.; Eisenstein, O.; Bosque, R.; Maseras, F. *J. Am. Chem. Soc.* **1996**, *118*, 10936-10937. (b) Muhoro, C. N.; Hartwig, J. F. *Angew. Chem., Int. Ed. Engl.* **1997**, *36*, 1510-1512. (c) Muhoro, C. N.; He, X. M.; Hartwig, J. F. *J. Am. Chem. Soc.* **1999**, *121*, 5033-5046. (d) Lam, W. H.; Lin, Z. Y. *Organometallics* **2000**, *19*, 2625-2628.

(8) Schlecht, S.; Hartwig, J. F. *J. Am. Chem. Soc.* **2000**, *122*, 9435-9443.

(9) Crestani, M. G.; Muñoz-Hernández, M.; Arévalo, A.; Acosta-Ramírez, A.; García, J. J. *J. Am. Chem. Soc.* **2005**, *127*, 18066-18073.

(10) (a) Montiel-Palma, V.; Lumbierres, M.; Donnadieu, B.; Sabo-Etienne, S.; Chaudret, B. *J. Am. Chem. Soc.* **2002**, *124*, 5624-5625. (b) Lachaize, S.; Essalah, W.; Montiel-Palma, V.; Vendier, L.; Chaudret, B.; Barthelat, J. C.; Sabo-Etienne, S. *Organometallics* **2005**, *24*, 2935-2943. (c) Alcaraz, G.; Grellier, M.; Sabo-Etienne, S. *Acc. Chem. Res.* **2009**, *42*, 1640-1649.

(11) Hebden, T. J.; Denney, M. C.; Pons, V.; Piccoli, P. M. B.; Koetzle, T. F.; Schultz, A. J.; Kaminsky, W.; Goldberg, K. I.; Heinekey, D. M. *J. Am. Chem. Soc.* **2008**, *130*, 10812-10820.

(12) (a) Esteruelas, M. A.; López, A. M.; Mora, M.; Oñate, E. *Chem. Commun.* **2013**, *49*, 7543-7545. (b) Esteruelas, M. A.; López, A. M.; Mora, M.; Oñate, E. *Organometallics* **2015**, *34*, 941-946.

(13) Hartwig, J. F.; Cook, K. S.; Hapke, M.; Incarvito, C. D.; Fan, Y. B.; Webster, C. E.; Hall, M. B. *J. Am. Chem. Soc.* **2005**, *127*, 2538-2552.

(14) Alcaraz, G.; Sabo-Etienne, S. *Coord. Chem. Rev.* **2008**, *252*, 2395-2409.

(15) (a) Pontiggia, A. J.; Chaplin, A. B.; Weller, A. S. *J. Organomet. Chem.* **2011**, *696*, 2870-2876. (b) Dallanegra, R.; Chaplin, A. B.; Weller, A. S. *Organometallics* **2012**, *31*, 2720-2728.

(16) (a) Pawley, R. J.; Moxham, G. L.; Dallanegra, R.; Chaplin, A. B.; Brayshaw, S. K.; Weller, A. S.; Willis, M. C. *Organometallics* **2010**, *29*, 1717-1728. (b) Esteruelas, M. A.; Honczek, N.; Oliván, M.; Oñate, E.; Valencia, M. *Organometallics* **2011**, *30*, 2468-2471. (c) Miloserdov, F. M.; Grushin, V. V. *Angew. Chem., Int. Ed.* **2012**, *51*, 3668-3672. (d) Alós, J.; Bolaño, T.; Esteruelas, M. A.; Oliván, M.; Oñate, E.; Valencia, M. *Inorg. Chem.* **2013**, *52*, 6199-6213. (e) Esteruelas, M. A.; Oliván, M.; Vélez, A. *Inorg. Chem.* **2013**, *52*, 12108-12119. (f) Johnson, H. C.; Leitao, E. M.; Whitten, G. R.; Manners, I.; Lloyd-Jones, G. C.; Weller, A. S. *J. Am. Chem. Soc.* **2014**, *136*, 9078-9093. (g) Alós, J.; Bolaño, T.; Esteruelas, M. A.; Oliván, M.; Oñate, E.; Valencia, M. *Inorg. Chem.* **2014**, *53*, 1195-1209. (h) Ren, P.; Pike, S. D.; Pernik, I.; Weller, A. S.; Willis, M. C. *Organometallics* **2015**, *34*, 711-723. (i) Esteruelas, M. A.; Oliván, M.; Vélez, A. *Organometallics* **2015**, *34*, 1911-1924. (j) Esteruelas, M. A.; Oliván, M.; Vélez, A. *J. Am. Chem. Soc.* **2015**, *137*, 12321-12329. (k) Esteruelas, M. A.; Nolis, P.; Oliván, M.; Oñate, E.; Vallribera, A.; Vélez, A. *Inorg. Chem.* **2016**, *55*, 7176-7181.

(17) Esteruelas, M. A.; García-Yebra, C.; Martín, J.; Oñate, E. *Inorg. Chem.* **2017**, *56*, 676-683.

(18) Buil, M. L.; Cardo, J. J. F.; Esteruelas, M. A.; Fernández, I.; Oñate, E. *Inorg. Chem.* **2016**, *55*, 5062-5070.

(19) Jessop, P. G.; Morris, R. H. *Coord. Chem. Rev.* **1992**, *121*, 155-284.

(20) (a) Irvine, G. J.; Roper, W. R.; Wright, L. J. *Organometallics* **1997**, *16*, 2291-2296. (b) Rickard, C. E. F.; Roper, W. R.; Williamson, A.; Wright, L. J. *Organometallics* **1998**, *17*, 4869-4874. (c) Rickard, C. E. F.; Roper, W. R.; Williamson, A.; Wright, L. J. *Angew. Chem., Int. Ed.* **1999**, *38*, 1110-1113. (d) Rickard, C. E. F.; Roper, W. R.; Williamson, A.; Wright, L. J. *Organometallics* **2000**, *19*, 4344-4355. (e) Irvine, G. J.; Rickard, C. E. F.; Roper, W. R.; Williamson, A.; Wright, L. J. *Angew. Chem., Int. Ed.* **2000**, *39*, 948-950. (f) Rickard, C. E. F.; Roper, W. R.; Williamson, A.; Wright, L. J. *Organometallics* **2002**, *21*, 1714-1718. (g) Rickard, C. E. F.; Roper, W. R.; Williamson, A.; Wright, L. J. *Organometallics* **2002**, *21*, 4862-4872. (h) Rickard, C. E. F.; Roper, W. R.; Williamson, A.; Wright, L. J. *J. Organomet. Chem.* **2004**, *689*, 1609-1616. (i) Buil, M. L.; Esteruelas, M. A.; Garcés, K.; Oñate, E. *J. Am. Chem. Soc.* **2011**, *133*, 2250-2263. (j) Esteruelas, M. A.; Fernández, I.; López, A. M.; Mora, M.; Oñate, E. *Organometallics* **2012**, *31*, 4646-4649. (k) Esteruelas, M.

A.; López, A. M.; Mora, M.; Oñate, E. *Organometallics* **2012**, *31*, 2965-2970. (l) Buil, M. L.; Esteruelas, M. A.; Fernández, I.; Izquierdo, S.; Oñate, E. *Organometallics* **2013**, *32*, 2744-2752. (m) Braunschweig, H.; Légare, M. A.; Matler, A.; Wennemann, B. *Eur. J. Inorg. Chem.* **2016**, 3376-3379. (n) McQueen, C. M. A.; Hill, A. F.; Sharma, M.; Singh, S. K.; Ward, J. S.; Willis, A. C.; Young, R. D. *Polyhedron* **2016**, *120*, 185-195.

(21) Alós, J.; Esteruelas, M. A.; Oliván, M.; Oñate, E.; Puylaert, P. *Organometallics* **2015**, *34*, 4908-4921.

(22) $\Delta G/RT_c = 22.96 + Ln(T_c/\delta\nu)$.

(23) Morris, R. H. *Chem. Rev.* **2016**, *116*, 8588-8654.

(24) Bénac-Lestrille, G.; Helmstedt, U.; Vendier, L.; Alcaraz, G.; Clot, E.; Sabo-Etienne, S. *Inorg. Chem.* **2011**, *50*, 11039-11045.

(25) Frisch, M. J.; Trucks, G. W.; Schlegel, H. B.; Scuseria, G. E.; Robb, M. A.; Cheeseman, J. R.; Scalmani, G.; Barone, V.; Mennucci, B.; Petersson, G. A.; Nakatsuji, H.; Caricato, M.; Li, X.; Hratchian, H. P.; Izmaylov, A. F.; Bloino, J.; Zheng, G.; Sonnenberg, J. L.; Hada, M.; Ehara, M.; Toyota, K.; Fukuda, R.; Hasegawa, J.; Ishida, M.; Nakajima, T.; Honda, Y.; Kitao, O.; Nakai, H.; Vreven, T.; Montgomery, J. A., Jr.; Peralta, J. E.; Ogliaro, F.; Bearpark, M.; Heyd, J. J.; Brothers, E.; Kudin, K. N.; Staroverov, V. N.; Kobayashi, R.; Normand, J.; Raghavachari, K.; Rendell, A.; Burant, J. C.; Iyengar, S. S.; Tomasi, J.; Cossi, M.; Rega, N.; Millam, N. J.; Klene, M.; Knox, J. E.; Cross, J. B.; Bakken, V.; Adamo, C.; Jaramillo, J.; Gomperts, R.; Stratmann, R. E.; Yazyev, O.; Austin, A. J.; Cammi, R.; Pomelli, C.; Ochterski, J. W.; Martin, R. L.; Morokuma, K.; Zakrzewski, V. G.; Voth, G. A.; Salvador, P.; Dannenberg, J. J.; Dapprich, S.; Daniels, A. D.; Farkas, Ö.; Foresman, J. B.; Ortiz, J. V.; Cioslowski, J.; Fox, D. J. Gaussian 09, Revision B.01; Gaussian, Inc.: Wallingford, CT, 2009.

(26) Zhao, Y.; Schultz, N. E.; Truhlar, D. G. *J. Chem. Theory Comput.* **2006**, *2*, 364-382.

(27) Weigend, F.; Ahlrichs, R. *Phys. Chem. Chem. Phys.* **2005**, *7*, 3297-3305.

(27) Grimme, S.; Antony, J.; Ehrlich, S.; Krieg, H. *J. Chem. Phys.* **2010**, *132*.

(29) (a) Foster, J. P.; Weinhold, F. *J. Am. Chem. Soc.* **1980**, *102*, 7211-7218. (b) Reed, A. E.; Weinhold, F. *J. Chem. Phys.* **1985**, *83*, 1736-1740. (c) Reed, A. E.; Weinstock, R. B.; Weinhold, F. *J. Chem. Phys.* **1985**, *83*, 735-746. (d) Reed, A. E.; Curtiss, L. A.; Weinhold, F. *Chem. Rev.* **1988**, *88*, 899-926.

(30) (a) Huzinaga, S.; Miguel, B. *Chem. Phys. Lett.* **1990**, *175*, 289-291. (b) Huzinaga, S.; Kolbukowski, M. *Chem. Phys. Lett.* **1993**, *212*, 260-264.

(31) Cabeza, J. A.; Van der Maelen, J. F.; García-Granda, S. *Organometallics* **2009**, *28*, 3666-3672 and references therein.

(31) Keith, T. A., AIMA11, 2010, http://tkgristmill.com

(33) Mitoraj, M. P.; Michalak, A.; Ziegler, T. *J. Chem. Theory Comput.* **2009**, *5*, 962-975.

(34) For a recent review see: von Hopffgarten, M.; Frenking, G. *Wiley Interdisciplinary Reviews-Computational Molecular Science* **2012**, *2*, 43-62.

(34) Mitoraj, M.; Michalak, A. *J. Mol. Model.* **2007**, *13*, 347-355.

(36) See for instance: (a) Mitoraj, M. P.; Michalak, A.; Ziegler, T. *Organometallics* **2009**, *28*, 3727-3733. (b) Thi, A. N. N.; Frenking, G. *Chem. Eur. J.* **2012**, *18*, 12733-12748. (c) Parafiniuk, M.; Mitoraj, M. P. *Organometallics* **2013**, *32*, 4103-4113. (d) Mondal, K. C.; Samuel, P. P.; Roesky, H. W.; Carl, E.; Herbst-Irmer, R.; Stalke, D.; Schwederski, B.; Kaim, W.; Ungur, L.; Chibotaru, L. F.; Hermann, M.; Frenking, G. *J. Am. Chem. Soc.* **2014**, *136*, 1770-1773.

(37) Krijn, A.; Baerends, E. J.; Fit Functions in the HFS-Method, Internal Report (in Dutch), Vrije Universiteit Amsterdam, The Netherlands, **1984**.

(38) (a) van Lenthe, E.; Baerends, E. J.; Snijders, J. G. *J. Chem. Phys.* **1993**, *99*, 4597-4610. (b) van Lenthe, E.; Baerends, E. J.; Snijders, J. G. *J. Chem. Phys.* **1994**, *101*, 9783-9792. (c) van Lenthe, E.; Ehlers, A.; Baerends, E. J. *J. Chem. Phys.* **1999**, *110*, 8943-8953.

(39) Blessing, R. H. *Acta Cryst.* **1995**, A*51*, 33-38. SADABS: Area-detector absortion correction; Bruker-AXS, Madison, WI, **1996**.

(40) SHELXL-2016/6. Sheldrick, G. M. *Acta Cryst.* **2008**, *A64*, 112-122.

Table of Contents

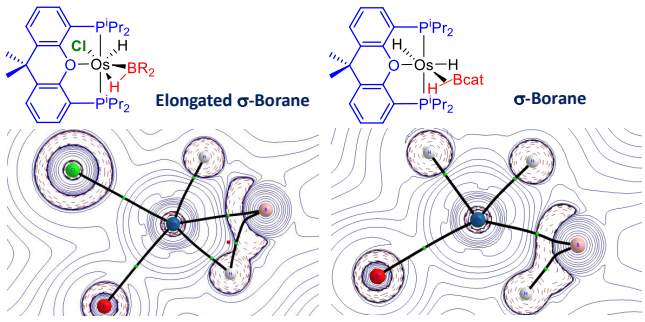

Supporting Information For

Elongated σ-Borane versus σ-Borane in Pincer-POP-Osmium Complexes

Miguel A. Esteruelas,[†] Israel Fernández,[‡] Cristina García-Yebra,[†] Jaime Martín,[†] and Enrique Oñate[†]*

[†]Departamento de Química Inorgánica, Instituto de Síntesis Química y Catálisis Homogénea (ISQCH), Centro de Innovación en Química Avanzada (ORFEO – CINQA), Universidad de Zaragoza – CSIC, 50009 Zaragoza, Spain

[‡]Departamento de Química Orgánica I, Facultad de Ciencias Químicas, Centro de Innovación en Química Avanzada (ORFEO-CINQA), Universidad Complutense de Madrid, 28040 Madrid, Spain

* Corresponding author's e-mail address: maester@unizar.es

Contents:

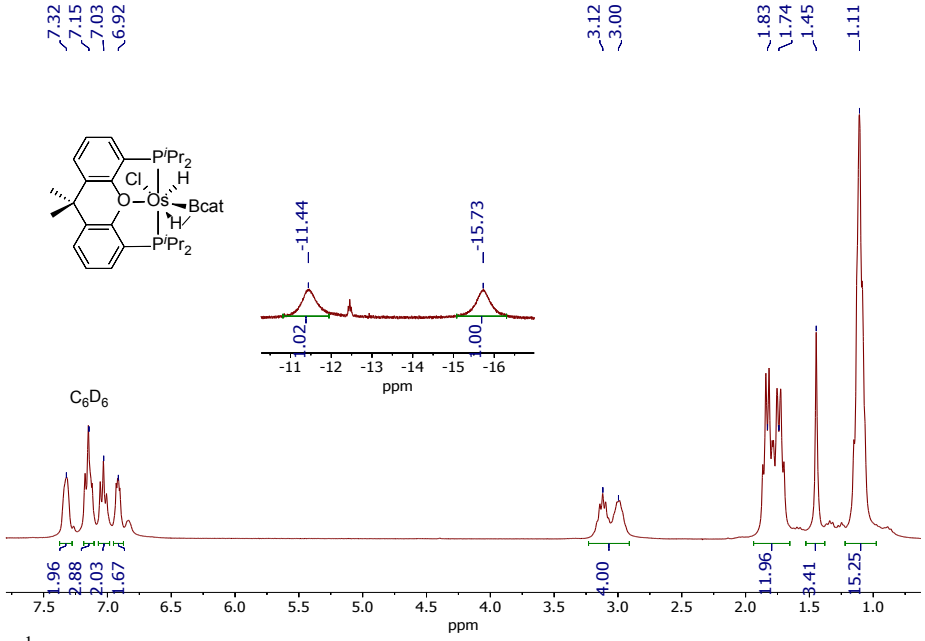

Figure S1. ^{1}H NMR (300.13 MHz, C_6D_6, 293 K) spectrum of complex **4**.

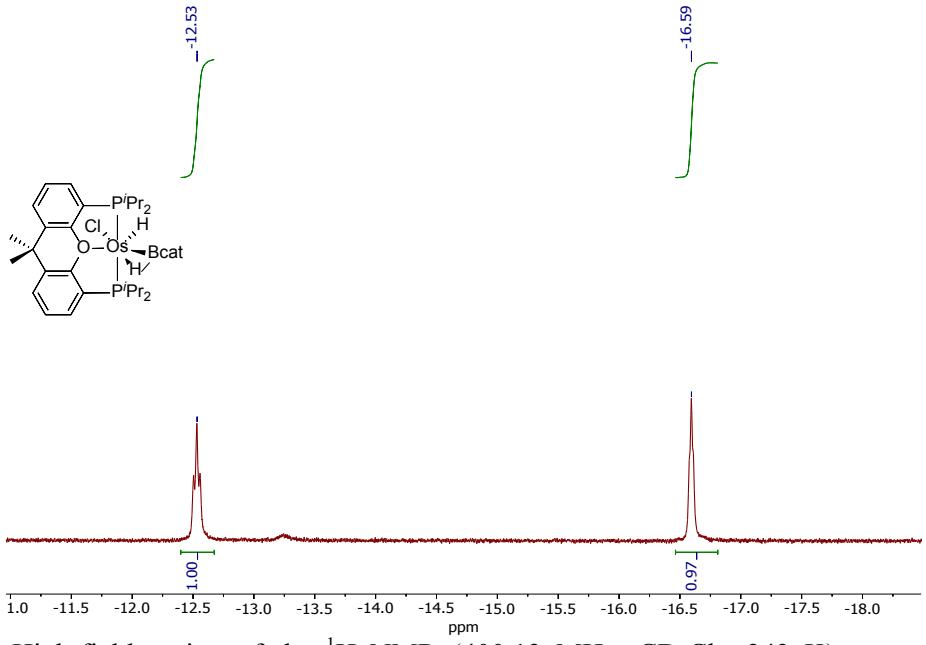

Figure S2. High-field region of the ^{1}H NMR (400.13 MHz, CD_2Cl_2, 243 K) spectrum of complex **4**.

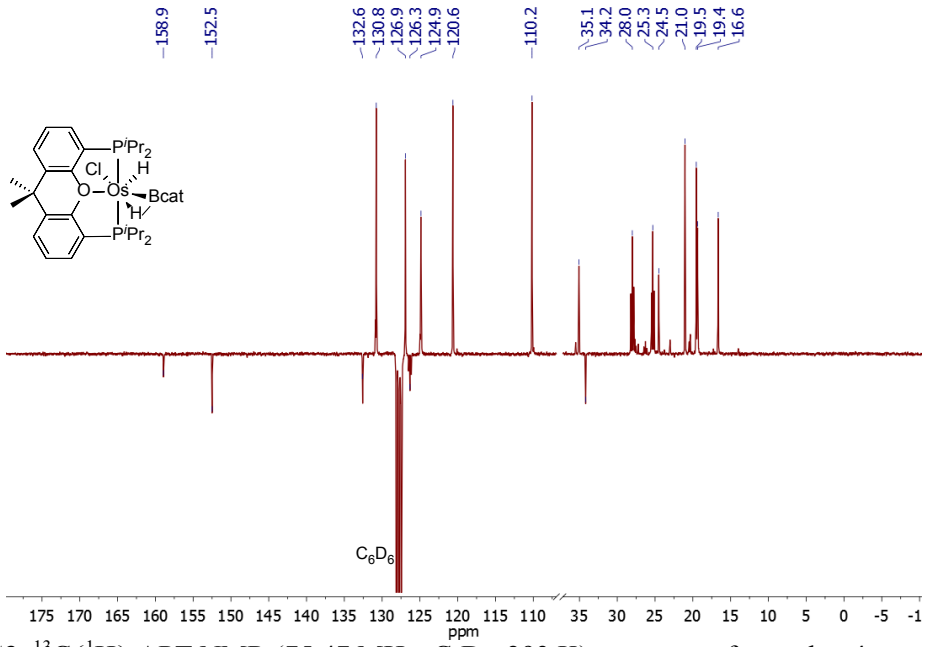

Figure S3. $^{13}C\{^1H\}$ APT NMR (75.47 MHz, C_6D_6, 293 K) spectrum of complex **4**.

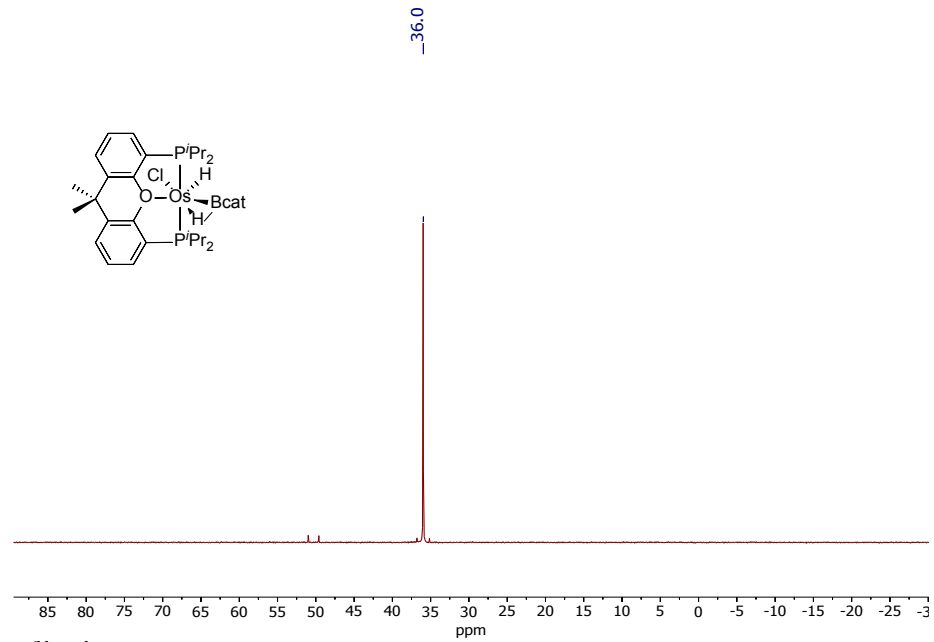

Figure S4. $^{31}P\{^1H\}$ NMR (121.49 MHz, C_6D_6, 293 K) spectrum of complex **4**.

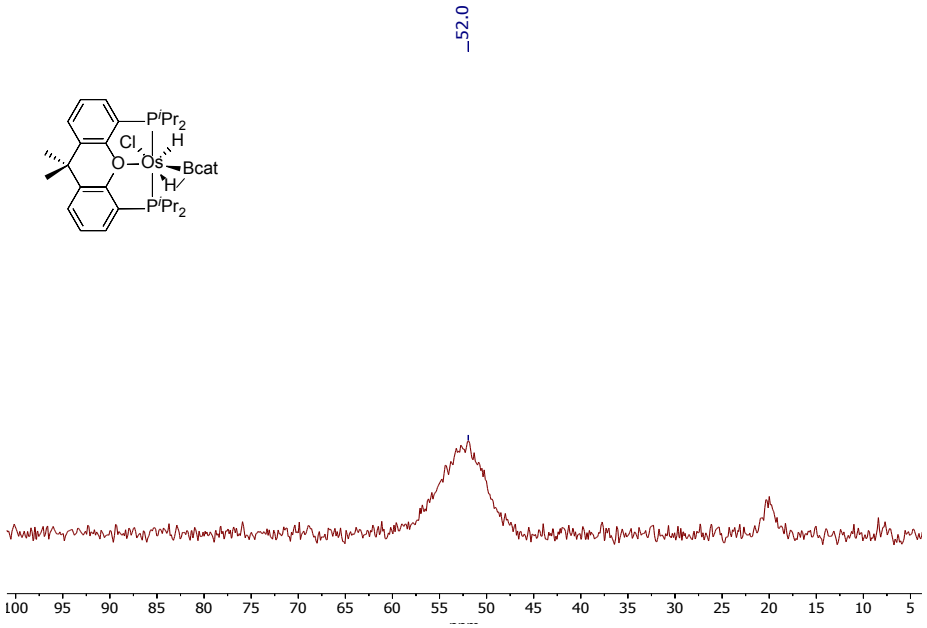

Figure S5. ^{11}B NMR (96.29 MHz, C_6D_6, 293 K) spectrum of complex **4**.

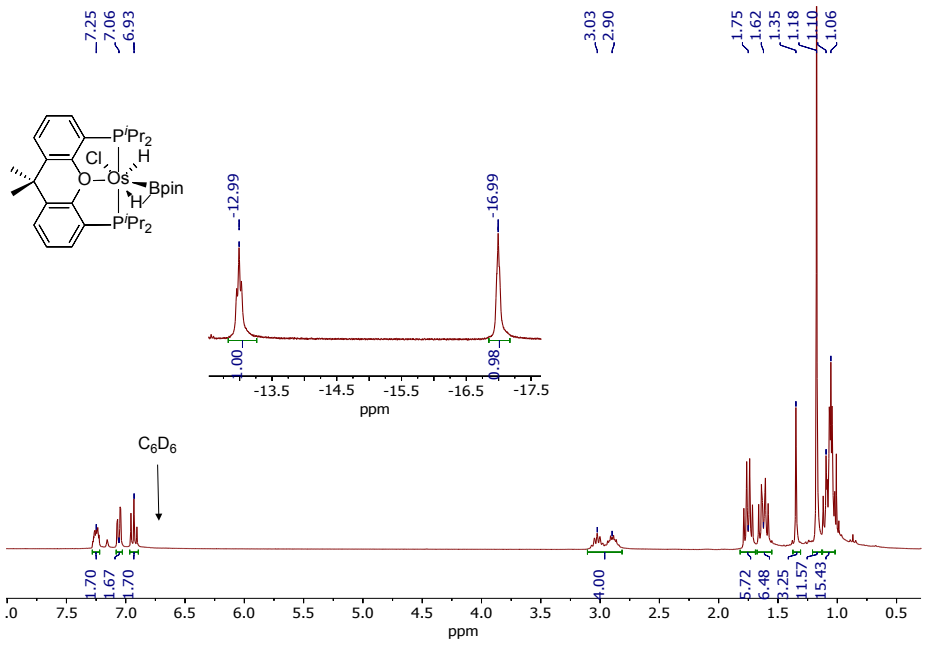

Figure S6. ^{1}H NMR (300.13 MHz, C_6D_6, 293 K) spectrum of complex **5**.

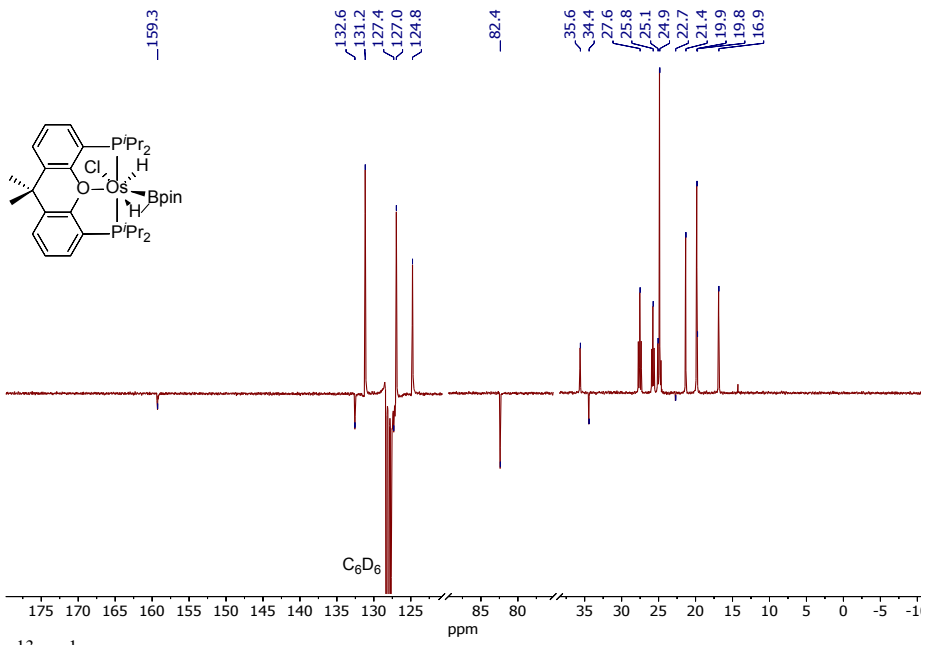

Figure S7. ^{13}C{^{1}H} APT NMR (75.48 MHz, C_6D_6, 293 K) spectrum of complex **5**.

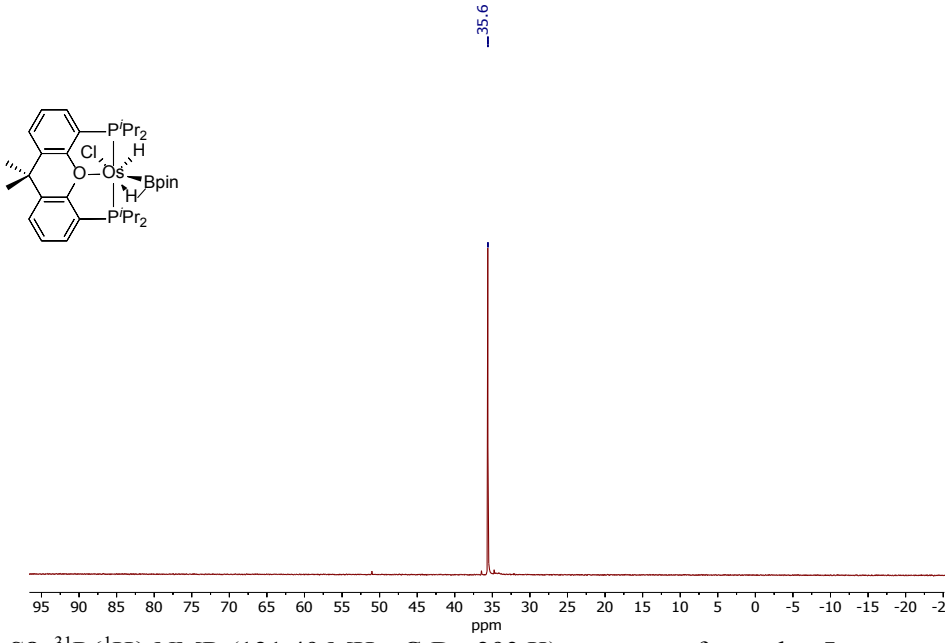

Figure S8. $^{31}P\{^1H\}$ NMR (121.49 MHz, C_6D_6, 293 K) spectrum of complex **5**.

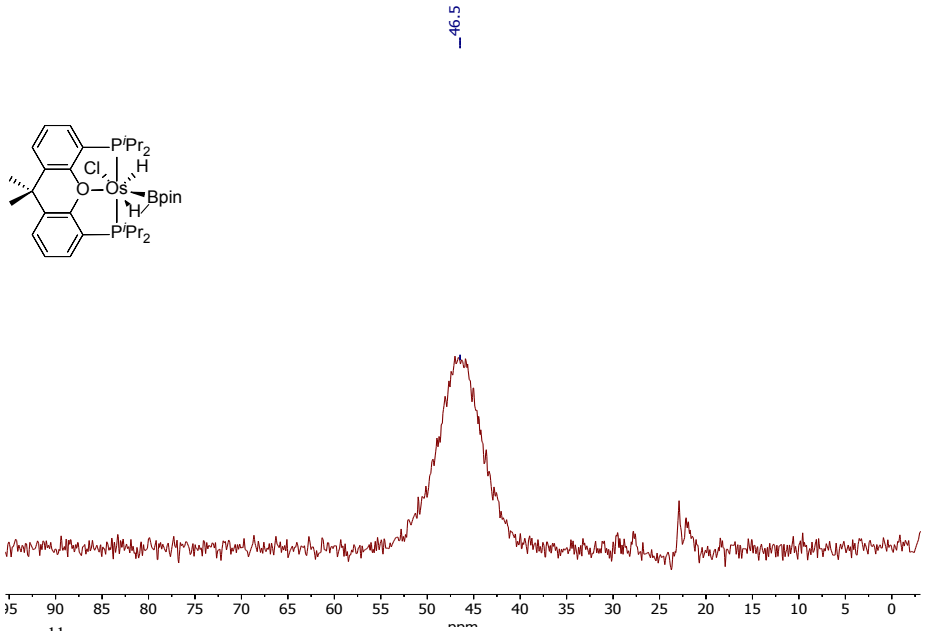

Figure S9. ^{11}B NMR (96.29 MHz, C_6D_6, 293 K) spectrum of complex **5**.

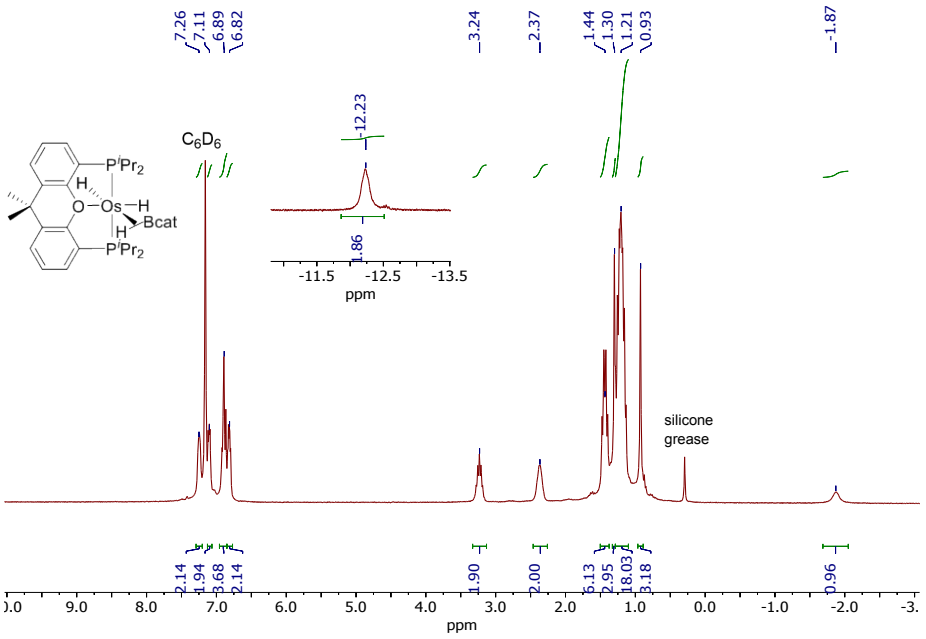

Figure S10. ^{1}H NMR (300.13 MHz, C_6D_6, 298 K) spectrum of complex **7**.

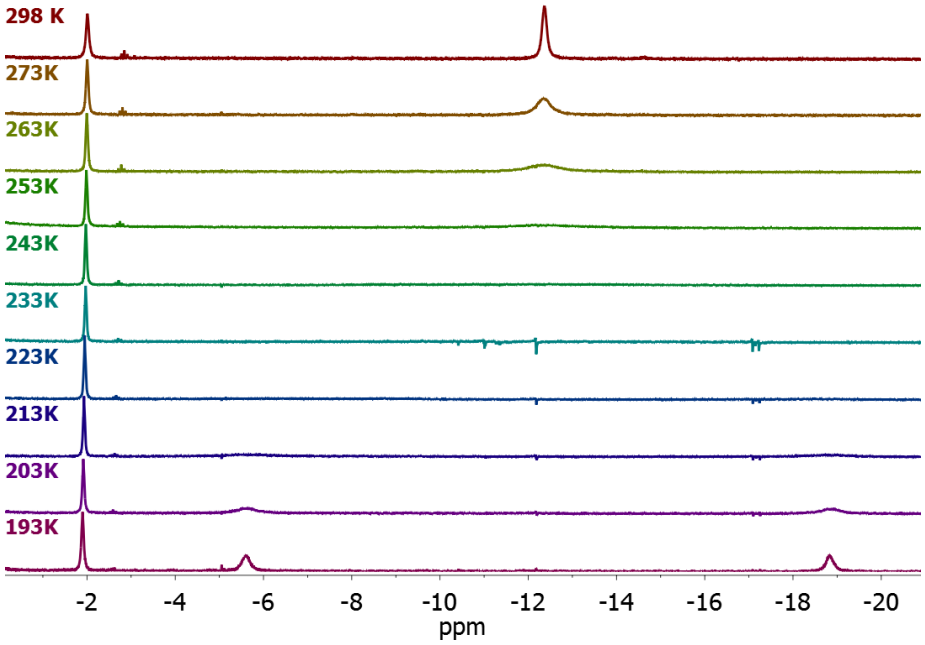

Figure S11. High-field region of the ^{1}H NMR (400.13 MHz, C_7D_8) spectrum of complex **7** between 298 and 193 K.

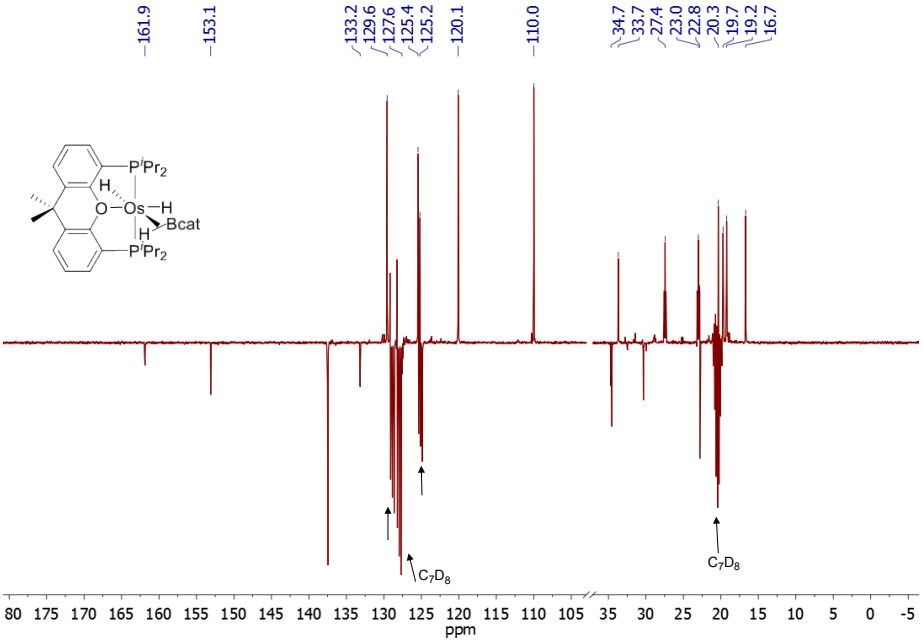

Figure S12. $^{13}C\{^1H\}$ APT NMR (100.62 MHz, C_7D_8, 298 K) spectrum of complex **7**.

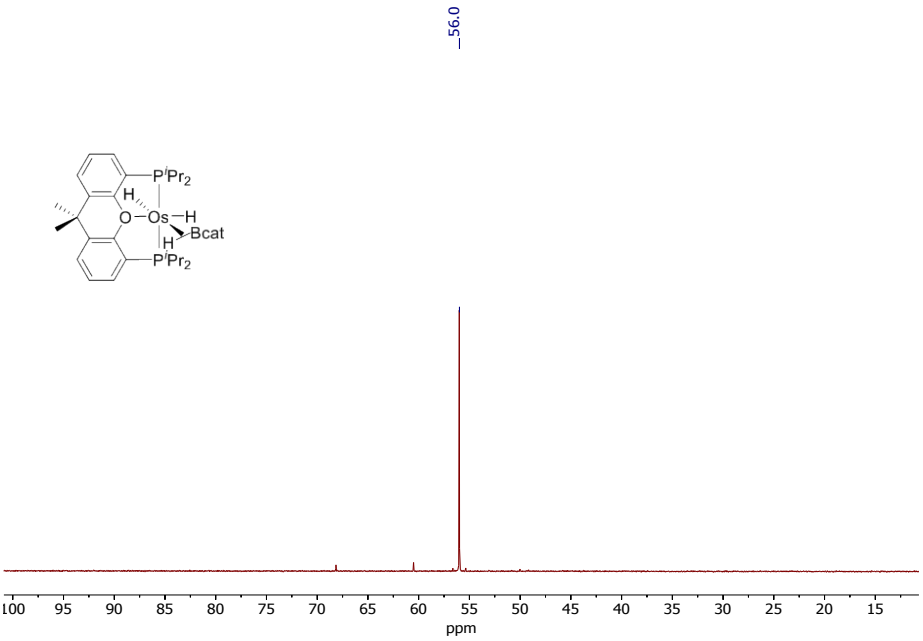

Figure S13. $^{31}P\{^1H\}$ NMR (161.98 MHz, C_7D_8, 298 K) spectrum of complex **7**.

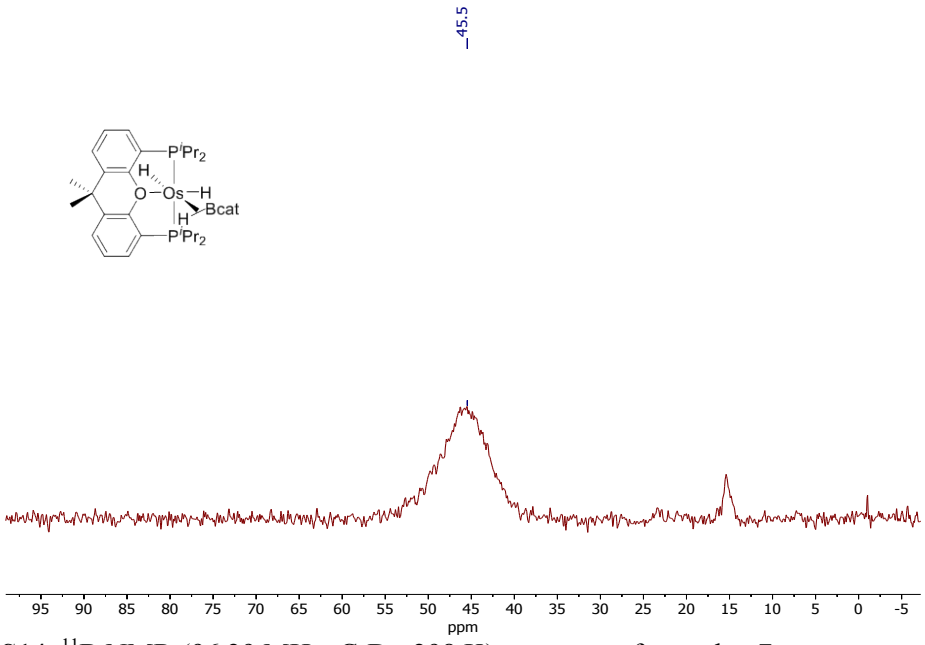

Figure S14. ^{11}B NMR (96.29 MHz, C_6D_6, 298 K) spectrum of complex **7**.

Total energies (in a. u., non corrected zero-point vibrational energies included) of complexes **4**, **5** and **7** (BP86-D3/def2-SVP level).

4: E= -2767.814532

5: E= -2772.558982

7: E= -2308.246144

Reactions of an Osmium(IV)-Hydroxo Complex with Amino-Boranes: Formation of Boroxide Derivatives

Antonio Antiñolo,[†,*] Miguel A. Esteruelas,[‡,*] Cristina García-Yebra,[‡,§] Jaime Martín,[‡] Enrique Oñate,[‡] and Alberto Ramos[†]

[†]Departamento de Química Inorgánica, Orgánica y Bioquímica-Centro de Innovación en Química Avanzada (ORFEO-CINQA), Universidad de Castilla-La Mancha, Campus Universitario, E-13071 Ciudad Real, Spain

[‡]Departamento de Química Inorgánica, Instituto de Síntesis Química y Catálisis Homogénea (ISQCH), Centro de Innovación en Química Avanzada (ORFEO-CINQA), Universidad de Zaragoza-CSIC, 50009 Zaragoza, Spain

ABSTRACT: The discovery of a reaction, which allows to prepare boroxide complexes of platinum group metals and to study their behavior under CO atmosphere, is described. The trihydride-osmium(IV)-hydroxo complex $OsH_3(OH)\{\kappa^3$-P,O,P-[xant(P^iPr_2)$_2$]} (**1**, xant(P^iPr_2)$_2$ = 4,5-bis(diisopropylphosphino)xanthene) reacts with the amino-boranes ^{i}Pr(H)NBCy$_2$ and ^{i}Pr(H)NBBN to give the osmium(IV)-boroxide derivatives $OsH_3(OBR_2)\{\kappa^3$-P,O,P-[xant(P^iPr_2)$_2$]} (BR_2 = BCy_2 (**2**), BBN (**3**); BBN = 9-borabicyclo[3.5.1]nonane) and ^{i}PrNH$_2$, as a consequence of the addition of the O-H bond of the hydroxo ligand of **1** to the B-N bond of the amino-boranes. At room temperature, under CO atmosphere, complexes **2** and **3** eliminate H_2 to afford the osmium(II)-boroxide compounds $OsH(OBR_2)(CO)_2\{\kappa^2$-P,P-[xant($P^iPr_2$)$_2$]} ($BR_2$ = BCy_2 (**4**), BBN (**5**)) bearing a κ^2-P,P-coordinated ether-diphosphine. The subsequent reductive elimination of the borinic acids R_2BOH needs heating and long time and leads to the tricarbonyl-osmium(0) derivative $Os(CO)_3\{\kappa^2$-P,P-[xant(P^iPr_2)$_2$]} (**6**), with the phosphorus atoms of the diphosphine lying in the equatorial plane of a pentagonal bypiramid of donor atoms around the metal center. In contrast to **2** and **3**, under CO atmosphere, precursor **1** eliminates water to initially give the *trans*-dihydride $OsH_2(CO)\{\kappa^3$-P,O,P-[xant(P^iPr_2)$_2$]} (**7**), which subsequently evolves to the *cis*-dihydride-*cis*-dicarbonyl derivative $OsH_2(CO)_2\{\kappa^2$-P,P-[xant(P^iPr_2)$_2$]} (**8**) and finally into the tricarbonyl **6**.

INTRODUCTION

Hydroxide complexes of platinum group metals[1] are a rare and particularly fascinating group of weak hydroxoacids, which have an oxo derivative as a conjugate base and are at the same time the strong conjugate base of an aquo-complex (Scheme 1). The exciting nature of these species is not corresponded with a rich chemistry, which is by contrast underdeveloped, in particular for osmium. In addition to a few dimers,[2] the mononuclear compounds of this element include: nitride complexes,[3] half-sandwich species,[4] and hydride-hydroxo derivatives.[5] The latter are particularly challenging since the reductive elimination of water is generally favored from a thermodynamic point of view.[6] Compounds of this class are generally osmium(II)-derivatives and only very recently a hydride-osmium(IV)-hydroxo complex has been isolated.[5f] In agreement with the marked ability of pincer ligands to stabilize uncommon species,[7] it contains the POP group 4,5-bis(diisopropylphosphino)xanthene (xant(P^iPr_2)$_2$).[8]

Scheme 1. Brønsted-Lowry Equilibria for a Metal Hydroxoacid

$$[L_nM(OH_2)]^n \overset{-H^+}{\rightleftharpoons} [L_nM(OH)]^{n-1} \overset{-H^+}{\rightleftharpoons} [L_nM(O)]^{n-2}$$

The previously mentioned duality of the hydroxide complexes is expressed in the respective nucleophilicity and electrophilicity of the oxygen and hydrogen atoms of the hydroxo group in the scarce performed reactions,[9] as the addition of aldehydes to [OsH(OH)(CPh)(IPr)(P^iPr_3)]OTf (IPr = 1,3-bis(2,6-diisopropylphenyl)imidazolylidene, OTf = CF_3SO_3) which affords the corresponding carboxylate derivatives and molecular hydrogen (Scheme 2).[10]

Scheme 2. Reactions of an Osmium-hydroxo Complex with Aldehydes

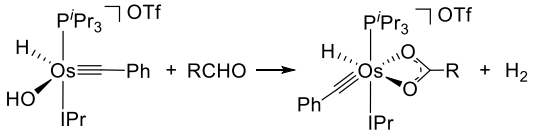

R = Et, CH=CH$_2$, CH=CHPh, Ph

Boroxide groups have been proposed as promising alternative to the alkoxide ligands, in order to better modulate the electronic and steric properties of catalyst precursors of interesting reactions of organic synthesis.[11] The empty p-orbital on the boron allows electron donation from the oxygen lone-lone pairs, which gives rise to a poorer electron donating oxygen group. In addition, although the boroxide ligand bears twice as many carbon substituents as an alkoxide group, the presence of an additional space converts it into sterically less demanding.[12] Boroxide compounds of metal of s and p blocks[13] and complexes of transition elements of all groups[11,14] have been reported. Nevertheless, one could think that there is a "boroxide wall" around the platinum group metals since the species of these elements are unknown until now. Two main procedures have been employed to generate this type of compounds:

reactions of a metal halide with a lithium boroxide and protonolysis of metal-carbon, -nitrogen, or –oxygen bonds with a borinic acid[12] (a and b in Scheme 3).

Scheme 3. Synthetic procedures to prepare boroxide compounds

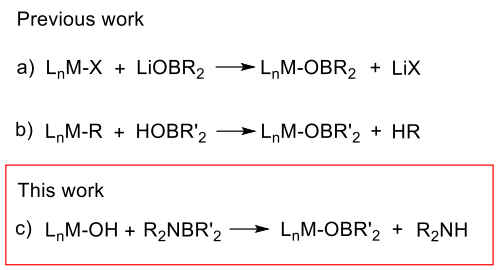

Boron shows higher affinity for oxygen than for nitrogen, which is consistent with the higher dissociation energy of the B-O bonds with regard to the B-N bonds in tricoordinate boron-species.[15] This, along with the oxygen nucleophilicity and the hydrogen electrophilicity of the hydroxo ligand in hydroxide complexes, prompted us to try the formation of boroxide species of a platinum group metal by means of the displacement of the amino group of amino-boranes by the conjugate base of a hydroxoacid (c in Scheme 3), in reactions that resemble that shown in scheme 2. Here, we report a novel procedure which allowed us to isolate the first boroxide complexes of a platinum group metal.

RESULTS AND DISCUSSION

Osmium(IV)-Boroxide Derivatives: Formation and Characterization. Metal ions in high oxidation state form strong bonds with oxygen, increasing the electrophilicity of the hydrogen atom of the hydroxo ligand. This fact led us to select the osmium(IV) complex $OsH_3(OH)\{\kappa^3\text{-}P,O,P\text{-}[xant(P^iPr_2)_2]\}$ (**1**) as starting point to achieve our goal. Treatment of toluene solutions of **1** with 1.0 equiv of the amino-boranes ^{i}Pr(H)NBCy$_2$ and ^{i}Pr(H)NBBN (BBN = 9-borabicyclo[3.3.1]nonane), at room temperature, for 30 min produces the release of isopropylamine and the formation of the desired osmium(IV)-boroxide derivatives $OsH_3(OBR_2)\{\kappa^3\text{-}P,O,P\text{-}[xant(P^iPr_2)_2]\}$ (BR_2 = BCy$_2$ (**2**), BBN (**3**)), which were isolated as pale yellow solids in 50-65% yield (Scheme 4).

Scheme 4. Formation of Boroxide Complexes 2 and 3

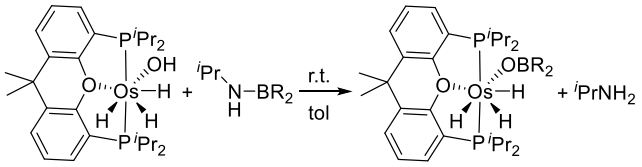

The formation of **2** and **3** is strongly supported by the X-ray diffraction structure of **2** (Figure 1a). The Os(POP) skeleton shows the typical T-shaped with the osmium atom situated in the common vertex and P1-Os-P2, P1-Os-O2, and P2-Os-O2 angles of 160.90(4)º, 81.75(7)º, and 80.53(7)º, respectively. The coordination geometry around the metal center can be rationalized as a distorted pentagonal bipyramid with the boroxide group and the hydride ligands lying in the perpendicular plane to the P-Os-P direction along with the oxygen atom of the diphosphine, which is situated between the boroxide O1 atom and the hydride H01 (O1-Os-O2 = 81.89(10)º). The osmium-boroxide distance of 2.089(3) Å is long. It compares well with the higher part of the range of the reported osmium(IV)-alkoxide bond lengths (1.90-2.10 Å),[16] whereas the Os-O1-B1 angle of 137.9(3)º significantly deviates from the expected value for sp^2 hybridized oxygen. This angle is about 20º larger than the Os-S-B angle in the borothiolate compounds $OsH(SBR_2)(\eta^2\text{-}H_2)(CO)(P^iPr_3)_2$ (113-119º).[17] This is consistent with that observed by Braunschweig and coworkers for the M-chalcogene-B angle, in the borachalcogene complexes $Cp(CO)_2Mn[EB^tBu(IMe)]$ (E = S, Se, Te), which increases by going up in the group; i.e., in the sequence Te < Se < S.[18] However, in contrast to the Braunschweig's compounds the O1-B bond length of 1.332(6) Å reveals a short chalcogene-boron single bond.[19] The DFT optimized structure (Figure 1b) confirms the trihydride character of the OsH_3 unit, although the calculated separations between H01 and H02 and between H02 and H03 of 1.57 and 1.64 Å, respectively, suggest the presence of weak nonclassical interactions between the hydride ligands.[20]

The ^{1}H NMR spectra of **2** and **3** in toluene-d_8 also support the presence of weak nonclassical interactions between the hydride ligands. At room temperature they display only one resonance (δ_{1H}, ≃ -13), indicating that are involved in two thermally activated site exchange processes. At temperatures lower than 223 K, three signals are however observed (δ_{1H}, -11.60, -11.71, -13.49 (**2**); -11.63, -11.75, -13.61 (**3**)) in agreement with the structures shown in Figure 1. Two of them form an AB spin system with a large *cis* J_{AB} coupling constant of 46.9 Hz for **2** and 98.5 Hz for **3** at 193 K, which slightly decreases as the temperature increases, as expected for quantum-mechanical exchange coupling between the involved hydrides.[21] According to equivalent P^{i}Pr$_2$ groups, the ^{31}P{^{1}H} NMR spectra contain a singlet at 44.2 ppm for **2** and 45.6 ppm for **3**, which is temperature invariant. In the ^{11}B spectra, the boroxide ligands give rise to a broad resonance centered at 48.3 ppm for **2** and at 50.6 ppm for **3**.

Osmium(II)-Boroxide Derivatives: Reactions with CO. Complexes **2** and **3** are not only novel examples of boroxide derivatives but also notable polyhydrides bearing a monodentate monoanionic oxygen-donor ligand.[20] The stability of the H-Os-OBR$_2$ unit is certainly noticeable. In this context, it should be pointed out that the reductive elimination of molecular hydrogen is kinetically favored with regard to the release of the borinic acid. Thus, the stirring of toluene solutions of both compounds, under 1 atmosphere of CO, at room temperature, for 24 h leads to the respective *cis*-dicarbonyl-hydride-osmium(II)-boroxide derivatives $OsH(OBR_2)(CO)_2\{\kappa^2\text{-}P,P\text{-}[xant(P^iPr_2)_2]\}$ (BR_2 = BCy$_2$ (**4**), BBN (**5**)), and molecular hydrogen (Scheme 5). The elimination of the borinic acid takes place after the elimination of H_2 on the hydride-osmium(II)-boroxide species and requires heating and time. In toluene, under 1 atmosphere of CO, complex **4** loses HOBCy$_2$, to quantitatively afford the tricarbonyl compound $Os(CO)_3\{\kappa^2\text{-}P,P\text{-}[xant(P^iPr_2)_2]\}$ (**6**), after 4 days at 110 ºC. The C-substituents attached to the boron atom influence on the elimination rate of the borinic acid. The bicyclic system of **5** favors the reductive elimination with regard to the

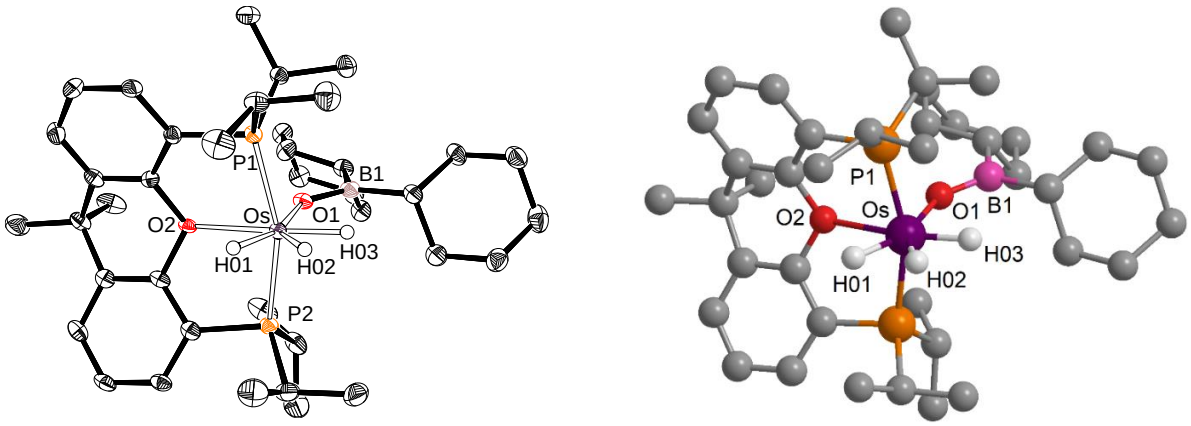

Figure 1. a) Molecular diagram of complex **2** with 50% probability ellipsoids. Hydrogen atoms (except hydrides) are omitted for clarity. Selected bond lengths (Å) and angles (deg): Os-O2 = 2.304(3), Os-O1 = 2.089(3), Os-H03 = 1.580(10), Os-H02 = 1.580(10), Os-H01 = 1.580(10), Os-P1 = 2.2893(11), Os-P2 = 2.2891(11), O1-B1 = 1.332(6); P1-Os-P2 = 160.90(4), P1-Os-O2 = 81.75(7), P2-Os-O2 = 80.53(7), O1-Os-O2 = 81.89(10), Os-O1-B1 = 137.9(3). **b)** DFT optimized structure of **2**. Selected bond lengths (Å) and angles (deg): Os-O2 = 2.351, Os-O1 = 2.088, Os-H03 = 1.594, Os-H02 = 1.598, Os-H01 = 1.633, Os-P1 = 2.322, Os-P2 = 2.321, O1-B1 = 1.330, H01-H02 = 1.57, H02-H03 = 1.64; P1-Os-P2 = 160.5, P1-Os-O2 = 81.5, P2-Os-O2 = 80.3, O1-Os-O2 = 78.1, Os-O1-B1 = 140.7.

cyclohexyl groups of **4**. As a consequence complex **5** cannot be isolated as an analytically pure solid, since amounts of the tricarbonyl derivative **6** are formed before the quantitative transformation of **3** into **5** has taken place, even at room temperature.

Complex **4** was isolated as a white solid in 64% yield and characterized by X-ray diffraction analysis. The structure (Figure 2) proves the reduction of the metal center from +4 to +2, involving the replacement of two hydride ligands by two carbonyl groups. The reduction produces a change in the coordination mode of the diphosphine from κ^3-P,O,P to κ^2-P,P, in agreement with the flexibility of the ether-diphosphines, which allows them to adapt to the requirements of the particular complex.[8c,8i,8j,22] The formation of **4** and **5** enlarges into osmium(II) the range of osmium(VI) and osmium(IV) species stabilized by κ^2-P,P-coordinated ether-diphosphines. The coordination polyhedron around the osmium atom can be rationalized as a distorted octahedron with the boroxide ligand disposed *trans* to a carbonyl group O1-Os-C1 = 174.90(8)º. The perpendicular plane is formed by the other carbonyl group, the hydride ligand, and the phosphorus atoms of the chelate diphosphine (P1-Os-P2 = 108.33(2)º). The coordination of the boroxide ligand does not show any difference with regard to the coordination in **2**. Thus, the Os-O1 and O1-B bond lengths of 2.0857(15) and 1.331(3) Å, respectively, and the Os-O1-B angle of 135.33(16)º are almost identical as those of **2**.

The IR and $^{13}C\{^1H\}$, ^1H, and $^{31}P\{^1H\}$ NMR spectra of **4**, in toluene-d_8, at 203 K are consistent with the structure shown in Figure 2. As expected for a *cis* disposition of the carbonyl groups, the IR contains the characteristic two ν(CO) bands corresponding to a C_{2v} point group, at 1998 and 1914 cm^{-1}. In the $^{13}C\{^1H\}$ NMR spectrum, these ligands display double doublets at 186.0 ($^2J_{C\text{-}P\ trans}$ = 99.8 Hz, $^2J_{C\text{-}P\ cis}$ = 1.0 Hz) and 181.8 ($^2J_{C\text{-}P\ cis}$ = 10.5 and 2.1 Hz) ppm. In agreement with the presence of a hydride ligand disposed *trans* to a phosphorus atom and *cis* to other one, the high field region of the ^1H NMR spectrum shows at -6.30 ppm a double doublet with H-P coupling constants of 115.1 and 33.6 Hz, whereas the $^{31}P\{^1H\}$ NMR spectrum contains two doublets at 3.4 and 1.5 ppm with a P-P coupling constant of 26.2 Hz. In accordance with **2**, the ^{11}B NMR spectrum, in toluene-d_8, at room temperature shows a broad resonance centered at 50.0 ppm.

Complex **5** exists in solution as a 1:1 mixture of two conformers, which may be related to the disposition of the xanthene linker of the diphosphine with regard to the ligands situated along the boroxide-osmium-carbonyl axis. Their presence is strongly supported by the ^1H and $^{31}P\{^1H\}$ NMR spectra, in toluene-d_8, at 203 K. Thus, in agreement with the ^1H NMR spectrum of **4**, the ^1H NMR spectrum of **5** shows two double doublets at -5.94 ($^2J_{P\text{-}H\ trans}$ = 99.0 Hz, $^2J_{P\text{-}H\ cis}$ = 29.94 Hz) and -6.31 ($^2J_{P\text{-}H\ trans}$ = 107.5 Hz, $^2J_{P\text{-}H\ cis}$ = 32.5 Hz) ppm, corresponding to the hydride ligand of each conformer, whereas the $^{31}P\{^1H\}$ NMR spectrum contains four doublets at 20.7 and 11.4 ($^2J_{P\text{-}P}$ = 24.5 Hz) ppm and 13.1 and 12.0 ($^2J_{P\text{-}P}$ = 24.5 Hz) ppm, two for each conformer.

The osmium(0)-tricarbonyl complex **6** was isolated as a yellow solid in 41 % yield and characterized by X-ray diffraction analysis. Figure 3 shows a view of the molecule. The coordination polyhedron around the osmium atom can be rationalized as a distorted trigonal bipyramid with two carbonyl groups at the apices (C1-Os-C3 = 175.12(19)º). The phosphorus atoms of the κ^2-coordinated ether-diphosphine and the remaining carbonyl group lie in the equatorial plane forming P1-Os-P2, P2-Os-C2, and C2-Os-P1 angles of 114.10(4)º, 123.63(17)º, and 122.09(17)º, respectively. The distances between the metal center and the apical carbonyl groups of 1.928(5) (Os-C1) and 1.931(5) (Os-C3) Å are about 0.08 Å longer than the distance between the osmium atom and the equatorial carbonyl group of 1.856(5) (Os-C2) Å. In agreement with the disposition of the carbonyl ligands, the IR in toluene contains three ν(CO) bands at 2003, 1916, and 1900 cm^{-1} with weak, very strong, and strong intensities, respectively. The equivalent phosphorus atoms of the diphosphine display a singlet at 4.5 ppm in the $^{31}P\{^1H\}$ NMR spectrum, in dichloromethane, at room temperature. Complex **6** is notable by two reasons: (i) it enlarges into osmium(0) the range of

Scheme 5. Carbonylation of complexes 2 and 3 in toluene

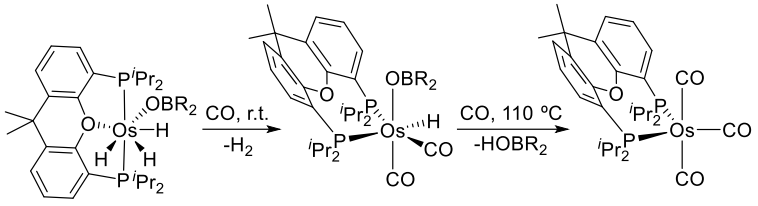

compounds involving a κ^2-P,P-coordinated ether-diphosphine and (ii) it is a rare example of $Os(CO)_3P_2$ compound with the phosphorus atoms lying in the equatorial plane of the bipyramid, since they always occupy apical positions in the complexes of this class previously reported.[23]

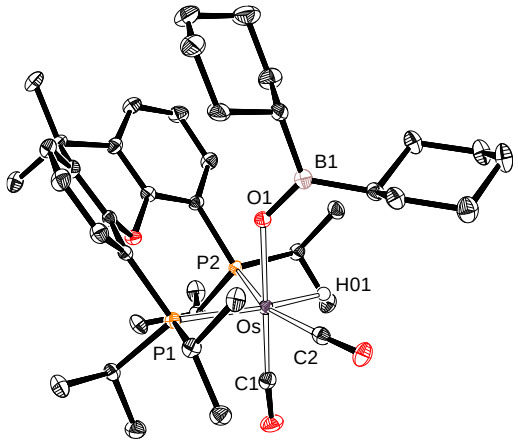

Figure 2. Molecular diagram of complex **4** with 50% probability ellipsoids. Hydrogen atoms (except the hydride) are omitted for clarity. Selected bond lengths (Å) and angles (deg): Os-O1 = 2.0857(15), Os-H01 = 1.584(10), Os-C2 = 1.886(2), Os-C1 = 1.865(2), Os-P1 = 2.5092(6), Os-P2 = 2.4522(6), O1-B = 1.331(3); O1-Os-C1 = 174.90(8), P1-Os-P2 = 108.33(2), Os-O1-B = 135.33(16).

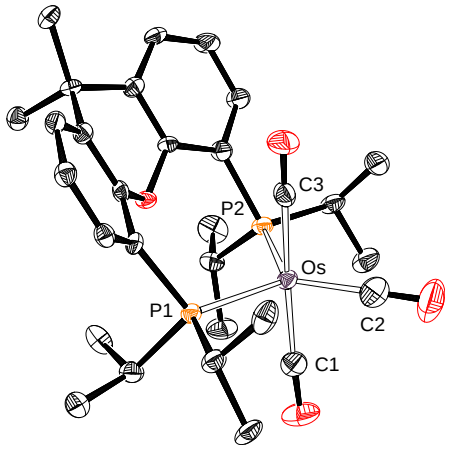

Figure 3. Molecular diagram of complex **6** with 50% probability ellipsoids. Hydrogen atoms are omitted for clarity. Selected bond lengths (Å) and angles (deg): Os-C3 = 1.931(5), Os-C2 = 1.856(5), Os-C1 = 1.928(5), Os-P1 = 2.3582(11), Os-P2 = 2.3677(11); C1-Os-C3 = 175.12(19), P1-Os-P2 = 114.10(4), P2-Os-C2 = 123.63(17), P1-Os-C2 = 122.09(17).

Reactions of 1 with CO: Reductive Elimination of H_2O. There are marked differences in behavior between the hydroxo precursor **1** and the boroxide derivatives **2** and **3**, under 1 atmosphere of CO. In contrast to the latter, complex **1** eliminates the oxygen donor group and a hydride ligand to quantitatively yield the previously described *trans*-dihydride compound $OsH_2(CO)\{\kappa^3$-P,O,P-[xant($P^iPr_2)_2$]$\}$[8h] (**7**) and water after 24 h, in toluene, at room temperature (Scheme 6). At 110 ºC, complex **7** evolves into the *cis*-dicarbonyl derivative $OsH_2(CO)_2\{\kappa^2$-P,P-[xant($P^iPr_2)_2$]$\}$ (**8**), as a result of the displacement of the oxygen atom of the diphosphine by a second carbon monoxide molecule and the *trans* to *cis* isomerization of the hydride ligands. Complex **8**, which is a new example of osmium(II) species with a κ^2-P,P-coordinated ether-diphosphine, is a dihydride counterpart of **4** and **5** bearing a hydride ligand in the position of the boroxide group. Like its analogous, it undergoes reduction into the tricarbonyl derivative **6**, under carbon monoxide atmosphere.

The κ^2-P,P-coordination of the diphosphine in **8** is strongly supported by the ^{1}H NMR spectrum of the complex, in toluene-d_8, at room temperature, which shows two double doublets at 0.97 and 0.89 ppm, for the methyl groups of the phosphine isopropyl substituents, instead of the characteristic doublet of virtual triplets of the κ^3-P,O,P-*mer* mode. In addition, in the high field region, the spectrum contains two doublet of doublet of doublets at -7.92 (hydride *cis* to both P atoms) and -10.01 (hydride *trans* to a P atom and *cis* to the other one) ppm with P-P coupling constants of 19.6 and 26.4 and 67.5 and 35.5 Hz, respectively, and a H-H coupling constant of 6.1 Hz. The $^{13}C\{^1H\}$ NMR spectrum also supports the structure proposed for **8** in Scheme 6, showing the carbonyl resonances at 188.0 (CO *trans* to a P atom and *cis* to the other one) and 186.0 (CO *cis* to P atoms) ppm as double doublets with C-P coupling constants of 74.1 and 3.4 Hz and 10.0 and 3.6 Hz, respectively. In the $^{31}P\{^1H\}$ NMR spectrum, the inequivalent P^iPr_2 groups display at 4.2 and 1.9 ppm doublets with a P-P coupling constant of 25.6 Hz.

CONCLUDING REMARKS

This study shows a novel reaction in the chemistry of hydroxo-transition metal complexes, reveals the existence of boroxide derivatives of platinum group metals, demonstrates that the reductive elimination of borinic acids from hydride metal-boroxide compounds is disfavored with regard to the release of molecular hydrogen and to the reductive elimination of water from hydride-metal-hydroxo counterparts, and enlarges the range of metal ions stabilizing compounds with κ^2-P,P-coordinated ether-diphosphines.

Scheme 6. Carbonylation of complex 1 in toluene

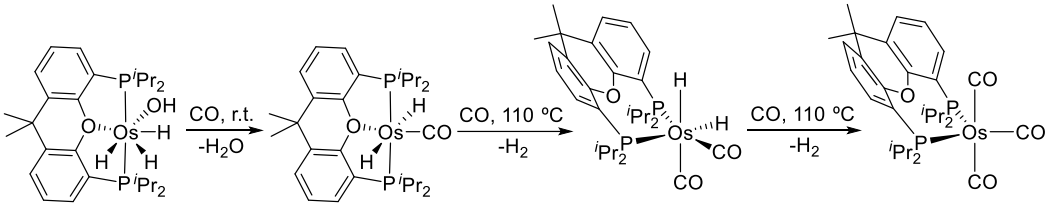

The oxygen nucleophilicity and hydrogen electrophilicity of hydroxo ligands coordinated to transition metals allow the hydroxo ligand to displace the amino group of $R_2NBR'_2$ amino-boranes. The reactions afford boroxide derivatives, including compounds of a platinum group metal as osmium. Complexes of this class containing hydride co-ligands are stable towards the elimination of borinic acids, in contrast to hydride-metal-hydroxo species which show a high tendency to release water. Under carbon monoxide atmosphere, the elimination of molecular hydrogen is observed. The elimination of the borinic acid also occurs but is always a subsequent process and needs heating and long time. The ether-diphosphine 4,5-bis(diisopropylphosphino)xanthene stabilizes the resulting species of the above mentioned processes, when the metal center is osmium, adapting its coordination mode to the electronic and steric requirements of each particular complex. As a consequence, the range of compounds bearing the diphosphine κ^2-P,P-coordinated has been enlarged into osmium(II) and osmium(0) derivatives.

In conclusion, a novel reaction in the chemistry of transition metal-hydroxo complexes has been discovered, which has led us to the preparation of the first boroxide derivatives of a platinum group metal and to study their behavior under carbon monoxide atmosphere.

EXPERIMENTAL SECTION

All reactions were performed under argon using Schlenk tube or glovebox techniques and dried solvents. Instrumental methods, NMR spectra, X-ray diffraction analysis information and DFT computational details are given in the Supporting Information. Complex $OsH_3(OH)\{\kappa^3$-P,O,P-[xant(P^iPr_2)$_2$]} (**1**) was prepared as published.[5f] Chemical shifts (expressed in parts per million) are referenced to residual solvent peaks (^{1}H, ^{13}C{^{1}H}) or external H_3PO_4 (^{31}P{^{1}H}) and $BF_3{\cdot}OEt_2$ (^{11}B). Coupling constants, J and N ($N = J_{PH} + J_{P'H}$ for ^{1}H; $N = J_{PC} + J_{P'C}$ for ^{13}C) are given in Hertz.

Preparation of ^{i}PrNHBCy$_2$. A 1.6 M solution of ^{n}BuLi in hexane (3.2 mL, 5.12 mmol) was slowly added to a colorless solution of isopropylamine (430 µL, 5.00 mmol) in diethyl ether (10 mL) kept at -78 ºC with an acetone/liquid N_2 bath. Upon finishing the addition, formation of a white precipitate (LiN^iPrH) was observed, then the cold bath was removed and the mixture was further stirred at room temperature for 1 h. Then, the white suspension thus obtained was again cooled at -78 ºC and a 1.0 M solution of $ClBCy_2$ in hexane (5.0 mL, 5.00 mmol) was slowly added. Once more, the bath was removed when the addition was finished and the mixture was further stirred for 2 h at room temperature to ensure reaction completion, after which time was left standing for 1 h to allow deposition of solid LiCl at the bottom of the flask. Then, the solution was filtered with a cannula and a small amount of celite®, and the solvents were subsequently removed under vacuum to afford the amino-borane ^{i}PrNHBCy$_2$ as a colorless viscous oil (950 mg, 81%). ^{1}H NMR (500 MHz, C_6D_6, 298 K): δ 3.61 (d, br, J_{HH} = 11.1, 1H, N*H*), 3.51 (dsept, 1H, J_{HH} = 11.1, 6.3, 1H, C*H*-^{i}Pr), 1.9 – 0.9 (m, 22H, Cy), 0.93 (d, J = 6.3, 6H, CH_3-^{i}Pr). ^{13}C{^{1}H} NMR (101 MHz, C_6D_6, 298 K): δ 43.2 (s *C*H-^{i}Pr), 30.2, 29.5 (2 x s, 2 x C^{2,3}-Cy), 29.3 (br, C^1-Cy), 28.6 (s, 2 x C^{2,3}-Cy), 27.7, 27.6 (2 x s, 2 x C^4-Cy), 26.7 (s, *C*H$_3$-^{i}Pr). ^{11}B NMR (160 MHz, C_6D_6) δ 44.7 (s, $\Delta\nu_{1/2}$ ca. 260 Hz, B).

Preparation of ^{i}PrNHBBN. A toluene solution (15 mL) containing (H-BBN)$_2$ (610 mg, 2.50 mmol) and excess isopropylamine (470 µL, 5.47 mmol) was stirred for 20 h at 60 ºC. Then, the solvent was removed under vacuum to yield the amino-borane ^{i}PrNHBBN as a colorless viscous oil (640 mg, 71%). ^{1}H NMR (400 MHz, C_6D_6, 298 K): δ 3.54 (br, 1H, N*H*), 3.39 (dsept, J = 10.1, 6.4, 1H, C*H*-^{i}Pr), 2.10 – 0.95 (m, 14H, BBN), 0.90 (d, J = 6.4, 6H, CH_3-^{i}Pr).^{13}C{^{1}H} NMR (101 MHz, C_6D_6, 298 K): δ 43.6 (s *C*H-^{i}Pr), 34.0, 33.6 (2 x s, 2 x *C*H$_2$-BBN), 27.1 (br, *C*H-BBN), 26.6 (s, *C*H$_3$-^{i}Pr), 24.1 (s, *C*H$_2$-BBN), 22.3 (br, *C*H-BBN). ^{11}B NMR (128 MHz, C_6D_6, 298 K): δ 47.9 (s, $\Delta\nu_{1/2}$ ca. 120 Hz, B).

Reaction of 1 with ^{i}PrNHBCy: Preparation of $OsH_3(OBCy_2)\{\kappa^3$-*P,O,P*-[xant(P^iPr_2)$_2$]} (2). Amino-borane ^{i}PrNHBCy$_2$ (43 mg, 0.184 mmol) was added to a solution of **1** (120 mg, 0.184 mmol) in toluene (5 mL). After 30 min, at room temperature, the solution was concentrated and 2 mL of acetone was added at -50 ºC to afford a pale yellow solid, which was washed twice with acetone (1 mL) and dried under reduced pressure. Yield: 95 mg (62 %). Anal. Calcd. for $C_{39}H_{65}BO_2OsP_2$: C, 56.51; H, 7.90. Found: C, 56.92; H, 7.91. ^{1}H NMR (300.13 MHz, C_4D_8O, 298 K): δ 7.60 (dd, $^3J_{HH}$ = 7.7, $^4J_{HH}$ = 1.2, 2H, C*H*-arom POP), 7.50 (m, 2H, C*H*-arom POP), 7.27 (dd, $^3J_{HH}$ = 7.6, $^3J_{HH}$ = 7.5, 2H, C*H*-arom POP), 2.51 (m, 2H, PC*H*(CH$_3$)$_2$), 2.26 (m, 2H, PC*H*(CH$_3$)$_2$), 1.89 (s, 3H, C*H*$_3$ POP), 1.63-1.52 (10H, C*H*$_2$ Cy), 1.48 (s, 3H, C*H*$_3$ POP), 1.21-0.94 (10H, C*H*$_2$ Cy; 18H, PCH(C*H*$_3$)$_2$), 0.81 (m, 2H, C*H* Cy), 0.73 (dvt, $^3J_{HH}$ = 6.9, N = 14.2, 6H, PCH(C*H*$_3$)$_2$), -12.72 (t, $^3J_{HP}$ = 11.4, 3H, Os*H*). ^{1}H NMR (400.13 MHz, C_7D_8, 193 K): $\delta\ \upsilon_A$ = -11.60 and υ_B = -13.49 (AB system, $^2J_{AB}$ = 46.9, 2H, Os*H*), -11.71 (br, 1H, Os*H*). ^{13}C{^{1}H}-APT NMR (75.47 MHz, C_4D_8O, 298 K): δ 159.8 (vt, N = 13.3, *C*-arom POP), 133.5 (vt, N = 5.6, *C*-arom POP), 131.0 (s, *C*H-arom POP), 129.8 (vt, N = 27.9, *C*-arom POP), 127.6 (s, *C*H-arom POP), 125.7 (s, *C*H-arom POP), 36.1 (br, *C*H Cy), 35.5 (s, *C*(CH$_3$)$_2$ POP), 34.5 (s, C(*C*H$_3$)$_2$ POP), 30.3 and 29.4 (s, *C*H$_2$ Cy), 28.6 (vt, N = 19.2, PC*H*(CH$_3$)$_2$), 28.4 (s, *C*H$_2$ Cy), 26.7 (vt, N = 33.2, PC*H*(CH$_3$)$_2$), 26.4 (s, C(*C*H$_3$)$_2$ POP), 21.1 (vt, N = 10.8, PCH(*C*H$_3$)$_2$), 20.8 (s, PCH(*C*H$_3$)$_2$), 20.5 (s, PCH(*C*H$_3$)$_2$), 20.0 (vt, N = 4.5, PCH(*C*H$_3$)$_2$). ^{31}P{^{1}H} NMR (161.98 MHz, C_7D_8, 298 K): 44.2 (s, POP). ^{11}B NMR (96.30 MHz, C_6D_6, 298 K): δ 48.3 (br). T_1 (min) (ms, Os*H*, 400.13 MHz, C_7D_8, 263 K): 74 ± 4 (-12.39 ppm). Crystals suitable for X-ray diffraction analysis were obtained by slow diffusion of pentane into a toluene solution of the complex at -30 ºC.

Reaction of 1 with ^{i}PrNHBBN: Preparation of $OsH_3(OBBN)\{\kappa^3$-*P,O,P*-[xant(P^iPr_2)$_2$]} (3). Amino-borane ^{i}PrNHBBN (35 mg, 0.195 mmol) was added to a solution of **1** (120 mg, 0.184 mmol) in toluene (5 mL). After 30 min, at room temperature, the solution was concentrated and 2 mL of acetone was added at -50 ºC to afford a pale yellow solid, which was washed twice with acetone (1 mL) and dried under reduced pressure. Yield: 73 mg (51 %). Anal. Calcd. for $C_{35}H_{57}BO_2OsP_2$: C, 54.40; H, 7.43. Found: C, 54.76; H, 7.16. ^{1}H NMR (300.13 MHz, C_4D_8O, 298 K): δ 7.59 (dd, $^3J_{HH}$ = 7.6, $^4J_{HH}$ = 1.2, 2H, C*H*-arom POP), 7.51 (m, 2H, C*H*-arom POP), 7.29 (dd, $^3J_{HH}$ = 7.6, $^3J_{HH}$ = 7.5, 2H, C*H*-arom POP), 2.48 (m, 2H, PC*H*(CH$_3$)$_2$), 2.36 (m, 2H, PC*H*(CH$_3$)$_2$), 1.93 (s, 3H, C*H*$_3$ POP), 1.87-1.73 (10H, C*H*$_2$ BBN), 1.39 (m, 2H, C*H*$_2$ BBN), 1.33 (s, 3H, C*H*$_3$ POP), 1.22-1.14 (12H, PCH(C*H*$_3$)$_2$), 1.10 (dvt, $^3J_{HH}$ = 7.2, N =

14.9, 6H, PCH(CH_3)$_2$), 0.86 (br, 2H, CH BBN), 0.76 (dvt, $^3J_{HH}$ = 7.0, N = 14.5, 6H, PCH(CH_3)$_2$), -12.78 (t, $^3J_{HP}$ = 11.8, 3H, OsH). ^{1}H NMR (400.13 MHz, C_7D_8, 193 K): δ υ_A = -11.63 and υ_B = -13.61 (AB system, $^2J_{AB}$ = 98.5, 2H, OsH), -11.75 (br, 1H, OsH). ^{13}C{^{1}H}-APT NMR (75.47 MHz, C_4D_8O, 298 K): δ 161.2 (vt, N = 13.4, C-arom POP), 134.2 (vt, N = 5.7, C-arom POP), 130.3 (s, CH-arom POP), 129.3 (vt, N = 28.5, C-arom POP), 126.8 (s, CH-arom POP), 126.0 (vt, N = 4.8, CH-arom POP), 35.7 (s, C(CH$_3$)$_2$ POP), 35.2 (s, CH$_2$ BBN), 34.0 (s, C(CH$_3$)$_2$ POP), 32.5 (br, CH BBN), 28.1 (vt, N = 19.3, PCH(CH$_3$)$_2$), 25.5 (s, CH$_2$ BBN), 24.9 (vt, N = 32.3, PCH(CH$_3$)$_2$), 23.8 (s, C(CH$_3$)$_2$ POP), 20.6 (d, $^2J_{PC}$ = 6.0, PCH(CH$_3$)$_2$), 20.4 (d, $^2J_{PC}$ = 6.6, PCH(CH$_3$)$_2$), 20.0 (s, PCH(CH$_3$)$_2$). ^{31}P{^{1}H} NMR (161.98 MHz, C_7D_8, 293 K): 45.6 (s, POP). ^{11}B NMR (96.30 MHz, C_6D_6, 298 K): δ 50.6 (br). T_1 (min) (ms, OsH, 400.13 MHz, C_7D_8, 233 K): 77 ± 4 (-12.39 ppm).

Reaction of 2 with CO: Preparation of OsH(CO)$_2$(OBCy$_2$){κ^2-*P,P*-[xant(P^{i}Pr$_2$)$_2$]} (4). A solution of **2** (85 mg, 0.103 mmol) in toluene (5 mL) was stirred for 24 h under 1 atmosphere of CO. The resulting solution was concentrated and pentane (1 mL) at 0 ºC was added to afford an off-white solid, which was washed twice with pentane (1 mL) and dried under reduced pressure. Yield: 58 mg (64 %). Anal. Calcd. for $C_{41}H_{63}BO_4OsP_2$: C, 55.77; H, 7.19. Found: C, 55.90; H, 7.30. IR (Toluene, cm^{-1}): ν (CO) 1998 (s), ν (CO) 1914 (s). ^{1}H NMR (300.13 MHz, C_6D_6, 298 K): δ 7.21 (m, 2H, CH-arom POP), 6.99-6.88 (4H, CH-arom POP), 2.63-2.28 (4H, PCH(CH$_3$)$_2$), 1.78-1.58 (6H, CH_2 Cy), 1.62 (s, 3H, CH_3 POP), 1.45-0.85 (36H, CH Cy, CH_2 Cy, PCH(CH_3)$_2$), 1.16 (s, 3H, CH_3 POP), 0.35 (m, 4H, CH$_2$), -6.51 (m,1H, OsH). ^{1}H NMR (400.13 MHz, C_7D_8, 203 K): -6.30 (dd, $^2J_{HH}$ = 33.6, $^2J_{HH}$ = 115.1, 1H, OsH).^{13}C{^{1}H} NMR (75.48 MHz, C_6D_6, 298 K): δ 185.7 (d, $^2J_{CP}$ = 98.0, CO), 181.9-181.7 (CO), 156.2 (d, $^2J_{CP}$ = 6.0, C-arom POP), 155.4 (d, $^2J_{CP}$ = 6.2, C-arom POP), 134.6 (vt, N = 3.8, C-arom POP), 134.0 (vt, N = 3.6, C-arom POP), 131.3 (s, CH-arom POP), 131.0 (s, CH-arom POP), 126.1 (s, CH-arom POP), 125.6 (s, CH-arom POP), 123.5 (s, CH-arom POP), 123.4 (s, CH-arom POP), 118.2 (d, $^1J_{CP}$ = 26.9, C-arom POP), 113.7 (d, $^1J_{CP}$ = 28.6, C-arom POP), 35.9 (s, C(CH$_3$)$_2$ POP), 35.0 (br, CH-Cy), 32.0 (s, C(CH$_3$)$_2$ POP), 30.2 (d, $^1J_{CP}$ = 16.6, PCH(CH$_3$)$_2$), 28.7, 28.7, 28.6, 28.5, 27.8 (all s, CH$_2$-Cy), 27.5 (d, $^1J_{CP}$ = 22.3, PCH(CH$_3$)$_2$), 23.9 (m, PCH(CH$_3$)$_2$), 23.3 (m, PCH(CH$_3$)$_2$), 22.6 (s, C(CH$_3$)$_2$ POP), 20.6 (d, $^2J_{CP}$ = 4.1, PCH(CH$_3$)$_2$), 19.4 (m, PCH(CH$_3$)$_2$), 19.1 (s, PCH(CH$_3$)$_2$), 18.8 (d, $^2J_{CP}$ = 6.3, PCH(CH$_3$)$_2$), 18.6 (br, PCH(CH$_3$)$_2$), 18.1 (d, $^2J_{CP}$ = 2.2, PCH(CH$_3$)$_2$), 18.0 (d, $^2J_{CP}$ = 4.3, PCH(CH$_3$)$_2$), 17.7 (m, PCH(CH$_3$)$_2$). ^{13}C{^{1}H} NMR (100.62 MHz, C_7D_8, 203 K): δ 186.0 (dd, $^2J_{CP}$ = 99.8, $^2J_{CP}$ = 1.0, CO), 181.8 (dd, $^2J_{CP}$ = 10.5, $^2J_{CP}$ = 2.1, CO), ^{31}P{^{1}H} NMR (121.50 MHz, C_6D_6, 298 K): δ 3.2 (br, POP). ^{31}P{^{1}H} NMR (161.98 MHz, C_7D_8, 203 K): 3.4 (d, $^2J_{PP}$ = 26.2, POP), 1.5 (d, $^2J_{PP}$ = 26.2, POP). ^{11}B NMR (96.30 MHz, C_6D_6, 298 K): δ 50.0 (br). Crystals suitable for X-ray diffraction analysis were obtained from a concentrated solution of the complex in benzene.

Reaction of 3 with CO: Formation of OsH(CO)$_2$(OBBN){κ^2-*P,P*-[xant(P^{i}Pr$_2$)$_2$]} (5). Complex **3** (25 mg, 0.035 mmol) in toluene-d_8 (0.5 mL) was placed in a NMR tube equipped with a Teflon screw cap, at room temperature, under 1 atmosphere of CO. After 24 h, a mixture of **5** and **6** was formed in a 1:1 ratio. Selected spectroscopic data for **5**: ^{1}H NMR (300.13 MHz, C_7D_8, 298 K): -6.69 (dd, $^2J_{HP}$ = 31.7, $^2J_{HP}$ = 110.5, 1H, OsH). ^{1}H NMR (400.13 MHz, C_7D_8, 203 K): -5.64 (dd, $^2J_{HP}$ = 29.4, $^2J_{HP}$ = 99.0, 1H, OsH), -6.31 (dd, $^2J_{HP}$ = 32.5, $^2J_{HP}$ = 107.5, 1H, OsH). ^{13}C{^{1}H} NMR (75.48 MHz, C_7D_8, 298 K): δ 185.4 (dd, $^2J_{CP}$ = 98.0, $^2J_{CP}$ = 3.3, CO), 182.1 (dd, $^2J_{CP}$ = 10.3, $^2J_{CP}$ = 4.5, CO). ^{31}P{^{1}H} NMR (121.49 MHz, C_7D_8, 298 K): δ 10.8 (br, POP). ^{31}P{^{1}H} NMR (161.98 MHz, C_7D_8, 203 K): 20.7 (d, $^2J_{PP}$ = 24.5, POP), 13.1 (d, $^2J_{PP}$ = 24.5, POP), 12.0 (d, $^2J_{PP}$ = 24.5, POP), 11.4 (d, $^2J_{PP}$ = 24.5, POP). ^{11}B NMR (96.29 MHz, C_7D_8, 298 K): δ 51.3 (br).

Preparation of Os(CO)$_3${κ^2-*P,P*-[xant(P^{i}Pr$_2$)$_2$]} (6). A solution of **4** (150 mg; 0.170 mmol) in toluene (5 mL) was placed in a schlenk tube provided equipped with a Teflon screw cap. The solution was stirred at 110 ºC under, 1 atmosphere of CO, for 4 days. After this time, a dark powder and a yellow solution were formed. The yellow solution was filtered and the solvent was evaporated to obtain a yellow oil. Its treatment with methanol (2 mL) at -50 ºC afforded a yellow solid which was dried under reduced pressure. Yield: 50 mg (41 %). Anal. Calcd. for $C_{30}H_{40}O_4OsP_2$: C, 50.27; H, 5.62. Found: C, 49.93; H, 5.81. IR (Toluene, cm^{-1}): ν (CO) 2003 (w), ν (CO) 1916 (s), ν (CO) 1900 (s). ^{1}H NMR (300.13 MHz, CD_2Cl_2, 298 K): δ 7.51 (dd, $^3J_{HH}$ = 7.3, $^4J_{HH}$ = 1.7 ,2H, CH-arom POP), 7.28 (m, 2H, CH-arom POP), 7.22 (dd, $^3J_{HH}$ = 7.7, $^3J_{HH}$ = 7.3, 2H, CH-arom POP), 2.50 (m, 4H, PCH(CH$_3$)$_2$), 1.57 (s, 6H, CH_3 POP), 1.11 (dvt, $^3J_{HH}$ = 6.9 , N = 16.6, 12H, PCH(CH_3)$_2$), 1.02 (dvt, $^3J_{HH}$ = 6.8, N = 15.3, 12H, PCH(CH_3)$_2$). ^{31}P{^{1}H} NMR (121.50 MHz, CD_2Cl_2, 298 K): 4.5 (s, POP). Crystals suitable for X-ray diffraction analysis were obtained by slow diffusion of pentane into a toluene solution of the complex at -30 ºC.

Reaction of 1 with CO: Formation of OsH$_2$CO{κ^3-*P,O,P*-[xant(P^{i}Pr$_2$)$_2$]} (7). A solution of **1** (0.100 g, 0.153 mmol) in toluene (5 mL) was stirred, under 1 atmosphere of CO, for 24h. The resulted solution was concentrated and pentane (2 mL) at 0 ºC was added to afford a yellow solid which was washed with pentane (2 x 2 mL) and dried under reduced pressure. Yield: 50 mg (49 %). The solid was characterized as **7** by comparison of its spectroscopic data with those reported in reference 8h.

Reaction of 7 with CO: Formation of OsH$_2$(CO)$_2${κ^2-*P,P*-[xant(P^{i}Pr$_2$)$_2$]} (8). A toluene-d_8 solution of **7** (40 mg, 0.06 mmol, in 0.6 mL) was placed in a NMR tube bearing a Teflon screw cap, under 1 atmosphere of CO, and was heated at 110 ºC for 8 h. After that, a mixture of **8** and **6** was formed in a 3:1 molar ratio. Spectroscopic data for **8**: ^{1}H NMR (300.13 MHz, C_7D_8, 298 K): δ 7.10 (d, $^3J_{HP}$ = 7.5, 2H, CH-arom POP), 6.96 (m, 2H, CH-arom POP), 6.93 (m, 2H, CH-arom POP), 2.52 (m, 1H, PCH(CH$_3$)$_2$), 2.36 (m, 1H, PCH(CH$_3$)$_2$), 2.22 (m, 1H, PCH(CH$_3$)$_2$), 2.18 (m, 1H, PCH(CH$_3$)$_2$), 1.40 (s, 3H, CH_3 POP), 1.31 (dd, $^3J_{HH}$ = 7.3, $^3J_{HP}$ = 15.0, 3H, PCH(CH_3)$_2$), 1.28-1.10 (m, 15H, PCH(CH_3)$_2$), 1.20 (s, 3H, CH_3 POP), 0.97 (dd, $^3J_{HH}$ = 7.1, $^3J_{HP}$ = 12.8, 3H, PCH(CH_3)$_2$), 0.89 (dd, $^3J_{HH}$ = 7.1, $^3J_{HP}$ = 13.8, 3H, PCH(CH_3)$_2$), -7.92 (ddd, $^2J_{HH}$ = 6.1, $^2J_{HP}$ = 19.6, $^2J_{HP}$ = 26.4, 1H, OsH), -10.01 (ddd, $^2J_{HH}$ = 6.1, $^2J_{HP}$ = 35.5, $^2J_{HP}$ = 67.5, 1H, OsH). ^{13}C{^{1}H} NMR (75.48 MHz, C_7D_8, 298 K): δ 188.0 (dd, $^2J_{CP}$ = 3.4, $^2J_{CP}$ = 74.1, CO), 186.0 (dd, $^2J_{CP}$ = 3.6, $^2J_{CP}$ = 10.0, CO), 156.0 (d, $^2J_{CP}$ = 6.7, C-arom POP), 155.8 (d, $^2J_{CP}$ = 6.9, C-arom POP), 134.8 (d, $^3J_{CP}$ = 3.0, C-arom POP), 134.4 (d, $^3J_{CP}$ = 3.0, C-arom POP), 129.4 (s, CH-arom POP), 125.8 (s, CH-arom POP), 125.8 (s, CH-arom POP), 125.5 (s, CH-arom POP), 123.0 (s, CH-arom POP), 123.0 (s, CH-arom POP), 122.9 (s, CH-arom POP), 122.9 (s, CH-arom POP), 122.4 (d, $^1J_{CP}$ = 26.4, C-arom POP), 121.1 (d, $^1J_{CP}$ = 27.9, C-arom POP), 36.1 (s, C(CH$_3$)$_2$ POP), 30.6 (s, C(CH$_3$)$_2$ POP), 30.0 (d, $^1J_{CP}$ = 25.2, PCH(CH$_3$)$_2$), 29.1 (d, $^1J_{CP}$ = 21.5, PCH(CH$_3$)$_2$), 26.5 (dd, $^3J_{CP}$ = 2.5, $^1J_{CP}$ = 27.8, PCH(CH$_3$)$_2$), 25.4 (dd, $^3J_{CP}$ = 4.8, $^1J_{CP}$ = 35.4, PCH(CH$_3$)$_2$), 24.6 (s, C(CH$_3$)$_2$ POP), 20.6 (s, PCH(CH$_3$)$_2$), 20.3 (s, PCH(CH$_3$)$_2$), 19.8 (d, $^2J_{CP}$ = 1.7, PCH(CH$_3$)$_2$), 18.8 (d, $^2J_{CP}$ = 5.0, PCH(CH$_3$)$_2$), 18.7 (dd, $^4J_{CP}$ = 1.9, $^2J_{CP}$ = 2.8, PCH(CH$_3$)$_2$), 18.1 (s, PCH(CH$_3$)$_2$), 18.0 (d, $^2J_{CP}$ = 2.3, PCH(CH$_3$)$_2$), 17.6 (d, $^2J_{CP}$ = 3.0, PCH(CH$_3$)$_2$). ^{31}P{^{1}H} NMR (121.49 MHz, C_7D_8, 298 K): 4.2 (d, $^2J_{PP}$ = 25.6, POP), 1.9 (d, $^2J_{PP}$ = 25.6, POP).

ASSOCIATED CONTENT

Supporting Information

The Supporting Information is available free of charge.

Instrumental methods, NMR spectra of complexes **2**, **3**, **4**, **5**, **6** and **8**, IR spectra of complexes **4** and **6**, structural analysis of complexes **2**, **4** and **6**, and computational details (PDF)

Cartesian coordinates of the optimized structures (XYZ)

Accession Codes

CCDC 1871559-1871561 contain the supplementary crystallographic data for this paper. These data can be obtained free of charge via www.ccdc.cam.ac.uk/data_request/cif, or by emailing data_request@ccdc.cam.ac.uk, or by contacting The Cambridge Crystallographic Data Centre, 12 Union Road, Cambridge CB2 1EZ, UK; fax: +44 1223 336033.

AUTHOR INFORMATION

Corresponding Author

*E-mail for A.A.: antonio.antinolo@uclm.es
M.A.E.: maester@unizar.es.

ORCID
Antonio Antiñolo: 0000-0002-4417-6417
Miguel A. Esteruelas: 0000-0002-4829-7590
Cristina García-Yebra: 0000-0002-5545-5112
Jaime Martín: 0000-0003-0909-3509
Enrique Oñate: 0000-0003-2094-719X
Alberto Ramos: 0000-0001-7993-7864

Present Adress

§Departamento de Química Orgánica y Química Inorgánica, Universidad de Alcalá, 28871 Alcalá de Henares, Spain.

Notes

The authors declare no competing financial interest.

ACKNOWLEDGMENT

Financial support from the MINECO of Spain (Projects CTQ2017-82935-P, CTQ2016-77614-P and Red de Excelencia Consolider CTQ2016-81797-REDC), the Diputación General de Aragón (E06_17R), FEDER, and the European Social Fund is acknowledged. A.R. acknowledges a postdoctoral contract funded by the "Plan Propio de I + D + i" of the Universidad de Castilla-La Mancha.

REFERENCES

(1) (a) Roesky, H. W.; Singh, S.; Yusuff, K. K. M.; Maguire, J. A.; Hosmane, N. S. Organometallic Hydroxides of Transition Elements. *Chem. Rev.* **2006**, *106*, 3813-3843. (b) Nelson, D. J.; Nolan, S. P. Hydroxide Complexes of the Late Transition Metals: Organometallic Chemistry and Catalysis. *Coord. Chem. Rev.* **2017**, *353*, 278-294.

(2) (a) Gould, R. O.; Jones, C. L.; Stephenson, T. A.; Tocher, D. A. Structural Characterization of Hydroxo-Bridged Arene-Ruthenium and -Osmium Complexes: Further Reactions of Hydroxo-Bridged Complexes. *J. Organomet. Chem.* **1984**, *264*, 365-378. (b) Cabeza, J. A.; Mann, B. E.; Maitlis, P. M.; Brevard, C. The Synthesis of Di-Nuclear and Tetra-Nuclear *p*-Cymene-Osmium Hydride Complexes - Characterization by ^{1}H (^{187}Os) Reverse INEPT Two-Dimensional Nuclear Magnetic-Resonance Spectroscopy. *J. Chem. Soc., Dalton Trans.* **1988**, 629-634. (c) Esteruelas, M. A.; García-Yebra, C.; Oliván, M.; Oñate, E. Reaction of a Cationic Osmium(IV) Dihydride with Ethylene: Formation and Structure of the Novel Tetraethylene Dimer Complex $[\{(P^{i}Pr_3)(\eta^2\text{-}C_2H_4)_2Os\}_2(\mu\text{-}OH)_2(\mu\text{-}O_2CCH_3)]BF_4$. *Organometallics* **2000**, *19*, 3260-3262. (d) Peacock, A. F. A.; Habtemariam, A.; Fernández, R.; Walland, V.; Fabbiani, F. P. A.; Parsons, S.; Aird, R. E.; Jodrell, D. I.; Sadler, P. J. Tuning the Reactivity of Osmium(II) and Ruthenium(II) Arene Complexes under Physiological Conditions. *J. Am. Chem. Soc.* **2006**, *128*, 1739-1748.

(3) (a) Wu, A.; Dehestani, A.; Saganic, E.; Crevier, T. J.; Kaminsky, W.; Cohen, D. E.; Mayer, J. M. Reactions of Tp-Os Nitrido Complexes with the Nucleophiles Hydroxide and Thiosulfate. *Inorg. Chim. Acta.* **2006**, *359*, 2842-2849. (b) Kiefer, A. M.; Giles, J. A.; Shapley, P. A. Synthesis, Structure, and Reactivity of Organometallic Osmium(VI) Hydroxo Compounds. *Organometallics* **2007**, *26*, 1881-1887.

(4) (a) Castarlenas, R.; Esteruelas, M. A.; Oñate, E. Preparation, X-ray Structure, and Reactivity of an Osmium-Hydroxo Complex Stabilized by an N-Heterocyclic Carbene Ligand: A Base-Free Catalytic Precursor for Hydrogen Transfer from 2-Propanol to Aldehydes. *Organometallics* **2008**, *27*, 3240-3247. (b) Buil, M. L.; Cadierno, V.; Esteruelas, M. A.; Gimeno, J.; Herrero, J.; Izquierdo, S.; Oñate, E. Selective Hydration of Nitriles to Amides Promoted by an Os-NHC Catalyst: Formation and X-ray Characterization of κ^2-Amidate Intermediates. *Organometallics* **2012**, *31*, 6861-6867. (c) Buil, M. L.; Esteruelas, M. A.; Herrero, J.; Izquierdo, S.; Pastor, I. M.; Yus, M. Osmium Catalyst for the Borrowing Hydrogen Methodology: *α*-Alkylation of Arylacetonitriles and Methyl Ketones. *ACS Catal.* **2013**, *3*, 2072-2075.

(5) (a) Gotzig, J.; Werner, R.; Werner, H. Basic Metals: 53. Ruthenium- and Osmium-Complexes with Dimethylphosphinomethanide-Anion as Ligands. *J. Organomet. Chem.* **1985**, *290*, 99-114. (b) Edwards, A. J.; Elipe, S.; Esteruelas, M. A.; Lahoz, F. J.; Oro, L. A.; Valero, C. Synthesis and Reactivity of the Unusual Five-Coordinate Hydrido-Hydroxo Complex $OsH(OH)(CO)(P^{i}Pr_3)_2$. *Organometallics* **1997**, *16*, 3828-3836. (c) Renkema, K. B.; Huffman, J. C.; Caulton, K. G. Characterization and Structure of $OsH(OH)(CO)(PBu_2Me)^{t}Bu_2$. *Polyhedron* **1999**, *18*, 2575-2578. (d) Prokopchuk, D. E.; Collado, A.; Lough, A. J.; Morris, R. H. Structural Properties of *trans* Hydrido-Hydroxo $M(H)(OH)(NH_2CMe_2CMe_2NH_2)(PPh_3)_2$ (M = Ru, Os) Complexes and their Proton Exchange Behaviour with Water in Solution. *Dalton Trans.* **2013**, *42*, 10214-10220. (e) Buil, M. L.; Cardo, J. J. F.; Esteruelas, M. A.; Fernández, I.; Oñate, E. Hydroboration and Hydrogenation of an Osmium-Carbon Triple Bond: Osmium Chemistry of a Bis-*σ*-Borane. *Organometallics* **2015**, *34*, 547-550. f) Esteruelas, M. A.; García-Yebra, C.; Martín, J.; Oñate, E. Dehydrogenation of Formic Acid Promoted by a Trihydride-Hydroxo-Osmium (IV) Complex: Kinetics and Mechanism. *ACS Catal.* **2018**, 8, 11314−11323.

(6) Ozerov, O. V. Oxidative Addition of Water to Transition Metal Complexes. *Chem. Soc. Rev.* **2009**, *38*, 83-88.

(7) *Pincer Compounds: Chemistry and Applications*; Ed.: Morales-Morales, D. Elsevier, 2018.

(8) For complexes of platinum group metals bearing this ligand see: (a) Asensio, G.; Cuenca, A. B.; Esteruelas, M. A.; Medio-Simón, M.; Oliván, M.; Valencia, M. Osmium(III) Complexes with POP Pincer Ligands: Preparation from Commercially Available $OsCl_3{\cdot}3H_2O$ and Their X-ray Structures. *Inorg. Chem.* **2010**, *49*, 8665-8667. (b) Esteruelas, M. A.; Oliván, M.; Vélez, A. Xantphos-Type Complexes of Group 9: Rhodium versus Iridium. *Inorg. Chem.* **2013**, *52*, 5339-5349. (c) Alós, J.; Bolaño, T.; Esteruelas, M. A.; Oliván, M.; Oñate, E.; Valencia, M. POP-Pincer Osmium-Polyhydrides: Head-to-Head (*Z*)-Dimerization of Terminal Alkynes. *Inorg. Chem.* **2013**, *52*, 6199-6213. (d) Esteruelas, M. A.; Oliván, M.; Vélez, A. POP-Pincer Silyl Complexes of Group 9: Rhodium versus Iridium. *Inorg. Chem.* **2013**, *52*, 12108-12119. (e) Alós, J.; Bolaño, T.; Esteruelas, M. A.; Oliván, M.; Oñate, E.; Valencia, M. POP-Pincer Ruthenium Complexes: d^6 Counterparts of Osmium d^4 Species. *Inorg. Chem.* **2014**, *53*, 1195-1209. (f) Esteruelas, M. A.; Oliván, M.; Vélez, A. POP-Rhodium-Promoted C-H and B-H Bond Activation and C-B Bond Formation. *Organometallics* **2015**, *34*, 1911-1924. (g) Esteruelas, M. A.; Oliván, M.; Vélez, A. Conclusive Evidence on the Mechanism of the Rhodium-Mediated Decyanative Borylation. *J. Am. Chem. Soc.* **2015**, *137*, 12321-12329. (h) Alós, J.; Esteruelas, M. A.; Oliván, M.; Oñate, E.; Puylaert, P. C-H Bond Activation Reactions in Ketones and Aldehydes Promoted by POP-Pincer Osmium and Ruthenium Complexes. *Organometallics* **2015**, *34*, 4908-4921. (i) Esteruelas, M. A.; Nolis, P.; Oliván, M.; Oñate, E.; Vallribera, A.; Vélez, A. Ammonia Borane Dehydrogenation Promoted by a Pincer-Square-Planar Rhodium(I) Monohydride: A Stepwise Hydrogen Transfer from the Substrate to the Catalyst. *Inorg. Chem.* **2016**, *55*, 7176-7181. (j) Esteruelas, M. A.; García-Yebra, C.; Martín, J.; Oñate, E. *mer*, *fac*, and Bidentate Coordination of an Alkyl-POP Ligand in the Chemistry of Nonclassical Osmium Hydrides. *Inorg. Chem.* **2017**, *56*, 676-683. (k) Curto, S. G.; Esteruelas, M. A.; Oliván, M.; Oñate, E.; Vélez, A. Selective C-Cl Bond Oxidative Addition of Chloroarenes to a POP-Rhodium Complex. *Organometallics* **2017**, *36*, 114-128. (l) Esteruelas, M. A.; Fenández, I.; García-Yebra, C.; Martín, J.; Oñate, E. Elongated *σ*-Borane versus *σ*-Borane in Pincer-POP-Osmium Complexes. *Organometallics* **2017**, *36*, 2298-2307. (m) Curto, S. G.; Esteruelas, M. A.; Oliván, M.; Oñate, E.; Vélez, A. β-Borylalkenyl *Z*-*E* Isomerization in Rhodium-Mediated Diboration of Nonfunctionalized Internal Alkynes. *Organometallics* **2018**, *37*, 1970-1978. (n) Esteruelas, M. A.; Oliván, M. Osmium Complexes with POP Pincer Ligands. In *Pincer Compounds*; 1st ed.; Morales-Morales, D.; Elsevier: 2018.

(9) See for example: Cuesta, L.; Hevia, E.; Morales, D.; Pérez, J.; Riera, L.; Miguel, D. Reactivity of Molybdenum and Rhenium Hydroxo Complexes toward Organic Electrophiles: Reactions that Afford Carboxylato Products. *Organometallics* **2006**, *25*, 1717-1722.

(10) Buil, M. L.; Cardo, J. J. F.; Esteruelas, M. A.; Oñate, E. Dehydrogenative Addition of Aldehydes to a Mixed NHC-Osmium-Phosphine Hydroxide Complex: Formation of Carboxylate Derivatives. *Organometallics* **2016**, *35*, 2171-2173.

(11) (a) Cole, S. C.; Coles, M. P.; Hitchcock, P. B. A Step too Far? Assessment of the Boroxide Ligand in Ring-Opening Polymerization. *Organometallics* **2004**, *23*, 5159-5168. (b) Cole, S. C.; Coles, M. P.; Hitchcock, P. B. Boroxide Complexes of the Group 4 Metals: A "Noninnocent" Ligand in Olefin Polymerization. *Organometallics* **2005**, *24*, 3279-3289. (c) Nasr, A.; Breuil, P. A. R.; Silva, D. C.; Berthod, M.; Dellus, N.; Jeanneau, E.; Lemaire, M.; Olivier-Bourbigou, H. New Boron-Containing Molybdenum Imido Alkylidene Complexes for Linear Olefin Homometathesis. *Organometallics* **2013**, *32*, 5320-5325.

(12) Coles, M. P. Metal Compounds of Boron-Substituted Alkoxide ('Boroxide') Ligands. *Coord. Chem. Rev.* **2016**, *323*, 52-59.

(13) (a) Beck, G.; Hitchcock, P. B.; Lappert, M. F.; Mackinnon, I. A. Lipophilic Lithium Alkoxides or Dialkylboroxides - X-Ray Structures of $[Li(\mu\text{-}OR')]_2$ and $Li(OBR_2)(tmeda)$, [tmeda = $(Me_2NCH_2)_2$, R = $CH(SiMe_3)_2$, R' = C^tBu_3 or BR_2]. *J. Chem. Soc., Chem. Comm.* **1989**, 1312-1314. (b) Murphy, D.; Sheehan, J. P.; Spalding, T. R.; Ferguson, G.; Lough, A. J.; Gallagher, J. F. Compounds Containing B-O-X Bonds (X = Si, Ge, Sn, Pb). Part 4. Crystal-Structures of $B(SiPh_3)_3$, $PhB(OSiPh_3)_2$ and $PhB(OGePh_3)_2$. *J. Mater. Chem.* **1993**, *3*, 1275-1283. (c) Anulewicz-Ostrowska, R.; Luliński, S.; Serwatowski, J. Synthesis and Characterization of Dialkylmetal Boryloxides $[(\mu\text{-}9\text{-}BBN\text{-}9\text{-}O)MMe_2]_2$, M = Al, Ga, In. *Inorg. Chem.* **1999**, *38*, 3796-3800. (d) Anulewicz-Ostrowska, R.; Luliński, S.; Serwatowski, J.; Suwińska, K. Diverse Reactivity of Dialkylaluminum Dimesitylboryloxides $[(\mu\text{-}Mes_2BO)AlR_2]_2$. Synthetic and Structural Study. *Inorg. Chem.* **2000**, *39*, 5763-5767. (e) Vidovic, D.; Moore, J. A.; Jones, J. N.; Cowley, A. H. Synthesis and Characterization of a Coordinated Oxoborane: Lewis Acid Stabilization of a Boron-Oxygen Double Bond. *J. Am. Chem. Soc.* **2005**, *127*, 4566-4567. (f) Le Coz, E.; Dorcet, V.; Roisnel, T.; Tobisch, S.; Carpentier, J. F.; Sarazin, Y. Low-Coordinate Barium Boryloxides: Synthesis and Dehydrocoupling Catalysis for the Production of Borasiloxanes. *Angew. Chem., Int. Ed.* **2018**, *57*, 11747-11751. (g) Someşan, A. A.; Le Coz, E.; Roisnel, T.; Silvestru, C.; Sarazin, Y. Stable Lead(II) Boroxides. *Chem. Commun.* **2018**, *54*, 5299-5302.

(14) (a) Weese, K. J.; Bartlett, R. A.; Murray, B. D.; Olmstead, M. M.; Power, P. P. Synthesis and Spectroscopic and Structural Characterization of Derivatives of the Quasi-Alkoxide Ligand $[OBMes_2]$-(Mes = 2,4,6-$Me_3C_6H_2$). *Inorg. Chem.* **1987**, *26*, 2409-2413. (b) Chen, H.; Power, P. P.; Shoner, S. C. Synthesis and Spectroscopic and X-Ray Structural Characterization of the First Homoleptic Transition-Metal Boryloxides $[Mn(OBTrip_2)(\mu\text{-}OBTrip_2)]_2$ and $[Fe(OBMes_2)(\mu\text{-}OBMes_2)]_2$. *Inorg. Chem.* **1991**, *30*, 2884-2888. (c) Chisholm, M. H.; Folting, K.; Haubrich, S. T.; Martin, J. D. Triple Bonds between Tungsten Atoms with Ancillary Dimesitylboroalkoxide Ligands. Preparations, Properties and Structures of $W_2(NMe_2)_4[OB(Mes)_2]_2$ and $W_2(OBu^t)_4[OB(Mes)_2]_2$ *Inorg. Chim. Acta.* **1993**, *213*, 17-24. (d) Gibson, V. C.; Redshaw, C.; Clegg, W.; Elsegood, M. R. J. Synthesis and Structural Characterization of some Novel Metalloboroxides Bearing Boron-Bound Mesityl and Fluoromesityl Substituents: The Molecular Structure of the First Metallaboroxane Complex. *Polyhedron* **1997**, *16*, 2637-2641. (e) Cole, S. C.; Coles, M. P.; Hitchcock, P. B. Transition-Metal Imido-Boroxide Complexes: a Structural and Spectroscopic Investigation of the Influence of Boron. *J. Chem. Soc., Dalton Trans.* **2002**, 4168-4174. (f) Cole, S. C.; Coles, M. P.; Hitchcock, P. B. Neutral and Zwitterionic Group 4 Metal Alkyls with Ancillary Boroxide Ligands. *Dalton Trans.* **2004**, 3428-3430.

(15) Luo, Y. R. Comprehensive Handbook of Chemical Bond Energies. CRC Press: Boca Raton, FL, 2007.

(16) (a) Che, C. M.; Huang, J. S.; Li, Z. Y.; Poon, C. K.; Tong, W. F.; Lai, T. F.; Cheng, M. C.; Wang, C. C.; Wang, Y. Dialkoxyosmium(IV) Porphyrins. Crystal and Molecular-Structures of Diethoxy-, Diphenoxy-, and Bis(2-propanolato) (*meso*-tetraphenylporphyrinato)osmium(IV). *Inorg. Chem.* **1992**, *31*, 5220-5225. (b) Kuhlman, R.; Streib, W. E.; Huffman, J. C.; Caulton, K. G. Site Selectivity in Electrophilic (H^+,CH_3^+) abstraction on $Os(H)_2X_2(P^iPr_3)_2$. *J. Am. Chem. Soc.* **1996**, *118*, 6934-6945. (c) Cheung, W. M.; Zhang, Q. F.; Williams, I. D.; Leung, W. H. Synthesis, Crystal Structures, and Reactivity of Osmium(II) an -(IV) Complexes Containing a Dithioimidodiphosphinate Ligand. *Inorg. Chem.* **2007**, *46*, 5754-5762. (d) Esteruelas, M. A.; García-Raboso, J.; Oliván, M. Preparation of Half-Sandwich Osmium Complexes by Deprotonation of Aromatic and Pro-aromatic Acids with a Hexahydride Brønsted Base. *Organometallics* **2011**, *30*, 3844-3852.

(17) Esteruelas, M. A.; López, A. M.; Mora, M.; Oñate, E. B-H Activation and H-H Formation: Two Consecutive Heterolytic Processes on an Osmium-Hydrogensulfide Bond. *Chem. Commun.* **2013**, *49*, 7543-7545.

(18) Liu, S. Y.; Légaré, M. A.; Auerhammer, D.; Hofmann, A.; Braunschweig, H. The First Boron-Tellurium Double Bond: Direct Insertion of Heavy Chalcogens into a Mn=B Double Bond. *Angew. Chem., Int. Ed.* **2017**, *56*, 15760-15763.

(19) Wang, Y.; Hu, H. F.; Zhang, J. Y.; Cui, C. M. Comparison of Anionic and Lewis Acid Stabilized N-Heterocyclic Oxoboranes: Their Facile Synthesis from a Borinic Acid. *Angew. Chem., Int. Ed.* **2011**, *50*, 2816-2819.

(20) Esteruelas, M. A.; López, A. M.; Oliván, M. Polyhydrides of Platinum Group Metals: Nonclassical Interactions and *σ*-Bond Activation Reactions. *Chem. Rev.* **2016**, *116*, 8770-8847.

(21) See for example: (a) Castillo, A.; Esteruelas, M. A.; Oñate, E.; Ruíz, N. Dihydrido and Trihydrido Diolefin Complexes Stabilized by the $Os(P^iPr_3)_2$ Unit: New Examples of Quantum Mechanical Exchange Coupling in Trihydrido Osmium Compounds. *J. Am. Chem. Soc.* **1997**, *119*, 9691-9698. (b) Casarrubios, L.; Esteruelas, M. A.; Larramona, C.; Muntaner, J. G.; Oñate, E.; Sierra, M. A. 2-Azetidinones as Precursors of Pincer Ligands: Preparation, Structure, and Spectroscopic Properties of CC'N-Osmium Complexes. *Inorg. Chem.* **2015**, *54*, 10998-11006.

(22) (a) Pontiggia, A. J.; Chaplin, A. B.; Weller, A. S. Cationic Iridium Complexes of the Xantphos Ligand. Flexible Coordination Modes and the Isolation of the Hydride Insertion Product with an Alkene. *J. Organomet. Chem.* **2011**, *696*, 2870-2876. (b) Dallanegra, R.; Chaplin, A. B.; Weller, A. S. Rhodium Cyclopentyl Phosphine Complexes of Wide-Bite-Angle Ligands DPEphos and Xantphos. *Organometallics* **2012**, *31*, 2720-2728. (c) Johnson, H. C.; Torry-Harris, R.; Ortega, L.; Theron, R.; McIndoe, J. S.; Weller, A. S. Exploring the Mechanism of the Hydroboration of Alkenes by Amine-Boranes Catalysed by $[Rh(Xantphos)]^+$. *Catal. Sci. Technol.* **2014**, *4*, 3486-3494. (d) Johnson, H. C.; Leitao, E. M.; Whitten, G. R.; Manners, I.; Lloyd-Jones, G. C.; Weller, A. S. Mechanistic Studies of the Dehydrocoupling and Dehydropolymerization of Amine-Boranes Using a $[Rh(Xantphos)]^+$ Catalyst. *J. Am. Chem. Soc.* **2014**, *136*, 9078-9093. (e) Johnson, H. C.; Weller, A. S. P-C-Activated Bimetallic Rhodium Xantphos Complexes: Formation and Catalytic Dehydrocoupling of Amine-Boranes. *Angew. Chem., Int. Ed.* **2015**, *54*, 10173-10177. (f) Ren, P.; Pike, S. D.; Pernik, I.; Weller, A. S.; Willis, M. C. Rh-POP Pincer Xantphos Complexes for C-S and C-H Activation. Implications for Carbothiolation Catalysis. *Organometallics* **2015**, *34*, 711-723. (g) Adams, G. M.; Weller, A. S. POP-Type Ligands: Variable Coordination and Hemilabile Behaviour. *Coord. Chem. Rev.* **2018**, *355*, 150-172. (h) Adams, G. M.; Colebatch, A. L.; Skornia, J. T.; McKay, A. I.; Johnson, H. C.; Lloyd-Jones, G. C.; Macgregor, S. A.; Beattie, N. A.; Weller, A. S. Dehydropolymerization of $H_3B{\cdot}NMeH_2$ To Form Polyaminoboranes Using [Rh(Xantphos-alkyl)] Catalysts. *J. Am. Chem. Soc.* **2018**, *140*, 1481-1495.

(23) (a) Stalick, J. K.; Ibers, J. A. Crystal and Molecular Structure of Tricarbonylbis(triphenylphosphine)osmium(0), $Os(CO)_3(P(C_6H_5)_3)_2$. *Inorg. Chem.* **1969**, *8*, 419-423. (b) Fiedler, T.; Bhuvanesh, N.; Hampel, F.; Reibenspies, J. H.; Gladysz, J. A. Gyroscope Like Molecules Consisting of Trigonal or Square Planar Osmium Rotators within Three-Spoked Dibridgehead Diphosphine Stators: Syntheses, Substitution Reactions, Structures, and Dynamic Proper-

ties. *Dalton Trans.* **2016**, *45*, 7131-7147. (c) Bissert, R.; Braunschweig, H.; Dewhurst, R. D.; Schneider, C. Metal-Only Lewis Pairs Based on Zerovalent Osmium. *Organometallics* **2016**, *35*, 2567-2573.

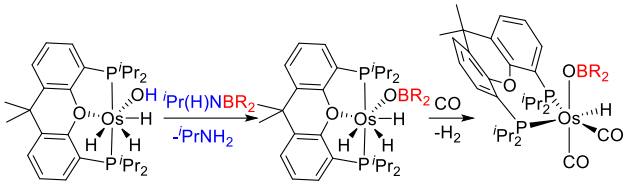

BR$_2$ = BCy$_2$, BBN

Supporting Information For

Reactions of an Osmium(IV)-Hydroxo Complex with Amino-Boranes: Formation of Boroxide Derivatives

Antonio Antiñolo,[†,] Miguel A. Esteruelas,[‡,*] Cristina García-Yebra,[‡,§] Jaime Martín,[‡] Enrique Oñate,[‡] and Alberto Ramos[†]*

[†]Departamento de Química Inorgánica, Orgánica y Bioquímica-Centro de Innovación en Química Avanzada (ORFEO-CINQA), Universidad de Castilla-La Mancha, Campus Universitario, E-13071 Ciudad Real, Spain

[‡]Departamento de Química Inorgánica, Instituto de Síntesis Química y Catálisis Homogénea (ISQCH), Centro de Innovación en Química Avanzada (ORFEO-CINQA), Universidad de Zaragoza-CSIC, 50009 Zaragoza, Spain

[§]Departamento de Química Orgánica y Química Inorgánica, Universidad de Alcalá, 28871 Alcalá de Henares, Spain

*Corresponding authors' e-mail address: antonio.antinolo@uclm.es , maester@unizar.es

Contents:

Instrumental Methods. Solvents were dried using standard procedures and distilled under argon atmosphere or obtained dry from an MBraun solvent purification apparatus. Pentane and dichloromethane were subsequently stored over P_2O_5 in the glovebox. Toluene and benzene were stored over sodium in the glovebox. Commercial chemicals were used as received, except where otherwise noted. NMR spectra were recorded on either a Bruker Avance 300, 400 or 500 MHz instrument. Signals were assigned using also bidimensional NMR experiments (^{1}H-^{1}H COSY, ^{1}H-^{13}C{^{1}H} HMBC and ^{1}H-^{13}C{^{1}H} HSQC). Elemental analyses were carried out using a Perkin-Elmer 2400 CHNS/O analyzer, and IR spectra were measured using a PerkinElmer Spectrum 100 FT-IR spectrometer.

NMR Spectra of Amino-Boranes

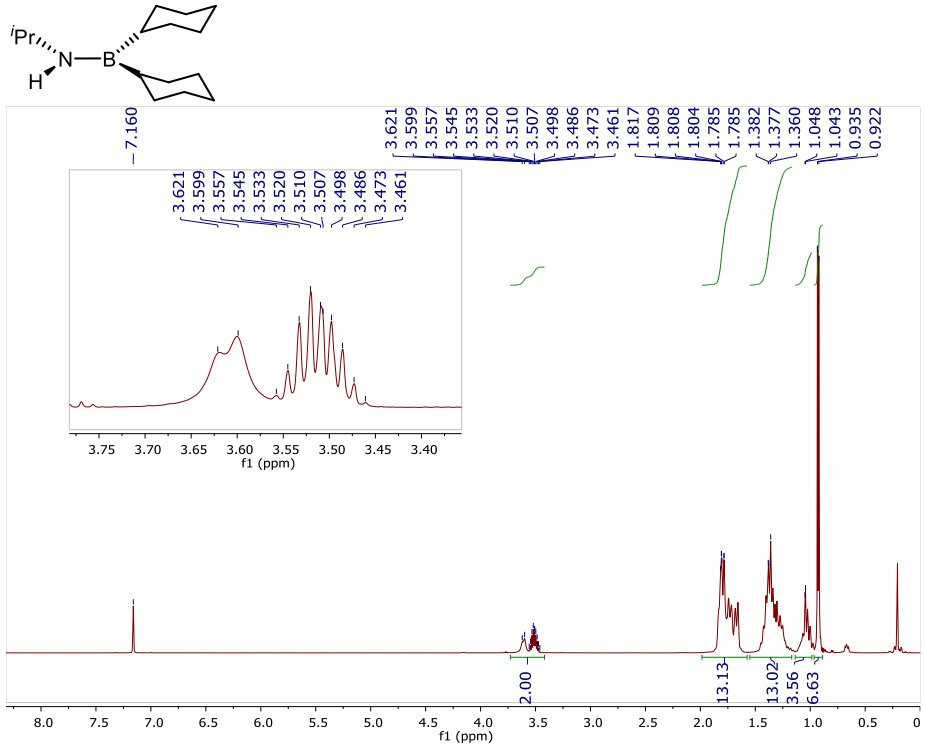

Figure S1. ^{1}H NMR (500 MHz, C_6D_6, 298 K) spectrum of amino-borane ^{i}**PrNHBCy$_2$**.

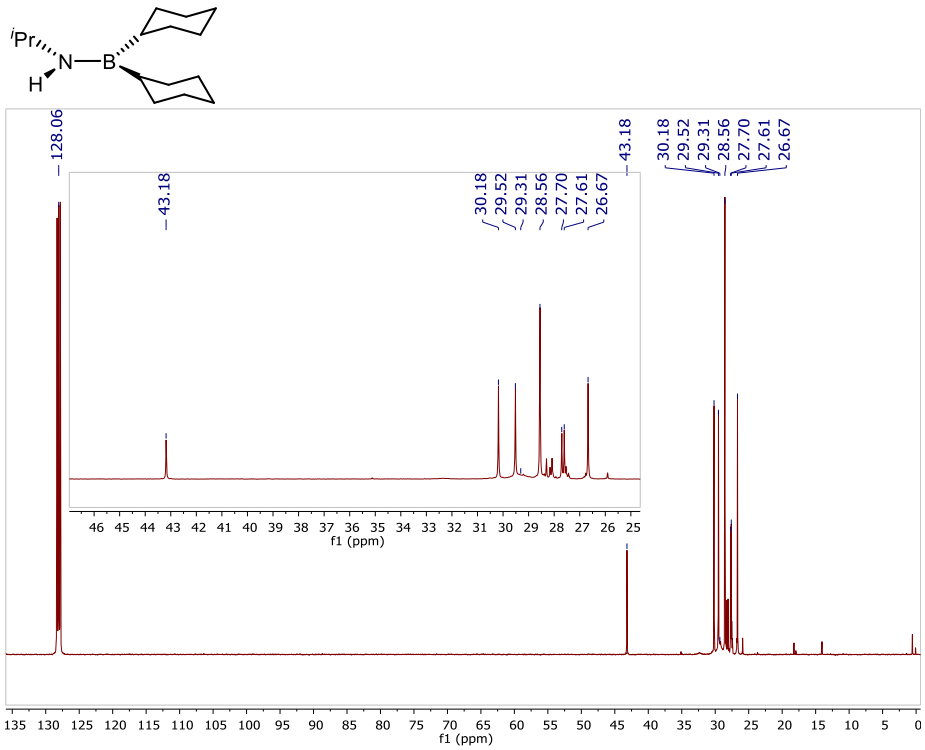

Figure S2. ^{13}C{^{1}H} NMR (101 MHz, C_6D_6, 298 K) spectrum of amino-borane ^{i}**PrNHBCy$_2$**.

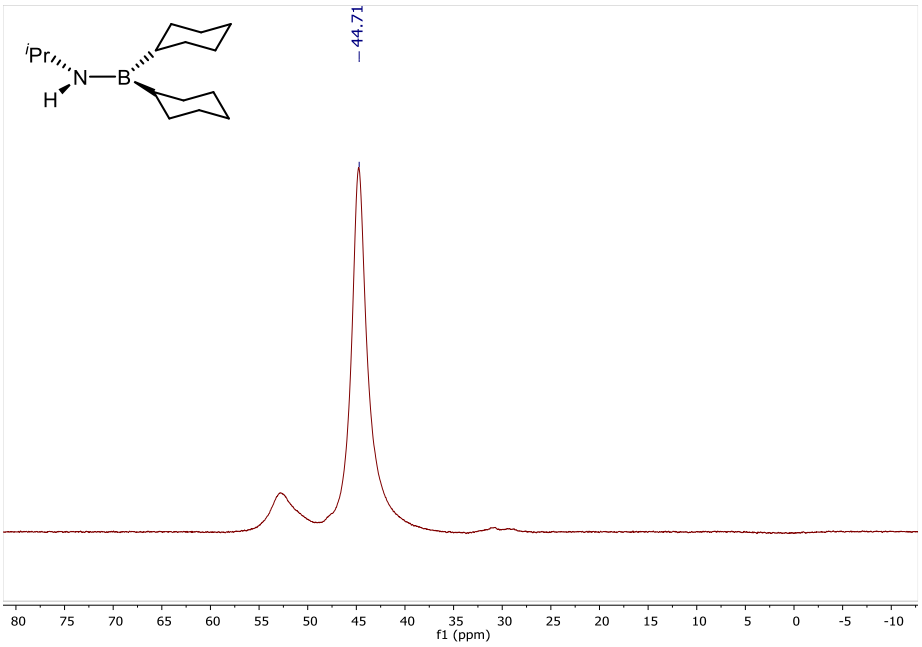

Figure S3. ^{11}B NMR (160 MHz, C_6D_6, 298 K) spectrum of amino-borane ^{i}**PrNHBCy$_2$**.

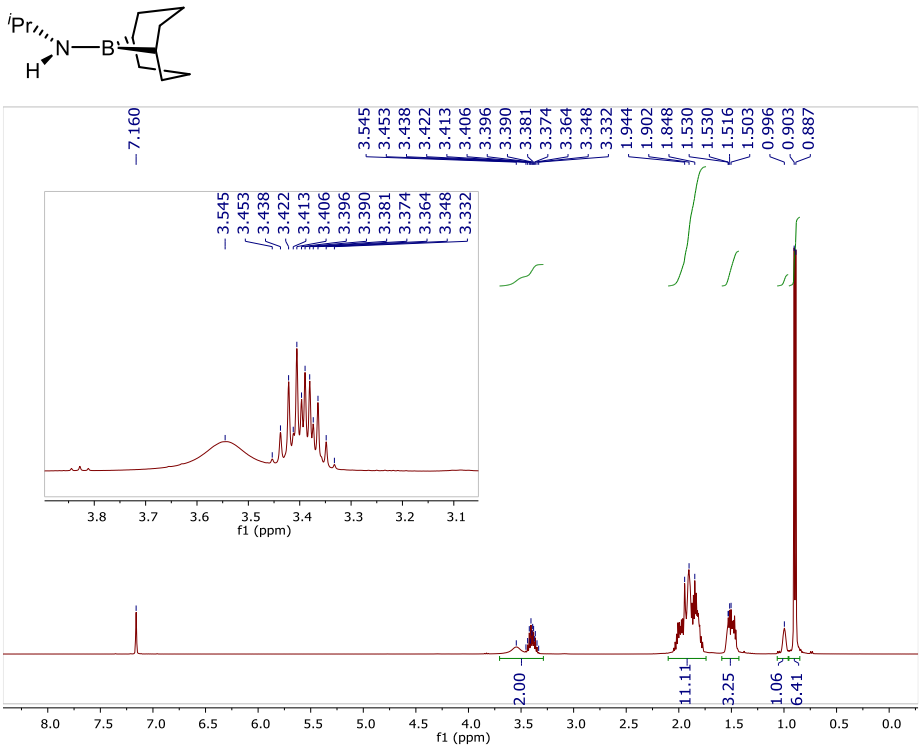

Figure S4. ^{1}H NMR (400 MHz, C_6D_6, 298 K) spectrum of amino-borane ^{i}**PrNHBBN**.

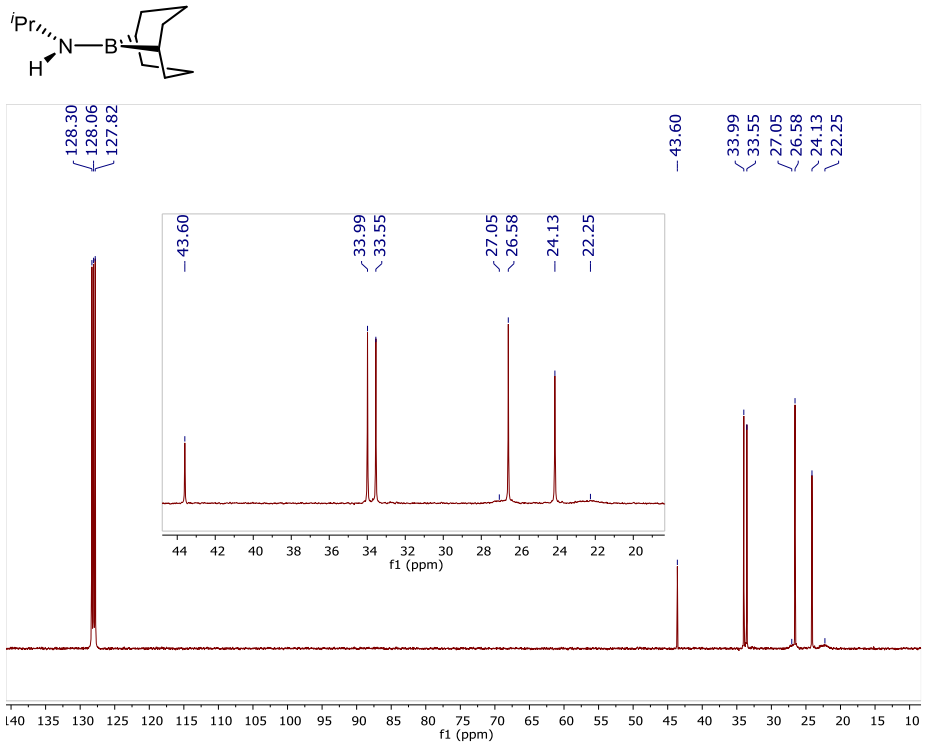

Figure S5. $^{13}C\{^{1}H\}$ NMR (101 MHz, C_6D_6, 298 K) spectrum of amino-borane **^{i}PrNHBBN**.

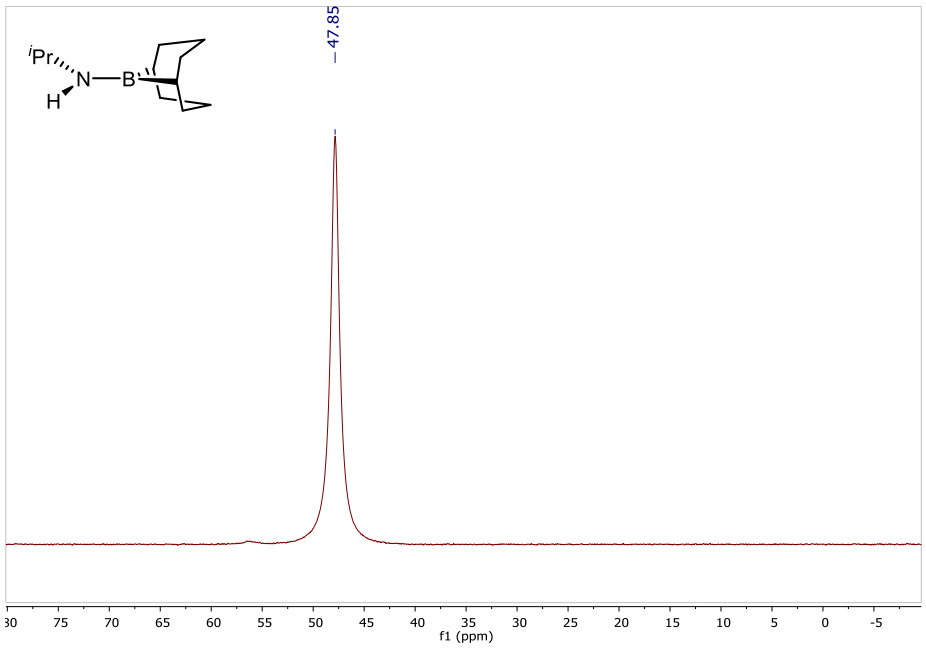

Figure S6. ^{11}B NMR (128 MHz, C_6D_6, 298 K) spectrum of amino-borane **^{i}PrNHBBN**.

NMR Spectra of Complexes 2, 3, 4, 5, 6 and 8.

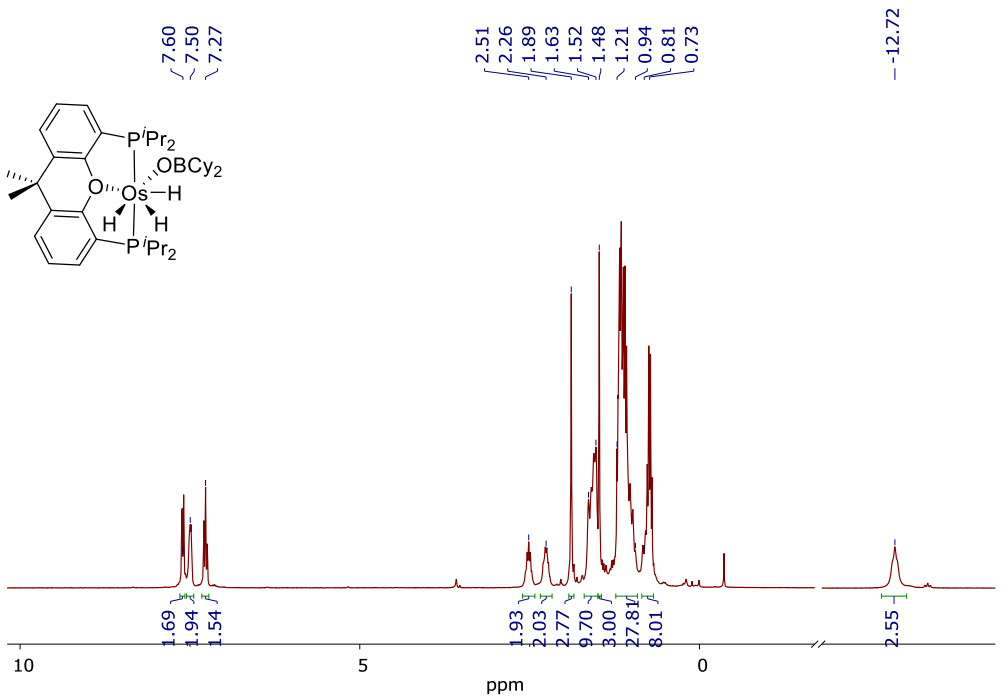

Figure S7. ^{1}H NMR (300.13 MHz, C_4D_8O, 298 K) spectrum of complex **2**.

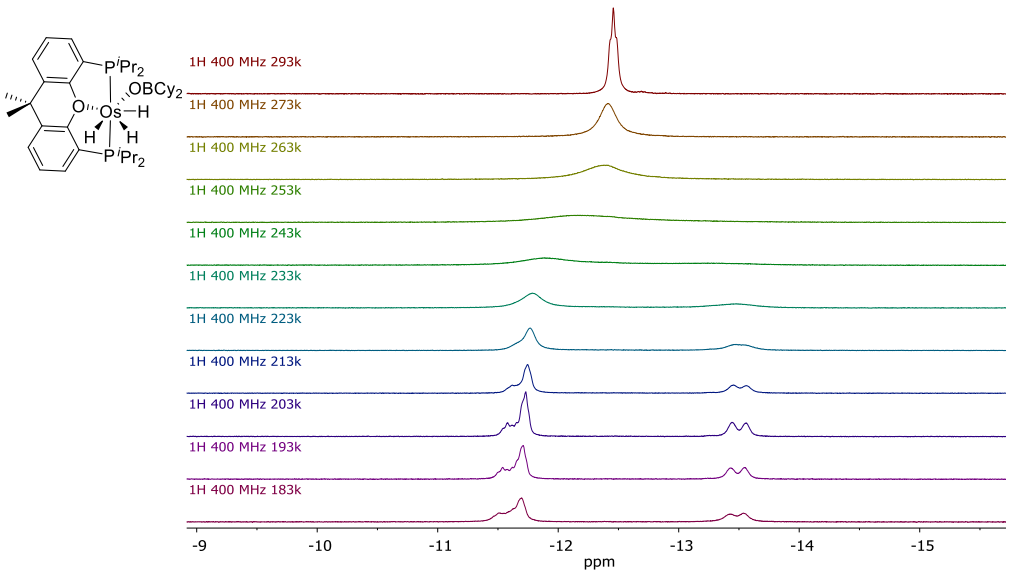

Figure S8. High-field region of the ^{1}H NMR (400.13 MHz, C_7D_8) spectrum of complex **2** between 293 and 183 K.

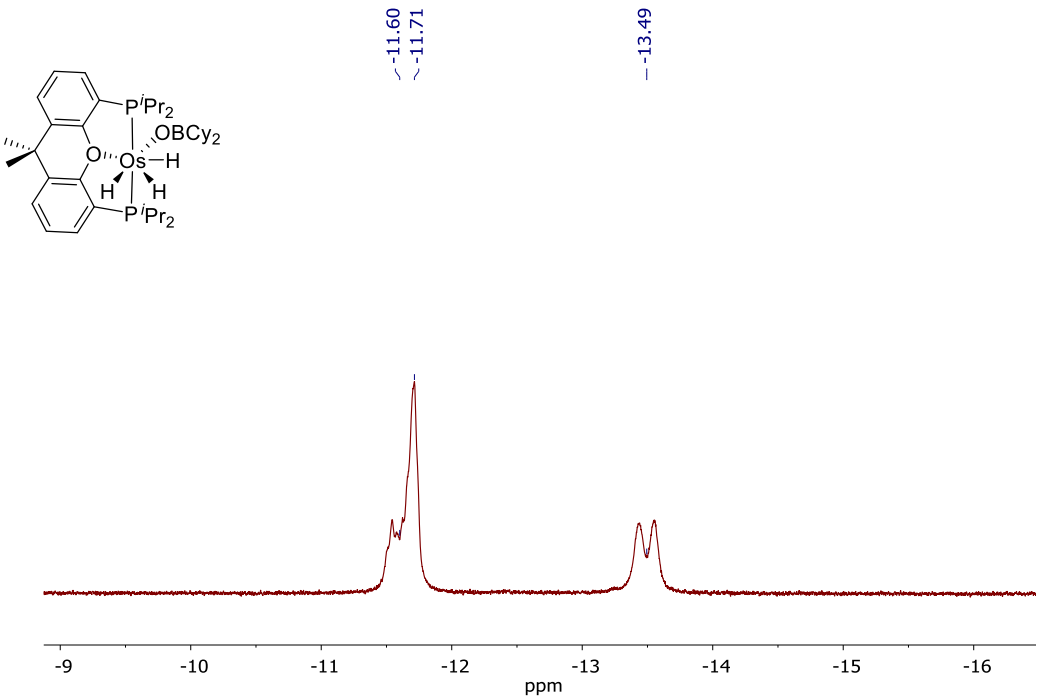

Figure S9. High-field region of the ^{1}H NMR (400.13 MHz, C_7D_8, 193 K) spectrum of complex **2**.

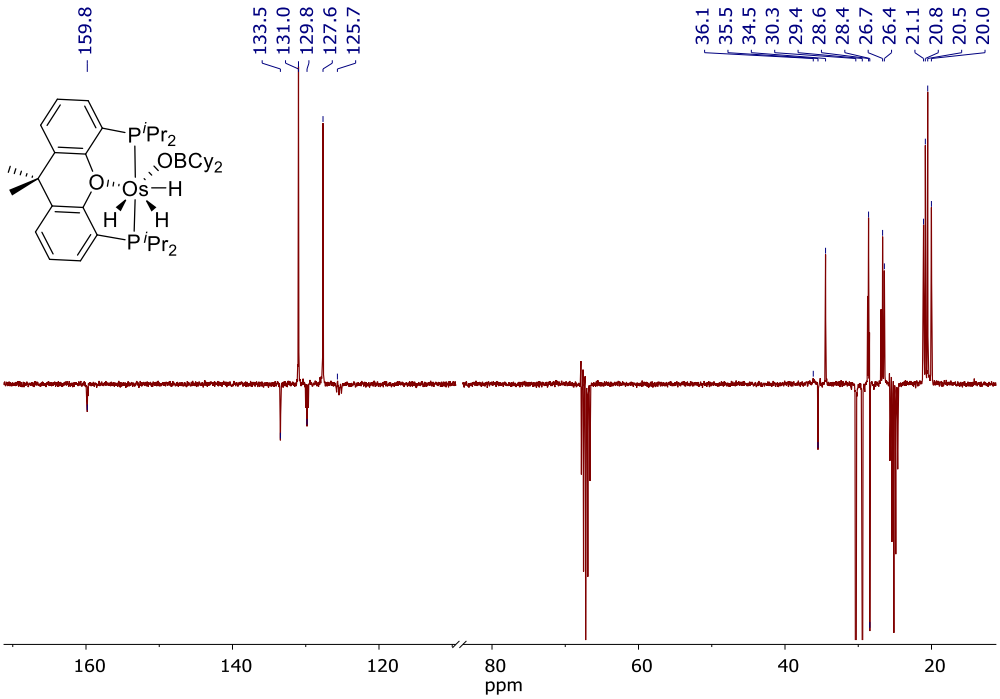

Figure S10. ^{13}C{^{1}H}-APT NMR (75.47 MHz, C_4D_8O, 298 K) spectrum of complex **2**.

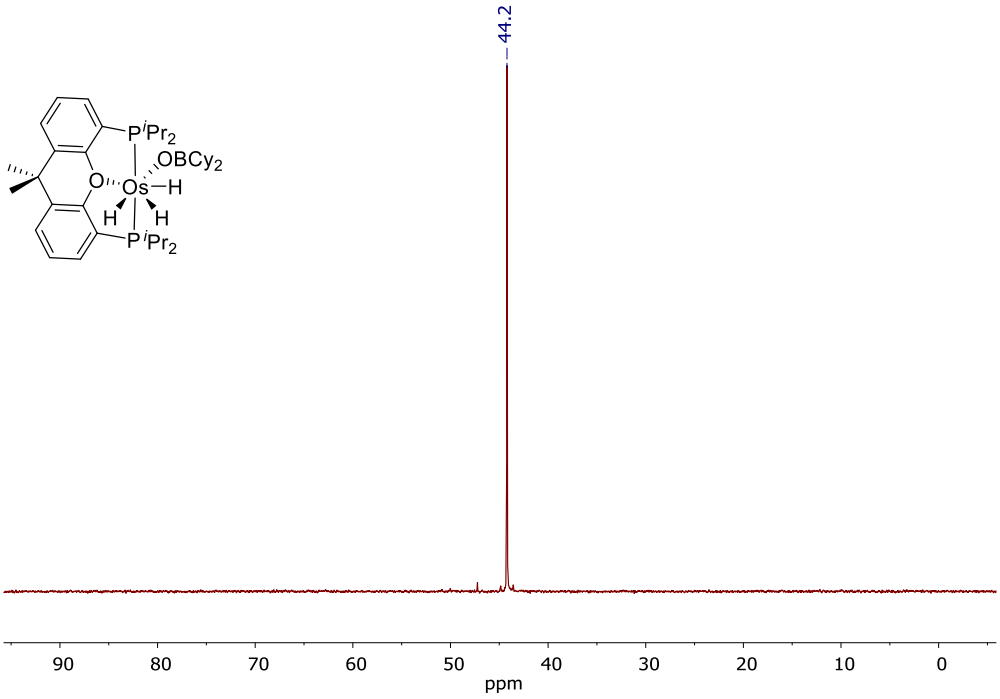

Figure S11. $^{31}P\{^{1}H\}$ NMR (161.98 MHz, C_7D_8, 298 K) spectrum of complex **2**.

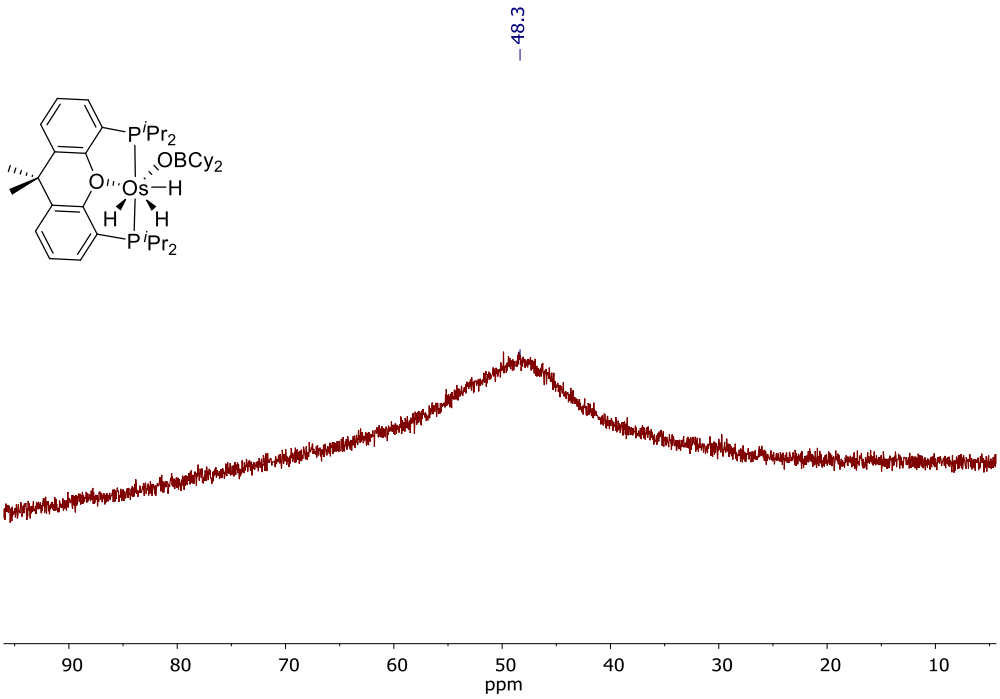

Figure S12. ^{11}B NMR (96.30 MHz, C_6D_6, 298 K) spectrum of complex **2**.

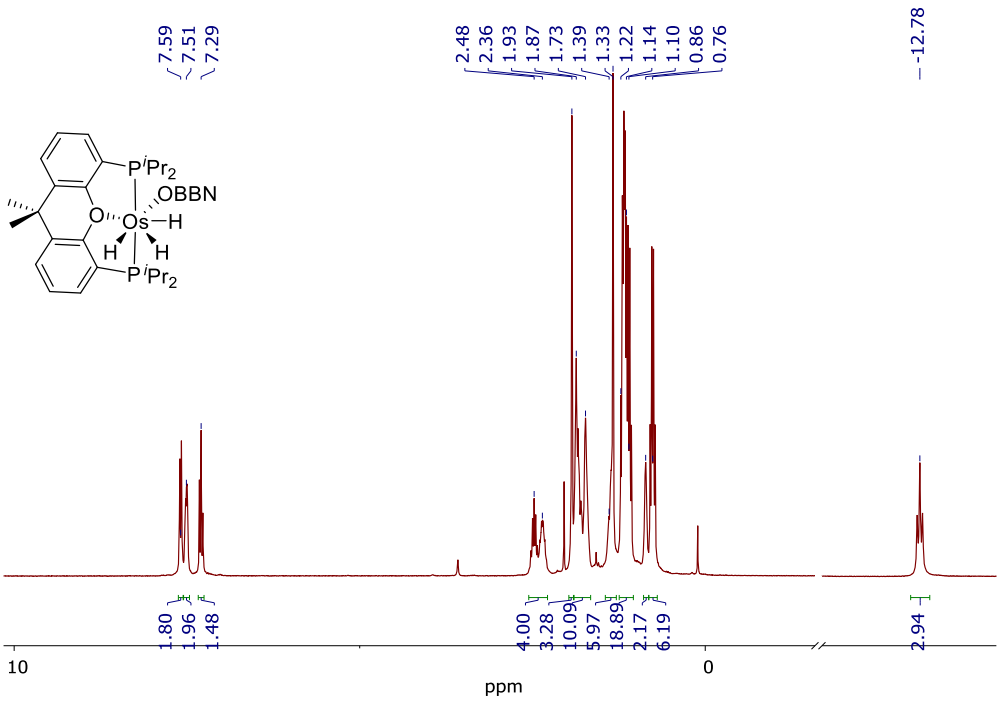

Figure S13. ^{1}H NMR (300.13 MHz, C_4D_8O, 298 K) spectrum of complex **3**.

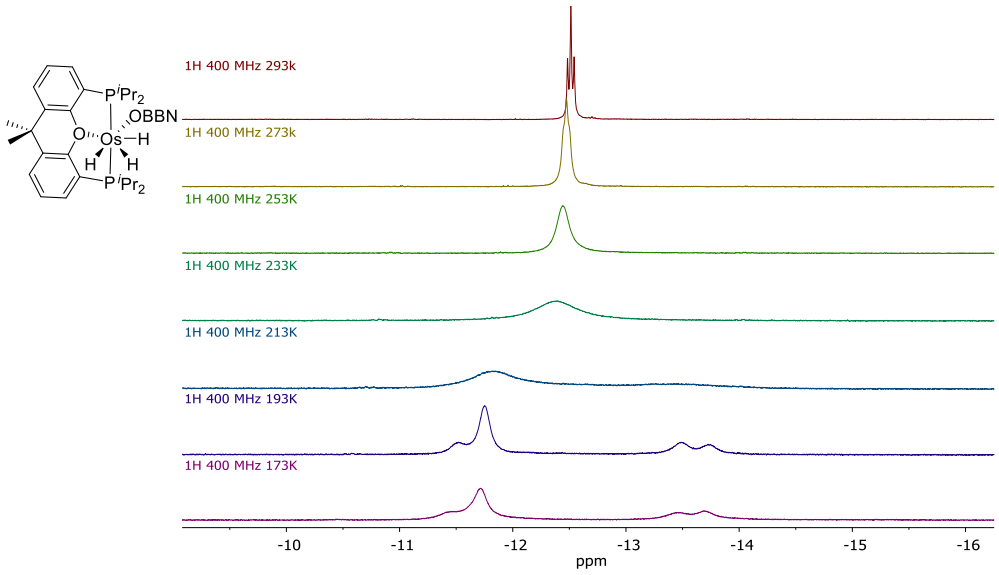

Figure S14. High-field region of the ^{1}H NMR (400.13 MHz, C_7D_8) spectrum of complex **3** between 293 and 173 K.

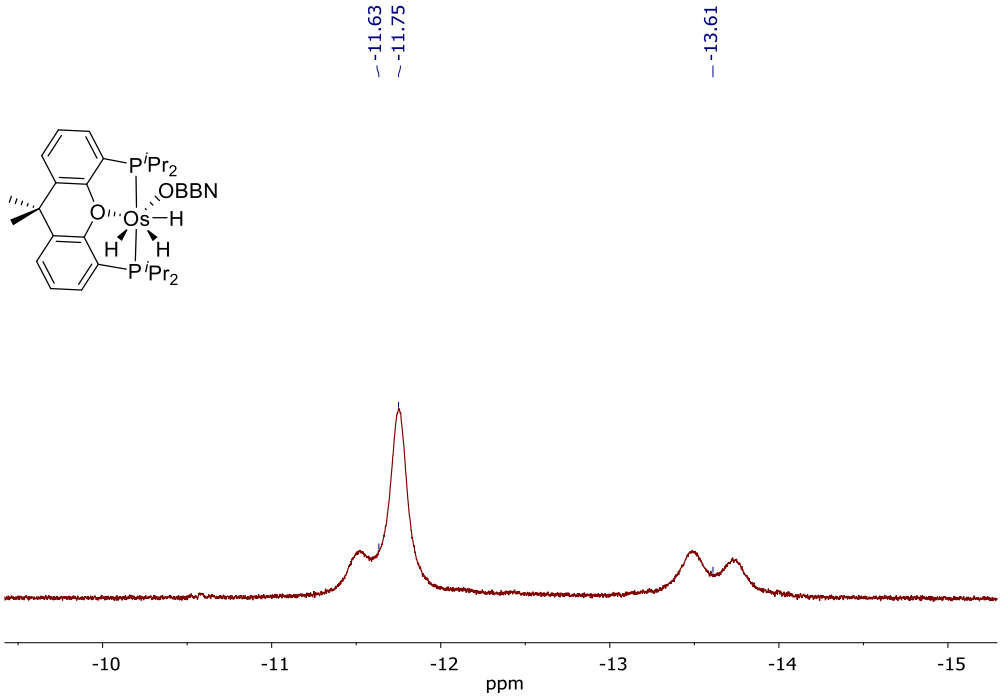

Figure S15. High-field region of the ^{1}H NMR (400.13 MHz, C_7D_8, 193 K) spectrum of complex **3**.

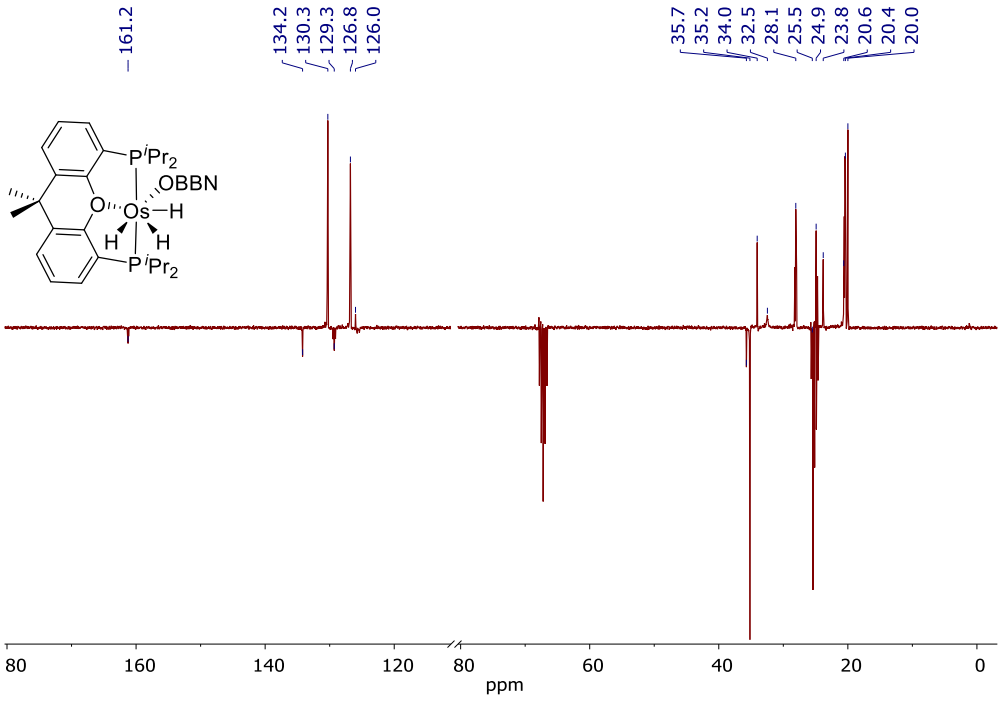

Figure S16. $^{13}C\{^1H\}$-APT NMR (75.47 MHz, C_4D_8O, 298 K) spectrum of complex **3**.

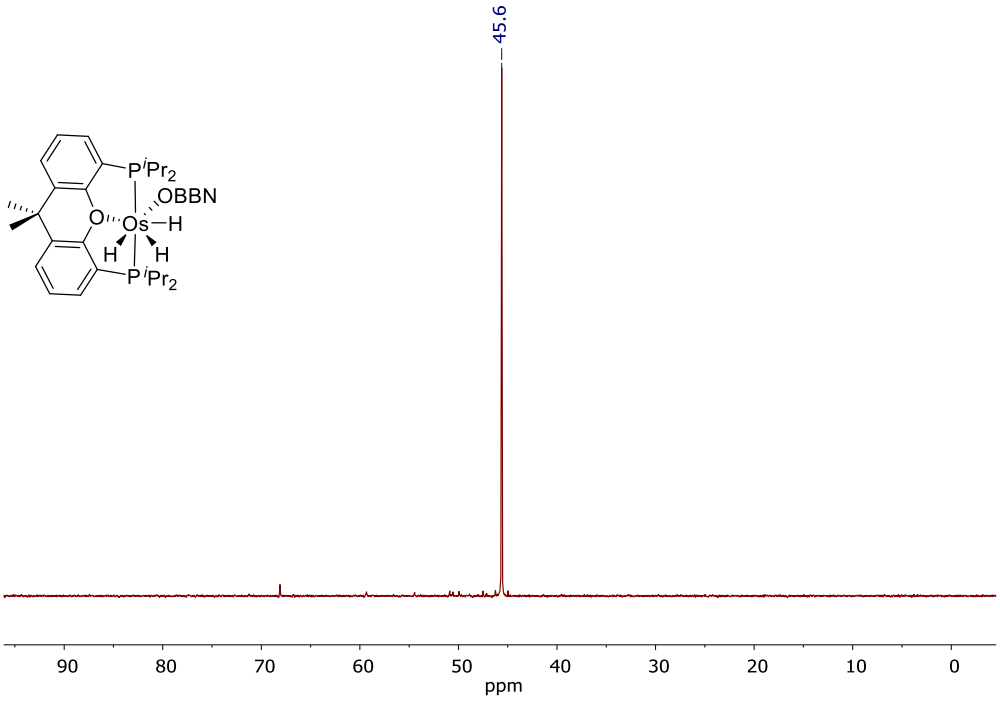

Figure S17. $^{31}P\{^1H\}$ NMR (161.98 MHz, C_7D_8, 298 K) spectrum of complex **3**.

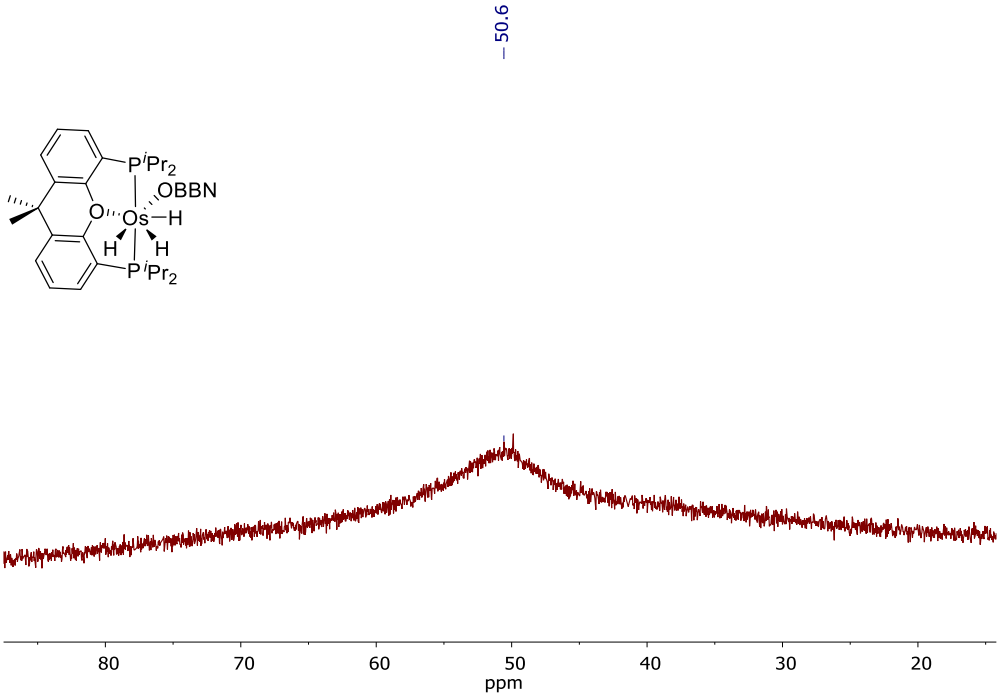

Figure S18. ^{11}B NMR (96.30 MHz, C_6D_6, 298 K) spectrum of complex **3**.

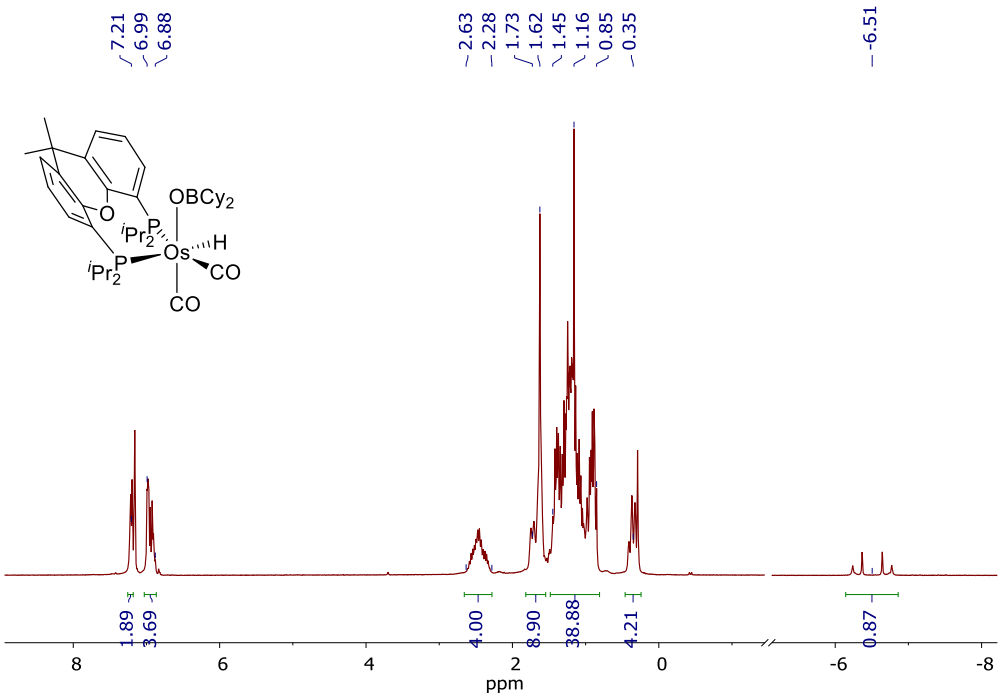

Figure S19. ^{1}H NMR (300.13 MHz, C_6D_6, 298 K) spectrum of complex **4**.

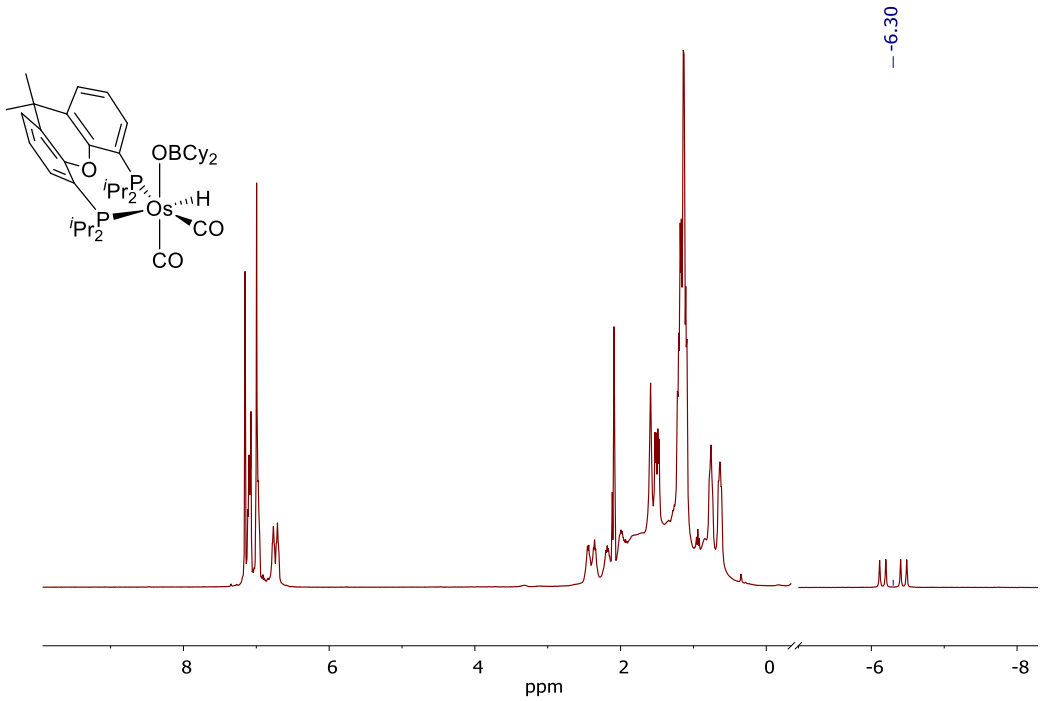

Figure S20. ^{1}H NMR (400.13 MHz, C_7D_8, 203K) spectrum of complex **4**.

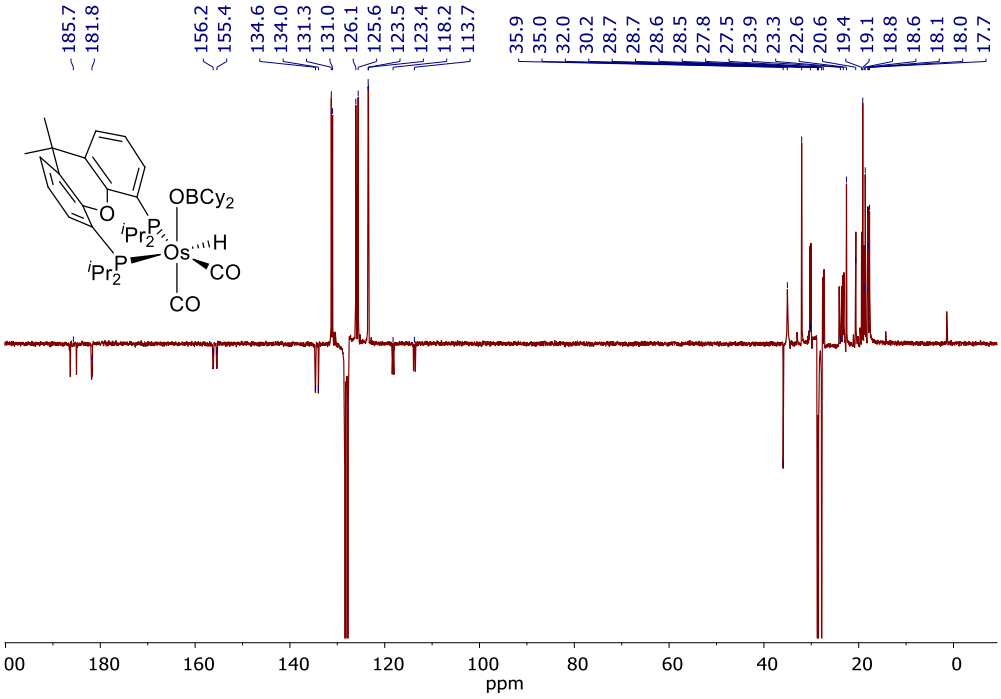

Figure S21. $^{13}C\{^{1}H\}$-APT NMR (75.48 MHz, C_6D_6, 298 K) spectrum of complex **4**.

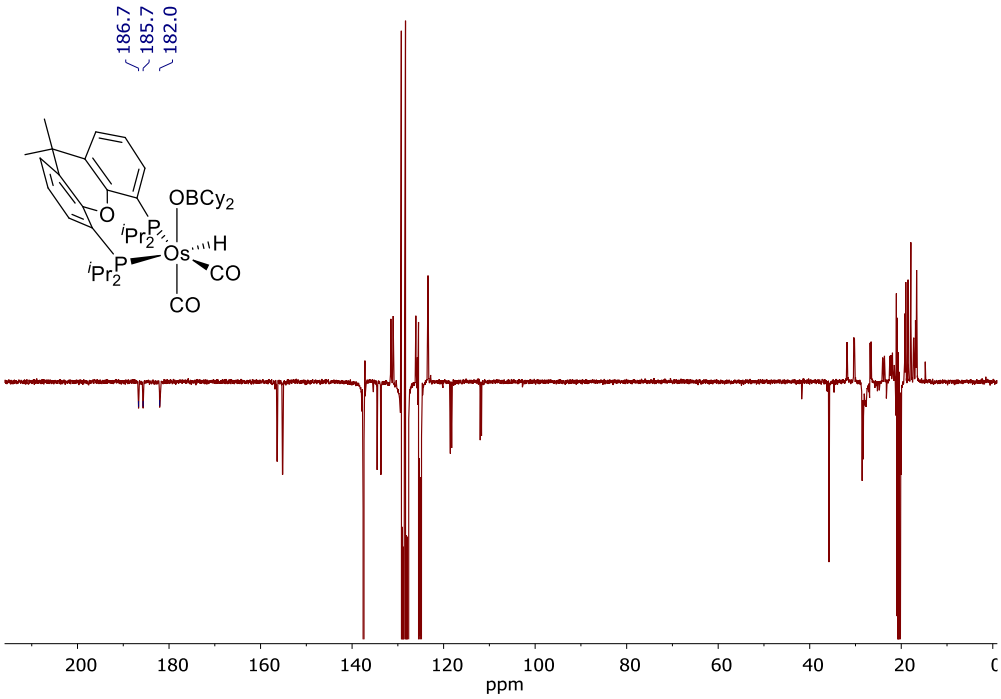

Figure S22. $^{13}C\{^{1}H\}$-APT NMR (100.62 MHz, C_7D_8, 203 K) spectrum of complex **4**

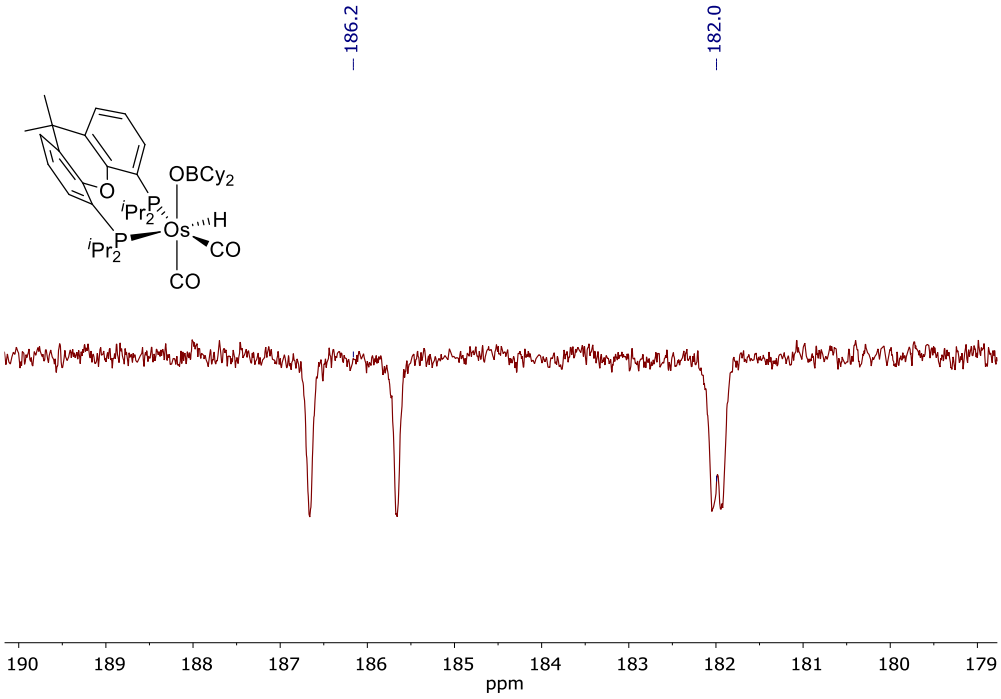

Figure S23. Low-field region of the $^{13}C\{^{1}H\}$-APT NMR (100.62 MHz, C_7D_8, 203 K) spectrum of complex **4**.

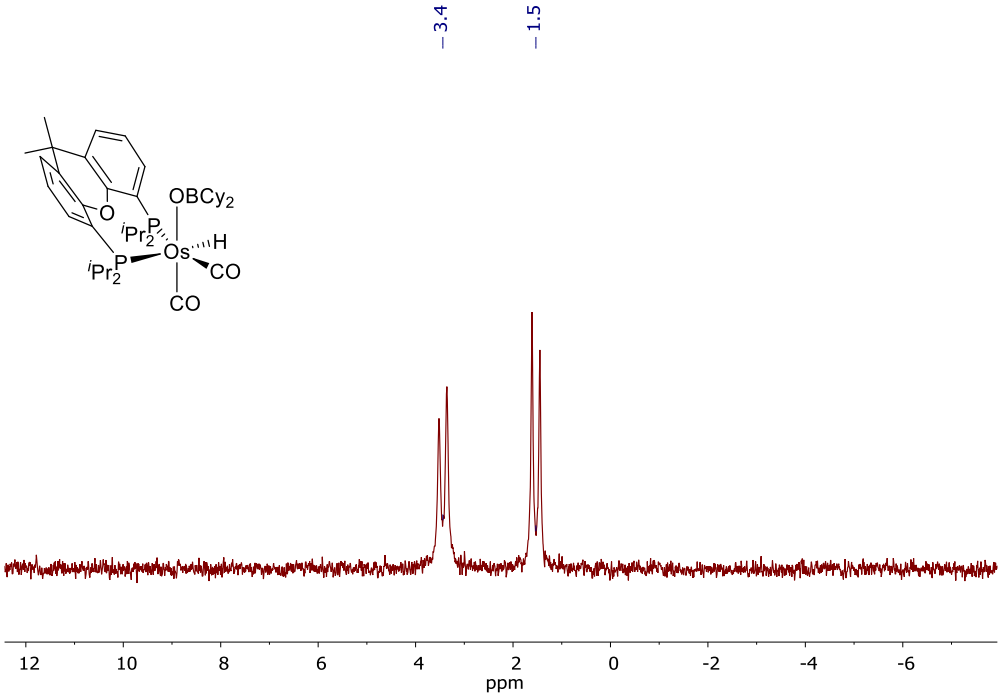

Figure S24. $^{31}P\{^{1}H\}$ NMR (161.98 MHz, C_7D_8, 203 K) spectrum of complex **4**.

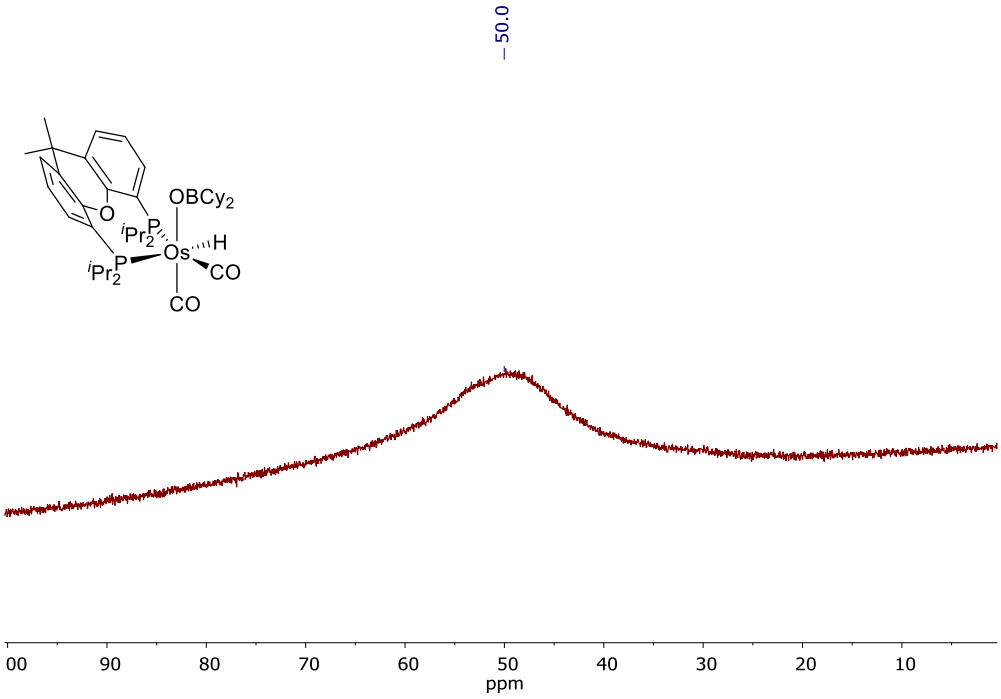

Figure S25. ^{11}B NMR (96.30 MHz, C_6D_6, 298 K) spectrum of complex **4**.

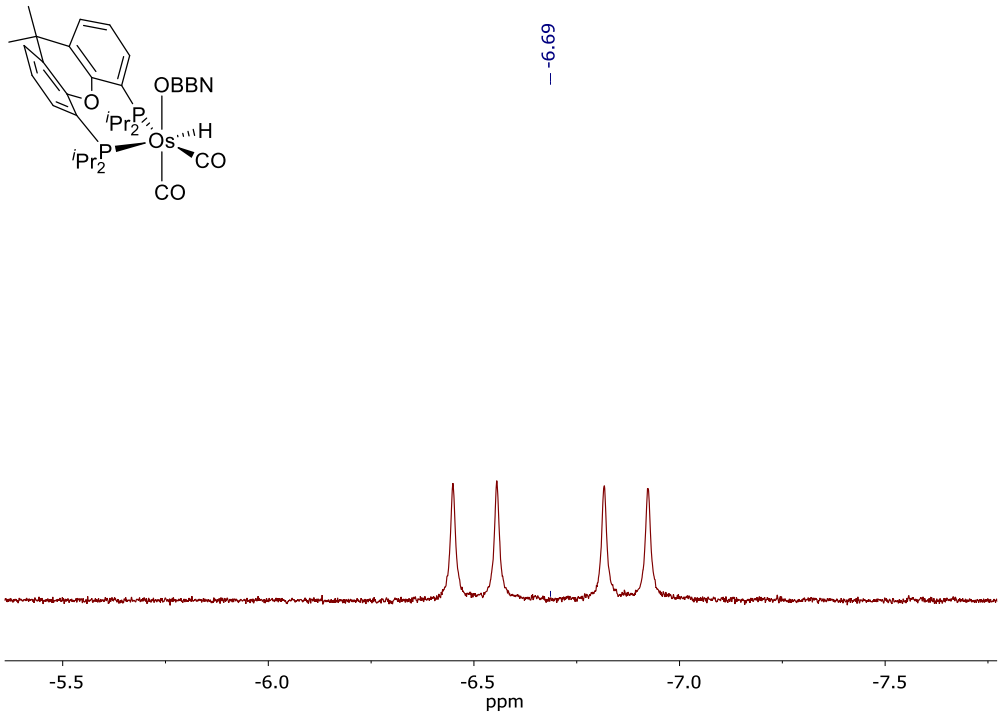

Figure S26. High-field region of the ^{1}H NMR (300.13 MHz, C_7D_8, 298 K) spectrum of complex **5**.

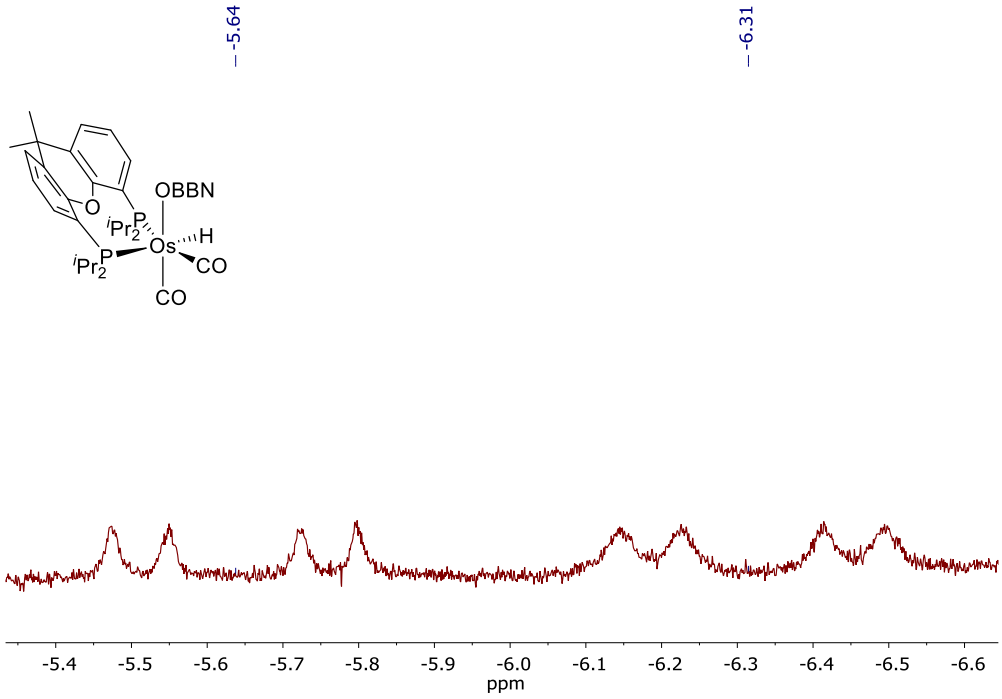

Figure S27. High-field region of the ^{1}H NMR (400.13 MHz, C_7D_8, 203 K) spectrum of complex **5**.

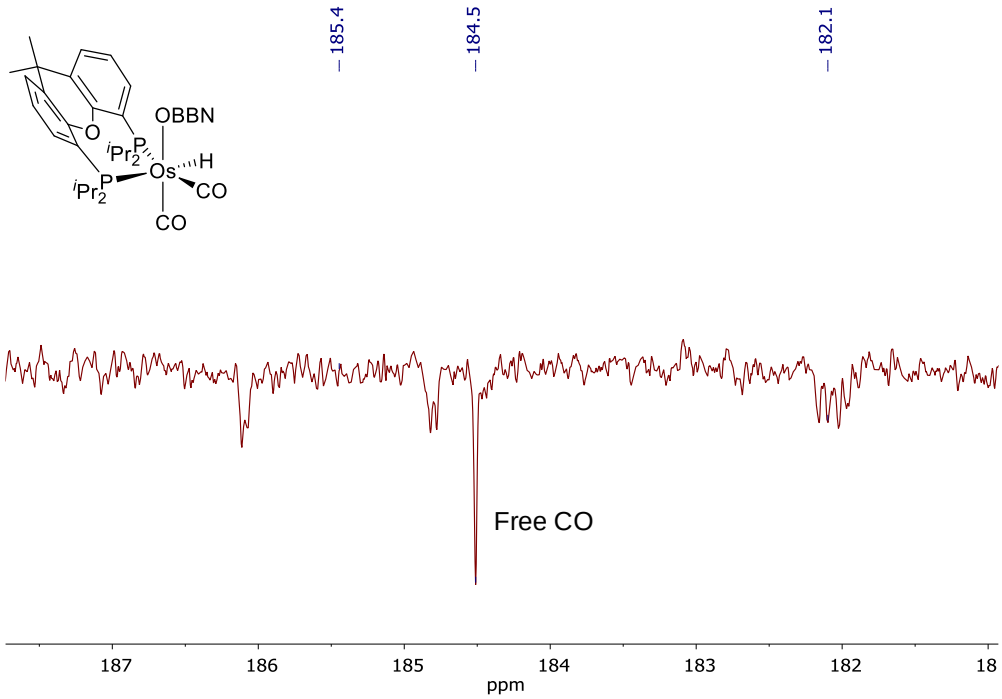

Figure S28. Low-field region of the $^{13}C\{^{1}H\}$-APT NMR (75.48 MHz, C_7D_8, 298 K) spectrum of complex **5**.

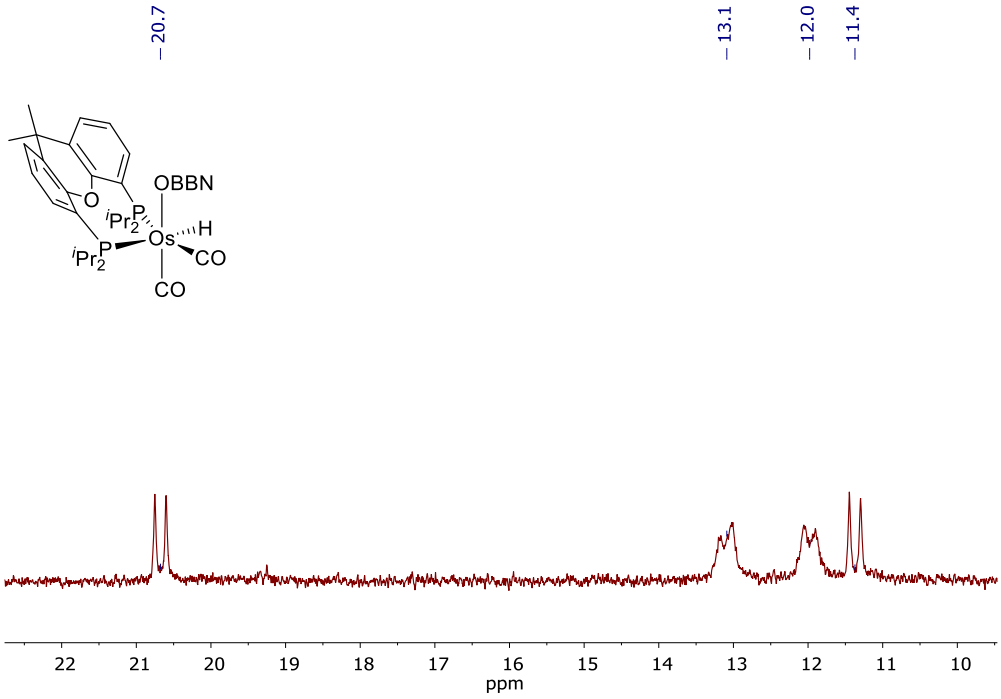

Figure S29. $^{31}P\{^{1}H\}$ NMR (161.98 MHz, C_7D_8, 203 K) spectrum of complex **5**.

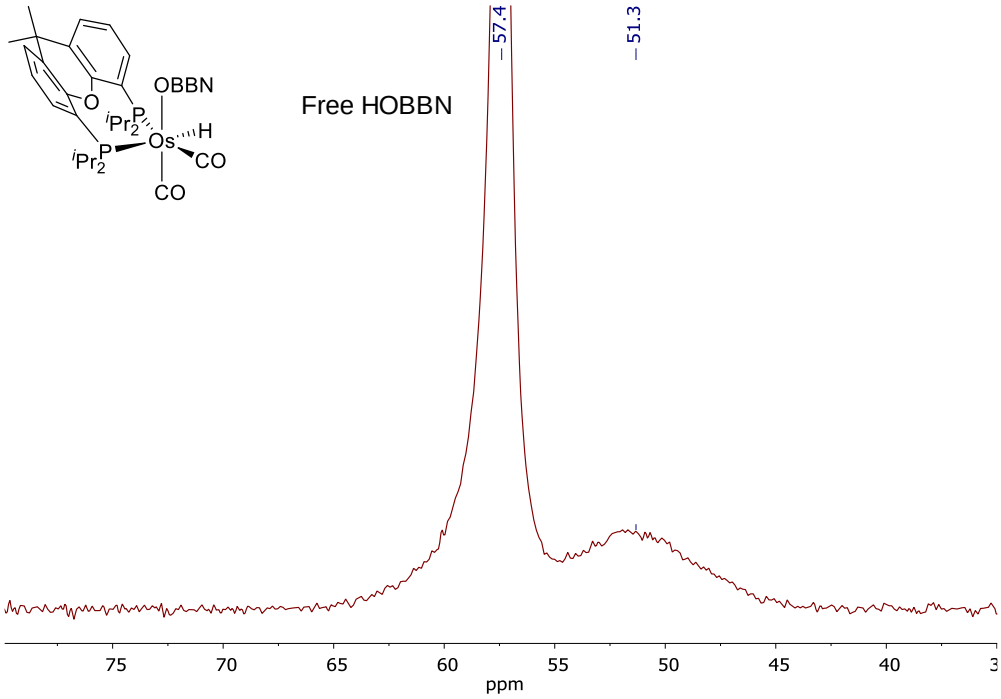

Figure S30. ^{11}B NMR (96.29 MHz, C_7D_8, 298 K) spectrum of complex **5**.

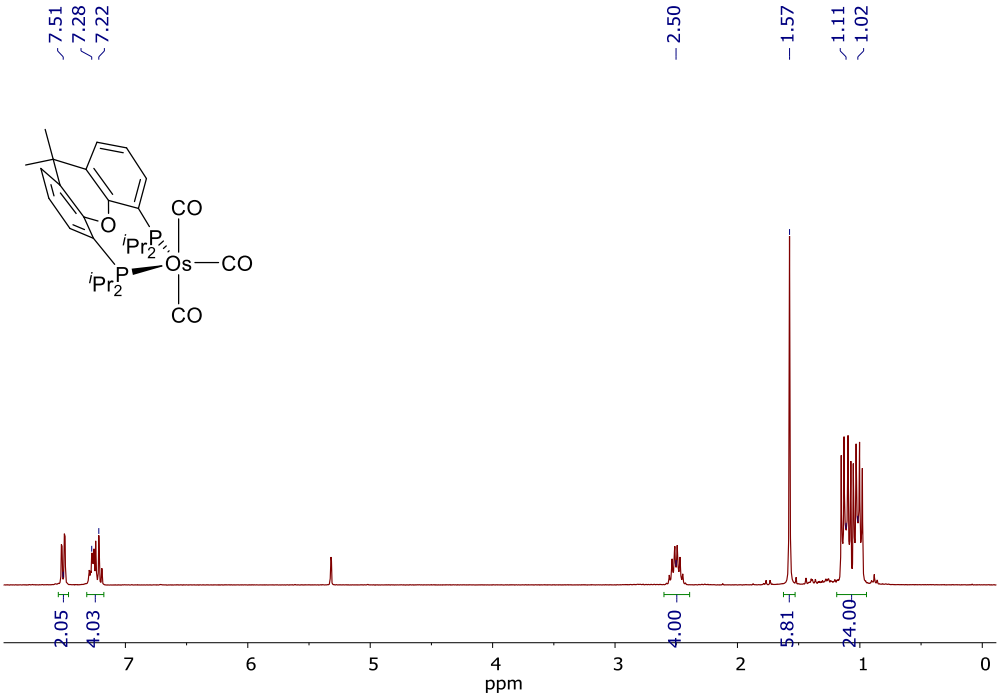

Figure S31. ^{1}H NMR (300.13 MHz, CD_2Cl_2, 298 K) spectrum of complex **6**.

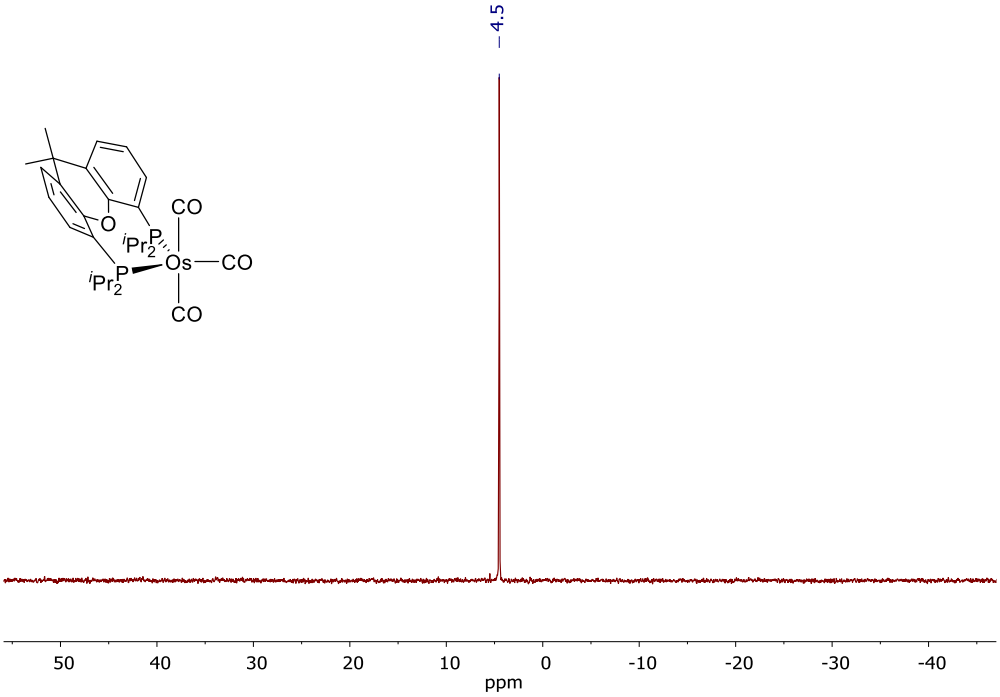

Figure S32. $^{31}P\{^{1}H\}$ NMR (121.50 MHz, CD_2Cl_2, 298 K) spectrum of complex **6**.

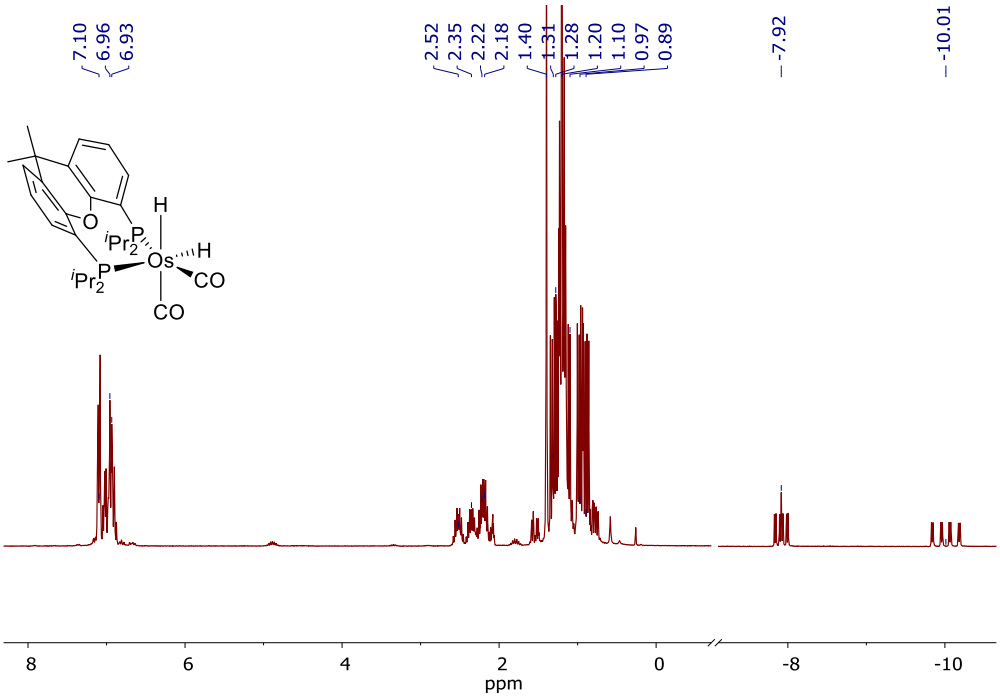

Figure S33. ^{1}H NMR (300.13 MHz, C_7D_8, 298 K) spectrum of complex **8**.

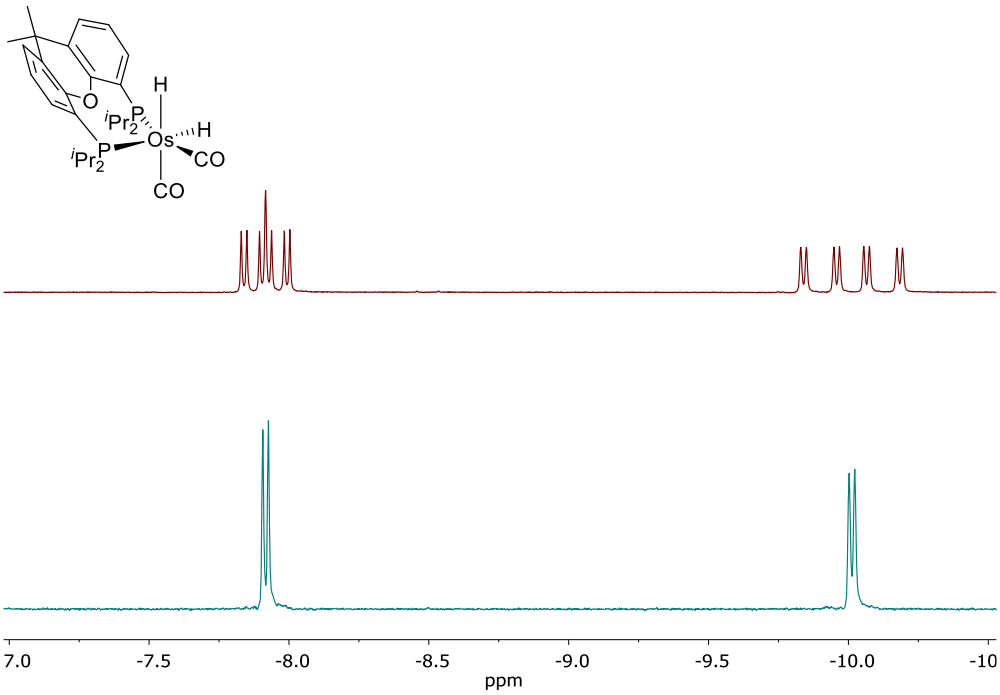

Figure S34. High-field region of the ^{1}H vs ^{1}H{^{31}P} NMR (300.13 MHz, C_7D_8, 298 K) spectra of complex **8**.

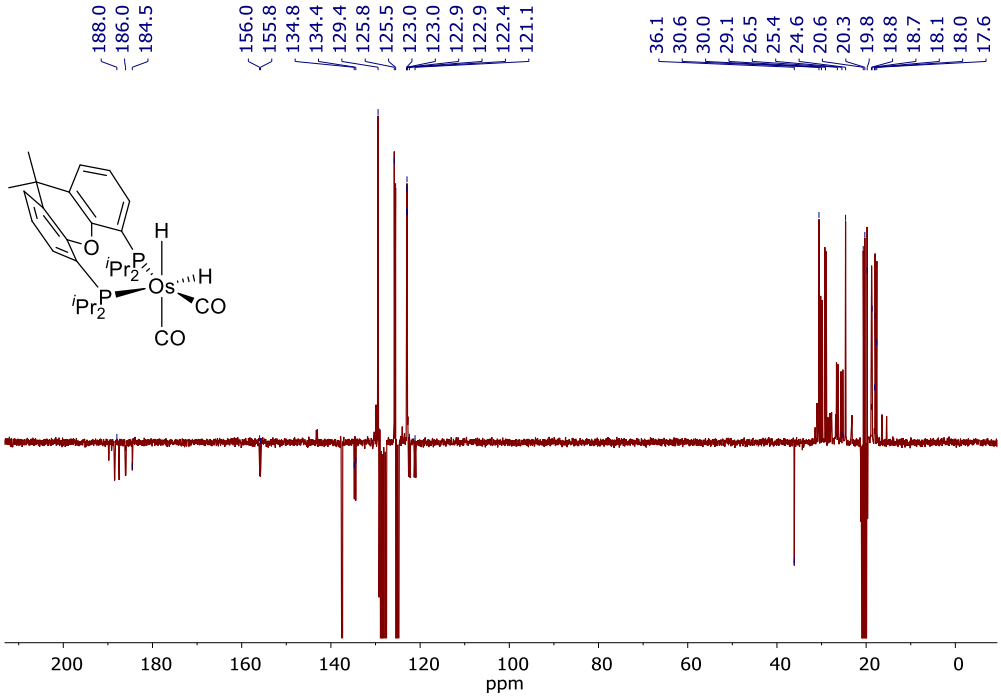

Figure S35. $^{13}C\{^{1}H\}$-APT NMR (75.48 MHz, C_7D_8, 298 K) spectrum of complex **8**.

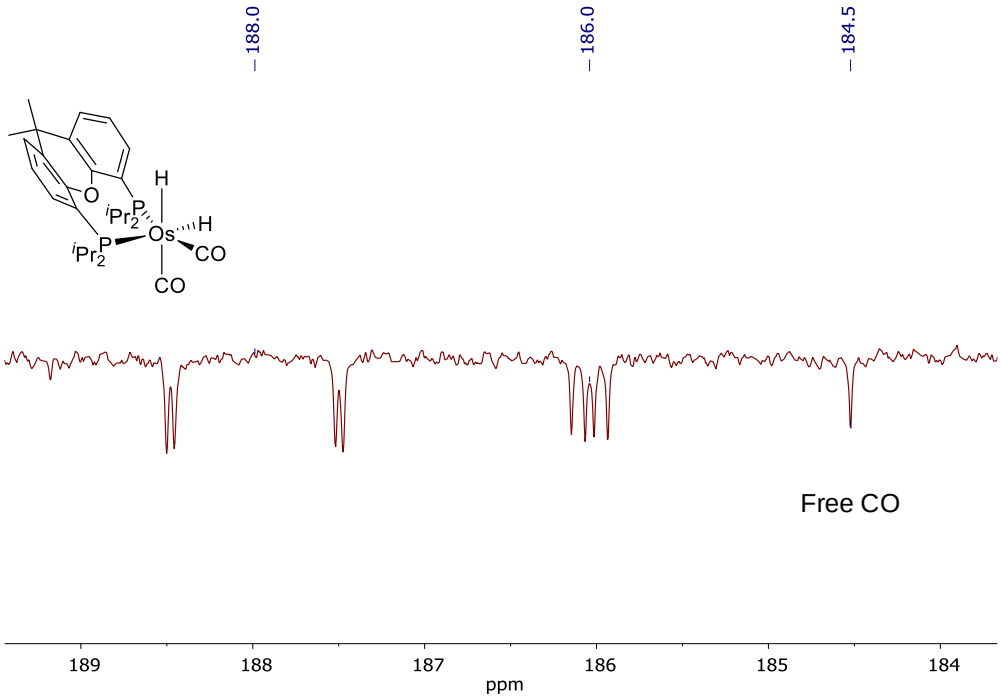

Figure S36. Low-field region of the $^{13}C\{^{1}H\}$-APT NMR (75.48 MHz, C_7D_8, 298 K) spectrum of complex **8**.

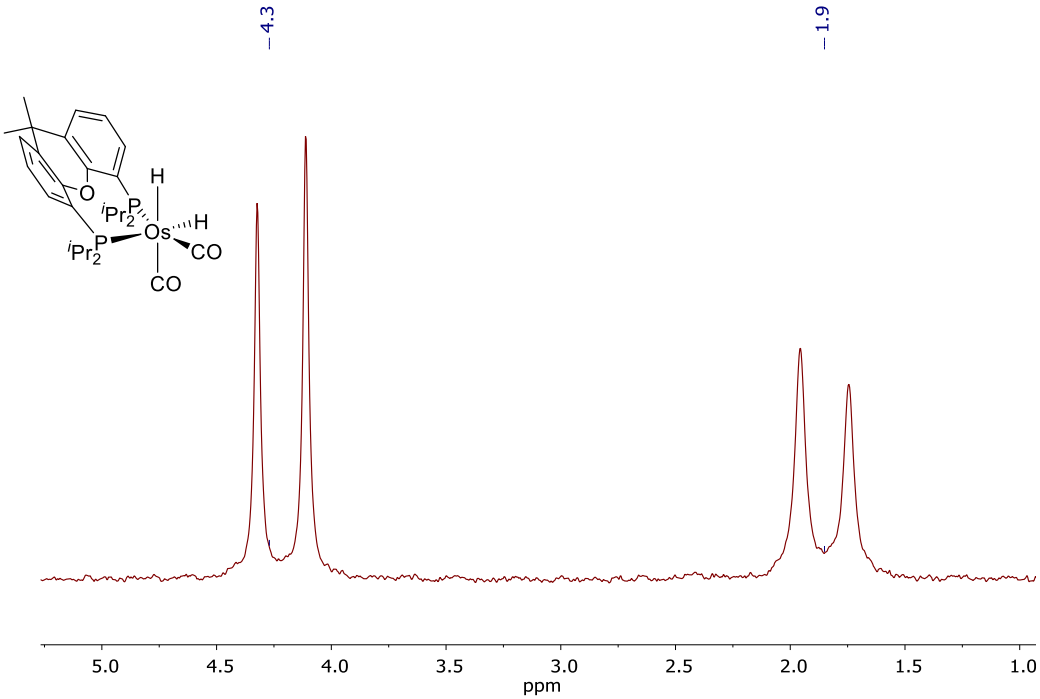

Figure S37. $^{31}P\{^{1}H\}$ NMR (121.49 MHz, C_7D_8, 298 K) spectrum of complex **8**.

IR Spectra of Complexes 4 and 6

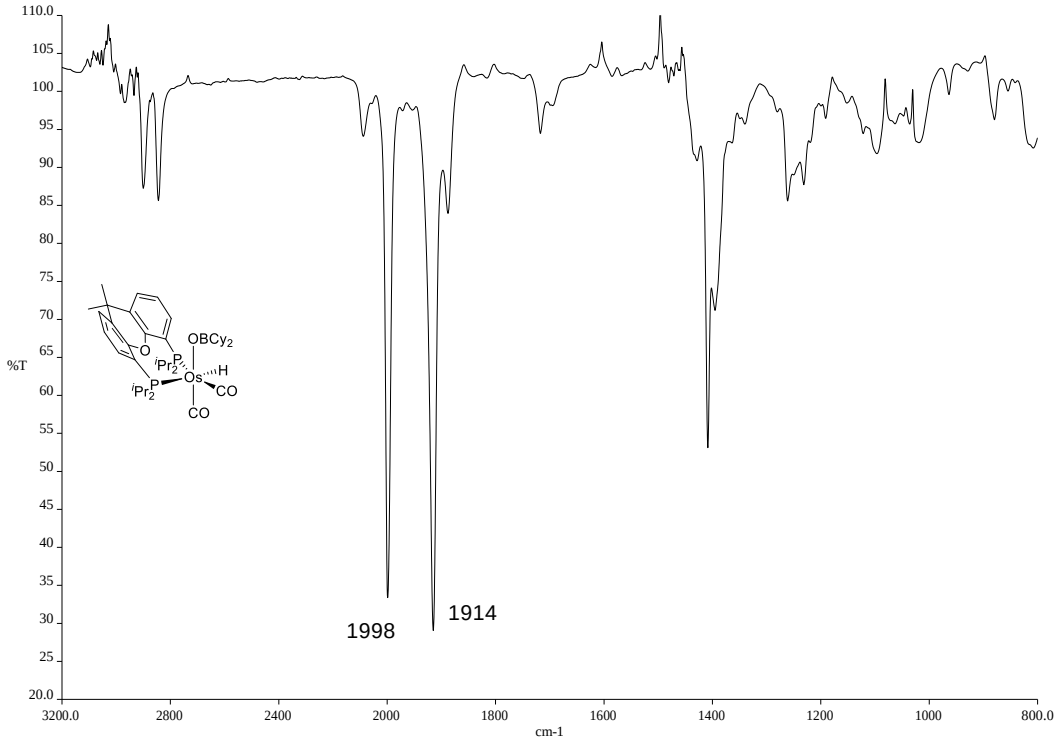

Figure S38. Infrared Spectrum of Complex **4** in Toluene.

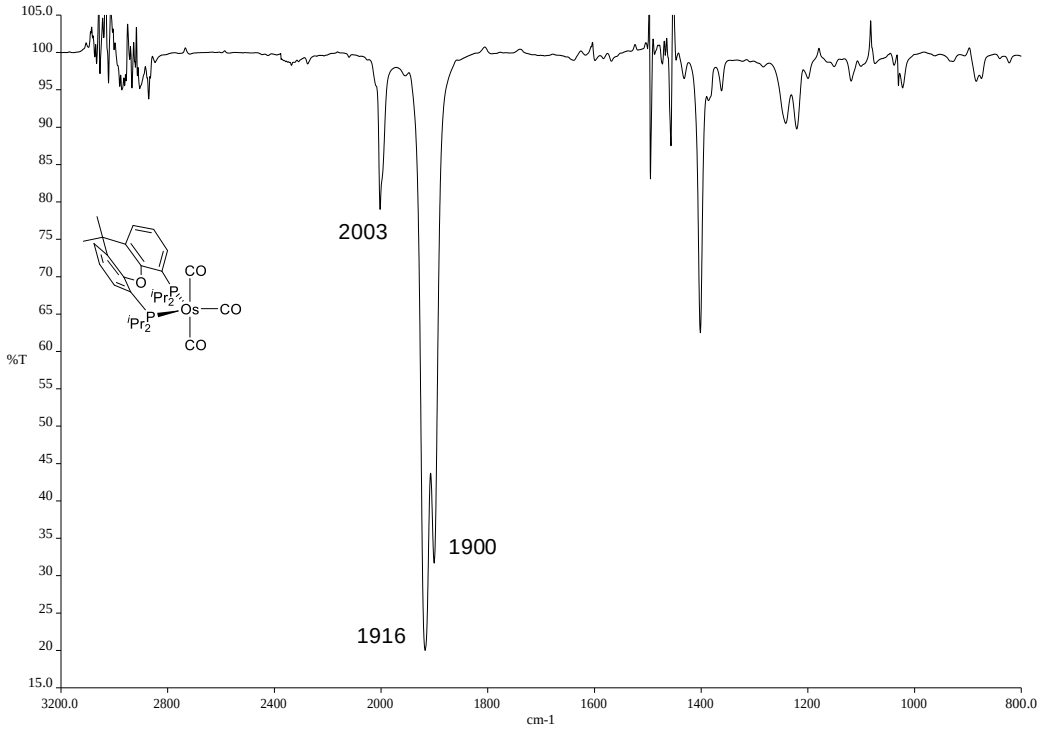

Figure S39. Infrared Spectrum of Complex **6** in Toluene.

Structural Analysis of Complexes 2, 4 and 6. X-ray data were collected for the complexes on a Bruker Smart APEX diffractometer equipped with a normal focus, and 2.4 kW sealed tube source (Mo radiation, l = 0.71073 Å). Data were collected over the complete sphere covering 0.3º in w. Data were corrected for absorption by using a multiscan method applied with the SADABS program.[1] The structures were solved by Patterson or direct methods and refined by full-matrix least squares on F^2 with SHELXL2016,[2] including isotropic and subsequently anisotropic displacement parameters. The hydrogen atoms were observed in the least Fourier Maps or calculated, and refined freely or using a restricted riding model. The hydride ligands were located in the last difference Fourier maps and refined with retrained distances to metal atoms (d_{Os-H} = 1.59(1) Å).

Crystal data for **2**: $C_{39}H_{65}BO_2OsP_2$, M_W 828.86, colourless, irregular block (0.137 x 0.114 x 0.074 mm^3), monoclinic, space group $P2_1/c$, *a*: 16.4953(11) Å, *b*: 10.8229(7) Å, *c*: 21.7324(14) Å, *β*: 95.2710(10)°, *V* = 3863.4(4) $Å^3$, *Z* = 4, *Z'* = 1, D_{calc}: 1.425 g cm^{-3}, F(000): 1704, T = 100(2) K, m 3.415 mm^{-1}. 54948 measured reflections (2θ: 3-57º, w scans 0.3º), 9400 unique (R_{int} = 0.0598); min./max. transm. Factors 0.719/0.862. Final agreement factors were R^1 = 0.0389 (7686 observed reflections, I > 2s(I)) and wR^2 = 0.0848; data/restraints/parameters 9400/3/425; GoF = 1.060. Largest peak and hole 2.647 (close to osmium atoms) and -1.329 e/ $Å^3$.

Crystal data for **4**: $C_{41}H_{63}BO_4OsP_2$, 1.5 x (C_6H_6), M_W 1000.02, colourless, irregular block (0.214 x 0.135 x 0.124 mm^3), tricilinic, space group P-1, *a*: 11.3211(6) Å, *b*: 11.9091(6) Å, *c*: 19.8390(13) Å, *a*: 103.7350(10)°, *β*: 95.1730(10)°, *γ*: 111.2730(10)°, *V* = 2374.9(2) $Å^3$, *Z* = 2, *Z'* = 1, D_{calc}: 1.398 g cm^{-3}, F(000): 1030, T = 100(2) K, m 2.794 mm^{-1}. 42117 measured reflections (2θ: 3-57º, w scans 0.3º), 11362 unique (R_{int} = 0.0350); min./max. transm. Factors 0.716/0.862. Final agreement factors were R^1 = 0.0235 (10335 observed reflections, I > 2s(I)) and wR^2 = 0.0486; data/restraints/parameters 11362/1/536; GoF = 0.992. Largest peak and hole 0.931 (close to osmium atoms) and -0.783 e/ $Å^3$.

Crystal data for **6**: $C_{30}H_{40}O_4OsP_2$, M_W 716.76, yellow, irregular block (0.142 x 0.102 x 0.050 mm^3), monoclinic, space group $P2_1/c$, *a*: 10.9699(11) Å, *b*: 8.9521(9) Å, *c*: 29.950(3) Å, *β*: 90.3490(10)°, *V* = 2941.1(5) $Å^3$, *Z* = 4, *Z'* = 1, D_{calc}: 1.619 g cm^{-3}, F(000): 1432, T = 100(2) K, m 4.477 mm^{-1}. 27723 measured reflections (2θ: 3-57°, w scans 0.3°), 7029 unique (R_{int} = 0.0625); min./max. transm. Factors 0.628/0.862. Final agreement factors were R^1 = 0.0363 (5237 observed reflections, I > 2s(I)) and wR^2 = 0.0641; data/restraints/parameters 7029/0/ 344; GoF = 1.011. Largest peak and hole 1.160 (close to osmium atoms) and -0.780 e/ $Å^3$.

Computational details. All calculations were performed at the DFT level using the B3LYP functional[3] supplemented with the Grimme's dispersion correction D3[4] as implemented in Gaussian09.[5] Os atoms were described by means of an effective core potential SDD for the inner electron[6] and its associated double-ζ basis set for the outer ones, complemented with a set of f-polarization functions for osmium.[7] The 6-31G** basis set was used for the H, C, B, O and P atoms.[8] All minima were verified to have no negative frequencies. The geometries were fully optimized in vacuum.

References

(1) Blessing, R. H. An Empirical Correction for Absorption Anisotropy. *Acta Crystallogr., Sect. A: Found. Crystallogr.* **1995**, *51*, 33-38.

(2) Sheldrick, G. M. A Short History of SHELX. *Acta Crystallogr., Sect. A: Found. Crystallogr.* **2008**, *64*, 112-122.

(3) (a) Lee, C. T.; Yang, W. T.; Parr, R. G. Development of the Colle-Salvetti Correlation-Energy Formula into a Functional of the Electron-Density. *Phys. Rev. B* **1988**, *37*, 785-789. (b) Becke, A. D. A New Mixing of Hartree-Fock and Local Density-Functional Theories. *J. Chem. Phys.* **1993**, *98*, 1372-1377. (c) Stephens, P. J.; Devlin, F. J.; Chabalowski, C. F.; Frisch, M. J. Ab-Initio Calculation of Vibrational Absorption and Circular-Dichroism Spectra Using Density-Functional Force-Fields. *J. Phys. Chem.* **1994**, *98*, 11623-11627.

(4) Grimme, S.; Antony, J.; Ehrlich, S.; Krieg, H. A Consistent and Accurate *ab initio* Parametrization of Density Functional Dispersion Correction (DFT-D) for the 94 Elements H-Pu. *J. Chem. Phys.* **2010**, *132*.

(5) Gaussian 09, Revision D.01, Frisch, M. J.; Trucks, G. W.; Schlegel H. B.; Scuseria, G. E.; Robb, M. A.; Cheeseman, J. R.; Scalmani, G.; Barone, V.; Mennucci, B.; Petersson, G. A.; Nakatsuji, H.; Caricato, M.; Li, X.; Hratchian, H. P.; Izmaylov, A. F.; Bloino, J.; Zheng, G.; Sonnenberg, J. L.; Hada, M.; Ehara, M.; Toyota, K.; Fukuda, R.; Hasegawa, J.; Ishida, M.; Nakajima, T.; Honda, Y.; Kitao, O.; Nakai, H.; Vreven, T.; Montgomery, J. A.; Peralta, Jr., J. E.; Ogliaro, F.; Bearpark, M.; Heyd, J. J.; Brothers, E.; Kudin, K. N.; Staroverov, V. N.; Keith, T.; Kobayashi, R.; Normand, J.; Raghavachari, K.; Rendell, A.; Burant, J. C.; Iyengar, S. S.; Tomasi, J.; Cossi, M.; Rega, N.; Millam, J. M.; Klene, M.; Knox, J. E.; Cross, J. B.; Bakken, V.; Adamo, C.; Jaramillo, J.; Gomperts, R.; Stratmann, R. E.; Yazyev, O.; Austin, A. J.; Cammi, R.; Pomelli, C.; Ochterski, J. W.; Martin, R. L.; Morokuma, K.; Zakrzewski, V. G.; Voth, G. A.; Salvador, P.; Dannenberg, J. J.; Dapprich, S.; Daniels, A. D.; Farkas, O.; Foresman, J. B.; Ortiz, J. V.; Cioslowski, J.; Fox, D. J. Gaussian, Inc., Wallingford CT, 2013.

(6) Andrae, D.; Häußermann, U.; Dolg, M.; Stoll, H.; Preuß, H. Energy-Adjusted *ab initio* Pseudopotentials for the Second and Third Row Transition Elements. *Theor. Chim. Acta* **1990**, *77*, 123-141.

(7) Ehlers, A. W.; Bohme, M.; Dapprich, S.; Gobbi, A.; Hollwarth, A.; Jonas, V.; Kohler, K. F.; Stegmann, R.; Veldkamp, A.; Frenking, G. A Set of F-Polarization Functions for Pseudo-Potential Basis-Sets of the Transition-Metals Sc-Cu, Y-Ag and La-Au. *Chem. Phys. Lett.* **1993**, *208*, 111-114.

(8) (a) Hehre, W. J.; Ditchfield, R.; Pople, J. A. Self-Consistent Molecular-Orbital Methods. XII. Further Extensions of Gaussian-Type Basis Sets for Use in Molecular-Orbital Studies of Organic-Molecules. *J. Chem. Phys.,* **1972**, *56*, 2257-2261. (b) Francl, M. M.; Pietro, W. J.; Hehre, W. J.; Binkley, J. S.; Gordon, M. S.; Defrees, D. J.; Pople, J. A. Self-Consistent Molecular-Orbital Methods .23. A Polarization-Type Basis Set for 2nd-Row Elements. *J. Chem. Phys.* **1982**, *77*, 3654-3665.

Cycloosmathioborane Compounds: Other Manifestation of the Hückel Aromaticity

Miguel A. Esteruelas,*[,†] Israel Fernández,[‡] Cristina García-Yebra,[†,§] Jaime Martín,[†] and Enrique Oñate[†]

[†]Departamento de Química Inorgánica, Instituto de Síntesis Química y Catálisis Homogénea (ISQCH), Centro de Innovación en Química Avanzada (ORFEO-CINQA), Universidad de Zaragoza-CSIC, 50009 Zaragoza, Spain

[‡]Departamento de Química Orgánica I, Facultad de Ciencias Químicas, Centro de Innovación en Química Avanzada (ORFEO-CINQA), Universidad Complutense de Madrid, 28040 Madrid, Spain

ABSTRACT: The discovery of cycloosmathioborane compounds is reported. These species, which are prepared by simultaneous dehydrogenation of a trihydride-hydrogensulfide-osmium(IV) complex and a BH_3NHR_2 amine-borane, bear an Os, S, B three-membered ring, being a manifestation of 4n + 2 Hückel aromaticity in which n = 0 and where the two π-electrons of the ring are provided by the S atom.

Aromaticity is a classical concept in chemistry which is continually evolving.[1] It was initially introduced to account for the special properties of some unsaturated hydrocarbons and conjugated heterocycles. In 1979, Thorn and Hoffmann proposed to extend it to organic aromatic compounds where a CH unit is replaced by an isolobal transition metal fragment[2] and, three years later, Roper's group reported the first metallabenzene.[3] Since then, a significant number of aromatic derivatives based on both carbon and transition elements have been isolated and characterized,[4] most of them, as Hückel aromatic species.[4c]

Frogly and Wright have recently defined metallaaromatic compounds as those bearing at least a transition metal in the ring[4d] whereas, in 1979, Bursten and Fenske used the term "*metalloaromaticity*" to describe the aromatic behavior appeared to have been induced into cyclobutadiene as a result of its coordination to the $Fe(CO)_3$ metal fragment.[5] Nevertheless, metalloaromaticity has been employed by some authors without distinction for both situations.[6] In addition, the term all-metal aromaticity has been invoked to address different aspects of the behavior of clusters of both main-groups elements and transition metals.[7]

Cyclo-gallene dianion $[Ga_3L_3]^{2-}$ (L = $Mes_2C_6H_3$) was the first compound of this class.[8] Today, homoleptic aromatic 3-10 membered rings with elements of group 2 as well as of groups 13-16 are known,[9] besides tripalladium[10] and trigold cations.[11] Three-membered ring compounds are certainly the most challenging due to the strain imposed by the small size of the ring. Computational methods have revealed that the aromaticity of group 14 cyclopropenylium analogues ($E_3H_3^+$) decreases in the sequence C > Si > Ge > Sn > Pb.[12] In addition to homoleptic species, a few heteroleptic ones with two different main-group elements are also known. Cummins and coworkers have reported EP_2 triangles (E = Ge, Sn, Pb), which are stabilized within the coordination sphere of a sterically protected diniobium unit[13] whereas the Guha's group has computationally predicted that the substitution of a boron atom in the triangle $[B_3H_3]^{2-}$ by a group 15 element should afford neutral aromatic H_2B_2XH rings (X = N, P).[14] Herein, we take one step forward in this fascinating field by reporting the preparation and full characterization of the first aromatic triangles having three different vertexes, namely two main-group elements, S and B, and a transition metal with its associated ligands.

Scheme 1 summarizes the preparation of the new compounds, which starts from the 9,9-dimethyl-4,5-bis(diisopropylphosphine)xanthene complex $OsH_3(OTf)\{\kappa^3$-P,O,P-[xant(P^iPr_2)$_2$]} (**1**) and takes place through the hydrogensulfide derivative $OsH_3(SH)\{\kappa^3$-P,O,P-[xant(P^iPr_2)$_2$]} (**2**). The synthesis of the latter was inspired by the recent preparation of its hydroxo counterpart $OsH_3(OH)\{\kappa^3$-P,O,P-[xant(P^iPr_2)$_2$]},[15] which is stable towards the reductive elimination of water in spite of that this process is generally favored from a thermodynamic point of view.[16] Similarly to the OH^- group, SH^- replaces the trifuoromethanesulfonate anion ($[OTf]^-$) from **1** to give **2**, which was isolated as red crystals in 47 % yield. The coordination of the SH^- group to the osmium atom is demonstrated by the X-ray diffraction analysis structure (Figure 1). The osmium(IV) center shows the expected pentagonal bipyramidal arrangement with axial P^iPr_2 groups and the oxygen atom of the diphosphine and the SH^-anion in the perpendicular plane, along with the *cisoid* inequivalent hydrides which display three resonances at -8.07, -13.01, and -13.78 ppm in the ^1H NMR spectrum, in toluene-d_8, at 193 K. The $^{31}P\{^1H\}$ NMR spectrum shows a singlet at 48.1 ppm for the equivalent P^iPr_2 groups. Complexes of platinum group metals bearing terminal hydrogensulfide ligands are rare due to the high tendency of this group to act as a bridging ligand.[17] The five-coordinate catecholboryl derivative $Os(Bcat)(SH)(CO)(P^iPr_3)_2$ was the first mononuclear SH-complex of these metals characterized by X-ray diffraction analysis. It was prepared by reaction of the monohydride $OsH(SH)(CO)(P^iPr_3)_2$[18] with HBcat via the dihydrogen intermediate $OsH(SBcat)(\eta^2$-$H_2)(CO)(P^iPr_3)_2$.[19] Braun and co-workers have recently reported the rhodium(I) derivative $Rh(SH)\{\kappa^3$-P,O,P-xant(^{t}Bu$_2$)$_2$]}, which has been also characterized by X-ray diffraction analysis.[20]

Scheme 1. Synthetic Strategy for the Preparation of Cycloosmathioborane Complexes

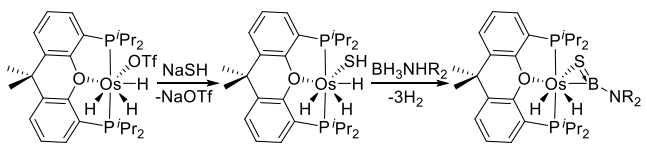

1 **2** NR_2 = NH^tBu (**3**), $N(CH_3)_2$ (**4**)

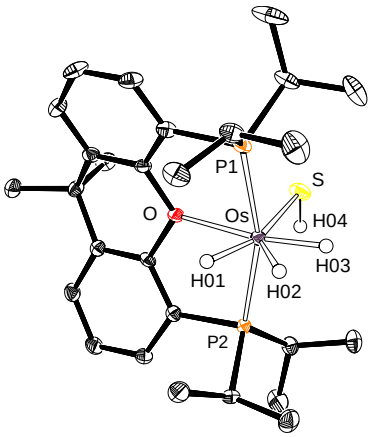

Figure 1. Molecular drawing of complex **2**. Hydrogen atoms (except hydrides and H04) are omitted for clarity. Selected distances and angles: Os-S = 2.4483(6) Å, S-H04 = 1.16(3) Å, Os-S-H = 105.8(13)º, O1-Os-S = 80.92(4)º, P1-Os-P2 = 162.26(2)º.

Complex **2** reacts with BH_3NHR_2 amine-boranes to give the unprecedented cycloosmathioborane derivatives $OsH_2\{\kappa^2\text{-S,B-}[SBNR_2]\}\{\kappa^3\text{-P,O,P-[xant(P}^i\text{Pr}_2)_2]\}$ (NR_2 = NH^tBu (**3**), NMe_2 (**4**)), as a result of the releasing of H_2 from both the metal center and the amine-boranes. The dehydrogenation is favored by the polyhydride character of **2**[21] and by the presence of the hydrogensulfide ligand, which traps the resulting amino-borane monomer.[22] The capture facilitates the complete extraction of the hydrogen atoms attached to the boron atom. Complex **3** and **4** were isolated as yellow solids in about 60 % yield. The X-ray diffraction analysis structure of **3** (Figure 2) proves the triangular shape of the ring determined by the Os, S, and B atoms. The most noticeable feature of the triangle is the B-S distance of 1.782(6) Å, which suggests a significant double bond character. It is only about 0.03 Å longer than the B-S bond length reported in the manganese complex $Mn(\eta^5\text{-}C_5H_5)\{S=B(^t\text{Bu})\text{IMe}\}(CO)_2$ (IMe = 1,3-dimethylimidazolylidene; 1.747(3) Å)[23] and in the thioxoboranes $S=B\{\kappa^2\text{-N,N-[N(2,6-Me}_2C_6H_3)C(Me)CHC(Me)N(2,6\text{-Me}_2C_6H_3)]\}$ (1.741(2) Å)[24] and $S=B\{\kappa^2\text{-N,N-[N(2,4,6-Me}_3C_6H_2)P(Ph)_2NP(Ph)_2N(2,4,6\text{-Me}_3C_6H_2)]\}$ (1.752(5) Å),[25] and about 0.07 Å longer than that found in the cation $S=B\{\kappa^2\text{-N,N-[N(L}^{Mes})CH_2CH_2N(L^{Mes})]\}^+$ (L^{Mes} = 1,3-dimesitylimidazolinylidene; 1.710(5) Å),[26] species reported as the first ones featuring a B-S double bond. The three-membered rings of **3** and **4** resemble that of the intermediate recently proposed by Braunschweig and co-workers for the reaction of the alkylborylene complex $Mn(\eta^5\text{-}C_5H_5)(=B^t\text{Bu})(CO)_2$, with $SPPh_3$, which yields the metathesis product $Mn(\eta^5\text{-}C_5H_5)(CO)_2(PPh_3)$. This intermediate has been suggested to be a κ^2-S,B-[SB^tBu] derivative.[27] The Os-S distance of 2.5572(14) Å is scarcely 0.08 Å longer than that of **2**, whereas the Os-B bond length of 2.073(6) Å is consistent with an Os(IV)-B single bond.[28] In fact, the OsH_2(POP) moiety can be described as a 16-electron valence *cis*-dihydride L_5Os(IV) fragment, which gives rise to the typical pentagonal bipyramidal arrangement around the metal center, with a *mer*-coordination of the POP-pincer. This arrangement generates two high field signals at about -9 and -18 ppm in the ^{1}H NMR spectra and a singlet at about 47 ppm in the $^{31}P\{^1H\}$ NMR spectra. A broad resonance at 56.3 ppm for **3** and at 62.0 ppm for **4** in the ^{11}B NMR spectra are also characteristic features of these compounds.

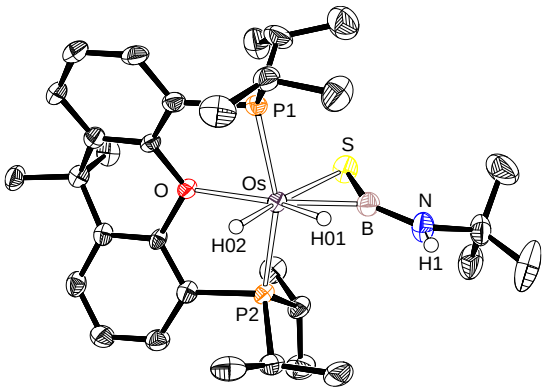

Figure 2. Molecular drawing of complex **3**. Hydrogen atoms (except hydrides and H1) are omitted for clarity. Selected distances and angles: B-N = 1.391(7) Å, Os-S-B = 53.5(2)º, S-B-Os = 82.8(2)º, B-Os-S = 43.7(2)º.

Density Functional Theory (DFT) calculations at the dispersion corrected BP86-D3/def2-TZVPP level were carried out on **3** to gain more insight into the bonding situation in the three-membered ring. Theoretical support for a significant double character of the B-S bond is given by the corresponding computed Wiberg Bond Index (WBI) of 1.40 and by the shape of HOMO-7 and HOMO-8. They can be viewed as π-molecular orbitals delocalized within the ring, also involving the lone pair of the attached nitrogen atom (Figure 3). According of the Natural Bond Order (NBO) method, the multiple bond character of the B-S bond derives from the delocalization of the lone pair of the sulfur atom into the vacant p_z atomic orbital of the boron (associated second-order perturbation energy of -55.7 kcal/mol). In addition, the NBO method also locates a significant delocalization of a doubly-occupied d_π(Os) atomic orbital to this vacant p_z(B) (associated energy of -21.3 kcal/mol), which is also fully consistent with the delocalized π-orbitals depicted in Figure 3.

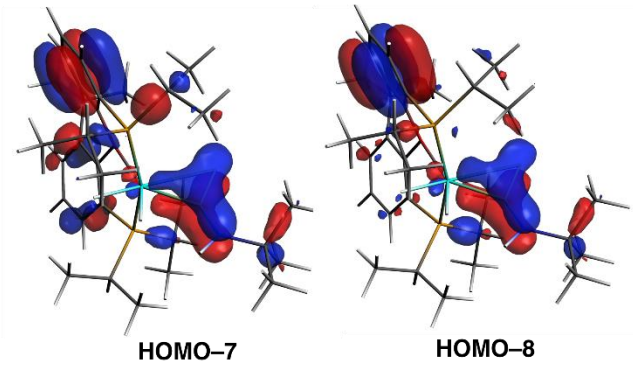

Figure 3. Computed π-molecular orbitals delocalized into the Os-B-S metallacycle of **3** (isosurface value of 0.04 a.u.).

The previous mentioned findings are consistent with a formally 4n + 2 Hückel aromatic system in which n = 0 and where the two π-electrons of the ring are provided by the sulfur atom. To confirm the aromaticity of the novel Os, S, B three-membered ring, we first computed the Nuclear Independent Chemical Shift (NICS) values at the center of the ring. A highly negative value of NICS (0) = -32.1 ppm was found, which would at first glance support the aromatic nature of the metallacycle. Nevertheless, it is well-known that isotropic NICS values, particularly in small rings, are usually contaminated by local shielding effects of the nearby bonds and therefore are not always reliable.[12a] The situation is even more dramatic if a transition metal is present in the ring.[4c] For this reason, we also computed the out-of-plane tensor

contribution to the NICS value at 1 Å above and below the ring center, which has been recommended as a reliable measure of the magnetic aromaticity.[29] The highly negative computed values, $NICS(1)_{zz}$ = -17.9 and -18.4 ppm are overwhelming evidence of the aromatic nature of the Os-S-B metallacycle. In addition, the Anisotropy of the Induced Current Density (ACID)[30] method was applied to visualize the aromatic ring current in the metallacycle. As depicted in Figure 4, the ACID method, computed for a model system where the bulky isopropyl and *tert*-butyl groups were replaced by hydrogen atoms ($NICS(1)_{zz}$ = -15.9 ppm), clearly shows the occurrence of a diatropic (clockwise vectors) ring current within the three-membered ring, therefore confirming the aromatic nature of this novel metallacycle.

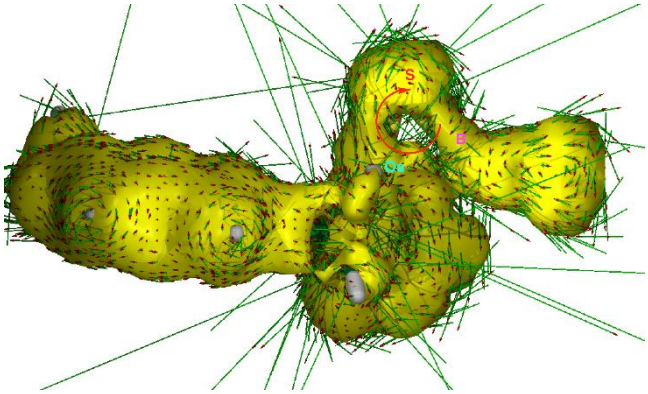

Figure 4. ACID plot for the model compound $OsH_2\{\kappa^2$-S,B-$[SBNH_2]\}\{\kappa^3$-P,O,P-$[xant(PH_2)_2]\}$ with a 0.04 a.u. isosurface value.

We have obtained additional support for the aromatic character of complexes **3** and **4** by means of energetic descriptors. However, the application of the energetic methods (ASE or ISE methods)[4c] typically used in other aromatic compounds, including those having transition-metals in their structures, is not possible for these particular species. We have carried out two alternative isodesmic reactions, namely the hydrogenation and the reductive elimination depicted in Scheme 2. For both reactions, the cleavage of the three-membered ring is computed to be endothermic, which is fully consistent with the thermodynamic stability (due to aromaticity) of the metallacycle.

Scheme 2. Computed Isodesmic Reactions Involving Complex 3. Energies (in kcal/mol) Were Computed at the BP86-D3/def2-TZVPP Level

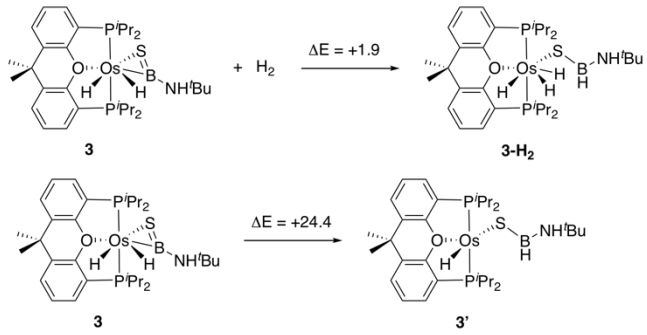

In conclusion, the assembly of a 16-electron valence $L_5Os(IV)$ metal fragment, a sulfur atom, and a B-NR_2 moiety gives rise to three-membered π-aromatic rings, which are formed by different vertexes, representing a novel manifestation of 4n + 2 Hückel aromaticity in which n = 0. These cycloosmathioborane compounds are prepared by simultaneous dehydrogenation of a trihydride-hydrogensulfide-osmium(IV) complex and a BH_3NHR_2 amine-borane.

ASSOCIATED CONTENT

Supporting Information

The Supporting Information is available free of charge on the ACS Publications website.
General information, instrumental methods, preparation and characterization of **2**, **3** and **4**, NMR spectra, structural analysis of **2** and **3**, and computational details (PDF)
Crystallographic information for **2** (CCDC 1878692) (CIF)
Crystallographic information for **3** (CCDC 1878693) (CIF)
Cartesian coordinates (xyz)

AUTHOR INFORMATION

Corresponding Author

*E-mail: maester@unizar.es.
ORCID
Miguel A. Esteruelas: 0000-0002-4829-7590
Israel Fernández: 0000-0002-0186-9774
Cristina García-Yebra: 0000-0002-5545-5112
Jaime Martín: 0000-0003-0909-3509
Enrique Oñate: 0000-0003-2094-719X

Present Addresses

C. G.-Y. §Departamento de Química Orgánica y Química Inorgánica, Universidad de Alcalá, 28871 Alcalá de Henares, Spain.

Notes

The authors declare no competing financial interests.

ACKNOWLEDGMENT

We thank MINECO of Spain (Projects CTQ2017-82935-P, CTQ2016-78205-P, and Red de Excelencia Consolider CTQ2016-81797-REDC), Diputación General de Aragón (No. E06_17R), FEDER, and the European Social Fund for financial support.

DEDICATION

Dedicated to Professor Pablo Espinet by his outstanding contribution to the field of the organometallic compounds, on the occasion of his 70th birthday.

REFERENCES

(1) (a) Stanger, A. What is ... Aromaticity: a Critique of the Concept of Aromaticity-Can it Really be Defined? *Chem. Commun.* **2009**, 1939-1947. (b) Solà, M. Why Aromaticity Is a Suspicious Concept? Why? *Front. Chem.* **2017**, *5*, 22.

(2) Thorn, D. L.; Hoffmann, R. Delocalization in Metallocycles. *Nouv. J. Chim.* **1979**, *3*, 39-45.

(3) Elliott, G. P.; Roper, W. R.; Waters, J. M. Metallacyclohexatrienes or "Metallabenzenes". Synthesis of Osmabenzene Derivatives and X-Ray Crystal Structure of $[Os(CSCHCHCHCH)(CO)(PPh_3)_2]$. *J. Chem. Soc., Chem. Comm.* **1982**, 811-813.

(4) (a) Bleeke, J. R. Metallabenzenes. *Chem. Rev.* **2001**, *101*, 1205-1227. (b) Cao, X.-Y.; Zhao, Q.; Lin, Z.; Xia, H. The Chemistry of Aromatic Osmacycles. *Acc. Chem. Res.* **2014**, *47*, 341-354. (c) Fernández, I.; Frenking, G.; Merino, G. Aromaticity of Metallabenzenes and Related Compounds. *Chem. Soc. Rev.* **2015**, *44*, 6452-6463. (d) Frogley, B. J.; Wright, L. J. Recent Advances in Metallaaromatic Chemistry. *Chem. - Eur. J.* **2018**, *24*, 2025-2038. (e) Zhu, C.; Xia, H. Carbolong Chemistry: A Story of Carbon Chain Ligands and Transition Metals. *Acc. Chem. Res.* **2018**, *51*, 1691-1700.

(5) Bursten, B. E.; Fenske, R. F. Molecular Orbital Studies on Cyclobutadienemetal Complexes: The Concept of Metallooaromaticity. *Inorg. Chem.* **1979**, *18*, 1760-1765.

(6) (a) Masui, H. Metalloaromaticity. *Coord. Chem. Rev.* **2001**, *219*, 957-992. (b) Feixas, F.; Matito, E.; Poater, J.; Solà, M. Metalloaromaticity. *WIREs Comput. Mol. Sci.* **2013**, *3*, 105-122.

(7) (a) Boldyrev, A. I.; Wang, L. S. All-Metal Aromaticity and Antiaromaticity. *Chem. Rev.* **2005**, *105*, 3716-3757. (b) Tsipis, C. A. DFT Study of "All-Metal" Aromatic Compounds. *Coord. Chem. Rev.* **2005**, *249*, 2740-2762. (c) Zubarev, D. Y.; Averkiev, B. B.; Zhai, H.-J.; Wang, L.-S.; Boldyrev, A. I. Aromaticity and Antiaromaticity in Transition-Metal Systems. *Phys. Chem. Chem. Phys.* **2008**, *10*, 257-267. (d) Li, L.-J.; Ali, B.; Chen, Z.; Sun, Z.-M. Recent Advances in Aromatic Antimony Clusters. *Chin. J. Chem.* **2018**, *36*, 955-960.

(8) (a) Li, X.-W.; Pennington, W. T.; Robinson, G. H. A Metallic System with Aromatic Character. Synthesis and Molecular Structure of $Na_2[(Mes_2C_6H_3)Ga]_3$ (Mes=2,4,6-$Me_3C_6H_2$): The First Cyclogallane. *J. Am. Chem. Soc.* **1995**, *117*, 7578-7579. (b) Li, X. W.; Xie, Y. M.; Schreiner, P. R.; Gripper, K. D.; Critendon, R. C.; Campana, C. F.; Schaefer, H. F.; Robinson, G. H. Cyclogallanes and Metalloaromaticity. Synthesis and Molecular Structure of Dipotassium Tris((2,6-dimesityphenyl)cyclogallene), $K_2[(Mes_2C_6H_3)Ga]_3$ (Mes=2,4,6-$Mes_2C_6H_3$): A Structural and Theoretical Examination. *Organometallics* **1996**, *15*, 3798-3803. (c) Robinson, G. H. Gallanes, Gallenes, Cyclogallenes, and Gallynes: Organometallic Chemistry about the Gallium−Gallium Bond. *Acc. Chem. Res.* **1999**, *32*, 773-782. (d) Wang, Y. Z.; Robinson, G. H. Organometallics of the Group 13 M-M Bond (M = Al, Ga, In) and the Concept of Metalloaromaticity. *Organometallics* **2007**, *26*, 2-11.

(9) Maslowsky, E. Inorganic Metallocenes: The Structures and Aromaticity of Sandwich Compounds of the Transition Elements with Inorganic Rings. *Coord. Chem. Rev.* **2011**, *255*, 2746-2763.

(10) Blanchard, S.; Fensterbank, L.; Gontard, G.; Lacôte, E.; Maestri, G.; Malacria, M. Synthesis of Triangular Tripalladium Cations as Noble-Metal Analogues of the Cyclopropenyl Cation. *Angew. Chem., Int. Ed.* **2014**, *53*, 1987-1991.

(11) Robilotto, T. J.; Bacsa, J.; Gray, T. G.; Sadighi, J. P. Synthesis of a Trigold Monocation: An Isolobal Analogue of $[H_3]^+$. *Angew. Chem., Int. Ed.* **2012**, *51*, 12077-12080.

(12) (a) Fernández, I.; Duvall, M.; I-Chia Wu, J.; Schleyer, P. v. R.; Frenking, G. Aromaticity in Group 14 Homologues of the Cyclopropenylium Cation. *Chem. - Eur. J.* **2011**, *17*, 2215-2224. (b) Fernández, I.; Wu, J. I.; Schleyer, P. v. R. Substituent Effects on "Hyperconjugative" Aromaticity and Antiaromaticity in Planar Cyclopolyenes. *Org. Lett.* **2013**, *15*, 2990-2993.

(13) Figueroa, J. S.; Cummins, C. C. Triatomic EP_2 Triangles (E = Ge, Sn, Pb) as μ^2: η^3,η^3-Bridging Ligands. *Angew. Chem., Int. Ed.* **2005**, *44*, 4592-4596.

(14) Ullah, S. S.; Mazumder, L. J.; Kaushik, S.; Das, N.; Brahma, M. S.; Sharma, P. K.; Guha, A. K. Electronic Structure, Stability, and Aromaticity of H_2B_2XH (X=N, P) molecules: A Theoretical Study. *Comput. Theor. Chem.* **2017**, *1113*, 120-125.

(15) Esteruelas, M. A.; García-Yebra, C.; Martín, J.; Oñate, E. Dehydrogenation of Formic Acid Promoted by a Trihydride-Hydroxo-Osmium(IV) Complex: Kinetics and Mechanism. *ACS Catal.* **2018**, *8*, 11314-11323.

(16) Ozerov, O. V. Oxidative Addition of Water to Transition Metal Complexes. *Chem. Soc. Rev.* **2009**, *38*, 83-88.

(17) For osmium complexes bearing bridging SH groups see: (a) Au, Y.-K.; Cheung, K.-K.; Wong, W.-T. Synthesis and Structural Characterization of Ruthenium and Osmium Carbonyl Clusters Containing 4,6-Dimethylpyrimidine-2-thione. *Inorg. Chim. Acta.* **1995**, *228*, 267-275. (b) Au, Y.-K.; Cheung, K.-K.; Wong, W.-T. Synthesis, Structural Characterization and Thermal Reactivities of Osmium Carbonyl Clusters Containing 4,6-Dimethylpyrimidine-2-thione. *J. Chem. Soc., Dalton Trans.* **1995**, 1047-1057. (c) Reyes-López, O. R.; Leyva, M. A.; Rosales-Hoz, M. J. Structural Characterization of $[(\mu\text{-H})Os_3(CO)_{10}(\mu\text{-NH}_2)]$ and a New Polymorphic form of $[(\mu\text{-H})Os_3(CO)_{10}(\mu\text{-SH})]$. Influence of the Bridging Group on the Geometry of Compounds $[(\mu\text{-H})Os_3(CO)_{10}(\mu\text{-X})]$ (X=NH_2, NRH, PRH, SbR_2, OH, SH, SR, SeR, Cl, Br). Reactions of $[(\mu\text{-H})Os_3(CO)_{10}(\mu\text{-X})]$ (X=OH and SH) with Proton Sponge. *J. Mol. Struct.* **2011**, *985*, 134-138.

(18) Buil, M. L.; Elipe, S.; Esteruelas, M. A.; Oñate, E.; Peinado, E.; Ruiz, N. Five-Coordinate Complexes $MHCl(CO)(P^iPr_3)_2$ (M = Os, Ru) as Precursors for the Preparation of New Hydrido− and Alkenyl−Metallothiol and Monothio−*β*-Diketonato Derivatives. *Organometallics* **1997**, *16*, 5748-5755.

(19) Esteruelas, M. A.; López, A. M.; Mora, M.; Oñate, E. B-H Activation and H-H Formation: Two Consecutive Heterolytic Processes on an Osmium-Hydrogensulfide Bond. *Chem. Commun.* **2013**, *49*, 7543-7545.

(20) Wozniak, M.; Braun, T.; Ahrens, M.; Braun-Cula, B.; Wittwer, P.; Herrmann, R.; Laubenstein, R. Activation of SF_6 at a Xantphos-Type Rhodium Complex. *Organometallics* **2018**, *37*, 821-828

(21) (a) Esteruelas, M. A.; López, A. M.; Mora, M.; Oñate, E. Ammonia-Borane Dehydrogenation Promoted by an Osmium Dihydride Complex: Kinetics and Mechanism. *ACS Catal.* **2015**, *5*, 187-191. (b) Esteruelas, M. A.; López, A. M.; Oliván, M. Polyhydrides of Platinum Group Metals: Nonclassical Interactions and *σ*-Bond Activation Reactions. *Chem. Rev.* **2016**, *116*, 8770-8847.

(22) Esteruelas, M. A.; Fernández, I.; López, A. M.; Mora, M.; Oñate, E. Osmium-Promoted Dehydrogenation of Amine-Boranes and B-H Bond Activation of the Resulting Amino-Boranes. *Organometallics* **2014**, *33*, 1104-1107.

(23) Liu, S. Y.; Légaré, M.-A.; Auerhammer, D.; Hofmann, A.; Braunschweig, H. The First Boron-Tellurium Double Bond: Direct Insertion of Heavy Chalcogens into a Mn=B Double Bond. *Angew. Chem., Int. Ed.* **2017**, *56*, 15760-15763.

(24) Wang, H.; Zhang, J. Y.; Hu, H. F.; Cui, C. M. Access to B=S and B=Se Double Bonds via Sulfur and Selenium Insertion into a B-H Bond and Hydrogen Migration. *J. Am. Chem. Soc.* **2010**, *132*, 10998-10999.

(25) Jaiswal, K.; Prashanth, B.; Ravi, S.; Shamasundar, K. R.; Singh, S. Reactivity of a Dihydroboron Species: Synthesis of a Hydroborenium Complex and an Expedient Entry into Stable Thioxo- and Selenoxo-Boranes. *Dalton Trans.* **2015**, *44*, 15779-15785.

(26) Franz, D.; Irran, E.; Inoue, S. Isolation of a Three-Coordinate Boron Cation with a Boron-Sulfur Double Bond. *Angew. Chem., Int. Ed.* **2014**, *53*, 14264-14268.

(27) Bauer, J.; Braunschweig, H.; Damme, A.; Carlos, J. O.; Kramer, J.-H. T.; Radacki, K.; Shang, R.; Siedler, E.; Ye, Q. Metathesis Reactions of a Manganese Borylene Complex with Polar Heteroatom-Carbon Double Bonds: A Pathway to Previously Inaccessible Carbene Complexes. *J. Am. Chem. Soc.* **2013**, *135*, 8726-8734.

(28) (a) Esteruelas, M. A.; Fernández, I.; López, A. M.; Mora, M.; Oñate, E. Preparation, Structure, Bonding, and Preliminary Reactivity of a Six-Coordinate d^4 Osmium-Boryl Complex. *Organometallics* **2012**, *31*, 4646-4649. (b) Buil, M. L.; Esteruelas, M. A.; Fernández, I.; Izquierdo, S.; Oñate, E. Cationic Dihydride Boryl and Dihydride Silyl Osmium(IV) NHC Complexes: A Marked Diagonal Relationship. *Organometallics* **2013**, *32*, 2744-2752.

(29) Fallah-Bagher-Shaidaei, H.; Wannere, C. S.; Corminboeuf, C.; Puchta, R.; Schleyer, P. v. R. Which NICS Aromaticity Index for Planar π Rings is Best? *Org. Lett.* **2006**, *8*, 863-866.

(30) (a) Herges, R.; Geuenich, D. Delocalization of Electrons in Molecules. *J. Phys. Chem. A.* **2001**, *105*, 3214-3220. (b) Geuenich, D.; Hess, K.; Köhler, F.; Herges, R. Anisotropy of the Induced Current Density (ACID), a General Method to Quantify and Visualize Electronic Delocalization. *Chem. Rev.* **2005**, *105*, 3758-3772.

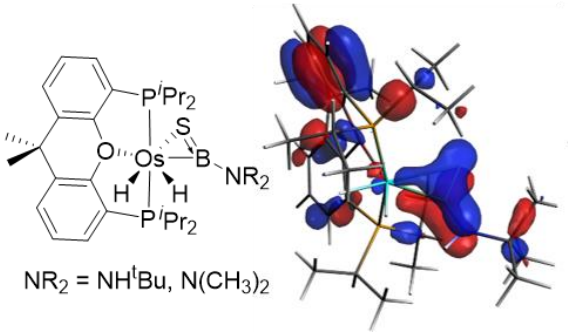

Cycloosmathioboranes bearing an Os, S, B three-membered ring are a manifestation of 4n + 2 Hückel aromaticity in which n = 0 and where the two π-electrons of the ring are provided by the S atom.

Supporting Information For

Cycloosmathioborane Compounds: Other Manifestation of the Hückel Aromaticity

Miguel A. Esteruelas,[†] Israel Fernández,[‡] Cristina García-Yebra,[†,§] Jaime Martín,[†] and Enrique Oñate[†]*

[†]Departamento de Química Inorgánica, Instituto de Síntesis Química y Catálisis Homogénea (ISQCH), Centro de Innovación en Química Avanzada (ORFEO-CINQA), Universidad de Zaragoza-CSIC, 50009 Zaragoza, Spain

[‡]Departamento de Química Orgánica I, Facultad de Ciencias Químicas, Centro de Innovación en Química Avanzada (ORFEO-CINQA), Universidad Complutense de Madrid, 28040 Madrid, Spain

[§]Departamento de Química Orgánica y Química Inorgánica, Universidad de Alcalá, 28871 Alcalá de Henares, Spain

*Corresponding author e-mail address: maester@unizar.es

Contents:

General Information and Instrumental Methods. All reactions were performed under argon using Schlenk tube or glovebox techniques. Solvents were dried using standard procedures and distilled under argon atmosphere or obtained dry from an MBraun solvent purification apparatus. Pentane was subsequently stored over P_2O_5 in the glovebox. Toluene, benzene and THF were stored over sodium in the glovebox. Commercial chemicals were used as received, except where otherwise noted. NMR spectra were recorded on either a Bruker Avance 300 or 400 MHz instrument. Chemical shifts (expressed in ppm) are referenced to residual solvent peaks (^{1}H, ^{13}C{^{1}H}) or external H_3PO_4 (^{31}P{^{1}H}) and $BF_3{\cdot}OEt_2$ (^{11}B). Coupling constants, J and N ($N = J_{PH} + J_{P'H}$ for ^{1}H; $N = J_{PC} + J_{P'C}$ for ^{13}C), are given in Hz. Signals were assigned using also bidimensional NMR experiments (^{1}H-^{1}H COSY, ^{1}H-^{13}C{^{1}H} HMBC and ^{1}H-^{13}C{^{1}H} HSQC). Elemental analyses were carried out using a Perkin-Elmer 2400 CHNS/O analyzer.

Preparation and Characterization of Complexes 2, 3 and 4. Complexes $OsH_3(OTf)\{\kappa^3$-P,O,P-[xant($P^iPr_2)_2$]} (**1**) was prepared as published.[1]

Synthesis of $OsH_3(SH)\{\kappa^3$-P,O,P-[xant($P^iPr_2)_2$]} (2). A solution of NaSH (58 mg, 1.03 mmol) in MeOH (2 mL) was added dropwise to a solution of complex **1** (200 mg, 0.255 mmol) in THF (8 mL). The resulting red solution was stirred for 1 hour, at room temperature, and it was concentrated to dryness. Toluene (10 mL) was added and the suspension was filtered through Kieselguhr. The filtrate was concentrated under reduced pressure, and 2 mL of pentane at -50 ºC was added to afford a pale red solid. The solid was washed with pentane at -50 ºC (3 x 2 mL) and was dried under vacuum. Yield: 80 mg (47 %). Red crystals suitable for X-ray diffraction analysis were obtained by vapor diffusion of pentane into a toluene solution of the complex at -30 ºC. Anal. Calcd. for $C_{27}H_{44}OOsP_2S$: C, 48.48; H, 6.63; S, 4.79. Found: C, 48.80; H, 6.69; S, 4.50. ^{1}H NMR (300.13 MHz, C_6D_6, 298 K): δ 7.22 (m, 2H, C*H*-arom POP), 7.04 (dd, $^3J_{HH} = 7.6$, $^4J_{HH} = 1.4$, 2H, C*H*-arom POP), 6.92 (dd, $^3J_{HH} = 7.5$, $^3J_{HH} = 7.5$, 2H, C*H*-arom POP), 2.62 (m, 2H, PC*H*$(CH_3)_2$), 2.02 (m, 2H, PC*H*$(CH_3)_2$), 1.54 (dvt, $^3J_{HH} = 7.5$, $N = 15.8$, 6H, PCH(C*H*$_3)_2$), 1.41

(dvt, $^3J_{HH}$ = 6.9, *N* = 14.0, 6H, PCH(C*H*$_3$)$_2$), 1.35 (s, 3H, C*H*$_3$ POP), 1.23 (s, 3H, C*H*$_3$ POP), 1.14 (dvt, $^3J_{HH}$ = 6.9, *N* = 16.4, 6H, PCH(C*H*$_3$)$_2$), 0.81 (dvt, $^3J_{HH}$ = 6.9, *N* = 14.7, 6H, PCH(C*H*$_3$)$_2$), -0.39 (t, $^3J_{HP}$ = 10.7, 1H, S*H*), -11.73 (br, 3H, Os*H*). ^{1}H NMR (400.13 MHz, C_7D_8, 193 K): δ -8.07 (m, 1H, Os*H*), -13.01 (br, 1H, Os*H*), -13.78 (br, 1H, Os*H*). ^{13}C{^{1}H}-APT NMR (75.47 MHz, C_6D_6, 298K): δ 157.8 (vt, *N* = 13.1, *C*-arom POP), 132.4 (vt, *N* = 5.5, *C*-arom POP), 131.2 (vt, *N* = 28.0, *C*-arom POP), 130.7 (s, *C*H-arom POP), 127.2 (s, *C*H-arom POP), 125.0 (vt, *N* = 4.6, *C*H-arom POP), 35.7 (s, *C*(CH$_3$)$_2$ POP), 34.6 (s, C(*C*H$_3$)$_2$ POP), 27.4 (vt, *N* = 23.0, P*C*H(CH$_3$)$_2$), 26.8 (vt, *N* = 31.4, P*C*H(CH$_3$)$_2$), 26.6 (s, C(*C*H$_3$)$_3$ POP), 23.5 (vt, *N* = 5.3, PCH(*C*H$_3$)$_2$), 20.8 (vt, *N* = 10.2, PCH(*C*H$_3$)$_2$), 20.6 (s, PCH(*C*H$_3$)$_2$), 19.5 (vt, *N* = 3.0, PCH(*C*H$_3$)$_2$). ^{31}P{^{1}H} NMR (121.49 MHz, C_6D_6, 298K): δ 48.1 (s, POP). T_1 (min) (ms, Os*H*, 400.13 MHz, C_7D_8, 233 K): 90 ± 5 (-8.16 ppm), 105 ± 5 (-13.49 ppm).

Synthesis of OsH$_2${κ^2-S,B-[SBNH^{t}Bu]{κ^3-P,O,P-[xant(P^{i}Pr$_2$)$_2$]} (3). Amine-borane $BH_3NH_2{}^tBu$ (13 mg, 0.149 mmol) was added to a solution of **2** (72 mg, 0.108 mmol) in 5 mL of toluene. The resulting solution was stirred for 1 day, at room temperature, and subsequently concentrated under vaccum to yield a brown residue, which was treated with pentane at -50 ºC (2 x 3 mL). The formed suspension was filtered and the solution evaporated to afford a yellow solid which was dried under reduced pressure. Yield: 52 mg (65 %). Yellow crystals suitable for X-ray diffraction analysis were obtained from a concentrated solution of the complex in pentane at room temperature. Anal. Calcd. for $C_{31}H_{52}BNOOsP_2S$: C, 49.66; H, 6.99; N, 1.87; S, 4.28. Found: C, 49.92; H, 6.77; N, 2.17; S, 4.66. ^{1}H NMR (300.13 MHz, C_6D_6, 298K): δ 7.17 (m, 2H, C*H*-arom POP), 6.98 (dd, $^3J_{HH}$ = 7.5, $^4J_{HH}$ = 1.3, 2H, C*H*-arom POP), 6.90 (dd, $^3J_{HH}$ = 7.4, $^3J_{HH}$ = 7.4, 2H, C*H*-arom POP), 4.08 (s, 1H, N*H*), 2.86 (m, 2H, PC*H*(CH$_3$)$_2$), 2.07 (m, 2H, PC*H*(CH$_3$)$_2$), 1.53 (s, 9H, C(C*H*$_3$)$_3$), 1.40 (dvt, $^3J_{HH}$ = 7.0, *N* = 15.0, 6H, PCH(C*H*$_3$)$_2$), 1.36 (s, 3H, C*H*$_3$ POP), 1.36-1.26 (12H, PCH(C*H*$_3$)$_2$), 1.06 (s, 3H, C*H*$_3$ POP), 0.94 (dvt, $^3J_{HH}$ = 7.0, *N* = 14.4, 6H, PCH(C*H*$_3$)$_2$), -9.03 (dt, $^2J_{HH}$ = 2.3, $^3J_{HP}$ = 18.7, 1H, Os*H*), -18.76 (dt, $^2J_{HH}$ = 1.9, $^3J_{HP}$ = 9.3, 1H, Os*H*). ^{13}C{^{1}H}-APT NMR (75.47 MHz, C_6D_6, 298K): δ 161.6 (vt, *N* = 14.1, *C*-arom POP), 133.7 (vt, *N* = 5.6, *C*-arom POP), 130.0 (s, *C*H-arom POP), 129.6 (vt, *N* = 26.6, *C*-arom POP), 125.7 (s, *C*H-arom

POP), 125.4 (s, *C*H-arom POP), 51.5 (s, *C*(CH_3)$_3$), 35.0 (s, *C*(CH_3)$_2$ POP), 34.0 (s, C(*C*H_3)$_2$ POP), 32.6 (s, C(*C*H_3)$_3$), 28.8 (vt, *N* = 21.6, P*C*H(CH_3)$_2$), 26.4 (vt, *N* = 32.2, P*C*H(CH_3)$_2$), 23.5 (s, C(*C*H_3)$_2$ POP), 21.2 (vt, *N* = 11.2, PCH(*C*H_3)$_2$), 20.5 (s, PCH(*C*H_3)$_2$), 20.1 (vt, *N* = 3.2, PCH(*C*H_3)$_2$), 20.0 (s, PCH(*C*H_3)$_2$). $^{31}P\{^1H\}$ NMR (121.49 MHz, C_6D_6, 298K): δ 46.8 (s, POP). ^{11}B NMR (96.29 MHz, C_6D_6, 298K): 56.8 (br).

Synthesis of OsH$_2${κ^2-S,B-[SBN(CH$_3$)$_2$]}{κ^3-P,O,P-[xant(P^{i}Pr$_2$)$_2$]} (4). Amine-borane complex $BH_3NH(CH_3)_2$ (40 mg, 0.716 mmol) was added to a solution of complex **2** (80 mg, 0.120 mmol) in 5 mL of toluene and it was stirred for 3 days. After that time, the solvent was evaporated and the resulting brown residue was extracted of with pentane at -50 ºC (2 x 3 mL) affording a yellow solution, which was filtered and evaporated to yield a yellow solid that was dried under reduced pressure. Yield: 50 mg (58 %). Anal. Calcd. for $C_{29}H_{48}BNOOsP_2S$: C, 48.26; H, 6.70; N, 1.94; S, 4.44. Found: C, 48.22; H, 6.34; N, 1.78; S, 4.50. ^1H NMR (300.13 MHz, C_6D_6, 298K): δ 7.16 (m, 2H, C*H*-arom POP), 7.00 (dd, $^3J_{HH}$ = 7.6, $^4J_{HH}$ = 1.3, 2H, C*H*-arom POP), 6.91 (dd, $^3J_{HH}$ = 6.9, $^3J_{HH}$ = 6.9, 2H, C*H*-arom POP), 3.44 (s, 3H, NC*H*$_3$), 3.29 (s, 3H, NC*H*$_3$), 2.82 (m, 2H, PC*H*(CH_3)$_2$), 2.00 (m, 2H, PC*H*(CH_3)$_2$), 1.42-1.22 (18H, PCH(C*H*$_3$)$_2$), 1.37 (s, 3H, C*H*$_3$ POP), 1.07 (s, 3H, C*H*$_3$ POP), 0.91 (dvt, $^3J_{HH}$ = 6.9, *N* = 14.2, 6H, PCH(C*H*$_3$)$_2$), -8.98 (dt, $^2J_{HH}$ = 1.0, $^3J_{HP}$ = 18.8, 1H, Os*H*), -17.88 (dt, $^2J_{HH}$ = 1.0, $^3J_{HP}$ = 9.5, 1H, Os*H*). $^{13}C\{^1H\}$-APT NMR (75.47 MHz, C_6D_6, 298K): δ 161.2 (vt, *N* = 14.2, *C*-arom POP), 133.5 (vt, *N* = 5.7, *C*-arom POP), 130.3 (s, *C*H-arom POP), 129.7 (vt, *N* = 26.6, *C*-arom POP), 125.9 (s, *C*H-arom POP), 125.4 (vt, *N* = 4.5, *C*H-arom POP), 46.7 (s, N(*C*H_3)$_3$), 41.8 (s, N(*C*H_3)$_3$), 35.0 (s, *C*(CH_3)$_2$ POP), 34.4 (s, C(*C*H_3)$_2$ POP), 29.5 (vt, *N* = 22.0, P*C*H(CH_3)$_2$), 26.8 (vt, *N* = 32.3, P*C*H(CH_3)$_2$), 23.7 (s, C(*C*H_3)$_2$ POP), 21.4 (vt, *N* = 11.2, PCH(*C*H_3)$_2$), 20.5 (s, PCH(*C*H_3)$_2$), 20.3 (s, PCH(*C*H_3)$_2$), 19.6 (vt, *N* = 3.6, PCH(*C*H_3)$_2$). $^{31}P\{^1H\}$ NMR (121.49 MHz, C_6D_6, 298K): δ 47.8 (s, POP). ^{11}B NMR (96.29 MHz, C_6D_6, 298K): 62.0 (br).

NMR Spectra of Complexes 2, 3 and 4

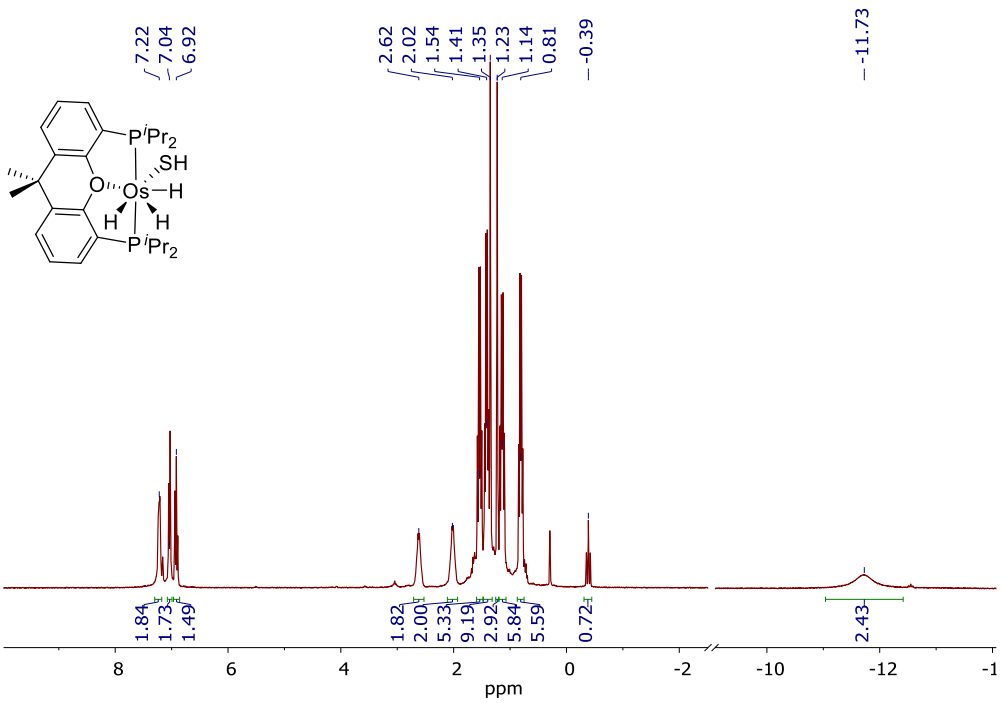

Figure S1. ^{1}H NMR (300.13 MHz, C_6D_6, 298 K) spectrum of complex **2**.

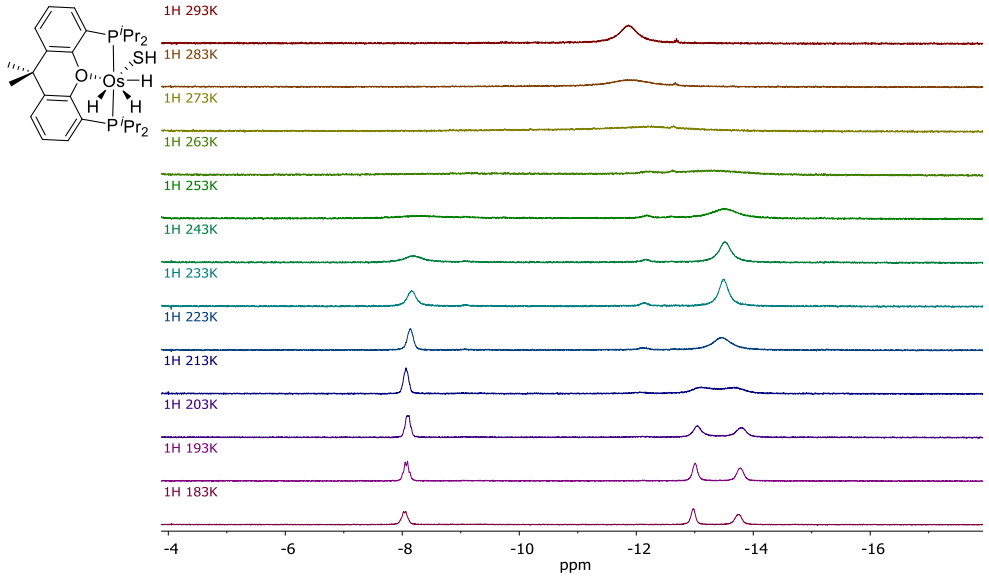

Figure S2. High-field region of the ^{1}H NMR (400.13 MHz, C_7D_8) spectrum of complex **2** between 293 and 183 K.

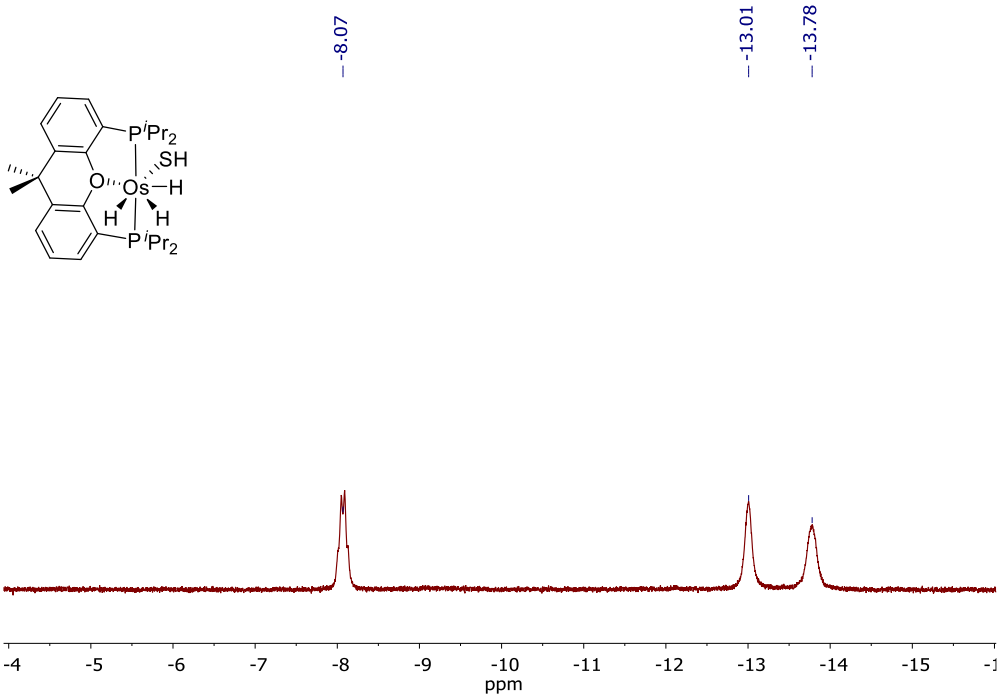

Figure S3. High-field region of the ^{1}H NMR (400.13 MHz, C_7D_8, 193 K) spectrum of complex **2**.

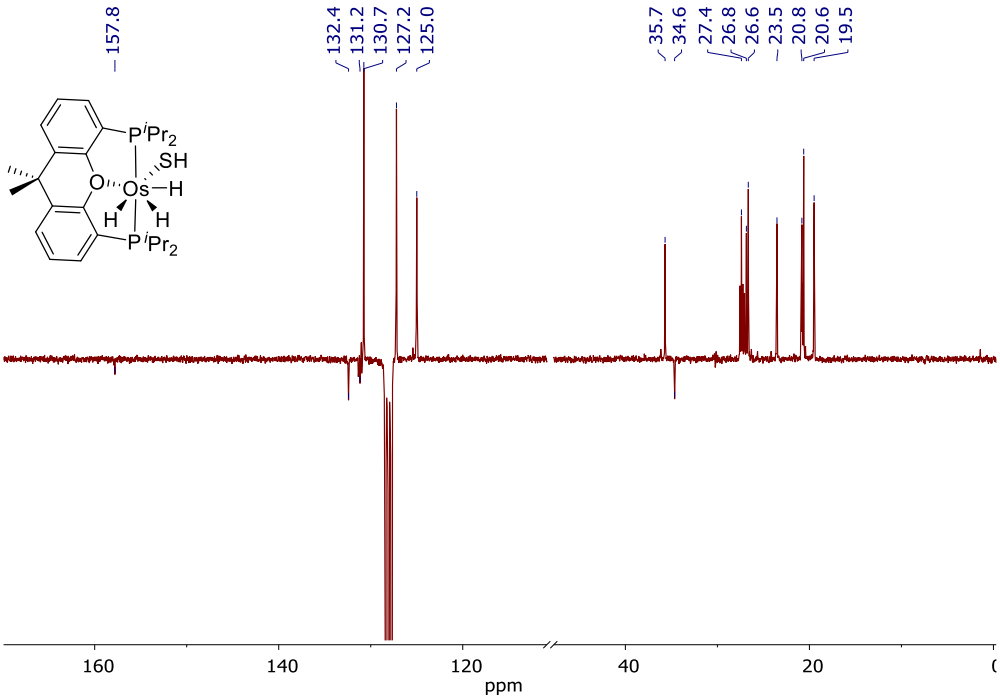

Figure S4. $^{13}C\{^1H\}$-APT NMR (75.47 MHz, C_6D_6, 298 K) spectrum of complex **2**.

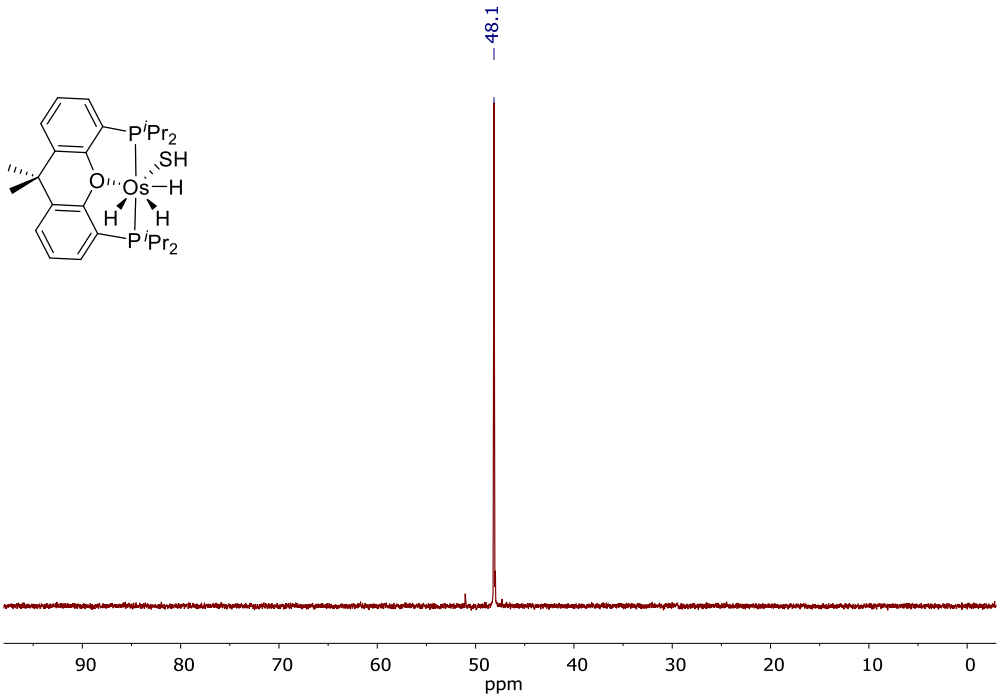

Figure S5. $^{31}P\{^{1}H\}$ NMR (121.49 MHz, C_6D_6, 298 K) spectrum of complex **2**.

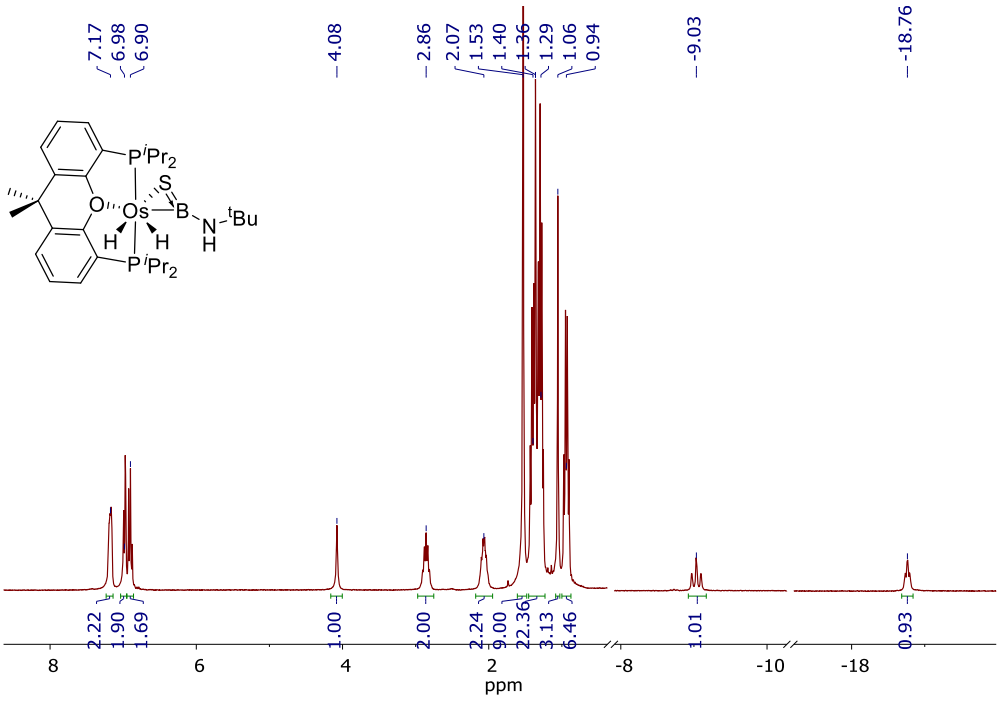

Figure S6. ^{1}H NMR (300.13 MHz, C_6D_6, 298 K) spectrum of complex **3**.

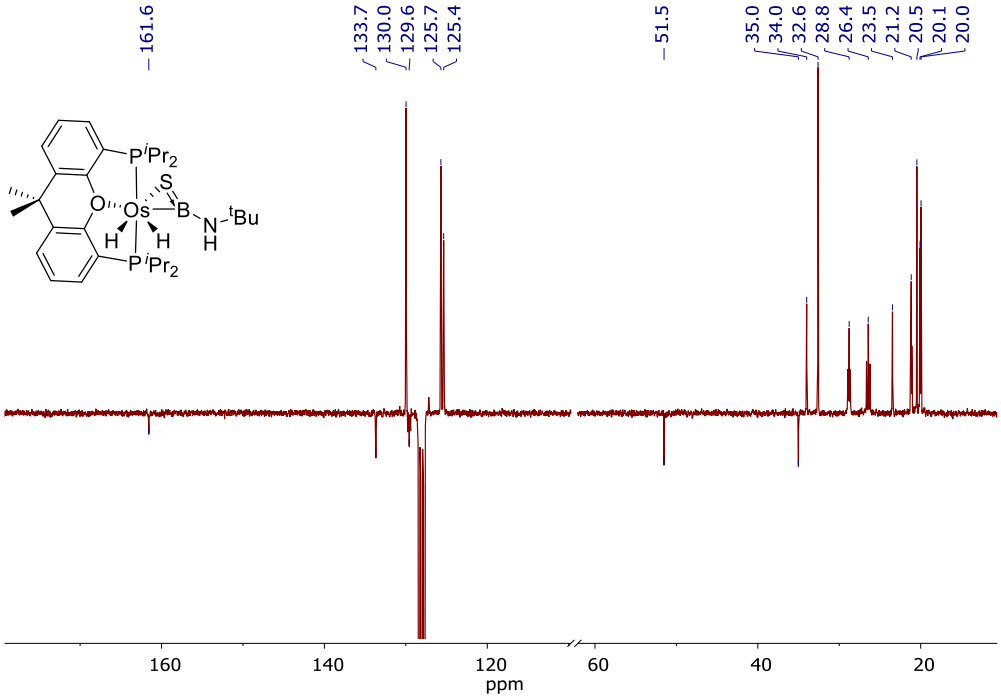

Figure S7. $^{13}C\{^1H\}$-APT NMR (75.47 MHz, C_6D_6, 298 K) spectrum of complex **3**.

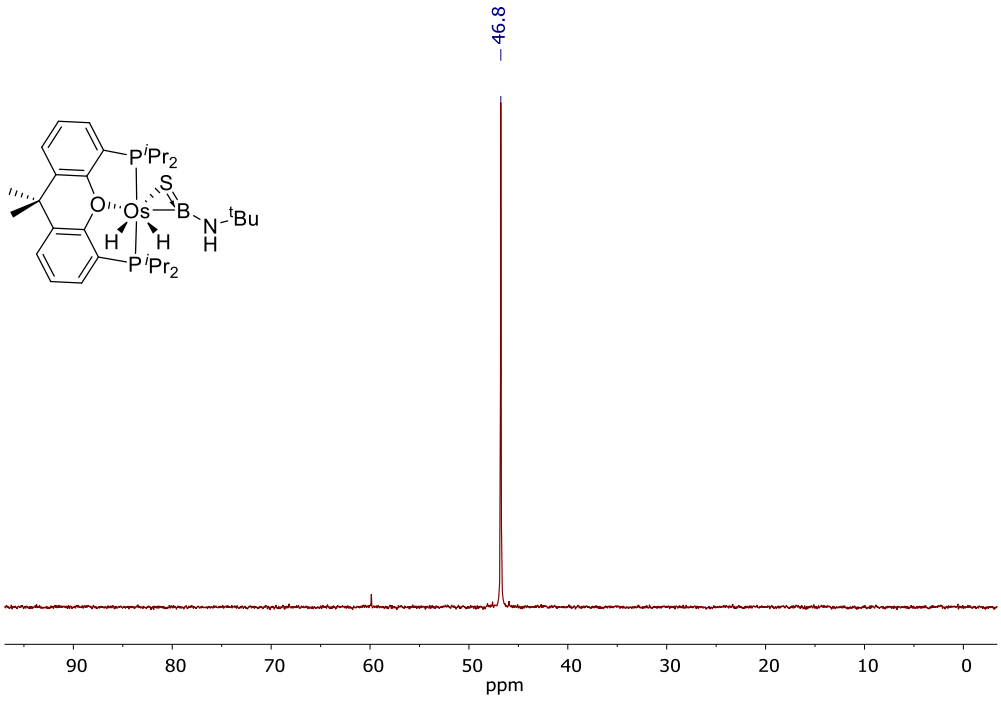

Figure S8. $^{31}P\{^1H\}$ NMR (121.49 MHz, C_6D_6, 298 K) spectrum of complex **3**.

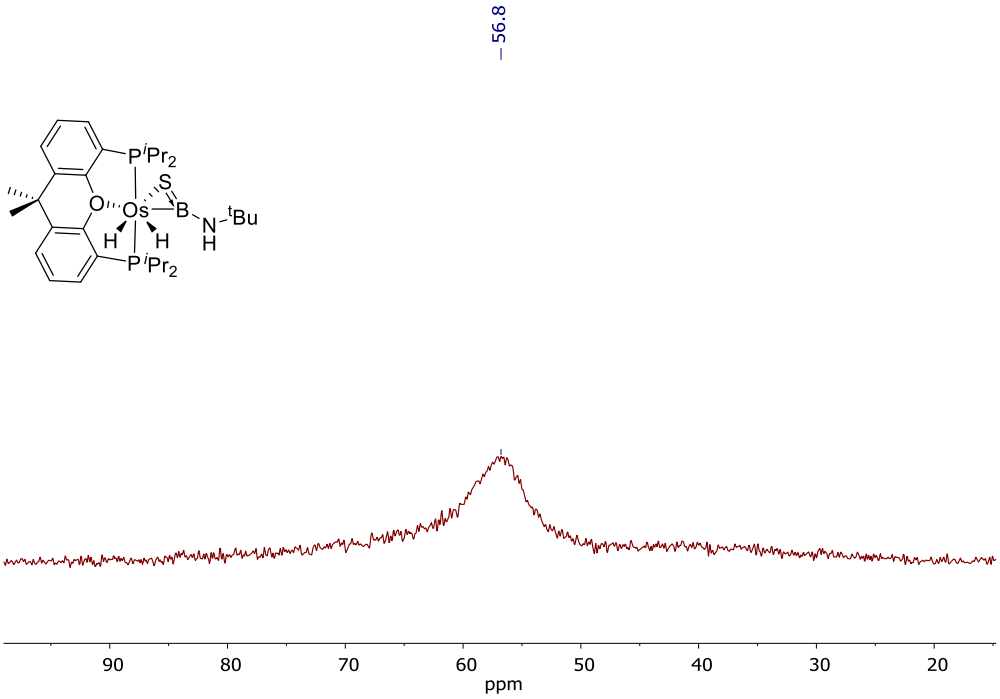

Figure S9. ^{11}B NMR (96.29 MHz, C_6D_6, 298 K) spectrum of complex **3**.

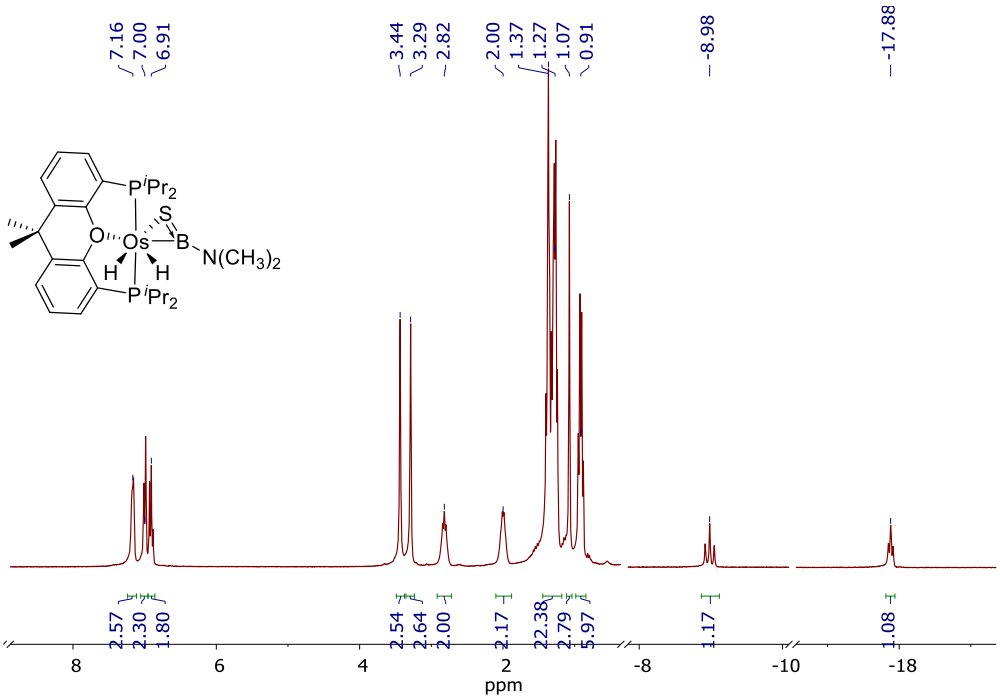

Figure S10. ^{1}H NMR (300.13 MHz, C_6D_6, 298 K) spectrum of complex **4**.

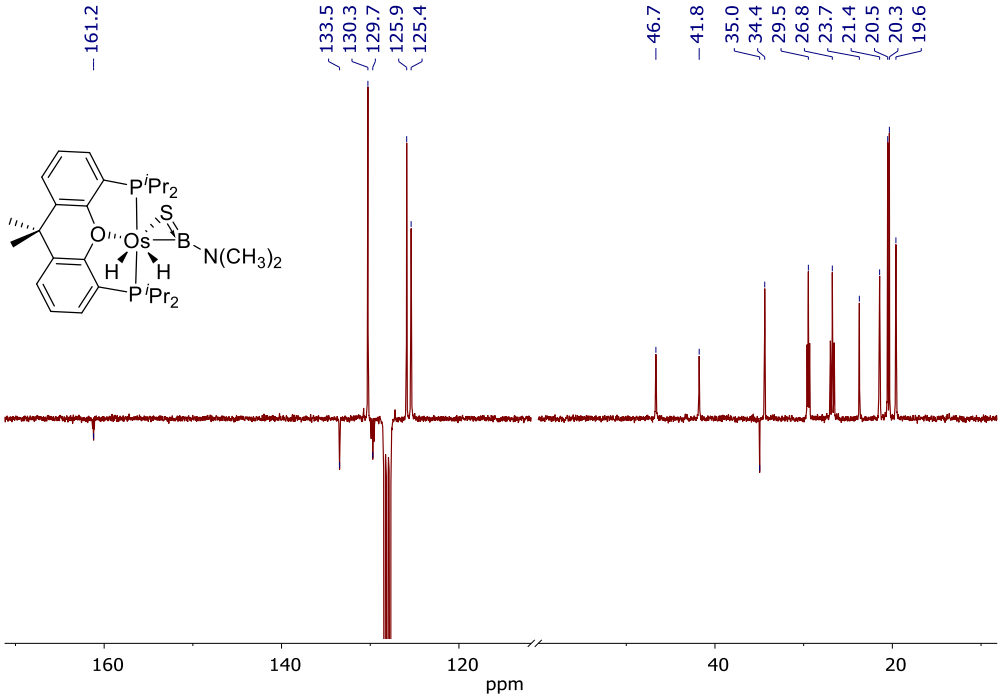

Figure S11. $^{13}C\{^1H\}$-APT NMR (75.47 MHz, C_6D_6, 298 K) spectrum of complex **4**.

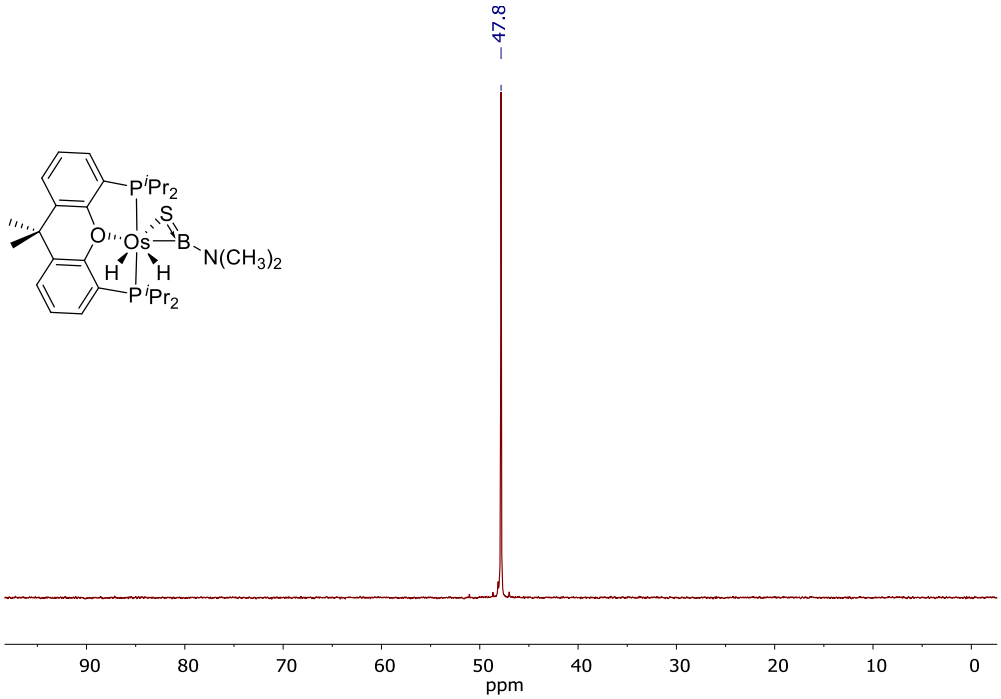

Figure S12. $^{31}P\{^1H\}$ NMR (121.49 MHz, C_6D_6, 298 K) spectrum of complex **4**.

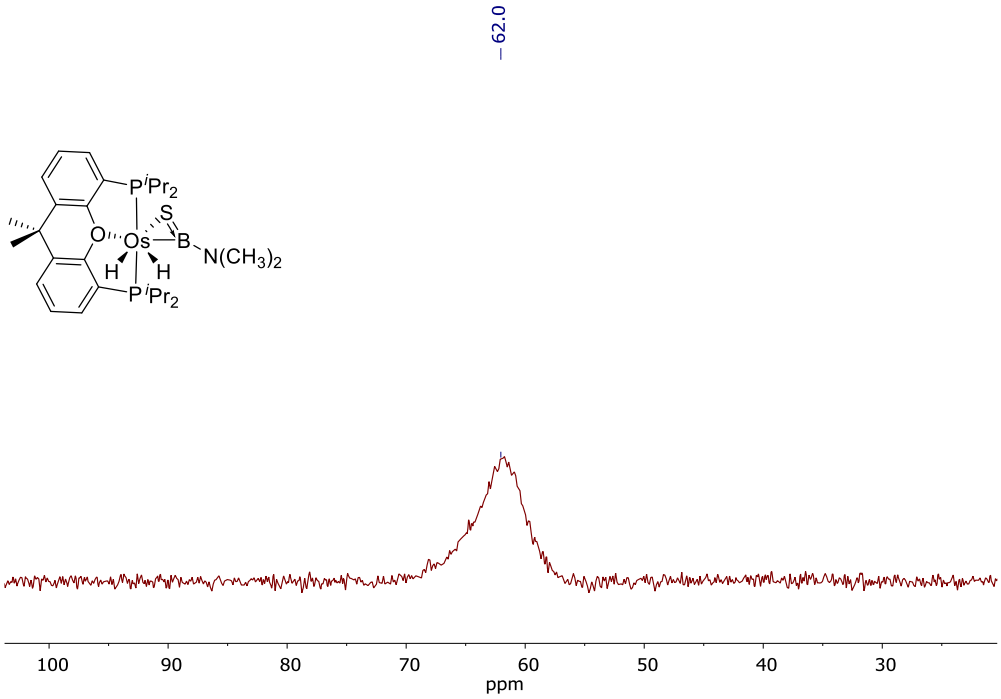

Figure S13. ^{11}B NMR (96.29 MHz, C_6D_6, 298 K) spectrum of complex **4**.

Structural Analysis of Complexes 2 and 3. X-ray data were collected for the complexes on a Bruker Smart APEX diffractometer equipped with a normal focus, and 2.4 kW sealed tube source (Mo radiation, λ = 0.71073 Å). Data were collected over the complete sphere covering 0.3° in ω. Data were corrected for absorption by using a multiscan method applied with the SADABS program.[2] The structures were solved by Patterson or direct methods and refined by full-matrix least squares on F^2 with SHELXL2016,[3] including isotropic and subsequently anisotropic displacement parameters. The hydrogen atoms were observed in the least Fourier Maps or calculated, and refined freely or using a restricted riding model. The hydride ligands were located in the last difference Fourier maps and refined with retrained distances to metal atoms (d_{Os-H} = 1.59(1) Å).

Crystal data for **2**: $C_{27}H_{44}OOsP_2S$, M_W 668.82, yellow, irregular block (0.171 x 0.140 x 0.129 mm^3), monoclinic, space group $P2_1/c$, *a*: 12.2836(6) Å, *b*: 11.9379(5) Å, *c*: 19.3225(9) Å, *β*: 98.3090(10)°, *V* = 2803.7(2) $Å^3$, *Z* = 4, *Z'* = 1, D_{calc}: 1.584 g cm^{-3}, F(000): 1344, T = 100(2) K, μ 4.754 mm^{-1}. 48768 measured reflections (2θ: 3-57°, ω scans 0.3°), 6937 unique (R_{int} = 0.0322); min./max. transm. Factors 0.687/0.862. Final agreement factors were R^1 = 0.0187 (6301 observed reflections, I > 2σ(I)) and wR^2 = 0.0437; data/restraints/parameters 6937/3/311; GoF = 1.033. Largest peak and hole 1.314 (close to osmium atoms) and -0.501e/ $Å^3$.

Crystal data for **3**: $C_{31}H_{52}BNOOsP_2S$, M_W 749.74, colourless, irregular block (0.128 x 0.098 x 0.033 mm^3), orthorhombic, space group Pbca, *a*: 20.8731(14) Å, *b*: 14.7433(10) Å, *c*: 21.7077(14) Å, *V* = 6680.3(8) $Å^3$, *Z* = 8, *Z'* = 1, D_{calc}: 1.491 g cm^{-3}, F(000): 3040, T = 100(2) K, μ 4.000 mm^{-1}. 93145 measured reflections (2θ: 3-57°, ω scans 0.3°), 8337 unique (R_{int} = 0.0665); min./max. transm. Factors 0.643/0.862. Final agreement factors were R^1 = 0.0409 (6495 observed reflections, I > 2σ(I)) and wR^2 = 0.0848; data/restraints/parameters 8337/2/365; GoF = 1.090. Largest peak and hole 1.664 (close to osmium atoms) and -1.387 e/ $Å^3$.

Computational Details. Geometry optimizations were performed without symmetry constraints using the Gaussian09[4] suite of programs at the BP86[5]/def2-TZVPP[6] level of theory using the D3 dispersion correction suggested by Grimme et al.[7] This level is denoted BP86-D3/def2-def2-TZVPP. All species were characterized by frequency calculations, and have positive definite Hessian matrices thus confirming that the computed structures are minima on the potential energy surface. Wiberg Bond Indices (WBIs) and Second-Order Perturbation Energies (SOPT) have been computed using the natural bond orbital (NBO6) method.[8]

The aromaticity of the considered species has been assessed by the computation of the NICS[9] values computed using the gauge invariant atomic orbital (GIAO) method,[10] at the dispersion corrected B3LYP level using the def2-SVP basis set,[6] with the optimized BP86-D3/def2-def2-TZVPP geometries. This scheme is denoted as GIAO-B3LYP/def2-SVP// BP86-D3/def2-def2-TZVPP.

Total energies (in a. u., ZPVE included) computed at the BP86-D3/def2-TZVPP level).

3: E= -2539.425077

3(model): E= -1831.933915

3-H2: E= -2540.590060

3': E= -2539.386766

ACID plot for the model compound $OsH_2\{\kappa^2$-S,B-$[SBNH_2]\{\kappa^3$-P,O,P-$[xant(PH_2)_2]\}$ using only the π orbitals.

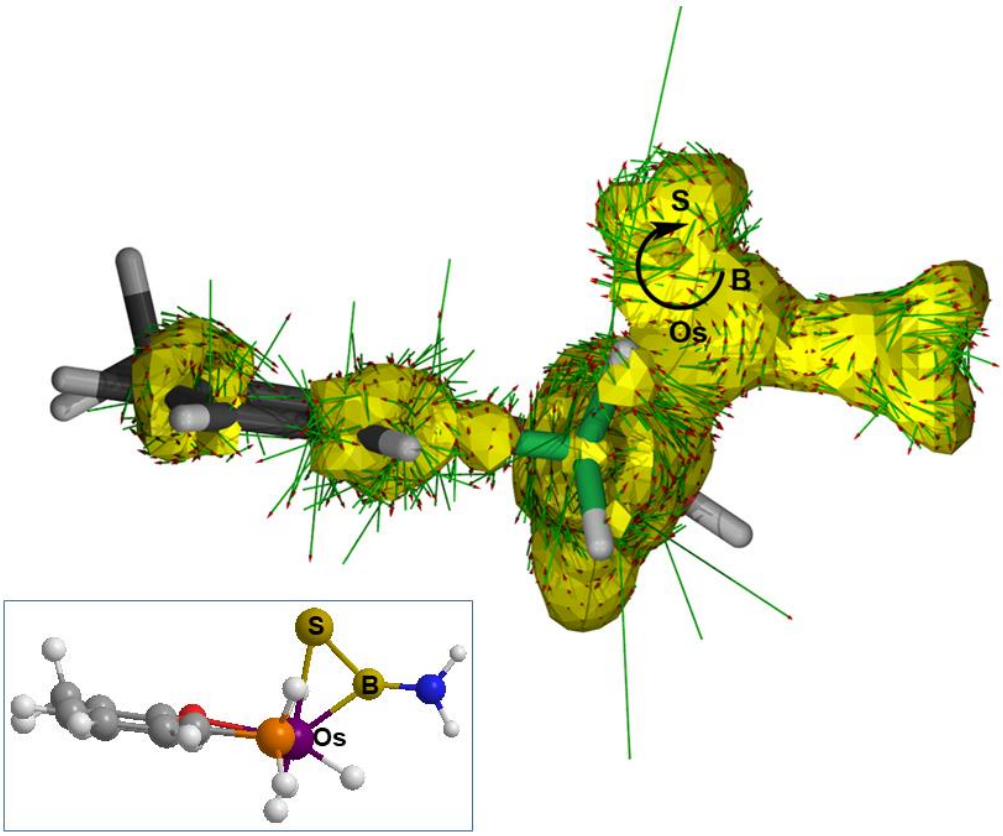

Figure S14. ACID plot for the model compound $OsH_2\{\kappa^2$-S,B-$[SBNH_2]\{\kappa^3$-P,O,P-$[xant(PH_2)_2]\}$ with a 0.04 a.u. isosurface value using only the π orbitals.

References

(1) Esteruelas, M. A.; García-Yebra, C.; Martín, J.; Oñate, E. Dehydrogenation of Formic Acid Promoted by a Trihydride-Hydroxo-Osmium(IV) Complex: Kinetics and Mechanism. *ACS Catal.* **2018**, *8*, 11314-11323.

(2) Blessing, R. H. An Empirical Correction for Absorption Anisotropy. *Acta Crystallogr., Sect. A: Found. Crystallogr.* **1995**, *51*, 33-38.

(3) Sheldrick, G. M. A Short History of SHELX. *Acta Crystallogr., Sect. A: Found. Crystallogr.* **2008**, *64*, 112-122.

(4) Gaussian 09, Revision D.01, Frisch, M. J.; Trucks, G. W.; Schlegel H. B.; Scuseria, G. E.; Robb, M. A.; Cheeseman, J. R.; Scalmani, G.; Barone, V.; Mennucci, B.; Petersson, G. A.; Nakatsuji, H.; Caricato, M.; Li, X.; Hratchian, H. P.; Izmaylov, A. F.; Bloino, J.; Zheng, G.; Sonnenberg, J. L.; Hada, M.; Ehara, M.; Toyota, K.; Fukuda, R.; Hasegawa, J.; Ishida, M.; Nakajima, T.; Honda, Y.; Kitao, O.; Nakai, H.; Vreven, T.; Montgomery, J. A.; Peralta, Jr., J. E.; Ogliaro, F.; Bearpark, M.; Heyd, J. J.; Brothers, E.; Kudin, K. N.; Staroverov, V. N.; Keith, T.; Kobayashi, R.; Normand, J.; Raghavachari, K.; Rendell, A.; Burant, J. C.; Iyengar, S. S.; Tomasi, J.; Cossi, M.; Rega, N.; Millam, J. M.; Klene, M.; Knox, J. E.; Cross, J. B.; Bakken, V.; Adamo, C.; Jaramillo, J.; Gomperts, R.; Stratmann, R. E.; Yazyev, O.; Austin, A. J.; Cammi, R.; Pomelli, C.; Ochterski, J. W.; Martin, R. L.; Morokuma, K.; Zakrzewski, V. G.; Voth, G. A.; Salvador, P.; Dannenberg, J. J.; Dapprich, S.; Daniels, A. D.; Farkas, Ö.; Foresman, J. B.; Ortiz, J. V.; Cioslowski, J.; Fox, D. J. Gaussian, Inc., Wallingford CT, 2009.

(5) Zhao, Y.; Schultz, N. E.; Truhlar, D. G. Design of Density Functionals by Combining the Method of Constraint Satisfaction with Parametrization for Thermochemistry, Thermochemical Kinetics, and Noncovalent Interactions. *J. Chem. Theory Comput.* **2006**, *2*, 364-382.

(6) Weigend, F.; Ahlrichs, R. Balanced Basis Sets of Split Valence, Triple Zeta Valence and Quadruple Zeta Valence Quality for H to Rn: Design and Assessment of Accuracy. *Phys. Chem. Chem. Phys.* **2005**, *7*, 3297-3305.

(7) Grimme, S.; Antony, J.; Ehrlich, S.; Krieg, H. A Consistent and Accurate *Ab Initio* Parametrization of Density Functional Dispersion Correction (DFT-D) for the 94 Elements H-Pu. *J. Chem. Phys.* **2010**, *132*, 154104-154119.

(8) (a) Foster, J. P.; Weinhold, F. Natural Hybrid Orbitals. *J. Am. Chem. Soc.* **1980**, *102*, 7211-7218. (b) Reed, A. E.; Weinhold, F. Natural Localized Molecular-Orbitals. *J. Chem. Phys.* **1985**, *83*, 1736-1740. (c) Reed, A. E.; Weinstock, R. B.; Weinhold, F. Natural-Population Analysis. *J. Chem. Phys.* **1985**, *83*, 735-746. (d) Reed, A. E.; Curtiss, L. A.; Weinhold, F. Intermolecular Interactions from a Natural Bond Orbital, Donor-Acceptor Viewpoint. *Chem. Rev.* **1988**, *88*, 899-926.

(9) Chen, Z. F.; Wannere, C. S.; Corminboeuf, C.; Puchta, R.; Schleyer, P. v. R. Nucleus-Independent Chemical Shifts (NICS) as an Aromaticity Criterion. *Chem. Rev.* **2005**, *105*, 3842-3888.

(10) Wolinski, K.; Hinton, J. F.; Pulay, P. Efficient Implementation of the Gauge-Independent Atomic Orbital Method for NMR Chemical-Shift Calculations. *J. Am. Chem. Soc.* **1990**, *112*, 8251-8260.